UAB
Universitat Autònoma de Barcelona

Unraveling the locomotor behavior of extinct primates: A morphofunctional analysis of three tarsal bones using 3D geometric morphometrics

ORIOL MONCLÚS GONZALO

ADVERTIMENT. L'accés als continguts d'aquesta tesi queda condicionat a l'acceptació de les condicions d'ús establertes per la següent llicència Creative Commons: https://creativecommons.org/licenses/?lang=ca

ADVERTENCIA. El acceso a los contenidos de esta tesis queda condicionado a la aceptación de las condiciones de uso establecidas por la siguiente licencia Creative Commons: https://creativecommons.org/licenses/?lang=es

WARNING. The access to the contents of this doctoral thesis it is limited to the acceptance of the use conditions set by the following Creative Commons license: https://creativecommons.org/licenses/?lang=en

Institut Català de Paleontologia
Miquel Crusafont

UAB
Universitat Autònoma
de Barcelona

Unraveling the locomotor behavior of extinct primates:

A morphofunctional analysis of three tarsal bones using 3D geometric morphometrics

ORIOL MONCLÚS GONZALO



PhD Dissertation

Universitat Autònoma de Barcelona
PhD Program in Geology

2025

Supervisors
Judit Marigó
David M. Alba

Cover: Leonardo Sorbelli



Institut Català de Paleontologia
Miquel Crusafont

UAB
Universitat Autònoma
de Barcelona

Unraveling the locomotor behavior of extinct primates:

A morphofunctional analysis of three tarsal bones using 3D geometric morphometrics

ORIOL MONCLÚS GONZALO

PhD Dissertation

Universitat Autònoma de Barcelona

PhD Program in Geology

2025

Supervisors: Judit Marigó

David M. Alba

Unraveling the locomotor behavior of extinct primates:

A morphofunctional analysis of three tarsal bones using 3D geometric morphometrics

Dissertation submitted by **Oriol Monclús Gonzalo** to the PhD Program in Geology, Department of Geology, in fulfillment of the requirements for obtaining the degree of Doctor by the Universitat Autònoma de Barcelona, and elaborated under the supervision of:

Dr. Judit Marigó, Universitat Autònoma de Barcelona, Department of Geology.

Dr. David M. Alba, Institut Català de Paleontologia Miquel Crusafont, Universitat Autònoma de Barcelona.

Signed in Bellaterra on November 4th, 2025:

Dr. Judit Marigó	Dr. David M. Alba	Oriol Monclús Gonzalo
Supervisor	Supervisor & tutor	PhD candidate

Res no uneix tant com una bestiesa compartida.

Joan Fuster (*Judicis finals*, 1985)

Y así, del poco dormir y del mucho leer, se le secó el celebro, de manera que vino a perder el juicio.

Miguel de Cervantes (*El ingenioso hidalgo don Quijote de la Mancha*, 1605)

For the most part we have little pride in our feet and it is a pity that this is so.

Frederic Wood Jones (*Structure and function as seen in the foot*, 1944)

Per correr miglior acque alza le vele
omai la navicella del mio ingegno,
che lascia dietro a sé mar sì crudele.

Dante Alighieri (*Purgatorio*, c. 1321)

Vae, puto deus fio.

Suetonius (*De vita Caesarum*, c. 121 A.D.)

Index

Index 7
Abstract 11
Acknowledgments 17
Chapter 1. Introduction 25
1.1. Non-human primate locomotion 25
1.1.1. What is a primate? 25
1.1.2. Extant non-human primate locomotor diversity 29
1.2. Functional morphology of the hindfoot and the navicular bone 38
1.2.1. The primate foot 38
1.2.2. The astragalus 43
1.2.3. The calcaneus 50
1.2.4. The navicular 57
1.3. Case study 1: The adaptive origin of primates 63
1.3.1. Plesiadapiforms 63
1.3.2. Adapiforms and omomyiforms 65
1.3.3. Early anthropoids 66
1.3.4. Hypotheses on euprimate origins 68
1.4. Case study 2: Hominoid locomotor evolution in the light of pedal evidence 72
1.4.1. The foot of Miocene apes: A general review 72
1.4.2. The great apes of the Vallès-Penedès Basin 74
1.5. Aims, scope, and structure 78
1.5.1. Scope and specific aims 78
1.5.2. Structure of this work 79
Chapter 2. Materials and Methods 85
2.1. Sample composition 85
2.1.1. Studied fossil sample for case study 1 and 2 85
2.1.2. Extant comparative sample for case study 1 and 2 88
2.2. Shape analysis 91
2.2.1. Geometric morphometrics 91
2.2.2. Phylogenetic Comparative Methods 100
2.2.3. Statistical shape analyses 105
Chapter 3. Early euprimates already had a diverse locomotor repertoire: Evidence from ankle bone morphology 121
Abstract 121
Introduction 121
Materials and methods 122
Sample composition, data collection, and phylogenetic tree 122
Quantification of shape, impact of size, and navicular shape variation 123
Covariation between navicular shape and locomotion in extant euprimate species 123
Reconstruction of early euprimate locomotor behavior 124
Navicular morphological evolution 125
Shape visualization 125
Results 126

Navicular shape variation among primates ... 126
Navicular shape as a proxy for locomotion ... 126
Reconstruction of the locomotor repertoire of early primates ... 126
Navicular evolution across the archaic primate–euprimate transition ... 127
Discussion ... 128
Understanding variation in navicular shape among primates ... 128
The diverse locomotion of early euprimates ... 130
The archaic primate–euprimate transition ... 132
Conclusions ... 132
Acknowledgments ... 132
References ... 133
Supplementary Online Material ... 135
Chapter 4. Reconstruction of the locomotor repertoire of early primates in the light of astragalar and calcaneal shape ... 165
Abstract ... 165
Introduction ... 165
Materials and methods ... 167
Sample composition and data collection ... 167
Quantification of shape, astragalar/calcaneal shape variation, and influence of size ... 167
Covariation between astragalar/calcaneal shape and locomotor behavior in extant euprimates ... 171
Reconstruction of extinct primate locomotor behavior ... 171
Rates of morphological evolution ... 173
Shape visualization ... 173
Results ... 173
Astragalar shape variation ... 173
Calcaneal shape variation ... 176
Astragalar shape as a predictor for locomotion ... 178
Calcaneal shape as a predictor for locomotion ... 180
Variation in the locomotor behavior of Paleogene primates ... 181
The evolution of astragalar and calcaneal shape in relation to locomotor changes among early primates ... 181
Discussion ... 183
Functional morphology of the astragalocalcaneal complex ... 183
The locomotor behavior of Paleogene primates ... 188
Origin and diversification of euprimates in the light of locomotor behavior ... 190
Summary and conclusions ... 191
Acknowledgments ... 191
References ... 192
Supplementary online material ... 197
Chapter 5. A dryopithecine talus from Abocador de Can Mata (Vallès-Penedès Basin, NE Iberian Peninsula): Morphometric affinities and evolutionary implications for hominoid locomotion ... 259
Abstract ... 259
Introduction ... 260
The talus of Miocene apes ... 260
Age and geological background ... 261

Materials and methods 261
Studied material and comparative sample 261
Surface scanning 261
Geometric morphometrics 261
Body mass estimation 263
Partial least-squares regression 264
Results 267
Description 267
Comparison with stem catarrhine and other Miocene ape tali 267
Morphometric comparisons 268
Body mass estimation 270
Partial least-squares regression 271
Discussion 274
Body size, sex assignment, and taxonomic attribution 274
Morphofunctional inferences and quantitative comparisons with extant anthropoids 275
Implications for the evolution of crown hominoid positional behaviors 276
Conclusions 277
Acknowledgments 278
References 278
Supplementary information 285
Chapter 6. Discussion 317
6.1. Functional morphology of the hindfoot and the navicular bone 317
6.1.1. The astragalus 318
6.1.2. The calcaneus 327
6.1.3. The navicular 333
6.2. Reconstruction of the locomotor behavior of Paleogene primates 336
6.2.1. Plesiadapiforms 336
6.2.2. Adapiforms 338
6.2.3. Omomyiforms 341
6.2.4. Early anthropoids 342
6.3. Insights into primate origins and early evolution from tarsal evidence 344
6.4. The evolution of crown-hominoid positional behaviors in the light of a dryopithecine astragalus from Abocador de Can Mata 346
6.4.1. Morphometric affinities, locomotor reconstruction and taxonomic attribution 346
6.4.2. Evolutionary implications for hominoid locomotion 351
Chapter 7. Conclusions 357
References 361

Abstract [English]

Primates display greater locomotor diversity than most other mammals and also exhibit remarkably versatile locomotor repertoires (combining multiple locomotor modes, such as quadrupedalism, climbing, clambering, leaping, suspension, and bipedalism). Albeit a few species are terrestrial, such locomotor diversity is mostly related to the extensive use of arboreal substrates. To make locomotor inferences about extinct species, it is critical to characterize the morphological adaptations that are functionally related to each locomotor mode. Foot elements are particularly informative in this regard, as they play an important role in locomotion, participating in body weight transfer, stability and mobility across multiple joints.

This dissertation focuses on the study of three tarsal bones (astragalus, calcaneus, and navicular) in primates, within the framework of two case studies. The first one examines the origin, early diversification and locomotor diversity of euprimates (primates of modern aspect), while the second one describes an unpublished isolated dryopithecine astragalus and discusses its morphofunctional implications for crown-hominoid locomotor evolution. The specific aims of this dissertation are the following: (I) to quantify the shape of these three tarsal bones using landmark-based 3D geometric morphometrics and assess whether shape variation among species covaries with distinct locomotor behaviors; (II) to quantitatively infer, via partial least-squares regression (PLSR), the locomotor repertoire of a comprehensive sample of early primates, providing a nuanced representation of the primate locomotor spectrum; (III) to investigate the origin and early radiation of euprimates based on tarsal evidence; and (IV) to investigate the functional morphology of the aforementioned dryopithecine astragalus.

The results are presented as three published articles, which are subsequently discussed together in relation to the relevant scientific literature and with regard to future research directions. The main conclusions can be summarized as follows: (I) the shape of the astragalus, calcaneus, and navicular is functionally related to locomotor behavior in extant primates, indicating that these bones can be used to make locomotor inferences in extinct primates; (II) plesiadapiforms (likely a paraphyletic assemblage of stem primates) are inferred to have been primarily quadrupedal, although to some extent they also engaged in other behaviors (particularly based on calcaneal shape); (III) among early euprimates, which are characterized by moderate leaping adaptations, adapiforms exhibited the most diverse locomotor repertoires, greater pedal mobility, and emphasis on inverted postures compared with omomyiforms, which appear to have been more proficient leapers; (IV) Asian early anthropoids are reconstructed as

generalized arboreal quadrupeds (combining quadrupedal locomotion with other behaviors such as leaping, climbing, and suspension), whereas Afro-Arabian parapithecoids are reconstructed as above-branch quadrupeds and horizontal leapers; and (V) the dryopithecine astragalus shows a mosaic of derived and plesiomorphic features compared with crown hominoids and yields an estimated locomotor repertoire consistent with previous inferences based on other anatomical areas.

Future lines of research should aim at incorporating additional types of morphological information, such as internal bone microstructure (to examine bone ecophenotypic plasticity) and biomechanical analyses (to test observed correlations between form and function). Such a holistic approach, coupled with discoveries of additional postcranial remains of fossil primates, would hopefully provide a more comprehensive framework for deciphering further the origin of locomotor adaptations during primate evolution.

Resum [Català]

Els primats presenten una major diversitat locomotora que la majoria dels altres mamífers i també exhibeixen repertoris locomotors notablement versàtils (combinant múltiples modes de locomoció, com ara el quadrupedisme, la grimpada, el salt, la suspensió i el bipedisme). Encara que algunes espècies són terrestres, aquesta diversitat locomotora es relaciona sobretot amb l'ús extensiu de substrats arboris. Per tal de realitzar inferències locomotores sobre espècies extintes, és fonamental caracteritzar les adaptacions morfològiques que estan funcionalment relacionades amb cada mode de locomoció. Els elements del peu són especialment informatius en aquest sentit, ja que tenen un rol important en la locomoció, participant en la transmissió del pes corporal, l'estabilitat i la mobilitat a través de múltiples articulacions.

Aquesta tesi doctoral se centra en l'estudi de tres ossos del tars (l'astràgal, el calcani i el navicular) en primats, en el marc de dos casos pràctics. El primer examina l'origen, la diversificació inicial i la diversitat locomotora dels euprimats (primats d'aspecte modern), mentre que el segon descriu un astràgal de driopitecí inèdit i n'analitza les implicacions morfofuncionals per a l'evolució locomotora dels hominoïdeus corona. Els objectius específics d'aquesta tesi són els següents: (I) quantificar la forma d'aquests tres ossos del tars mitjançant morfometria geomètrica en 3D basada en *landmarks* i avaluar si la variació de la forma entre espècies covaria amb els diferents comportaments locomotors; (II) inferir quantitativament, mitjançant la regressió per mínims quadrats parcials (PLSR), el repertori locomotor d'una mostra àmplia de primats primerencs, proporcionant una representació més contínua de l'espectre locomotor dels primats; (III) investigar l'origen i la radiació inicial dels euprimats a partir de l'evidència proporcionada pel tars; i (IV) investigar la morfologia funcional de l'astràgal de driopitecí esmentat anteriorment.

Els resultats es presenten com a tres articles publicats, els quals posteriorment es discuteixen en relació amb la literatura científica rellevant i fent referència a futures línies de recerca. Les principals conclusions es poden resumir de la següent manera: (I) la forma de l'astràgal, el calcani i el navicular està relacionada funcionalment amb el comportament locomotor en els primats actuals, la qual cosa indica que aquests ossos poden utilitzar-se per a realitzar inferències locomotores en primats extints; (II) s'infereix que els plesiadapiformes (probablement, un conjunt parafilètic de primats basals) eren principalment quadrúpedes, tot i que també duien a terme altres comportaments locomotors (sobretot a partir de la forma del calcani); (III) entre els euprimats primerencs, caracteritzats per adaptacions moderades al salt, els adapiformes mostraven els repertoris locomotors més diversos, una major mobilitat del peu i un major èmfasi

en postures invertides en comparació amb els omomiformes, que probablement eren saltadors més eficients; (IV) els antropoïdeus asiàtics primerencs són reconstruïts com a quadrúpedes arboris generalitzats (combinant la locomoció quadrúpeda amb altres comportaments com el salt, la grimpada i la suspensió), mentre que els parapitecoïdeus d'Afro-Aràbia són reconstruïts com a quadrúpedes que es desplaçaven damunt les branques i saltadors horitzontals; i (V) l'astràgal de driopitecí presenta un mosaic de trets derivats i plesiomòrfics en comparació amb els hominoïdeus corona, i indica un repertori locomotor coherent amb inferències funcionals prèvies basades en altres àrees anatòmiques.

Les futures línies de recerca haurien d'intentar incorporar fonts addicionals d'informació morfològica, com ara la microestructura interna de l'os (per examinar-ne la seva plasticitat ecofenotípica), i realitzar anàlisis biomecàniques (per testar les correlacions observades entre forma i funció). Aquest enfocament holístic, combinat amb troballes de restes postcranials addicionals de primats fòssils, hauria de poder oferir un marc de treball més complet per estudiar amb major profunditat l'origen de les adaptacions locomotores durant l'evolució dels primats.

Resumen [Castellano]

Los primates presentan una mayor diversidad locomotora que la mayoría de los otros mamíferos y también muestran repertorios locomotores notablemente versátiles (combinando múltiples modos de locomoción, como cuadrupedismo, trepada, salto, suspensión y bipedismo). Aunque algunas especies son terrestres, esta diversidad locomotora se relaciona sobre todo con el uso extensivo de sustratos arbóreos. Para poder realizar inferencias locomotoras sobre especies extintas, es fundamental caracterizar las adaptaciones morfológicas que están funcionalmente relacionadas con cada modo de locomoción. Los elementos del pie son especialmente informativos en este sentido, ya que desempeñan un papel importante en la locomoción, participando en la transmisión del peso corporal, la estabilidad y la movilidad a través de múltiples articulaciones.

Esta tesis doctoral se centra en el estudio de tres huesos del tarso (el astrágalo, el calcáneo y el navicular) en primates, en el marco de dos casos prácticos. El primero examina el origen, la diversificación inicial y la diversidad locomotora de los euprimates (primates de aspecto moderno), mientras que el segundo describe un astrágalo de driopitecino inédito y analiza las implicaciones morfofuncionales para la evolución locomotora de los hominoideos corona. Los objetivos específicos de esta tesis son los siguientes: (I) cuantificar la forma de estos tres huesos del tarso mediante morfometría geométrica en 3D basada en *landmarks* y evaluar si la variación de la forma entre especies covaría con los distintos comportamientos locomotores; (II) inferir cuantitativamente, mediante la regresión por mínimos cuadrados parciales (PLSR), el repertorio locomotor de una amplia muestra de primates primitivos, proporcionando una representación más continua del espectro locomotor de los primates; (III) investigar el origen y la radiación inicial de los euprimates a partir de la evidencia proporcionada por el tarso; e (IV) investigar la morfología funcional del astrágalo del driopitecino mencionado anteriormente.

Los resultados se presentan en forma de tres artículos publicados, que posteriormente se discuten en relación con la literatura científica relevante y haciendo referencia a futuras líneas de investigación. Las principales conclusiones pueden resumirse de la siguiente manera: (I) la forma del astrágalo, el calcáneo y el navicular está funcionalmente relacionada con el comportamiento locomotor en los primates actuales, lo que indica que estos huesos pueden utilizarse para realizar inferencias locomotoras en primates extintos; (II) se infiere que los plesiadapiformes (probablemente, un conjunto parafilético de primates basales) eran principalmente cuadrúpedos, aunque también realizaban otros comportamientos locomotores (sobre todo a partir de la forma

del calcáneo); (III) entre los euprimates tempranos, caracterizados por adaptaciones moderadas al salto, los adapiformes mostraban los repertorios locomotores más diversos, una mayor movilidad del pie y un mayor énfasis en posturas invertidas en comparación con los omomiformes, que probablemente eran saltadores más eficientes; (IV) los antropoideos asiáticos tempranos se reconstruyen como cuadrúpedos arborícolas generalizados (combinando la locomoción cuadrúpeda con otros comportamientos como el salto, la trepa y la suspensión), mientras que los parapitecoideos de Afro-Arabia se reconstruyen como cuadrúpedos que se desplazaban sobre las ramas y saltadores horizontales; y (V) el astrágalo del driopitecino presenta un mosaico de rasgos derivados y plesiomórficos en comparación con los hominoideos corona, e indica un repertorio locomotor coherente con inferencias funcionales previas basadas en otras áreas anatómicas.

Las futuras líneas de investigación deberían intentar incorporar fuentes adicionales de información morfológica, como la microestructura interna del hueso (para examinar su plasticidad ecofenotípica), y realizar análisis biomecánicos (para comprobar las correlaciones observadas entre forma y función). Este enfoque holístico, combinado con hallazgos de restos postcraneales adicionales de primates fósiles, debería ofrecer un marco de trabajo más completo para estudiar con mayor profundidad el origen de las adaptaciones locomotoras durante la evolución de los primates.

Acknowledgments

Aquesta tesi s'ha realitzat amb el suport de l'AGAUR (Agència de Gestió d'Ajuts Universitaris i de Recerca) amb els ajuts Joan Oró per a la contractació de personal investigador predoctoral en formació (2021 FI_B 00524, 2022 FI_B1 00131, 2023 FI-3 00131), amb el suport de la Secretaria d'Universitats i de Recerca de la Generalitat de Catalunya i el Fons Social Europeu. Els treballs realitzats en el context d'aquesta tesi doctoral s'han realitzat en el marc dels projectes R+I+D (PID2020-116908GB-I00, PID2024-159434NB-I00 i PID2024-157557NB-I00), finançats per la Agencia Estatal de Investigación del Ministerio de Ciencia e Innovación (MCIN/AEI/10.13039/501100011033/) i en el context del grup de recerca consolidat de Paleoprimatologia i Paleontologia Humana (2021 SGR 01188). A més, també ha estat clau en la meva formació com a paleontòleg poder participar en diferents campanyes d'excavació, gràcies als projectes "El Paleogen català i l'origen dels primats" (CLT0009-22-000022) i "La transició Aragonià/Vallesià a la conca del Vallès-Penedès" (CLT0009_22_000018), finançats pel Departament de Cultura de la Generalitat de Catalunya. També m'agradaria agrair al coordinador del programa de doctorat en Geologia, en Joan Reche, per la seva ajuda en dubtes i qüestions que han anat sorgint al llarg d'aquests anys, així com al comitè de seguiment de doctorat, pels seus consells durant totes les sessions de seguiment: M. Luisa Arboleya, Mercè Corbella, Marc Furió, Albert Griera i Arnau Bolet. Així mateix, també m'agradaria expressar la meva gratitud als següents investigadors per acceptar formar part del tribunal titular i suplent de la defensa d'aquesta tesi: Tracy Kivell, Júlia Arias-Martorell, Raef Minwer-Barakat, Josep M. Potau, Marta Pina i Nicole Torres-Tamayo. A més, de nou voldria donar les gràcies a la Tracy Kivell i la Nicole Torres-Tamayo per també acceptar ser avaluadores externes de la tesi.

A títol personal, m'agradaria començar per agrair i expressar la meva admiració als meus dos directors, a qui dec el meu creixement com a científic al llarg d'aquests gairebé cinc anys de feina:

Judit, ja durant el màster vas guiar-me en els meus primers passos per la morfometria geomètrica i l'estudi del peu dels primats, i, més endavant, has seguit aconsellant-me i supervisant el meu treball, sovint més enllà del que és estrictament científic, la qual cosa valoro moltíssim i ha sigut cabdal en el meu aprenentatge. El que m'has transmès aquests anys és el nucli del meu coneixement com a científic. Estic molt feliç d'haver estat el teu primer estudiant de doctorat i confio que puguem seguir treballant junts d'ara en endavant!

David, gràcies per haver confiat en mi i donat suport incomptables vegades, sovint quan jo mateix no les tenia totes o, potser per inexperiència o voler córrer massa, no podia encara afrontar-les. Et dec haver crescut i madurat (una mica, ni que sigui) com a investigador aquests darrers anys. M'has demostrat com de profund i interessant és aquest camp, a no conformar-me i a intentar excel·lir en el que faig i, sobretot, a raonar, raonar i raonar; confio en poder seguir col·laborant i aprenent de tu. En tot el que faci com a investigador a partir d'ara, espero que hi puguis veure la teva empremta com el mentor que has estat per mi.

També m'agradaria mencionar els/les següents investigador/es i col·laborador/es, que han contribuït en diferents aspectes del meu treball al llarg d'aquests anys, i a qui, per tant, també els/les dec moltíssim. Anne-Claire, I'm very grateful to have had you as my master co-supervisor, your guidance and inspiration introduced me to several methods that have now become central to my research. Merci beaucoup! Raef, ha sido un placer excavar contigo a lo largo de estos años, agradezco muchísimo tus charlas y buen humor y cervezas (¡también en Benevento!), y, por supuesto, que accedieras a formar parte del tribunal (¡gracias Maribel!). Sole, admiro muchísimo el proyecto del Bridges (del que pude formar parte y aprender muchísimo gracias a ti) y también los diferentes cursos de Transmitting Science, donde he tenido la oportunidad de formarme en nuevas metodologías y mejorar como investigador; gracias por siempre ser tan amable conmigo. Marc, gràcies per la teva tasca orientadora durant el màster, sempre preocupant-te per intentar-nos aconsellar de cara al futur. Júlia, has estat importantíssima per mi com a mentora i persona de confiança en aquest darrer tram de la tesi; t'agraeixo moltíssim totes les oportunitats que m'has donat per treballar plegats i confio poder-ho seguir fent d'ara endavant. Per descomptat, gràcies també per accedir a formar part del tribunal! Alessandro, siempre te has preocupado por ayudarme y aconsejarme como si fueras mi "hermano mayor científico", te lo agradezco muchísimo y espero que nos sigamos viendo en congresos, excavaciones y colaboraciones! Marta, me gustaría agradecerte tu ayuda en establecer nuevas colaboraciones, así como en siempre querer compartir tus experiencias y aconsejarme en cómo afrontar algunos de los retos de la investigación, ¡muchísimas gracias! I per últim, Josep Manel, et vull donar les gràcies per la teva amabilitat, pel teu esforç en les excavacions, i per compartir la teva enorme i admirable passió pels fòssils amb els altres.

Als coautors dels articles que conformen aquesta tesi, també els voldria agrair la seva paciència i dedicació. Sergio, moltes gràcies pels teus comentaris sobre l'article de l'astràgal del driopitec; Thomas, te agradezco muchísimo tus consejos sobre algunos aspectos metodológicos de la tesis y, sobre todo, por proponerme venir a Oxford para trabajar contigo; ¡espero que muy pronto

podamos trabajar juntos en nuevos proyectos! Anaïs, I'd like to thank you for your help with the phylogenetic discriminant analysis, it was a real highlight of the navicular paper!

L'edifici de l'ICP (peculiar, tots ho sabem; una mena de *Skynet* en potència si un dia decideix fer quelcom més que apagar les llums i obrir les finestres quan vol) ha estat casa meva durant aquests anys de tesi. Això és gràcies a tothom amb qui he compartit espai i que, d'una manera o altra, han contribuït en ajudar-me en el meu benestar i/o recerca. Moltes gràcies, companyes i companys, per ser-hi durant aquests anys; als passadissos, als paleovermuts, a les "colònies" amb l'IBE, a les graellades i a les calçotades. També voldria mencionar i agrair la feina a l'equip de treballador/es que mantenen l'edifici, l'oficina i, en particular, el meu escriptori (un lloc força entròpic) net i en condicions. En especial, gràcies Pepi per tenir sempre un amable bon dia de benvinguda per començar la jornada.

Aquests darrers anys han estat molt més que landmarks i peus de primats. Com diu aquesta màxima apòcrifa de Cervantes: "siempre es mejor el camino que la posada", i, sens dubte, aquest és el major regal que em podia oferir el doctorat. Moltes gràcies a tots els que heu estat aquí: Souzanna, Leo, Florian, Chabi, Andrea, Elpiniki, Maria, Georgina, Carmen, Raquel, Jordi, Kelly, Laia, Jesús, Omar, Ane, Álex, Bernat, David, Júlia J., Marina, Ana, Albert, Júlia R., Tiziana, Chara, Mattia i Nikoleta.

Menció especial als meus actuals (i històrics) companys de despatx, la Georgina, el Florian i el Jesús, que han hagut de compartir espai amb algú tan desordenat com jo. Als que us quedeu i pels que vinguin, espero que seguiu incrementant la col·lecció de mems de la porta; així no caldrà mirar-se fixament als ulls amb cada persona que passa o surt de l'ascensor. También me gustaría agradecer a Raquel por siempre estar en todas las buenas ocasiones e ir conmigo a tantas clases del SAF (las de "mortal kombat" en concreto fueron geniales, ¡aún no he tenido ocasión de ponerlas en práctica en la vida real!); a Carmen, por esos inolvidables podcasts y por ser siempre tan amable y dar tan buenos consejos con todo, eres un modelo para mí; a la Maria, per ajudar-nos amb els dubtes burocràtics i animar-nos un a l'altre a escriure la tesi en aquest darrer tram del doctorat; a la Georgina, per la bona energia que sempre transmet i per estar tan disposada a col·laborar i donar-me un cop de mà en el que sigui; to Elpiniki, for welcoming me last year in Perugia during the jazz festival, an "oriolic" experience for sure!; a la Marina, la Júlia i l'Ana, per sempre poder comptar amb elles per fer unes birres al bar dels ferros (i, a vegades, a bars força curiosos de Sabadell); a l'Andrea, el Chabi i el Florian, "this is the way", i, evidentment, "tot anirà bé"!; gràcies per fer més amens aquests anys de tesi amb vosaltres, amics; al Leonardo, con cui sono rinato a Muntaner con Travessera de Gràcia, grazie anche per la magnifica copertina, amico

mio; and last, thank you, Souzanna, for being so great and for helping and listening to me all these years. Είσαι φίλος μου και θα είμαι πάντα εδώ αν με χρειαστείς.

No m'oblido de Montpeller ni de tothom que va fer possible que l'estada durant aquells tres mesos i escaig a Occitània fos més amena i divertida. I'd like to thank Rodolphe Tabuce for his diligent help with all the Erasmus bureaucracy; Laurent Marivaux for the insightful discussions on paleoprimatology; Maëva Orliac, Céline Robinet, and Mehdi Mouana for their help with the collections facility; Renaud Lebrun for his assistance during the CT-scanning sessions; Sylvie Agret for her kindness and for helping me improve my French; and PierrO for his friendliness and enthusiasm with the running group. Lastly, I would also like to thank all my colleagues there for making my stay so enjoyable: Lucas, Fleur, Felix, José, Moritz, Hamilcar, and Alba. També voldria agrair als meus companys peninsulars, Óscar, Lucía i Vincent, per les creps, les birres i la companyia durant el darrer mes de l'estada; gràcies!

Tot i que la tesi ha ocupat gran part de la meva atenció, altres projectes i ocupacions també han marcat aquesta etapa. En destaquen dos: un llibre de divulgació sobre el registre fòssil d'animals vertebrats dels Països Catalans i la plaça de professor substitut a la Unitat d'Antropologia del BABVE. Roc, moltes gràcies per invitar-me a participar en un projecte tan interessant. Ha estat una feina dura i, en paral·lel a la tesi, a vegades creia que no ho aconseguiria, però m'alegro del resultat que hem aconseguit plegats! Francesc, Gemma, Núria i Jèssica, us agraeixo moltíssim la vostra paciència i amabilitat a l'hora d'ajudar-me a preparar les classes durant el curs passat.

Si bé la tesi ha estat una nova etapa, això no vol dir que no hagi rebut l'escalf d'aquells a qui vaig conèixer abans de "complicar-me" la vida amb astràgals i naviculars. Julia, gracias por haber compartido conmigo la aventura de Nomen Dubium y por haber estado confidente de mis preocupaciones y metas durante los primeros compases de la tesis; També voldria donar les gràcies als meus infatigables bioquímics, Francesc, Andreu i Vadim, pel seu constant estímul intel·lectual i per la seva amistat incondicional, encara que jo a vegades estigués una mica desconnectat i amb baixa energia social (sense ATP, vaja...). Per últim, gràcies als meus amics molinencs, Berni, Juni, Minijuni, Forni i Muñi, amb qui he jugat partits de futsal contra tots els municipis de Catalunya i compartit més gintònics dels que em fa vergonya reconèixer. Vosaltres, després d'haver-me conegut a l'escola, ja podíeu intuir que alguna cosa així acabaria passant...

Per últim, m'agradaria agrair a la meva família l'entusiasme que sempre ha mostrat per tot el que feia, i com, des de ben petit, han intentat incentivar-ho. Gràcies als meus cosins i cunyat: Izan, Georgina, Julia, Pablo, Marina (i Noa!); i als meus tiets i tietes: Sergi, Loli, Esperanza i Ricardo. Estic

d'acord amb la Jane Austen, les tietes i els tiets (i això és extensible als altres) sou pilars, "persones de conseqüència", en fi, fonts incommensurables de suport i guia.

A la meva àvia Mercè, que ja des de petit em comprava llibres de dinosaures i animals prehistòrics, i que sempre ha estat incondicional en tot el que feia.

Als meus pares, Núria i Enric, a qui els dec tant, de fet tot, i que sempre m'han facilitat l'accés al coneixement i a la cultura; no puc pensar en un millor llegat que aquest per a un fill. M'heu donat suport, m'heu protegit, però també m'heu deixat equivocar-me quan ho he necessitat; gràcies.

A la meva germana, la Mar, per ser un model i una font d'inspiració; mai dubtis de tu mateixa, ets brillant i aconseguiràs tot el que et proposis!

Per últim, m'agradaria donar les gràcies a l'Eva-Mercè, la persona que m'ha acompanyat i m'ha donat les majors alegries durant aquest darrer any i escaig. T'admiro i m'inspires en tot el que fas; des que formes part de la meva vida ho has canviat tot.

Chapter 1:

Introduction

Chapter 1. Introduction

1.1. Non-human primate locomotion

1.1.1. What is a primate?

Primates are a mammalian order of moderate taxonomic diversity but marked morphological and ecological disparity (e.g. Fleagle and Seiffert, 2020; Fleagle et al., 2025). Comprising more than 300 species, extant non-human primates are distributed across a broad geographic range, spanning Africa, Asia, and South America (Groves, 2001). Primates exhibit a wide array of dietary and locomotor behaviors, life history patterns, and habitat preferences (Campbell et al., 2010). This is exemplified, for instance, by primates as ecologically and morphologically disparate as mouse lemurs (*Microcebus* spp.), slow lorises (*Nycticebus* spp.), squirrel galagos (*Sciurocheirus* spp.), spider monkeys (*Ateles* spp.), baboons (*Papio* spp.), or orangutans (*Pongo* spp.). Extant primates are classified into two groups, the suborder Strepsirrhini—comprising Malagasy lemurs, lorises, and bushbabies—and the suborder Haplorrhini—comprising tarsiers and anthropoids, which in turn include monkeys, apes, and humans (Groves, 2001; Table 1.1).

Four major adaptive complexes (Fig. 1.1) are characteristic of primates of modern aspect (Euprimates sensu Hoffstetter, 1977; discussed in Le Gros Clark, 1959; Napier and Napier, 1967; Martin, 1968; Szalay et al., 1987; Cartmill, 1992, 2012).

The first adaptive complex is related to improvements in the visual apparatus (Fig. 1.1A). This includes the possession of a postorbital bar (or septum in haplorrhines), large eyes, and convergent orbits. In addition, euprimates exhibit proportionally larger and more complex brains compared with other mammals (Martin, 1990; Silcox et al., 2009, 2010), which have been associated with the more complex social behavior exhibited by primates (Dunbar, 1998; Dunbar and Shultz, 2007), the selective pressures derived from arboreal environments (Falk, 2015), or selection for increased foraging efficiency (DeCasien et al., 2017). Moreover, the evolution of the visual apparatus was accompanied by a greater development of brain areas related to the visual apparatus (Kirk et al., 2006), along with other modifications, such as the shortening of the snout, a decrease in the complexity of nasal turbinates, and the presence of an interorbital septum (Smith et al., 2007).

The second adaptive complex includes a series of adaptations for habitual leaping behavior—ubiquitous among primates except for some groups, such as lorises, pottos, angwantibos, and great apes—such as elongated hindlimbs and modified foot bones (Fig.1.1B; Dagosto, 1988; 2007).

The third includes features related to enhanced grasping capabilities (Fig.1.1C), such as elongated manual and pedal phalanges, an opposable hallux (big toe) and pollex (thumb), and flat nails instead of bilaterally flattened, pointed claws on the big toe (and often on the other digits in most primate families). Additionally, primates have tactile pads with skin ridges, called dermatoglyphs, which, in combination with Meissner's corpuscles, enhance the sense of touch and provide better traction on arboreal substrates (Cartmill, 1974a).

Finally, the fourth adaptive complex encompasses features associated with herbivory (Fig.1.1D). Compared with the ancestral tribosphenic morphology exhibited by early eutherians, the dentition of primates is typically low-crowned, characterized by the addition of the hypocone on the upper molars, the hypoconid and hypoconulid on the lower molars, and the reduction or absence of the paraconid, resulting in increased occlusal complexity and functional adaptation to a more frugivorous diet (Szalay, 1968; Swindler, 2002). Nevertheless, primates are characterized by a wide range of dietary preferences, spanning from strict faunivores (such as tarsiers and some lorises) to specialized folivores (including bamboo lemurs, sifakas, indris, howler monkeys, langurs, colobus monkeys, and mountain gorillas), yet the diet of most species includes variable quantities of fruit (Fleagle et al., 2025). Primate diet may consist of other food items, such as seeds, gums, bark, nectar, or exudates (Ankel-Simons, 2007). Several factors influence primate foraging behavior, including body size, metabolic requirements, gut size, food passage rate, home range size, and the cost of locomotion (Kay, 1984; Garber, 1987). The influence of these different factors is reflected in their anatomy, such as the sharp, pointed teeth of tarsiers, an adaptation for chewing and breaking down the chitinous exoskeletons of certain insects, or the complex stomach and enlarged intestine of langurs, which facilitates the digestion of fibrous, low-quality plant material (Lambert, 1998). Additionally, the presence of a bulla constituted by the petrosal bone has often been cited as a unique euprimate synapomorphy, although its adaptive significance remains unclear (Szalay et al., 1987).

There is a broad consensus about the systematic position of primates within the Mammalia. They are included, together with the orders Dermoptera (colugos or flying lemurs) and Scandentia (tree shrews), within the superorder Euarchonta (Adkins and Honeycutt, 1991; Waddell et al., 1999;Liu et al., 2001; Murphy et al., 2001a, b; Springer et al., 2003, 2004). However, the internal

Table 1.1. Taxonomic classification of extant and extinct Primates down to superfamily rank, including taxon rank, name, and authority. Modified from Marigó et al. (2014). A dagger indicates extinct taxa.

Order Primates Linnaeus, 1758

Semiorder Plesiadapiformes Simons and Tatterstall, 1972†

Superfamily Paromomyoidea Simpson, 1940†

Superfamily Plesiadapoidea Trouessart, 1897†

Semiorder Euprimates Hoffstetter, 1977

Suborder Strepsirrhini Geoffroy Saint-Hilaire, 1812

Infraorder Adapiformes Hoffstetter, 1977†

Superfamily Adapoidea Trouessart, 1879†

Infraorder Lemuriformes Gregory, 1915

Superfamily Lemuroidea Gray, 1821

Superfamily Daubentonioidea Gray, 1863

Infraorder Lorisiformes Gregory, 1915

Superfamily Lorisoidea Gray, 1821

Suborder Haplorrhini Pocock, 1918

Infraorder Tarsiiformes Gregory, 1915

Superfamily Omomyoidea Trouessart, 1879†

Superfamily Tarsioidea Gray, 1825

Infraorder Anthropoidea Mivart, 1864 (=Simiiformes Hofftsetter, 1977)

Pavorder incertae sedis

Superfamily Parapithecoidea Schlosser, 1911†

Pavorder Platyrrhini Geoffroy Saint-Hilaire, 1812

Superfamily Pithecoidea Mivart, 1865

Superfamily Ceboidea Bonaparte, 1831

Pavorder Catarrhini Geoffroy Saint-Hilaire, 1812

Superfamily Propliopithecoidea Strauss, 1961†

Superfamily Pliopithecoidea Zapfe, 1960†

Superfamily Cercopithecoidea Gray, 1821

Superfamily Hominoidea Gray, 1825

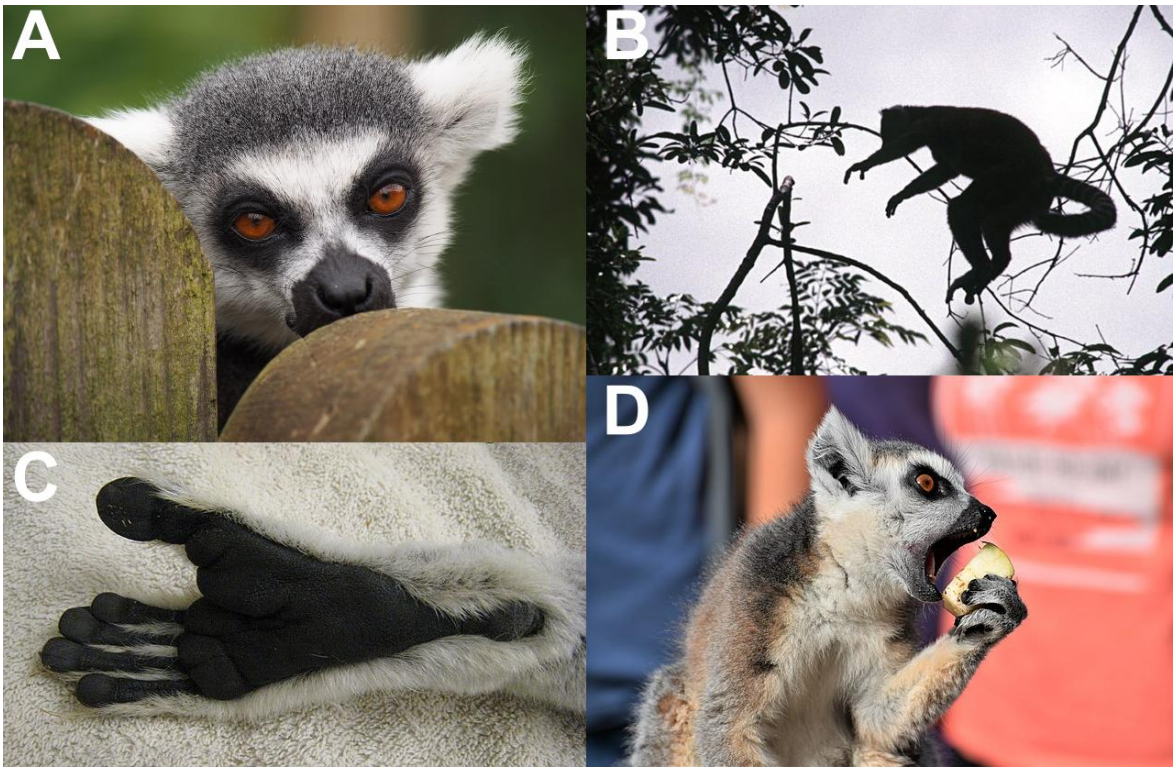


Figure 1.1. The four major adaptive complexes of euprimates depicted by a ring-tailed lemur (*Lemur catta*): (A) enhanced visual apparatus (© Francis C. Franklin / CC-BY-SA-3.0); (B) adaptations for leaping behavior (© Tom Junek / CC BY-SA 3.0); (C) enhanced grasping capabilities (© Zina Suljić / CC BY-SA 4.0); (D) herbivory (© Alex Dunkel / CC BY-SA 3.0).

phylogenetic relationships of euarchontans have been subject to extensive debate (Silcox et al., 2015). Either the Dermoptera (Janecka et al., 2007), the Scandentia (Novacek, 1992; Godinot, 2007; Song et al., 2012), or a clade comprising both (Sundatheria; Springer et al. 2003, 2004; Bloch et al. 2007; O'Leary et al., 2013) have been proposed as the sister taxon of Primates, based on various sources of evidence. In turn, a major issue when addressing the definition of primates is the inclusion of fossils. The earliest unequivocal primates (euprimates) are first recorded during the Paleocene–Eocene transition (~55.8 Ma; Ni et al., 2004; Smith et al., 2006; Beard, 2008; Rose et al., 2011). A more contentious putative early euprimate, *Altiatlasius koulchii*, has been recovered from even older layers, stretching out the origin of euprimates to the late Paleocene (Sigé et al., 1990; but see alternative interpretations in Godinot, 1994; Hooker et al., 1999). This age would concur with some molecular estimates that suggest that the last common ancestor of euprimates lived just after the K/Pg boundary, during the early Paleocene (Chatterjee et al., 2009; Springer et al., 2012), although other studies yield older age estimates (reviewed in Raaum, 2015). The inclusion of plesiadapiforms within Primates is also contentious. Early researchers classified them as primates based on dental similarities (e.g., Gidley 1923; Le Gros Clark, 1959; see also Szalay, 1968;

Szalay et al. 1987), albeit other alternative phylogenetic relationships—mainly between paromomyid plesiadapiforms and dermopterans (see Beard, 1990, 1993a, b; Kay et al., 1990, 1992)—have been suggested, challenging this view during the last two decades of the past century. More recently, however, new and better-informed phylogenetic analyses (thanks to the recovery of more complete plesiadapiform skeletons) evinced that this group exhibits closer ties with euprimates than with either colugos or tree shrews, favoring again the view that plesiadapiforms are a paraphyletic assemblage of stem primates (Silcox, 2001, 2007; Bloch and Boyer, 2002, 2007; Bloch et al., 2007; Boyer and Bloch, 2008).

1.1.2. Extant non-human primate locomotor diversity

The positional behaviors of extant primates are highly diverse and combine an extensive array of locomotor modes, including quadrupedal walking and running, climbing, clambering, leaping, different types of suspensory behaviors, and bipedalism (Campbell et al., 2010; Fleagle et al., 2025). This remarkable locomotor diversity is, to a large extent, linked to the use of arboreal substrates and considered essential for the diversification and evolutionary success of the order (Cartmill, 1974a; Vilensky and Larson, 1989; Cant, 1992; Schmitt et al., 2016; Granatosky, 2018). Some primates, particularly catarrhines, are also partly or fully terrestrial (e.g., Gebo, 1996; Benefit, 1999), yet all species are still capable of engaging in substantial arboreal locomotion when needed. Traveling across thin and flexible arboreal substrates represents an important biomechanical challenge, as the body of the animal will tend to pitch or roll (Cartmill, 1985; Cant, 1992; Preuschoft, 2002; Schmitt et al., 2016). To maintain balance, grasping extremities are used to generate opposite torques, which has a profound impact in the type of gait utilized by primates (Hildebrand, 1967, 1985; Cartmill, 1974a; Lemelin, 1999; Schmitt and Lemelin, 2002; Lemelin et al., 2003; Cartmill et al., 2007a, b; Lemelin and Schmitt, 2007). Compared to most non-primate mammals, which exhibit lateral-sequence (LS) gaits—each hind footfall is followed by the ipsilateral fore footfall—primates habitually employ diagonal sequence (DS) gaits to travel across the arboreal canopy. In DS gaits, the hindfoot contacts the substrate first, followed by the contralateral forefoot. This minimizes bipedal support on ipsilateral limbs (i.e., supporting the body weight with two limbs in the same side of the body) and allows the descending forelimb to assess new substrates while grasping them underneath the center of mass (Hildebrand, 1967, 1985; Vilensky and Larson, 1989; Larson, 1998a; Cartmill et al., 2002, 2007a, b; Lemelin et al., 2003). Additionally, primates also display a more protracted arm position of the humerus at touchdown,

enhancing their reach when grasping arboreal substrates and facilitating activities such as grabbing food items with their hands (Larson, 1998a; Larson et al., 2000, 2001). As a result of these grasping adaptations to deal with the fine branch niche, most of the weight-bearing function has shifted from the forelimbs to the hindlimbs (Reynolds, 1985a, b; Demes et al., 1994; Schmitt and Hanna, 2004; Schmidt, 2005). Similarly, primates exhibit greater limb compliance compared to most other non-primate mammals, enhancing their ability to balance and improving their maneuverability on the arboreal supports (Jenkins, 1974; Cartmill, 1985; Schmitt, 1999; Larney and Larson, 2004). Altogether, the evolution of grasping extremities has been linked to the exploitation of the fine-branch milieu by primates, resulting in all the aforementioned unusual locomotor characteristics of this group (Larson, 1998a).

Strepsirrhine primates display a very diverse array of locomotor behaviors (Fig. 1.2), from specialized vertical clingers and leapers (VCL; indris, sifakas, wooly lemurs, and some bushbaby species) to slow climbers (aye-ayes, lorises, pottos, and angwantibos; Walker, 1974; Gebo, 1987a; Oxnard et al., 1990). Additionally, some species, like the ring-tailed lemur (*Lemur catta*), habitually spend a lot of time on the ground, while others, such as the fork-crowned lemur (*Phaner* spp.) or the needle-clawed bushbaby (*Euoticus* spp.), possess keeled nails that allow them to cling on vertical trunks (Ward and Sussman, 1979; Forbanka, 2018).

Among lorisiforms, lorisids (lorises, pottos, and angwantibos) engage in a cautious and slow locomotion along the fine branch milieu, including hindlimb suspension and bridging across gaps of the arboreal canopy (Walker, 1969; Dykyj, 1980; Glassman and Wells, 1984; Gebo, 1987a; Oxnard et al., 1990; Nekaris and Setevens, 2007). Their specialized locomotor repertoire is reflected in various postcranial adaptations facilitating joint mobility, including those in the wrist, ankle, and lumbar spine (Grand, 1967; Cartmill and Milton, 1977; Gebo, 1989a; Runestad, 1997; Shapiro, 2007; Yapuncich and Granatosky, 2021). Bridging is particularly important in these animals, as they lack the ability to leap across gaps in the arboreal canopy. Bridging is accomplished by grasping the terminal end of a support and pulling it towards themselves until it can bear their body weight. Moreover, lorisid kinematics depart from that of most other primates, as they habitually exhibit relatively higher peak forces on their forelimbs and have been observed to utilize lateral-sequence gaits more frequently (Hilderbrand, 1967; Dykyj, 1980; Schmitt and Lemellin, 2004). In contrast, most galagids (bushbabies) are described as very agile leapers, ranging from specialized VCL, such as the squirrel bushbabies (*Sciurocheirus* spp.) to above-branch arboreal quadrupeds and horizontal leapers like the thick-tailed bushbabies (*Otolemur* spp.; Hall-Craggs, 1965a; Crompton, 1983; Gebo, 1987a; Oxnard et al., 1990; Off and Gebo, 2005). Their postcranial anatomy, particularly the hindlimbs, exhibit several adaptations

associated with leaping performance (Hall-Craggs, 1965b, 1966; Stevens et al., 1971; Gebo, 1989a; Lewton et al., 2020).

Among Malagasy lemurs, indriids (indris, sifakas and wooly lemurs) and sportive lemurs (*Lepilemur* spp.) are also characterized by engaging in specialized VCL behaviors (Napier and Walker, 1967; Gebo, 1987a; Oxnard et al., 1990; Warren and Crompton, 1997; Dagosto and Yamashita, 1998; Lawler, 2006). Like bushbabies and tarsiers (see below), these species possess markedly elongated hindlimbs, which increase the distance over which takeoff forces can be applied during hindlimb extension (Demes and Gunther, 1989). However, due to scale limitations imposed by body size—namely, muscle force increases as a function of area and weight force is proportional to volume—indriids and sportive lemurs have relatively abbreviated feet. Therefore, the feet of these large-bodied leapers are believed to be merely force transducers, instead of propulsive levers as in smaller-sized leapers (Gebo and Dagosto, 1988; Demes and Gunther, 1989, Demes et al., 1996). Conversely, the proximal segment of the hindlimb is proportionally very elongate in both indriids and sportive lemurs—hence their designation as "thigh-powered" leapers (Anemone, 1990; Demes et al., 1991). Although generally regarded as more quadrupedal than the former species, lemurids (including true lemurs, ring-tailed lemurs, ruffed lemurs, and bamboo lemurs) exhibit a diverse array of locomotor behaviors (Walker, 1974; Gebo, 1987a; Oxnard et al., 1990; Terranova, 1996; Dagosto and Yamashita, 1998). For instance, bamboo lemurs (*Hapalemur* spp. and *Prolemur simus*) frequently employ VCL behaviors to travel across the bamboo forest they inhabit, which are mainly composed of tall, narrow, vertical culms (Hemingway et al., 2020). In contrast, the larger-bodied ruffed lemurs (*Varecia* spp.; up to 4 kg) habitually move using above-branch quadrupedalism, sometimes practicing some degree of hindlimb suspension (Pereira et al., 1988; Meldrum et al., 1997). All cheirogaleids, irrespective of their leaping preferences—grading from very active species such as mouse lemurs (*Microcebus* spp.) to mostly quadrupedal on relatively large horizontal supports like dwarf lemurs (*Cheirogaleus* spp.)—display habitual suspensory locomotion (Walker, 1974; Gebo, 1987a; Oxnard et al., 1990; Toussaint et al., 2015). Like lorisids, cheirogaleids also employ cantilevering, a specific type of suspensory locomotion in which the grasping feet maintain contact with the substrate while the body extends across a gap to reach another support or capture animal prey (Granatosky et al., 2014). Aye-ayes (*Daubentonia madagascariensis*), the sister taxon of all the remaining lemuroids, are characterized by some unique features—superficially rodent-like dentition, large and globular braincase, clawed digits except for the hallux, and an extremely long and slender third digit of each hand—because of their specialized ecology based on preying on insect larvae hidden within wood (Erickson, 1991). This is reflected in their locomotor behavior, as aye-ayes

usually move more cautiously than other lemurs, resembling lorisids in this regard (Curtis and Feistner, 1991).

Among haplorrhines, tarsiers are characterized by a suit of features in the postcranial skeleton—including an extremely elongated feet with a distinct morphology to achieve foot inversion—that facilitate their specialized VCL behavior (Fig. 1.3; MacKinnon and MacKinnon, 1980; Crompton and Andau, 1986; Gebo, 1987a; Dagosto et al., 2001; Crompton et al., 2010). Tarsiers prefer stiff, highly angled, large diameter supports for takeoff to perform long leaps and minimize energy loss. Contrarily, they habitually choose more compliant medium-sized supports for landing, as a strategy to absorb impact and dissipate shock (Crompton et al., 2010).

Compared to strepsirrhines and tarsiers, most field studies indicate that anthropoids exhibit greater emphasis on quadrupedal locomotion, which correlates with several postcranial anatomical features favoring this locomotor mode at the expense of climbing and grasp-leaping behaviors (Gebo, 1986, 1989b, 1993a; Ford, 1988; Gebo and Dagosto, 2004). Additionally, the generally larger body mass of extant anthropoids plays a significant role in determining their locomotor and habitat preferences, resulting in the more extensive use of below-branch suspensory locomotion in atelids and apes (Cant, 1992; Preuschoft et al., 1996; Hunt, 1991, 2016), as well as increased utilization of terrestrial substrates in some catarrhine lineages (Cartmill, 1985; Gebo, 1996).

Among New World monkeys (Fig. 1.3), medium-sized cebids and pitheciids (e.g., capuchins, squirrel monkeys, titis, sakis and uakaris) inhabit different forest types and strata, exhibiting a relatively compliant quadrupedal locomotion characterized by flexed limbs and greater axial rotation during gait, as well as frequent horizontal leaping (Fleagle and Mittermeier, 1980; Fleagle and Meldrum, 1988; Boinski, 1989; Gebo, 1992a; Walker and Ayres, 1996; Youlatos, 1998, 1999; Wright, 2007; Bezanson, 2009; Youlatos and Meldrum, 2011). The smaller-sized callitrichids (tamarins and marmosets) diverge from this pattern, and, instead, display a distinct locomotor repertoire that includes different degrees of clawed scansorial locomotion and rapid, scurrying quadrupedal progression—similar to some non-primate mammals such as tree shrews (Garber, 1980, 1992; Rosenberger and Stafford, 1994; Youlatos, 1999; Garber and Leigh, 2001; Schmitt, 2003; Youlatos and Meldrum, 2011). The remaining and largest-bodied platyrrhine family, the Atelidae, habitually dwell in the uppermost branches of the arboreal canopy and primarily employ a combination of climbing, clambering, and suspensory locomotion, which is reflected in postcranial adaptations such as elongated forelimbs and a trunk morphology reminiscent of extant apes (Erickson, 1963; Lockwood, 1999). However, unlike apes, atelids possess fully

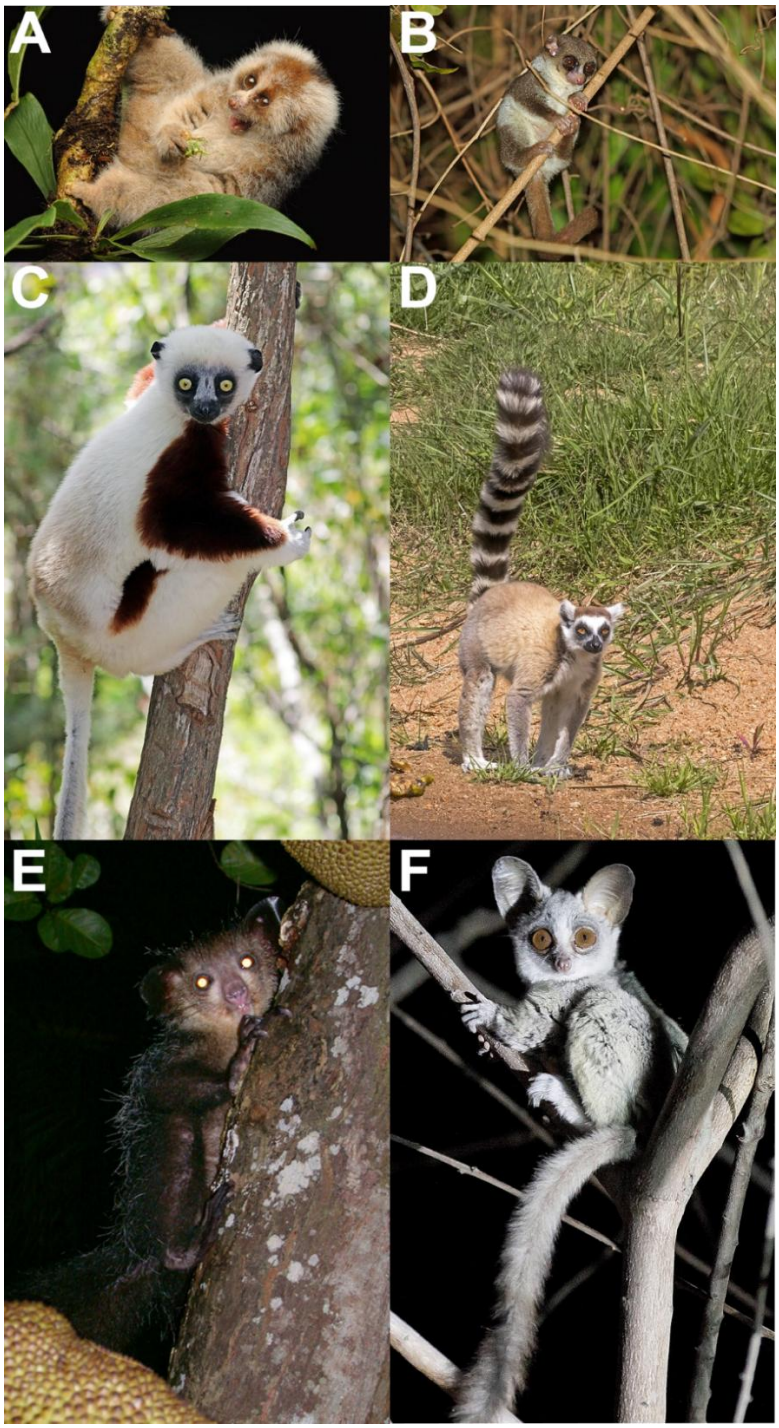


Figure 1.2. Locomotor diversity of strepsirrhine primates: (A) a Bangka slow loris (*Nycticebus bancanus*) engaging in cantilevering to catch an arthropod prey (© Gunay M.E. / CC BY-SA 4.0); (B) a western fat-tailed dwarf lemur (*Cheirogaleus medius*) climbing a small oblique support (© Nigel Voaden / CC BY 4.0); (C) a Coquerel's sifaka (*Propithecus coquereli*) practicing vertical clinging on a large vertical support (© Charles J. Sharp / CC BY-SA 4.0); (D) a ring-tailed lemur (*Lemur catta*) standing quadrupedally on the ground (© Charles J. Sharp / CC BY-SA 4.0); (E) an aye-aye (*Daubentonia madagascariensis*) vertical clinging on a large trunk using its claws to forage for wood boring insect larvae (© Tom Junek / CC BY-SA 3.0); (F) a Mohol bushbaby (*Galago moholi*) standing on a small oblique support (© Andrey Giljov / CC BY-SA 4.0).

prehensile tails with sensitive tactile pads on the ventral surface that are used as supporting "fifth limbs" during arboreal locomotion (Rosenberger, 1983). Within atelids, howler monkeys (*Alouatta* spp.) engage in substantially less suspensory locomotion than the other genera, relying more on quadrupedal and clambering locomotion (Fleagle and Mittermeier, 1980; Schön Ybarra and Schön, 1987; Gebo, 1992a; Youlatos and Meldrum, 2011). Conversely, spider monkeys (*Ateles* spp.), muriquis (*Brachyteles* spp.), and, to a lesser degree, wooly monkeys (*Lagothrix* spp.), engage in highly agile, tail-assisted suspensory locomotion, including tail-assisted brachiation, especially in *Ateles* (Mittermeier and Fleagle, 1976; Mittermeier, 1978; Cant, 1986; Fontaine, 1990; Cant et al., 2001; Youlatos, 2008; Youlatos and Meldrum, 2011).

Old World monkeys inhabit a wide range of habitats characterized by diverse climates and vegetation types. They are classified into two distinct families: cercopithecines, a predominantly African group, and colobines, mostly distributed across Asia (Fleagle et al., 2025). Cercopithecines display a striking diversity in body size, ranging from the small, arboreal talapoin monkeys (less than 1 kg) to the predominantly terrestrial baboons and mandrills, which can reach a body mass up to 50 kg (Fig. 1.3; Fleagle et al., 2025). Most cercopithecines exhibit varying degrees of terrestriality, with substantial differences even within the same genus (e.g., *Macaca*; Cant, 1988; Wells and Turnquist, 2001; Chatani, 2003). Most large-bodied cercopithecines (papionins) are generally terrestrial, moving primarily on the ground using quadrupedal walking and running. However, they still habitually climb trees or rocky cliffs for resting and refuge (Rose, 1977; Hunt, 1991). When moving quadrupedally, arboreal cercopithecines rely on palmigrade quadrupedalism, whereas terrestrial species tend to utilize digitigrade quadrupedalism, which allows for faster and more efficient cursorial locomotion, more adequate in open environments (Rose, 1973; Anapol et al., 2005; Zihlman and Underwood, 2013). Colobines are generally smaller than cercopithecines, and, even the largest species, such as the gray langurs (*Semnopithecus* spp.) or proboscis monkeys (*Nasalis larvatus*), are more arboreal and exhibit greater leaping abilities than their cercopithecine counterparts (Fig. 1.3; Fleagle, 1977; Gebo and Chapman, 1995; McGraw, 1998; Zhu et al., 2015). Notably, some colobine species like the douc langurs (*Pygathrix* spp.), have been observed engaging in substantial bimanual locomotion and forelimb suspensory postures, resembling gibbons and siamangs in this regard (Fleagle, 1977; Byron and Covert, 2004; Wright et al., 2008).

Extant apes (non-human hominoids) are highly arboreal animals characterized by habitual use of climbing and suspensory behaviors (Fig. 1.4; Hunt, 1991). To accomplish this, hominoids are characterized by the possession of an orthograde body plan, comprising a series of traits for

increasing the mobility at several joints (particularly in the upper half of the body) and reducing the stresses derived from frequent suspensory and climbing behaviors (Stern, 1976; Hunt, 2016).

The lesser apes (gibbons and siamangs) predominantly use brachiation as their main locomotor mode (Fleagle, 1976, Gittins, 1983; Hunt, 1991, 2016; Vereecke, 2006; Fan et al., 2013). Brachiation is defined as a type of suspensory locomotion in which the animal swings from branch to branch using only its forelimbs, without the intervening aid of the tail or hindlimbs. Two types of brachiation are distinguished: brachiation with continuous contact, a slow form of brachiation with close handhold spacing; and ricochetal brachiation, a faster type of brachiation necessary for large handhold spacings in which periods of 'free flight' (without contact with the support) occur (Hollihn and Jungers, 1984; Usherwood and Bertram, 2003; Bertram, 2004). Hylobatids also use other locomotor modes, namely vertical climbing and clambering, arboreal and terrestrial bipedalism, and leaping (Fleagle, 1976, 1980; Gittins, 1983; Hunt, 1991, 2016; Vereecke, 2006; Fan et al., 2013). Differences between genera also exist, as the larger siamangs (up to 11 kg) habitually climb more and less frequently engage in ricochetal brachiation than the smaller gibbons (around 6 kg; Fleagle, 1976, 1980).

Orangutans are the largest fully arboreal primates, spending most of their times in the arboreal canopy—only Sumatran orangutans (*Pongo pygmaeus*) males tend to move terrestrially to cross canopy gaps (Susman, 1974; Sujardito and van Hoof, 1986; Cant, 1987, Hunt, 1991; Thorpe and Crompton, 2006). Orangutans habitually move using quadrumanous suspensory locomotion, vertical climbing and orthograde clambering in a varied array of combinations of the forelimbs and hindlimbs (Hunt, 1996). Orangutans can also move quadrupedally, albeit it represents a very small component of their overall locomotor repertoire. When forced to move on the ground, either under captivity or more infrequently in the wild (especially large males of Sumatran orangutans) employ different hand postures during quadrupedalism, such as fist-walking or palmigrade postures with the fingers flexed, providing stability while protecting their long, curved fingers adapted for below-branch suspension (Tuttle, 1967, 1969; Cant, 1987).

African apes, comprising gorillas (*Gorilla* spp.), chimpanzees (*Pan troglodytes*), and bonobos (*Pan paniscus*), depart from the locomotor behavior displayed by the Asian apes in their extensive use of terrestrial substrates (Hunt, 1991, 2016). While chimpanzees and bonobos also climb frequently (Hunt, 1991, 1992; Doran, 1993), gorillas—particularly males, which can weight up to 200 kg—habitually travel on the ground, and only occasionally use arboreal substrates (Hunt, 1991; Remis, 1995; Gebo, 1996). To move quadrupedally, African apes employ their characteristic knuckle-walking, representing a compromise between terrestrial quadrupedal locomotion and

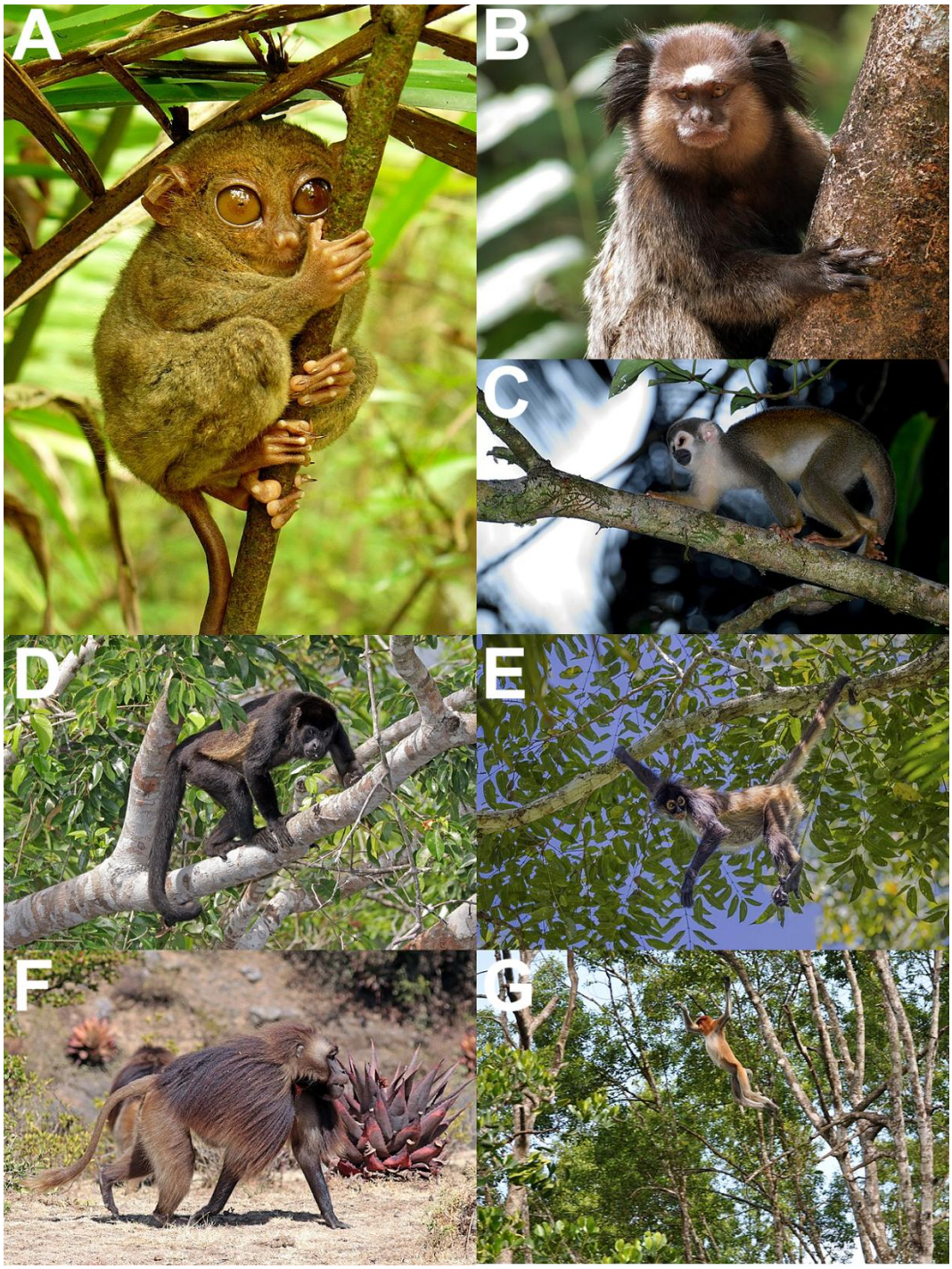


Figure 1.3. Locomotor diversity of non-hominoid haplorrhines. (A) Philippine tarsier (*Carlito syrichta*) clinging on a small vertical support (© Kok Leng Yeo / CC BY 2.0); (B) black-tufted marmoset (*Callithrix penicillata*) claw clinging a large vertical trunk (© User:Miguelrangeljr / CC BY-SA 3.0); (C) squirrel monkey (*Saimiri sciureus*) moving quadrupedally above a horizontal branch (© Geoff Gallice / CC BY 2.0); (D) Ecuadorian mantled howler monkey (*Alouatta palliata aequatorialis*) clambering on oblique supports while assisted by its prehensile tail (© Charles J. Sharp / CC BY-SA 4.0); (E) Geoffroy's spider monkey (*Ateles geoffroyi yucatanensis*) practicing below-branch suspension assisted by its prehensile tail (© Charles J. Sharp / CC BY-SA 4.0); (F) gelada (*Theropithecus gelada gelada*) walking quadrupedally on the ground (© Charles J. Sharp / CC BY-SA 4.0); (G) proboscis monkey (*Nasalis larvatus*) performing a spectacular leap (© User:Thesupermat2 / CC BY 2.0).

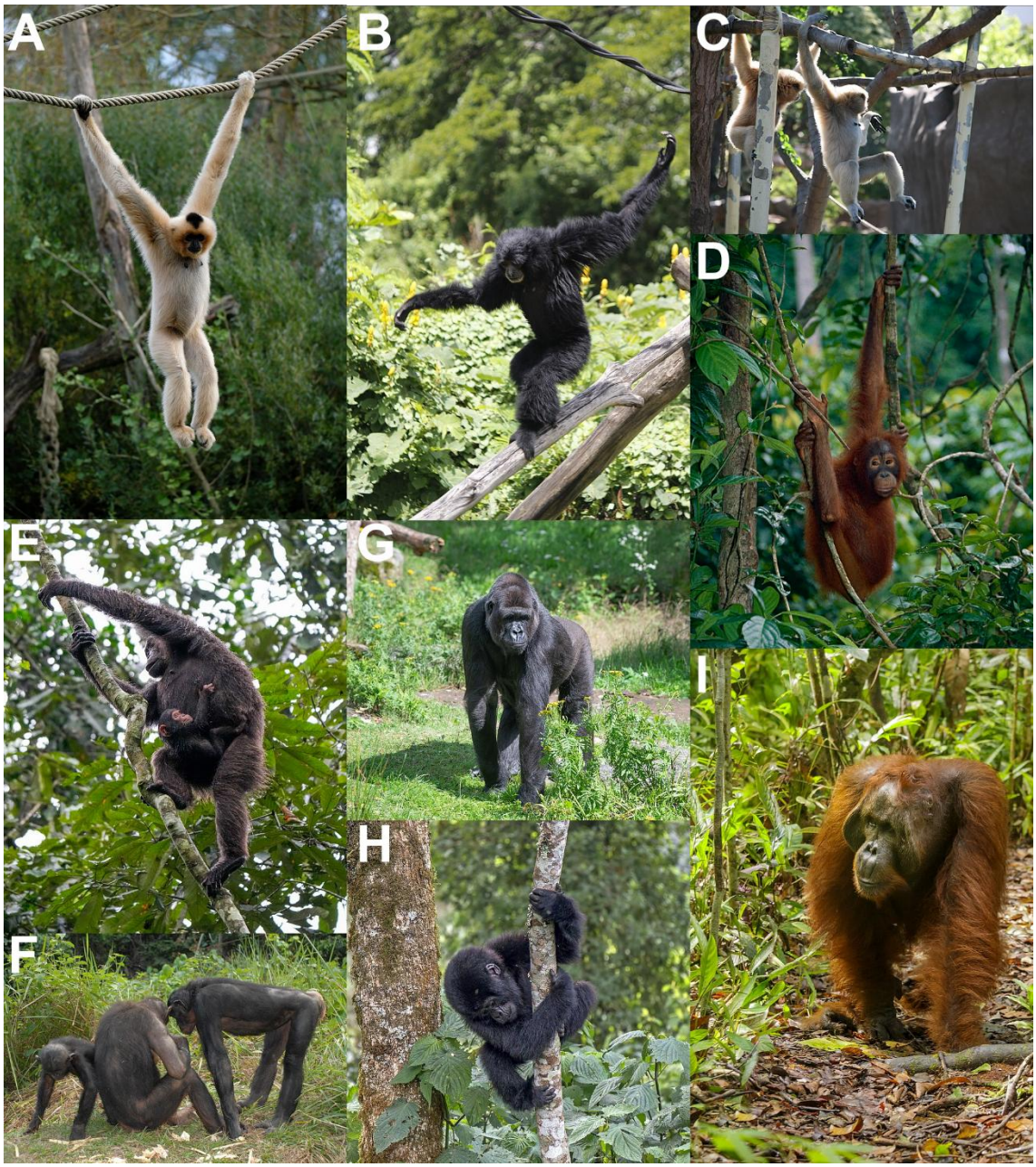


Figure 1.4. Locomotor diversity of extant non-human hominoids. (A) A white-cheeked gibbon (*Nomascus leucogenys*) suspending on a rope (© User:Musicaline / CC BY-SA 4.0); (B) a siamang (*Symphalangus syndactylus*) moving bipedally on a horizontal support (© User:Candramawa99 / Public Domain); (C) two white-handed gibbons (*Hylobates lar*) brachiating (© User:Petruss / CC BY 2.0); (D) a Bornean orangutan (*Pongo pygmaeus*) suspending by its four limbs (© Bernard Dupont / CC BY-SA 2.0); (E) an eastern chimpanzee (*Pan troglodytes schweinfurthii*) vertical climbing a tree with its baby clinging to her torso (© Giles Laurent / CC BY-SA 4.0); (F) a group of three bonobos (*Pan paniscus*) resting on the ground (© Pierre Fidenci / CC BY-SA 2.5); (G) a western lowland gorilla (*Gorilla gorilla gorilla*) knuckle-walking on the ground (© User:Tuxyso / CC-BY-SA-4.0); (H) a two-year-old mountain gorilla (*Gorilla beringei beringei*) climbing vertically a tree (© Charles J. Sharp / CC BY-SA 4.0); (I) a male Bornean orangutan (*Pongo pygmaeus*) fist-walking on the ground (© Thomas Fuhrmann / CC BY-SA 4.0).

arboreal suspensory behaviors (Tuttle, 1967, 1969, 2014). To this end, several purported adaptations have been identified in the wrist and hand of African apes, such as the presence of large dorsal ridges on the metacarpals (to limit phalangeal dorsiflexion at the metacarpophalangeal articular surface), a reduced ulnar styloid process, and scaphoid-centrale fusion to better withstands the high loads derived from knuckle-walking (Tuttle, 1967, 1969; Sarmiento, 1988; Kivell and Schmitt, 2009; Püschel et al., 2020).

1.2. Functional morphology of the hindfoot and the navicular bone

1.2.1. The primate foot

Primate feet are recognized as one of the hallmarks of the order Primates (e.g., Gregory, 1920; Morton, 1924; Le Gros Clark, 1959; Martin, 1968; Cartmill, 1974a; Dagosto, 1988; Gebo, 1993b). It is comprised of seven tarsal bones, five metatarsals, two phalanges in the hallux (or big toe), and three phalanges in the lateral digits (Fig. 1.5; Gebo, 1993b). Within the tarsals, four of them—the astragalus or talus, the calcaneus, the navicular, and the cuboid—are larger, while the remaining three—the entocuneiform, the mesocuneiform, and the ectocuneiform—are comparatively small.

All extant primates, with the exclusion of modern humans, possess a divergent hallux, an adaptation for more efficiently moving and foraging within the fine-branch niche of the arboreal environment (Martin, 1990). Euprimate-like grasping capability is achieved through the saddle-shaped joint between the hallux and the entocuneiform. In combination with the contraction of the main toe flexors (i.e., the flexor hallucis longus [FHL], the flexor digitorum longus, and the adductor hallucis), the position of the entocuneiform within the foot, and the proximodistal torsion of the first metatarsal, this saddle-shaped joint results in the abducted orientation of the hallux, facilitating its opposition to the lateral digits during grasping postures (Gebo, 1993b; Klenerman and Wood, 2006).

While the forefoot elements—metatarsals and phalanges—are mainly required for grasping, the larger tarsal bones—the astragalus, calcaneus, navicular, and cuboid—are primarily involved in the critical movements that occur at the main articular joints during primate locomotion on the arboreal canopy (Fig. 1.6; Lewis, 1980a, b). These joints are the upper ankle or talocrural joint(UAJ), which includes the articulation between the astragalus, tibia, and fibula; the lower ankle or

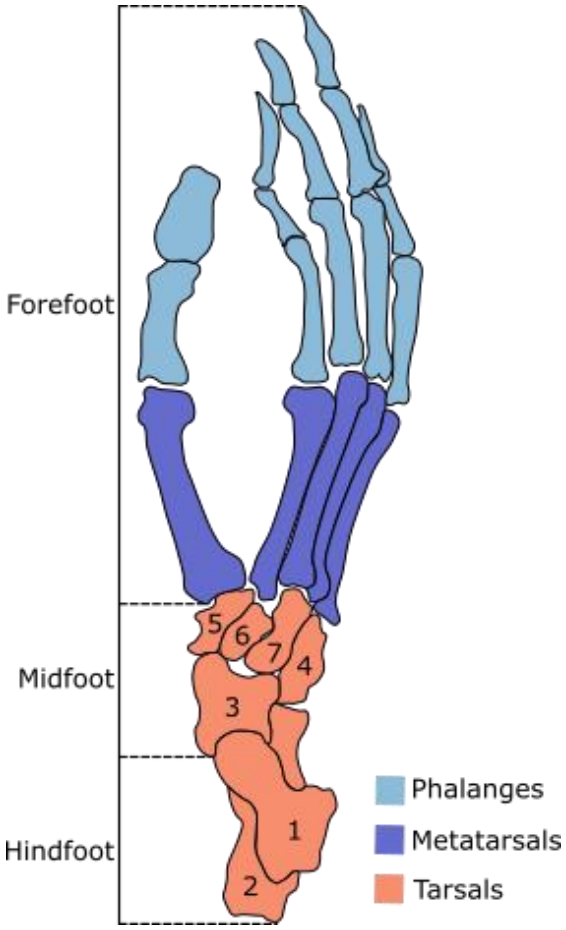


Figure 1.5. Dorsal view of an articulated foot of *Eulemur fulvus*, adapted from Gebo (1985). The different regions of the foot (tarsus, metatarsus and phalanges) are painted in different colors, as indicated by the legend. Tarsal bones are indicated by numbers: 1 = astragalus; 2 = calcaneus; 3 = navicular; 4 = cuboid; 5 = entocuneiform; 6 = mesocuneiform; 7 = ectocuneiform.

subtalar joint (LAJ), involving the astragalus, the calcaneus, and, to a lesser extent in some species, the navicular; and the transverse tarsal joint (TTJ), comprising the astragalonavicular (or talonavicular) and calcaneocuboid joints. The UAJ primarily facilitates dorsiflexion and plantarflexion of the foot relative to the leg, while the LAJ and TTJ allow for complex rotational movements, including inversion-eversion and adduction-abduction (Fig. 1.7; Gebo, 1993b).

Dorsiflexion and plantarflexion are the main movements occurring at the UAJ along the transverse axis of the foot (Aiello and Dean, 1990). During dorsiflexion, the dorsal surface of the foot moves closer to the anterior aspect of the leg, effectively decreasing the angle between them. Conversely, in plantarflexion, the foot is extended downward, increasing this angle (Gebo, 1993b). In dorsiflexion, the trochlea of the astragalus shifts proximally towards the tibia until contacting with the astragalar neck, where it locks and stabilizes the joint. Concurrently, the medial malleolus of the tibia meets the distal part of the medial tibial facet—which varies in concavity across

different primate groups (Harrison, 1987; Strasser, 1988; Boyer et al., 2015a). Furthermore, the mediolateral wedging of the astragalar trochlea, in particular the curvature of the medial rim, allows for some concomitant abduction and eversion during dorsiflexion. Contrarily, during plantarflexion, the astragalus moves distally relative to the tibia and fibula, stopping when the lateral and medial tubercles of the astragalus contact the corresponding malleoli. In this position, the mediolateral asymmetry of the trochlea permits concomitant adduction and inversion of the foot (Barnett and Napier, 1952; Lewis, 1980a; Scott and Winter, 1991; Michelson and Helgemo, 1995).

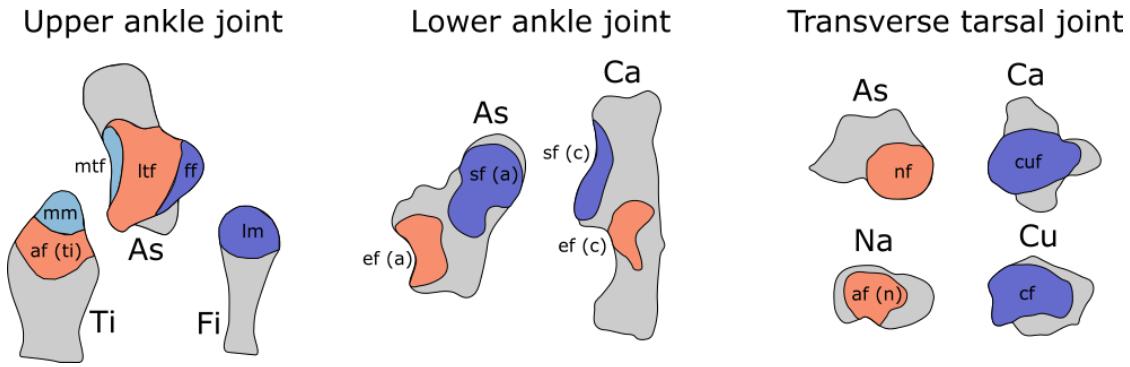


Figure 1.6. Main tarsal joints. Abbreviations: Ti = tibia; Fi = fibula; As = astragalus; Ca = calcaneus; Na = navicular; Cu = cuboid; lm = lateral malleolus; mm = medial malleolus; af (ti) = astragalar facet on the tibia (also called talar facet); ltf = lateral tibial facet; mtf = medial tibial facet; ff = fibular facet; ef (a) = ectal facet on the astragalus (also called posterior calcaneal facet); sf (a) = sustentacular facet on the astragalus (also called anterior calcaneal facet); ef (c) = ectal facet on the calcaneus (also called posterior astragalar facet); sf (c) = sustentacular facet on the calcaneus (also called anterior astragalar facet); nf = navicular facet; cuf = cuboid facet; af (n) = astragalar facet on the navicular (also called talar facet); cf = calcaneal facet. Adapted from Dagosto (1986).

Inversion and eversion allow the foot to be placed in a grasping position on arboreal substrates (Gebo, 1993b). These motions mainly occur at the LAJ and TTJ, along the longitudinal axis of the foot, albeit other more distal tarsal joints—such as those between the navicular, the cuboid, and the cuneiforms—also contribute to this movement (Aiello and Dean, 1990). In inversion, the flexor musculature pulls on the medial surface of the foot, rotating the navicular in a lateral direction. Simultaneously, the cuboid is drawn into the calcaneus at the calcaneocuboid joint, placing this joint more in line—transversely—to the astragalonavicular joint. This configuration facilitates the lateral rotation of the foot. The calcaneus is also rotated laterally, as facilitated by the short calcaneocuboid ligament, helping to lock the joint in a close-packed position. As a result, the astragalus shifts proximally, following the helical path along the ectal facet on the calcaneus. The

astragalar neck and head also move dorsally and medially, matching the lateral rotation of the navicular. Conversely, during eversion, the navicular and cuboid rotate medially, resulting in a medial rotation of the calcaneus as well. The astragalus slides distally, with its neck and head oriented plantarly (Lewis, 1980b; Gebo, 1993b; Jastifer and Gustafson, 2014).

Abduction and adduction of the foot primarily occur at the TTJ, along the long axis of the leg. These movements often accompany both dorsiflexion and plantarflexion as well as inversion and eversion. Abduction is defined as the horizontal rotation of the foot away—laterally—from the midline defined by the long axis of the leg, while adduction describes the opposite movement, the movement—medially—towards the midline of the long axis of the leg (Aiello and Dean, 1990).

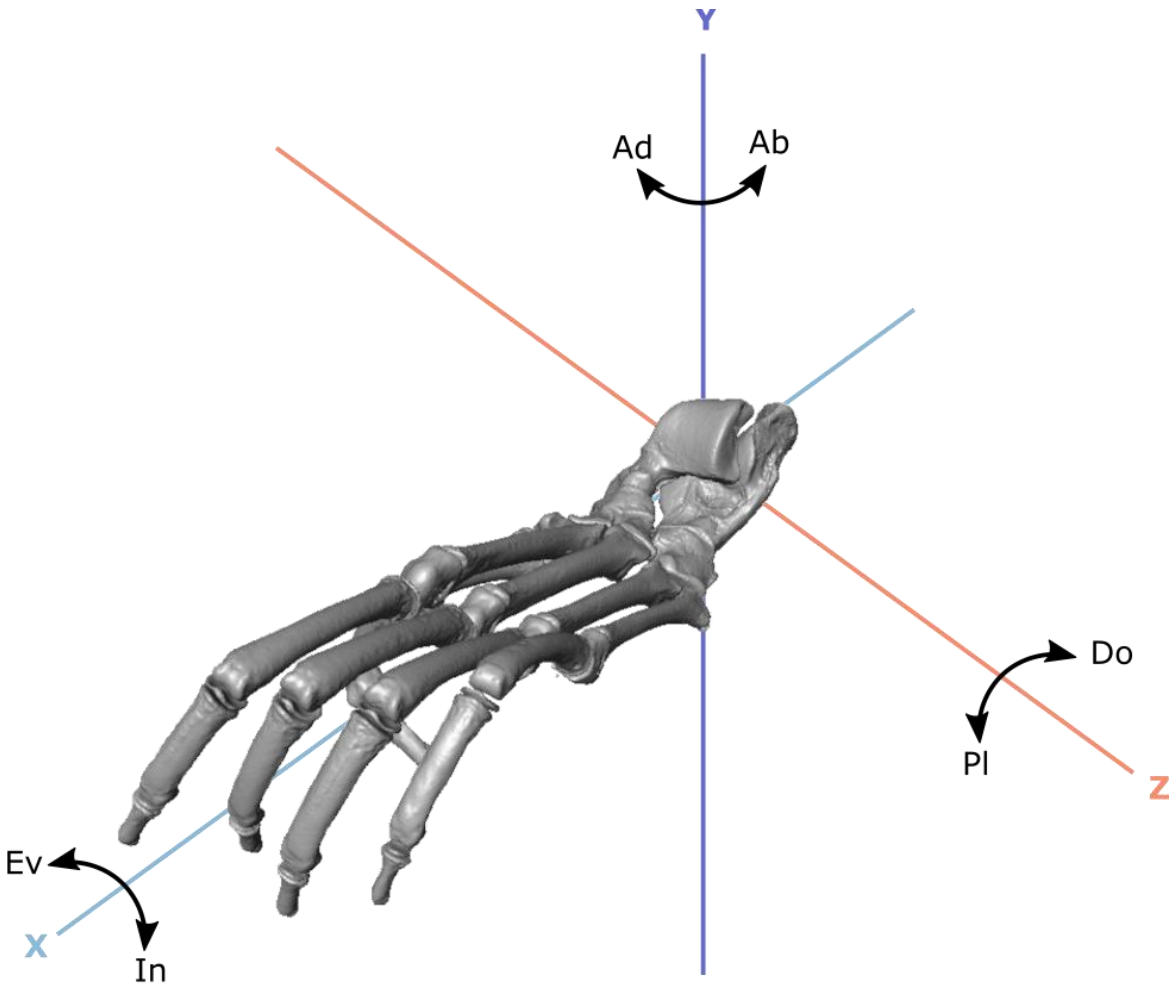


Figure 1.7. Foot movements. The X, Y and Z axes represent the longitudinal axis of the foot, the long axis of the leg, and the transverse axis of the ankle, respectively. The specimen represented belongs to *Alouatta seniculus* (AMNH 200554). Abbreviations: Ev = eversion; In = inversion; Do = dorsiflexion; Pl = plantarflexion; Ad = adduction; Ab = abduction.

Primate feet exhibit substantial morphological diversity, reflecting the different functional demands of different locomotor repertoires (e.g., Conroy and Rose, 1983; Gebo, 1988, 1993b; DeSilva et al., 2019). For instance, while most primates have flat and rounded nails instead of the primitive mammalian claws, some species—e.g., marmosets, tamarins, and several strepsirrhine species—have secondarily evolved keeled nails that resemble the claws of other arboreal mammals, allowing these species to cling on large vertical supports (Cartmill, 1974a; Garber, 1980, 1992). Furthermore, some primates—including lorises, pottos and angwantibos, indris, sifakas and wooly lemurs, as well as gibbons and siamangs—have modified the position and relative size of the hallux to expand the grasping span of the foot (Gebo, 1985, 1989a). Almost all primates employ a semiplantigrade foot posture in both arboreal and terrestrial substrates (Gebo, 1993b). However, African apes and humans utilize a full plantigrade posture, with the heel contacting the support (Gebo, 1992b). The relative length of the foot, particularly influenced by the elongation of the tarsus, is also extremely variable within primates, and has been extensively studied because of its important functional implications, particularly in relation with leaping proclivity and the position of the fulcrum of the foot (Morton, 1924; Hall-Craggs, 1965b; Lessertisseur and Jouffroy, 1973; Moyà-Solà et al., 2012; Boyer et al., 2013).

Another source of substantial morphological diversity, with profound functional implications, is the shape of the articular facets that constitute the joints of the foot. Articular facets can be described in terms of their outline morphology, curvature, and orientation (MacConaill, 1953, 1973; Hamrick, 1996). The surface morphology relates to the biomechanical demands required to withstand the force loadings transmitted through the joint and the need to provide sufficient range of motion at the joint (Hamrick, 1996). Consequently, facet morphology is significantly correlated with body mass, given the expectation that larger animals would require larger surface facet areas than smaller animals, as a result of the increased force transference (Ruff and Runestad, 1992). However, this relationship is not as straightforward, as larger species also tend to exhibit more extended hindlimb postures, leading to a decrease in the motion range of their joints facilitated by a reduction of the relative articular facet surface (Godfrey et al., 1991, 1995; Ruff and Runestad, 1992; Polk, 2002). Joint mobility can be increased by lengthening the articular facet or increasing its curvature. A long facet will increase the distance in which one bone can translate over another (Hamrick, 1996; Yapuncich and Granatosky, 2021). Alternatively, increasing the curvature of a facet will allow for an increase in the degree of rotation occurring at the joint (Rafferty and Ruff, 1994; Hamrick, 1996). Additionally, the orientation of articular facets maximizes the range of movements in the directions that best support the functional demands of a given

species, maximizing biomechanical efficiency across different locomotor modes (Conroy and Rose 1983; Tocheri et al., 2003).

1.2.2. The astragalus

The astragalus, also known as the talus or ankle bone, articulates with the tibia and fibula proximally, and with the calcaneus and navicular distally, thus representing an intermediate bone between the leg and the foot (Aiello and Dean, 1990; Gebo, 2014). It plays an important role in transferring the weight of the upper body and legs to the rest of the foot and the substrate. The astragalus is constituted almost entirely by articular surfaces that contribute to all three main tarsal joints: the UAJ, the LAJ, and the TTJ (Fig. 1.8; Lewis 1980a, b; Gebo, 1993b; Novacheck, 1998; Leardini et al., 1999). The astragalus can be divided into three main parts (Aiello and Dean, 1990; Gebo, 2014): (1) the body; (2) the neck; and (3) the head. In turn, the body constitutes most of the bone and includes the trochlea, the lateral and medial facets that articulate with the fibular and tibial malleolus, respectively, the proximal (or posterior) medial and lateral tubercles, and the ectal (or posterior calcaneal) facet; the neck encompasses the sustentacular facet (or anterior calcaneal facet) with the calcaneus, which may be divided in two separate facets in some primate species (in this case these are called middle and anterior calcaneal facets); and the head contacts the navicular via the navicular facet.

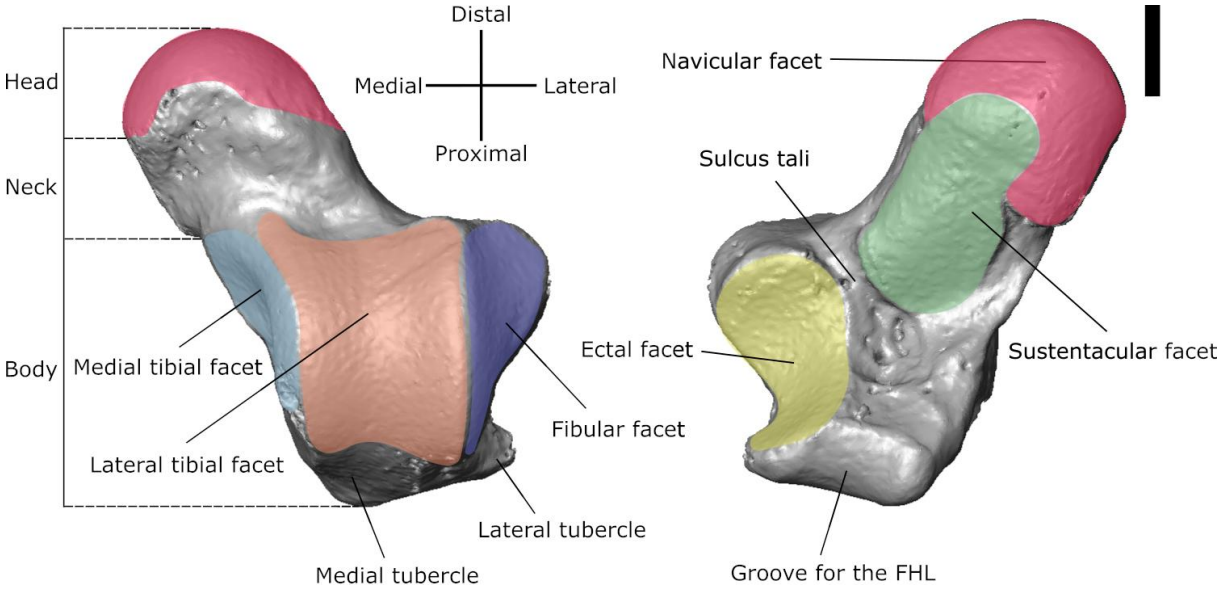


Figure 1.8. The astragalus. The specimen represented belongs to *Eulemur fulvus* (AMNH 100528). Scale bar equals 3 mm. Abbreviations: FHL = flexor hallucis longus.

The astragalar trochlea is a dorsal articular surface exhibiting a saddle shape with a central groove flanked by medial and lateral ridges, upon which the distal tibia articulates (Aiello and Dean, 1990; Gebo, 2014). The medial malleolus of the tibia and the lateral malleolus of the fibula fit on the corresponding medial and lateral sides of the talar body, constituting a two-pronged mortise that facilitates dorsiflexion and plantarflexion at the UAJ, while restricting excessive lateral movement (Lewis, 1980a). In primates, the degree of elongation of the trochlea reflects the amount of distance over which the tibia can translate over the astragalus, restricting or enhancing dorsi- and plantarflexion at the UAJ (Fig. 9A; Lewis, 1980a). Trochlear wedging can occur both mediolaterally (a shorter medial trochlear margin relative to the lateral margin) or proximodistally (a broader trochlear surface distally than proximally), resulting in increased degrees of concomitant movements during dorsi- and plantarflexion (Fig. 1.9B; Barnett and Napier, 1952; Langdon, 1986; Latimer et al., 1987). The relative height of the lateral and medial rims is also highly variable among primates. In some species, the lateral rim is higher than the medial rim, which could reflect the inverted posture of the grasping foot (Fig. 1.9C; Dagosto, 1988, 2007). However, as noted by Strasser (1988), Old World monkeys, particularly the most terrestrial, also display a very elevated lateral rim compared to the medial rim—stressing that the functional significance of this feature must be contextualized within a broader functional and phylogenetic framework. Similarly, the relative depth of the trochlear groove can reflect distinct locomotor repertoires. For instance, species that engage in more suspensory behaviors tend to exhibit relatively shallower trochlear grooves compared to those that require a more stable UAJ, such as specialized leapers or terrestrial quadrupeds (Fig. 1.9D; Dagosto, 1988, 2007). The latter functional group is also characterized by the presence of squatting facets on the dorsal side of the talar neck that act as bony stops for the tibia during dorsiflexion (Harrison, 1982; Conroy and Rose, 1983).

The fibular malleolus contacts the astragalus at the fibular facet, whose morphology distinguishes strepsirrhines from haplorrhines irrespective of their locomotor adaptations (Fig. 1.10A; Beard et al., 1988). Haplorrhines exhibit the ancestral eutherian condition, characterized by a very steep facet, whereas strepsirrhines exhibit a more angled, sloping facet (Dagosto, 1988). Within strepsirrhines, angles of slope can vary—for instance, bushbabies have steeper fibular facets compared to other strepsirrhines, while lorises, pottos, and angwantibos possess markedly less steep, gently sloping fibular facets—reflecting different locomotor adaptations (Gebo, 1988). In African apes, the fibular facet flares laterally, creating a surface which enables resisting excessive medial or lateral displacements. This provides greater stability at the ankle joint during weight-bearing in inverted or everted foot postures (Fig. 1.10B; Conroy and Rose, 1983; Gebo, 1992b; DeSilva, 2009). The medial tibial facet articulates with the tibial malleolus and can be

distinguished between extant strepsirrhines and tarsiers by its generally larger surface compared to the more restricted facet exhibited by anthropoids (Fig. 1.10C; Dagosto, 1988; Boyer et al., 2015a). Strepsirrhine species that engage in frequent leaping behavior can be differentiated from those with a lower leaping component in their locomotor repertoire by their relatively larger medial tibial facet (Boyer et al., 2015a). African apes and cercopithecoids—particularly the most terrestrial species—possess a medially flaring medial tibial facet with a well-developed malleolar cup, providing a stable ankle during dorsiflexion and inversion (Harrison, 1982, 1987; Strasser, 1988).

Primates exhibit considerable variation in the presence and development of the medial and lateral tubercles in the proximal region of the astragalar body (Fig. 1.11A; Harrison, 1982). Likewise, the morphology and position of the groove for the FHL tendon is distinctly expressed in different primate groups (Fig. 1.11B; Beard et al., 1988). In haplorrhines and most other eutherians, this groove lies in the midline of the proximal trochlea, whereas in strepsirrhines it is placed more laterally (Gebo, 1986; Yapuncich et al., 2017). Additionally, both a relatively wide and deep groove is functionally significant, as it is indicative of postures requiring powerful flexion of the pedal digits. Furthermore, the development of the lateral and medial tubercles is indicative of strong pedal grasping as well, as they serve as attachment sites for the posterior talofibular ligament and enhancing the mechanical load of the FHL muscle, respectively (Harrison, 1982; Leardini et al., 1999; Yapuncich et al., 2017). Species that engage in frequent hindlimb suspension and climbing behaviors exhibit deeper grooves and more prominent tubercles compared to specialized leapers and more generalized pronograde quadrupeds (Seiffert et al., 2015). The functional significance of the posterior trochlear shelf—considered a unique euprimate feature, albeit lacking or poorly developed in most haplorrhines—remains a subject of debate (Decker and Szalay, 1974; Dagosto, 1988; Yapuncich et al., 2019). Some proposed that it may act as a buttress during plantarflexion, aiding leaping behavior (Dagosto, 2007). Others suggested it functions as a cam mechanism that increases the effective length of the flexor fibularis tendon, improving digit flexion and pedal grasping during dorsiflexion on vertical supports (Yapuncich et al., 2019).

Euarchontans are characterized by several modifications at the LAJ. These include a continuous sustentacular facet with the navicular facet, an increased size of the ectal facet on the astragalus relative to its calcaneal counterpart, an ectal facet that is obliquely oriented with the long axis of the astragalus and the absence of a fibular facet on the calcaneus (Szalay and Decker, 1974; Szalay and Drawhorn, 1980; Chester et al., 2015). Altogether, these features enhance the range of motion at this joint during inversion and eversion, facilitating the exploitation of the arboreal milieu by

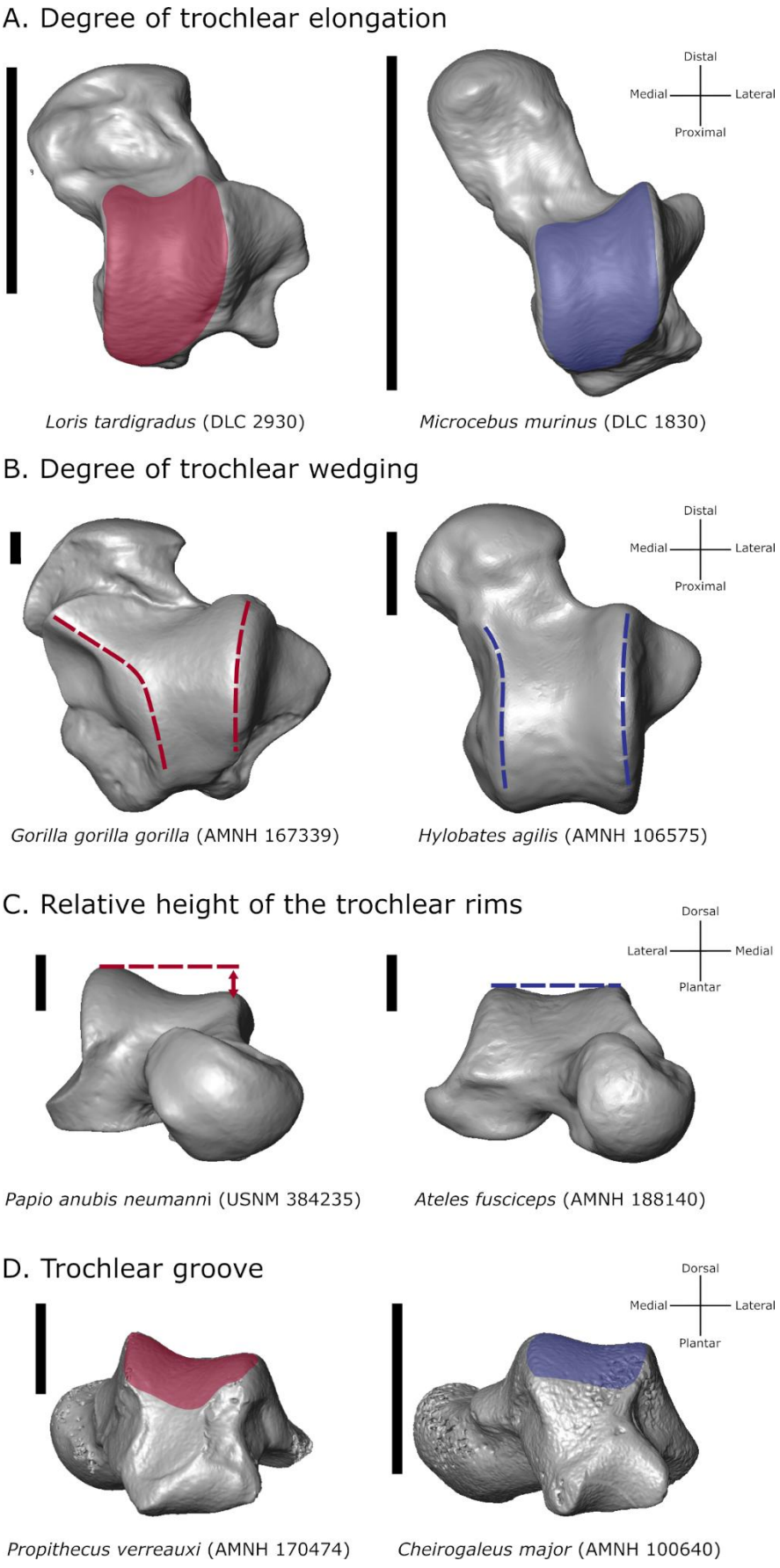


Figure 1.9. Features of the astragalar trochlea. (A) Degree of trochlear wedging; (B) relative height of the trochlear rims; (C) depth of the trochlear groove. Scale bar equals 5 mm.

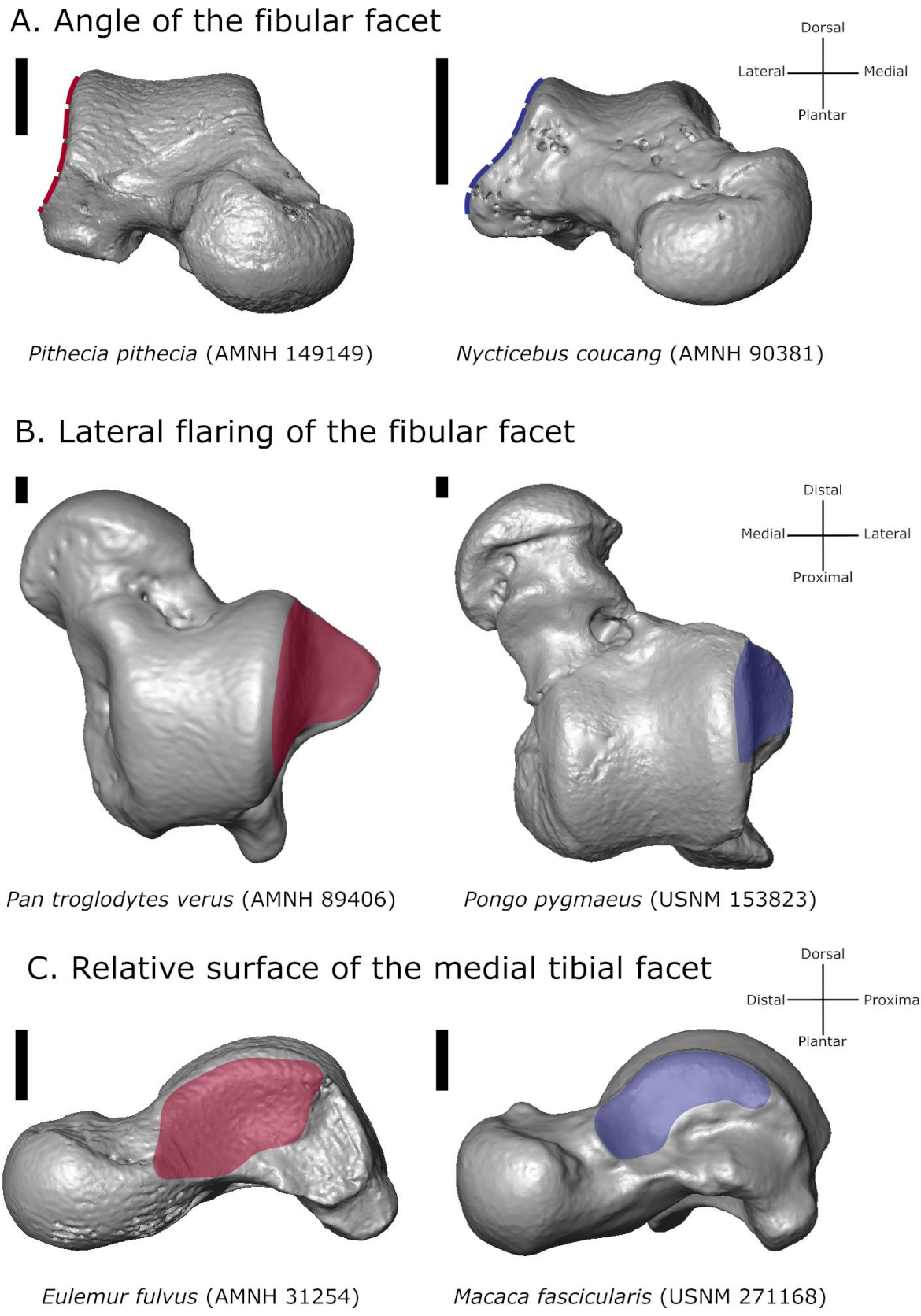


Figure 1.10. Features of the lateral and medial facets of the astragalar body. (A) Angle of the fibular facet; (B) lateral flaring of the fibular facet; (C) relative surface of the medial tibial facet. Scale bar equals 3 mm.

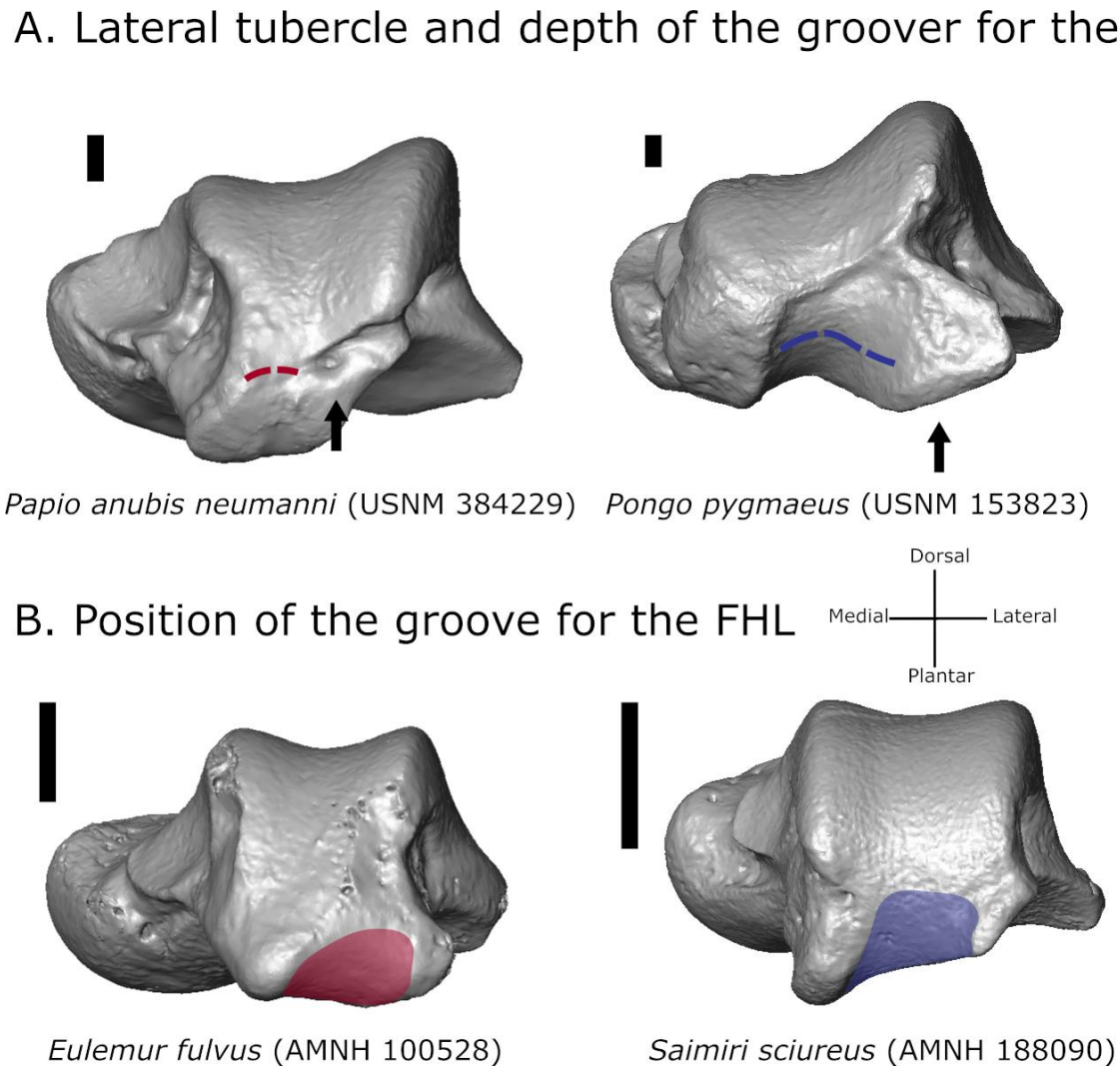


Figure 1.11. Features of the proximal region of the astragalar body. (A) Relative development of the lateral tubercle and depth of the groove for the FHL tendon; (B) position of the groove of the FHL tendon. Scale bar equals 3 mm. Abbreviations: FHL = flexor hallucis longus.

euarchontans, including primates (Lewis, 1980b; Conroy and Rose, 1983). Specifically, multiple studies across primates have found that a long and shallow ectal facet on the astragalus is associated with enhanced inversion capabilities at the LAJ (Fig. 1.12A; Langdon, 1986; Parr et al., 2014; Knigge et al., 2015; Püschel et al., 2017; Friesen et al., 2024). In addition, the orientation of the ectal facet on the astragalus influences the degree of screw motion of the astragalus at the LAJ, further contributing to the inversion and eversion capabilities of the foot (Conroy and Rose 1983). The sustentacular facet on the astragalus is much longer in primates than in other extant or extinct euarchontans and plesiadapiforms, which might be related to the overall lengthening of the tarsus that also characterizes primates and has been related to leaping behavior, as well as to be driven by allometric effects (Fig. 1.12B; Harrison, 1982; Dagosto, 1988, 2007; Boyer et al., 2013). However, other arboreal non-leaping animals—e.g., kinjakous, margays, pen-tailed

treeshrews—display relatively elongated astragalar necks as well, which might be also reflective of greater inversion and eversion capabilities at the LAJ (Jenkins and McClearn, 1984). Oraguntans also exhibit a relatively elongated astragalar neck, which has similarly been associated with increased motion at the LAJ (Harrison, 1982; Gebo, 1989b). In addition to elongation, the degree of medial angulation of the astragalar neck varies considerably among primates and is relevant for functional inferences (Barnett, 1955). For instance, a marked medial angulation of the astragalar neck facilitates the absorption of compressive forces toward the medial side of the foot—an adaptation consistent with enhanced pedal grasping (Barnett, 1955; Harrison, 1982; Szalay and Langdon, 1986).

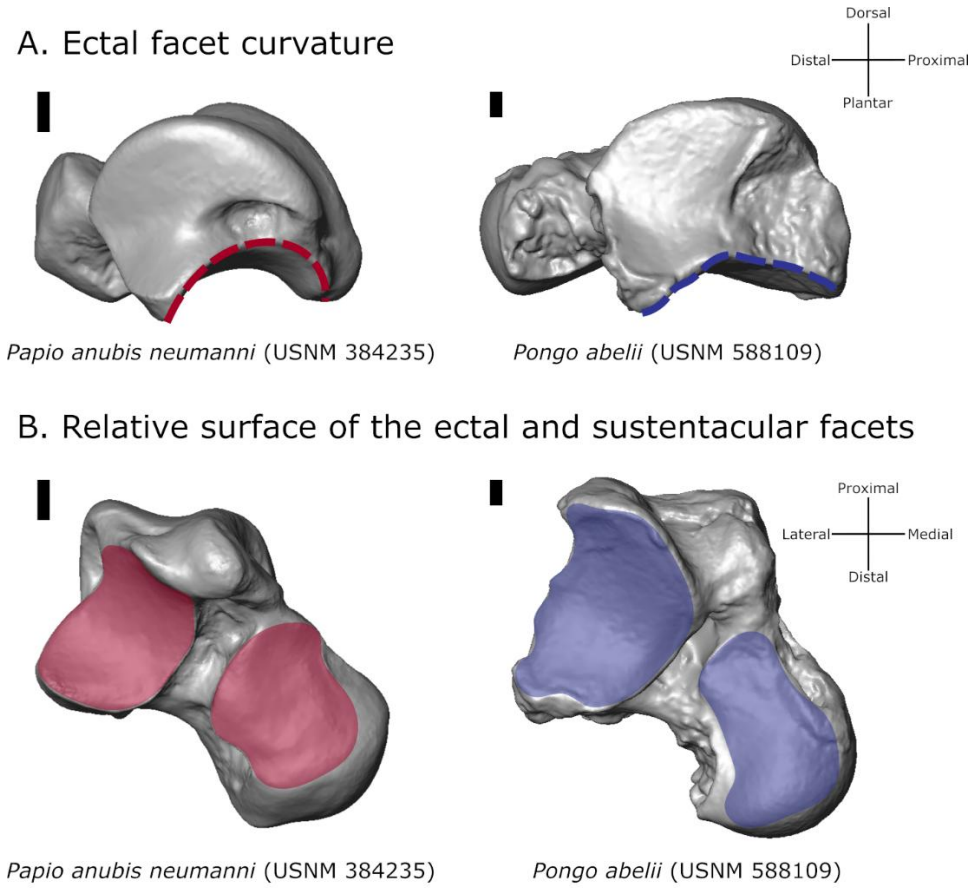


Figure 1.12. Features of the calcaneal facets and the astragalar neck. (A) Ectal facet curvature; (B) relative surface of the ectal and sustentacular facets. Scale bar equals 3 mm.

Compared to other mammals, the astragalar head in primates—encompassing the navicular facet—is more spherical than mediolaterally extended (Fig. 1.13; Szalay and Decker, 1974; Dagosto, 1988, 2007; Hooker, 2001; Chester et al., 2015). This morphology facilitates inversion and eversion at the TTJ, while reducing the concomitant mediolateral translation, an adaptation that

is probably related to the increase in relative size and mobility of the hallux in primates (Dagosto, 1988, 2007). Additional features of the astragalar head, such as its relative size and degree of torsion, are also functionally relevant. For instance, studies in extant catarrhines have shown that a relatively large and deviated astragalar head, like that of African apes, is associated with better withstanding large compressive forces—like those derived from vertical climbing. In contrast, the comparatively smaller and less deviated astragalar neck, such as that of Old World monkeys, is more consistent with habitual quadrupedalism (Szalay and Langdon 1986).

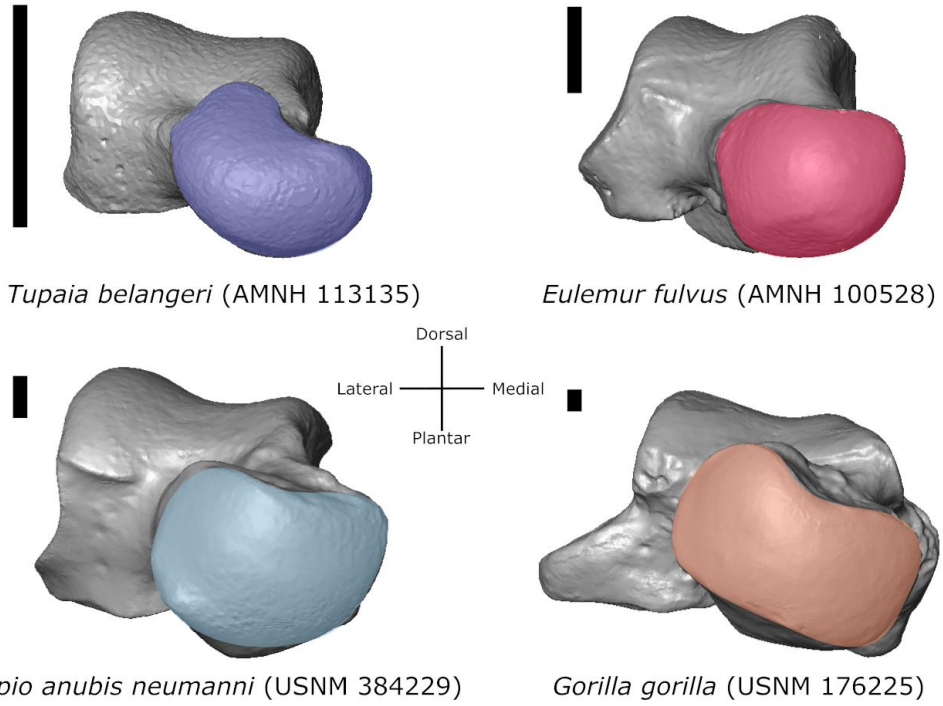


Figure 1.13. Morphology of the astragalar head across primates and other euarchontans. Scale bar equals 3 mm.

1.2.3. The calcaneus

The calcaneus or heel bone (Fig. 1.14) articulates with the astragalus dorsally, with the cuboid distally, and, in some species, with the navicular medially (Aiello and Dean, 1990; Gebo, 2014). The tuber calcanei acts as the lever for the plantarflexor muscles which attach to the proximal calcaneus via the calcaneal tendon. The ectal and sustentacular facets articulate with the astragalus and constitute the LAJ. Additionally, the sustentaculum tali emerges as a medial projection of the calcaneal body that serves as a bony shelf beneath the astragalar head and neck—contributing as a supportive structure—as well as a muscle pulley for the FHL tendon,

enhancing the mechanical efficiency of grasping in primates (Su and Zeininger, 2022). Lastly, the distal calcaneal end includes the cuboid facet, which constitutes part of the TTJ.

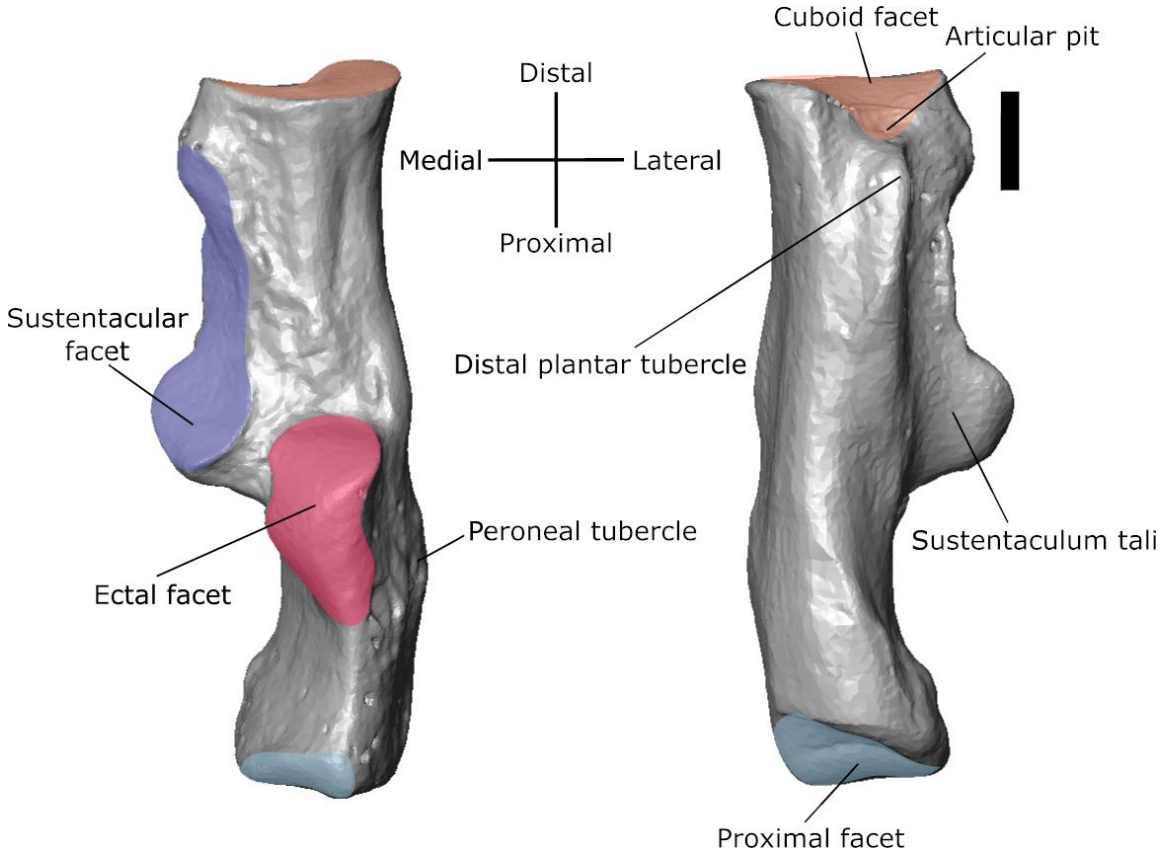


Figure 1.14. The calcaneus. The specimen represented belongs to *Eulemur fulvus* (AMNH 100528). Scale bar equals 3 mm.

Compared to other mammals, primates exhibit more elongated tarsal elements, particularly the navicular and the distal calcaneus (Fig. 1.15; Dagosto, 1988, 2007; Moyà-Solà et al., 2012; Boyer et al., 2013). The lengthening of the tarsus is considered a biomechanical innovation to effectively increase hindlimb length, reflecting adaptations for acrobatic leaping (Dagosto, 1988, 2007; Gebo, 1988). Nevertheless, calcaneal proportions in primates also exhibit an important allometric component, complicating their morphofunctional interpretation. Only small-bodied VCL species, such as tarsiers and bushbabies, deviate from the common allometric trend because of their extreme calcaneal elongation (Hall-Craggs, 1965b; Gebo, 1987b, 1989a; Moyà-Solà et al., 2012; Boyer et al, 2013). For instance, large-bodied VCL species—such as woolly lemurs, sifakas, and indris—overlap in calcaneal proportions with non-leaping lorises, pottos, and angwantibos, whereas other species with more limited leaping behaviors, such as aye-ayes and dwarf lemurs,

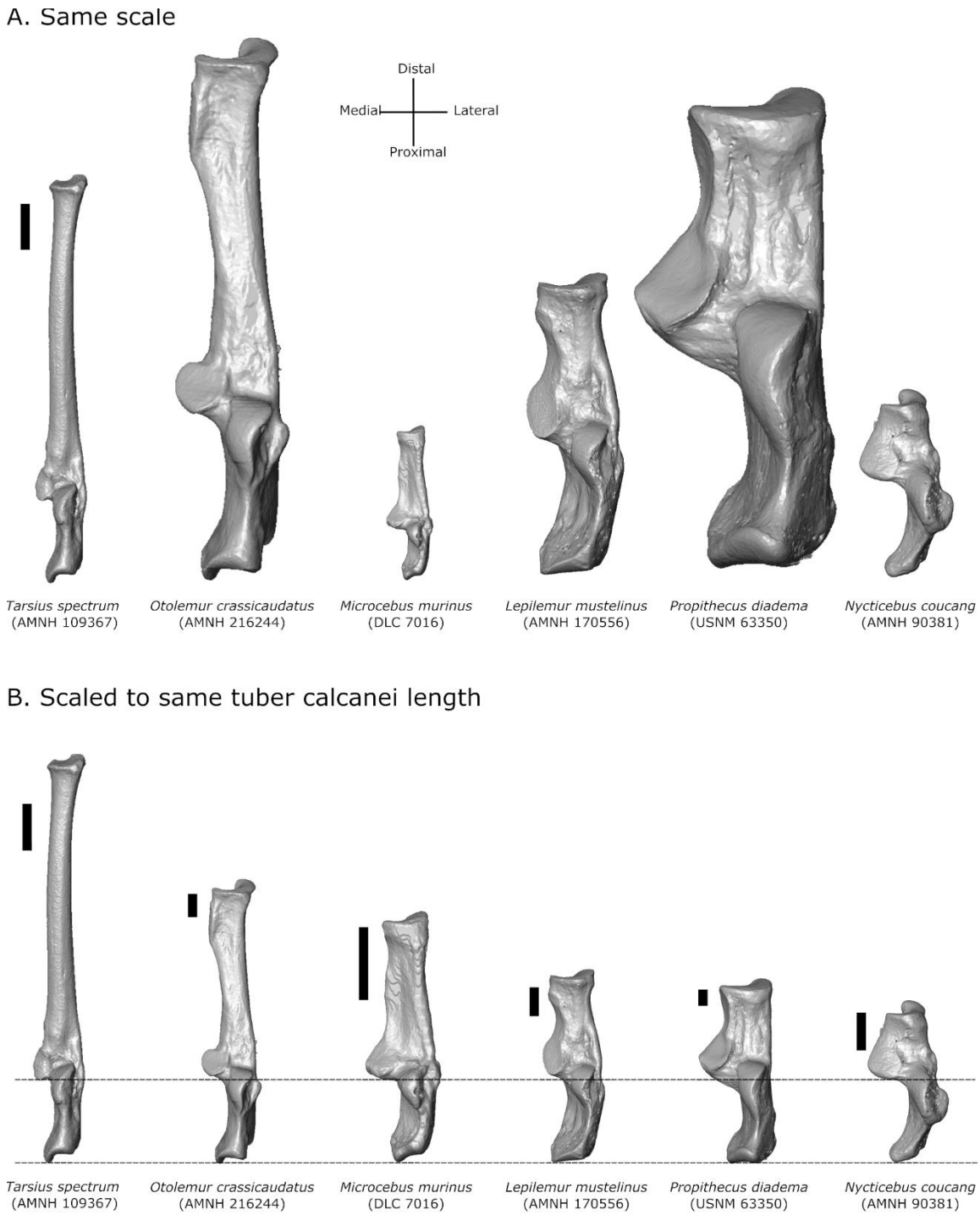


Figure 1.15. Extant primate calcanei diversity. (A) Calcanei represented at the same scale; (B) calcanei represented scaled at the same tuber calcanei length. Scale bar equals 3 mm.

exhibit greater calcaneal elongation than the former (Gebo and Dagosto, 1988). Furthermore, calcaneal elongation is more accentuated in strepsirrhines and tarsiers than in anthropoids (Boyer et al., 2013). This is explained by the distinct foot postures exhibit by these groups (Moyà-Solà et al., 2012). Compared to anthropoids and most non-primate generalized mammals, strepsirrhines and tarsiers have a foot characterized by a fulcrum placed on the end of the tarsus, enhancing its

grasping function at the cost of losing part of the lever arm constituted by the forefoot. Consequently, tarsi-fulcrumators require further elongation of the tarsal elements to compensate for the loss of load arm (Morton, 1924). In contrast, anthropoids, which exhibit a metatarsi-fulcrumating foot—with the fulcrum located more distally, on the metatarsal heads or even further, on the phalanges—do not have such reduction in the available load arm, and, therefore, do not require further elongation of the tarsus (Morton, 1924).

On the calcaneus, the convex and helically-inclined surface of the ectal facet, which is markedly prolonged proximally and medially, allows for a combination of rotation and translation movements along the joint axis—screw-like or helical motion—between the astragalus and the calcaneus (Fig. 1.16A; Manter, 1941; Szalay and decker, 1974; Lewis, 1980b; Conroy and Rose, 1983). Among primates, lorisids are distinguished by their long and convex ectal facet, which increases joint movement potential at the LAJ compared to other species (Gebo, 1988; Yapuncich and Granatosky, 2021). Similarly, in platyrrhines, a proximodistally elongated ectal facet on the calcaneus is associated with increased suspensory locomotion, likely reflecting with a more mobile LAJ (Püschel et al., 2017). In contrast, Old World monkeys exhibit highly curved and more dorsally than medially facing ectal facets, limiting the range of mediolateral movements and favoring plantarflexion at the ankle (Strasser, 1988; Harrison,1989). However, there are differences between the two cercopithecoid subfamilies: colobines possess longer ectal facets than cercopithecines, which has been related to increased inversion capabilities, as expected from their greater arboreal commitment (Strasser, 1988). Among non-primate euarchontans, tree shrews also display morphological differences on this facet depending on their locomotor ecology, with *Ptilocercus lowii*, the most arboreal species, exhibiting the longest and most helical ectal facet of all (Sargis, 2002). The sustentacular facet, typically confluent in euarchontans (including most primates), is located on the dorsal surface of the sustentaculum tali and extends distally through the calcaneal body, contacting the head and neck of the astragalus, as well as the navicular in some species (Fig. 1.16B; Lewis, 1980b). The sustentacular facet is distinctively separated into two facets in Old World monkeys, aye-ayes, as well as some fossil anthropoids such as *Apidium* (Gebo and Simons, 1987; Strasser, 1988; Fleagle and Simons, 1995). In Old World monkeys, those with more terrestrial habits exhibit more reduced sustentacular facets than those that are more committed to arboreality, suggesting reduced helical and rotational movements at the LAJ and TTJ (Gebo and Sargis, 1994). Similarly, in tree shrews, the sustentacular facet is only continuous in *P. lowii*, while tupaiids exhibit a gradient of decreasing relative surface in relation with increased terrestrial locomotor behavior (Sargis, 2002).

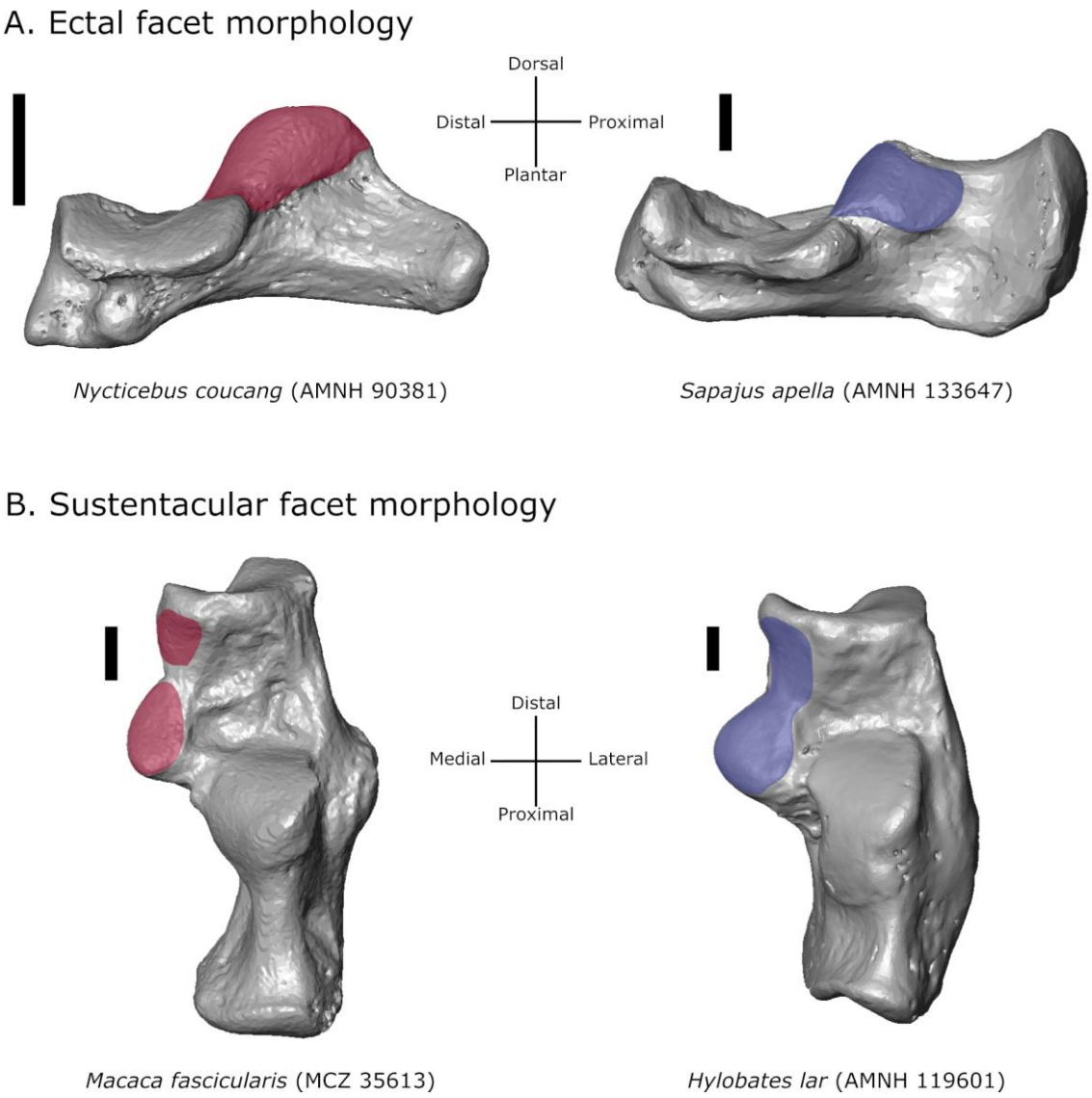


Figure 1.16. Features of the ectal and sustentacular facets on the calcaneus. (A) Ectal facet morphology; (B) Sustentacular facet morphology. Scale bar equals 3 mm.

The tuber calcanei—also known as calcaneal tuberosity—is the proximal projection of the calcaneus that serves as the attachment site for the triceps surae—the gastrocnemius and soleus muscles via the Achilles tendon (Aiello and Dean, 1990). The morphology of the tuber calcanei is very variable among primates, reflecting aspects of their positional behavior (Fig. 1.17A; Conroy and Rose, 1983; Strasser, 1988). For instance, terrestrial Old World monkeys possess a very long tuber calcanei, facilitating powerful loading of the foot during terrestrial quadrupedalism (Strasser, 1988; Youlatos, 2003). Conversely, apes exhibit a comparatively shorter tuber calcanei, although more terrestrial taxa—particularly gorillas and to a lesser extent chimpanzees and bonobos—possess more elongated tuber calcanei than Asian apes (Nozaki et al., 2021; Harper et al., 2022; Prang, 2024). Additionally, the morphology of the proximal facet of the tuber calcanei is

indicative of the length of the Achilles tendon (Fig. 1.17B). In habitual leapers, this facet is dorsoplantarly high, projecting dorsally to approximately the same level as the most dorsal surface of the ectal facet, effectively increasing the length of this tendon by expanding its attachment area and, therefore, enhancing its energy storage (Gebo, 1987b, 1993b). African apes exhibit a broadened proximal tuber calcanei region, in the lateral side of its plantar aspect, resembling that of humans and allowing for a larger contact area of the heel with the substrate (Gebo, 1992; Nozaki et al., 2021; Prang, 2024). Among anthropoids, the presence of an enlarged plantar tubercle on the tuber calcanei—in apes and some platyrrhine monkeys—is associated with enhanced grasping capabilities, as this region serves as the origin of the superficial head of the flexor digitorum brevis muscle (Fig. 1.17C; Sarmiento, 1983). A large flexor digitorum brevis muscle with a large origin process allows toe flexion independently of the position of the foot, facilitating different postures during deliberate climbing and suspension (Sarmiento, 1983). Within strepsirrhines, the slow climbing lorisids similarly possess an enlarged plantar tubercle, as well as a plantarly and medially oriented tuber calcanei, which are associated with increased mechanical advantage of the superficial head of the flexor digitorum brevis muscle (Sarmiento, 1983; Seiffert et al., 2015). The peroneal tubercle is situated more proximally in primates compared with other eutherians, including non-primate euarchontans (Fig. 1.17D; Dagosto, 1988). It acts as a muscle pulley for the peroneus longus tendon, an important hallux adductor (Gebo, 1993b; Godfrey et al., 1997). Compared to other anthropoids, extant apes exhibit a more prominent peroneal tubercle, indicative of an increase importance of the peroneal musculature to facilitate a strong hallucal grasping (Stern and Susman, 1983). Among strepsirrhines, lorisids also exhibit enlarged lateral peroneal tubercles, indicating a developed peroneal musculature as well (Gebo, 1989a).

Compared to other mammals, the calcaneocuboid joint is highly modified in primates, allowing for more extensive rotational movements at the TTJ (Fig. 1.18; Hall-Craggs, 1966; Decker and Szalay, 1974; Lewis, 1980b; Dagosto, 1988). Unlike the more obliquely oriented and ovoid articulation seen in non-primate mammals, the primate calcaneocuboid joint is oriented perpendicularly and exhibits a sellar (saddle-like) shape. Additionally, the cuboid bears a protuberance of moderate size with a corresponding depression on the calcaneus. Altogether, these modifications allow the calcaneocuboid joint to act as a pivot, enhancing the degree of adjunct inversion and eversion at the TTJ at the expense of a more mediolateral translation (Jenkins and McClearn, 1984). Among primates, lorisiforms and apes are characterized by a deep and dorsoplantarly high cuboid facet on the calcaneus (Conroy and Rose, 1983; Gebo, 1989a). In

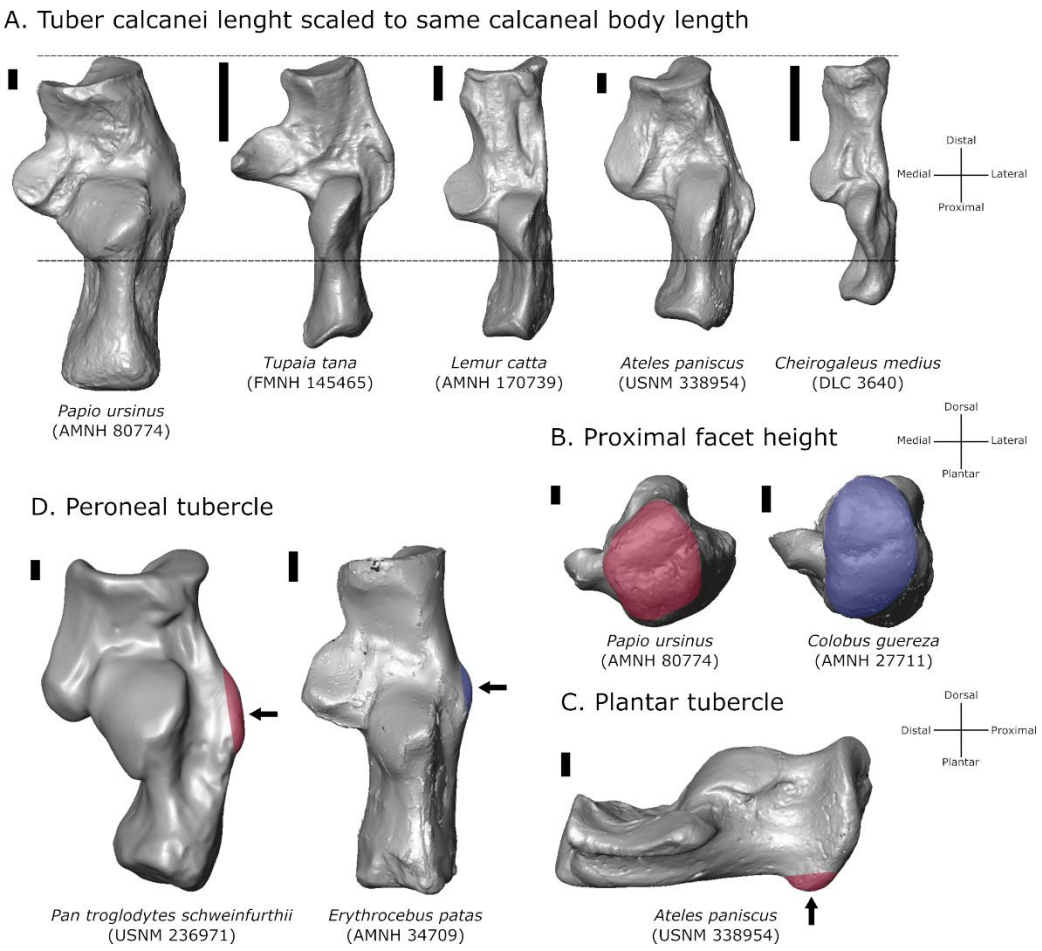


Figure 1.17. Features of the tuber calcanei, peroneal and plantar tubercles. (A) Tuber calcanei length scaled to same calcaneal body length; (B) relative height of the proximal facet on the tuber calcanei; (C) morphology of the plantar tubercle; (D) morphology of the peroneal tubercle. Scale bar equals 3 mm.

bushbabies, this deep calcaneal pit accommodates the cuboid protuberance and compensates for the restricted mobility caused by the extreme proximodistal elongation of the calcaneus and navicular (Gebo, 1987b). Midfoot rotation is further accomplished via a synovial joint between the distal region of the calcaneus and the navicular (Hall-Craggs, 1966). Conversely, tarsiers, which are also characterized by an extremely elongated tarsus, display the flattest and most ovoid cuboid facet on the calcaneus, lacking a pivot-like calcaneocuboid joint (Hall-Craggs, 1966; Gebo, 1987b). As a result, joint-mobility measures for tarsiers indicate a much lower rotational mobility at the calcaneocuboid joint. In fact, tarsiers do not habitually exhibit hindlimb suspension, which requires a lot of rotation between the calcaneus and the cuboid, as the latter bone needs to be locked into a non-existent calcaneal pit. Instead, tarsiers achieve the required midfoot rotation for their inverted positions while clinging on vertical substrates via an enhanced navicular rotation facilitated by highly modified cuneiform joints (Gebo, 1987b). Similarly to tarsiers, although for

very different functional requirements, Old World monkeys also exhibit a flat cuboid joint resulting in a less pivot-like calcaneocuboid joint. This indicates less rotational movements at the TTJ, expected for the more cursorial locomotion practiced by them, especially the most terrestrial species (Conroy and Rose, 1983). However, some differences exist between cercopithecoid taxa depending on their locomotor ecology, as the most arboreal species tend to have deeper cuboid pits and more laterally oriented cuboid facets than the most terrestrial species, facilitating the rotational movements at this joint as well as more divergent digits to better engage in arboreal substrates (Harrison, 1989).

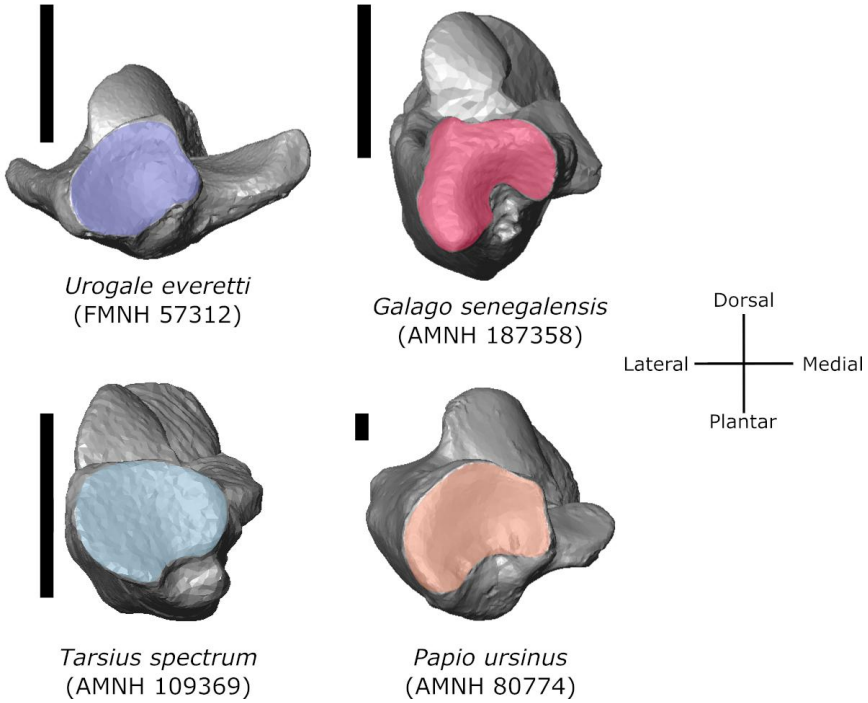


Figure 1.18. Morphology of the cuboid facet across primates and other euarchontans. Scale bar equals 3 mm.

1.2.4. The navicular

The navicular bone articulates proximally with the astragalus, distally with the three cuneiforms—namely the entocuneiform, mesocuneiform, and ectocuneiform—and plantarly with the cuboid (Fig. 1.19; Gebo, 2014). As a bridge between the ankle and the distal tarsal and metatarsal regions, the navicular is a key element of the primate midfoot, playing a critical role in locomotor biomechanics (Heard-Booth et al., 2022).

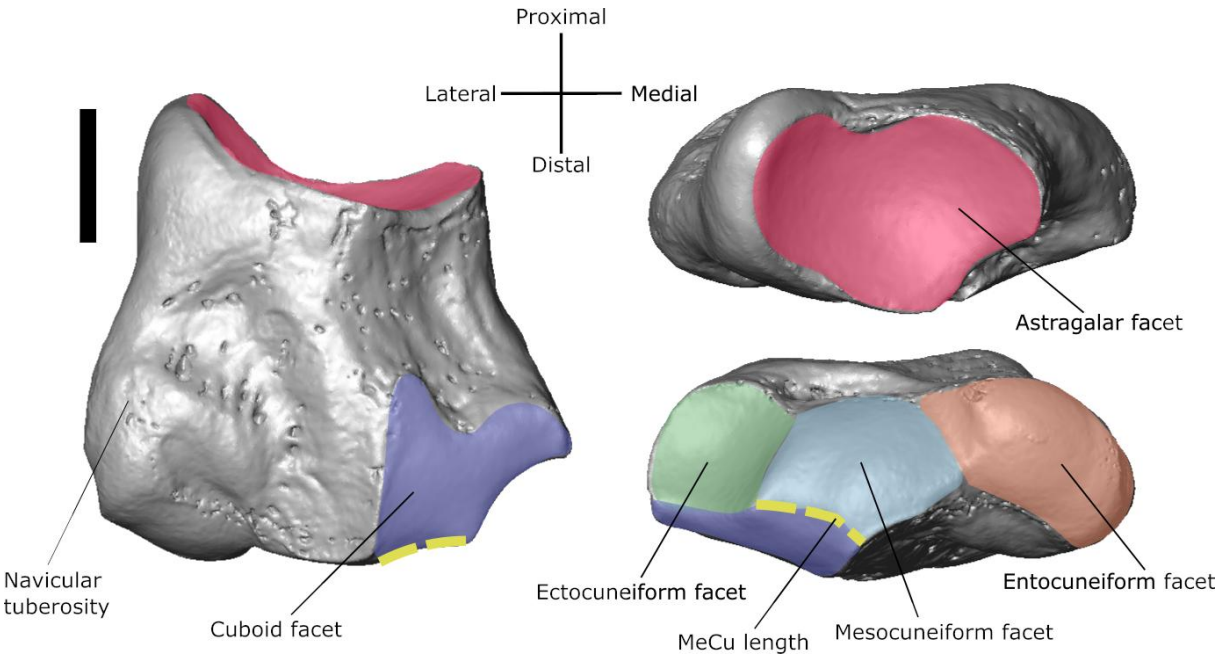


Figure 1.19. The navicular. The specimen represented belongs to *Eulemur fulvus* (USNM 589433). Scale bar equals 3 mm. Abbreviations: MeCu length = length of the contact between the cuboid and mesocuneiform facets.

Like other tarsal elements, the navicular exhibits varying degrees of proximodistal elongation across primate taxa (Fig. 1.20; Gebo, 1988; Marigó et al., 2020). The lengthening of the navicular, as with the calcaneus, is associated with a biomechanical requirement for increasing the lever arm of the foot to facilitate active leaping behavior in some primate species (Dagosto, 1988, 2007; Gebo, 1988). Nevertheless, similarly to the calcaneus, navicular proportions exhibit an important allometric component and are also affected by the type of foot posture—tarsi-fulcrumating or metatarsi-fulcrumating—complicating a straightforward functional interpretation of this feature (Morton, 1924; Moyà-Solà et al., 2012; Boyer et al, 2013). For instance, small-bodied VCL species such as bushbabies and tarsiers tend to have very elongated naviculars, while large-bodied VCL species, conversely, possess proximodistally short naviculars (Hall-Craggs, 1965b; Gebo, 1987b, 1989a; Gebo and Dagosto, 1988). Among those species with increased mobility demands at the transverse and subsequent tarsal joints, such as lorisids within strepsirrhines, or atelids and apes within anthropoids, the navicular is less elongated—being mediolaterally wider than proximodistally elongated (Marigó et al., 2020). This morphology evinces the role of the navicular as a facilitator of the mobility rather than that of a stiffer bridge between the ankle and the forefoot, as is the case in specialized leapers and terrestrial quadrupeds (Gebo, 1988; Prang, 2016).

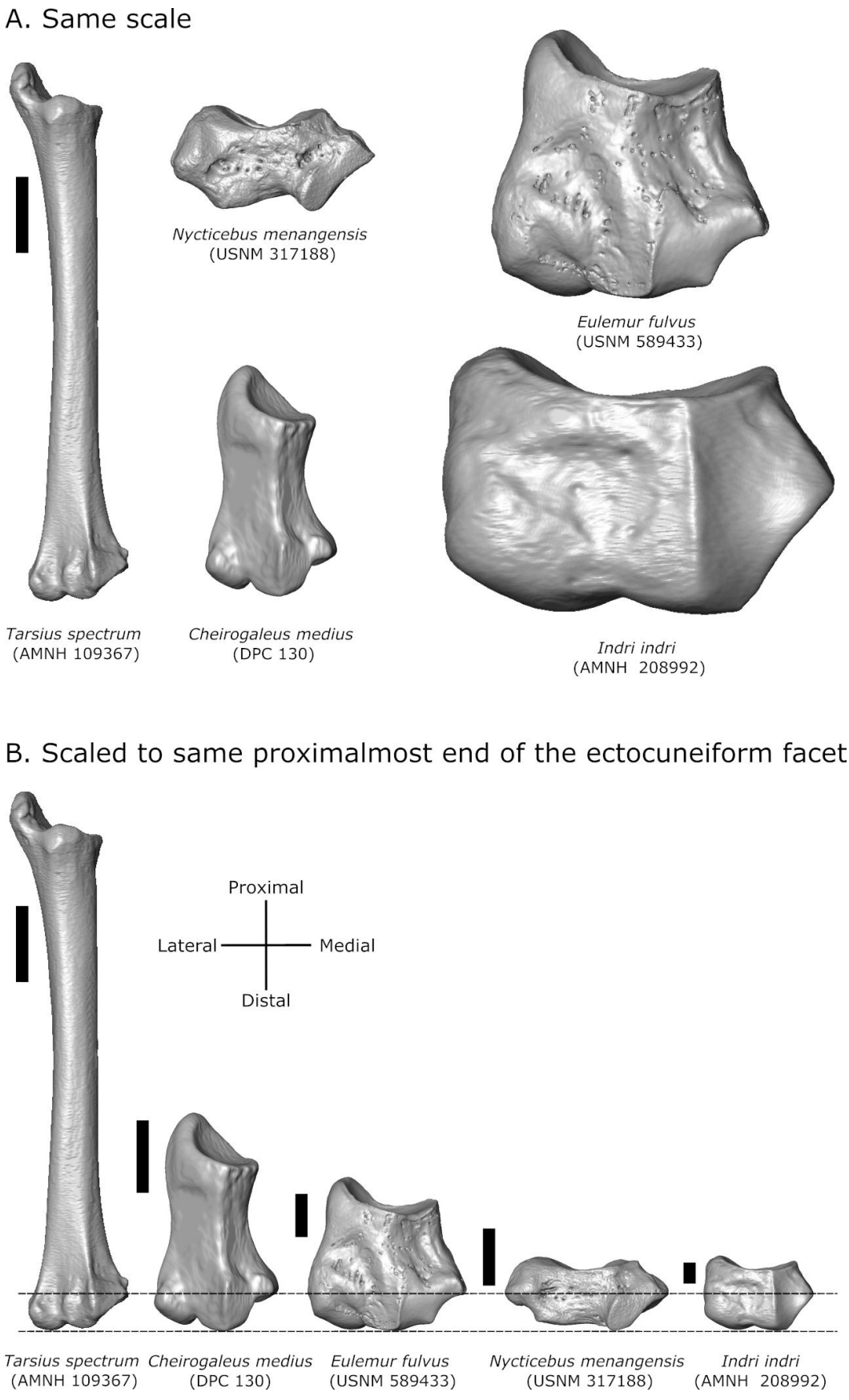


Figure 1.20. Extant primate navicular diversity. (A) Naviculars represented at the same scale; (B) naviculars represented scaled to the same proximalmost end of the entocuneiform facet. Scale bar equals 3 mm.

Together with the calcaneocuboid joint, the astragalonavicular joint (or talonavicular joint) is one of the main articulations that constitutes the TTJ. Compared to the condition in most other eutherians, in which the mediolateral width exceeds the dorsoplantar height, the astragalar facet on the navicular is ovoid in primates (Fig. 1.21A; Dagosto, 1988, 2007). This distinct morphology enables a more axial rotation in this articulation, facilitating inversion and eversion movements of the foot (Dagosto, 1986). Among primate species with greater climbing and suspensory components in their locomotor repertoire, the astragalar facet tends to be mediolaterally wider and shallower than that of more quadrupedal or specialized leaping species, which exhibit a deeper and more restricted facet that limits mobility at the TTJ (Decker and Szalay, 1974). Furthermore, in frequent leapers the medial wall of the navicular on the astragalar facet is proximodistally elongated, indicating that rotational movements accomplished along this joint are more limited as well (Fig. 1.21B). Conversely, less specialized leaping species exhibit comparatively less protruding medial walls (Decker and Szalay, 1974; Dagosto, 1986, 1988). The presence of an enlarged navicular tuberosity, which is the attachment site of the tendon of posterior tibialis muscle, is also very variable among primates (Lewis, 1964). In African apes, it has been suggested that this morphology could reflect that the medial column of the foot has a weight-bearing function during terrestrial locomotion (Sarmiento and Marcus, 2000; Harcourt-Smith and Aiello, 2004). Alternatively, a well-developed navicular tuberosity could reflect the presence of enlarged musculature associated with plantarflexion and inversion—particularly the posterior tibialis muscle. This interpretation is supported by the lack of clear association between the relative size of navicular tuberosity and arboreal behavior (Prang, 2016). For instance, some highly arboreal primates adapted to climbing and suspensory locomotion—such as atelids or hylobatids—possess an enlarged navicular tuberosity, suggesting that increased rotation of the navicular at the talonavicular joint could be facilitated by the pull of the tendon of the posterior tibialis muscle (Fig. 1.21C; Kuo et al., 2020).

Distally, the cuneiforms and the cuboid articulate with the navicular to constitute the transverse arch of the foot (Decker and Szalay, 1974). The articular facets for the entocuneiform and mesocuneiform are convex, whereas the facet for the ectocuneiform is concave. Strepsirrhines differ from haplorrhines by their more widely spaced and curved cuneiform facets, in contrast to the more confluent and flatter facets of the latter (Gebo, 1986a; Dagosto, 1988). The arrangement of the cuneiform facets on the navicular is related to the degree of opposability of the hallux against the other digits. In lorisids, their markedly adducted orientation of the hallux is facilitated by a more oblique orientation of the first metatarsal relative to the entocuneiform facet

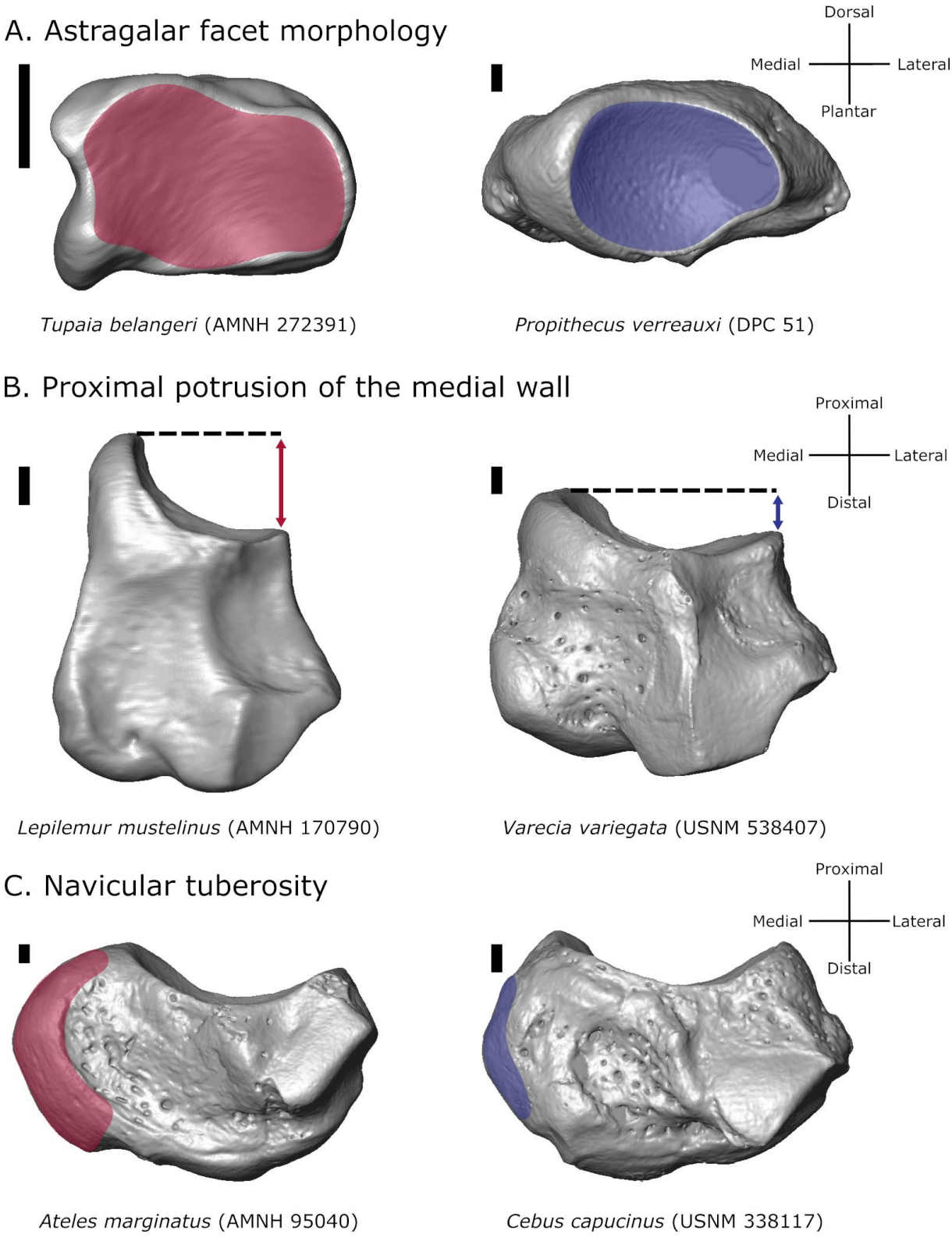


Figure 1.21. Features of the astragalar facet and navicular tuberosity. (A) Morphology of the astragalar facet; (B) proximal protrusion of the medial wall of the astragalar facet; (C) relative development of the navicular tuberosity. Scale bar equals 1 mm.

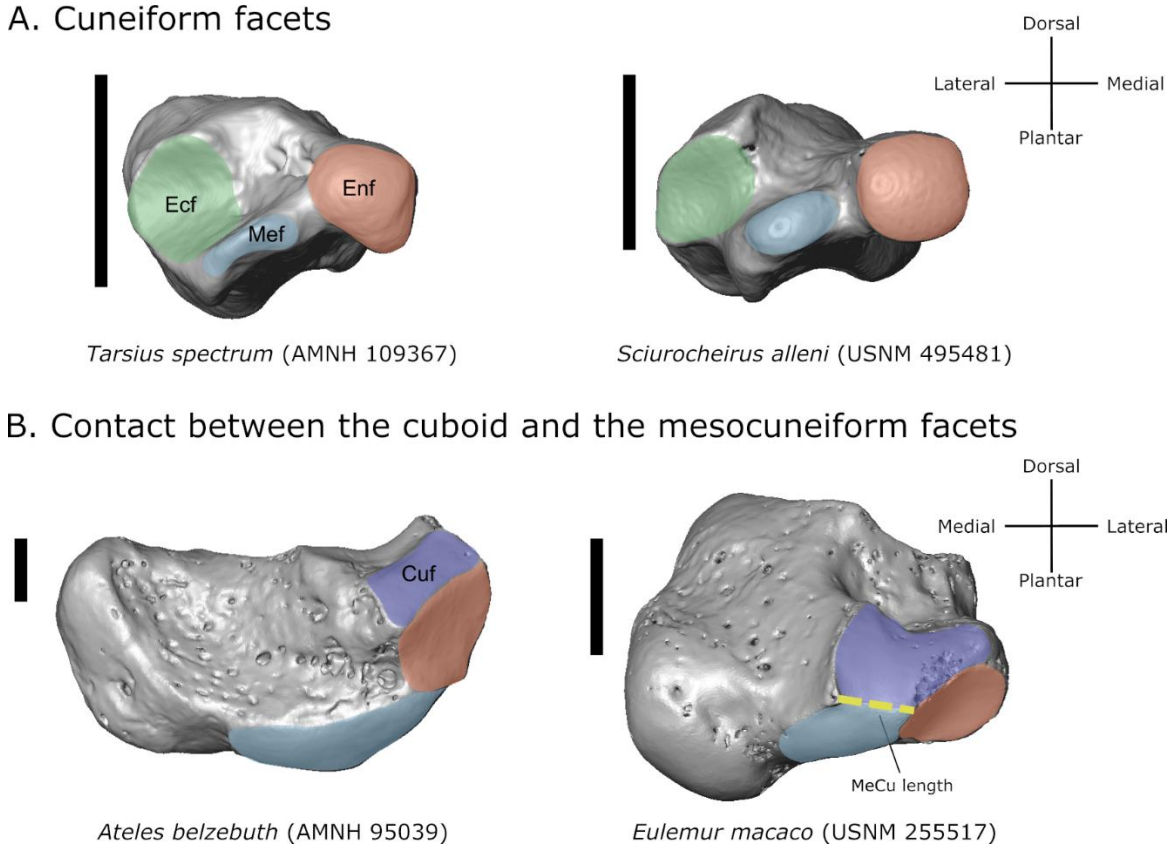


Figure 1.22. Features of the cuneiform and cuboid facets. (A) Distinct morphology between the cuneiform facets in tarsiers and bushbabies; (B) contact between the cuneiform and the mesocuneiform facets. Scale bar equals 3 mm. Abbreviations: Ecf = ectocuneiform facet; Mef = mesocuneiform facet; Enf = entocuneiform facet; Cuf = cuboid facet; MeCu length = MeCu length = length of the contact between the cuboid and mesocuneiform facets.

on the navicular, along with a broader and less convex morphology of the entocuneiform facet (Dagosto, 1986; Gebo, 1989a). In contrast, a reduced entocuneiform facet is associated with either a reduced hallux or reduced emphasis on weight transference through the hallux, as expected when everted foot postures are more frequently employed (Szalay and Dagosto, 1988; Sarmiento and Marcus, 2000). Within lorisiforms, bushabies exhibit a very restricted morphology of the cuneiform facets that enhances dorsiflexion and plantarflexion at these joints, at the cost of limiting the rotational mobility (Fig. 1.22A; Gebo, 1987b, 1989a). This is compensated by the presence of a synovial joint between the navicular and the calcaneus, providing a structural support for their very elongated tarsus while allowing enough flexibility to invert the foot (Hall-Craggs, 1966). Tarsiers, conversely, display a distal navicular morphology that allow for greater rotational movements than in bushbabies. For instance, while all three cuneiform facets in bushbabies articulate with their respective counterparts, in tarsiers the mesocuneiform facet only contacts the mesocuneiform during extreme plantarflexion, preventing dislocation of this joint

(Gebo, 1987b). Additionally, the entocuneiform facet is highly derived in tarsiers, allowing for greater rotational movements of the navicular to compensate the absence of a synovial joint between the navicular and the calcaneus, as in bushbabies. In strepsirrhines, the cuboid facet is larger than in haplorrhines, such that this facet also contacts the mesocuneiform—a condition not exhibited by haplorrhines and which constitutes a strepsirrhine synapomorphy (Fig. 1.22B; Beard, 1988). Multiple functional explanations have been proposed for this feature: it could stem from the morphology of the mesocuneiform itself (Gregory, 1920); be associated with the development of the transverse plantar arch, suggested to serve as a lateral wall to support the pedal flexors during grasping (Decker and Szalay, 1974); or facilitate foot inversion at the distal tarsal joints, whereby the cuboid shifts medially and plantarly during this movement, contacting the mesocuneiform (Dagosto, 1988).

1.3. Case study 1: The adaptive origin of primates

1.3.1. Plesiadapiforms

Plesiadapiforms are a diverse group of eutherians that inhabited North America, Europe and Asia from the earliest Paleocene to the late Eocene (Silcox and Gunnell, 2008). They are habitually considered broadly ancestral to or a paraphyletic assemblage of stem primates (Szalay, 1968; Szalay et al. 1987; Bloch et al., 2007; Silcox, 2007). However, some authors have advocated their exclusion from the order Primates, based on the absence of some or all the synapomorphic features exhibited by extant primates (Martin, 1968, 1986; Cartmill, 1974b, 1992). Additionally, most plesiadapiforms exhibit several derived features in their dentition (enlarged, blade-like third and fourth premolars; rodent-like, ever growing incisors; and reduced dental formulas) that exclude them from being directly ancestral to primates (Silcox et al., 2017). Alternative hypotheses proposing closer phylogenetic links between paromomyids and dermopterans were proposed some decades ago (Beard, 1990, 1993a, b; Kay et al., 1990, 1992), but more recent studies reject such link and uphold the closer ties between plesiadapiforms and euprimates (Silcox, 2001, 2007; Bloch et al., 2007; Chester et al., 2015). Most plesiadapiforms were relatively small-bodied, although some species are estimated to have reached a large body mass, up to several kilograms (Silcox et al., 2017; Boyer and Gingerich, 2019). Plesiadapiforms exhibit several dental features that link them to extant primates, including relatively low molar cusps and lower molars with low trigonids and broad talonids (Szalay, 1968). In addition, many plesiadapiform species possess

dental adaptations associated with specialized diets—including tree exudates, larvae and nectar—although most species are inferred to have had moderately varied diets that included insects, fruit and leaves (Szalay, 1968; Kay and Cartmill, 1977; Rose and Bown, 1996; Silcox et al., 2002, 2017; López-Torres et al., 2018; Wilson-Mantilla et al., 2021).

Taxonomically diverse—over 120 species across 10 families (Silcox et al., 2017; Crowell et al., 2024)—the postcranial morphology of plesidapiforms is not well known. Most early studies (Szalay and Decker, 1974; Szalay and Drawhorn, 1980) compared plesiadapiforms with other contemporaneous mammals, emphasizing features that facilitated arboreal lifestyle. Recent discoveries of multiple partial skeletons (Bloch and Boyer, 2002, 2007; Bloch et al., 2007; Chester et al., 2017, 2019, 2025; Boyer and Gingerich, 2019), along with some isolated bones (Chester et al., 2015), substantially enhanced our understanding of plesiadapiform postcranial morphology, shedding light on their locomotor adaptations. These findings suggest that plesiadapiforms exhibited a diverse array of distinct positional behaviors, from large-bodied, slow-moving taxa such as *Plesiadapis cookei*, to agile bounders among paromomyids, and even potential below-branch suspensory forms within micromomyids (Bloch and Boyer, 2007; Bloch et al., 2007). Foot elements from plesiadapiforms are known for 23 species representing eight families (Yapuncich et al., 2022). Compared to other Cretaceous and Paleocene eutherians, plesiadapiforms share several hindfoot and navicular features with other euarchontans—including euprimates—primarily associated with enhanced mobility at the LAJ and TTJ, as well as evidence of some degree of incipient pedal grasping (Szalay and Decker, 1974; Chester et al., 2015). Namely, these include (Szalay and Decker, 1974): a contiguous and more extended sustentacular facet on both the astragalus and calcaneus, a convex and helically inclined ectal facet on the calcaneus, and a more transversely oriented calcaneocuboid joint with a relatively well-developed pit for the cuboid protuberance. Furthermore, most plesiadapiforms also exhibit evidence of enhanced grasping capabilities, such as a saddle-shaped distal articular facet on the cuneiform and the morphology of the first metatarsal (Szalay and Dagosto, 1988; Bloch and Boyer, 2007; Sargis et al., 2007; Boyer and Gingerich, 2019). Notably, the discovery of a partial skeleton of *Carpolestes simpsoni* revealed that at least one plesiadapiform species possessed a divergent hallux with a nail rather than a claw—a feature resembling that of euprimates and likely associated with utilizing fine-branch arboreal substrates (Bloch and Boyer, 2002). All considered, plesiadapiforms are very informative for understanding what the ancestors of euprimates may have looked like, irrespective of their systematic position within Euarchonta and their specific relationship with euprimates.

1.3.2. Adapiforms and omomyiforms

Euprimates—or primates of modern aspect—are characterized by the presence of a suite of anatomical specializations, including adaptations for grasping, enhancement of the visual system, dental adaptations for increased frugivory, and postcranial features related to leaping behavior (Cartmill, 1974a, b, 1992; Szalay, 1987; Silcox et al., 2015). The earliest unambiguous euprimates appeared at the onset of the Eocene, shortly after the Paleocene-Eocene Thermal Maximum, rapidly expanding across the globe (Smith et al., 2006; Beard, 2008; Rose et al., 2011; Morse et al., 2019). These early euprimate species are divided into two groups, adapiforms and omomyiforms. The former are regarded a paraphyletic assemblage of stem strepsirrhines, usually divided into three main families (Godinot, 1998; Marigó et al., 2016; Ni et al., 2016): Notharctidae (comprising Notharctinae, Cercamoniinae and Asiadapinae, the latter two sometimes elevated to family rank); Adapidae (including Adapinae and Cercopithecinae); and Sivaladapidae, which persisted in Asia until the late Miocene. Adapiforms were generally larger-bodied than omomyiforms, possessed longer snouts, smaller orbits (suggesting diurnality), and dentitions indicative of folivorous or frugivorous diets (Gunnell et al., 2008; Franzen et al., 2009; Seiffert et al., 2009). Contrarily, omomyiforms are often regarded as stem haplorrhines or stem tarsiiforms, although their exact affinities with extant tarsiers and anthropoids remain debated (Rosenberger and Preuschoft, 2012; Ni et al., 2013, 2016; Rossie et al., 2018). Omomyiforms are usually divided into three subfamilies: Anaptomorphinae, Omomyinae and Microchoerinae, the latter sometimes referred to as a distinct family (Szalay, 1975; Gingerich, 1981; Gunnell and Rose, 2002). They were usually smaller-bodied than adapiforms, had shorter snouts, larger orbits, and dentitions that suggest an important component of insects and other arthropods in their diets (Gunnell et al., 2008). Postcranially, both adapiforms and omomyiforms are quite variable, albeit they also exhibit major differences. Adapiforms were larger and generally described as lemur-like, characterized by relatively mobile and likely habitually supinated forelimbs, as well as very elongated hindlimbs compared to the forelimbs, resulting in a low intermembral index. In contrast, omomyiforms were usually smaller-bodied than adapiforms, being regarded as similar to bushabies or tarsiers (Dagosto, 1993; Dagosto et al., 1999).

Foot elements have proven to be especially informative for understanding the locomotor adaptations of early euprimates (Yapuncich et al., 2022). Adapiform pedal morphology is particularly well known, with foot elements recovered for more than 30 species (e.g., Gregory, 1920; Decker and Szalay, 1974; Dagosto, 1983; Rose and Walker, 1985; Covert, 1988; Gebo et al., 1991, 1999, 2008; Beard et al., 2007; Franzen et al., 2009; Rose et al., 2009; Boyer et al., 2010a,

2017a; Marivaux et al., 2011, 2013; Seiffert et al., 2015; Dunn et al., 2016; Marigó et al., 2016, 2020). Based on their pedal remains, adapiforms exhibit considerable locomotor diversity (Gebo, 1988). For instance, some species display features associated with increased leaping proclivity, such as a deep trochlear groove on the astragalus, a well-developed posterior trochlear shelf, and a relatively elongated distal calcaneus and navicular, although tarsal elongation is less pronounced than in most omomyiforms (Gebo et al., 1991; Marivaux et al., 2011, 2013; Boyer et al., 2013, 2017a; Marigó et al., 2016, 2020). Contrarily, others exhibit features that correlate with a more cautious climbing behavior, resembling superficially extant lorisids, including a shallow trochlear groove on the astragalus, a mediolaterally expanded astragalar head, a relatively large medial tibial facet, the lack of an enlarged posterior trochlear shelf, and a short distal calcaneus and navicular (Dagosto, 1983; Rose et al., 2009; Boyer et al., 2010a; Seiffert et al., 2015; Dunn et al., 2016). Conversely, omomyiform pedal morphology is moderately less well known, with foot elements recovered for approximately 20 species (e.g., Szalay, 1975; Savage and Waters, 1978; Godinot and Dagosto, 1983; Gebo, 1988; Covert and Hamrick, 1993; Anemone and Covert, 2000; Gebo et al., 2001, 2012a, 2015a; Dunn et al., 2006; Dunn, 2010; Rose et al., 2011; Ni et al., 2013). Overall, omomyiforms exhibit relatively less diversity in pedal morphology than adapiforms, and most species are reconstructed as habitual leapers resembling bushbabies and mouse lemurs (Gebo, 1988). The most distinctive feature of the omomyiform foot is its relatively elongated tarsus, as evinced in the calcaneus, the navicular, and the neck of the astragalus. However, only certain microchoerine genera such as *Necrolemur* and *Microchoerus* approach the extreme elongation seen in extant tarsiers and bushbabies, exhibiting additional postcranial adaptations like distal tibiofibular fusion (Dagosto, 1985; Gebo, 1988; Boyer et al., 2013). Remarkably, adapiforms exhibit a more derived overall foot morphology compared to omomyiforms, which more closely resemble the plesiomorphic eutherian condition than the former. This is exemplified by the possession, in adapiforms, of several characters functionally associated with increased mobility at the main tarsal joints, including the sloping angle of the fibular facet, the lateral position of the groove for the FHL tendon, and the contact between the cuboid and the mesocuneiform facets on the navicular (Beard, 1988; Dagosto, 1988).

1.3.3. Early anthropoids

In general, most anthropoids are larger-bodied than other primates, exhibit several derived cranial traits (including a fused frontal bone and mandibular symphysis, postorbital closure,

relatively smaller orbits and larger brains than their strepsirrhine and tarsier counterparts), and are characterized by a suite of postcranial features related to increased quadrupedal locomotion and the use of horizontal substrates (Gebo, 1989b; Ross, 1996; Gebo and Dagosto, 2004; Williams et al., 2010).

Anthropoids are first known from the Eocene of Asia, with the oldest remains belonging to the family Eosimiidae (Beard et al., 1996; Jaeger et al., 1999; Bajpai et al., 2008). Eosimiids—sometimes referred as eosimiiforms together with the African family Afrotarsiidae (Chaimanee et al., 2012; Beard, 2016)—are a group of small-bodied anthropoids characterized by a mixture of features unknown among their extant counterparts, combining primitive euprimate characters with more derived anthropoid ones (Chaimanee et al., 2024). Multiple isolated foot bones of eosimiids have been recovered so far, including elements of the hindfoot (Gebo et al., 2000, 2001, 2002; Gebo et al., 2012b), midfoot (Gebo et al., 2017), and distal phalanges (Gebo et al., 2015b, 2017). Regarding pedal morphology, eosimiids resemble contemporaneous, similar-sized omomyiforms, but differ from adapiforms in possessing a vertical fibular facet and a reduced medial tibial facet (Gebo et al., 2000, 2001; Gebo et al., 2012b). In contrast, other features of the eosimiid hindfoot—such as a relatively angled astragalar neck, a broad sustentaculum on the calcaneus, and the lack of distal calcaneal elongation—align eosimiids more closely with later anthropoids (Gebo et al., 2000, 2001; Gebo et al., 2012b). These latter features have led some authors to reconstruct eosimiids as relatively generalized arboreal quadrupeds, differing from the more acrobatic behavior inferred for most omomyiforms (Gebo et al., 2000, 2001; Yapuncich et al., 2019).

Another group of putative early anthropoids from the Eocene and Oligocene of Asia are the amphipithecids, although their inclusion in the Anthropoidea has been extensively debated (Ciochon and Gunnell, 2002, 2004; Beard et al., 2009; Jaeger et al., 2020). The systematic position of amphipithecids is uncertain, having been proposed as the sister group of platyrrhines or parapithecoids (e.g., Bajpai et al., 2008; Beard et al., 2009; Seiffert et al., 2010; Ni et al., 2016; Jaeger et al., 2019; Marivaux et al., 2023). Recently, the status of amphipithecids as crown anthropoids or even as a monophyletic group has been challenged, with some studies proposing a more basal position for amphipithecids as stem anthropoids (Seiffert et al., 2009, 2018; Williams et al., 2010; Jaeger et al., 2020). Compared with eosimiids, amphipitheciids are generally larger-bodied—up to 10 kg in some species—but resemble the latter in the possession of a mixture of primitive and more derived characters (Jaeger et al., 2020). The foot of amphipithecids is solely known based on two astragali, which exhibit characteristic anthropoid features such as a steep fibular facet, a restricted medial tibial facet, and a medial position for the groove of the FHL tendon (Marivaux et al., 2003, 2010; Dagosto et al., 2010). The morphology of these two astragali is suggestive of a

locomotor behavior dominated by arboreal quadrupedalism with low emphasis on leaping behavior (Dagosto et al., 2010; Marivaux et al., 2010).

Early anthropoids from the late Eocene and early Oligocene of Afro-Arabia—parapithecoids, oligopithecids and propliopithecoids—display more unambiguous anthropoid synapomorphies, providing many insights into the initial diversification of Anthropoidea (Seiffert et al., 2010; Seiffert, 2012). Parapithecoids are usually regarded as stem anthropoids, as evinced by their retention of primitive dental formula, like in platyrrhines, as well as other cranial and postcranial features (Fleagle and Kay, 1987; Seiffert et al., 2005, 2020; Seiffert, 2012). Postcranially, parapithecoids resemble extant New World monkeys like the squirrel monkey (*Saimiri* spp.) and the capuchin monkey (*Cebus* spp.), being reconstructed as small- to medium-bodied above-branch quadrupeds and horizontal leapers (Gebo and Simons, 1987; Gebo, 1989b, 1993a; Simons and Seiffert, 1999; Seiffert et al., 2000; Seiffert and Simons, 2001; Gladman et al., 2013). Foot bones have been recovered for several parapithecoid genera, notably *Apidium* and *Proteopithecus*, displaying some similarities with earlier haplorrhines—such as omomyiforms and eosiimids—as well as with most extant non-atelid platyrrhines. These features include a symmetrical trochlea with parallel rims, a midline positioned groove for the tendon of the FHL, a steep fibular facet, a relatively narrow ectal facet on the astragalus, and a moderately long distal calcaneus, among other features (Conroy and Rose, 1983; Gebo and Simons, 1987; Gebo, 1993a; Fleagle and Simons, 1995; Seiffert and Simons, 2001; Boyer and Seiffert, 2013; Gladman et al., 2013). Contrarily, oligopithecids and propliopithecoids are usually included within crown anthropoids as stem catarrhines, based on the possession of more derived characters towards this group (Simons, 1962, 1995; Seiffert et al., 2010, 2020; Seiffert, 2012). Larger-bodied than parapithecoids, oligopithecids and propliopithecoids are reconstructed as more adept climbers, contrasting with the more active locomotion inferred for the former (Conroy and Rose, 1983; Gebo and Simons, 1987; Ankel-Simons et al., 1998; Seiffert and Simons, 2001; Patel et al., 2012). The recovered foot bones of oligopithecids and propliopithecoids resemble those of extant apes and atelids in some features associated with an ankle adapted for increased mobility ranges, in agreement with the rest of the postcranium (Simons, 1995; Seiffert and Simons, 2001).

1.3.4. Hypotheses on euprimate origins

Several adaptive hypotheses have been proposed to explain the emergence of euprimates. The first attempts to account for the suite of features that characterize euprimates focused on

their relationship with arboreal life. For instance, Smith (1924) proposed that euprimates evolved from shrew-like ancestors that developed significant brain enlargement in response to the higher demands of arboreal life compared to the terrestrial ones. Similarly, Jones (1916) argued that arboreality drove a functional differentiation of the limbs, with the feet becoming increasingly specialized for locomotion, effectively freeing the hands for tasks such as grasping. These early ideas were later synthesized into what became known as the "arboreal hypothesis" (Le Gros Clark, 1959). Under this hypothesis, tree shrews were considered primitive primates that only partially developed an incipient primate-like morphology—including traits such as a postorbital bar, partial reduction of the olfactory system alongside a relatively developed visual cortex, and minor adaptations for grasping (Fig. 1.23A). Initially, this view was framed in an orthogenetic context (Le Gros Clark, 1934) but later shifted to an adaptationist perspective (Le Gros Clark, 1959). As per the arboreal hypothesis, primate adaptive complexes were proposed to have been acquired independently in several lineages throughout primate evolution. This hypothesis was aligned with the prevailing view of higher taxa at the time, which did not distinguish between primitive and derived characters, or between traits that evolved independently across different lineages and those inherited from a common ancestor (Simpson, 1945; Cartmill, 2018).

An alternative hypothesis proposed by Szalay and colleagues (Szalay, 1968; Szalay and Dagosto, 1980; Szalay et al., 1987) suggests a two-stage model, regarded as the “grasp-leaping” hypothesis. According to this hypothesis, primates acquired adaptations for a more frugivorous diet first and later evolved postcranial features related to leaping and grasping behaviors. Among extant species, small, generalized primates such as mouse lemurs are relatively good analogues for the last common ancestor of extant primates (Charles-Dominique and Martin, 1970; Fig. 1.23B). Although leaping features are frequently found in the first adapiforms and omomyiforms (e.g., Walker, 1974; Gebo, 1988; Rose, 1994a), the fossil record also suggests that adaptations for grasping evolved earlier, weakening a concurrent evolution of these traits (Bloch and Boyer, 2002). However, the purported homology of the opposable, nail-bearing hallux of *C. simpsoni* with that of euprimates has been widely criticized by some (Kirk et al., 2003; Gebo, 2004, 2009). Furthermore, the “grasp-leaping” hypothesis has received some criticism regarding the adaptive implications for increased leaping in the locomotor repertoire of the earliest primates. Some have interpreted leaping behavior as a strategy to avoid predation (Crompton et al., 1993; Crompton,1995; Crompton and Sellers, 2007), although other possible benefits should be further studied in the future.

However, comparative evidence does not support neither the “arboreal” nor the “grasp-leaping” hypotheses. Most non-primate arboreal animals, such as squirrels, do not exhibit the

same set of features that euprimates do. Instead, they typically have sharp claws, a well-developed olfactory apparatus, laterally directed eyes, and non-opposable pollex and hallux. Therefore, something else other than arboreal life per se—or leaping behavior specifically—must have driven the acquisition of euprimate-like adaptive complexes (Cartmill, 1974b). Alternatively, Cartmill (1974a, b, 1992, 2012) proposed that both the visual adaptations and the grasping foot of euprimates evolved as adaptations for "visual predation" (Fig. 1.23C). More precisely, visual convergence is an adaptation for near-field vision that allows the predator to gauge the distance to the prey. Additionally, a grasping foot facilitates small animals—such as the earliest euprimates—to move cautiously along narrow supports, securing themselves on fine substrates while using their hand to capture prey (Cartmill 1974a, b). The visual predator hypothesis has undergone some criticisms based on the lack of orbital convergence in some visual predators (e.g., moongoses, tree shrews), while there are also taxa exhibiting orbital convergence despite not being visual predators (e.g., kinkajous, koalas, sloths; Rasmussen and Sussman, 2007; Sussman et al., 2013), leading to a reframe of this hypothesis to specifically refer to nocturnal visual predators (Cartmill, 1992, 2012).

A fourth model for primate origins is also focused on the role of visual adaptations, linking their emergence to the process of evolution of angiosperms (Sussman, 1991; Sussman and Raven, 1978; Sussman et al., 2013). Contrary to the "visual predation" hypothesis, the "angiosperm coevolution" hypothesis aligns more closely with the fossil record. Multiple studies suggest that both the plesiadapiforms and early euprimates exhibit dental traits indicating an important component of fruit and other vegetal products—leaves, seeds, gum, nectar—in their diets (Szalay, 1968, 1972; Gingerich, 1976; Boyer et al., 2010b; Silcox et al., 2017; López-Torres et al., 2018; Wilson-Mantilla et al., 2021). Therefore, the "angiosperm coevolution" hypothesis proposes that grasping adaptations are related to the acquisition of angiosperm products in the terminal branches, allowing the earliest primates to occupy this niche. This hypothesis has been criticized by some, based on the apparent lower visual demands required for fruit foraging on the terminal branches compared to insect preying (Cartmill, 1992, 2012; Kemp et al., 2024). However, others consider that the evolution of orbital convergence is consistent with an adaptation for detecting small, usually very inconspicuous angiosperm products in cluttered environments (Changizi and Shimojo, 2008). Additionally, Rasmussen (1990) proposed a composite model for primate origins, the "terminal branch feeding" hypothesis, based on his observations made on the woolly opossum (*Caluromys derbianus*), which exhibits "primate-like" adaptations compared to closely related didelphids, such as a more marked orbital convergence, larger brain size, and the presence of a postorbital process (Fig. 1.23D). This new model, including aspects of both the "visual predator"

hypothesis and the "angiosperm coevolution" hypothesis, argues that the earliest primates fed on both fruit growing in the terminal branches and insects, having developed grasping extremities to access the fine branch milieu and visual adaptations to catch the animal prey (Rasmussen, 1990). Moreover, this synthesis devises a more gradualistic model for primate origins, starting with feeding on the terminal branches and then adding other adaptations, including those for leaping behavior. This has led to subsequent stepwise models for the independent evolution of primate adaptive complexes, including a "*Caluromys*-like" stage before the acquisition of the full set of key primate adaptations (Gebo, 2004; Sargis et al., 2007).

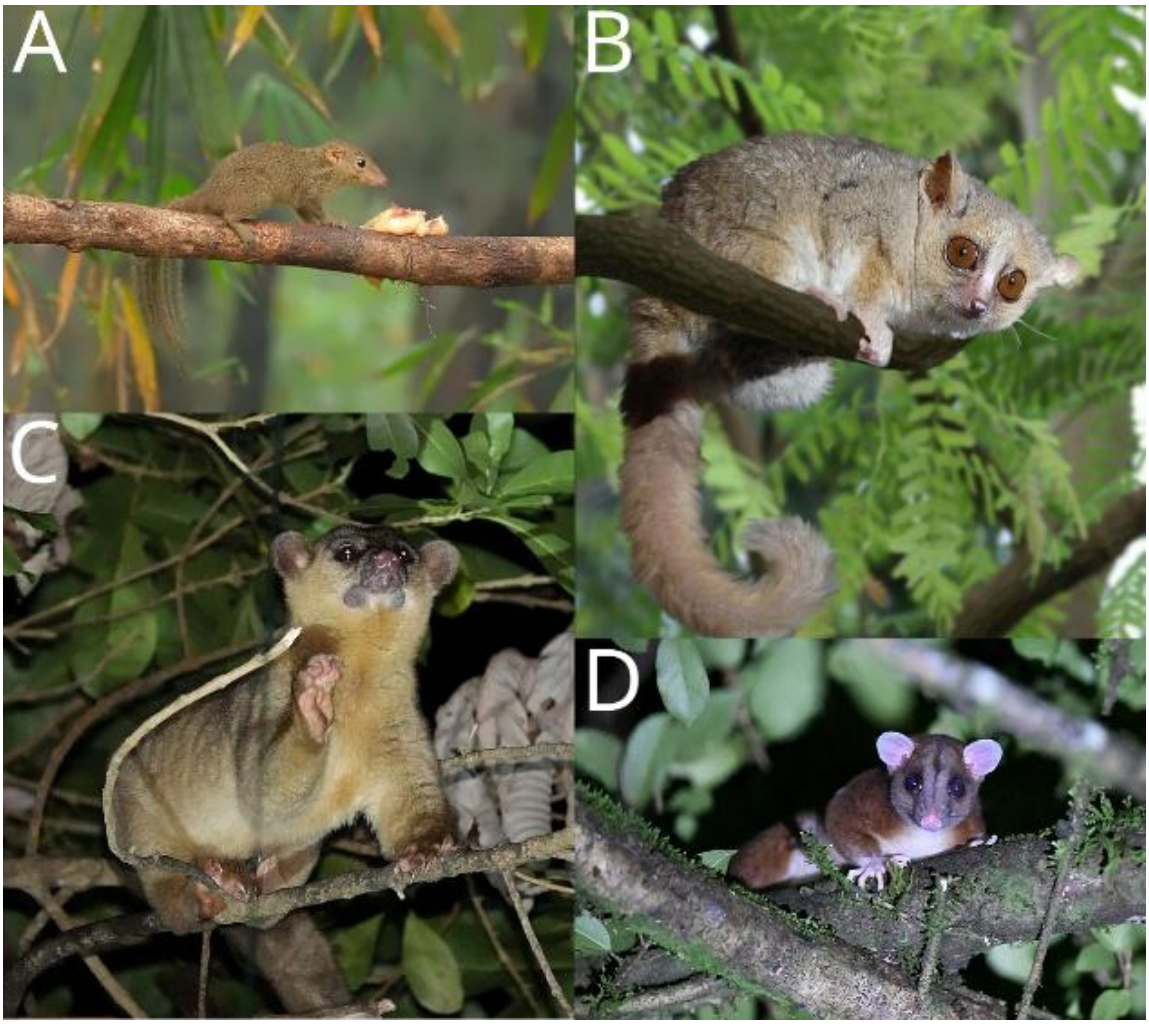


Figure 1.23. Extant analogues for each four main models on the origin of primates. (A) Northen treeshrew (*Tupaia belangeri*), from the "arboreal" hypothesis (© Tisha Mukherjee / CC BY-SA 4.0); (B) Gray mouse lemur (*Microcebus murinus*), from the "grasp-leaping" hypothesis (© Gabriella Skollar, photographer; Rebecca Lewis; editor / CC BY-SA 3.0); (C) Kinkajou (*Potos flavus*), from the "visual-predator" hypothesis (© desertnaturalist / CC BY 4.0); (D) Derby's Woolly Opossum (*Caluromys derbianus*), from the "angiosperm coevolution" and "terminal branch feeding" hypotheses (© Chloe and Trevor Van Loon / CC BY 4.0).

1.4. Case study 2: Hominoid locomotor evolution in the light of pedal evidence

1.4.1. The foot of Miocene apes: A general review

The locomotor behavior of most Miocene apes was markedly different from that exhibited by extant apes or extant Old World monkeys, as evinced by the combination of plesimorphic (i.e., monkey-like) and derived (i.e., ape-like) traits in their postcranial anatomy (Rose, 1983, 1993, 1994a; Ward, 2015). Current evidence supports a mosaic evolution of the hominoid postcranium, progressively transitioning from a locomotor repertoire dominated by above-branch arboreal quadrupedalism—resembling to that practiced by many extant monkeys—toward orthograde behaviors including frequent vertical climbing and suspension (Ward, 2015;). The mosaic nature of Miocene ape postcranial anatomy supports the view that homoplasy played a pervasive role in hominoid evolution, albeit the extent of convergent evolution among Miocene apes is still debated (Larson, 1998b; Alba, 2012; Almécija et al., 2021). This applies to pedal morphology as well, which is relatively well known for Early to Middle Miocene apes from Africa, albeit it is scarcer for Middle to Late Miocene Eurasian species (reviewed in Drapeau, 2022).

Compared with other anthropoids, the foot of extant apes is characterized by a greater range of mobility and prehensility, which can be related to the more varied and non-stereotypical locomotion of the latter (Conroy and Rose, 1983; Hunt, 2016). In contrast, most specialized features associated with a very mobile foot in extant apes are absent from the pedal elements of Miocene apes. Instead, these exhibit a remarkably plesiomorphic morphology (Harrison, 1982; Conroy and Rose, 1983; Rose, 1993, 1994b). The pedal morphology of Early to Middle Miocene apes from Africa—including proconsulids, nyanzapithecids and afropithecids—resembles that of stem catarrhines (e.g., pliopithecoids and dendropithecids), with a foot adapted for strong hallucal grasping but possessing less mobility in the main joints than extant apes (Langdon, 1986; Dunsworth, 2006; DeSilva, 2008). Despite the overall plesiomorphic morphology, several derived features toward the extant ape condition are already present in the feet of these species, such as a moderately laterally flaring fibular facet on the astragalus, a somewhat developed lateral posterior tubercle, and a relatively robust hallux associated with powerful grasping (Harrison, 1982; Conroy and Rose, 1983; Walker, 1997). However, other features are more monkey-like, including the relatively restricted and congruent surfaces of the main tarsal joints (limiting the mobility of these articulations), the lack of a plantar tubercle on the calcaneus, or the possession

of a narrow forefoot, contrasting with the more splayed forefoot of extant apes (Harrison, 1982; Conroy and Rose, 1983; Langdon, 1986; Rose, 1993; Ward et al., 1993; Ward, 1998; Dunsworth, 2006; DeSilva, 2008; Nakatsukasa et al., 2012; Patel et al., 2017). Consequently, Early and Middle Miocene apes from Africa are habitually reconstructed as arboreal quadrupeds that engaged in frequent climbing behaviors, albeit lacking specific adaptations for vertical climbing or suspensory locomotion, contrary to extant apes (Walker, 1997; Ward, 2015). Some species, such as *Proconsul major* or *Rangwapithecus gordoni*, exhibit ankle and midfoot features suggestive of enhanced climbing capabilities compared with other Early Miocene species (Harrison, 1982; Nengo and Rae, 1992; DeSilva, 2008; Patel et al., 2017). Conversely, other species like *Equatorius africanus* display pedal morphologies—as well as other postcranial adaptations—indicative of terrestrial quadrupedalism, similar to extant terrestrial cercopithecines (McCrossin and Benefit, 1997; McCrossin et al., 1998; Harrison, 2010).

Middle to Late Miocene apes from Eurasia exhibit pedal morphologies that more closely resemble extant apes than do their earlier, Early to Middle Miocene counterparts from Africa, although they still retain several primitive traits (Ward, 2015). Unfortunately, pedal remains are less abundant for Eurasian species, preventing a more detailed understanding of their foot anatomy. The available pedal evidence of dryopithecines (including *Hispanopithecus*, *Rudapithecus*, *Danuvius* and *Pierolapithecus*), has only been preliminarily described (Begun, 2002, 2009; Moyà-Solà et al., 2004; Böhme et al., 2019), exhibiting an admixture of ape-like and monkey-like characters, which concurs with the remaining postcranial evidence for these species (Alba, 2012). Foot bones attributed to the pongine *Sivapithecus* exhibit multiple ape-like features, including a proximodistally abbreviated tarsus, a relatively well-developed posterior talar tubercles with a deep groove for the FHL tendon, slightly less congruent joints allowing for increased mobility (permitting increased mobility at these articulations), and robust metatarsals, including the hallux, as in earlier Miocene ape species (Walker, 1997; Ward, 2015). However, in other features at the ankle and forefoot, such as a relatively high astragalar trochlea and the laterally adducted lateral metatarsals, evincing a narrow forefoot, resembled extant Old World monkeys (Pilbeam, 1980; Madar, 1996, 2002). This admixture of ape-like and monkey-like characters in the pedal morphology of dryopithecines is consistent with the remaining postcranial evidence for these species, which display adaptations for orthograde behaviors in the trunk and upper limbs (Moyà-Solà et al., 2004; Alba, 2012), despite the retention of other traits better suited for above-branch quadrupedalism (e.g., Almécija et al., 2007, 2009; Alba, 2012; Tallman et al., 2013; Pina et al., 2019). *Oreopithecus* exhibits a remarkably ape-like pedal morphology, including several features at the main tarsal joints indicative of a very mobile ankle and a splayed forefoot

(Szalay and Langdon, 1986; Köhler and Moyà-Solà, 1997). Most of the rest of the skeleton also shows striking similarities to extant apes, including the intermembral proportions (Jungers, 1987) and upper limb morphology (Harrison, 1987; Harrison and Rook, 1997). The lower torso does not exhibit a full rigid lumbar region and elongate ilium like those of extant great apes, resembling more extant hylobatids in that regard (Hammond et al., 2020).

1.4.2. The great apes of the Vallès-Penedès Basin

The Vallès-Penedès Basin (NE Iberian Peninsula) is a key reference area for the study of Miocene land mammal faunas of Europe (Agustí et al., 1997; Casanovas-Vilar et al., 2016a, b, 2022). Most of this basin, a half-graben limited by the Catalan (Prelittoral and Littoral) Coastal Ranges, originated as a consequence of the rifting of the NW Mediterranean during the Neogene (Cabrera et al., 2004; Casanovas-Vilar et al., 2016). The infill of this basin is predominantly composed of alluvial fan deposits, yielding an exceptionally rich fossil record of Early to Late Miocene continental vertebrates (Casanovas-Vilar et al., 2016, 2022). The Vallès-Penedès is one of the two basins (the other is the Seu d'Urgell Basin) where dryopithecines have been found in the Iberian Peninsula, co-occurring with pliopithecoid stem catarrhine (Alba, 2012; Marigó et al., 2014; Alba et al., 2017, 2022). These include various pliopithecoid species (Moyà-Solà et al., 2001; Alba et al., 2010a, 2015; Alba and Moyà-Solà, 2012): the pliopithecid *Pliopithecus canmatensis* and the crouzeliids *Egarapithecus narcisoi*, *Barberapithecus huerzeleri*, and *Pliobates cataloniae*. The latter species was initially described as a stem hominoid, based on postcranial similarities with modern apes, particularly in the elbow and wrist joints (Alba et al., 2015; Raventós-Izard et al., 2025), which are currently interpreted as convergences, as supported by dental similarities with other European crouzeliids (Bouchet et al., 2024a, b). Among dryopithecines, five species have been recorded (Begun, 1992a; Moyà-Solà and Köhler, 1993, 1995, 1996; Moyà-Solà et al., 2004, 2009a, b; Alba et al., 2012a, b). These include the middle Miocene dryopithecins *Dryopithecus fontani*, *Pierolapithecus catalaunicus*, and *Anoiapithecus brevirostris*, as well as the slightly younger late Miocene hispanopithecins *Hispanopithecus laietanus* and *Hispanopithecus crusafonti*.

There is broad consensus that dryopithecines are great apes (i.e., hominids) but their phylogenetic relationships have been controversial and doubts remain about their monophyly (Alba, 2012; Almécija et al., 2021; Pugh, 2022; see review in Urciuoli and Alba, 2023). In addition, considerable uncertainty persists regarding the systematic position of dryopithecines relative to

extant hominids (see reviews in Almécija et al., 2021; Urciuoli and Alba, 2023). Thus, dryopithecines have been variously interpreted as stem hominids predating the divergence between hominines and pongines (Andrews, 1992; Moyà-Solà et al., 2004, 2009a, b; Alba, 2012; Alba et al., 2015; Nengo et al., 2017; Gilbert et al., 2020; Pugh, 2022); as stem pongines (Moyà-Solà and Köhler, 1993, 1995, 1996; Agustí et al., 1996; Köhler et al., 2001a, b); or, alternatively, as stem hominines (Begun, 1992b, 2002, 2009, 2015; Begun et al., 1997, 2012). The latter interpretation has led Begun and coauthors to propose a Eurasian origin for the hominine clade (Begun, 1992b, 2009; Begun et al., 1997, 2012). Within the Dryopithecinae, dryopithecins appear to be slightly less derived than hispanopithecins in terms of their dental morphology (Moyà-Solà et al., 2009a, b; Alba et al., 2010b; Alba, 2012; Pérez de los Ríos et al., 2012). Additionally, the latter exhibit more clear-cut postcranial adaptations for suspensory locomotion than dryopithecins (Moyà-Solà and Köhler, 1996; Almécija et al., 2007; Alba, 2012; Alba et al., 2012b; Pina et al., 2012; Susanna et al., 2014). The distinctiveness of *Pierolapithecus*, *Anoiapithecus*, and *Dryopithecus* at the genus rank has also been questioned by some authors (e.g., Begun, 2002, 2009, 2015). Nonetheless, differences in craniodental morphology support their distinction (Moyà-Solà et al., 2004, 2009a, b; Alba, 2012; Pérez de los Ríos, 2013; Alba et al., 2013; Pugh et al., 2023). Similarly, the distinction between *H. crusafonti* and *H. laietanus* has also been challenged by some (Harrison, 1991; Andrews et al., 1996; Ribot et al., 1996), although there is considerable evidence favoring it as well (Alba, 2012; Alba et al., 2012b; Fortuny et al., 2021).

Dryopithecus is a large-bodied hominid, with an inferred body mass of 44–50 kg (Moyà-Solà et al., 2009a; Alba et al., 2011). In the Vallès-Penedès Basin, *Dryopithecus* is known from several dentognathic remains, including a face recovered from Abocador de Can Mata (ACM; Moyà-Solà et al., 1990; 2009a). The postcranial morphology of *Dryopithecus* is not very well known. It includes a juvenile humeral fragment (found at the type locality of the genus, Saint-Gaudens; Lartet, 1856; Pilbeam and Simons, 1971), and, tentatively, a partial distal humeral shaft and several pollical phalanges from the site of Castell de Barberà (Alba et al., 2011; Almécija et al., 2012), as well as a proximal femur from the ACM series (Moyà-Solà et al., 2009a; Pina et al., 2019). The recovered humeral remains exhibit a hominoid-like morphology, although it could be suggestive of both suspensory and quadrupedal behaviors (Rose, 1994b; Alba et al., 2011). Phalangeal morphology suggests strong pollical grasping, as in other Miocene apes (Almécija et al., 2012). The results derived from the analysis of the cortical bone distribution in the femoral neck are comparable with the pattern observed in extant quadrupedal primates, contrasting with the more homogeneous distribution exhibited by extant great apes (Pina et al., 2019) and other fossil apes interpreted as more suspensory, such as *H. laietanus* (Pina et al., 2012). Overall, the scarce

postcranial evidence of *Dryopithecus* suggests that it was predominantly an above-branch quadruped with powerful-grasping abilities that habitually engaged in cautious climbing behaviors.

Pierolapithecus was described based on a partial skeleton from the ACM sequence (Moyà-Solà et al., 2004). The facial morphology of *Pierolapithecus* bears strong resemblance to that of extant great apes, including reduced midfacial prognathism, setting *Pierolapithecus* apart from Early Miocene hominoids from Africa (Pugh et al., 2023). Postcranially, *Pierolapithecus* exhibits several ape-like traits indicative of an orthograde body plan, including the degree and type of rib curvature, an elongated clavicle, and the morphology of the lumbar vertebrae (Moyà-Solà et al., 2004; Susanna et al., 2010). The pelvic remains are also suggestive of orthograde adaptations, such as moderate iliac flaring (Hammond et al., 2013), while the patellar morphology indicates enhanced knee mobility (Pina et al., 2014, 2020). Additionally, the lack of ulnocarpal contact relates to enhanced ulnar deviation (i.e., displacement of the hand toward the ulnar side of the forearm) and improved stabilization of the wrist during load-bearing activities (Moyà-Solà et al., 2004). Contrarily, the metacarpals and manual phalanges of *Pierolapithecus* exhibit a more primitive morphology, consistent with quadrupedal palmigrady assisted by powerful grasping (Moyà-Solà et al., 2004, 2005; Almécija et al., 2009; Alba et al., 2010c; contra Begun and Ward, 2005; Deane and Begun, 2008, 2010). Altogether, the postcranial morphology of *Pierolapithecus* indicates a locomotor repertoire that combined above-branch quadrupedalism with vertical climbing, lacking specialized adaptations for suspensory locomotion. This supports the hypothesis that an orthograde body plan evolved prior to the emergence of suspensory behaviors in hominid evolution (Moyà-Solà et al., 2004; 2005; Alba, 2012; contra Begun and Ward, 2005).

Anoiapithecus, also recorded from the ACM sequence, is known solely on the basis of a partial face with an associated mandible (Moyà-Solà et al., 2009b). It is distinguished from both *Dryopithecus* and *Pierolapithecus* by its notable orthognathous facial profile, in addition to other cranial and dental features (Moyà-Solà et al., 2009b; Alba et al., 2013, 2024a).

Hispanopithecus laietanus has been recovered from several late Miocene localities of the Vallès-Penedès Basin (Villalta Comella and Crusafont Pairó, 1944; Begun et al., 1990; Golpe Posse, 1993; Moyà-Solà and Köhler, 1993, 1995, 1996; Köhler et al., 2001b; Almécija et al., 2007; Alba et al., 2012a, b, 2018; Tallman et al., 2013; Susanna et al., 2014). The craniodental morphology of *H. laietanus* indicates a more derived condition toward extant great apes than that of the Middle Miocene dryopithecins (Alba, 2012). Postcranial remains are primarily known from a partial skeleton from Can Llobateres 2 (Moyà-Solà et al., 1996) and an additional partial skeleton from Can Feu (Alba et al., 2012). Body mass estimates range from approximately 39–40 kg for the Can

Llobateres 2 male skeleton to around 22–25 kg for the Can Feu female individual (Moyà-Solà and Köhler, 1996; Moyà-Solà et al., 2009b; Alba et al., 2012a; Susanna et al., 2014). Vertebral, scapular and first rib morphology support the possession of an orthograde body plan, characterized by a broad, shallow thorax and a short and relatively stiff lumbar region (Moyà-Solà and Köhler, 1996; Köhler et al., 2001b; Alba et al., 2012; Susanna et al., 2014). Forelimb morphology indicates enhanced elbow mobility, facilitating adduction, pronation and flexion of the forearm, as required for habitual climbing and suspensory behaviors (Moyà-Solà and Köhler, 1996; Alba et al., 2012a). However, other features in the forelimb are instead suggestive of quadrupedal locomotion, resulting in a mixed locomotor signal (Alba et al., 2012a). Phalangeal morphology further reflects this mosaic morphology, including some traits associated with below-branch suspensory behaviors alongside with other features indicative of above-branch palmigrady (Moyà-Solà and Köhler, 1996; Almécija et al., 2007; Alba et al., 2010c). Similarly, the hindlimb displays an admixture of characters associated with both vertical climbing and quadrupedal locomotion (Moyà-Solà and Köhler, 1996; Köhler et al., 2002; Pina et al., 2012; Tallman et al., 2013). Combined with the high intermembral index inferred for the species, the mosaic postcranial morphology suggests that *H. laietanus* possessed unequivocal adaptations for below-branch suspension, while also retaining other features functionally associated with above-branch palmigrade quadrupedalism assisted by powerful-grasping (Moyà-Solà and Köhler, 1996; Almécija et al., 2007; Alba et al., 2012; Pina et al., 2012; Tallman et al., 2013; Susanna et al., 2014).

Hispanopithecus crusafonti is primarily known based on dentognathic remains from Can Poncic (Begun, 1992a), albeit an additional partial mandible from the Teuleria del Firal site (traditionally attributed to *D. fontani*; Vidal, 1913; Woodward, 1914; Simons and Pilbeam, 1965) was included into the hypodigm as well (Casanovas-Vilar et al., 2011; Alba, 2012; Alba et al., 2012b). The attribution of this material to *Hispanopithecus* is based on dental dental similarities with *H. laietanus* (including some that appear synapomorphic), although the absence of cranial remains for *H. crusafonti* makes the generic attribution somewhat provisional (Alba, 2012; Alba et al., 2012b). Compared with *H. laietanus*, the postcranial record of *H. crusafonti* is far more limited. In addition, most of the postcranial elements tentatively assigned to this species—including an isolated hamate and several metatarsals—have yet to be formally described or analyzed (Moyà-Solà et al., 1990; Alba, 2012). An additional partial femoral shaft—probably belonging to a juvenile or a small female—was preliminarily described and found to more closely resemble that of *H. laietanus* than *D. fontani* (Pina, 2016).

1.5. Aims, scope, and structure

1.5.1. Scope and specific aims

This dissertation focuses on the study of the functional morphology of the primate foot. Pedal elements are highly informative for understanding the evolution of primates, as some of its characteristics, such as the grasping hallux or the presence of nails rather than claws, have long been recognized as defining traits of the order (Cartmill, 1974; Szalay et al., 1987). In addition, taphonomic biases within the fossil record favors the preservation of certain skeletal elements, such as tarsal bones, resulting in a more complete representation of these elements in extinct primates compared to other parts of the skeleton. Consequently, considerable research has been devoted to the study of the foot bones of extinct primates, seeking to characterize the functional morphology of the primate foot to shed light on their locomotion and evolutionary history. However, thanks to the advent of novel methodologies to quantify the morphology of skeletal elements and to the availability of more extensive comparative datasets of both morphological and behavioral data, a more in-depth investigation of the primate foot is warranted. In light of these recent developments, this dissertation builds on the use of 3D geometric morphometrics and quantitative locomotor data derived from field studies on extant primates to reconstruct the locomotor repertoire of extinct primates, thereby offering new insights into primate origins and their evolutionary history.

This dissertation comprises two case studies. The first one investigates the origins of euprimates (i.e., primates of modern aspect), with particular emphasis on their locomotor diversity from a macroevolutionary perspective. This first case study employs shape data quantified from three tarsal bones: the astragalus, the calcaneus and the navicular. The second case study focuses on an isolated astragalus specimen, delving into its taxonomic attribution, functional morphology, and broader implications for the evolution of locomotor behavior in crown hominoids. The specific objectives are listed below:

I. To quantify the shape of three tarsal bones—the astragalus, the calcaneus, and the navicular—in extant primate species using various 3D geometric morphometric approaches, and to assess whether observed shape differences among different taxa significantly covary with their distinct locomotor behaviors.
II. To reconstruct the locomotor repertoire of an extensive sample of early primates—including all major groups from the Paleogene (plesiadapiforms, adapiforms,

omomyiforms, and early anthropoids)—using partial least-squares regression (PLSR). Thismethod builds on the same machinery as the traditional two-block partial least-squares (2B-PLS) by identifying the principal axes of covariation between different blocks of variables—tarsal shape and quantified locomotion, in the case of this dissertation—allowing the generation of predictive models. Compared to other approaches, the PLSR overcomes the limitations derived from using discrete locomotor categories, which, although valuable, are overly simplistic and do not allow to characterize the full locomotor spectrum of primates. Conversely, the PLSR accommodates the use of locomotor percentages, providing a more nuanced and continuous representation of primate locomotor behavior.

III. To investigate the evolutionary radiation of the earliest euprimates, with a particular emphasis on their locomotor diversity and morphological changes occurring in the hindfoot and navicular. This aim requires the use of evolutionary modeling and other phylogenetic comparative methods to assess macroevolutionary patterns of morphological and behavioral change. Additionally, it aims to critically evaluate the adequacy of the competing adaptive hypotheses proposed to explain the origin and early diversification of euprimates.

IV. To describe an unpublished isolated dryopithecine astragalus (IPS85037) recovered from the middle Miocene (11.7 Ma) Abocador de Can Mata locality ACM/C8-B* (Vallès-Penedès Basin, NE Iberian Peninsula), and study it from a morphofunctional viewpoint, including the estimation of its locomotor repertoire using the PLSR approach outlined in the second specific objective.

1.5.2. Structure of this work

This PhD dissertation is conceived as a compendium of scientific articles and is organized into various chapters: the Introduction (Chapter 1), the Materials and methods (Chapter 2), the Results (Chapters 3–5), the Discussion (Chapter 6), and the Conclusions (Chapter 7). References of Chapters 1, 2, and 6, are included at the end of the dissertation; Chapters 3–5, which consist of three published papers, contain their own references each one.

Chapter 1 is divided into four main sections. The first provides a general overview of the order Primates, with particular emphasis on their locomotor diversity. The second reviews the functional morphology of the primate foot, focusing on the three bones analyzed in this dissertation. The

third section corresponds to the presentation of the first case study, which focuses on the adaptive origins of euprimates. The final section presents the second case study, centered on the description and morphofunctional analysis of an isolated dryopithecine talus.

Chapter 2 details the composition of both the fossil and extant comparative sample used throughout this dissertation, including the unpublished dryopithecine talus. It also details the methodologies employed for shape quantification and visualization, along with the different analytical and statistical techniques utilized, including a detailed explanation on the development of the PLSR.

The chapters included in the Results section have been published in first quartile journals indexed by the Journal Citation Reports (Chapters 3-5). They are the following:

- Monclús-Gonzalo, O., Alba, D.M., Duhamel, A., Fabre, A.C., Marigó, J., 2023. Early euprimates already had a diverse locomotor repertoire: Evidence from ankle bone morphology. J. Hum. Evol. 181, 103395. https://doi.org/10.1016/j.jhevol.2023.103395
- Monclús-Gonzalo, O., Alba, D.M., Fabre, A.C., Marigó, J. 2025. Reconstruction of the locomotor repertoire of early primates in the light of astragalar and calcaneal shape. J. Hum. Evol. 206, 103370. https://doi.org/10.1016/j.jhevol.2025.103730
- Monclús-Gonzalo, O., Pal, S., Püschel, T.A., Urciuoli, A., Vinuesa, V., Robles, J.M., Almécija, S., Alba, D.M., 2025. A dryopithecine talus from Abocador de Can Mata (Vallès-Penedès Basin, NE Iberian Peninsula): Morphometric affinities and evolutionary implications for hominoid locomotion. Am. J. Biol. Anthropol. 186, e70043. https://doi.org/10.1002/ajpa.70043

Chapters 3 and 4 fulfill the specific aims (I), (II), and (III), by examining the covariation between tarsal shape and locomotion, reconstructing the locomotor repertoire of comprehensive sample of early primates, and investigating the origin and early diversification of euprimates in relation to their tarsal morphology and locomotor diversity. Chapter 5, in turn, fulfills the specific aims (I) and (IV), by assessing the covariation between astragalar shape and locomotion (employing a distinct comparative sample from that of Chapters 3 and 4), and describing and conducting a morphofunctional analysis of IPS85037.

In the Discussion provided in Chapter 6, the results are discussed around four main topics, which correspond to the aforementioned specific aims: quantification and assessment of the covariation between tarsal shape and locomotor behavior in extant primates; reconstruction of the locomotor repertoire of early primates; evaluation of the origin and early radiation of euprimates based on tarsal evidence; and description, morphofunctional analysis and taxonomic

attribution of an unpublished isolated dryopithecine astragalus from ACM. Finally, the general Conclusions of this dissertation are presented in Chapter 7, followed by the References cited in Chapters 1, 6, and 7.

Chapter 2:

Materials and Methods

Chapter 2. Materials and Methods

2.1. Sample composition

2.1.1. Studied fossil sample for case study 1 and 2

Three-dimensional (3D) models derived from μCT scans of 120 tarsal bones—including 38 astragali, 46 calcanei, and 36 naviculars—representing 36 genera across all major Paleogene primate groups were used in Chapters 3 and 4 (Tables 2.1–2.4). All but one of the 3D models were downloaded from the online repository MorphoSource (https://www.morphosource.org; Boyer et al., 2017b). A right astragalus of *Djebelemur martinezi* (CBI-1-545), was downloaded from MorphoMuseuM (www.morphomuseum.com; Lebrun and Orliac, 2016; Marivaux et al., 2018).

Table 2.1. Plesiadapiform, adapiform, omomyiform and early anthropoid specimens included in the fossil sample for case study 1 (Chapters 3 and 4).

Species	Family	Catalog No.	Pedal element
Ignacius graybullianus	Paromomyidae	USNM pal442235	Astragalus
Nannodectes gidleyi	Plesiadapidae	AMNH FM 17379	Astragalus
Plesiadapis cookei	Plesiadapidae	UMMP VP 87990	Astragalus
Plesiadapis rex	Plesiadapidae	UMMP VP 94816	Astragalus
Purgatorius sp.	Purgatoriidae	UCMP V 197509	Astragalus
Carpolestes simpsoni	Carpolestidae	UMMP VP 101963	Calcaneus
Tinimomys graybulliensis	Micromomyidae	USNM pal461201	Calcaneus
Phenacolemur sp.	Paromomyidae	USNM pal442240	Calcaneus
Plesiadapis cookei	Plesiadapidae	UMMP VP 87990	Calcaneus
Purgatorius sp.	Purgatoriidae	UCMP V 197517	Calcaneus
Carpolestes simpsoni	Carpolestidae	UMMP 101963	Navicular
Dryomomys szalayi	Micromomyidae	UMMP VP 41870	Navicular
Tinimomys graybulliensis	Micromomyidae	USNM pal530203	Navicular
Adapis parisiensis	Adapidae	UM ECA 1379	Astragalus
Adapis parisiensis	Adapidae	UM ECA 1377	Astragalus
Adapis parisiensis	Adapidae	PC-VI ESC 936	Astragalus
Adapis parisiensis	Adapidae	PC-VI ROS 4057	Astragalus
Adapis parisiensis	Adapidae	UM ROS-2 108	Astragalus
Leptadapis magnus	Adapidae	MNHN Qu1101	Astragalus
Marcgodinotius indicus	Notharctidae	GU 748	Astragalus
Anchomomys frontanyensis	Notharctidae	IPS 7713	Astragalus

Cantius trigonodus	Notharctidae	USGS 21832	Astragalus
Notharctus pugnax	Notharctidae	AMNH FM 12000	Astragalus
Notharctus pugnax	Notharctidae	AMNH FM 12570	Astragalus
Notharctus tenebrosus	Notharctidae	AMNH FM 11474	Astragalus
Notharctus sp.	Notharctidae	AMNH FM 129382	Astragalus
Smilodectes sp.	Notharctidae	AMNH FM 131763	Astragalus
Djebelemur martinezi	Djebelemuridae	CBI-1-545	Astragalus
Adapis parisiensis	Adapidae	NMB QE 644	Calcaneus
Adapis parisiensis	Adapidae	NMB QE 741	Calcaneus
Adapis parisiensis	Adapidae	NMB QF 558	Calcaneus
Adapis parisiensis	Adapidae	NMB QH 640	Calcaneus
Adapis sp.	Adapidae	NMB QE 530	Calcaneus
Leptadapis magnus	Adapidae	NMB QE 604	Calcaneus
Leptadapis magnus	Adapidae	NMB QE 920	Calcaneus
Leptadapis magnus	Adapidae	NMB QF 421	Calcaneus
Caenopithecus lemuroides	Adapidae	NMB EH 719	Calcaneus
Marcgodinotius indicus	Notharctidae	GU 709	Calcaneus
Marcgodinotius indicus	Notharctidae	GU 1644	Calcaneus
Marcgodinotius indicus	Notharctidae	GU 710	Calcaneus
Anchomomys frontanyensis	Notharctidae	IPS 7748	Calcaneus
Cantius abditus	Notharctidae	USGS 6783	Calcaneus
Cantius trigonodus	Notharctidae	USGS 21829	Calcaneus
Cantius trigonodus	Notharctidae	AMNH FM 16852	Calcaneus
Copelemur tutus	Notharctidae	UCMP V 135001	Calcaneus
Notharctus sp.	Notharctidae	AMNH FM 131956	Calcaneus
Notharctus sp.	Notharctidae	AMNH FM 55061	Calcaneus
Notharctus sp.	Notharctidae	AMNH FM 129382	Calcaneus
Notharctus tenebrosus	Notharctidae	AMNH FM 131945	Calcaneus
Notharctus tenebrosus	Notharctidae	AMNH FM 11474	Calcaneus
Smilodectes gracilis	Notharctidae	AMNH FM 131774	Calcaneus
Smilodectes sp.	Notharctidae	AMNH FM 131763	Calcaneus
Anchomomys frontanyensis	Notharctidae	IPS 46392	Navicular
Anchomomys frontanyensis	Notharctidae	IPS 46393	Navicular
Anchomomys frontanyensis	Notharctidae	IPS 46394	Navicular
Anchomomys frontanyensis	Notharctidae	IPS 46395	Navicular
Anchomomys frontanyensis	Notharctidae	IPS 46396	Navicular
Anchomomys frontanyensis	Notharctidae	IPS 7700	Navicular
Anchomomys frontanyensis	Notharctidae	IPS 7705	Navicular
Anchomomys frontanyensis	Notharctidae	IPS 7709	Navicular
Cantius ralstoni	Notharctidae	UW 21450	Navicular
Copelemur tutus	Notharctidae	UCMP V 134990	Navicular
Notharctus robustior	Notharctidae	CM 11910	Navicular
Notharctus robustior	Notharctidae	UCM 69992	Navicular
Notharctus tenebrosus	Notharctidae	AMNH FM 11474	Navicular
Notharctus tenebrosus	Notharctidae	DPC 25453	Navicular
Notharctus tenebrosus	Notharctidae	AMNH FM 129382	Navicular

Smilodectes gracilis	Notharctidae	USNM V 25686	Navicular
Smilodectes gracilis	Notharctidae	AMNH FM 131762	Navicular
Smilodectes gracilis	Notharctidae	AMNH FM 131774	Navicular
Smilodectes mcgrewi	Notharctidae	UM 95526	Navicular
Arapahovius gazini	Omomyidae	IRSNB M 1235	Astragalus
Teilhardina belgica	Omomyidae	GU 800	Astragalus
Vastanomys major	Omomyidae	UM BFI 811	Astragalus
Necrolemur sp.	Omomyidae	AMNH FM 12613	Astragalus
Hemiacodon gracilis	Omomyidae	AMNH FM 29185	Astragalus
Hemiacodon gracilis	Omomyidae	UMMP VP 98648	Astragalus
Omomys carteri	Omomyidae	UMMP VP 38321	Astragalus
Omomys carteri	Omomyidae	CM 69756	Astragalus
Shoshonius cooperi	Omomyidae	CM 67297	Astragalus
Shoshonius cooperi	Omomyidae	UMMP VP 99074	Astragalus
Washakius insignis	Omomyidae	USNM 598483	Astragalus
Absarokius sp.	Omomyidae	UCM 67907	Calcaneus
Arapahovius gazini	Omomyidae	UCM 67850	Calcaneus
Teilhardina belgica	Omomyidae	IRSNB M 1247	Calcaneus
Omomys carteri	Omomyidae	UCM 68745	Calcaneus
Omomys carteri	Omomyidae	UCM 69065	Calcaneus
Omomys carteri	Omomyidae	UCM 67678	Calcaneus
Omomys sp.	Omomyidae	AMNH FM 29164	Calcaneus
Ourayia uintensis	Omomyidae	SDNH 4020-60933	Calcaneus
Shoshonius cooperi	Omomyidae	CM 69765	Calcaneus
Washakius insignis	Omomyidae	AMNH FM 88824	Calcaneus
Arapahovius gazini	Omomyidae	UCMP V 142021	Navicular
Arapahovius gazini	Omomyidae	UCMP V 118500	Navicular
Chipetaia lamporea	Omomyidae	CM 070904	Navicular
Omomyidae incertae sedis	Omomyidae	UCMP V 134984	Navicular
Omomys carteri	Omomyidae	UMMP V 32279	Navicular
Omomys carteri	Omomyidae	UMMP V 32319	Navicular
Omomys carteri	Omomyidae	UMMP V 32319	Navicular
Omomys carteri	Omomyidae	UMMP V 98604	Navicular
Omomys carteri	Omomyidae	UMMP V 99000	Navicular
Omomys carteri	Omomyidae	UMMP V 32259	Navicular
Ourayia uintensis	Omomyidae	CM 070917	Navicular
Teilhardina brandti	Omomyidae	USNM 542002	Navicular
Tetonius homunculus	Omomyidae	UCMP V 142018	Navicular
Apidium sp.	Parapithecidae	DPC 3054	Astragalus
Apidium sp.	Parapithecidae	DPC 5027	Astragalus
Apidium sp.	Parapithecidae	DPC 5416	Astragalus
Simonsius grangeri	Parapithecidae	DPC 1001	Astragalus
Eosimias sinensis	Eosimiidae	IVPP V 12303	Astragalus
Eosimias sinensis	Eosimiidae	IVPP V 11849	Astragalus
Ganlea sp.	Amphipithecidae	NMMP 39	Astragalus
Eosimias incertae sedis	Eosimiidae	IVPP V 11848	Calcaneus

Eosimias sp.	Eosimiidae	IVPP V 12313	Calcaneus
Eosimias sp.	Eosimiidae	IVPP V 11851	Calcaneus
Parapithecidae incertae sedis	Parapithecidae	DPC 8810	Calcaneus
Parapithecidae incertae sedis	Parapithecidae	DPC 2381	Calcaneus
Parapithecidae incertae sedis	Parapithecidae	DPC 1003	Calcaneus
Proteopithecus sylviae	Proteopithecidae	DPC 24776	Calcaneus

Abbreviations: USNM = National Museum of Natural History; AMNH = American Museum of Natural History; UMMP = University of Michigan Museum of Paleontology; UCMP = University of California Museum of Paleontology; ISEM = Institute des Sciences de l'Évolution de Montpellier; ESC = Private Collection of Mr Dominique Vidalenc; MNHN = Muséum National d'Histoire Naturelle ; GU = HNB Garhwal University; IPS = Institut Català de Paleontologia Miquel Crusafont; USGC = United States Geological Survey; CBI = Museum of the Office National des Mines; NMB = Naturhistorisches Museum Basel; UW = University of Wyoming; CM = Carnegie Museum of Natural History; UCM = University of Colorado Museum of Natural History; DPC = Duke Lemur Center Museum of Natural History; IRSNB = Royal Belgian Institute of Natural Sciences; SDNH = San Diego Natural History Museum; IVVP = Institute of Vertebrate Paleontology and Paleoanthropology; NMMP = National Museum of Myanmar Primates.

The fossil specimen analyzed in case study 2 (Chapter 5) is an unpublished astragalus (IPS85037), recovered from the Middle Miocene (11.7 Ma) ACM locality ACM/C8-B* (Vallès-Penedès Basin, NE Iberian Peninsula). IPS85037 was scanned using a NextEngineTM3D scanner HD (NextEngine Inc., Santa Monica, USA) using high definition (HD) settings following the protocol detailed by Hammond et al. (2016).

For comparative purposes, an astragalus of the Early Miocene stem hominoid *Ekembo heseloni* (KMN-RU2036) was also included in the sample (Walker and Pickford 1983) and scanned using the same procedure as for IPS85037.

2.1.2. Extant comparative sample for case study 1 and 2

The 3D models derived from the µCT scans of 936 tarsal bones (440 astragali, 412 calcanei, and 84 naviculars) for the extant comparative sample for case study 1 (Chapters 3 and 4). It comprises 43 primate genera, representing all major extant primate groups except catarrhines, and six non-primate euarchontan genera. All 3D models used in Chapters 3 and 4 were downloaded from the online repository MorphoSource.

Table 2.2. Summary of the extant comparative sample utilized in the fossil sample for case study 1 (Chapters 3 and 4). Sample size is given for each species.

Family	Species	Astragali	Calcanei	Naviculars
Ptilocerciidae	*Ptilocercus lowii*	3	4	0
Tupaiidae	*Dendrogale murina*	0	1	0
Tupaiidae	*Tupaia belangeri*	2	6	0
Tupaiidae	*Tupaia minor*	1	1	0
Tupaiidae	*Tupaia palawanensis*	1	0	0
Tupaiidae	*Tupaia tana*	0	1	0
Tupaiidae	*Urogale everetti*	2	1	0
Cynocephalidae	*Cynocephalus volans*	5	2	0
Cynocephalidae	*Galeopterus variegatus*	1	1	0
Cheirogaleidae	*Cheirogaleus major*	3	4	2
Cheirogaleidae	*Cheirogaleus medius*	2	7	1
Cheirogaleidae	*Microcebus griseorufus*	12	0	0
Cheirogaleidae	*Microcebus murinus*	4	10	1
Cheirogaleidae	*Microcebus rufus*	3	10	2
Cheirogaleidae	*Mirza coquereli*	0	0	1
Cheirogaleidae	*Mirza zaza*	3	12	1
Daubentoniidae	*Daubentonia madagascariensis*	6	7	5
Galagidae	*Galago moholi*	12	9	1
Galagidae	*Galago senegalensis*	8	7	0
Galagidae	*Galagoides demidovii*	5	3	0
Galagidae	*Otolemur crassicaudatus*	11	4	0
Galagidae	*Otolemur garnettii*	3	4	0
Galagidae	*Paragalago zanzibaricus*	2	2	0
Galagidae	*Sciurocheirus alleni*	1	2	1
Indriidae	*Avahi laniger*	6	6	5
Indriidae	*Indri indri*	3	2	1
Indriidae	*Propithecus coquereli*	2	2	0
Indriidae	*Propithecus diadema*	2	2	1
Indriidae	*Propithecus verreauxi*	6	3	1
Lemuridae	*Eulemur fulvus*	22	20	4
Lemuridae	*Eulemur macaco*	0	2	1
Lemuridae	*Eulemur mongoz*	5	6	3
Lemuridae	*Hapalemur griseus*	19	21	4
Lemuridae	*Lemur catta*	8	7	2
Lemuridae	*Varecia variegata*	3	4	1
Lepilemuridae	*Lepilemur leucopus*	3	5	0
Lepilemuridae	*Lepilemur mustelinus*	5	0	2
Lorisidae	*Arctocebus calabarensis*	4	2	1
Lorisidae	*Loris* sp.	7	8	1
Lorisidae	*Nycticebus bengalensis*	0	0	2
Lorisidae	*Nycticebus coucang*	7	7	2
Lorisidae	*Nycticebus javanicus*	1	1	0
Lorisidae	*Nycticebus menangensis*	2	4	1

Lorisidae	*Nycticebus pygmaeus*	4	5	0
Lorisidae	*Perodicticus sp.*	16	10	3
Tarsiidae	*Carlito syrichta*	4	2	0
Tarsiidae	*Cephalopachus bancanus*	2	2	0
Tarsiidae	*Tarsius spectrum*	3	4	1
Atelidae	*Alouatta caraya*	7	2	0
Atelidae	*Alouatta palliata*	9	8	3
Atelidae	*Alouatta seniculus*	5	0	0
Atelidae	*Ateles belzebuth*	5	4	1
Atelidae	*Ateles fusciceps*	15	12	4
Atelidae	*Ateles geoffroyi*	7	10	0
Atelidae	*Ateles marginatus*	0	0	1
Atelidae	*Ateles paniscus*	3	4	0
Atelidae	*Lagothrix* sp.	15	14	1
Callitrichidae	*Callimico goeldii*	12	11	0
Callitrichidae	*Callithrix geoffroyi*	2	2	0
Callitrichidae	*Callithrix jacchus*	7	7	0
Callitrichidae	*Callithrix penicillata*	2	0	0
Callitrichidae	*Cebuella pygmaea*	9	10	1
Callitrichidae	*Leontocebus fuscicollis*	10	10	1
Callitrichidae	*Leontopithecus rosalia*	9	9	1
Callitrichidae	*Mico* sp.	4	4	0
Callitrichidae	*Saguinus midas*	7	4	1
Callitrichidae	*Saguinus mystax*	3	3	0
Callitrichidae	*Saguinus oedipus*	10	9	5
Cebidae	*Cebus capucinus*	2	2	1
Cebidae	*Cebus olivaceus*	3	2	2
Cebidae	*Saimiri boliviensis*	3	3	0
Cebidae	*Saimiri oerstedii*	2	2	1
Cebidae	*Saimiri sciureus*	7	6	1
Cebidae	*Sapajus apella*	6	3	0
Pitheciidae	*Cacajao calvus*	12	10	2
Pitheciidae	*Callicebus personatus*	1	2	0
Pitheciidae	*Cheracebus torquatus*	2	2	0
Pitheciidae	*Chiropotes* sp.	10	9	2
Pitheciidae	*Pithecia monachus*	2	5	0
Pitheciidae	*Pithecia pithecia*	8	7	3
Pitheciidae	*Plecturocebus* sp.	17	13	2

The 3D models included in the extant comparative sample for case study 2 (Chapter 5) were kindly provided by Sergio Almécija (ICP). This sample comprises 64 astragali from 14 anthropoid genera, including all hominids, all hylobatids except for *Hoolock*, and several cercopithecoids and platyrrhines, providing good phylogenetic coverage (Table 2.3). All specimens were scanned via

the Geomagic Capture scanner (3D Systems, Rock Hill, USA) and subsequently cleaned using Geomagic Wrap (v. 2019; 3D Systems).

Table 2.3. Summary of the extant comparative sample utilized for case study 2 (Chapter 5). Sample size is given for each species.

Family	Species	Astragali
Atelidae	*Alouatta palliata*	2
Atelidae	*Alouatta seniculus*	2
Atelidae	*Ateles fusciceps*	4
Cebidae	*Cebus apella*	4
Cercopithecidae	*Colobus guereza*	4
Cercopithecidae	*Nasalis larvatus*	2
Cercopithecidae	*Macaca arctoides*	1
Cercopithecidae	*Macaca fascicularis*	1
Cercopithecidae	*Macaca mulatta*	2
Cercopithecidae	*Papio anubis*	2
Cercopithecidae	*Papio hamadryas*	1
Hylobatidae	*Hylobates agilis*	1
Hylobatidae	*Hylobates klossii*	1
Hylobatidae	*Nomascus concolor*	1
Hylobatidae	*Symphalangus syndactylus*	3
Hominidae	*Pongo abelii*	2
Hominidae	*Pongo pygmaeus*	6
Hominidae	*Gorilla beringei*	7
Hominidae	*Gorilla gorilla*	6
Hominidae	*Pan paniscus*	4
Hominidae	*Pan troglodytes*	8

2.2. Shape analysis

2.2.1. Geometric morphometrics

The analysis of shape plays a crucial role in interpreting distinct biological processes responsible for morphological variation between species, including evolution and development (Gould, 1970; Klingenberg, 2010; Dryden and Mardia, 2016). In turn, morphometrics is the quantitative description, analysis and interpretation of shape (Rohlf, 1990). Linear morphometrics are characterized by the application of different statistical methods to a set of quantitative variables, which provide an initial approximation to both size (when scalar variables such as

distances, areas or volumes are used) and shape (when dimensionless variables like angles and ratios are used; Raup, 1966; Gould, 1970; Mosimann, 1970, 1975; Oxnard, 1978; Alberch et al., 1979; Reyment, 1985; Marcus, 1990; Bookstein, 1996). Although linear morphometrics allows easy comparisons with previous studies and normally utilizes variables that are very intuitive and easy to interpret biologically, it also faces several limitations that constrain its effectiveness in capturing the morphological information of the structures under study, particularly their geometric information (Bookstein, 1991; Zelditch et al., 2012). First, distance measurements in linear morphometrics tend to overemphasize the size component of variance at the expense of the shape component, thereby obscuring meaningful shape differences among individuals, which are often entangled with size (Bookstein et al., 1985; Bookstein, 1989). Size scaling is an important factor for understanding variation in many biological traits, including shape. When there is no correlation between shape and size (such that shape is preserved at different sizes), their relationship is termed 'isometric' and implies that metrical variables scale in a linear fashion relative to size. However, this is the exception rather than the rule; most frequently, metrical variables are correlated in a non-linear fashion, so that shape varies as a function of size. In these cases, the relationship between shape and size is qualified as 'allometric' (Gould, 1966; Jungers et al., 1995). Allometry (size-related shape changes or, more broadly, size-scaling effects) has been extensively studied in evolutionary biology, developmental biology, and paleobiology, as it reflects developmental and phylogenetic constraints that not only restrain but also channel shape variation along pre-existing routes, thereby resulting in recurrent evolutionary patterns of morphological change (Gould, 1966; Alberch et al., 1979; Klingenberg, 1998). To account for the size-scaling effects, several size-adjustment approaches have been developed in the context of linear morphometrics, from simple bivariate ratios to Mosimann shape variables (dividing multiple variables by their geometric mean), to allometric residuals computed after linearizing the allometric relationship between two variables by applying logarithms (Rohlf, 1967; Mosimann, 1970, 1975; Rohlf and Bookstein, 1987; Albrecht et al., 1993; Jungers et al., 1995). However, Mosimann shape variables only remove the isometric (linear) size variation whereas allometric residuals further remove the non-linear scaling component (which does not preserve shape but may be interesting depending on the aims of the study, such as for example testing biomechanical hypotheses). The main problems of linear morphometrics are caused by the fact that they rely on a limited set of isolated linear measurements. Given that shape is inherently multidimensional, this is insufficient to adequately capture the details of biological structures. Furthermore, these measurements are not geometrically related (i.e., position within a coordinate system), so that linear morphometrics performs poorly in capturing spatial relationships, hindering a global interpretation of the overall shape configuration (Klingenberg and Monteiro, 2005).

Consequently, an equivalent set of measures could be yield by two distinct shapes (or, on the contrary, two distinct sets of measures could be interpreted as the same shape) due to the absence of information regarding the spatial relationships between points (Adams et al., 2004). As a result, linear morphometrics are also unsuitable to provide a graphical representation of shape variation, because the geometry of the structure is not recorded (Strauss and Bookstein, 1982; Rohlf and Marcus, 1993; Adams et al., 2004).

In contrast to linear morphometrics, in two- and three-dimensional geometric morphometrics (2DGM and 3DGM, respectively) shape is defined as all the geometric information that remains when location, scale and rotational effects are filtered out from an object (Kendall, 1977, 1984). Traditional geometric morphometrics employ Cartesian coordinates derived from homologous anatomical landmarks to quantify the shape of the studied structures, albeit more recent alternative methods, such as semilandmarks and diffeomorphic deformation (see below), do not require the use of homologous coordinates (Bookstein, 1991; Gunz et al., 2005; Durrlemann et al., 2012). Shape quantification in geometric morphometrics is achieved through what is called the 'Procrustes paradigm[1]' which encompasses the unified statistical theory for shape (Kendall, 1977), along with the required analytical procedures to superimpose landmark configurations and obtain shape variables (Bookstein, 1986; Rohlf and Slice, 1990; Goodall, 1991; Rohlf, 1999). Ideally, landmarks should be anatomically homologous points that maintain consistent topological positions relative to one another, provide comprehensive coverage of the structure's morphology, and be reliably and repeatedly identifiable across individuals (Bookstein, 1991; Zelditch et al., 2012). However, some of these criteria can sometimes conflict. For instance, a particular region may lack sufficient anatomically homologous points, resulting in either the acceptance of sparse coverage or the relaxation of the homology criterium to provide a comprehensive sampling of morphology so that the features of biological significance can be discovered. In this regard, Bookstein (1991) defined three types of landmarks based on their degree of homology and the type of biological or geometrical information they convey. Type I landmarks correspond to points that can be reliably identified across specimens and are anatomically homologous, such as discrete tissue juxtapositions. Type II landmarks account for local geometrical relationships, such as points of minimum or maximum curvature or the tips of a structure, reflecting shape relationships. Type III landmarks, in contrast, are defined solely by mathematical or geometrical

[1] In Greek mythology, Procrustes was a rogue smith and bandit from Attica, son of Poseidon, who assaulted travelers by forcing them to fit a special bed of his own making—either by stretching their limbs or cutting them down. Ironically, Procrustes met his end in the same manner, compelled by the hero Theseus to make his own body fit his bed as well.

criteria—such as centroids or midpoints—being the least reliable in terms of anatomical homology (Bookstein, 1991). Therefore, type I landmarks are preferred because of their high biological homology and reproducibility, while type III landmarks are often used with caution and are sometimes referred to as semilandmarks rather than true anatomical landmarks (Bookstein, 1991; Adams et al., 2004). This dissertation uses 3DGM based on anatomical landmarks to quantify tarsal shape in Chapters 3 and 5 (Fig. 2.1), while Chapter 4 adopts an alternative approach employing high-density sliding semilandmarks (see below for more detailed explanations).

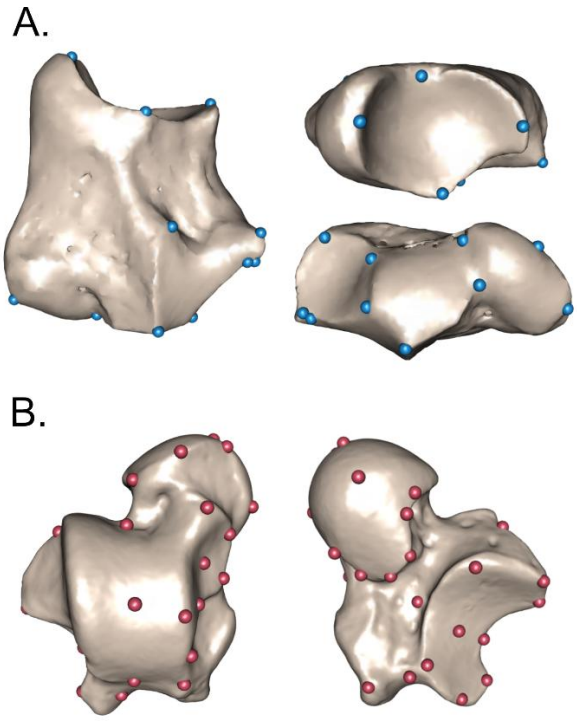


Figure 2.1. Anatomical landmark-based configurations employed in this dissertation. (A) Navicular (Chapter 3); (B) Astragalus (Chapter 5). The navicular corresponds to the specimen of *Eulemur fulvus* USNM 542489, while the astragalus corresponds to the specimen of *Pan paniscus* RMCA 27698. Plantar, proximal, and distal views are shown from left to right and from top to bottom for the navicular, and dorsal and plantar views are shown from left to right for the astragalus.

Landmark configurations are aligned using Procrustes superimposition, a procedure that standardizes them by position, scale and orientation, transforming geometric distances into Procrustes distances (Fig. 2.2A; Bookstein, 1996; Goodall, 1991). Each configuration is translated so that its centroid—the average of its landmark coordinates—coincides with the origin of the configuration. Next, configurations are scaled to the same centroid size, rendering them size-invariant (though this does not eliminate the allometric component of shape variation). Centroid size (CS), defined as the square root of the summed squared distances of the coordinates of a

given configuration to its centroid, is a scalar variable habitually employed as the size variable in geometric morphometrics studies (Bookstein, 1989, 1991). In the specific case of superimposing two landmark configurations, one of them is used as a reference to rotate the other so the sum squared of Euclidean distances between the homologous landmarks of both configurations is minimal. For more than two configurations, several methods exist, the most widely used being the generalized Procrustes analysis (GPA), in which the rotation step is treated in an iterative fashion (Gower, 1975; Rohlf and Slice, 1990; Goodall, 1991). All translated and scaled configurations are rotated around their centroid to one arbitrary configuration of the sample using a least-squares approach. Subsequently, the new coordinates are averaged and rotated again to fit the new consensus configuration iteratively until convergence among all configurations is achieved. Several variants of the original Procrustes superimposition method exist, differing in how size is computed for scaling and how the configurations are fitted to one another during the rotation step (Zelditch et al., 2012). Some approaches rely on what is known as 'partial Procrustes superimposition', in which configurations are scaled to unit centroid size and posteriorly projected onto a tangent space from the original non-Euclidean Kendall shape space (Rohlf, 1990, 1999). An alternative approach, known as 'full Procrustes superimposition', scales the configurations to cos (ρ) instead, where ρ are the Procrustes distances, allowing for a total minimization of the sum of squared distances (Goodall, 1991; Rohlf, 1999; Dryden and Mardia, 2016). It is important to acknowledge the reduction in degrees of freedom after performing a Procrustes superimposition (Bookstein, 1991; Goodall, 1991; Rohlf, 1999). After removing the effects of scale, translation and orientation, the resulting configurations have fewer degrees of freedom. For 2D data, four dimensions are lost, while for 3D data, seven dimensions are lost (Mitteroecker and Gunz, 2009). As a result of the loss of dimensionality, after the Procrustes superimposition landmark configurations are distributed in a curved, non-Euclidean Riemannian manifold (a particular type of manifold that generalizes Euclidean geometry to curved spaces) known as the Kendall shape space (Fig. 2.2B; Kendall, 1977, 1984). The Kendall shape space is curved and non-Euclidean, while most conventional statistical tools assume linear, Euclidean spaces, precluding the use of conventional statistical techniques (Marcus, 1990; Zelditch et al., 2012). To address this, configurations are often projected onto a Euclidean tangent space at the mean shape on the Kendall shape space (Kendall, 1984; Rohlf, 1999). Although projecting the shapes onto the Euclidean tangent space can cause some degree of distortion, most biological shape variation is constrained around the tangent point, making such potential distortion mathematically trivial unless comparing very dissimilar configurations located far from the tangent point (Fig. 2.2C; Rohlf, 1999; Slice, 2001; Klingenberg, 2020). Subsequently, standard multivariate techniques can be then applied to the resulting shape variables—commonly referred

to as 'Procrustes shape coordinates', a denomination that will be employed in the course of this dissertation. However, caution must be taken when analyzing these data, as sample sizes are habitually unbalanced and shape variation hardly ever meets the normality assumptions. Consequently, non-parametric tests are generally recommended (Zelditch et al., 2012).

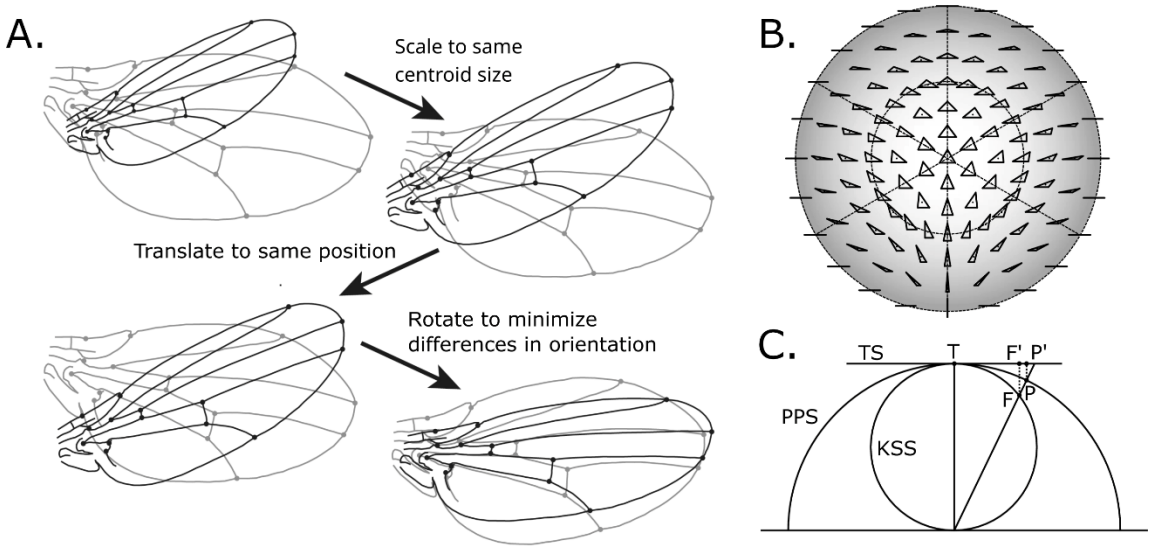


Figure 2.2. (A) Procrustes superimposition of two landmark configurations; (B) Representation of Kendall's shape space for 2D configuration of three landmarks; (C) schematic cross-section of Kendall's shape space for the previous configuration, the hemisphere of landmark configurations aligned by a partial Procrustes superimposition, and the tangent space. The points F and P correspond to the same shape aligned by full Procrustes superimposition and partial Procrustes superimposition, respectively. All three panels are modified after Klingenberg (2020). Abbreviations: TS = tangent space; T = mean shape of the sample; PPS = hemisphere of landmark configurations aligned by a partial Procrustes superimposition; KSS = Kendall's shape space; F' = tangent projection of F; P' = tangent projection of P'.

The major strength of geometric morphometrics is the visualization of shape differences (Zelditch et al., 2012; Mitteroecker et al., 2013). After several unsuccessful attempts, Bookstein (1989, 1991) introduced the thin-plate spline (TPS) interpolation to compute deformation grids in the style of D'Arcy Thompson's (1915, 1917) shear mapping (which was, in turn, inspired in the work of the famous Renaissance painter Albrecht Dürer). The TPS algorithm models the differences between two shapes by computing a mapping function between two-point configurations while the space in between is smoothly interpolated (Mitteroecker and Gunz, 2009). To do so, bending energy of the deformation (defined as a scalar quantity based on the second derivatives of the deformation function) is minimized, which is also critical to the sliding

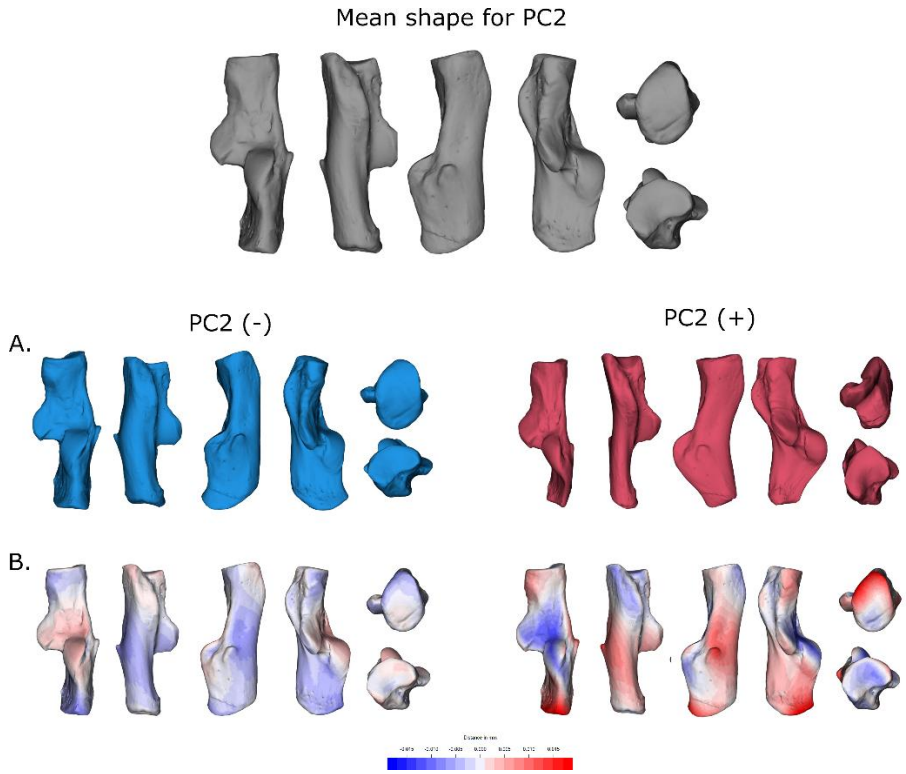


Figure 2.3. Two examples for the visualization of shape differences between landmark configurations of the calcaneus (Chapter 4, Figs. 8 and 9). (A) Deformation-based approach; (B) Heat map approach. For the heat map approach, blue and red indicate regions of contraction and expansion based on the position of the extreme calcaneal shapes (minimum or maximum values) relative to the mean shape.

of semilandmarks (see below). In 2D landmark datasets, TPS grids are very useful to visualize shape differences (Bookstein, 1991, 1997). In 3D configurations, however, shape differences are better illustrated by deforming the mean landmark configuration along a shape vector (Fig. 2.3A; which can be derived from different types of multivariate analyses, such as PCA) or by using wireframes connecting the homologous landmarks (Mitteroecker and Gunz, 2009). These deformation-based approaches, nevertheless, require dense and evenly distributed landmark coverage of the shape of the structure studied—which is habitually accomplished via the use of semilandmarks (see below). Color or heat maps are an alternative option to deformation, which is based on translating the differences between homologous landmark positions into colors, including orthogonal distances to the surface between homologous locations, currents, or magnitudes of deformation or bending (Fig. 2.3B). Although visually intuitive, color maps reduce complex multidimensional data to scalar values, resulting in a considerable loss of information. Therefore, they are best used in conjunction with deformation grids or reconstructed shapes to provide a more complete depiction of shape variation (Mitteroecker and Schaefer, 2022). Unlike the former, other visualization tools, such as landmark displacement vectors or superimposed

surfaces, are generally less effective to show shape changes, as some parts of the structures may not be visible. For this reason, their use is less recommended.

One important limitation of geometric morphometrics is the loss of information about some critical aspects that constitute shape, such as curvature, which remains after removing position, scale and rotational effects, but it is not always adequately captured by landmark coordinates alone (Zelditch et al., 2012). Additionally, the shape of many structures cannot be properly quantified by means of traditional geometric morphometrics employing solely anatomical landmarks, due to the absence of enough homologous points to be located consistently across the sample (Gunz and Mitteroecker, 2013). Several methods have been developed to address the limitations of traditional geometric morphometrics based on the use of anatomical landmarks, including outline analysis (such as elliptical Fourier analysis; Foote, 1989; Bookstein, 1997; Haines and Crampton, 2000), surface and volume-based analyses (like spherical harmonics analysis; Shen et al., 2009), diffeomorphic deformation/diffeomorphic surface matching (Durrleman et al., 2012; Beaudet, 2025), pseudolandmarks (Boyer et al., 2015b), and semilandmarks (Bookstein, 1997; Gunz et al., 2005; Gunz and Mitteroecker, 2013). Each of these approaches has advantages and limitations depending on the type of structure studied, the available computational resources, or the type of downstream analysis intended (Mitteroecker and Schaefer, 2022; Goswami and Clavel, 2025). In this dissertation, in addition to traditional anatomical landmark-based geometric morphometrics (Chapter 3 and 5), a high-density sliding semilandmark approach is also employed (Chapter 4). This method incorporates curve and surface semilandmarks placed in a semiautomatic manner (Fig. 2.4; Bardua et al., 2019). Sliding semilandmarks were first proposed by Bookstein (1991, 1997) for 2D structures to minimize variation resulting from arbitrary placement. Later, Gunz et al. (2005) extended this approach to 3D surfaces (reviewed in Pérez et al., 2006; Gunz and Mitteroecker, 2013; Botton-Divet et al., 2015; Bardua et al., 2019). To slide semilandmarks, two alternative approaches can be employed: minimize either bending energy or Procrustes distance. Bending energy, derived from the TPS algorithm, quantifies the magnitude of local shape deformation (Gunz et al., 2005). Sliding semilandmarks is an iterative process that includes three main steps (Mitteroecker and Gunz, 2009): (1) computation of both a sample mean shape and the tangent vectors to slide each semilandmark in each specimen; (2) sliding of the semilandmarks along the tangent vectors to minimize either bending energy or Procrustes distances to the mean; (3) projecting slid semilandmarks back onto the nearest point of the curve if they slipped of the curvature. Both metrics, Procrustes distances and bending energy, have their trade-offs. Procrustes distances are computationally cheaper than bending energy and therefore

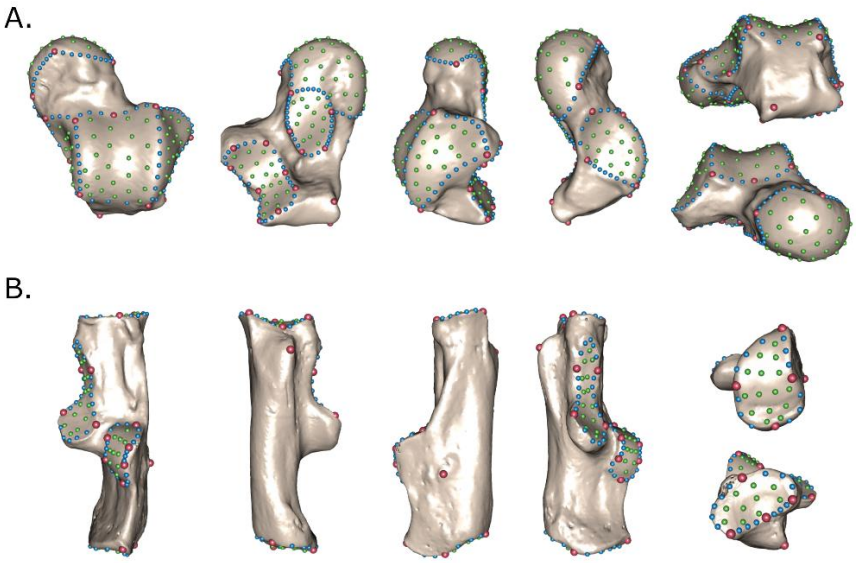


Figure 2.4. High-density sliding semilandmark configurations employed in this dissertation (in Chapter 4). (A) Astragalus; (B) Calcaneus. Red points represent anatomical landmarks, blue points represent curve semilandmarks, and light green points represent surface semilandmarks. Both specimens used as a reference correspond to *Lemur catta*: (A) DLC 6848; (B) AMNH 170739. Dorsal, plantar, lateral, medial, proximal, and distal views are shown from left to right and from top to bottom for both bones.

can be applied to a large amount of landmarks; however, for structures with larger shape discrepancies this approach can lead to important distortions. In contrast, bending energy is computationally more demanding, but ensures smooth displacement in all cases (Mitteroecker and Schaefer 2022). One of the problems of using high-density sliding semilandmark approaches, in addition to the higher computational demands and time consumption, is that it can create issues regarding data dimensionality. Increasing the number of landmarks inflates measurement error, which can artificially increase Procrustes distances—especially when shape differences are small. Since it is improbable that measurement error will be identical across specimens, even subtle inconsistencies can create spurious variation (Fruciano, 2016; Bardua et al., 2019; Rolfe et al., 2021). This will be negligible when large shape differences exist. However, it can become relevant if the number of landmarks is large and the magnitude of shape difference is not. This problem has been especially discussed during the last years in the context of some dimension-reduction techniques like between-group PCA (bgPCA) and CVA, in which group separation tends to increase with the number of measured variables, potentially leading to spurious grouping (Mitteroecker and Bookstein, 2011; Bookstein, 2019; Cardini et al., 2019; Rohlf, 2021; Courtenay, 2023). Additionally, high dimensionality also complicates the implementation of many types of multivariate analyses, including phylogenetic comparative methods (PCMs), which suffer from low statistical performance when the number of variables approaches the number of individuals.

When the number of variables equals or exceeds the number of individuals, these analyses are precluded (Adams, 2014a; Adams and Collyer, 2018). For this reason, new statistical frameworks are emerging to address the limitations of working with high-dimensional datasets (Clavel et al., 2015, 2019; Adams and Collyer, 2019; Clavel and Morlon, 2020).

2.2.2. Phylogenetic Comparative Methods

Phylogenetic comparative methods (PCMs) encompass a set of analytical tools designed to analyze traits across species while accounting for their shared evolutionary history and the diversification of lineages (Paradis, 2014). Although early comparative studies during the 19th and early 20th centuries already considered the shared evolutionary history of species as a central aspect of their investigation, the formal development of PCMs began during the 1980s, alongside the emergence of geometric morphometrics (reviewed in Pagel and Harvey, 1988), after the publication of a series of seminal papers introducing the first methods to account for the evolutionary history of species and incorporate it into the statistical analyses (e.g., Felsenstein, 1985; Grafen, 1989). The main tenet of such approaches is that, as a result of their shared evolutionary history, species cannot be treated as statistically independent data points. Due to the assumption of independence by most traditional statistical methods, overlooking the shared ancestry of closely related species could lead to misleading results, including inflated Type I error rates—as traits from closely related species will tend to be autocorrelated and will resemble because of shared ancestry, not as a result of other types of relationships. Therefore, the main critique of comparative studies at the time was their failure to account for the non-independence of species due to their shared evolutionary history (Felsenstein, 1985). Currently, PCMs are broadly categorized into two main categories (Pennell and Harmon, 2013). The first one focuses on the macroevolutionary dynamics of diversification in different clades and the changes in speciation and extinction rates through times across groups. The second one investigates the tempo and mode of evolution of traits across phylogenies (Cornwell and Nagakawa, 2017). This dissertation solely employs the latter category of PCMs.

To address the issue of the non-independence of observations in comparative data, it is assumed that pairs of observations are related through a covariance parameter. These parameters quantify the expected similarity between trait values of two distinct species and are organized into a symmetric variance-covariance matrix (VCV), where the diagonal elements represent the variances of individual species and the off-diagonal elements correspond to the

covariances between species (Symonds and Blomberg, 2014). In comparative analyses dealing with multiple species, the covariance parameters among trait values can be estimated a priori by assuming that the traits have evolved under a specific evolutionary model. There are two main evolutionary models to characterize trait evolution (Paradis, 2014): Brownian motion (BM) and Orstein-Uhlenbeck (OU). Additionally, several extended models derived from the modification of the former two have been developed to characterize more complex scenarios. These often involve additional parameters and may have limitations depending on the type and structure of the data (e.g., Butler and King, 2004; Venditti et al., 2011; Freckleton, 2012; O'Meara, 2012; Ho and Ané, 2014; Mazel et al., 2016; Smaers et al., 2016; Cornwell and Nakagawa, 2017).

The BM evolutionary model (Fig. 2.5) is named after Robert Brown, who first described the movement of the pollen grains suspended in water (Brown, 1828). Although BM was later characterized as a stochastic process (Wiener, 1923), foundational contributions had already been made by Bachelier (1900) and Einstein (1905). However, it was not until the 1970s that BM was introduced as a model of quantitative character evolution (Felsenstein, 1973) as well as a model into phylogenetic comparative regression analyses (Felsenstein, 1985). Under a BM model, trait evolution is simulated following a random walk—represented mathematically as σdB(t)—where σ is the scale of change and dB(t) is the scatter generator as a function of time. This implies that trait variance increases uniformly with time, and that phenotypic divergence between species grows proportional to the sum of branch lengths separating them (Wiener, 1923; Cavalli-Sforza and Edwards, 1967; Felsenstein, 1973). Therefore, BM models can be described completely by only two parameters: the starting value of the population mean trait (μ) and the evolutionary rate parameter (σ^2), which determines how fast traits can change through time (Blomberg et al., 2020). However, there is no biological reason to assume that the variance of a trait should increase linearly with time, as it would indicate that shape changes through time are not constrained—either internally (by physical boundaries) or externally (by selective pressures)—an assumption that is unlikely to be true for any real trait (McGhee, 2015). Brownian motion models can be interpreted as either implying no selection (i.e., random drift) or as indicative of strong directional selective pressures (e.g., Hansen and Martins, 1996). Although both scenarios can be modeled using a BM model, they may be distinguishable based on their evolutionary rates—random drifts would exhibit lower rates than selective drifts (Harmon et al., 2003). While the traditional BM model assumes a single, constant evolutionary rate across the phylogeny, this assumption has been recently expanded through the use of reversible-jump Markov chain Monte Carlo (rjMCMC) procedures, which enable the estimation of multi-rate BM models, where rates vary across branches (expanded in the next section; O'Meara et al., 2006; Eastman et al., 2011; Venditti et al.,

2011; Revell et al., 2012). Another relevant extension of the BM model is the Early Burst (EB) model, which describes scenarios of adaptive radiation, where the rates of evolutionary change are initially high but decay exponentially over time (Foote, 1997; Blomberg et al., 2003; Harmon et al., 2010).

The OU model describes trait evolution under stabilizing selection by incorporating the effect of friction (Fig. 2.5; e.g., Uhlenbeck and Ornstein, 1930; Felsenstein, 1988; Hansen and Martins, 1996; Hansen, 1997; Martins and Hansen, 1997). In addition to the random walk component, σdB(t), two additional parameters are included in an OU model: the attraction to the selective optimum (ϑ), and the strength of this attraction (α), which can be interpreted as the strength of the selection (Butler and King, 2004). Additionally, the OU model has been expanded to describe multi-regime scenarios, much more realistic than modeling evolution toward a single optimum—which is often an oversimplification in empirical contexts. These extended OU models allow parameters to vary across the phylogeny, offering a more realistic representation of evolutionary processes (e.g., Hansen, 1997; Butler and King, 2004; Beaulieu et al., 2012).

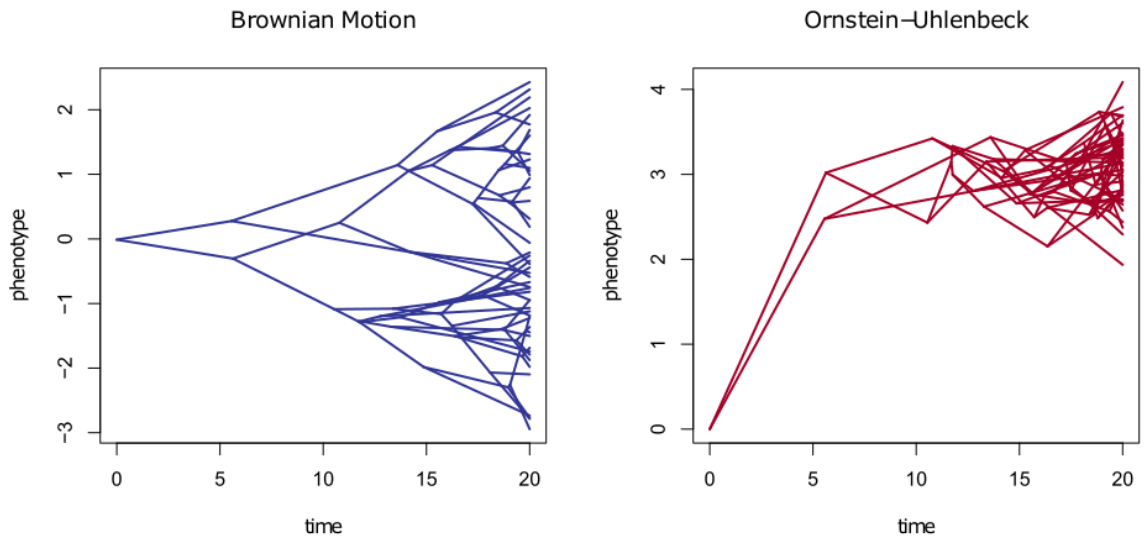
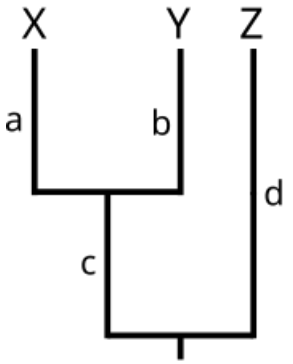


Figure 2.5. Phenograms based on a quantitative trait simulation on a simulated phylogeny (50 tips) under a BM model (left; $\sigma^2 = 0.2$) and an OU model (right; $\sigma^2 = 0.2$; $\vartheta = 3$; $\alpha = 0.5$).

The most commonly used methods for studying trait evolution are phylogenetic independent contrasts (PIC; Felsenstein, 1985) and phylogenetic generalized least-squares (PGLS; Grafen, 1989; and later expanded by Martins and Hansen, 1997; Pagel, 1997, 1999; Rohlf, 2001), which is also referred to as phylogenetic regression or phylogenetic general linear models. The rationale behind PIC is that differences between closely related species (also called contrasts) can reflect

independent evolutionary pathways. Therefore, regressing the independent contrasts of one trait against those of another allows to calculate a regression coefficient that accounts for phylogenetic relatedness among species (Felsenstein, 1985).

When described for the first time, PGLS was defined as a generalization of PIC, as both approaches stem from the recognition of the statistical non-independence of species as data points (Grafen, 1989). The simplest way to interpret the PGLS is as a weighted regression. In a standard regression (e.g., an ordinary least-squares; OLS), all classical linear model assumptions, constant variance of errors (homoscedasticity), and independence of errors are held. Contrarily, PGLS models heteroscedasticity and non-independence by incorporating phylogenetic relationships into the structure of the error VCV matrix. This VCV matrix includes: a series of diagonal elements, representing the total length of the branches from the root to the tips (which would be the same in ultrametric trees), and the off-diagonal covariance elements, representing the shared evolutionary history between two tips of the tree (Fig. 2.6). Based on this VCV matrix, PGLS minimizes the weighted sum of squared residuals obtained from the regression, weighting data points based on the covariance structure of the model (Grafen, 1989; Rohlf, 2001). Compared to PIC, PGLS is more flexible (Symonds and Blomberg, 2014). Under a BM model, PGLS is identical to PIC. However, unlike the latter, PGLS can accomodate alternative models like OU or EB (Hansen, 1997; Butler and King, 2004; Harmon et al., 2010). In addition, it also allows the transformation of the VCV matrix (e.g., by employing Pagel's branch length transformations; Pagel, 1999; Freckleton et al., 2002), adjusting the amount of phylogenetic covariance exhibited by the data (see below). Thus, PGLS allows the utilization of different covariance matrices to represent alternative evolutionary models. In turn, these models can be compared to evaluate their fit to the data and determine which model best explains the evolutionary history of the trait, using criteria such as the Akaike Information Criterion (AIC; e.g., Butler and King, 2004). Phylogenetic generalized least-squares models are also well suited to deal with multivariate data, which is the habitual case in geometric morphometrics studies (Adams, 2014a; Clavel et al., 2015, 2019; Adams and Collyer, 2018, 2019). However, high-dimensional phenotypes are challenging to analyze, particularly when the number of variables approaches or exceeds the number of observations. This can inflate Type I errors and complicate the estimation of the determinant of the VCV matrix. To circumvent these issues, several methods have been developed recently, based on different approaches like penalized-likelihood (PL) and distance approaches (for a more detailed explanation see next section; Clavel et al., 2015, 2019; Adams and Collyer, 2018, 2019).



	X	Y	Z
X	var(X)	covar(XY)	covar(XZ)
Y	covar(XY)	var(Y)	covar(YZ)
Z	covar(XZ)	covar(YZ	var(Z)

	X	Y	Z
X	a+c	c	0
Y	c	b+c	0
Z	0	0	d

Figure 2.6. Example of a phylogenetic VCV matrix. Uppercase letters indicate the tips of the phylogenetic tree (species) while lowercase letters indicate the phylogenetic distance (as a function of time). Modified from Kamilar and Cooper (2013).

Determining the degree of phylogenetic autocorrelation of the trait data is critical, because when the phylogeny or assumed evolutionary model is inaccurate, and there is little or no phylogenetic covariance in the residuals (as expected by the OLS model), the assumption that the amount of evolutionary change along a branch is proportional to the branch length (as assumed under the BM model) can be misleading (Symonds and Blomberg, 2014). This issue can be addressed by calculating metrics of phylogenetic signal, which inform about the extent to which closely related species tend to resemble each other (Blomberg et al., 2003). Several analytical approaches have been developed to estimate phylogenetic signal, including Pagel's λ (Pagel, 1997) and Blomberg's K (Blomberg et al., 2003), which are also extended to accommodate multivariate data (Pagel, 1999; Adams, 2014b). These two approaches are distinguished by how they characterize the dependency between trait covariation among species. Blomberg's K expresses the strength of phylogenetic signal as a ratio between the observed mean squared error of trait values and the expected mean squared error under a BM model (Blomberg et al., 2003). Therefore, if K<1, traits are less similar among related species than expected under a BM, whereas if K>1, traits are more similar among related species than expected under a BM; K=1 indicates that trait evolution is consistent with a BM model. In contrast, Pagel's λ can be understood as a scaling parameter that adjusts the off-diagonal elements of the phylogenetic VCV to down-weight the effect of the phylogeny on the error structure of the model (Pagel, 1997). To estimate λ, maximum likelihood estimation (MLE) is used to maximize the fit of the model to the observed data (Freckleton et al., 2002). One of the key advantages of PGLS is that it enables to adjust the amount of phylogenetic signal in the data by means of modifying the properties of the

VCV matrix—unlike PIC, which assumes that the phylogeny accurately describes the error structure of the data (Symonds and Blomberg, 2014). With Pagel's λ, the off-diagonal elements of VCV matrix can be rescaled according to the estimated strength of phylogenetic signal (Fig. 2.7). If λ = 0, the branches of the phylogenetic tree are rescaled into a star phylogeny, indicating no phylogenetic signal. In contrast, if λ = 1, trait data is consistent with a BM model (Pagel, 1999). Low phylogenetic signal (habitually when K < 1 and λ < 1) is interpreted as indicative of evolutionary lability or, conversely, as stable selection pressures over time. Adaptive radiations, characterized by high rates of trait evolution leading to large differences among close relative species, are also expected to be characterized by relatively low phylogenetic signal. Pervasive homoplasy can also result in a pattern in which close relatives are less similar than distant ones, resulting in low phylogenetic signals as well. In contrast, high phylogenetic signal (when K or λ are equal to 1 or, in the case of K, surpasses it) is expected under neutral evolution, as this process approximate the BM model of evolution. Alternatively, high phylogenetic signal can also be interpreted as phylogenetic conservatism resulting from stabilizing selection, pleiotropy, limited genetic variation, or architectural constraints limiting the evolutionary lability of the trait.

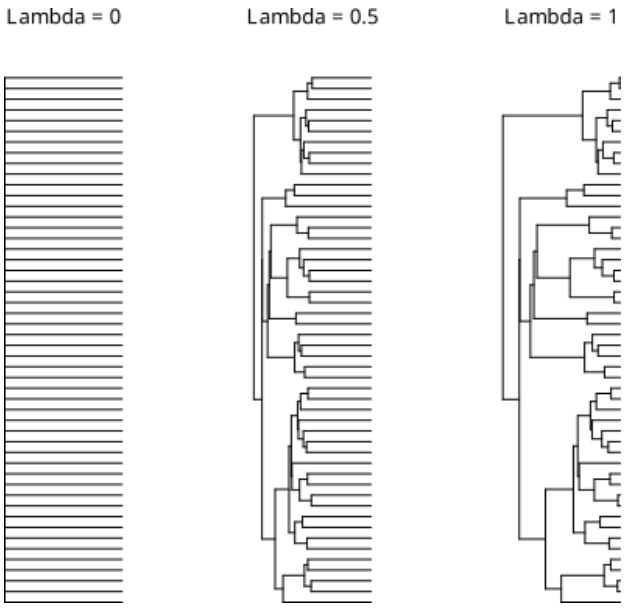


Figure 2.7. Example of a simulated tree (50 tips) rescaled with three different lambda values.

2.2.3. Statistical shape analyses

Ordination methods In geometric morphometrics, shape variables (Procrustes shape coordinates) are inherently correlated (as a result of overlapping anatomical structures and the

shared influence of genetic, developmental, and functional factors), exhibit reduced degrees of freedom, and are highly multidimensional (Mitteroecker and Gunz, 2009; Zelditch et al., 2012). To address these aforementioned issues, Procrustes shape coordinates are habitually transformed into new variables though dimensionality reduction techniques. The most common approach is to carry out a principal component analysis (PCA), in which the Procrustes shape coordinates are projected onto a latent space defined by a set of new linear combinations of the original variables, the principal components (PCs; (Polly et al., 2013). A PCA thus aims to calculate a new set of variables, the PCs, whose variances account for all the variances and covariances of the original variables and follow two conditions: (1) PCs are orthogonal, which means that their pairwise covariances are equal to zero; and (2) each successive PC accounts for the highest possible amount of variance not accounted for by the previous ones (Dryden and Mardia, 2016). Each PC is defined by an eigenvalue (indicating the proportion of variance accounted for) and an eigenvector (representing the direction of maximum variance), such that PCs can be understood as eigenvectors scaled by their corresponding eigenvalues (Polly et al., 2013). The resulting PC scores serve as the new shape variables, having the proper number of degrees of freedom and being uncorrelated with one another (Hotelling, 1933; Jollife, 1986). Alternatively, it is also possible to carry out a relative warps analysis (RWA; Bookstein, 1991, Rohlf, 1993; Bookstein et al., 2003). Partial warps describe the shape changes arising from local deformations (the “nonaffine” part; Bookstein, 1991) while the uniform shape components are the “affine” part of the transformation, describing the global deformation—scaling, rotation, shear, and translation (Bookstein, 1996; Rohlf and Bookstein, 2003). If the partial warps and the uniform component scores are equally weighted, employing a RWA becomes equivalent to performing a PCA on the projected Procrustes shape coordinates onto the tangent space (Rohlf, 1993). Several extensions of PCA have been proposed to address specific analytical needs. These include analyses of the form space (i.e., size-shape space, resulting from the inclusion of size, either by skipping the scaling step of the GPA or by including the natural log-transformed [ln] CS as an additional variable before computing the PCA; Mitteroecker et al., 2004; Dryden and Mardia, 2016), between-group PCA (bgPCA; Mitteroecker and Bookstein, 2011), and several approaches that employ the phylogenetic structure of the sample, such as the phylogenetic PCA (pPCA; Revell, 2009; Polly et al., 2013), and the phylogenetically-aligned component analysis (PACA; Collyer and Adams, 2021). Additionally, phylomorphospaces (Bookstein et al., 1985; Klingenberg and Ekau, 1996; Sidlauskas, 2008) can be employed to project the phylogeny of a group or a clade onto the morphospace. Among the former methods, this dissertation employs the bgPCA (Chapter 5), the pPCA (Chapters 3 and 4), and the phylomorphospace (Chapter 3), which will be briefly discussed below.

Compared to standard PCA, bgPCA is designed to maximize the variance between a priori defined groups. To do so, a standard PCA is carried out on the covariance matrix of the groups means, and the original individual observations are projected a posteriori onto the latent space (Mitteroecker and Bookstein, 2011). Compared to a standard PCA, which is primarily an exploratory technique to assess the overall pattern in the distribution of the sample, bgPCA emphasizes the distinctiveness of a series of groups defined a priori and, thus, can be used for classification. In bgPCA, the morphological affinities between fossil specimens and groups defined a priori can also be assessed using typicality probabilities. Compared to posterior probabilities, which account for the probability of membership in a restricted sense, typicality probabilities assess if a particular individual fits within the multivariate normal distribution of each a priori defined group, without being constrained to belong to any of them (Albrecht, 1992). Like posterior probabilities, typicality probabilities also rely on the Mahalanobis squared distances (D^2) between the a posteriori projected individuals and the centroids of each a priori defined group. However, in typicality probabilities, D^2 are compared independently to a chi-square distribution for each a priori defined group separately and interpreted as a p-value. In this case, the null hypothesis is that the specimen fits with the distribution of the group. Thus, a small p-value (e.g., < 0.05) means the specimen is an outlier for that group. Because every test is performed independently for each group (unlike in posterior probabilities), typicality probabilities must be considered a non-comparative measure (e.g., p-values does not sum up to 1) for outlier detection rather than group membership.

Recently, concerns have been raised about the application of bgPCA in geometric morphometrics, particularly when the number of variables is larger than the number of groups, which might result in spurious grouping (Bookstein, 2019; Cardini, 2019). To ensure that the grouping is not spurious, several precautions must be taken (Chapter 5). First, the sample should be designed to ensure that all groups defined a priori contain a sufficiently large number of individuals (Rohlf, 2021). Second, an additional cross-validated bgPCA (CV-bgPCA) should be conducted on the same set of shape variables used in the standard bgPCA (Cardini and Polly, 2020). CV-bgPCA uses a leave-one-out cross-validation approach (LOOCV), which iteratively resamples the data by excluding one individual at a time while using the remaining individuals to calculate the latent space that is used afterwards to classify the excluded individual. Additionally, non-parametric permutational-based tests of the variance, such as the permutational analysis of variance (PERMANOVA; Anderson, 2001) or randomized residual permutation procedures (RRPP; Collyer and Adams, 2018), can be employed to assess the amount of variance (R^2) explained by group differences and calculate their statistical significance (p-value). By comparing the R^2 values

and statistical significance levels of each bgPCA approach (standard and cross-validated) and the raw shape data, it is possible to verify if the bgPCA is introducing spurious grouping or not. For instance, if the differences among the a priori defined groups are significant in the bgPCA—but not in the CV-bgPCA or the raw shape data—or if R^2 is substantially higher in the bgPCA compared to the CV-bgPCA or the raw shape data, this would indicate potential spurious grouping (Cardini and Polly, 2020).

The phylogenetic PCA (pPCA) allows to control for phylogenetic covariance while computing a PCA-like ordination of the data (Revell, 2009). Unlike a standard PCA, the major axes of a pPCA are not the major axes of shape variation, but the major axes of the non-phylogenetic residual variation resulting from the removal of the phylogenetic covariation within the sample (Revell, 2009; Polly et al., 2013). To compute a pPCA, the first step is the estimation of the ancestral states for each internal node in the phylogeny, in an equivalent manner than it is done with the phylomorphospace. These include the squared-change parsimony (Maddison, 1991) and MLE (Schluter et al., 1997), the latter allowing for the assumption of different evolutionary models to estimate the ancestral node values (Revell, 2009). The ancestral root value is used to center the pPCA. Although using other values rather than the arithmetic mean may potentially distort the results, due to the non-Euclidean nature of shape space (Rohlf, 1998), shape variation in biological datasets is usually small enough to make such risk negligible (Rohlf, 2002). The next step is the computation of the evolutionary VCV matrix—which is equivalent to the trait VCV matrix except for that taxa are downweighted by their shared phylogenetic story. As in standard PCA, eigenvalues and eigenvectors are calculated from this matrix. However, contrary to the standard PCA, their sum does not equal to the sum of variances of the original traits due to the phylogenetic correction (Polly et al., 2013). Lastly, species are projected onto the latent space defined by the eigenvectors (Revell, 2009). Notwithstanding, although the eigenvectors themselves are orthogonal, the resulting pPCA scores are not uncorrelated. This occurs due to the influence of the phylogenetic VCV matrix, which reintroduces correlations among the scores, resulting in a mixture of non-phylogenetic components and residual phylogenetic signal (Revell, 2009; Polly et al., 2013). Despite this, pPCA scores are valuable as shape variables and can be used in subsequent analyses to test evolutionary hypotheses on trait convergence and adaptive radiation, for instance (see below).

Phylomorphospaces are a very useful approach for visualizing the morphological diversification of a clade or group of organisms by projecting their phylogeny into a multivariate morphospace (Bookstein et al., 1985; Klingenberg and Ekau, 1996; Sidlauskas, 2008). Phylomorphospaces can be employed for different visualization purposes, including investigating

morphological convergence (e.g., Stayton 2005), the ecomorphological adaptations of different clades (e.g., Klingenberg and Ekau 1996), and characterize adaptive radiations (e.g., Fabre et al., 2020, 2021). To build a phylomorphospace it is necessary to estimate the ancestral states for all internal nodes in the tree, including the root. These reconstructed ancestral morphotypes are then projected onto a multivariate morphospace, which is usually defined by a PCA or another similar ordination method. The tree is visualized by connecting all nodes with the tips that correspond to the topology of the phylogeny (Schluter et al., 1997; Revell, 2014). Several methods can be used to estimate the ancestral states of the internal nodes of the tree (Rohlf, 2002). Parsimony-based approaches estimate the ancestral states by minimizing the amount of evolutionary changes required on the tree. While some methods (such as linear parsimony) are not invariant to rotation, squared-change parsimony satisfies this constraint and estimates ancestral states by minimizing the sum of squared branch lengths over the tree (Maddison,1991; Rohlf, 2002). Alternatively, MLE methods can be employed for continuous trait data under the assumption that these traits evolve accordingly to a given model of evolution. These include BM, OU, EB, as well as their extensions or tree transformations (e.g., Harmon et al., 2008; Revell, 2012; Clavel et al., 2015). Furthermore, by computing the ancestral shape states, it is possible to provide valuable insights into the morphology of the ancestors of extant clades (Rohlf, 2002). When the projection of the phylogenetic tree is done in a space defined by phenotype and time (which can be two or three-dimensional), it is named traitgram (Evans et al., 2009; Revell, 2014).

Linear regression and analysis of variance Due to the multivariate nature of geometric morphometrics, shape variables nearly never meet the assumptions of parametric tests (i.e, data must be symmetrical and normally distributed). Therefore, statistical significance is typically assessed using permutation tests (e.g., Mitteroecker and Gunz, 2009; Adams and Collyer, 2015; Collyer and Adams, 2018). To analyze shape variation and its covariation with other variables, two main statistical approaches are commonly employed: linear regression and analysis of variance (ANOVA). The latter includes its multivariate extensions—multivariate analysis of variance (MANOVA) and multivariate analysis of covariance (MANCOVA)—as well as permutational analysis of variance (PERMANOVA; Anderson, 2001). Linear regressions are habitually used to test whether shape is related to a continuous variable (e.g., body mass or CS), while ANOVA and its extensions are used to evaluate the amount of variation within each group to the amount of variation between the group means (e.g., shape differences between two or more categories).

The nonlinear relationship between shape and size, known as allometry, is one of the most extensively studied phenomena in the context of evolutionary biology, developmental biology and

paleontology (Gould, 1966; Alberch et al., 1979; Klingenberg, 1998). In the context of geometric morphometrics, allometry is habitually referred to the relationship between shape variables (which are high-dimensional, as they are habitually based on the Procrustes shape coordinates) and size (commonly measured as the CS, a scalar variable). Due to the multivariate nature of geometric morphometrics, reporting graphical summaries that adequately describe the multivariate relationship between shape and size has proven challenging. To do so, one possibility is to compute the form space by carrying out a PCA based on the shape data matrix (Procrustes shape coordinates) and size (the ln CS values) or by performing the Procrustes alignment without the scaling step (Mitteroecker et al., 2004; Dryden and Mardia, 2016). The major direction of variation in the form space often reveals the allometric relationship followed by the sample. An alternative approach involves employing a dimensionality reduction technique, such as PCA or bgPCA, on the Procrustes shape coordinates alone, and subsequently plot the PC or bgPC scores against centroid size to visualize the allometric relationship. The corresponding loadings of the PCs can be used to visualize the shape differences occurring along the allometric regression via TPS deformation, allowing a better interpretation of such morphological changes. This approach has been employed in Chapter 4 (using PCs) and Chapter 5 (using bgPCs). One limitation is that allometric shape variation can be distributed across less important PCs and thus go undetected (Mitteroecker et al., 2004). However, if the first PCs are already explanatory of a large amount of variation (e.g., > 90%), the remaining shape variation would likely be residual. The other group of techniques refer to multivariate regressions of shape on size (e.g., Mitteroecker et al., 2004; Drake and Klingenberg, 2008; Adams, 2014b; Klingenberg, 2016). In this case, the regression model is a multivariate regression in which Procrustes shape coordinates serve as the dependent variables, with ln CS as the independent variable. To visualize the allometric relationship, the residuals derived from projecting the shape data onto the vector of the regression coefficients are plotted against ln CS. This provides a clear one-dimensional view of the shape and size relationship. Another visualization option is to represent the predicted values from the allometric regression (Adams and Nistri, 2010). As with the previous technique, multivariate regressions of shape on size also allow to calculate the shape changes along the allometric regression via TPS.

When analyzing the relationship between shape and size across species, it may be important to account for the phylogenetic non-independence of the species (Felsenstein, 1985; Paradis, 2014; Cornwell and Nakagawa, 2017). In the dimensionality reduction approach (Chapter 4), standard (univariate) PGLS regression between the first few PCs and ln CS can be computed to assess the relationship between shape and size while recognizing the statistical non-independence of species as data points (Grafen, 1989; Rohlf, 2001). Additionally, the phylogenetic

signal can be adjusted and optimized by finding the maximum-likelihood transformation of the phylogenetic tree (e.g., employing Pagel's λ), allowing the model to best fit the data (Pagel, 1999; Freckleton et al., 2002). Due to the high dimensionality of morphometric data, multivariate regressions of shape on size are more difficult to compute under a PCM framework (Adams and Collyer, 2018, 2019). To circumvent this limitation, there is the option to use distance matrices rather than covariance matrices (which become unstable in the context of high-dimensional datasets where the number of variables approaches or exceeds the number of observations). A phylogenetic transformation matrix is then obtained under a BM model and used to transform the original variables and compute every factor of the model (Adams, 2014b). Statistical estimates are obtained via permutation and compared to the observed values to assess significance (Adams and Collyer 2018). While this approach is useful under a BM model, distance matrices do not allow for parametric computation and lack a likelihood framework, precluding model selection. Moreover, reducing high-dimensional shape data to a single distance matrix can result in reduced statistical power (Clavel et al., 2019). Alternatively, Clavel et al.'s (2015, 2019) PL approach offers a distinct statistical framework more suitable for evolutionary hypothesis testing, supporting likelihood-based inference, parameter estimation, and model comparison across a range of evolutionary models (e.g., BM, OU, EB, etc). The main limitations of the PL approach are their high sensitivity to the estimation of the regularization parameters and that can be computationally intensive, particularly when dealing with large datasets. In Chapter 3, this approach was employed to compute a phylogenetic multivariate regression between navicular shape and ln CS.

In geometric morphometrics, CS can also be used as a predictor of body mass (Parr et al., 2014). To estimate body mass, the ln body mass (dependent variable) of each specimen can be regressed onto the ln CS (independent variable) via OLS (Chapter 5). Afterwards, body mass estimates are derived from the resulting best-fit line. However, because the regression is based on logarithmically transformed data, the predicted BM values must be corrected for logarithmic transformation bias (Smith, 1993). This can be addressed by computing the quasi-maximum likelihood estimator (QMLE), which is defined as QMLE = exp(SEE 2 /2), where SEE is the standard error of estimate of the regression (Egi et al., 2004).

Partial least-squares regression Also known as two-block PLS (2B-PLS), PLS is employed to examine the patterns of covariation between two or more sets of variables (Wold, 1966; Rohlf and Corti, 2000). This method finds pairs of linear combinations (latent variables) computed from the original variables that maximize the covariation of the original sets of variables. This is done via singular value decomposition of the covariance matrix between the blocks, yielding paired

singular vectors (one for each set of variables) that successively capture the strongest covariation patterns between blocks and a diagonal matrix of singular values that can be understood as the weights expressing the strength of covariation between each vector pair (Rohlf and Corti, 2000; Bookstein et al., 2003). Each PLS axis is only correlated to the corresponding axis in the other sets of variables but uncorrelated with the remaining axes in that set. The axes of every set are orthogonal to one another, and their squared coefficients sum up to one—thus, PLS can be understood as a rigid rotation of two or more sets of variables, being analogous to PCA in this regard (Rohlf and Corti, 2000). However, while PCA aims to find linear combinations that successively maximize the amount of variation within the sample, in PLS the new latent variables are aimed to find the maximum covariance between the sets of variables. The importance of each pair of axes can be assessed by computing the percentage of the sum squared covariances (singular values) between the blocks, which are again analogous to the percentage of variance accounted for by each PC in a PCA (Mitteroecker and Gunz, 2009). To assess if there is significant covariation between each pair of linear combinations, a sampling distribution of singular values is obtained by resampling the original blocks of data. If the singular value is higher (habitually >95%) than those obtained from permutated blocks, the covariance between the pair of latent variables is considered significant (Rohlf and Corti, 2000). In morphometrics, PLS may be used to address different research questions. When all blocks of variables are comprised by shape coordinates, PLS can be used to test the degree of morphological integration (e.g., Bookstein et al., 2003; Bastir and Rosas, 2006). This includes both within-configuration integration (e.g., covariation between blocks of the same landmark configuration) and between-configuration integration (e.g., covariation between different anatomical structures). Additionally, other types of variables—including functional, behavioral (such as locomotor behavior) or environmental—can be employed to assess their covariation with a block of shape variables (e.g., Almécija et al., 2015; Fabre et al., 2017, 2018, 2019; Püschel et al., 2017). An important feature that PLS shares with PCA is that the computed latent variables correspond to meaningful deformation patterns that can be visualized via TPS deformation (Rohlf and Corti, 2000).

While the standard implementation of PLS in morphometric literature is an exploratory analysis ideal for testing hypotheses about morphological integration or covariation between shape and other variables (Rohlf and Corti, 2000; Zelditch et al., 2012), there is a type of PLS technique, known as partial least-squares regression (PLSR; Wold et al. 2001), that enables the generation of predictive models (i.e., the prediction of continuous outcomes from shape data). Originally developed for use in fields like econometrics, social sciences, and later chemometrics (e.g., Wold, 1966; Wold et al., 2001; Abdi, 2010), PLSR has been applied in the context of geometric

morphometrics studies to predict one block of shape variables from another one (e.g., Schlager, 2017; Archer et al., 2018; Bastir et al., 2019; Torres-Tamayo et al., 2020). PLSR combines aspects of both PCA—by projecting the original variables onto a latent space—and multiple linear regression—by finding the multidimensional direction in the latent space that explains the maximum variance direction of the predicted block of variables. Compared to other methods, PLSR is particularly well suited for morphometric predictive modeling, where predictors (e.g., Procrustes shape coordinates) are often highly collinear. Traditional methods like OLS suffer in such contexts, as multicollinearity inflates the variance of regression coefficients and may lead to matrix inversion problems. In contrast, PLSR projects the original variables onto a latent space defined by orthogonal latent variables, which are uncorrelated by definition, circumventing these issues (Wold et al., 2001; Abdi, 2010). PLSR is sometimes compared to principal component regression (PCR). However, the two approaches differ in a critical way: PCR reduces dimensionality based only on the variance of the first block of data (predictor), thus solving the problem of multicollinearity but ignoring the second block of data (response). This can result in retaining components (the first PCs, which explain the most variance) that explain little about the second block of data, while, potentially, discarding lower-variance PCs that are more informative of the second block of data (Jolliffe, 1982). In contrast, PLSR incorporates the covariance between the first (predictor) and the second (response) blocks of data when computing the latent variables, typically requiring fewer components and offering greater predictive power. Under the PLSR framework, new values corresponding to the first block of data (predictor) are projected onto the latent space defined by the original training data and then multiplied by a matrix of coefficients derived from the linear regression between the scores of the original data projected onto the latent space. Then, the resulting values can be projected back into the original space to obtain the resulting values for the second block (response). To evaluate PLSR predictive performance, cross-validation methods (such as LOOCV) are habitually employed (Abdi, 2010). These approaches enable to handle overfitting, especially if the second block of variables (response) contains a lot of noise, as well as to explore the accuracy of the model to predict the response variables across the data. Different statistics can be utilized, including the mean absolute error (MAE; i.e., the arithmetic average of the absolute errors; Willmott and Matsuura 2005) and the predicted residual sum of square (PRESS; Abdi, 2010).

In this dissertation, PLSR is employed to infer the locomotor repertoire in fossil primates based on tarsal shape. To so do, two blocks of data are employed, consisting of (1) tarsal shape—navicular shape in Chapter 3; astragalar/calcaneal shape in Chapter 4; and astragalar shape in Chapter 5—averaged by species, and (2) locomotor percentages for the species included in the

extant comparative sample. Tarsal shape was defined as the first block of data (predictor) and locomotor percentages as the second block (response). Different locomotor modes were distinguished in every chapter depending on the composition of the extant comparative sample. For example, Chapter 4 includes clawed climbing/clinging behaviors as one of the locomotor categories, as locomotor predictions are made for plesiadapiforms, which have been interpreted as scansorial by some authors (e.g., Bloch and Boyer, 2007; Bloch et al., 2007). Conversely, Chapter 5, which focuses on a Miocene ape astragalus, places greater emphasis on other types of locomotion, such as vertical climbing and bipedalism (e.g., Almécija et al., 2021). Because locomotor data can come from different sources and authors, and these may report small amounts of specific locomotor behaviors not included in the study, locomotor percentages must be standardized to ensure that they add up to 1 or 100%. Proportion data (i.e., values that range from 0 to 1, or 0% to 100%) habitually violate some assumptions of standard parametric methods, such as normality and homoscedasticity (normal distribution of variances), as they are bounded in a limited range and their variance depends on the mean. To address these issues and make the distribution of the locomotor behavior data more symmetric and suitable for subsequent analyses, two types of data transformations were employed: (1) Arcsine square root transformation (Chapters 3 and 4), and (2) Logit transformation (Chapter 5). Both data transformations pull out the ends of the distribution, thereby stabilizing the variance of the data. The arcsine square root transformation preserves the 0–1 (or 0–100%) bounds, whereas the logit transformation produces an unbounded output (Sokal and Rohlf, 1995; Warton and Hui, 2011). As a result of the application of these data transformations, the obtained predictions need to be transformed back by applying a squared sinus or an inverse logit transformation, respectively. Finally, the predictions obtained are rounded up again to ensure that they add to 1 or 100%.

Phylogenetic discriminant function analysis Discriminant function analyses (DFA), habitually called canonical variate analyses (CVA) in the literature, comprise a set of multivariate statistical methods used to classify observations into a priori defined groups (Sokal and Rohlf, 1995). To do so, DFAs seek to compute new linear combinations of predictor variables (discriminant functions; DFs) that maximize the between-group variance while minimizing within-group variance (Campbell and Atchley, 1981). Although DFA is closely related to PCA in that both compute linear combinations of the original variables to better explain the data and reduce dimensionality, the two differ fundamentally in how they deal with shape space. PCA conducts a rigid, orthogonal rotation of the original space, thus preserving the Euclidean distances and angles between points, and yielding new linear combinations (PCs) that are orthogonal and uncorrelated between them. In

contrast, DFA reshapes the shape space using a non-rigid rotation of the original variables, potentially distorting within-group distances. Therefore, the new linear combinations of the original variables (DFs) are not orthogonal (Campbell and Atchley, 1981; Klingenberg and Monteiro, 2005). In geometric morphometrics, shape variables (Procrustes shape coordinates) are high-dimensional and rank-deficient due to alignment constraints derived from the GPA (Rohlf, 1999; Mitteroecker and Gunz, 2009). For this reason, conducting a DFA on the Procrustes shape coordinates directly can be problematic, both because of the problems derived from high-dimensionality (when the number of variables approach or exceed the number of observations) and the inherent multicollinearity of this type of shape data, requiring some type of regularization or dimensionality reduction (Mitteroecker and Bookstein, 2011). Therefore, in the context of geometric morphometrics it is a standard practice to perform a dimensionality reduction via a PCA and then compute a DFA on the most explanatory PCs (usually by employing the minimum number of PCs that enable the highest percentage of correct classification after LOOCV without overestimating the variance among groups; e.g., Zanolli et al., 2023).

As discussed above, not accounting for the shared evolutionary history between species can lead to inflated Type I error rates, as species should not be treated as statistically independent data points (Felsenstein, 1985). To address this in the context of DFA, Chapter 3 employs a recently developed phylogenetic discriminant function analysis (pDFA). This approach consists of integrating a generalized least-squares (GLS) model on the extant species dataset (training dataset) to predict the locomotor category of extinct species while accounting for phylogenetic covariance among species (Clavel and Morlon, 2020). Predictions are made under the assumption of equal prior probabilities for all locomotor categories, as no a priori information exists regarding the prevalence of these categories among extinct primates. Rather than relying on posterior probabilities—which are not necessarily a good estimate of group belonging as they may suffer from overfitting (Qiao et al., 2009)—estimates of group membership classification confidence were evaluated using different resampling techniques (e.g., LOOCV, k-fold). While LOOCV consists of removing one individual from the training set each time (and then predicting the locomotor category for the extinct species with the remaining dataset), the k-fold subsampling approach is based on removing one third of each locomotor class from the training set (and predict the locomotor category for the extinct species afterwards as well). Compared to LOOCV, the k-fold approach can potentially highlight more uncertainty in the predictions as it more strongly destabilizes the training. Similarly, the performance (calculated as the misclassification rate) of the pDFA was assessed by performing a LOOCV on the training set.

Evolutionary modeling Bayesian branch-specific rate estimation via reversible-jump Markov chain Monte Carlo (rjMCMC) is a powerful approach for exploring models with varying numbers of rate regimes, accommodating the possibility that different branches may evolve at distinct evolutionary rates, as well as for inferring the posterior distribution over these branch-specific rate configurations (Green, 1995; Pagel and Meade, 2008; Venditti et al., 2011). Therefore, in Chapters 3 and 4, bayesian branch-specific rate estimation via rjMCMC was employed to model the evolution of tarsal shape across the primate phylogenetic tree, with special emphasis on euprimate origins and early evolution. Markov chain Monte Carlo is a computational framework for Bayesian inference in cases where the posterior distribution is too complex to calculate analytically. It simulates a chain of parameter values that, after an initial "burn-in" period, approximate the posterior distribution (Geyer, 2011). In particular, Bayesian branch-specific rate estimation via rjMCMC models continuous traits under a BM evolutionary model, using GLS to compute the likelihood of trait values at the tips of the tree and the per branch evolutionary rates parameters. The rjMCMC algorithm allows to explore different models with varying numbers of rate regimes (i.e., some with few rates, simpler, and some with many). The posterior, model-averaged distribution incorporates all sampled models, yielding relative rate estimates per branch while averaging over the uncertainty regarding both the number of shifts and where they occurred (Venditti et al., 2011). An attractive feature of using rjMCMC is that it can directly highlight the regions of the tree—specific branches or clades—that exhibit remarkable changes in the evolutionary rates, permitting powerful testing for rate heterogeneity (Pagel and Meade, 2008). Following Venditti's et al. (2011) recommendations, the first pPCs (retaining up to 95% of the total variance) were employed in Chapters 3 and 4 to reduce dimensionality and ensure that traits approximate uncorrelated continuous variables with strong functional signal.

It is essential to perform a series of diagnostic analyses to verify that posterior estimates are reliable and that independent chains have converged and are well mixed (Cowles and Carlin, 1996; Kuhner, 2009). Convergence across independent chains is assessed via visual inspection of the trace plots and the Gelman-Rubin's convergence diagnostic test (Gelman and Rubin, 1992). Trace plots depict how parameter values change over the course of the MCMC simulation. Ideally, they should be stationary (i.e., the chain fluctuates around a stable mean) and well mixed (i.e., the chain moves smoothly though the parameter space). Persistent drifts or trends indicate that the chain is not convergent, while poor mixing or high autocorrelation between chains will be evinced by the presence of blocky or sticky patterns. In turn, the Gelman-Rubin's convergence diagnostic test compares the variance within each chain to the variance between chains (Gelman and Rubin, 1992). When all chains are sampling the same posterior distribution, the statistic is close to 1.

Values greater than 1.1 habitually suggest that the chains have not converged. Another important diagnostic test that must be performed when employing rjMCMC is the computation of the effective sample size (ESS) of each independent chain. Because MCMC are correlated, the raw sample size is not informative. Thus, computing the ESS of each independent chain allows to estimate how many independent samples a chain effectively represents. An acceptable ESS is >200 for most parameters. When ESS is low, it can be related to overly complex models or strong correlations between parameters (Kuhner, 2009). Some limitations of employing a rjMCMC models with too many rate shifts may still result in low ESS or poor mixing, especially in densely sampled or unbalanced trees, albeit it remains as a strong method for modeling evolutionary rate heterogeneity if all assumptions are met (Martínez-Gómez et al., 2024).

Chapter 3:

Early euprimates already had a diverse locomotor repertoire: Evidence from ankle bone morphology

Reproduced from:

Monclús-Gonzalo, O., Alba, D.M., Duhamel, A., Fabre, A.C., Marigó, J., 2023. Early euprimates already had a diverse locomotor repertoire: Evidence from ankle bone morphology. J. Hum. Evol. 181, 103395. https://doi.org/10.1016/j.jhevol.2023.103395

Journal of Human Evolution 181 (2023) 103395

Contents lists available at ScienceDirect

Journal of Human Evolution

journal homepage: www.elsevier.com/locate/jhevol

Early euprimates already had a diverse locomotor repertoire: Evidence from ankle bone morphology

Oriol Monclús-Gonzalo [a, 1], David M. Alba [a], Anaïs Duhamel [b], Anne-Claire Fabre [c, d, e, *, 1], Judit Marigó [f, a, *, 1]

[a] Institut Català de Paleontologia Miquel Crusafont, Universitat Autònoma de Barcelona, Edifici ICTA-ICP, c/ Columnes s/n, 08193 Cerdanyola del Vallès, Barcelona, Spain
[b] University of Lyon, ENSL, CNRS, LGL-TPE, Villeurbanne 69622, France
[c] Naturhistorisches Museum Bern, 3005 Bern, Switzerland
[d] Institute of Ecology and Evolution, University of Bern, 3012 Bern, Switzerland
[e] Life Sciences Department, Vertebrates Division, Natural History Museum, London SW7 5BD, UK
[f] Universitat Autònoma de Barcelona, Departament de Geologia, 08193 Cerdanyola del Vallès, Barcelona, Spain

ARTICLE INFO

Article history:
Received 9 August 2022
Accepted 8 May 2023
Available online 13 June 2023

Keywords:
Early euprimates
Locomotor repertoire
Geometric morphometrics
Functional morphology
Paleogene
Navicular

ABSTRACT

The morphological adaptations of euprimates have been linked to their origin and early evolution in an arboreal environment. However, the ancestral and early locomotor repertoire of this group remains contentious. Although some tarsal bones like the astragalus and the calcaneus have been thoroughly studied, the navicular remains poorly studied despite its potential implications for foot mobility. Here, we evaluate early euprimate locomotion by assessing the shape of the navicular—an important component of the midtarsal region of the foot—using three-dimensional geometric morphometrics in relation to quantified locomotor repertoire in a wide data set of extant primates. We also reconstruct the locomotor repertoire of representatives of the major early primate lineages with a novel phylogenetically informed discriminant analysis and characterize the changes that occurred in the navicular during the archaic primate–euprimate transition. To do so, we included in our study an extensive sample of naviculars (36 specimens) belonging to different species of adapiforms, omomyiforms, and plesiadapiforms. Our results indicate that navicular shape embeds a strong functional signal, allowing us to infer the type of locomotion of extinct primates. We demonstrate that early euprimates displayed a diverse locomotor behavior, although they did not reach the level of specialization of some living forms. Finally, we show that the navicular bone experienced substantial reorganization throughout the archaic primate–euprimate transition, supporting the major functional role of the tarsus during early primate evolution. This study demonstrates that navicular shape can be used as a reliable proxy for primate locomotor behavior. In addition, it sheds light on the diverse locomotor behavior of early primates as well as on the archaic primate–euprimate transition, which involved profound morphological changes within the tarsus, including the navicular bone.

© 2023 The Authors. Published by Elsevier Ltd. This is an open access article under the CC BY-NC-ND license (http://creativecommons.org/licenses/by-nc-nd/4.0/).

1. Introduction

Extant primates are very diverse in body size (from ~30 g in mouse lemurs to 200 kg in male gorillas) and locomotor behavior, including arboreal and terrestrial quadrupedalism, vertical clinging and leaping (VCL), climbing and suspensory behaviors, and terrestrial bipedalism, among others (Oxnard et al., 1990; Hunt et al., 1996; Fleagle, 2013). Several evolutionary scenarios have been proposed to explain the origin and evolution of primates of modern aspect (or euprimate, sensu Hoffstetter, 1977) locomotor diversity from an adaptive viewpoint, but they remain highly debated (Napier and Walker, 1967; Walker, 1974; Cartmill, 1974, 1992; Szalay and Dagosto, 1980; Dagosto, 1988, 2007; Rasmussen, 1990; Sussman, 1991). The early adaptive radiation of euprimates (adapiforms and omomyiforms) has been extensively investigated based on postcranial remains, especially ankle bones such as the

* Corresponding authors.
E-mail addresses: fabreac@gmail.com (A.-C. Fabre), judit.marigo@uab.cat (J. Marigó).
[1] O.M.G, A.-C.F., and J.M. contributed equally to this work.

https://doi.org/10.1016/j.jhevol.2023.103395
0047-2484/© 2023 The Authors. Published by Elsevier Ltd. This is an open access article under the CC BY-NC-ND license (http://creativecommons.org/licenses/by-nc-nd/4.0/).

calcaneus, astragalus, and navicular, as they are well represented in the fossil record and considered to be good proxies for locomotor habits among primates (e.g., Decker and Szalay, 1974; Szalay and Decker, 1974; Conroy and Rose, 1983; Rose and Walker, 1985; Covert, 1988; Gebo et al., 1991, 2015; Moyà-Solà et al., 2012; Boyer et al., 2013, 2015, 2017a; Llera Martín et al., 2022). The morphology of these bones suggests that the archaic primate–euprimate transition was characterized by a substantial reorganization of the foot (Dagosto, 1988, 2007). Nonetheless, an integrative study relating foot bone morphology with quantified locomotor data in a broad sample of living and extinct primates is currently missing.

Among early euprimates, basal omomyiforms have been proposed to be more active and prone to leaping than basal adapiforms (Walker, 1974; Gebo, 1988; Rose, 1994; Boyer et al., 2013). However, differences in body size between the members of these groups have hindered the interpretation of their morphological differences, as adapiforms (except for some small forms such as *Anchomomys frontanyensis*) are substantially larger than most omomyiforms (Rose, 1994), although within the latter group there are also larger-bodied species (Dunn et al., 2006; Dunn, 2010). For this reason, it has been suggested that some morphological differences between these groups might simply reflect size-scaling (allometric) effects instead of fundamental differences in locomotor behavior, although body mass and locomotor behavior are functionally interwoven (Walker, 1974). Furthermore, for biomechanical reasons, foot type has also been proposed as an important factor influencing tarsal morphology (Morton, 1924; Moyà-Solà et al., 2012). Foot types differ with respect to the location of the fulcrum, which is defined as the position in which the lever (in this case, the foot) pivots (Morton, 1924). Anthropoids and most nonprimate mammals have a metatarsi-fulcrumating foot, with the fulcrum placed on the heads of the metatarsals, associated with an increased load arm (Morton, 1924). In contrast, extant strepsirrhines and tarsiers have a tarsi-fulcrumating foot, where the fulcrum is located on the distal tarsal bones; this provides them increased grasping abilities but results in a reduced load arm, which is compensated by the elongation of the tarsus, especially the calcaneus and the navicular (Moyà-Solà et al., 2012). In addition, indriids are specialized VCLs that depart from the tarsi-fulcrumating condition, being described as 'tarsi-rotators' because their foot displays a greater range of inversion–eversion and acts solely as a force transducer instead of as a propulsive lever (Demes et al., 1996; Ankel-Simons, 2007). Moreover, they possess a derived adductor grasping mode (sensu Gebo, 1985; Gebo and Dagosto, 1988) characterized by an enhanced grasping action of the hallux and the second digit that enables the exploitation of the vertical support niche despite their large body size compared to other vertical clingers and leapers.

The functional morphology of the tarsus has been extensively studied for the calcaneus and astragalus of extinct primates (e.g., Decker and Szalay, 1974; Szalay and Decker, 1974; Lewis, 1980a,b; Godinot and Dagosto, 1983; Dagosto, 1988, 2007; Gebo, 1988; Gebo et al., 2000, 2001, 2012, 2015; Seiffert and Simons, 2001; Dunn et al., 2006; Dagosto et al., 2010; Dunn, 2010; Marivaux et al., 2010, 2011; Moyà-Solà et al., 2012; Boyer et al., 2013, 2015, 2017a, 2019; Gladman et al., 2013; Chester et al., 2015; Seiffert et al., 2015; Marigó et al., 2016; Yapuncich et al., 2017, 2019). These two bones account for the 31% and 38% of the fossil primate pedal remains preserved in the fossil record, respectively, indicating a strong bias toward their study compared with other foot elements (Yapuncich et al., 2022). They have been the most informative for our understanding of foot function, as they present several traits related to pedal grasping, load transmission, and degree of movements at the crural, subtalar, and transverse tarsal joints (Su and Zeiniger, 2022), allowing us to produce strong inferences about the locomotor behavior of extinct species. In contrast, the navicular remains comparatively poorly studied despite being important for midfoot mobility as an intermediate between the astragalus and the distal tarsals and metatarsals (Lewis, 1980b; Su and Zeiniger, 2022). Only a handful of studies have investigated the functional signal of the navicular (Covert, 1988; Dagosto, 1988, 2007; Gebo et al., 1991; Anemone and Covert, 2000; Dunn, 2010; Rose et al., 2011; Marigó et al., 2020), and none have used a geometric morphometrics approach, quantified locomotor data, or phylogenetic comparative methods. Differences in proximodistal elongation as well as in the morphology of the navicular facets among extant taxa with varied locomotor behaviors suggest that this bone may be useful for inferring the locomotor behavior of extinct primates and, hence, might provide additional insight into the reconstruction of the ancestral euprimate morphotype from an adaptive viewpoint.

We aim to investigate the evolution and diversification of the locomotor behavior of early euprimates. To do so, we use a three-dimensional (3D) geometric morphometric approach focused on the navicular and based on a large sample of extant and extinct species. These include representatives of the plesiadapiforms, as they are considered an early paraphyletic radiation of stem primates (Bloch et al., 2007; Silcox et al., 2015, 2017). We generated a novel data set including representatives of living lemuriforms and noncatarrhine haplorrhines, as well as a large sample of early primates from the Paleocene and Eocene (plesiadapiforms, adapiforms, and omomyiforms). We hypothesize that navicular morphology is functionally linked to the locomotor behavior of primates. Specifically, we predict that navicular shape (quantified by means of a 3D geometric morphometrics approach) is a reliable predictor of the locomotor repertoire of extant primates and, thus, can be used to infer the locomotion of extinct primate species for which this bone has been recovered. With regards to early euprimates, we hypothesize that their locomotor repertoire was already diverse early on in their evolution as they rapidly diversified in the arboreal niche, exploring different ecological strategies within the arboreal milieu. Notwithstanding, we predict that their locomotor adaptations were less specialized than the ones present in some extant species. Finally, we hypothesize that the locomotor mode played a critical role during the archaic primate–euprimate transition, leading to substantial morphological changes in the foot anatomy that can be traced on the navicular bone.

2. Materials and methods

2.1. Sample composition, data collection, and phylogenetic tree

The analyzed sample is composed of 121 naviculars belonging to 46 extant and 17 extinct primate species (alongside one specimen attributed to Omomyidae indet. [UCMP V 134984]). The extant taxa represent nearly the entire genus diversity of strepsirrhines (cheirogaleids: $n = 8$; galagids: $n = 2$; indriids: $n = 8$; lemurids: $n = 15$; lorisids: $n = 10$; daubentoniids: $n = 5$; and lepilemurids: $n = 2$) and a representative sample of extant noncatarrhine haplorrhines (atelids: $n = 10$; callitrichids: $n = 10$; cebids: $n = 5$; pitheciids: $n = 9$; and tarsiids: $n = 1$). Due to the semi(terrestrial) locomotor behavior of several catarrhine species, which is not adequate for comparison with early euprimates, this group has not been included in the sample. The extinct taxa correspond to 13 omomyiforms, 19 adapiforms, and four plesiadapiforms. The 3D models of all specimens were downloaded from the online repository MorphoSource (www.MorphoSource.org; Boyer et al., 2017b). The complete list of specimens analyzed is provided in Supplementary Online Material (SOM) Table S1, the list of living species and their locomotor data in SOM Table S2, and the list of extinct species in SOM Table S3.

A phylogenetic tree (SOM Fig. S1) comprising all extant primates in our study was downloaded from the 10kTrees Project v. 3 (Arnold et al., 2010). The criteria used to place the extinct taxa are explained in SOM S1. Unless otherwise stated, all analyses were performed in R v. 4.2.2 (R Core Team, 2022), and the alpha level of significance was set at $p < 0.05$.

2.2. Quantification of shape, impact of size, and navicular shape variation

Quantification of shape using three-dimensional geometric morphometrics To accurately depict navicular shape, a series of 16 homologous anatomical landmarks (Fig. 1; Table 1) was placed on the 3D surface of each specimen using the software Landmark v. 3.0.0.6 (Wiley, 2006). For those specimens belonging to the left foot, a mirroring of the mesh was performed before placing the landmarks in order to have the same orientation for all specimens. A generalized Procrustes analysis was carried out with the function 'gpagen' of the package geomorph v. 4.0.3 (Adams and Otárola-Castillo, 2013) to obtain the Procrustes shape coordinates (Rohlf and Slice, 1990; Mitteroecker and Gunz, 2009). A mean shape was calculated for each species, and species means were used as input in all further analyses.

Impact of size on navicular shape To assess the impact of navicular size on navicular shape in the analyzed sample, we first examined the correlation between navicular size and body mass (SOM Fig. S2). After that, we computed a series of allometric regressions of species-mean Procrustes shape coordinates vs. $\log_{10}$-transformed centroid size (CS; Goodall, 1991) in the entire sample and two subsets: only euprimates (excluding plesiadapiforms) and euprimates except for the small vertical clingers and leapers (*Tarsius spectrum*, *Galago moholi*, and *Sciurocheirus alleni*). We fitted a multivariate phylogenetic linear model with a Pagel's lambda by penalized likelihood using the 'mvgls' function of the package mvMORPH v. 1.1.6 (Clavel et al., 2015; Clavel and Morlon, 2020). A penalized-likelihood approach is a modern formulation of the regularization/shrinkage approaches, which are commonly used to constrain the estimates of parameters such as the maximum likelihood error, to address analyses in which the number of variables exceed the sample number (Clavel et al., 2019). Next, we tested for significant correlation between shape and centroid size using the function 'manova.gls'.

Navicular shape variation To assess navicular shape variation across the sample, a principal component analysis (PCA) was performed using the species-mean Procrustes shape coordinates. The phylogeny was plotted along with the results of the PCA, building a phylomorphospace using the function 'phylomorphospace' of the package phytools v. 0.7–20 (Revell, 2012).

2.3. Covariation between navicular shape and locomotion in extant euprimate species

To test the correlation between navicular shape and locomotor behavior, a quantified locomotor data set was compiled from the available literature. To assemble this data set, six different locomotor categories were used, following several field studies as well as the descriptions for standardized primate locomotor and postural modes presented by Hunt et al. (1996): quadrupedalism (Q), leaping (L), climbing (C), suspension (S), bridging (B), and scrambling/clambering (S/C; see SOM S1 for further details). We next performed a PCA to assess if the locomotor categories described in SOM Table S2 were suitable for describing the locomotor repertoire described in the field studies from which the locomotor percentages were retrieved (SOM Fig. S3).

A two-block partial least squares (2B-PLS) analysis (Rohlf and Corti, 2000) was performed to study the covariation between navicular shape and quantified locomotor data (SOM Table S2) in extant taxa. To do so, the function 'two.b.pls' from the package geomorph v. 4.0.3 (Adams and Otárola-Castillo, 2013) was used. This method uses 3D landmark data and performs a singular value decomposition, which decomposes the covariance matrix of the two blocks of variables into two matrices of eigenvectors (each one

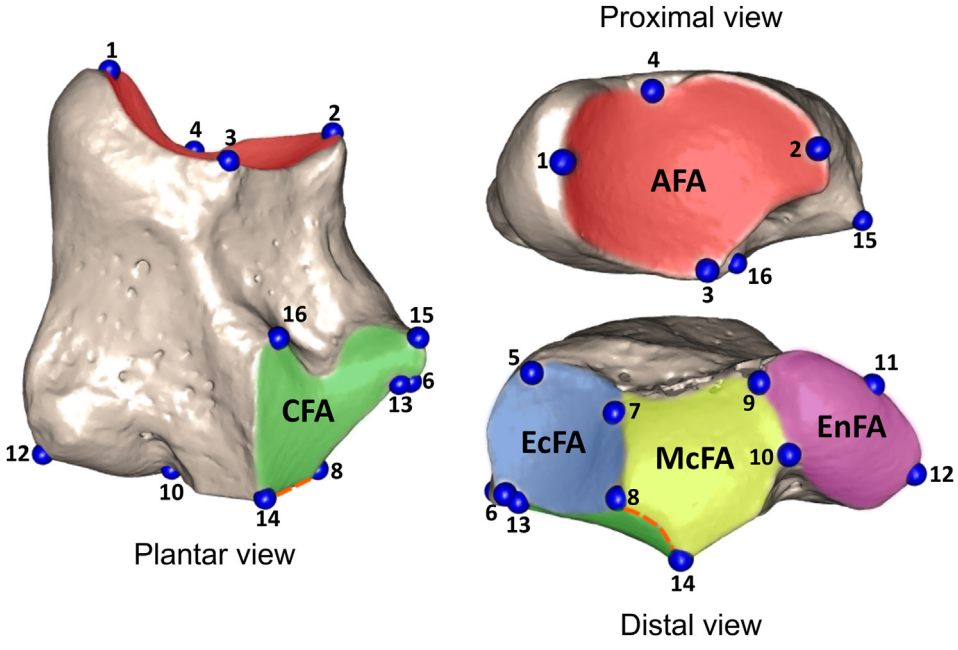


Figure 1. Landmark configuration and anatomy of the navicular bone. Plantar, proximal, and distal views of the navicular of *Eulemur fulvus* (USNM 542489, https://doi.org/10.17602/M2/M15828). McCuLength (mesocuneiform-cuboid contact length), depicting the contact between the McFA (mesocuneiform facet area) and CFA (cuboid facet area), is shown as an orange dotted line (between landmarks 8 and 14). Abbreviations: AFA = astragalar facet area; EnFA = entocuneiform facet area; EcFA = ectocuneiform facet area. See Table 1 for landmark definitions. (For interpretation of the references to color in this figure legend, the reader is referred to the Web version of this article.)

Table 1
Definition of the anatomical landmarks used in this study. To visualize placement of the landmarks on the navicular bone, see Figure 1.

Landmark	Definition
1	Most proximomedial point of the AFA
2	Most proximolateral point of the AFA
3	Plantarmost point of maximum curvature between LM1 and LM2
4	Dorsalmost point of maximum concavity between LM1 and LM2
5	Dorsolateralmost point of the EcFA
6	Plantarlateralmost point of the EcFA
7	Dorsalmost point of the contact between the EcFA and the McFA
8	Plantarmost point of the contact between the EcFA and the McFA
9	Dorsalmost point of the contact between the McFA and the EnFA
10	Plantarmost point of the contact between the McFA and the EnFA
11	Dorsomedialmost point of the EnFA
12	Plantarmedialmost point of the EnFA
13	Distolateralmost point of the CFA
14	Distomedialmost point of the CFA
15	Proximolateralmost point of the CFA
16	Proximomedialmost point of the CFA

Abbreviations: AFA = astragalar facet area; LM = landmark; EcFA = ectocuneiform facet area; McFA = mesocuneiform facet area; EnFA = entocuneiform facet area; CFA = cuboid facet area.

for one block of data) and a matrix of eigenvalues (the square-roots of eigenvectors; Rohlf and Corti, 2000; Bookstein et al., 2003). The significance of each linear combination is assessed by comparing the singular value to those obtained after resampling. If the partial least squares (PLS) covariation coefficient (r-PLS) is higher than the ones obtained from permutated blocks, its associated *p*-value is significant.

2.4. Reconstruction of early euprimate locomotor behavior

Prediction of the locomotor percentages To reconstruct the locomotor repertoire of early euprimates, we used the two sets of eigenvectors generated by the singular warp analysis performed on the previous covariance analysis (which was exclusively carried out on extant species). Similar approaches have previously been applied to reconstruct one block of shape variables from another block (e.g., Torres-Tamayo et al., 2020). We projected the species-means Procrustes shape coordinates belonging to the early euprimate species into the latent space generated after the singular warp analysis. We then used the coefficients obtained from the linear regression of the original latent variables to estimate the latent variables corresponding to the second block (derived from the quantified locomotor behavior data). The resulting variables can be projected back to obtain the quantified locomotor behavior of the early euprimate species. Finally, the locomotor percentages were predicted after reversing the arcsin square-root transformation and normalization (to ensure that their total sum was equal to 100).

To check the accuracy of this method, we performed a leave-one-out cross-validation (LOOCV) on the extant species set to predict their quantified locomotor behavior and compare it with their actual quantified locomotor behavior. We calculated the mean absolute error (MAE; Willmott and Matsuura, 2005) and plotted the estimated values against the original ones in a bivariate plot for each locomotor variable to compare them and assess if the predictive performance of this method varied depending on the estimated locomotor variable or the degree of locomotor specializations of some species (SOM Figs. S4 and S5; SOM Table S4).

Phylogenetic multivariate analysis of variance To assess the differences between navicular shape and foot type, taxonomic groups, and locomotor categories, we used a type II phylogenetic multivariate analysis of variance (MANOVA) with the function 'manova.gls' of the package mvMORPH v 1.1.6 (Clavel et al., 2015). The multivariate phylogenetic linear models were fitted with a Pagel's lambda by penalized likelihood using the 'mvgls' function of the package mvMORPH v1.1.6 (Clavel et al., 2015). In comparison to other modes, the advantage of using Pagel's lambda is that it provides more flexibility in estimating the error structure, as if we were fitting a phylogenetic mixed model while accounting for departure from Brownian motion (Clavel and Morlon, 2020). Significance was assessed using a Pillai statistic and 1000 permutations.

Phylogenetic discriminant function analysis To predict the locomotor category of fossil euprimates, we carried out a recently developed phylogenetic discriminant analysis. This consists of fitting a generalized least-squares model on the extant species data (training data set) to predict the locomotor category of each extinct euprimate species using both its Procrustes shape coordinates and its phylogenetic position. This new method is the first linear discriminant analysis which is both phylogeny-informed and applicable to high dimensional data sets (i.e., data sets containing more traits than individuals). The fitting of the model on the training data set was performed using the function 'mvgls.dfa' from the package mvMORPH v. 1.1.6 (Clavel et al., 2015), and the performance (misclassification rate) of the phylogenetic discriminant function analysis (pDFA) was assessed by performing a LOOCV on the training set. It consists of removing each individual one by one from the training set, performing the pDFA only on the remaining individuals, and checking if the locomotor category of the removed individual is well predicted. Then, we compared it to 1000 randomized predictions on the training set (SOM Fig. S6). Group membership to a locomotor class and posterior probabilities for fossil taxa were calculated using the function 'predict.mvgls.dfa' of the package mvMORPH v. 1.1.6 (Clavel et al., 2015). The predictions were made assuming an equal prior probability of belonging to the different locomotor categories since we do not have a priori knowledge of the prevalence of those categories in the geological period in which the extinct primates lived. Posterior probabilities are not necessarily a good estimate of the classification uncertainty because they may suffer from overfitting and do not accurately reflect out-of-sample prediction uncertainty (Qiao et al., 2009). As we previously did to evaluate the discriminant model performances, we assessed the classification uncertainty by using resampling techniques. For each fossil, we repeated the class prediction several times from models trained on different subsamples of the training set, and we computed the proportions in which the fossil was assigned to each locomotor class. Each training set was obtained using two different subsampling approaches inspired from leave-one-out and K-fold cross-validation. The leave-one-out subsampling approach consisted in removing one by one each extant individual from the training set and predicting the fossils' classes from a model trained on the remaining extant individuals. The K-fold subsampling approach consisted in randomly removing one-third of each locomotor class from the training set—since the smaller class contains three individuals—and predicting the fossils' classes from a model trained on the remaining extant individuals. The three-fold random subsampling was repeated 200 times. The K-fold approach tends to highlight more uncertainty in the predictions because it destabilizes more consequently the training set.

Convergence analyses To identify morphological convergence depending on similar locomotor behaviors, we utilized a phylogenetic ridge regression method of the package RRPhylo v. 2.5.8 (Castiglione et al., 2019). First, a phylogenetic ridge regression was performed on the tree with the species-means Procrustes shape

coordinates of the navicular, using the 'RRPhylo' function to obtain the branch-wise evolutionary rates and the ancestral character estimates at each node. After that, morphological convergence was tested using the function 'search.conv' of the package RRPhylo v. 2.5.8. Finally, the mean angle and the *p*-value of the mean angle were retrieved.

2.5. Navicular morphological evolution

Ancestral state reconstruction To assess the evolutionary model that best depicts the evolution of the first two principal components (PCs) of the PCA performed on the species-means Procrustes shape coordinates (Fig. 2), a maximum-likelihood approach was used with the functions 'mvBM,' 'mvOU,' 'mvEB,' and 'aicw' of the package mvMORPH v. 1.1.6 (Clavel et al., 2015). The ancestral morphotype for each node of the phylogenetic tree was estimated with the function 'estim' of the package mvMORPH v. 1.1.6 (Clavel et al., 2015). Finally, a phenogram plot, a projection of the phylogenetic tree in a space defined by a shape variable (y axis) and time (x axis), was performed using the function 'pheno' of the package phytools v. 0.7–20 (Revell, 2012) for each PC.

Rates of morphological evolution To test the morphological evolution of the navicular, we estimated the branch-specific evolutionary rates and rate shifts using the variable rates model applied in BayesTraits v. 3 (http://www.evolution.rdg.ac.uk/). The shifts in the rate of continuous trait evolution, which was modeled using a Brownian motion model, were detected with a reversible-jump Monte Carlo algorithm. The first 10 PCs of the phylogenetic PCA on the species-mean Procrustes shape coordinates, computed using the function 'phyl.pca' of the package phytools v. 0.7–20 (Revell, 2012) accounting for >99% of the overall variation in navicular shape, were used as an input. Ten independent chains were run for 200,000,000 iterations, sampling every 10,000 iterations, and the first 25,000,000 iterations were discarded as burn-in (SOM Table S5). Trace plots were examined, and the 10 independent chains that were stationary after burn-in were kept (SOM Fig. S7). The effective sample size (ESS) of the posterior samples (ESS < 100) as well as the convergence of the chains were assessed with a Gelman and Rubin's convergence diagnostic (SOM Tables S5 and S6), with the functions 'effectiveSize' and 'Gelman.diag' implemented in the package coda v. 0.19–4 (Plummer et al., 2005). Assessing the convergence of chains is critical to detect large deviations among the different chains (non-convergence) and ensure similar between-chain variances (Gelman and Rubin, 1992). The results were plotted on the tree using the function 'mytreebybranch' (https://github.com/anjgoswami/salamanders/blob/master/mytreerateplotter.R). Branch-specific average rates and the posterior probability of rate shifts (the mean of all ten independent chains) were summarized using the 'rjpp' and 'plotShift' functions of the package btrtools v. 0.0.0.9000 (https://github.com/hferg/btrtools/tree/master/R).

2.6. Shape visualization

To visualize shape differences in navicular shape between the extremes of the axes of the different analyses carried out, a thin-plate spline deformation of the 3D model of a navicular bone was carried out. Shape visualization of the effects of PCs, PLS, and discriminant function values was performed using the functions 'shape.predictor' and 'plotRefToTarget' of the package geomorph v. 4.0.3 (Adams and Otárola-Castillo, 2013) and 'shade3d' of the package rgl v. 0.100.47 (Adler and Murdoch, 2020). The specimen used as the reference was the navicular bone of *Eulemur fulvus* (USNM 542489), which is adequate to represent the mean shape of the sample.

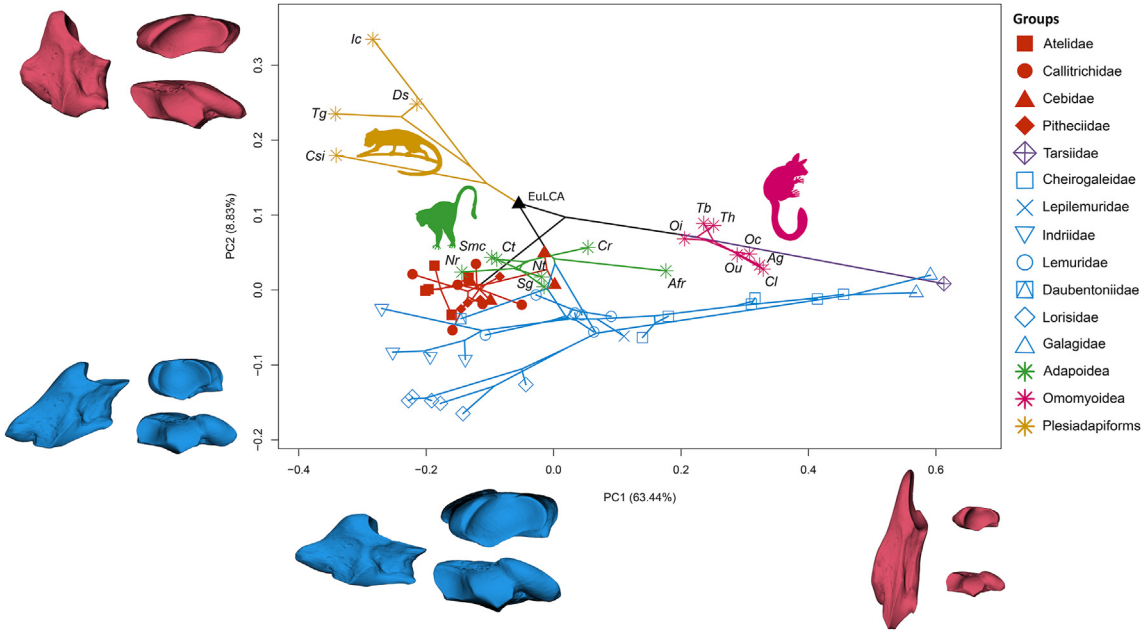


Figure 2. Phylomorphospace based on the first and second principal components (PCs of the principal component analysis carried out on the species-mean adjusted shape coordinates). Data points are color-coded by taxonomic group. The amount of variance explained by each PC is depicted below the axis in parenthesis. Navicular shapes associated with minimum (blue) and maximum (red) values along each PC (plantar, proximal, and distal views are shown from left to right and from top to bottom, as shown in Fig. 1). Thin plate splines correspond to the specimen of *Eulemur fulvus* USNM 542489. Abbreviations: EuLCA = euprimate last common ancestor; Th = *Tetonius homunculus*; Ag = *Arapahovius gazini*; Oi = Omomyidae indet.; Oc = *Omomys carteri*; Ou = *Ourayia uintensis*; Cl = *Chipetaia lamporea*; Tb = *Teilhardina brandti*; Afr = *Anchomomys frontanyensis*; Nr = *Notharctus robustior*; Nt = *Notharctus tenebrosus*; Ct = *Copelemur tutus*; Sg = *Smilodectes gracilis*; Smc = *Smilodectes mcgrewi*; Cr = *Cantius ralstoni*; Ic = *Ignacius clarforkensis*; Cs = *Carpolestes simpsoni*; Ds = *Dryomomys szalayi*; Tg = *Tinimomys graybulliensis*. (For interpretation of the references to color in this figure legend, the reader is referred to the Web version of this article.)

3. Results

3.1. Navicular shape variation among primates

No significant correlation is found between navicular shape and $\log_{10}$-transformed centroid size in the entire sample (Pillai's trace = 0.470, $p = 0.756$) or among euprimates alone (Pillai's trace = 0.561, $p = 0.415$). Although navicular centroid size and body mass are significantly correlated ($r^2 = 0.299$, $p < 0.001$; see SOM Fig. S2), three species of vertical clingers and leapers (*T. spectrum*, *G. moholi*, and *S. alleni*) are clear outliers of the linear regression, displaying larger navicular centroid sizes than expected given their body masses. Thus, we repeated the allometric analysis on euprimates excluding these three species and found a significant correlation between navicular shape and $\log_{10}$-transformed centroid size, indicating intrinsic allometric effects (smaller naviculars are relatively proximodistally longer compared to larger ones) in most euprimates (Pillai's trace = 0.594, $p = 0.031$).

The phylomorphospace of the first two PCs of a PCA based on the species-mean Procrustes shape coordinates differentiates species by locomotor behavior and foot type (Fig. 2). PC 1 (63.44% of the total variance) separates species depending on the degree of proximodistal elongation of the navicular, hence denoting a much wider distribution in tarsi-fulcrumating species (comprising extant strepsirrhines, tarsiers, and the extinct adapiforms and omomyiforms) than in metatarsi-fulcrumating ones (extant platyrrhines and plesiadapiforms). Slow climbers (SC, lorisids), large vertical clingers and leapers (LVCL, indriids), suspensors/clamberers (SUS/CLA, atelids), clawed-leapers (CL, callitrichids), and many arboreal quadrupeds/large leapers (AQ/LL, cebids, pitheciids, and *Daubentonia madagascariensis*) display negative scores with a proximodistally short navicular. In contrast, the small-sized vertical clingers and leapers (tarsiids and galagids), which possess a very proximodistally elongated navicular, display positive scores. Species with a moderate proximodistal elongation, such as the cheirogaleids, the lemurids, and the large VCL *Lepilemur mustelinus*, display intermediate scores. Extinct species are distributed along the first axis, forming three differentiated clusters: omomyiforms overlap with cheirogaleids, displaying moderate proximodistal elongation without reaching the extreme shown by tarsiids and galagids; adapiforms occupy the same range as lemurids and *L. mustelinus*; and plesiadapiforms fall apart of the other species, exhibiting a proximodistally short navicular outside the euprimate morphospace.

Principal component 2 (8.83% of the total variance) reflects changes in the shape of the astragalar facet as well as the arrangement of the cuneiform facets. Plesiadapiforms differ from the other species in displaying a more transversely elongated astragalar facet on the medial side and having a medially and plantarly extended entocuneiform facet. In contrast, all euprimates display an ovoid astragalar facet and more aligned cuneiform facets, though some small leapers like tarsiers possess a small and plantarly compressed mesocuneiform facet, and others, such as several anthropoids, display an L-shaped arrangement of the facets.

3.2. Navicular shape as a proxy for locomotion

Phylogenetic MANOVA results indicate that among living euprimate species, there are significant shape differences between locomotor categories (Pillai's trace = 3.732, $p = 0.003$) and foot type (Pillai's trace = 1.246, $p = 0.046$), thus indicating that both locomotor behavior and type of foot posture impact navicular shape.

The first two blocks of the 2B-PLS analysis for the entire extant sample (Fig. 3A) show significant covariation between navicular shape and locomotion (r-PLS = 0.435, $p = 0.041$). Proximodistally elongated naviculars with a more proximally projecting medial side at the astragalar facet are correlated with leaping, whereas proximodistally short and mediolaterally wide naviculars are associated with preference for scrambling and clambering, bridging, and quadrupedal behaviors. However, among large VCL species, indriids (indicated in the figure) depart from the general trend and display proximodistally shortened naviculars despite their proclivity for leaping, thus indicating that proximodistal elongation is indicative of leaping behavior in tarsi-fulcrumating species but not in tarsi-rotator ones. Because of the importance of taking the type of foot posture into account, we repeated the analysis, including only the tarsi-fulcrumating species. When tarsi-fulcrumators are considered alone (Fig. 3B), a stronger correlation is found between navicular shape and locomotion. Again, proximodistal elongation of the navicular is related to leaping proclivity, whereas a proximodistally short and mediolaterally broader navicular is characteristic of more suspensory, bridging, and quadrupedal animals (r-PLS = 0.824, $p < 0.001$).

3.3. Reconstruction of the locomotor repertoire of early primates

The estimated locomotor percentages (Fig. 3A, B; Table 2) for early euprimate species depict two main patterns of locomotor repertoires. Omomyiforms as well as *A. frontanyensis* are characterized by intermediate to high reliance on leaping (34–65%), moderate degrees of quadrupedalism and climbing (13–32%), and more modest values for the other locomotor variables (<10%, most of them <5%). Among extant species, the locomotor repertoires of *Microcebus* and *Mirza* are the ones that more closely resemble the reconstructed ones for these taxa. Except for *A. frontanyensis*, the other adapiforms display higher percentages of quadrupedalism (30–50%) and climbing (21–40%) and variable reliance on leaping (7–33%), although always below the percentages displayed by omomyiforms. Some species, like *Notharctus robustior*, also display moderate percentages of suspension (17%), whereas bridging and scrambling/clambering percentages are very low for all species (less than 6%). These species are reconstructed as above-branch quadrupeds and climbers, and the better analogues for their locomotor repertoire are the lemurids, especially the larger forms such as *Lemur catta* or *Varecia variegata*. There are no important differences between the predictions obtained from the analysis carried out on the entire extant sample and the sample comprised only by tarsi-fulcrumators, although the latter are slightly less scattered across the fossil sample (omomyiforms and *A. frontanyensis* on the one hand, and the other adapiforms on the other, show more consistent within-group percentages) and yielded smaller MAEs for all locomotor variables (SOM Table S4).

The phylogenetically informed discriminant analysis has a misclassification rate of 0.152 after performing a LOOCV on the training set (extant ones). Two estimates of group membership classification confidence for each extinct species (comparing two subsampling techniques: leave-one-out and K-fold cross-validation) are presented in Table 3. Figure 4 is the graphical result of the pDFA (the plot of the species on the principal discriminant axes, which are those that better discriminate among the different locomotor categories). Omomyiforms are classified as cheirogaleid generalists (*Omomys carteri*, *Ourayia uintensis*, *Chipetaia lamporea*, and Omomyidae indet.), arboreal quadrupeds/large leapers (*Tetonius homunculus*), or small VCL (*Teilhardina brandti* and *Arapahovius gazini*). Conversely, all adapiforms fall into the arboreal quadrupeds/large leapers category except for *A. frontanyensis*, which is classified as a large VCL.

Convergence analyses (Table 4) confirmed the similarities between adapiforms and extant arboreal quadrupeds/large leapers

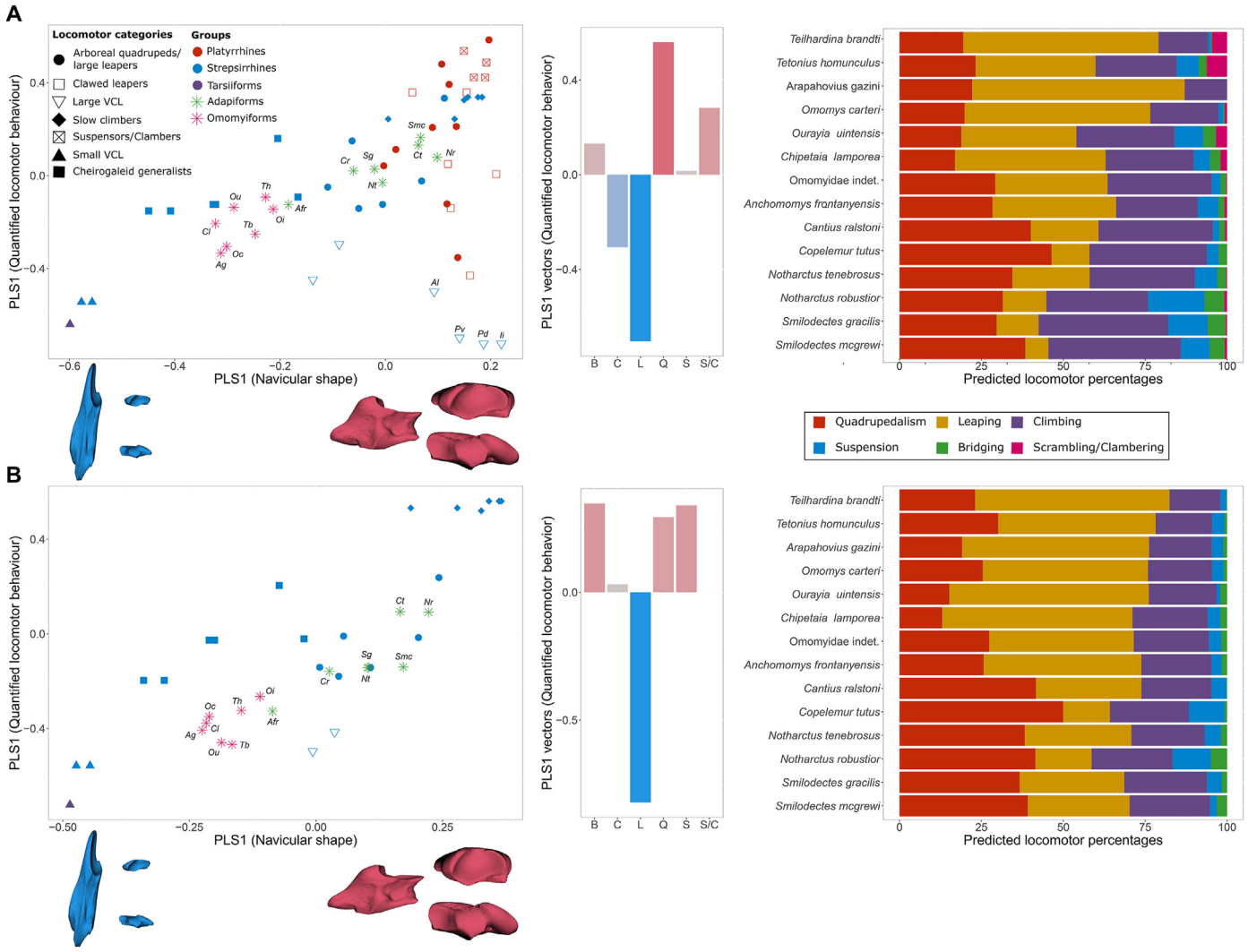


Figure 3. Results of the two-block partial least squares (2B-PLS) between the species-mean Procrustes shape coordinates and quantified locomotor data for all extant species included in this study (A) and tarsi-fulcrumating ones (B). Data points are color coded by taxonomic group and shape is coded by locomotor category. The vectors of the first PLS axis of the locomotor variables are plotted in the right side of the figure. The predicted locomotor percentages for the fossil species are presented in a bar chart located next to the vectors for the first PLS axis for each condition. Navicular shapes associated with minimum (blue) and maximum (red) values of covariation are plotted below each scatterplot (plantar, proximal, and distal views are shown, from left to right and from top to bottom, as shown in Fig. 1). Thin plate splines correspond to the specimen of *Eulemur fulvus* USNM 542489. Abbreviations: Q = quadrupedalism; B = bridging; C = climbing; L = leaping; S = suspension; S/C = scrambling/clambering; Th = *Tetonius homunculus*; Ag = *Arapahovius gazini*; Oi = Omomyidae indet.; Oc = *Omomys carteri*; Ou = *Ourayia uintensis*; Cl = *Chipetaia lamporea*; Tb = *Teilhardina brandti*; Afr = *Anchomomys frontanyensis*; Nr = *Notharctus robustior*; Nt = *Notharctus tenebrosus*; Ct = *Copelemur tutus*; Sg = *Smilodectes gracilis*; Smc = *Smilodectes mcgrewi*; Cr = *Cantius ralstoni*; Al = *Avahi laniger*; Ii = *Indri indri*; Pd = *Propithecus diadema*; Pv = *Propithecus verreauxi*. (For interpretation of the references to color in this figure legend, the reader is referred to the Web version of this article.)

and indicated a greater degree of convergence with lemurids than with platyrrhines. In contrast, no convergence was found between adapiforms (excluding *A. frontanyensis*) and cheirogaleids. Among adapiforms, the middle Eocene notharctid genera (*Smilodectes* and *Notharctus*) also presented significant convergence with the group of specialized large VCL (indriids, *Hapalemur griseus*, and *L. mustelinus*). Conversely, *A. frontanyensis* is classified as a large VCL in the previous pDFA but shows no convergence with this group. Omomyiforms show convergence with the small VCL (*T. spectrum* and the galagids), with the cheirogaleids, and with *A. frontanyensis*. No convergence was found between omomyiforms and either the extant arboreal quadrupeds/large leapers or the adapiforms excluding *A. frontanyensis*. Lastly, no convergence was found between the plesiadapiforms and the callitrichids (clawed leapers) and the lorisids (slow climbers).

3.4. Navicular evolution across the archaic primate–euprimate transition

An 'Early Burst' model is the one that best explains the evolution of PC1, showing a diversification of the proximodistal elongation of the navicular early in euprimate evolutionary history (Fig. 5A; Table 5). By contrast, PC2 evolution is best described by an 'Ornstein–Uhlenbeck' model, depicting stabilizing selection toward an euprimate-like navicular, with more ovoid astragalar facet and straighter arrangement of the cuneiform facets (Fig. 5B; Table 5). Important shifts in rates of navicular evolution occur early in primate evolution (Fig. 6; SOM Fig. S7). Remarkably, mean evolutionary rates are extremely high in the branch leading to the euprimate ancestor. Other significant shifts occur earlier, during the radiation of plesiadapiforms, and across the clade composed of the

Table 2
Predicted locomotor repertoire for each extinct euprimate species. Locomotor percentages were calculated after normalization and reversion of the arcsin square root transformation on the estimated quantified locomotor behavior (see Materials and methods).

Species	Q		L		C		S		B		S/C	
	Entire sample	Tf	Entire sample	Tf	Entire sample	Tf	Entire sample	Tf	Entire sample	Tf	Entire sample	Tf
Tetonius homunculus	23.221	30.124	36.652	48.074	24.660	17.220	6.793	3.765	2.359	0.816	6.315	0.000
Arapahovius gazini	22.171	19.091	64.924	57.098	12.728	19.130	0.077	3.464	0.009	1.217	0.091	0.000
Omomyidae indet.	29.220	27.367	34.317	44.136	31.738	22.899	2.723	3.829	1.714	1.769	0.289	0.000
Omomys carteri	19.860	25.412	56.697	50.419	20.832	19.552	1.401	3.537	0.434	1.080	0.776	0.000
Ourayia uintensis	18.866	15.187	35.114	60.949	29.972	20.677	8.752	1.133	3.850	2.046	3.447	0.008
Chipetaia lamporea	16.930	13.006	45.972	58.101	26.900	22.981	4.923	3.858	3.283	2.053	1.992	0.001
Teilhardina brandti	19.444	23.082	59.632	59.353	15.167	15.456	0.792	1.823	0.314	0.285	4.651	0.000
Anchomomys frontanyensis	28.382	25.683	37.752	48.149	24.857	21.311	6.372	3.192	1.796	1.660	0.842	0.004
Notharctus robustior	31.520	41.483	13.308	17.143	31.011	24.745	17.279	11.622	6.010	5.003	0.872	0.003
Notharctus tenebrosus	34.429	38.204	23.614	32.606	32.127	22.408	6.809	4.899	2.699	1.880	0.323	0.003
Copelemur tutus	46.422	49.954	11.553	14.285	35.858	24.122	3.597	10.889	2.554	0.747	0.016	0.004
Smilodectes gracilis	29.627	36.695	12.842	31.928	39.545	25.238	12.076	4.470	5.456	1.665	0.455	0.004
Smilodectes mcgrewi	38.388	39.151	7.067	31.088	40.396	24.539	8.793	2.028	4.595	3.181	0.761	0.014
Cantius ralstoni	40.079	41.644	20.684	32.194	34.811	21.307	1.979	4.621	1.774	0.233	0.673	0.001

Abbreviations: Tf = tarsi-fulcrumators; Q = quadrupedalism; L = leaping; C = climbing; S = suspension; B = bridging; S/C = scrambling/clambering.

Table 3
Results of the phylogenetic discriminant analysis. Locomotor category predicted for each species and two estimates of group membership classification confidence (LOOCV and K-fold) are provided.[a]

Species	Classification	AQ/LL		CG		CL		LVCL		SC		SVCL		SUS/CLA	
		LOOCV	K-fold	LOOCV	K-fold	LOOCV	K-fold	LOOCV	K-fold	LOOCV	K-fold	LOOCV	K-fold	LOOCV	K-fold
Tetonius homunculus	AQ/LL	**0.891**	0.447	0.109	**0.478**	0.000	0.000	0.000	0.000	0.000	0.000	0.000	0.075	0.000	0.000
Arapahovius gazini	SVCL	0.000	0.000	0.022	0.433	0.000	0.000	0.000	0.000	0.000	0.000	**0.978**	**0.567**	0.000	0.000
Omomyidae indet.	CG	0.022	0.190	**0.978**	**0.752**	0.000	0.000	0.000	0.007	0.000	0.000	0.000	0.052	0.000	0.000
Omomys carteri	CG	0.000	0.000	**0.978**	**0.842**	0.000	0.000	0.000	0.000	0.000	0.000	0.022	0.158	0.000	0.000
Ourayia uintensis	CG	0.000	0.000	**0.978**	**0.877**	0.000	0.000	0.000	0.000	0.000	0.000	0.022	0.123	0.000	0.000
Chipetaia lamporea	CG	0.000	0.000	**0.870**	0.395	0.000	0.000	0.000	0.000	0.000	0.000	0.130	**0.605**	0.000	0.000
Teilhardina brandti	SVCL	0.000	0.107	0.435	**0.563**	0.000	0.000	0.000	0.010	0.000	0.000	**0.565**	0.320	0.000	0.000
Anchomomys frontanyensis	LVCL	0.065	0.357	0.000	0.222	0.000	0.000	**0.935**	**0.422**	0.000	0.000	0.000	0.000	0.000	0.000
Notharctus robustior	AQ/LL	**0.978**	**0.702**	0.000	0.000	0.000	0.007	0.022	0.278	0.000	0.000	0.000	0.000	0.000	0.013
Notharctus tenebrosus	AQ/LL	**1.000**	**0.988**	0.000	0.000	0.000	0.000	0.000	0.012	0.000	0.000	0.000	0.000	0.000	0.000
Copelemur tutus	AQ/LL	**1.000**	**0.982**	0.000	0.000	0.000	0.018	0.000	0.000	0.000	0.000	0.000	0.000	0.000	0.000
Smilodectes gracilis	AQ/LL	**1.000**	**0.875**	0.000	0.000	0.000	0.000	0.000	0.125	0.000	0.000	0.000	0.000	0.000	0.000
Smilodectes mcgrewi	AQ/LL	**1.000**	**0.985**	0.000	0.000	0.000	0.008	0.000	0.007	0.000	0.000	0.000	0.000	0.000	0.000
Cantius ralstoni	AQ/LL	**1.000**	**0.995**	0.000	0.000	0.000	0.000	0.000	0.005	0.000	0.000	0.000	0.000	0.000	0.000

Abbreviations: LOOCV = leave-one-out cross-validation; K-fold = K-fold cross-validation; AQ/LL = arboreal quadrupeds/large leapers; CG = cheirogaleid generalists; CL = clawed leapers; LVCL = large vertical clingers and leapers; SC = slow climbers; SVCL = small vertical clingers and leapers; SUS/CLA = suspensors/clamberers.
[a] The highest estimate for each method is marked in bold.

early to middle Eocene notharctid species and within groups characterized by a particular locomotor behavior, such as the indriids, the lorisids, and the atelids.

4. Discussion

The study of early euprimate locomotor diversity is essential to understand the factors that led to their origin and early diversification. A substantial reorganization of the postcranial skeleton, including the tarsus, has been observed during the archaic primate–euprimate transition (Dagosto, 1988, 2007). Our study provides new clues on such a transition, shedding light on the remarkably diverse locomotor behavior of early euprimates on the basis of navicular shape, which emerges as a reliable proxy for primate locomotor behavior.

4.1. Understanding variation in navicular shape among primates

The elongation of different tarsal elements, such as the talar neck, the cuboid, the navicular, or the distal part of the calcaneus, is informative about the locomotor behavior of extinct taxa (Decker and Szalay, 1974; Gebo, 1988; Dagosto, 1988, 2007; Moyà-Solà et al., 2012; Boyer et al., 2013). However, the functional association between tarsal elongation and leaping does not hold for some groups, such as indriids, which are highly committed leapers despite possessing a proximodistally short navicular (Gebo and Dagosto, 1988). Other taxa, such as lemurids and anthropoids, display a wide variation in leaping frequency among taxa with similar navicular shape, thus hampering locomotor inferences solely on this basis (Crompton et al., 1987; Gebo, 1987a; Oxnard et al., 1990). Biomechanical studies of leaping have shown there are various constraints related to the size of the animal (Demes and Günther, 1989; Demes et al., 1996, 1999), leading to different anatomical solutions (Alfaro et al., 2005; Wainwright et al., 2005). Small-bodied leapers like tarsiers or small galagids must accelerate over small distances and hence need to maximize the time and distance required to generate enough impulse during takeoff. For this reason, small leapers possess very elongated feet, including the navicular in the midtarsal region (Hall-Crags, 1965; Demes and Günther, 1989). In contrast, large VCL species are constrained by the more limited force available to accelerate (muscle force increases as a function of area, whereas weight increases as a function

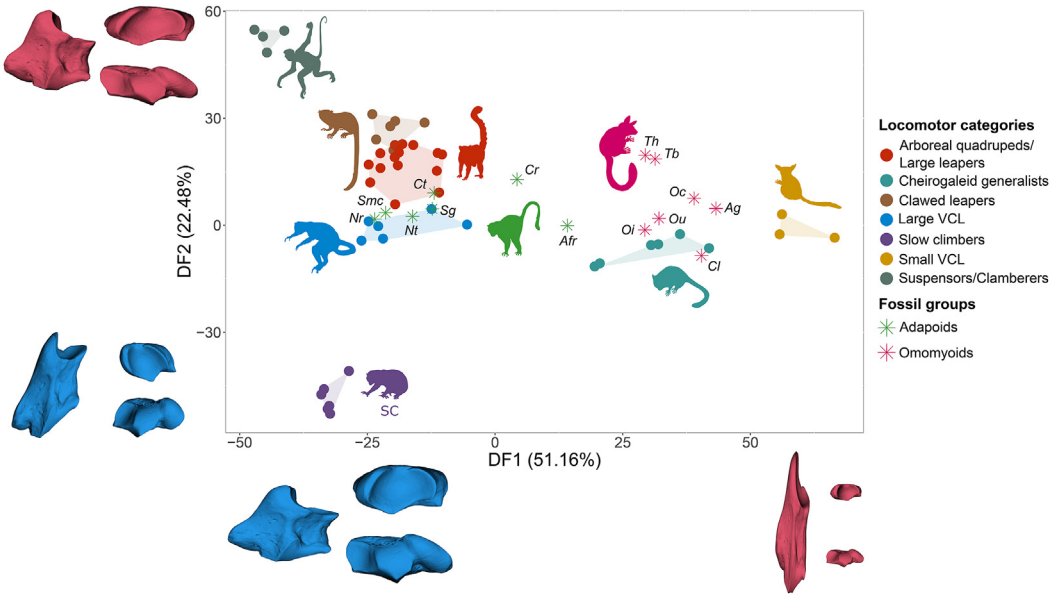


Figure 4. Phylogenetic discriminant analysis based on the species mean-adjusted shape coordinates and locomotor categories. Data points are color coded by locomotor category (extant species) or taxonomic group (extinct species). Navicular shapes associated with minimum (blue) and maximum (red) values of each discriminant function (DF; plantar, proximal, and distal views are shown, from left to right and from top to bottom, as shown in Fig. 1). Thin plate splines correspond to the specimen of *Eulemur fulvus* USNM 542489. Abbreviations: Th = *Tetonius homunculus*; Ag = *Arapahovius gazini*; Oi = Omomyidae indet.; Oc = *Omomys carteri*; Ou = *Ourayia uintensis*; Cl = *Chipetaia lamporea*; Tb = *Teilhardina brandti*; Afr = *Anchomomys frontanyensis*; Nr = *Notharctus robustior*; Nt = *Notharctus tenebrosus*; Ct = *Copelemur tutus*; Sg = *Smilodectes gracilis*; Smc = *Smilodectes mcgrewi*; Cr = *Cantius ralstoni*. (For interpretation of the references to color in this figure legend, the reader is referred to the Web version of this article.)

Table 4
Results of the convergence analyses performed on species-mean adjusted shape coordinates between extinct and living primate species.[a]

Comparison	Mean angle	*p*-value
Adapiforms and arboreal quadrupeds/ large leapers	13.332	**0.001**
Adapiforms and arboreal quadrupeds/ large leapers (Lemuridae)	9.494	**0.009**
Adapiforms and arboreal quadrupeds/ large leapers (Cebidae and Pitheciidae)	12.396	**0.049**
Adapiforms and cheirogaleid generalists	15.643	0.162
Middle Eocene notharctids (*Smilodectes* and *Notharctus*) and large vertical clingers and leapers	8.532	**0.002**
Anchomomys frontanyensis and large vertical clingers and leapers	18.470	**0.32**
Omomyiforms and small vertical clingers and leapers	11.429	**0.011**
Omomyiforms and cheirogaleid generalists	9.103	**0.006**
Omomyiforms and arboreal quadrupeds/large leapers	15.683	0.172
Omomyiforms and North American notharctids (*Cantius*, *Copelemur*, *Smilodectes* and *Notharctus*)	15.475	0.162
Omomyiforms and *Anchomomys frontanyensis*	8.330	**0.002**
Plesiadapiforms and clawed leapers	20.396	0.518
Plesiadapiforms and small climbers	22.371	0.687

[a] Significant results are indicated in bold for $p < 0.05$.

of volume) and hence do not show such an elongation of the tarsal elements (Gebo and Dagosto, 1988; Demes and Günther, 1989; Demes et al., 1996).

Foot-type posture also impacts the degree of proximodistal elongation of the navicular. Tarsi-fulcrumating species display a broader range of navicular elongation, as shown by their distribution along PC1 of the phylomorphospace (Fig. 2), and significant shape differences are found between groups. This distinction is linked to the loss of available load arm, that tarsi-fulcrumators compensate for by means of a greater elongation of the tarsal region (Morton, 1924; Moyà-Solà et al., 2012).

Covariation analyses confirm the relationship between navicular shape and locomotor behavior, as well as the importance of considering foot-type posture. Both 2B-PLS analyses (Fig. 3) relate proximodistal elongation of the navicular with leaping proclivity, whereas proximodistally short naviculars are associated with quadrupedalism, bridging, and scrambling and clambering (Gebo, 1988). However, proximodistal elongation is only correlated with locomotor behavior among tarsi-fulcrumating species (Fig. 3B). For example, indriids display a very proximodistally short navicular despite their high proclivity toward leaping, with broad and shallow astragalar and cuneiform facets, as well as a more sellar-shaped cuboid facet, features more related to climbing rather than leaping behavior (Gebo and Dagosto, 1988). This set of features is likely related to their particular foot type, in which the foot does not act as a propulsor but as a force transducer (Demes et al., 1996). Among metatarsi-fulcrumators, suspensors, scramblers, and clamberers also display broader naviculars with wide and shallow astragalar and cuneiform facets, whereas more quadrupedal and leaping species possess narrow naviculars with deeper facets that enhance the stability of the astragalonavicular joint (Decker and Szalay, 1974). Cuneiform facets (in particular the entocuneiform facet) are also broader and shallower in more suspensory or climbing primates like lorisids (Gebo, 1989), compared to the narrower and more protuberant facets displayed by more quadrupedal or leaping species, such as galagids, in which the arrangement and shape of the facets limit rotational movements (Hall-Craggs, 1966; Gebo, 1987b). Tarsiers are an exception to this trend, as they possess a navicular capable of rotating in both its proximal and distal ends to achieve foot inversion (Gebo, 1987b). Differences in the shape of the cuboid facet also exist between saltatory or more suspensory species as well as climbing taxa, the latter presenting broader and

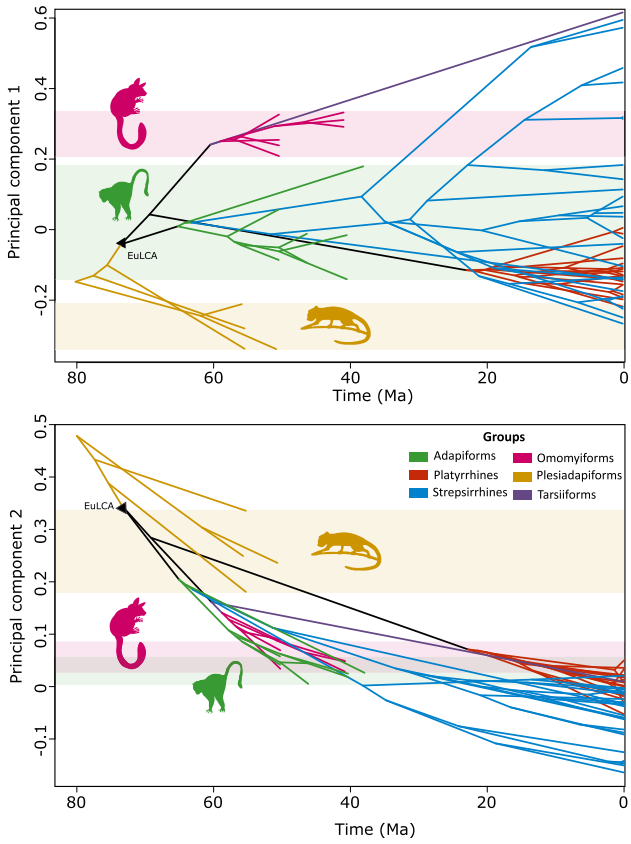


Figure 5. Phenogram based on the (A) first and (B) second principal components (Fig. 2) for all extant and fossil species and the reconstructed internal nodes following an 'Early Burst' (A) or an 'Ornstein-Uhlenbeck' (B) evolutionary model (see also Table 5). Tree branches are color-coded by taxonomic group. The euprimate last common ancestor is indicated by a black triangle in its corresponding node. Adapiform, omomyiform, and plesiadapiform ranges and their overlap with the other groups are indicated by blue, green, and yellow shades, respectively. (For interpretation of the references to color in this figure legend, the reader is referred to the Web version of this article.)

Table 5
Results of the evolutionary model comparison for the first and second principal components (PC) of the principal component analysis performed on the species-mean adjusted shape coordinates. The highest AICw for each PC is in bold.

Axis	Evolutionary model	Loglikelihood	AIC	AICw
PC1	BM	47.210	−90.224	0.026
	OU	47.867	−87.056	0.007
	EB	**51.849**	**−97.297**	**0.968**
PC2	BM	103.954	−203.712	0.001
	OU	**113.198**	**−217.718**	**0.996**
	EB	106.559	−206.718	0.004

Abbreviations: AICc = Akaike Information Criterion corrected; AICw = weighted AIC; BM = Brownian motion; OU = Ornstein-Uhlenbeck; EB = Early Burst.

mediolaterally extended cuboid facets. This last feature is also relevant from a phylogenetic viewpoint, as the contact between the cuboid and mesocuneiform facets is a strepsirrhine synapomorphy that has been related to increased midtarsal folding of the foot, an adaptation toward the use of vertical supports (Beard et al., 1988; Dagosto, 1988).

4.2. The diverse locomotion of early euprimates

Among early euprimates, omomyiforms have been described as agile climbing and running animals, with active arboreal locomotion and high proclivity for leaping (Gebo, 1988; Anemone and Covert, 2000; Rose et al., 2011; Gebo et al., 2012, 2015; Boyer et al., 2013). This is revealed in the phylomorphospace (Fig. 2), in which omomyiforms display relatively similar scores to some extant small-bodied leapers (such as *Microcebus* or *Mirza*), although they do not overlap with any extant species and do not reach the extreme values displayed by specialized small VCL forms like *T. spectrum* or the galagids, suggesting that they lacked a specialized VCL locomotion. Moreover, the results from the prediction of their locomotor repertoire (Fig. 3; Table 2) indicate a moderate to high proclivity for leaping, combined with lower percentages of quadrupedalism and climbing. Phylogenetic discriminant analysis classifies omomyiform species either as cheirogaleid generalists (*C. lamporea*, *O. uintensis*, *Omomys carteri*, and Omomyidae indet. [UCMP V 134984]) or small VCL (*T. brandti* and *A. gazini*), apart from *T. homunculus*, which falls in the arboreal quadrupeds/large leapers category (Table 3). The scatterplot of the discriminant analysis (Fig. 4) and the results of the convergence analyses (Table 4) illustrate overall similarities between omomyiforms and both small VCL species and cheirogaleid generalists, indicating an active (yet not specialized for VCL) locomotor behavior for these species (Gebo, 1988). Interestingly, when the robustness of each classification is assessed by means of a subsampling technique (LOOCV and K-fold cross-validation), we find that the locomotor category that better suits to all omomyiforms is cheirogaleid generalists, whereas some specimens (belonging to *T. homunculus* and Omomyidae indet.) show moderate propensity for the arboreal quadrupeds/large leapers category, and others (including *A. gazini*, *T. brandti*, or *C. lamporea*) are more frequently classified as small VCL. The relatively elongated navicular of omomyiforms, which falls within the cheirogaleid range, is the most important feature related with increased leaping behavior (Gebo, 1988; Boyer et al., 2013). In addition, the proximal protrusion of the proximomedial side of the astragalar facet and the shallower and reduced cuneiform facets without a contact between the mesocuneiform and the cuboid facets likely limit the degree in which rotational movements were accomplished along these articulations (Dagosto, 1988; Marigó et al., 2020). The smaller estimated body size for most omomyiforms is also an important feature that has been related to a more agile locomotor repertoire (Rose, 1994). However, larger-sized omomyiforms such as *O. uintensis* and *C. lamporea* are still classified in our analyses as relatively agile unspecialized leapers. This agrees with previous studies (Dunn et al., 2006; Dunn, 2010) and indicates that an increased leaping behavior was a shared feature within the omomyiform locomotor repertoire. *Tetonius homunculus*, which compared to other omomyiforms shows in our analyses more propensity for quadrupedal and climbing locomotion, is also the one displaying less navicular proximodistal elongation, in accordance with other features in the calcaneus and the astragalus, such a slightly shorter distal calcaneus and a mediolaterally broader astragalar head (Gebo, 1988). One omomyiform genus, *Necrolemur*, for which the navicular is unknown, displays similar tarsier-like morphological specialization in its hindlimbs, and likely had a different locomotor repertoire than the species present in our study. This would add more locomotor diversity to this group, which likely included from active arboreal quadrupeds to specialized VCL in the case of some later forms (Dagosto, 1985; Gebo, 1987b).

Adapiforms are considered basal strepsirrhines by most cladistic analyses (Seiffert et al., 2005; Williams et al., 2010). Moreover, adapiforms share derived pedal traits with extant strepsirrhines, whereas omomyiforms usually retain a more primitive condition (Decker and Szalay, 1974; Gebo, 1986, 1988; Dagosto, 1988, 2007). Adapiforms are generally larger than omomyiforms and characterized by less elongated tarsal bones, indicating that they were predominantly above branch arboreal quadrupeds with less proclivity for leaping (Rose and Walker, 1985; Covert, 1988; Gebo,

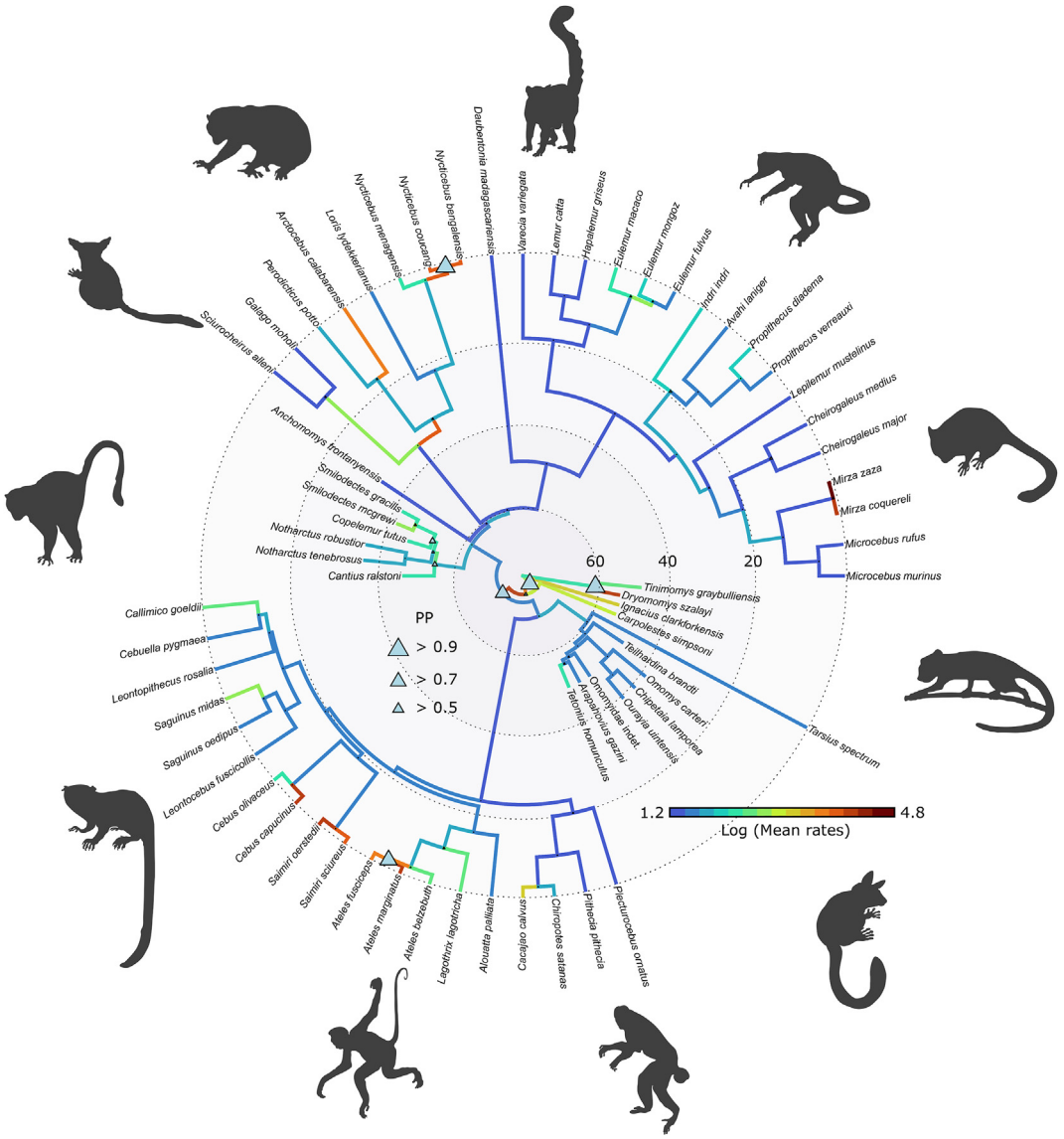


Figure 6. Evolutionary rates and rate shifts for navicular shape in extant and extinct primates. Branch rates are color-coded (warmer colors indicate faster evolutionary rates while cooler colors represent slower evolutionary rates). High probability shifts in evolutionary rates are indicated by blue triangles. The relative size of the triangles represents the posterior probabilities (PP) of the rate shifts (see SOM Fig. S7 to visualize the PP of rate shifts). (For interpretation of the references to color in this figure legend, the reader is referred to the Web version of this article.)

1988; Gebo et al., 1991; Boyer et al., 2013), as supported by our results (Figs. 3–5; Tables 2–4). The only exception is the small-bodied adapiform *A. frontanyensis*, which possesses an omomyiform-like tarsal elongation (Marigó et al., 2016, 2020). This is indicated in the phylomorphospace (Fig. 2), in which *A. frontanyensis* falls very close to the omomyiform cluster. Despite these morphological similarities, there is no doubt that *A. frontanyensis* is a basal strepsirrhine instead of an omomyiform. Apart from the dental characters that identify *A. frontanyensis* as a strepsirrhine (Marigó et al., 2011), its navicular displays an unambiguous strepsirrhine synapomorphy: a contact between the mesocuneiform and the cuboid facets (Dagosto, 1988). Interestingly, the contact between these facets in *A. frontanyensis* is more restricted than in most extant strepsirrhines, probably a primitive retention from the ancestral euprimate, given that *Cantius ralstoni*, the most basal adapiform of our sample, also displays a very short contact (Beard et al., 1988; Marigó et al., 2020). The prediction of its locomotor repertoire, similar to that of some omomyiform species (Fig. 3; Table 2), and the results from the convergence analyses (Table 4) also highlight the similarities in navicular shape between *A. frontanyensis* and omomyiforms. Nevertheless, the more bulbous cuneiform facets and the contact between the mesocuneiform and cuboid facets in *A. frontanyensis* are likely related to a more inverted foot posture than in omomyiforms, which some authors have interpreted as an adaptation for the small branch niche (Marigó et al., 2020). Considering this, an active arboreal locomotion for *A. frontanyensis*, similar to that of *Cheirogaleus* or *Mirza*, is the best interpretation for its locomotor behavior. Interestingly, convergence analyses also yielded significant convergence between adapiforms and extant large VCL species. This is at odds with our prediction of the notharctid locomotor repertoire, which is dominated by quadrupedalism and climbing (Table 4), and thus is closer to that of above-branch quadrupeds than specialized VCL. In addition, some authors have noted that the foot of notharctids lacked some morphological adaptations required to engage in VCL locomotion, such as a derived adductor grasping mode (sensu

Gebo, 1985; Gebo and Dagosto, 1988), thus strengthening our view that these animals were more likely non-specialized arboreal quadrupeds, like the ringtail (*Lemur catta*) and ruffed lemurs (*V. variegata*). Similarly, the phylogenetic discriminant analysis classifies *A. frontanyensis* as a large VCL, in disagreement with the results of other analyses for this taxon. We hypothesize that some similarities in navicular shape and elongation between *A. frontanyensis* and the non-indriid large VCL (*H. griseus* and *L. mustelinus*) might have led to this result. In addition, when resampling techniques (LOOCV and K-fold CV) are performed to assess the classification uncertainty of the pDFA, *A. frontanyensis* shows moderate propensity for the AQ/LL and CG categories, thus indicating a more agile arboreal locomotor behavior.

4.3. The archaic primate–euprimate transition

Our results support that early euprimates underwent a rapid adaptive diversification very early in their evolutionary history, which allowed them to occupy different arboreal niches (Figs. 5 and 6; Table 5). The postcranial remains of plesiadapiforms are scarce and usually belong to derived species, such as *Carpolestes simpsoni*, *Plesiadapis cookei*, or *Ignacius clarkforkensis* (Bloch and Boyer, 2002; Bloch et al., 2007; Boyer and Gingerich, 2019), that are not representative of the early evolution of this group. However, a recent study carried out on the astragalus and calcaneus of the most basal plesiadapiform, *Purgatorius*, confirms that these animals were arboreal but did not possess a euprimate-like grasp-leaping behavior (Chester et al., 2015). Instead, they are viewed as arboreal clawed-climbers similar to the living scandentian *Ptilocercus lowi*, which is also regarded as a good analogue for the ancestral euarchontan (Szalay and Dagosto, 1988; Sargis, 2002, 2004; Nyakatura, 2019). A remarkable exception is *C. simpsoni*, whose partial skeleton displays euprimate-like hallucal grasping features (Bloch and Boyer, 2002). The transition from an archaic primate to the ancestral euprimate is marked by a substantial increase in the proximodistal elongation of the navicular bone (extensive to the whole midtarsal region), together with the acquisition of a more ovoid proximal facet as well as the rearrangement of the cuneiform and cuboid facets, allowing the foot to engage in more complex rotational movements at the astragalonavicular joint and reducing the mediolateral translation of the foot (Szalay and Decker, 1974; Szalay and Drawhorn, 1980; Dagosto, 1988, 2007). These profound morphological changes explain the major shifts that occurred early in primate evolution, during the radiation of plesiadapiforms and in the branch leading to the ancestral euprimate (Fig. 6; SOM Fig. S7).

The acquisition of a tarsi-fulcrumating foot by the ancestral euprimate, presumably as an adaptation to access the fine-branch milieu, would have led to proximodistal elongation of the midtarsal region to compensate for the decreased load arm, followed by a rapid diversification of locomotor behaviors (Morton, 1924). Omomyiforms retained a small body size and an active arboreal locomotor behavior for which cheirogaleids, particularly the agile *Microcebus* and *Mirza* rather than the more cautious *Cheirogaleus*, might be good analogues (Gebo et al., 1991, 2012, 2015; Anemone and Covert, 2000; Rose et al., 2011). Omomyiforms show lower evolutionary rates than adapiforms, which experienced a body size increase that led to the acquisition of a different type of locomotion than the ancestral euprimate, arguably emphasizing above-branch quadrupedalism, as in extant lemurids (Rose and Walker, 1985; Covert, 1988; Gebo et al., 1991). Some adapiforms, such as the small-bodied *A. frontanyensis*, converged toward the omomyiform condition by displaying a more proximodistally elongated navicular as a result of more active arboreal locomotor behaviors (Marigó et al., 2016, 2020).

5. Conclusions

Our study demonstrates that navicular shape is a reliable indicator of the locomotor behavior in primates and can be used as a predictor to infer the locomotor adaptations of extinct species. Most notably, proximodistal elongation of this bone is related to leaping proclivity, although type of foot posture needs to be considered, as it can influence navicular morphology. Our research also shows that early euprimates displayed a diverse array of locomotor adaptations early on their evolution, although they did not reach the level of specialization displayed by some living groups. Finally, we have assessed the archaic primate—euprimate transition by studying the morphological changes occurred in the navicular bone. Initial increases in navicular elongation, as well as other morphological features such as an ovoid astragalar facet, might be related to the acquisition of a tarsi-fulcrumating foot type and a euprimate-like hallucal grasping, indicating a shift toward a more active locomotor behavior. Collectively, our results provide evidence that early euprimates emerged from a small and unspecialized grasp-leaper animal, but soon diversified into a broad range of locomotor behaviors that allowed the occupation of different arboreal niches.

Acknowledgments

This work has been supported by CERCA Programme/Generalitat de Catalunya, research projects PID2020-116908GB-I00 and PID2020-117289GB-I00 financed by MCIN/AEI/10.13039/501100011033, and project CLT_2022_EXP_ARQ001SOLC_00000197 financed by the Culture Department of the Generalitat de Catalunya, as well as the consolidated research groups 2022 SGR 01188 and 2022 SGR 00620 (Generalitat de Catalunya), Ramón y Cajal grant (RYC2021-034366-I to J.M.) funded by MCIN/AEI/10.13039/501100011033 and by the European Union NextGenerationEU/PRTR, FI AGAUR fellowship (2021 FI_B 00524 and 2022 FI_B1 00131 to O.M.G.) funded by the Secretaria d'Universitats i Recerca de la Generalitat de Catalunya and the European Social Fund. We want to thank our colleagues Doug M. Boyer and Stephen G. B. Chester for providing insightful comments and suggestions that greatly improved an earlier version of the manuscript. We thank Julien Clavel for providing the script for the discriminant analysis. We thank the team of the online repository Morphosource and the following US institutions for providing access to specimens: Museum of Natural History (NY), Duke Lemur Center Division of Fossil Primates (NC), National Museum of Natural History (Washington DC), University of California, Berkeley Museum of Paleontology (CA), University of Michigan Museum of Paleontology (MI), University of Wyoming (WY), and Stony Brook University (NY). We also thank the Leakey Foundation General Research Grant (to Stephen G. B. Chester). This article is part of the Ph.D. dissertation of O.M.G. within the Geology Ph.D. program of the Universitat Autònoma de Barcelona.

Author contributions

O.M.G., A.-C.F., and J.M. designed the research; O.M.G., A. D., A.-C.F., and J.M. carried out the research; O.M.G. and J.M. performed data collection; O.M.G., A.-C.F., and J.M. analyzed the data; and O.M.G., D.M.A., A.-C.F., and J.M. wrote the paper.

Supplementary Online Material

Supplementary Online Material to this article can be found online at https://doi.org/10.1016/j.jhevol.2023.103395.

References

Adams, D.C., Otárola-Castillo, E., 2013. Geomorph: An r package for the collection and analysis of geometric morphometric shape data. Methods Ecol. Evol. 4, 393–399. https://doi.org/10.1111/2041-210X.12035.

Adler, D., Murdoch, D., 2020. Rgl: 3D visualization using openGL. https://github.com/dmurdoch/rgl. https://dmurdoch.github.io/rgl/.

Alfaro, M.E., Bolnick, D.I., Wainwright, P.C., 2005. Evolutionary consequences of many-to-one mapping of jaw morphology to mechanics in labrid fishes. Am. Nat. 165, E140–E154. https://doi.org/10.1086/429564.

Anemone, R.L., Covert, H.H., 2000. New skeletal remains of *Omomys* (Primates, Omomyidae): Functional morphology of the hindlimb and locomotor behavior of a Middle Eocene primate. J. Hum. Evol. 38, 607–633. https://doi.org/10.1006/jhev.1999.0371.

Ankel-Simons, F., 2007. Primate Anatomy, 3rd ed. Academic Press, Burlington.

Arnold, C., Matthews, L.J., Nunn, C.L., 2010. The 10kTrees website: A new online resource for primate phylogeny. Evol. Anthropol. 19, 114–118. https://doi.org/10.1002/evan.20251.

Beard, K.C., Dagosto, M., Gebo, D.L., Godinot, M., 1988. Interrelationships among primate higher taxa. Nature 331, 712–714. https://doi.org/10.1038/331712a0.

Bloch, J.I., Boyer, D.M., 2002. Grasping primate origins. Science 298, 1606–1610. https://doi.org/10.1126/science.1078249.

Bloch, J.I., Silcox, M.T., Boyer, D.M., Sargis, E.J., 2007. New Paleocene skeletons and the relationship of plesiadapiforms to crown-clade primates. Proc. Natl. Acad. Sci. USA 104, 1159–1164. https://doi.org/10.1073/pnas.0610579104.

Bookstein, F.L., Gunz, P., Mitterœcker, P., Mitteroecker, P., Prossinger, H., Schaefer, K., Horst, S., 2003. Cranial integration in *Homo*: Singular warps analysis of the midsagittal plane in ontogeny and evolution. J. Hum. Evol. 44, 167–187. https://doi.org/10.1016/S0047-2484(02)00201-4.

Boyer, D.M., Gingerich, P.D., 2019. Skeleton of late Paleocene *Plesiadapis cookei* (Mammalia, Euarchonta): life history, locomotion, and phylogenetic relationships. Univ. Michigan Pap. Paleontol. 38, 1–269.

Boyer, D.M., Seiffert, E.R., Gladman, J.T., Bloch, J.I., 2013. Evolution and allometry of calcaneal elongation in living and extinct primates. PLoS One 8, e67792. https://doi.org/10.1371/journal.pone.0067792.

Boyer, D.M., Yapuncich, G.S., Butler, J.E., Dunn, R.H., Seiffert, E.R., 2015. Evolution of postural diversity in primates as reflected by the size and shape of the medial tibial facet of the talus. Am. J. Phys. Anthropol. 157, 134–177. https://doi.org/10.1002/ajpa.22702.

Boyer, D.M., Toussaint, S., Godinot, M., 2017a. Postcrania of the most primitive euprimate and implications for primate origins. J. Hum. Evol. 111, 202–211. https://doi.org/10.1016/j.jhevol.2017.07.005.

Boyer, D.M., Gunnell, G.F., Kaufman, S., McGeary, T.M., 2017b. Morphosource: Archiving and sharing 3-d digital specimen data. Paleontol. Soc. Pap. 22, 157–181. https://doi.org/10.1017/scs.2017.13.

Boyer, D.M., Yapuncich, G.S., Dunham, N.T., McNamara, A., Shapiro, L.J., Hieronymus, T.L., Young, J.W., 2019. My branch is your branch: Talar morphology correlates with relative substrate size in platyrrhines at Tiputini Biodiversity Station, Ecuador. J. Hum. Evol. 133, 23–31. https://doi.org/10.1016/j.jhevol.2019.05.012.

Cartmill, M., 1974. Rethinking primate origins. Science 184, 14–21. https://doi.org/10.1126/science.184.4135.436.

Cartmill, M., 1992. New views on primate origins. Evol. Anthropol. 1, 105–111. https://doi.org/10.1002/evan.1360010308.

Castiglione, S., Serio, C., Tamagnini, D., Melchionna, M., Mondanaro, A., Di Febbraro, M., Profico, A., Piras, P., Barattolo, F., Raia, P., 2019. A new, fast method to search for morphological convergence with shape data. PLoS One 14, e0226949. https://doi.org/10.1371/journal.pone.0226949.

Chester, S.G.B., Bloch, J.I., Boyer, D.M., Clemens, W.A., 2015. Oldest known euarchontan tarsals and affinities of Paleocene *Purgatorius* to primates. Proc. Natl. Acad. Sci. USA 112, 1487–1492. https://doi.org/10.1073/pnas.1421707112.

Clavel, J., Escarguel, G., Merceron, G., 2015. mvMORPH: An R package for fitting multivariate evolutionary models to morphometric data. Methods Ecol. Evol. 6, 1311–1319. https://doi.org/10.1111/2041-210X.12420.

Clavel, J., Aristide, L., Morlon, H., 2019. A penalized likelihood framework for high-dimensional phylogenetic comparative methods and an application to new-world monkeys brain evolution. Syst. Biol. 68, 93–116. https://doi.org/10.1093/sysbio/syy045.

Clavel, J., Morlon, H., 2020. Reliable phylogenetic regressions for multivariate comparative data: Illustration with the MANOVA and application to the effect of diet on mandible morphology in phyllostomid bats. Syst. Biol. 69, 927–943. https://doi.org/10.1093/sysbio/syaa010.

Conroy, G.C., Rose, M.D., 1983. The evolution of the primate foot from the earliest primates to the Miocene hominoids. Foot Ankle 3, 342–364. https://doi.org/10.1177/107110078300300604.

Covert, H.H., 1988. Ankle and foot morphology of *Cantius mckennai*: Adaptations and phylogenetic implications. J. Hum. Evol. 17, 57–70. https://doi.org/10.1016/0047-2484(88)90049-8.

Crompton, R.H., Lieberman, S.S., Oxnard, C.E., 1987. Morphometrics and niche metrics in prosimian locomotion: An approach to measuring locomotion, habitat, and diet. Am. J. Phys. Anthropol. 73, 149–177. https://doi.org/10.1002/ajpa.1330730203.

Dagosto, M., 1985. The distal tibia of primates with special reference to the Omomyidae. Int. J. Primatol. 6, 45–75. https://doi.org/10.1007/BF02693696.

Dagosto, M., 1988. Implications of postcranial evidence for the origin of euprimates. J. Hum. Evol. 17, 35–56. https://doi.org/10.1016/0047-2484(88)90048-6.

Dagosto, M., 2007. The postcranial morphotype of primates. In: Ravosa, M.J., Dagosto, M. (Eds.), Primate Origins: Adaptations and Evolution. Springer US, Boston, pp. 489–534. https://doi.org/10.1007/978-0-387-33507-0_15.

Dagosto, M., Marivaux, L., Gebo, D.L., Beard, K.C., Chaimanee, Y., Jaeger, J.-J., Marandat, B., Soe, A.N., Kyaw, A.A., 2010. The phylogenetic affinities of the Pondaung tali. Am. J. Phys. Anthropol. 143, 223–234. https://doi.org/10.1002/ajpa.21308.

Decker, R.L., Szalay, F.S., 1974. Origins and function of the pes in the Eocene Adapidae (Lemuriformes, Primates). In: Jenkins, F.A. (Ed.), Primate Locomotion. Academic Press, New York, pp. 261–291. https://doi.org/10.1016/B978-0-12-384050-9.50014-3.

Demes, B., Günther, M.M., 1989. Biomechanics and allometric scaling in primate locomotion and morphology. Folia Primatol. 53, 125–141. https://doi.org/10.1159/000156412.

Demes, B., Jungers, W.L., Fleagle, J.G., Wunderlich, R.E., Richmond, B.G., Lemelin, P., 1996. Body size and leaping kinematics in Malagasy vertical clingers and leapers. J. Hum. Evol. 31, 367–388. https://doi.org/10.1006/jhev.1996.0066.

Demes, B., Fleagle, J.G., Jungers, W.L., 1999. Takeoff and landing forces of leaping strepsirhine primates. J. Hum. Evol. 37, 279–292. https://doi.org/10.1006/jhev.1999.0311.

Dunn, R.H., 2010. Additional postcranial remains of omomyid primates from the Uinta Formation, Utah and implications for the locomotor behavior of large-bodied omomyids. J. Hum. Evol. 58, 406–417. https://doi.org/10.1016/j.jhevol.2010.02.010.

Dunn, R.H., Sybalsky, J.M., Conroy, G.C., Rasmussen, D.T., 2006. Hindlimb adaptations in *Ourayia* and *Chipetaia*, relatively large-bodied omomyine primates from the Middle Eocene of Utah. Am. J. Phys. Anthropol. 131, 303–310. https://doi.org/10.1002/ajpa.20407.

Fleagle, J.G., 2013. Primate Adaptation and Evolution, 3rd ed. Academic Press, San Diego. https://doi.org/10.1016/B978-0-12-378632-6.00005-7.

Gebo, D.L., 1985. The nature of the primate grasping foot. Am. J. Phys. Anthropol. 67, 269–277. https://doi.org/10.1002/ajpa.1330670312.

Gebo, D.L., 1986. Anthropoid origins—The foot evidence. J. Hum. Evol. 15, 421–430. https://doi.org/10.1016/S0047-2484(86)80025-2.

Gebo, D.L., 1987a. Locomotor diversity in prosimian primates. Am. J. Primatol. 13, 271–281. https://doi.org/10.1002/ajp.1350130305.

Gebo, D.L., 1987b. Functional anatomy of the tarsier foot. Am. J. Phys. Anthropol. 73, 9–31. https://doi.org/10.1002/ajpa.1330730103.

Gebo, D.L., 1988. Foot morphology and locomotor adaptation in Eocene primates. Folia Primatol. 50, 3–41. https://doi.org/10.1159/000156332.

Gebo, D.L., 1989. Postcranial adaptation and evolution in Lorisidae. Primates 30, 347–367. https://doi.org/10.1007/BF02381259.

Gebo, D.L., Dagosto, M., 1988. Foot anatomy, climbing, and the origin of the Indriidae. J. Hum. Evol. 17, 135–154. https://doi.org/10.1016/0047-2484(88)90052-8.

Gebo, D.L., Dagosto, M., Rose, K.D., 1991. Foot morphology and evolution in early Eocene *Cantius*. Am. J. Phys. Anthropol. 86, 51–73. https://doi.org/10.1002/ajpa.1330860105.

Gebo, D.L., Dagosto, M., Beard, K.C., Qi, T., Wang, J., 2000. The oldest known anthropoid postcranial fossils and the early evolution of higher primates. Nature 404, 276–278. https://doi.org/10.1038/35005066.

Gebo, D.L., Dagosto, M., Beard, K.C., Qi, T., 2001. Middle Eocene primate tarsals from China: Implications for haplorhine evolution. Am. J. Phys. Anthropol. 116, 83–107. https://doi.org/10.1002/ajpa.1105.

Gebo, D.L., Smith, T., Dagosto, M., 2012. New postcranial elements for the earliest Eocene fossil primate *Teilhardina belgica*. J. Hum. Evol. 63, 205–218. https://doi.org/10.1016/j.jhevol.2012.03.010.

Gebo, D.L., Smith, R., Dagosto, M., Smith, T., 2015. Additional postcranial elements of *Teilhardina belgica*: The oldest European primate. Am. J. Phys. Anthropol. 156, 388–406. https://doi.org/10.1002/ajpa.22664.

Gelman, A., Rubin, D.B., 1992. Inference from iterative simulation using multiple sequences. Stat. Sci. 7, 457–511. https://doi.org/10.1214/ss/1177011136.

Gladman, J.T., Boyer, D.M., Simons, E.L., Seiffert, E.R., 2013. A calcaneus attributable to the primitive late Eocene anthropoid *Proteopithecus sylviae*: Phenetic affinities and phylogenetic implications. Am. J. Phys. Anthropol. 151, 372–397. https://doi.org/10.1002/ajpa.22266.

Godinot, M., Dagosto, M., 1983. The astragalus of *Necrolemur* (Primates, Microchoerinae). J. Paleontol. 57, 1321–1324.

Goodall, C., 1991. Procrustes methods in the statistical analysis of shape. J. R. Stat. Soc. B Stat. Methodol. 53, 285–339. https://doi.org/10.1111/j.2517-6161.1991.tb01825.x.

Hall-Crags, E.C.B., 1965. An analysis of the jump of the Lesser Galago (*Galago senegalensis*). Proc. Zool. Soc. 147, 20–29. https://doi.org/10.1111/j.1469-7998.1965.tb01874.x.

Hall-Craggs, E.C.B., 1966. Rotational movements in the foot of *Galago senegalensis*. Anat. Rec. 154, 287–293. https://doi.org/10.1002/ar.1091540211.

Hoffstetter, R., 1977. Phylogénie des Primates. Confrontation des résultats obtenus par les diverses voies d'approche du problème. Bull. Mem. Soc. Anthropol. Paris 13, 327–346. https://doi.org/10.3406/bmsap.1977.1886.

Hunt, K.D., Cant, J.G.H., Gebo, D.L., Rose, M.D., Walker, S.E., Youlatos, D., 1996. Standardized descriptions of primate locomotor and postural modes. Primates 37, 363–387. https://doi.org/10.1007/BF02381373.

Lewis, O.J., 1980a. The joints of the evolving foot. Part I. The ankle joint. J. Anat. 130, 527–543.

Lewis, O.J., 1980b. The joints of the evolving foot. Part II. The intrinsic joints. J. Anat. 130, 833–857.
Llera Martín, C.J., Rose, K.D., Sylvester, A.D., 2022. A morphometric analysis of early Eocene Euprimate tarsals from Gujarat, India. J. Hum. Evol. 164, 103141. https://doi.org/10.1016/j.jhevol.2022.103141.
Marigó, J., Minwer-Barakat, R., Moyà-Solà, S., 2011. New *Anchomomys* (Adapoidea, Primates) from the Robiacian (Middle Eocene) of northeastern Spain. Taxonomic and evolutionary implications. J. Hum. Evol. 60, 665–672. https://doi.org/10.1016/j.jhevol.2010.12.006.
Marigó, J., Roig, I., Seiffert, E.R., Moyà-Solà, S., Boyer, D.M., 2016. Astragalar and calcaneal morphology of the middle Eocene primate *Anchomomys frontanyensis* (Anchomomyini): Implications for early primate evolution. J. Hum. Evol. 91, 122—143. https://doi.org/10.1016/j.jhevol.2015.08.011.
Marigó, J., Minwer-Barakat, R., Moyà-Solà, S., Boyer, D.M., 2020. First navicular remains of a European adapiform (*Anchomomys frontanyensis*) from the Middle Eocene of the Eastern Pyrenees (Catalonia, Spain): Implications for early primate locomotor behavior and navicular evolution. J. Hum. Evol. 139, 102708. https://doi.org/10.1016/j.jhevol.2019.102708.
Marivaux, L., Beard, K.C., Chaimanee, Y., Dagosto, M., Gebo, D.L., Guy, F., Marandat, B., Khaing, K., Kyaw, A.A., Oo, M., Sein, C., Soe, A.N., Swe, M., Jaeger, J.-J., 2010. Talar morphology, phylogenetic affinities, and locomotor adaptation of a large-bodied amphipithecid primate from the late middle Eocene of Myanmar. Am. J. Phys. Anthropol. 143, 208–222. https://doi.org/10.1002/ajpa.21307.
Marivaux, L., Tabuce, R., Lebrun, R., Ravel, A., Adaci, M., Mahboubi, M., Bensalah, M., 2011. Talar morphology of azibiids, strepsirhine-related primates from the Eocene of Algeria: Phylogenetic affinities and locomotor adaptation. J. Hum. Evol. 61, 447–457. https://doi.org/10.1016/j.jhevol.2011.05.013.
Mitteroecker, P., Gunz, P., 2009. Advances in geometric morphometrics. Evol. Biol. 36, 235–247. https://doi.org/10.1007/s11692-009-9055-x.
Morton, D.J., 1924. Evolution of the human foot II. Am. J. Phys. Anthropol. 7, 1–52. https://doi.org/10.1002/ajpa.1330070114.
Moyà-Solà, S., Köhler, M., Alba, D.M., Roig, I., 2012. Calcaneal proportions in primates and locomotor inferences in *Anchomomys* and other Palaeogene Euprimates. Swiss J. Palaeontol. 131, 147–159. https://doi.org/10.1007/s13358-011-0032-5.
Napier, J.R., Walker, A.C., 1967. Vertical clinging and leaping — A newly recognized category of locomotor behaviour of primates. Folia Primatol. 6, 204–219. https://doi.org/10.1159/000155079.
Nyakatura, J.A., 2019. Early primate evolution: Insights into the functional significance of grasping from motion analyses of extant mammals. Biol. J. Linn. Soc. 127, 611–631. https://doi.org/10.1093/biolinnean/blz057.
Oxnard, C.E., Crompton, R.H., Lieberman, S.S., 1990. Animal Lifestyles and Anatomies. University of Washington Press, Seattle.
Plummer, M., Best, N., Cowles, K., Vines, K., 2005. CODA: Convergence diagnosis and output analysis for MCMC. R News 6, 7–11.
Qiao, Z., Zhou, L., Huang, J.Z., 2009. Sparse linear discriminant analysis with applications to high dimensional low sample size data. Int. J. Appl. Math. 39, 48–60.
R Core Team, 2022. R: A language and environment for statistical computing. R Foundation for Statistical Computing, Vienna.
Rasmussen, D.T., 1990. Primate origins: Lessons from a neotropical marsupial. Am. J. Primatol. 22, 263–277. https://doi.org/10.1002/ajp.1350220406.
Revell, L.J., 2012. phytools: An R package for phylogenetic comparative biology (and other things). Methods Ecol. Evol. 3, 217–223. https://doi.org/10.1111/j.2041-210X.2011.00169.x.
Rohlf, F.J., Slice, D., 1990. Extensions of the Procrustes method for the optimal superimposition of landmarks. Syst. Zool. 39, 40–59. https://doi.org/10.2307/2992207.
Rohlf, F.J., Corti, M., 2000. Use of two-block partial least-squares to study covariation in shape. Syst. Biol. 49, 740–753. https://doi.org/10.1080/106351500750049806.
Rose, K.D., 1994. The earliest primates. Evol. Anthropol. 3, 159–173. https://doi.org/10.1002/evan.1360030505.
Rose, K.D., Walker, A., 1985. The skeleton of early Eocene *Cantius*, oldest lemuriform primate. Am. J. Phys. Anthropol. 66, 73–89. https://doi.org/10.1002/ajpa.1330660107.
Rose, K.D., Chester, S.G.B., Dunn, R.H., Boyer, D.M., Bloch, J.I., 2011. New fossils of the oldest North American euprimate *Teilhardina brandti* (Omomyidae) from the Paleocene–Eocene thermal maximum. Am. J. Phys. Anthropol. 146, 281–305. https://doi.org/10.1002/ajpa.21579.
Sargis, E., 2002. The postcranial morphology of *Ptilocercus lowii* (Scandentia, Tupaiidae): An analysis of primatomorphan and volitantian characters. J. Mamm. Evol. 9, 137–160. https://doi.org/10.1023/A:1021387928854.
Sargis, E., 2004. New views on tree shrews: The role of tupaiids in primate supraordinal relationships. Evol. Anthropol. 13, 56–66. https://doi.org/10.1002/evan.10131.
Seiffert, E.R., Simons, E.L., 2001. Astragalar morphology of late Eocene anthropoids from the Fayum Depression (Egypt) and the origin of catarrhine primates. J. Hum. Evol. 41, 577–606. https://doi.org/10.1006/jhev.2001.0508.
Seiffert, E.R., Simons, E.L., Clyde, W.C., Rossie, J.B., Attia, Y., Bown, T.M., Chatrath, P., Mathison, M.E., 2005. Basal anthropoids from Egypt and the antiquity of Africa's higher primate radiation. Science 310, 300–304. https://doi.org/10.1126/science.1116569.
Seiffert, E.R., Costeur, L., Boyer, D.M., 2015. Primate tarsal bones from Egerkingen, Switzerland, attributable to the middle Eocene adapiform *Caenopithecus lemuroides*. PeerJ 3, e1036. https://doi.org/10.7717/peerj.1036.
Silcox, M.T., Sargis, E.J., Bloch, J.I., Boyer, D.M., 2015. Primate origins and supraordinal relationships: Morphological evidence. In: Henke, W., Tatterstall, I. (Eds.), Handbook of Paleoanthropology, 2nd ed. Springer, Heidelberg, pp. 1053–1081. https://doi.org/10.1007/978-3-642-39979-4_29.
Silcox, M.T., Bloch, J.I., Boyer, D.M., Chester, S.G.B., López-Torres, S., 2017. The evolutionary radiation of plesiadapiforms. Evol. Anthropol. 26, 74–94. https://doi.org/10.1002/evan.21526.
Su, A., Zeiniger, A., 2022. The primate ankle and hindfoot. In: Zeiniger, A., Hatala, K.G., Wunderlich, R.E., Schmitt, D. (Eds.), The Evolution of the Primate Foot. Anatomy, Function, and Palaeontological Evidence, 1st ed. Springer, Cham, pp. 21–45. https://doi.org/10.1007/978-3-031-06436-4_3.
Sussman, R.W., 1991. Primate origins and the evolution of angiosperms. Am. J. Primatol. 23, 209–223. https://doi.org/10.1002/ajp.1350230402.
Szalay, F.S., Decker, R.L., 1974. Origins, evolution, and function of the tarsus in late Cretaceous Eutheria and Paleocene primates. In: Jenkins, F.A. (Ed.), Primate Locomotion. Academic Press, New York, pp. 223–259. https://doi.org/10.1016/B978-0-12-384050-9.50013-1.
Szalay, F., Dagosto, M., 1980. Locomotor adaptations as reflected on the humerus of Paleogene primates. Folia Primatol. 34, 1–45. https://doi.org/10.1159/000155946.
Szalay, F.S., Drawhorn, G., 1980. Evolution and diversification of the Archonta in an arboreal milieu. In: Luckett, W.P. (Ed.), Comparative Biology and Evolutionary Relationships of Tree Shrews. Springer, Boston, pp. 133–169. https://doi.org/10.1007/978-1-4684-1051-8_4.
Szalay, F.S., Dagosto, M., 1988. Evolution of hallucial grasping in the primates. J. Hum. Evol. 17, 1–33. https://doi.org/10.1016/0047-2484(88)90047-4.
Torres-Tamayo, N., Schlager, S., García-Martínez, D., Sanchis-Gimeno, J.A., Nalla, S., Ogihara, N., Oishi, M., Martelli, S., Bastir, M., 2020. Three-dimensional geometric morphometrics of thorax-pelvis covariation and its potential for predicting the thorax morphology: A case study on Kebara 2 Neandertal. J. Hum. Evol. 147, 102854. https://doi.org/10.1016/j.jhevol.2020.102854.
Wainwright, P.C., Alfaro, M.E., Bolnick, D.I., Hulsey, C.D., 2005. Many-to-one mapping of form to function: A general principle in organismal design? Integr. Comp. Biol. 45, 256–262. https://doi.org/10.1093/icb/45.2.256.
Walker, A., 1974. Locomotor adaptations in past and present prosimian primates. In: Jenkins, F.A. (Ed.), Primate Locomotion. Academic Press, New York, pp. 349–381. https://doi.org/10.1016/B978-0-12-384050-9.50016-7.
Wiley, D., 2006. Landmark Editor 3.0. Institute for Data Analysis and Visualization, University of California, Davis.
Williams, B., Kay, R., Kirk, E., Ross, C., 2010. *Darwinius masillae* is a strepsirrhine—a reply to Franzen et al. (2009). J. Hum. Evol. 59, 567–573. https://doi.org/10.1016/j.jhevol.2010.01.003.
Willmott, C.J., Matsuura, K., 2005. Advantages of the mean absolute error (MAE) over the root mean square error (RMSE) in assessing average model performance. Clim. Res. 30, 79–82. https://doi:10.3354/cr030079.
Yapuncich, G.S., Seiffert, E.R., Boyer, D.M., 2017. Quantification of the position and depth of the *flexor hallucis longus* groove in euarchontans, with implications for the evolution of primate positional behavior. Am. J. Phys. Anthropol. 163, 367–406. https://doi.org/10.1002/ajpa.23213.
Yapuncich, G.S., Feng, H.F., Dunn, R.H., Seiffert, E.R., Boyer, D.M., 2019. Vertical support use and primate origins. Sci. Rep. 9, 12341. https://doi.org/10.1038/s41598-019-48651-x.
Yapuncich, G.S., Chester, S.G.B., Bloch, J.I., Boyer, D.M., 2022. The feet of Paleogene primates. In: Zeiniger, A., Hatala, K.G., Wunderlich, R.E., Schmitt, D. (Eds.), The Evolution of the Primate Foot. Anatomy, Function, and Palaeontological Evidence, 1st ed. Springer, Cham, pp. 277–319. https://doi.org/10.1007/978-3-031-06436-4_12.

Supplementary Online Material (SOM):

Early euprimates already had a diverse locomotor repertoire: Evidence from ankle bone morphology

Oriol Monclús-Gonzalo[a,1], David M. Alba[a], Anaïs Duhamel[b], Anne-Claire Fabre[c,d,e,1,*], Judit Marigó[f,a,1,*]

[a] *Institut Català de Paleontologia Miquel Crusafont, Universitat Autònoma de Barcelona, Edifici ICTA-ICP, c/ Columnes s/n, 08193 Cerdanyola del Vallès, Barcelona, Spain*

[b] *University of Lyon, ENSL, CNRS, LGL-TPE, Villeurbanne 69622, France*

[c] *Naturhistorisches Museum Bern, 3005 Bern, Switzerland*

[d] *Institute of Ecology and Evolution, University of Bern, 3012 Bern, Switzerland*

[e] *Life Sciences Department, Vertebrates Division, Natural History Museum, London SW7 5BD, UKu*

[f] *Universitat Autònoma de Barcelona, Departament de Geologia, 08193 Cerdanyola del Vallès, Barcelona, Spain*

[1]O.M.G, A.-C.F. and J.M. contributed equally to this work.

[*]**Corresponding authors.**

Email addresses: judit.marigo@uab.cat (J. Marigó), fabreac@gmail.com (A.-C. Fabre).

Author contributions

O.M.G., A.-C.F., and J.M. designed the research, O.M.G., A. D., A.-C.F., and J.M. carried out the research, O.M.G., and J.M. performed data collection; O.M.G., A.-C.F., and J.M. analyzed the data and O.M.G., D.M.A., A.-C.F., and J.M. wrote the paper.

SOM S1

Supplementary methods

Phylogenetic tree

A phylogenetic tree comprising all extant primates was downloaded from 10kTrees Project v.3 (Arnold et al., 2010). The fossil taxa were added to the tree using the function 'bind.tip' of the package phytools v. 0.7-20 (Revell, 2012). The branch lengths of extinct species were estimated from their chronostratigraphic range as reported in The Paleobiology Database (https://paleobiodb.org/). Extinct branches were grafted onto the base tree by sampling randomly within the length of the sister branch. Although there are phylogenetic uncertainties about many extinct taxa (especially omomyiforms and plesiadapiforms; Rose et al., 1994; Silcox et al., 2017) and disagreements between divergence times estimated from molecular and fossil data, recent molecular estimates tend to approach our current knowledge of the fossil record (Springer et al., 2012). Omomyidae indet. (UCMP V 134984, doi:10.17602/M2/M11994) was placed as the outgroup of *Arapahovius gazini* and *Tetonius homunculus* given similarities in navicular shape.

Type of foot posture

Biomechanically, the foot can be understood as a second-class lever, in which the muscular force (effort) is applied in the most proximal region of the calcaneus (tuber calcis), in order to raise the body mass (load) at the ankle joint by means of the rotation of the fulcrum. Primate foot posture type can be classified depending on the localization of the fulcrum (Morton, 1924). Animals that have a metatarsi-fulcrumating foot, such as the anthropoids and most living mammals, possess the fulcrum located in the metatarsal heads of the foot, whereas the tarsi-fulcrumating condition, represented by prosimians, is characterized by having the fulcrum located at the distal tarsal bones. Within the lemuriforms, however, indriids stand out

presenting a different type of foot posture (Gebo and Dagosto, 1988; Demes et al., 1996). Specifically, the indriid foot is not used as a propulsor but as a force transducer; it accommodates the extensive hip movements thanks to its increased midtarsal rotatory mobility. For this reason, in this study we classify indriids in a separate category of tarsi-rotators. Type of foot posture for each species is indicated in SOM Table S2.

Quantified locomotor behavior

Quantified locomotor behavior was based on percentages of locomotor behaviors compiled from the available literature and reviewed in Granatosky (2018). Compilation was done in order to include the minimum number of different authors, as an attempt to standardize the data. Still, different categories were used in the several field studies included in the dataset, hence we organized the percentages in six broad locomotor categories, following the descriptions for standardized primate locomotor modes presented in Hunt et al. (1996):

1. Leaping Leaping is characterized by a propulsive phase in which the hindlimbs are flexed back and extended from a first support, followed by an extended time of free flight and a relatively precise landing on a second support. The leap can be performed from a pronograde or vertical position. This category included 'Leaping' and 'Vertical leap', the latter used in studies that differentiated the support from which the leap was performed.
2. Quadrupedalism Quadrupedalism is the most common locomotor behavior observed in primates. It can be performed in an arboreal or terrestrial environment and on horizontal or oblique (<45º) supports. The torso should be pronograde or roughly parallel to the support and the gait must be regular and symmetrical. This category included 'Quadrupedal walking' (slow to medium speed), 'Quadrupedal running', 'Galloping,' and 'Bounding' (increasing the speed of the movement respectively).

Climbing Climbing is defined as a progression (ascent or descent) on supports angled >45º. All four limbs move in an irregular pattern with diverse hand and foot movements and positions. This category included 'Climbing', 'Vertical descent' (which encompasses both rump-first and head-first types of descent), and 'Scansorial' (referring to the habitual clinging positions displayed by callitrichids).

3. Suspension Suspension describes the locomotor activity in which the animal's body is held by at least one of the limbs in tension. This category included 'Bimanual suspension' and 'Quadrupedal suspension'.

4. Bridging Bridging is a gap-closing movement that involves the hands reaching out for another support followed by the rest of the body and finally by the two feet, allowing the animal to reach the new support and cross the gap. This category included 'Bridging' and 'Inverted bridging', which is the opposite movement (starting with the feet or tail reaching the distant support, followed by the body and finally the hands).

5. Scrambling/Clambering 'Scrambling' is defined as a pronograde and non-suspensory progression lacking a regular gait. Similarly, 'Clambering' is also a non-suspensory progression that is not accompanied by a regular gait, yet the body is held in an orthograde position. This category included 'Scrambling/Clambering'.

We obtained the locomotor percentages of extant species from Granatosky (2018) for each locomotor variable designed in our study, an arcsine square root transformation of the data was performed. This is a standard procedure for analyzing proportional ecological data that makes the variances more constant throughout the sample and approximate the data to a more normal distribution (Sokal and Rohlf, 1995).

Locomotor categories

Living euprimate species have been classified in seven different locomotor categories regarding their observed locomotor behavior (see references in SOM Table S2). A principal component analysis was performed to assess if these categories matched the locomotor percentages directly derived from field studies (SOM Table S2; SOM Fig. S3).

1. Arboreal quadrupeds/large leapers This category encompasses those primates whose main locomotor mode is quadrupedalism, although they can engage in other activities such as leaping, climbing, or suspension. This category included the lemurids (except for *Hapalemur griseus*), *Daubentonia madagascariensis*, the cebids, the pitheciids, and the atelid *Alouatta palliatta*.

2. Cheirogaleid generalists This category includes all the representatives of Cheirogaleidae in our study: *Microcebus murinus*, *Microcebus rufus*, *Mirza coquereli*, *Mirza zaza*, *Cheirogaleus major*, and *Cheirogaleus medius*. Despite the different degrees of proclivity for leaping shown by cheirogaleids in their locomotor behavior (*Microcebus* and *Mirza* with the greatest proclivity for leaping, while *Cheirogaleus* relies less on leaping), all perform a diverse range of movements such as bridging, cantilevering, and climbing small supports, although scurrying with the body held close to the support is the main locomotor mode.

3. Clawed leapers This category includes the members of Callitrichidae, due to their very characteristic locomotor repertoire. Callitrichids are the smallest group of New World monkeys and display characteristic adaptations to clinging on tree trunks: all digits except for the great toe end in claw-like teguale. This trait allows them to engage in vertical clinging and leaping behavior on large vertical supports.

4. Large vertical clingers and leapers This category includes the indriids, *Lepilemur mustelinus* and *Hapalemur griseus*. They are all characterized by medium to large body mass and a dominant leaping component in their locomotor behavior as well as a clinging posture on vertical supports. Contrary to other primates that leap from one horizontal or oblique support to another, large

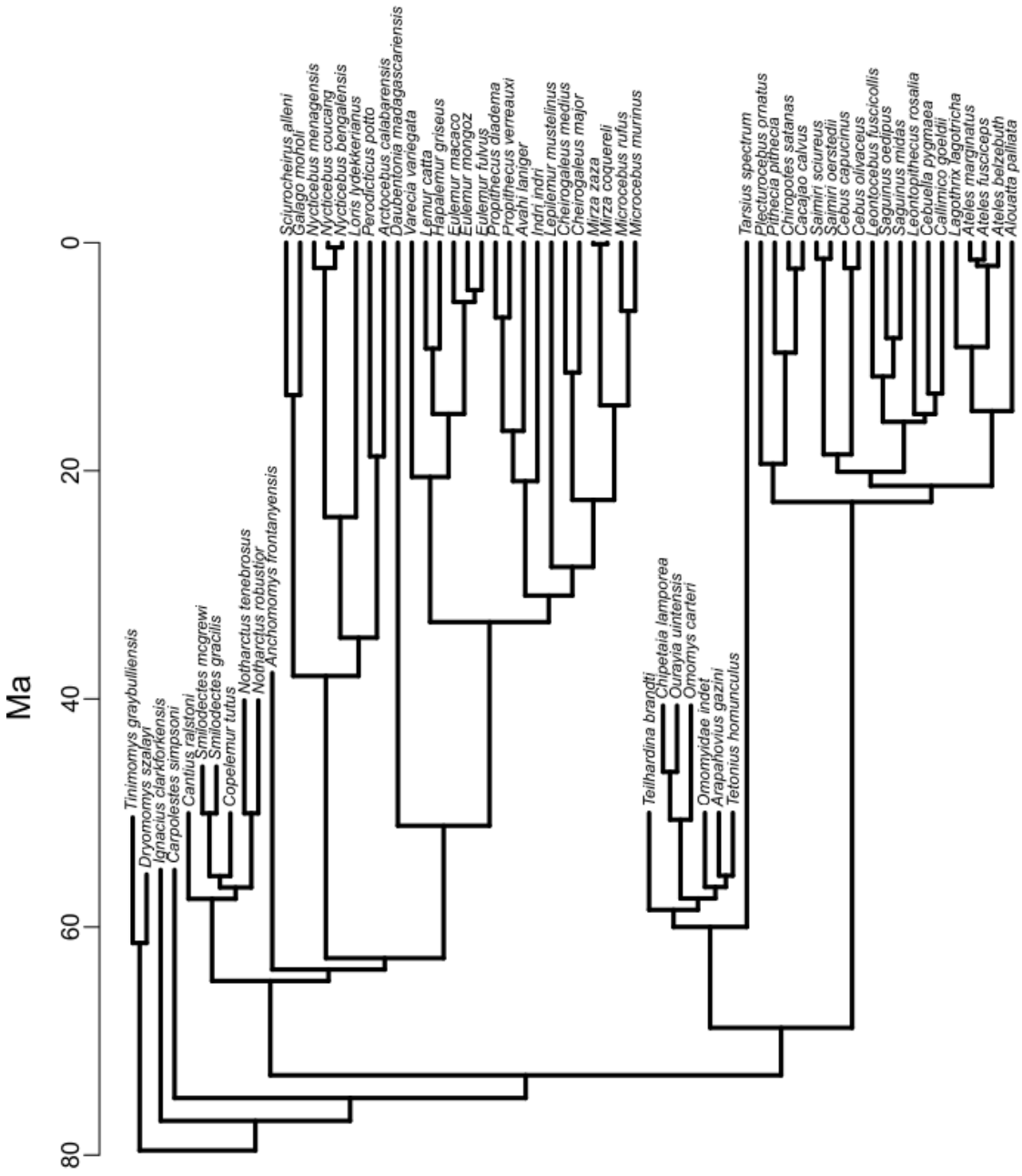
vertical clingers and leapers (LVCL) start their leap from a torso-orthograde clinging posture on vertical supports, with a propulsive force powered by their hindlimbs.

5. Slow climbers This category is represented by the species of Lorisidae. Lorisid locomotor repertoire resembles that of *Cheirogaleus*, but their movements are more deliberate and they never leap. They show the highest component of bridging and suspension among prosimians, although also move quadrupedally along horizontal supports.

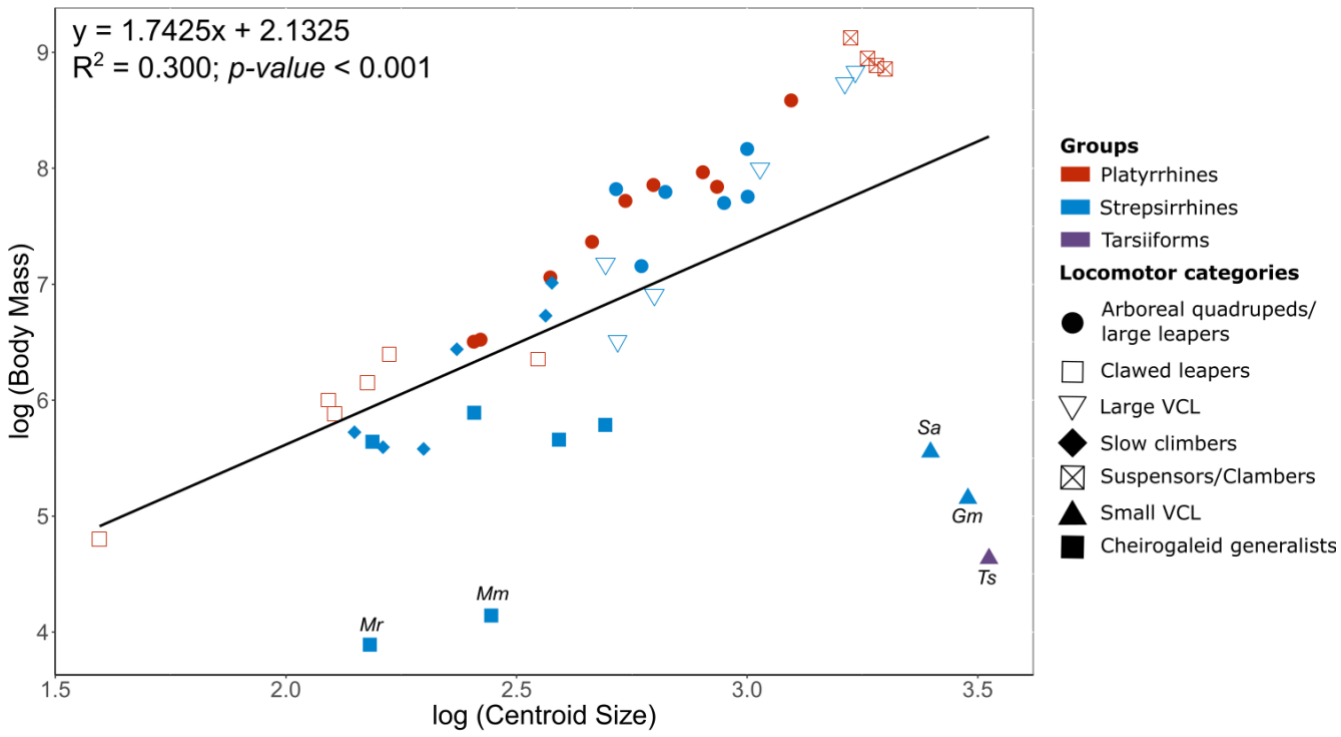
6. Small vertical clingers and leapers This category encompasses the small galagids and *Tarsius spectrum*. As with the LVCL, small galagids and *T. spectrum* are specialized leapers that perform large leaps with relatively high frequency from one vertical support to another, in which they cling between jumps. However, some forms like *Galago moholi* also display some degree of scurrying behavior, similar to the cheirogaleids.

7. Suspensors/Clambers This category includes the atelids except for *Alouatta palliata*. They engage in both quadrupedal and suspensory behaviors, the latter performed with the four limbs and the tail, which is prehensile. In some aspects of their locomotor behavior, they show convergence with apes.

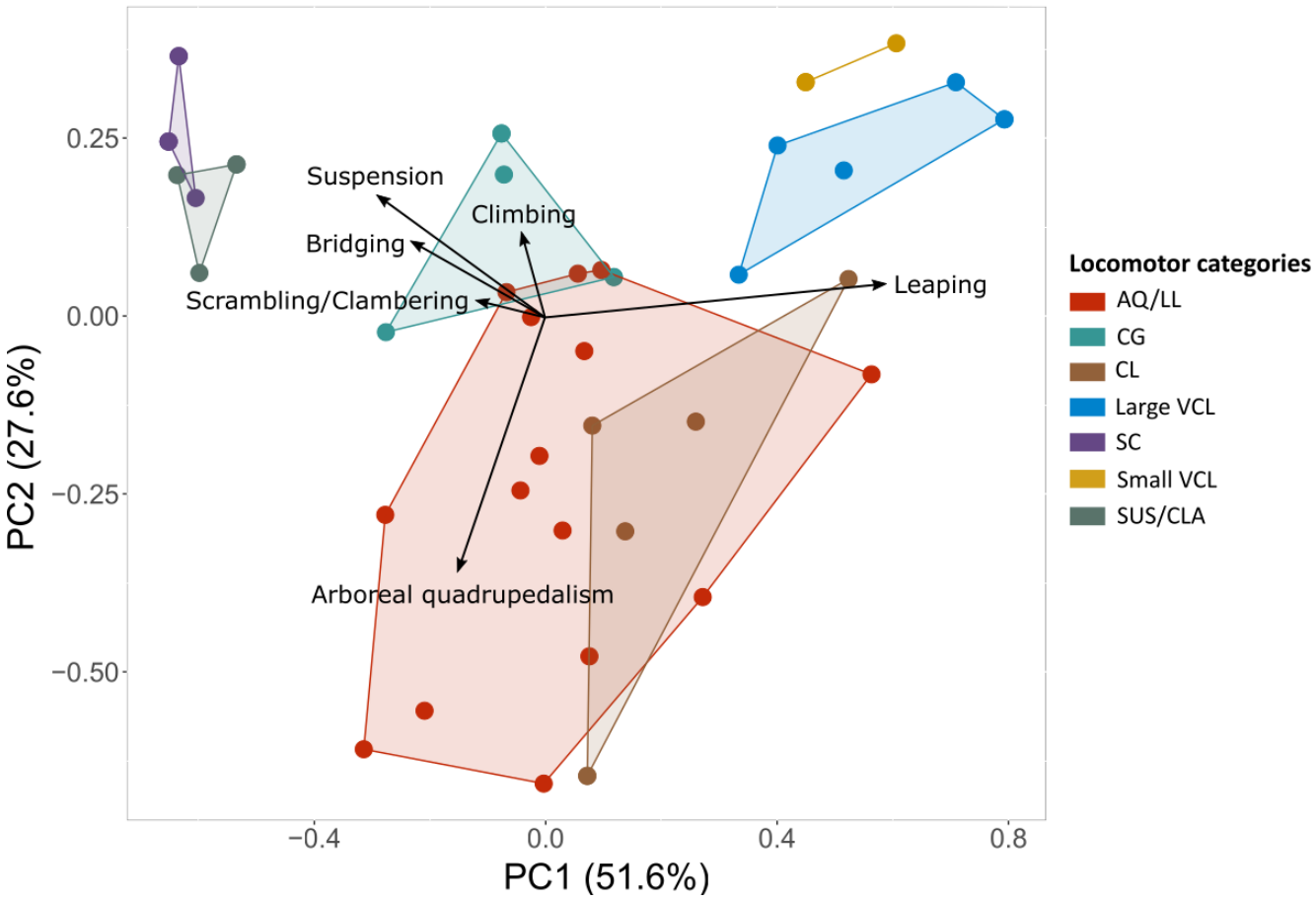
After performing the PCA on the quantified locomotor behavior of extant species (SOM Fig. S3), we confirmed that the locomotor categories attributed to each species fitted their quantified locomotor behavior as compiled in Granatosky (2018). Moreover, each locomotor category forms a distinct cluster; clawed leapers are the exception as they overlap with the arboreal quadrupeds/large leapers.



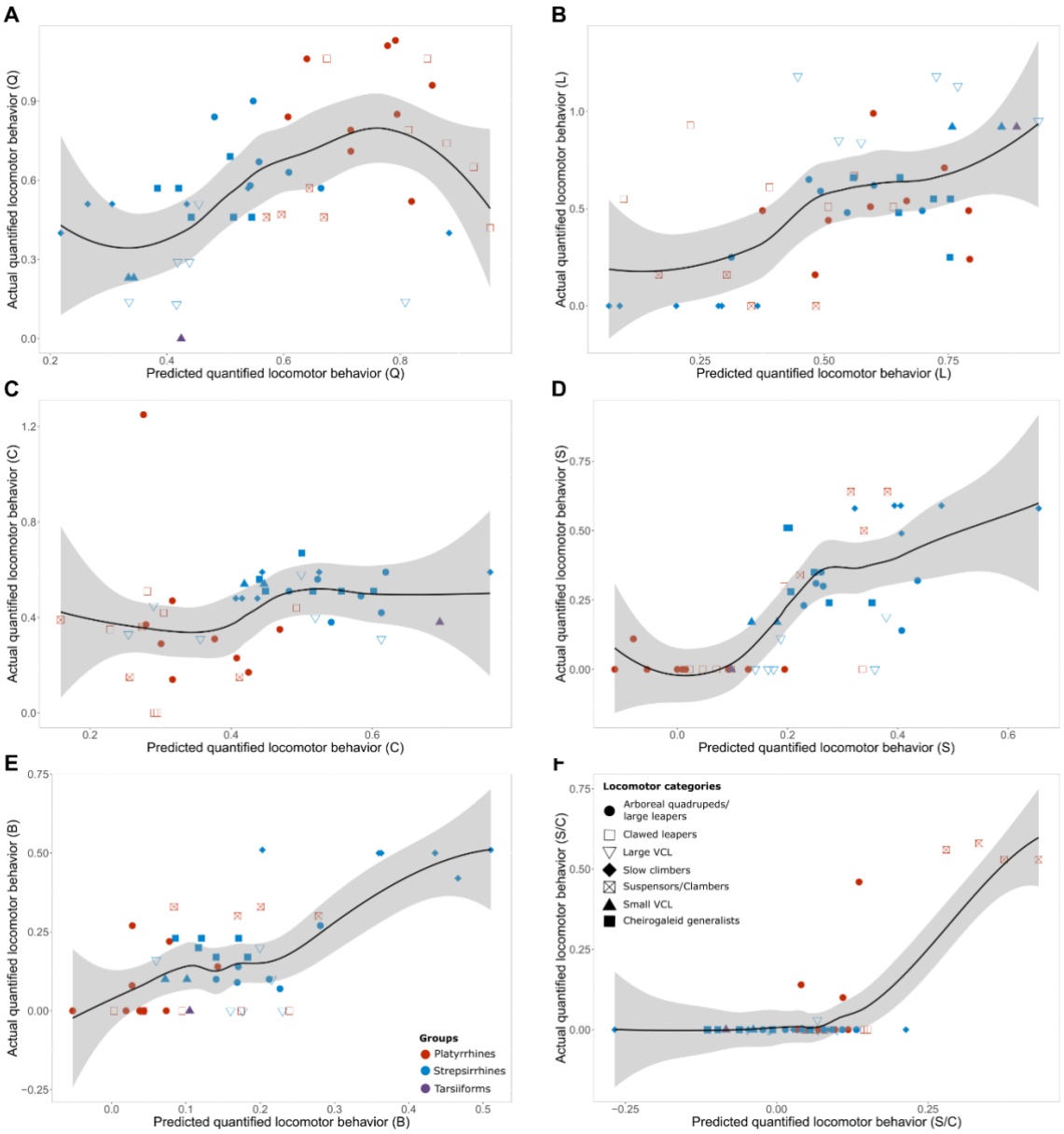
SOM Figure. S1. Phylogenetic tree of the extant and extinct species included in the analyses. The phylogenetic tree was downloaded from 10kTrees Project v. 3 (Arnold et al., 2010). The fossil taxa were added manually to the tree by sampling randomly within the length of the sister branch and following the chronostratigraphic range provided in The Paleobiology Database (https://paleobiodb.org/).



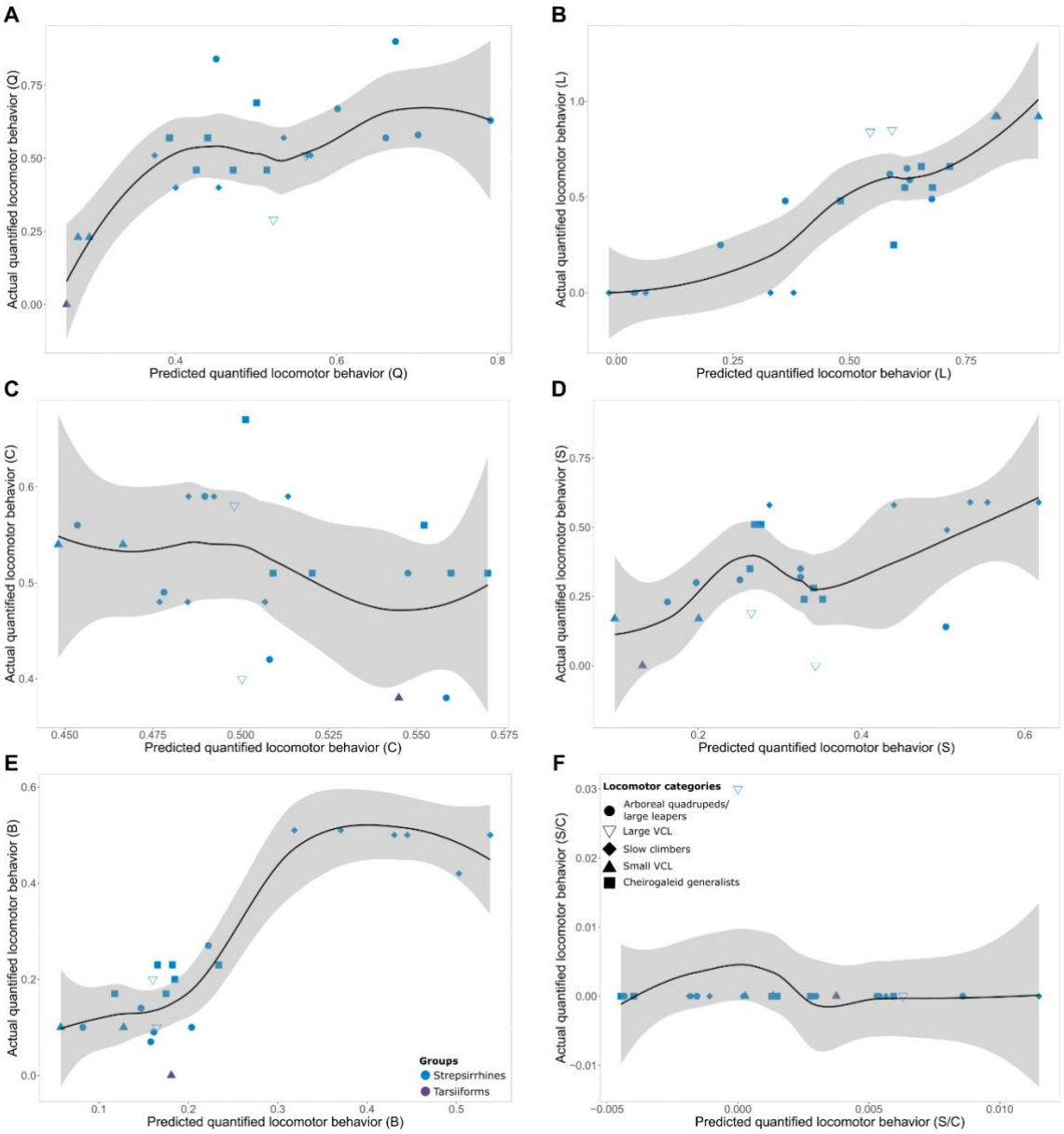
SOM Figure S2. Bivariate regression between the log_{10}-transformed centroid size and log_{10}-transformed body mass of the extant primate species of the sample. Data points are color-coded by taxonomic groups and shape-coded by locomotor category. The intercept and the slope, as well as the r^2 and the *p*-value are indicated in the scatterplot. The small vertical clingers and leapers (Ts = *Tarsius spectrum*; *Gm* = *Galago moholi*; *Sa* = *Sciurocheirus alleni*), as well as the small-sized generalists mouse lemurs (Mm = *Microcebus murinus*; Mr = *Microcebus rufus*) clearly depart from the best-fit line displayed by other species.



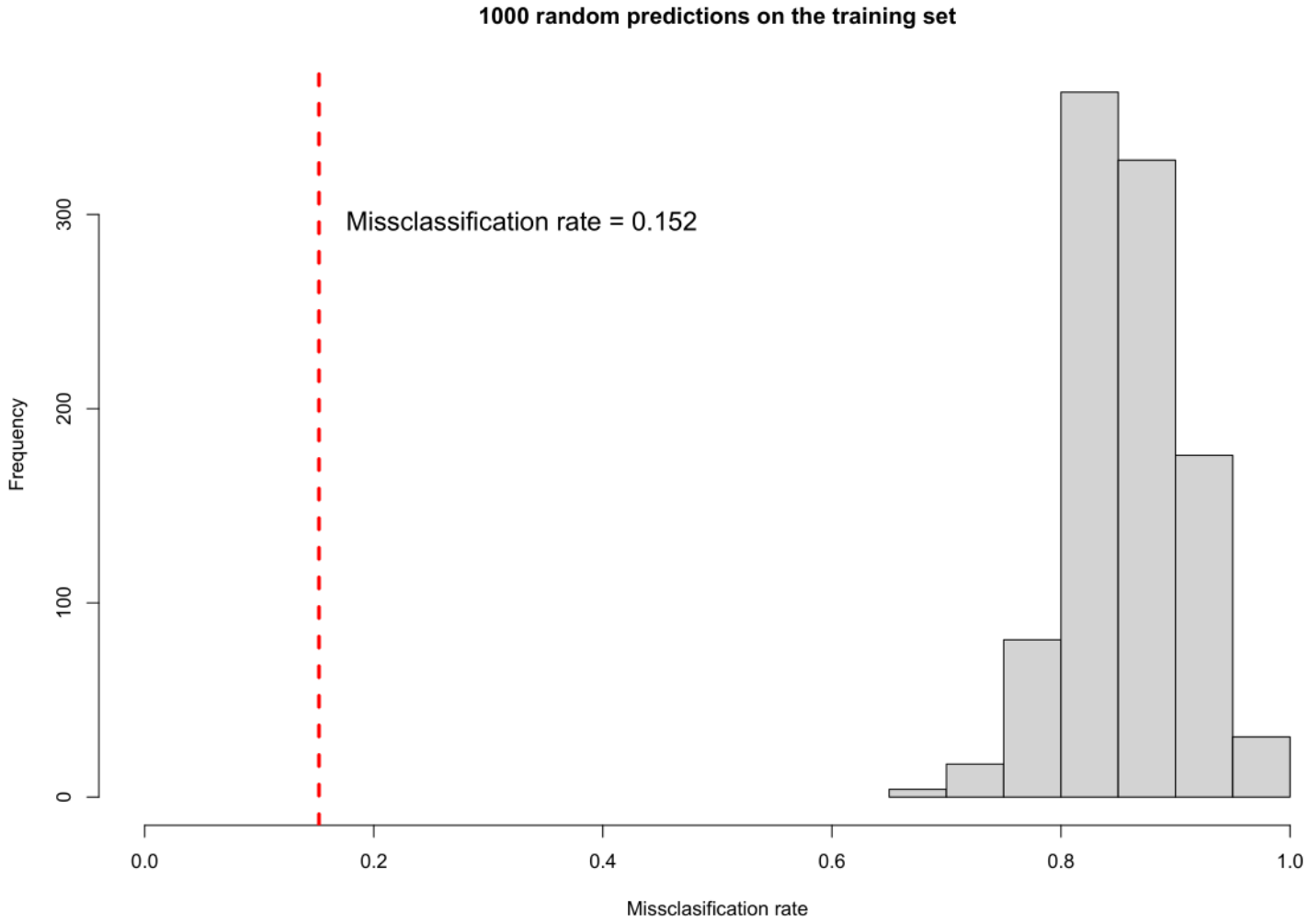
SOM Figure S3. Principal component analysis of the quantified locomotor data (SOM Table S2). Data points are color-coded by locomotor category. Loadings corresponding to each locomotor variable are displayed to show which locomotor variables influence more each locomotor category. Abbreviations: AQ/LL = arboreal quadrupeds/large leapers; CG = cheirogaleid generalists; CL = clawed leapers; Large VCL = large vertical clingers and leapers; SC = slow climbers; SUS/CLA = suspensors/clamberers.



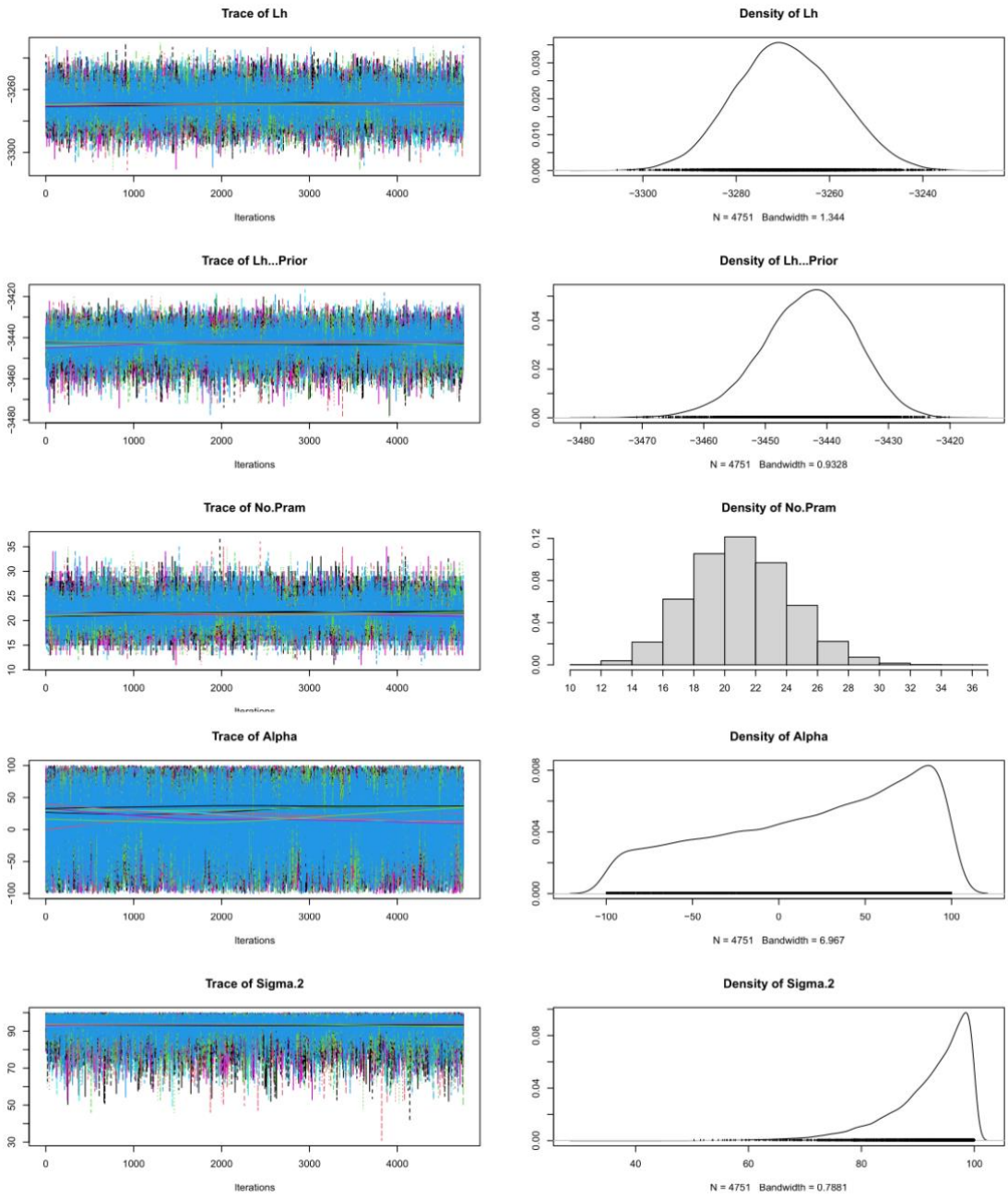
SOM Figure S4. Bivariate plots between the predicted and the actual quantified locomotor behavior among the entire extant sample. Estimation of the quantified locomotor behavior was assessed by performing a leave-one-out cross-validation on each extant species (see Materials and methods). The gray shadow represents the 95% confidence interval after performing a local polynomial regression fitting (Cleveland et al., 1992).



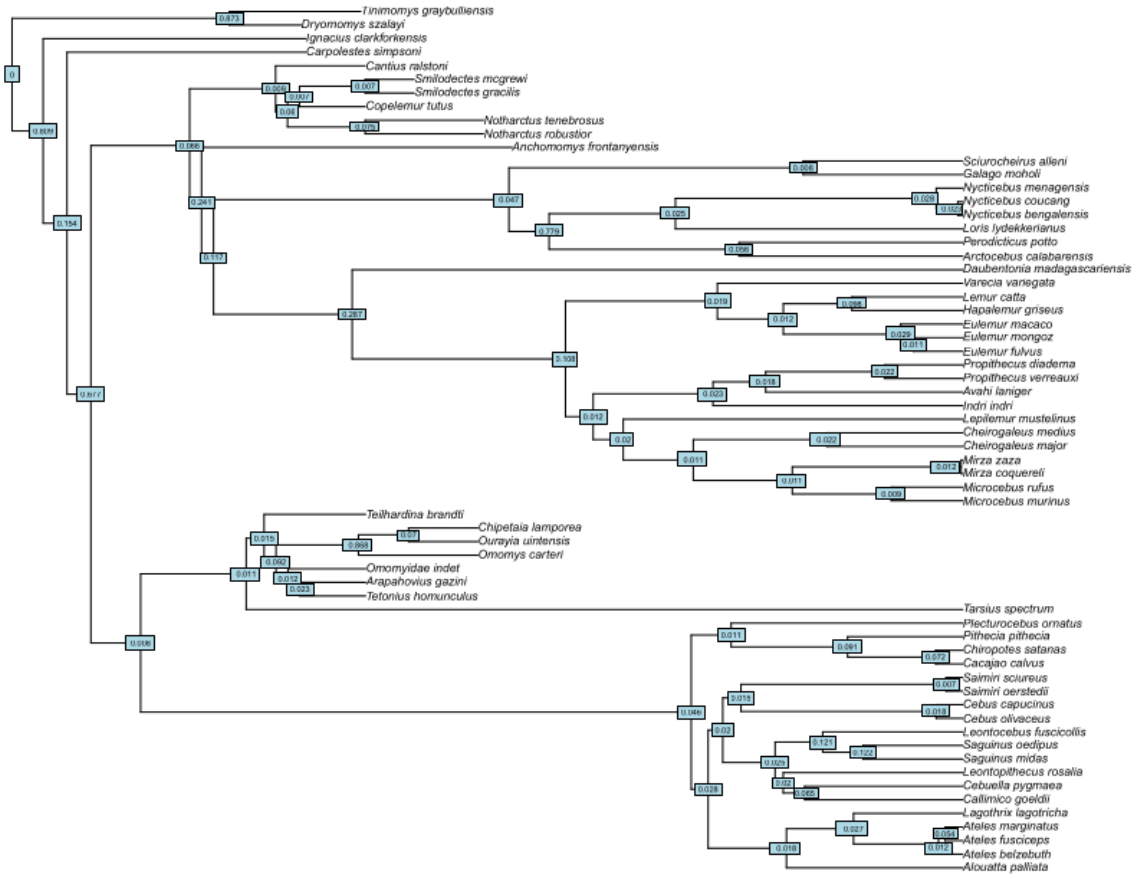
SOM Figure S5. Bivariate plots between the predicted and the actual quantified locomotor behavior among extant tarsi-fulcrumators. Estimation of the quantified locomotor behavior was assessed by performing a leave-one-out cross-validation on each extant tarsi-fulcrumator species (see Materials and methods). The gray shadow represents the 95% confidence interval after performing a local polynomial regression fitting (Cleveland et al., 1992).



SOM Figure S6. Missclassification rate for discriminant predictions compared to 1000 randomized predictions on the training set.



SOM Figure S7. Combined trace plots of the ten independent chains ran for the analysis (see Materials and methods). Supplementary Online Material Tables S4 and S5 provide the effective sample size of each independent chain and Gelman and Rubin's convergence diagnostic analysis (Gelman and Rubin, 1992) for the whole independent chains.



SOM Figure S7. Phylogenetic tree with the mean posterior probabilities of rate shifts in evolutionary rate for all ten independent chains.

SOM Table S1

Complete list of all the specimens used, institutions where they are housed, and scan details used to obtain the three-dimensional models, provided separately as an Excel file.

SOM Table S2

Type of foot, body mass, locomotor categories, and quantified locomotor behavior of living primate species included in this study.

Species	Family	Superfamily	Type of foot	Body mass (g)	Locomotor category[a]	Quantified locomotor behavior						References
						Arboreal quadrupedalism	Leaping	Climbing	Suspension	Bridging	Scrambling/clambering	
Alouatta palliata	Atelidae	Ceboidea	Metatarsi-fulcrumator	5350	AQ/LL	1.13	0.16	0.29	0	0.22	0	Bezanson (2009); Fleagle, (2013)
Ateles belzebuth	Atelidae	Ceboidea	Metatarsi-fulcrumator	7250	SUS/CLA	0.47	0	0.36	0.5	0.33	0.56	Cant et al. (2001, 2003); Fleagle (2013)
Ateles fusciceps[b]	Atelidae	Ceboidea	Metatarsi-fulcrumator	9160	SUS/CLA	0.46	0.16	0.15	0.64	0.30	0.53	Youlatos (2002); Fleagle (2013)
Ateles marginatus[b]	Atelidae	Ceboidea	Metatarsi-fulcrumator	7690	SUSU/CLA	0.46	0.16	0.15	0.64	0.30	0.53	Fleagle and Mittermeier (1980); Youlatos (2002); Fleagle, 2013)
Lagothrix lagotricha	Atelidae	Ceboidea	Metatarsi-fulcrumator	7020	SUS/CLA	0.57	0	0.39	0.34	0.33	0.58	Cant et al. (2001, 2003); Fleagle (2013)
Callimico goeldii	Callitrichidae	Ceboidea	Metatarsi-fulcrumator	468	CL	0.42	0.93	0.44	0	0	0	Garber and Leigh (2001); Fleagle (2013)
Cebuella pygmaea	Callitrichidae	Ceboidea	Metatarsi-fulcrumator	122	CL	0.79	0.55	0.42	0	0	0	Jackson (2011); Fleagle (2013)
Leontopithecus rosalia	Callitrichidae	Ceboidea	Metatarsi-fulcrumator	598	CL	0.74	0.61	0.35	0.30	0	0	Rosenberger and Stafford (1994); Fleagle (2013)
Saguinus midas	Callitrichidae	Ceboidea	Metatarsi-fulcrumator	575	CL	1.06	0.51	0	0	0	0	Fleagle and Mittermeier (1980); Fleagle (2013)
Saguinus oedipus[c]	Callitrichidae	Ceboidea	Metatarsi-fulcrumator	404	CL	1.06	0.51	0	0	0	0	Fleagle and Mittermeier (1980); Fleagle (2013)
Leontocebus fuscicollis	Callitrichidae	Ceboidea	Metatarsi-fulcrumator	358	CL	0.65	0.67	0.51	0	0	0	Garber and Leigh (2001); Fleagle 2013)

Cebus olivaceus	Cebidae	Ceboidea	Metatarsi-fulcrumator	2250	AQ/LL	0.79	0.54	1.25	0	0.27	0.14	Wright (2007); Fleagle (2013)
Cebus capucinus	Cebidae	Ceboidea	Metatarsi-fulcrumator	2540	AQ/LL	1.06	0.24	0.35	0	0.08	0.10	Bezanson (2009); Fleagle (2013)
Saimiri oerstedii	Cebidae	Ceboidea	Metatarsi-fulcrumator	680	AQ/LL	0.85	0.49	0.47	0.11	0	0	Johnson and Shapiro (1998); Fleagle (2013)
Saimiri sciureus	Cebidae	Ceboidea	Metatarsi-fulcrumator	668	AQ/LL	0.84	0.71	0.17	0	0	0	Fleagle and Mittermeier (1980); Fleagle (2013)
Cacajao calvus	Pitheciidae	Ceboidea	Metatarsi-fulcrumator	2880	AQ/LL	0.71	0.49	0.37	0	0.14	0.46	Walker (1996); Fleagle (2013)
Chiropotes satanas	Pitheciidae	Ceboidea	Metatarsi-fulcrumator	2580	AQ/LL	1.11	0.44	0.14	0	0	0	Fleagle and Mittermeier (1980); Fleagle (2013)
Pithecia pithecia	Pitheciidae	Ceboidea	Metatarsi-fulcrumator	1580	AQ/LL	0.52	0.99	0.23	0	0	0	Fleagle and Meldrum (1988); Fleagle (2013)
Plecturocebus ornatus[d]	Pitheciidae	Ceboidea	Metatarsi-fulcrumator	1163	AQ/LL	0.96	0.51	0.31	0	0	0	Lawler et al. (2006); Fleagle (2013)
Tarsius spectrum	Tarsiidae	Tarsioidea	Tarsi-fulcrumator	103	SVCL	0	0.92	0.38	0	0	0	MacKinnon and MacKinnon (1980); Fleagle (2013)
Microcebus murinus	Cheirogaleidae	Lemuroidea	Tarsi-fulcrumator	63	CG	0.57	0.66	0.51	0.24	0.17	0	Gebo (1987); Fleagle (2013)
Microcebus rufus[e]	Cheirogaleidae	Lemuroidea	Tarsi-fulcrumator	49	CG	0.57	0.66	0.51	0.24	0.17	0	Gebo (1987); Fleagle (2013)
Mirza coquereli	Cheirogaleidae	Lemuroidea	Tarsi-fulcrumator	326	CG	0.46	0.55	0.51	0.51	0.23	0	Gebo (1987); Fleagle (2013)
Mirza zaza[f]	Cheirogaleidae	Lemuroidea	Tarsi-fulcrumator	287	CG	0.46	0.55	0.51	0.51	0.23	0	Gebo (1987); Fleagle (2013)
Cheirogaleus major	Cheirogaleidae	Lemuroidea	Tarsi-fulcrumator	362	CG	0.69	0.25	0.67	0.28	0.2	0	Gebo (1987); Fleagle (2013)
Cheirogaleus medius	Cheirogaleidae	Lemuroidea	Tarsi-fulcrumator	282	CG	0.46	0.48	0.56	0.35	0.23	0	Gebo (1987); Fleagle (2013)

Lepilemur mustelinus[g]	Lepilemuridae	Lemuroidea	Tarsi-fulcrumator	1000	LVCL	0.29	0.84	0.58	0	0.2	0.03	Warren and Crompton (1997); Fleagle (2013)
Indri indri[h]	Indriidae	Lemuroidea	Tarsi-rotator	6840	LVCL	0.14	1.18	0.31	0	0	0	Dagosto and Yamashita (1998); Fleagle (2013)
Avahi laniger[i]	Indriidae	Lemuroidea	Tarsi-rotator	1307	LVCL	0.29	0.95	0.45	0	0.16	0	Warren and Crompton (1997); Fleagle (2013)
Propithecus verreauxi	Indriidae	Lemuroidea	Tarsi-rotator	2980	LVCL	0.13	1.13	0.33	0.11	0	0	Fleagle (2013); Furnell et al. (2015)
Propithecus diadema	Indriidae	Lemuroidea	Tarsi-rotator	6210	LVCL	0.14	1.18	0.31	0	0	0	Dagosto and Yamashita (1998); Fleagle (2013)
Eulemur fulvus	Lemuridae	Lemuroidea	Tarsi-rotator	2333	AQ/LL	0.67	0.62	0.42	0.31	0.09	0	Gebo (1987); Fleagle (2013)
Eulemur mongoz	Lemuridae	Lemuroidea	Tarsi-fulcrumator	1282	AQ/LL	0.57	0.65	0.49	0.3	0.14	0	Gebo (1987); Fleagle (2013)
Eulemur macaco	Lemuridae	Lemuroidea	Tarsi-fulcrumator	2430	AQ/LL	0.58	0.59	0.56	0.32	0.07	0	Gebo (1987); Fleagle (2013)
Hapalemur griseus	Lemuridae	Lemuroidea	Tarsi-fulcrumator	670	LVCL	0.51	0.85	0.4	0.19	0.1	0	Gebo (1987); Fleagle (2013)
Lemur catta	Lemuridae	Lemuroidea	Tarsi-fulcrumator	2210	AQ/LL	0.84	0.49	0.38	0.23	0.1	0	Gebo (1987); Fleagle (2013)
Varecia variegata	Lemuridae	Lemuroidea	Tarsi-fulcrumator	3520	AQ/LL	0.63	0.48	0.59	0.35	0.1	0	Gebo (1987); Fleagle (2013)
Daubentonia madagascariensis	Daubentoniidae	Lemuroidea	Tarsi-fulcrumator	2490	AQ/LL	0.9	0.25	0.51	0.14	0.27	0	Curtis and Feistner (1994); Fleagle (2013)
Arctocebus calabarensis[j]	Lorisidae	Lorisoidea	Tarsi-fulcrumator	306	SC	0.4	0	0.59	0.58	0.51	0	Gebo (1987); Fleagle (2013)
Perodicticus potto	Lorisidae	Lorisoidea	Tarsi-fulcrumator	836	SC	0.57	0	0.59	0.49	0.42	0	Gebo (1987); Fleagle (2013)
Loris lydekkerianus[j]	Lorisidae	Lorisoidea	Tarsi-fulcrumator	269	SC	0.4	0	0.59	0.58	0.51	0	Gebo (1987); Fleagle (2013)

Nycticebus bengalensis[k]	Lorisidae	Lorisoidea	Tarsi-fulcrumator	1110	SC	0.51	0	0.48	0.59	0.5	0	Gebo (1987); Fleagle (2013)
Nycticebus coucang	Lorisidae	Lorisoidea	Tarsi-fulcrumator	626	SC	0.51	0	0.48	0.59	0.5	0	Gebo (1987); Fleagle (2013)
Nycticebus menagensis[k]	Lorisidae	Lorisoidea	Tarsi-fulcrumator	265	SC	0.51	0	0.48	0.59	0.5	0	Gebo (1987); Fleagle (2013)
Galago moholi[l]	Galagidae	Lorisoidea	Tarsi-fulcrumator	173	SVCL	0.23	0.92	0.54	0.17	0.1	0	Gebo (1987); Fleagle (2013)
Sciurocheirus alleni[l]	Galagidae	Lorisoidea	Tarsi-fulcrumator	258	SVCL	0.23	0.92	0.54	0.17	0.1	0	Gebo (1987); Fleagle (2013)

Abbreviations: AQ/LL = arboreal quadruped/large leapers; CG = cheirogaleid generalists; CL = clawed leapers; LVCL =, large vertical clingers and leapers; SUS/CLA = suspensors/clambers; SC = slow climbers; SVCL = small vertical clingers and leapers.

[b]Quantified locomotor behavior based on *Ateles paniscus.*

[c]Quantified locomotor behavior based on *Saguinus midas.*

[d]Quantified locomotor behavior based on *Plecturocebus torquatus.*

[e]Quantified locomotor behavior based on *Microcebus murinus.*

[f]Quantified locomotor behavior based on *Mirza coquereli.*

[g]Quantified locomotor behavior based on *Lepilemur edwarsi.*

[h]Quantified locomotor behavior based on *Propithecus diadema.*

[i]Quantified locomotor behavior based on *Avahi occidentalis.*

[j]Quantified locomotor behavior based on *Loris tardigradus.*

[k]Quantified locomotor behavior based on *Nycticebus coucang.*

[l]Quantified locomotor behavior based on *Galago senegalensis.*

SOM Table S3

Extinct species included in the study.

Species	Group[a]	Family
Tetonius homunculus	Omomyiforms	Omomyidae
Arapahovius gazini	Omomyiforms	Omomyidae
Omomyidae indet. (UCMP V 134984, doi:10.17602/M2/M11994)	Omomyiforms	Omomyidae
Omomys carteri	Omomyiforms	Omomyidae
Ourayia uintensis	Omomyiforms	Omomyidae
Chipetaia lamporea	Omomyiforms	Omomyidae
Teilhardina brandti	Omomyiforms	Omomyidae
Anchomomys frontanyensis	Adapiforms	Notharctidae
Notharctus robustior	Adapiforms	Notharctidae
Notharctus tenebrosus	Adapiforms	Notharctidae
Copelemur tutus	Adapiforms	Notharctidae
Smilodectes gracilis	Adapiforms	Notharctidae
Smilodectes mcgrewi	Adapiforms	Notharctidae
Cantius ralstoni	Adapiforms	Notharctidae
Carpolestes simpsoni	Plesiadapiforms	Carpolestidae
Ignacius clarkforkensis	Plesiadapiforms	Paromomyidae
Dryomomys szalayi	Plesiadapiforms	Micromomyidae
Tinimomys graybulliensis	Plesiadapiforms	Micromomyidae

[a] Group and family based on Fleagle (2013).

SOM Table S4

Mean absolute errors calculated after comparing the predicted quantified locomotor behavior (estimated after performing a leave-one-out cross-validation for each species) against the actual quantified locomotor behavior for the entire extant sample and the extant tarsi-fulcrumators.

Locomotor variable	Mean absolute error	
	Entire extant sample	Tarsi-fulcrumators
Quadrupedalism	0.195	0.115
Leaping	0.220	0.116
Climbing	0.146	0.072
Suspension	0.131	0.116
Bridging	0.093	0.063
Scrambling/Clambering	0.091	0.005

SOM Table S5

Effective sample size for the ten independent chains ran for the Bayesian analysis performed to account for navicular morphological evolution (Fig. 6).

	Likelihood	Likelihood + prior	Number of parameters	Alpha	Sigma2
Run 1	1517.198	2910.148	1551.979	1803.192	3914.377
Run 2	3670.005	1782.128	1480.513	1041.694	3967.316
Run 3	3237.357	3086.443	2168.403	3126.606	4029.568
Run 4	3034.670	3627.174	2991.390	1702.741	4050.866
Run 5	3850.141	1661.152	2630.599	1090.848	4751.000
Run 6	2628.792	1846.964	2204.403	1009.416	4505.072
Run 7	3149.507	2728.294	2849.331	4039.032	3128.439
Run 8	1678.359	3682.195	2585.859	1100.621	4443.416
Run 9	3694.139	3348.263	2086.637	1686.353	3941.255
Run 10	1529.629	1110.907	680.916	2507.064	4441.577

SOM Table S6

Gelman and Rubin's convergence diagnostic test on the ten independent chains ran for the Bayesian analysis performed to account for navicular morphological evolution (Fig. 6). The multivariate potential scale reduction factor is equal to 1.02.

	Point estimation	Upper confidence limits
Likelihood	1	1.01
Likelihood + prior	1	1
Number of parameters	1	1.01
Alpha	1.01	1.02
Sigma2	1	1.01

SOM References

Arnold, C., Matthews, L.J., Nunn, C.L., 2010. The 10kTrees website: A new online resource for primate phylogeny. Evol. Anthropol. 19, 114–118. https://doi.org/10.1002/evan.20251

Bezanson, M., 2009. Life history and locomotion in *Cebus capucinus* and *Alouatta palliata*. Am. J. Phys. Anthropol. 140, 508–517. https://doi.org/10.1002/ajpa.21099

Cant, J.G.H., Youlatos, D., Rose, M.D., 2001. Locomotor behavior of *Lagothrix lagothricha* and *Ateles belzebuth* in Yasuní National Park, Ecuador: General patterns and nonsuspensory modes. J. Hum. Evol. 41, 141–166. https://doi.org/10.1006/jhev.2001.0485

Cant, J.G.H., Youlatos, D., Rose, M.D., 2003. Suspensory locomotion of *Lagothrix lagothricha* and *Ateles belzebuth* in Yasuní National Park, Ecuador. J. Hum. Evol. 44, 685–699. https://doi.org/10.1016/S0047-2484(03)00060-5

Cleveland, W.S., Grosse, E., Shyu, W.M., 1992. Local Regression Models. In: Hastie, T.J. (Ed.), Statistical Models in S, 1st ed. Routledge, New York. pp. 309–376.

Curtis, D.J., Feistner, A.T.C., 1994. Positional behaviour in captive aye-ayes (*Daubentonia madagascariensis*). Folia Primatol. 62, 155–159. https://doi.org/10.1159/000156772

Dagosto, M., Yamashita, N., 1998. Effect of habitat structure on positional behavior and support use in three species of lemur. Primates 39, 459–472. https://doi.org/10.1007/BF02557569

Demes, B., Jungers, W.L., Fleagle, J.G., Wunderlich, R.E., Richmond, B.G., Lemelin, P., 1996. Body size and leaping kinematics in Malagasy vertical clingers and leapers. J. Hum. Evol. 31, 367–388. https://doi.org/10.1006/jhev.1996.0066

Fleagle, J.G., 2013. Primate Adaptation and Evolution, 3rd ed. Academic Press, San Diego. https://doi.org/10.1016/B978-0-12-378632-6.00005-7

Fleagle, J.G., Meldrum, D.J., 1988. Locomotor behavior and skeletal morphology of two sympatric pitheciine monkeys, *Pithecia pithecia* and *Chiropotes satanas*. Am. J. Primatol. 16, 227–249. https://doi.org/10.1002/ajp.1350160305

Fleagle, J.G., Mittermeier, R.A., 1980. Locomotor behavior, body size, and comparative ecology of seven Surinam monkeys. Am. J. Phys. Anthropol. 52, 301–314. https://doi.org/10.1002/ajpa.1330520302

Furnell, S., Blanchard, M.L., Crompton, R.H., Sellers, W.I., 2015. Locomotor ecology of *Propithecus verreauxi* in Kirindy Mitea National Park. Folia Primatol. 86, 223–230. https://doi.org/10.1159/000377677

Garber, P.A., Leigh, S.R., 2001. Patterns of positional behavior in mixed-species troops of *Callimico goeldii*, *Saguinus labiatus*, and *Saguinus fuscicollis* in northwestern Brazil. Am. J. Primatol. 54, 17–31. https://doi.org/10.1002/ajp.1009

Gebo, D.L., 1987. Locomotor diversity in prosimian primates. Am. J. Primatol. 13, 271–281. https://doi.org/10.1002/ajp.1350130305

Gebo, D.L., Dagosto, M., 1988. Foot anatomy, climbing, and the origin of the Indriidae. J. Hum. Evol. 17, 135–154. https://doi.org/10.1016/0047-2484(88)90052-8

Gelman, A., Rubin, D.B., 1992. Inference from iterative simulation using multiple sequences. Stat. Sci. 7, 457–511. https://doi.org/10.1214/ss/1177011136

Granatosky, M.C., 2018. A Review of locomotor diversity in mammals with analyses exploring the influence of substrate use, body mass and intermembral index in primates. J. Zool. 306, 207–216. https://doi.org/10.1111/jzo.12608

Hunt, K.D., Cant, J.H.C., Gebo, D.L., Rose, M.D., Walker, S.E., Youlatos, D., 1996. Standardized Descriptions of Primate Locomotor and Postural Modes. Primates. 37, 363–387. https://doi.org/10.1007/BF02381373

Jackson, C.P., 2011. The positional behavior of pygmy marmosets (*Cebuella pygmaea*) in northwestern Bolivia. Primates 52, 171–178. https://doi.org/10.1007/s10329-011-0237-7

Johnson, S.E., Shapiro, L.J., 1998. Positional behavior and vertebral morphology in atelines and cebines. Am. J. Phys. Anthropol. 105, 333–354. https://doi.org/10.1002/(SICI)1096-8644(199803)105:3<333::AID-AJPA4>3.0.CO;2-S

Lawler, R.R., Ford, S.M., Wright, P.C., Easley, S.P., 2006. The Locomotor behavior of *Callicebus brunneus* and *Callicebus torquatus*. Folia Primatol. 77, 228–239. https://doi.org/10.1159/000091232

MacKinnon, J., MacKinnon, K., 1980. The behavior of wild spectral tarsiers. Int. J. Primatol. 1, 361–379. https://doi.org/10.1007/BF02692280

Morton, D.J., 1924. Evolution of the human foot II. Am. J. Phys. Anthropol. 7, 1–52. https://doi.org/10.1002/ajpa.1330070114

Revell, L.J., 2012. phytools: An R package for phylogenetic comparative biology (and other things). Methods Ecol. Evol. 3, 217–223. https://doi.org/10.1111/j.2041-210X.2011.00169.x

Rose, K.D., Godinot, M., Bown, T.M., 1994. The Early Radiation of Euprimates and the initial diversification of Omomyidae. In: Fleagle, J.G., Kay, R.F. (Eds.), Anthropoid Origins. Plenum Press, New York, pp. 1–28. https://doi.org/10.1007/978-1-4757-9197-6_1

Rosenberger, A.L., Stafford, B.J., 1994. Locomotion in captive *Leontopithecus* and *Callimico*: A multimedia study. Am. J. Phys. Anthropol. 94, 379–394. https://doi.org/10.1002/ajpa.1330940307

Silcox, M.T., Bloch, J.I., Boyer, D.M., Chester, S.G.B., López-Torres, S., 2017. The evolutionary radiation of plesiadapiforms. Evol. Anthropol. 26, 74–94. https://doi.org/10.1002/evan.21526

Sokal, R., Rohlf, F., 1995. Biometry: The Principles and Practice of Statistics in Biological Research, 3rd ed. Freeman, New York.

Springer, M.S., Meredith, R.W., Gatesy, J., Emerling, C.A., Park, J., Rabosky, D.L., Stadler, T., Steiner, C., Ryder, O.A., Janečka, J.E., Fisher, C.A., Murphy, W.J., 2012. Macroevolutionary dynamics and historical biogeography of primate diversification inferred from a species supermatrix. PLoS One 7, e49521. https://doi.org/10.1371/journal.pone.0049521

Walker, S.E., 1996. The evolution of positional behavior in the saki-uakaris (*Pithecia*, *Chiropotes*, and *Cacajao*). In: Norconk, M.A., Rosenberger, A.L., Garber, P.A. (Eds.), Adaptive Radiations of Neotropical Primates. Plenum Press, New York, pp. 335–367.

Warren, R.D., Crompton, R.H., 1997. Locomotor ecology of *Lepilemur edwardsi* and *Avahi occidentalis*. Am. J. Phys. Anthropol. 104, 471–486. https://doi.org/10.1002/(SICI)1096-8644(199712)104:4<471::AID-AJPA4>3.0.CO;2-V

Wright, K.A., 2007. The relationship between locomotor behavior and limb morphology in brown (*Cebus apella*) and weeper (*Cebus olivaceus*) capuchins. Am. J. Primatol. 69, 736–756. https://doi.org/10.1002/ajp.20391

Youlatos, D., 2002. Positional behavior of black spider monkeys (*Ateles paniscus*) in French Guiana. Int. J. Primatol. 23, 1071–1093. https://doi.org/10.1023/A:1019602116805

Chapter 4:

Reconstruction of the locomotor repertoire of early primates in the light of astragalar and calcaneal shape

Reproduced from:

Monclús-Gonzalo, O., Alba, D.M., Fabre, A.C., Marigó, J. 2025. Reconstruction of the locomotor repertoire of early primates in the light of astragalar and calcaneal shape. J. Hum. Evol. 206, 103370. https://doi.org/10.1016/j.jhevol.2025.103730

Journal of Human Evolution 206 (2025) 103730

Contents lists available at ScienceDirect

Journal of Human Evolution

journal homepage: www.elsevier.com/locate/jhevol

Reconstruction of the locomotor repertoire of early primates in the light of astragalar and calcaneal shape

Oriol Monclús-Gonzalo [a, *], David M. Alba [a], Anne-Claire Fabre [b, c, d], Judit Marigó [e, a, *]

[a] Institut Català de Paleontologia Miquel Crusafont (ICP-CERCA), Universitat Autònoma de Barcelona, Edifici ICTA-ICP, c/ Columnes s/n, 08193 Cerdanyola del Vallès, Barcelona, Spain
[b] Naturhistorisches Museum Bern, 3005 Bern, Switzerland
[c] Institute of Ecology and Evolution, University of Bern, 3012 Bern, Switzerland
[d] Life Sciences Department, Vertebrates Division, Natural History Museum, London SW7 5BD, UK
[e] Universitat Autònoma de Barcelona, Departament de Geologia, 08193 Cerdanyola del Vallès, Barcelona, Spain

ARTICLE INFO

Article history:
Received 7 June 2024
Accepted 23 June 2025
Available online 18 July 2025

Keywords:
Early euprimates
Plesiadapiforms
Astragalus
Calcaneus
Functional morphology
Locomotion

ABSTRACT

The locomotor behavior of the earliest euprimates is key to our understanding of the origin and early diversification of the group. Postcranial traits suggest that major locomotor shifts occurred during the early evolution of this clade. Two tarsal bones, the astragalus and the calcaneus, have been extensively studied because of their functional importance. To provide further insights into early primate evolution, we use a three-dimensional high-density sliding semilandmark geometric morphometric approach to quantify tarsal shape on an extensive (936) sample of astragali and calcanei from extant and extinct primates as well as other euarchontans. We reconstruct the locomotor repertoire for a total of 37 extinct taxa, representing all major Paleogene primate groups, using a partial least squares regression between astragalar/calcaneal shape and locomotor percentages compiled from the literature. Our results concur with previous studies and confirm that the astragalar/calcaneal shape exhibits a strong functional signal, allowing to accurately estimate the locomotor repertoire of extinct species. Locomotor estimates based on fossils indicate that early euprimates displayed a diverse array of locomotor repertoires comparable to extant species, highlighting cases of convergent evolution among distantly related groups. Locomotor differences between plesiadapiforms and early euprimates include a greater use of leaping by the latter, suggesting that the origin and early diversification of euprimates involved an important locomotor shift. Based on tarsal shape, this study improves our understanding of early primate locomotion and evolution, providing the most extensive taxonomic scope to date.
© 2025 The Authors. Published by Elsevier Ltd. This is an open access article under the CC BY-NC-ND license (http://creativecommons.org/licenses/by-nc-nd/4.0/).

1. Introduction

Primates of modern aspect (or euprimates, sensu Hoffstetter, 1977) are characterized by a group of distinct traits associated with grasping (e.g., nails instead of claws, opposable hallux, and pollex), improvement in the visual apparatus (e.g., postorbital bar, convergent orbits, and larger and more complex brains than other mammals), leaping (e.g., elongation of the tarsus), and frugivory (bunodont cusps and broad taloned basins; Cartmill, 1974, 1992; Szalay et al., 1987; reviewed in Silcox et al., 2015). The earliest euprimates, first recorded at the beginning of the Eocene (excluding the enigmatic *Altiatlasius* from the late Paleocene; Sigé et al., 1990), are represented by adapiforms and omomyiforms, which rapidly expanded across Eurasia and North America (Smith et al., 2006; Beard, 2008; Rose et al., 2011; Morse et al., 2019). Adapiforms are regarded as a paraphyletic assemblage of stem strepsirrhines (Godinot, 1998; Marigó et al., 2016; Ni et al., 2016). Compared with omomyiforms, adapiforms are generally larger and have longer snouts, smaller eye sockets (indicating a diurnal lifestyle), and dentitions suggesting mainly folivorous or frugivorous diets (Gunnell et al., 2008). Based on available partial skeletons and abundant isolated postcranial remains, most adapiforms are considered to have been generalized arboreal quadrupeds with some resemblances to extant lemurs (e.g. Gregory, 1920; Decker and Szalay, 1974; Dagosto, 1983; Rose and Walker, 1985; Covert, 1988; Gebo et al., 1991; Marigó et al., 2016, 2020; Llera Martín

* Corresponding authors.
E-mail addresses: oriol.monclus@icp.cat (O. Monclús-Gonzalo), judit.marigo@uab.cat (J. Marigó).

https://doi.org/10.1016/j.jhevol.2025.103730
0047-2484/© 2025 The Authors. Published by Elsevier Ltd. This is an open access article under the CC BY-NC-ND license (http://creativecommons.org/licenses/by-nc-nd/4.0/).

et al., 2022; Monclús-Gonzalo et al., 2023). Omomyiforms, on the other hand, are an extinct assemblage of stem haplorhines or stem tarsiiformes whose exact relationships with either tarsiers or anthropoids are still a matter of debate (Rosenberger and Preuschoft, 2012; Ni et al., 2013, 2016). They are usually referred to as 'tarsier-like', but current evidence indicates that omomyiforms differed substantially from tarsiers in their postcranial skeleton and likely occupied an ecological niche more similar to that of extant cheirogaleids and some galagids (Godinot and Dagosto, 1983; Gebo, 1988; Dagosto et al., 1999; Dunn et al., 2006; Gunnell et al., 2008).

Anthropoids are also first recorded during the Eocene. The oldest group, eosimiids, from the middle Eocene of Asia (and probably afrotarsiids; Chaimanee et al., 2012, 2024), are usually regarded as the most basal stem anthropoids, exhibiting a mixture of primitive haplorrhine features together with more derived anthropoid ones (Beard et al., 1994, 1996; Gebo et al., 2000, 2001; Beard and Wang, 2004; Chaimanee et al., 2012, 2024; but see Gunnell and Miller, 2001; Miller et al., 2005). Another group of likely stem anthropoids, the amphipithecids, also exhibit a combination of primitive and derived traits, as well as some resemblances to adapiforms, which have raised doubts on their inclusion within the Anthropoidea (Gunnell and Ciochcon, 2008), despite being favored by most authors (Kay et al., 2004; Beard et al., 2009; Marivaux et al., 2010; Coster et al., 2013; Jaeger et al., 2020; Chaimanee et al., 2024). Conversely, early anthropoids from the late Eocene and early Oligocene of Afro-Arabia (e.g., parapithecids and proteopithecids) display more clear-cut anthropoid synapomorphies (Fleagle and Kay, 1988; Simons and Seiffert, 1999; Seiffert et al., 2000, 2004, 2005). Early anthropoids generally differ from omomyiforms and most adapiforms in possessing adaptations for a more quadrupedal locomotion with higher utilization of larger and more horizontal substrates, thus departing from the more active grasp-leaping behavior exhibited by extant lemuriforms and tarsiers (Gebo, 1986; Dagosto, 1990; Kay et al., 1997).

There is a relatively diverse group of placentals, from the Paleocene and Eocene, which are usually regarded either as broadly ancestral to or as a paraphyletic assemblage of stem primates: plesiadapiforms (Silcox et al., 2007). Despite their considerable taxonomic diversity (including more than 120 species classified into 10 families; Silcox et al., 2017; Crowell et al., 2024), relatively little is known about the postcranial anatomy of these animals, except for a few partial skeletons (Bloch and Boyer, 2002, 2007; Bloch et al., 2007; Chester et al., 2017, 2019, 2025; Boyer and Gingerich, 2019) and some isolated bones (Chester et al., 2015), thus hampering efforts to reach a comprehensive understanding of their locomotor diversity. Although most authors agree that plesiadapiforms were arboreal (Szalay and Decker, 1974; Szalay and Dagosto, 1980; Szalay and Drawhorn, 1980; Beard, 1989; Godinot and Beard, 1991; Rose, 1994; Kirk et al., 2008; Chester et al., 2015, 2017, 2019), given that they lack most euprimate-like traits associated with locomotor behavior, their locomotor repertoire has been inferred to differ substantially from that of euprimates. Only *Carpolestes simpsoni* has been shown to exhibit adaptations related to grasping small branches, such as an opposable hallux with a nail instead of a claw (Bloch and Boyer, 2002). Altogether, the current evidence suggests that plesiadapiforms were probably as ecologically diverse as they were taxonomically, occupying a wide array of ecological niches, as defined by divergent dietary and locomotor adaptations (Bloch and Boyer, 2007; Prufrock et al., 2016; López-Torres et al., 2017; Silcox et al., 2017).

To explain the acquisition of euprimate distinct traits, several (not mutually exclusive) adaptive hypotheses have been proposed. These include the visual predation hypothesis (Cartmill, 1974, 1992), the angiosperm coevolution hypothesis (Sussman and Raven, 1978; Sussman, 1991; Sussman et al., 2012), and the grasp-leaping hypothesis (Szalay and Delson, 1979; Szalay and Dagosto, 1980; Kemp, 2024a, 2024b). Both the visual predation and the angiosperm coevolution hypotheses focus on selective pressures derived from the utilization of the fine branch milieu to access food resources, either small animal prey or angiosperm products. This led to their unification by Rasmussen (1990) based on the didelphid *Caluromys* as an extant analogue of the earliest euprimates. Conversely, the grasp-leaping hypothesis proposes that the modern primate morphotype, including the features related to the visual apparatus, is explained by the ability of the last common ancestor (LCA) of euprimates to engage in active leaping behavior (Szalay and Delson, 1979; Szalay and Dagosto, 1980). Increasing evidence from the last two decades (e.g., Bloch and Boyer, 2002; Bloch et al., 2007; Chester et al., 2015) indicates that distinctive euprimate traits did not appear simultaneously but in a stepwise manner. Accordingly, the origin of euprimates should be considered a protracted process rather than an abrupt event, allowing for the former adaptive hypotheses to fit into different stages along early primate (and euprimate) evolution (Gebo, 2004; Dagosto, 2007; Sargis et al., 2007; Silcox and López-Torres, 2017). Therefore, inferences about plesiadapiform locomotor abilities, irrespective of their exact phylogenetic position, are necessary to better understand the origin and early diversification of euprimates.

Among other elements of the postcranial skeleton, the hindfoot, composed by two tarsal bones (the astragalus and the calcaneus), has been extensively studied. This is because many astragalar and calcaneal features are informative about the locomotor adaptations of extinct species, given their critical role in important functional aspects of the foot. These include the leverage of many muscles and the mobility at the ankle joint and more distal tarsal joints, where most of the inversion and eversion of the foot, as well as its supination and pronation, occurs (Su and Zeiniger, 2022). In addition, the type of foot posture, defined by the location of the fulcrum of the foot (i.e., the position in which the lever comprised by the foot pivots), also influences the morphology of these two bones, particularly the calcaneus (Morton, 1924; Moyà-Solà et al., 2012). Tarsi-fulcrumators, including extant strepsirrhines and tarsiers, are characterized by a fulcrum located more proximally, at the distal part of the tarsus, resulting in increased grasping capabilities. However, the load arm of the lever is reduced and must be compensated via elongation of the midtarsal region. Conversely, metatarsi-fulcrumators, comprising extant anthropoids and most nonprimate mammals, exhibit a fulcrum that is placed more distally, in the metatarsal heads or the phalanges, and thus they do not require further elongation of the tarsus (Morton, 1924).

The relationship between the shape of these two bones and locomotor behavior, as a result of the strong functional signal embedded in their morphology, has been extensively addressed, mostly from a descriptive and qualitative perspective (e.g., Gregory, 1920; Decker and Szalay, 1974; Szalay and Decker, 1974; Walker, 1974; Conroy and Rose, 1983; Rose and Walker, 1985; Gebo, 1986, 1988; Covert, 1988; Dagosto, 1988, 1990; Gebo et al., 2000; Pina et al., 2011) or using morphometric approaches based on linear measurements and indices (e.g., Gebo and Simons, 1987; Gebo et al., 1991, 2001, 2012; Marivaux et al., 2003, 2010, 2011; Boyer et al., 2010, 2015; Moyà-Solà et al., 2012; Boyer and Seiffert, 2013; Seiffert et al., 2015; Dunn et al., 2016; Marigó et al., 2016; Yapuncich et al., 2017, 2019; Yapuncich and Granatosky, 2021). Only a handful of studies have tackled this question utilizing multivariate methods (Parr et al., 2014; Boyer et al., 2017a; Püschel et al., 2017, 2018, 2020; Llera Martín et al., 2022), albeit employing simplified locomotor categories that do not adequately represent

the complex spectrum of primate locomotor repertoires. Here, we quantitatively investigate the correlation between astragalar/calcaneal shape and locomotor behavior in extant primates to identify the main morphological correlates that span the extensive behavioral spectrum exhibited by this group (Bock and Von Wahlert, 1965). In particular, we use a three-dimensional (3D) high-density sliding semilandmark geometric morphometric approach to quantify the shape of the astragalus and the calcaneus. In addition, we use percentages of locomotor behaviors in extant primate species to quantify their locomotor repertoires and infer the locomotor repertoire of extinct primate species, which enables us to discuss the locomotor behavior exhibited by primates in the context of their early evolutionary history. As shown by previous studies (see references mentioned previously), we hypothesize that the shape of these two tarsal bones exhibits a strong correlation with locomotion so that they can be used as predictors to reconstruct the locomotor behavior of extinct primate species. Both the astragalus and the calcaneus are relatively well known for several Paleogene primate species (Yapuncich et al., 2022: Fig. 12.1) and hence are important as potential indicators of their locomotor behavior. In line with previous studies, we predict that the locomotor repertoire estimated for early primates will be substantially diverse, as evinced by previous studies carried out on the available postcranial remains (e.g., Walker, 1974; Conroy and Rose, 1983; Gebo, 1988; Covert, 1995; Bloch et al., 2007; Boyer et al., 2013a; Marigó et al., 2016, 2020; Monclús-Gonzalo et al., 2023; Monclús-Gonzalo et al., 2025). In addition, we also expect that locomotor estimates for euprimates will considerably differ from those for plesiadapiforms, emphasizing behaviors such as frequent leaping, which have been correlated with the morphological features that distinguish the euprimate ancestral morphotype from plesiadapiforms (Dagosto, 1988, 2007).

2. Materials and methods

2.1. Sample composition and data collection

Osteological sample The analyzed astragalar and calcaneal extant samples are composed of 440 and 412 specimens, respectively, representing nearly the entire diversity of the superorder Euarchonta at the family rank. In addition, we compiled surface models of astragali (38) and calcanei (46) of extinct specimens representing all major Paleogene primate groups (Table 1). Most adapine postcranial remains are referred to *Adapis parisiensis*. However, the lack of stratigraphic information for some of the oldest specimens, coupled with geochronological and morphological evidence, suggests that there are several species included within *A. parisiensis* (Godinot, 1998; Marigó et al., 2019). For this reason, apart from the slightly older and larger *Leptadapis magnus*, we informally refer the material previously assigned to *A. parisiensis* to the '*Adapis* group' (e.g., Marigó et al., 2019). All these surface models were downloaded from MorphoSource (www.morphosource.org; Boyer et al., 2017b), except for a right astragalus of *Djebelemur martinezi* (CBI-1-545), which was downloaded from MorphoMuseuM (www.morphomuseum.com; Lebrun and Orliac, 2016; Marivaux et al., 2018). The list of the specimens is provided in Supplementary Online Material (SOM) Table S1 (see Figs. 1–4 for a representative sample of extant and extinct astragali and calcanei). A phylogenetic tree (SOM Fig. S1) comprising all extant primates in our study was downloaded from the 10kTrees Project v. 3 (Arnold et al., 2010). The criteria used to place the extinct taxa are explained in SOM S1.

Locomotor data collection Behavioral data consist of percentages of locomotor behaviors compiled from the literature (SOM Table S2), divided into five categories based on Hunt et al.'s (1996) descriptions for standardized primate locomotor and postural modes (for more information on how the five locomotor categories were compiled, see SOM S1): quadrupedalism (Q), climbing (C), leaping (L), suspension (S), and clawed clinging/climbing (CC). To standardize the data, the minimum number of studies (provided that more than one study was available for a given extant species) was considered when compiling the locomotor percentages (SOM S1). Because of the lack of behavioral information for some categories in several extant species, data from closely related species were sometimes used (see SOM Table S2 for details). An arcsine square root transformation was applied to the locomotor percentages; this is a standard procedure for analyzing proportional ecological data that makes the variances more homogeneous throughout the sample and approximates the data to a more normal distribution (Sokal and Rohlf, 1995).

2.2. Quantification of shape, astragalar/calcaneal shape variation, and influence of size

Quantification of shape using three-dimensional geometric morphometrics A 3D high-density sliding semilandmark procedure (Bookstein, 1997; Gunz et al., 2005) was used to quantify the shape of the two tarsal bones (Fig. 5; Tables 2 and 3), following the pipeline presented in Bardua et al. (2019). This methodology allows semilandmarks to slide along the curves and the surfaces, previously predefined using a template, while minimizing the bending energy. As a result, semilandmarks, which are inherently

Table 1
List of the extinct primate species and astragali/calcanei included in this study.

Family	Species	Astragalus	Calcaneus
Plesiadapiformes:			
Purgatoriidae	*Purgatorius* sp.	1	1
Micromomyidae	*Tinimomys graybulliensis*	0	1
Paromomyidae	*Ignacius graybullianus*	1	0
Paromomyidae	*Phenacolemur* sp.	0	1
Plesiadapidae	*Nannodectes gidleyi*	1	0
Plesiadapidae	*Plesiadapis cookei*	1	1
Plesiadapidae	*Plesiadapis rex*	1	0
Carpolestidae	*Carpolestes simpsoni*	0	1
Omomyiformes:			
Incertae sedis	*Teilhardina belgica*	1	1
Incertae sedis	*Vastanomys major*	1	0
Omomyidae	*Absarokius* sp.	0	1
Omomyidae	*Arapahovius gazini*	1	1
Omomyidae	*Necrolemur* sp.	1	0
Omomyidae	*Hemiacodon gracilis*	2	0
Omomyidae	*Omomys carteri*	2	4
Omomyidae	*Ourayia uintensis*	0	1
Omomyidae	*Shoshonius cooperi*	2	1
Omomyidae	*Washakius insignis*	1	1
Adapiformes:			
Notharctidae	*Marcgodinotius indicus*	1	3
Notharctidae	*Cantius* sp.	1	3
Notharctidae	*Copelemur tutus*	0	1
Notharctidae	*Notharctus* sp.	4	5
Notharctidae	*Smilodectes* sp.	1	2
Notharctidae	*Anchomomys frontanyensis*	1	1
Adapidae	'*Adapis* group'	5	5
Adapidae	*Leptadapis magnus*	1	3
Adapidae	*Caenopithecus lemuroides*	0	1
Stem Lemuriformes:			
Djebelemuridae	*Djebelemur martinezi*	1	0
Stem Anthropoidea:			
Eosimiidae	*Eosimias* sp.	2	3
Amphipithecidae	*Ganlea* sp.	1	0
Parapithecidae	*Apidium* sp.	3	0
Parapithecidae	*Simonsius grangeri*	1	0
Parapithecidae	Parapithecidae indet.	0	3
Proteopithecidae	*Proteopithecus sylviae*	0	1

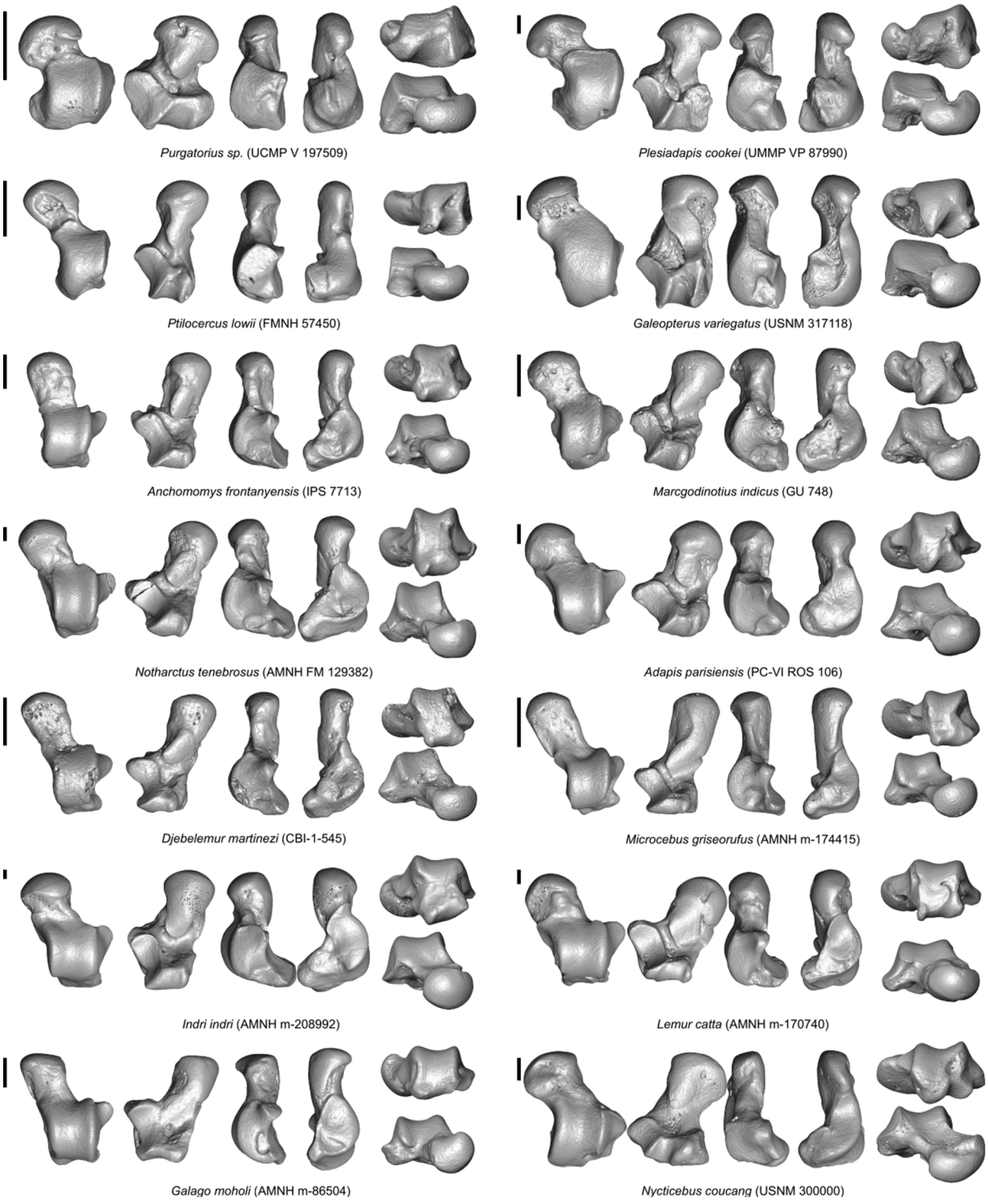


Figure 1. Selected sample of astragali belonging to plesiadapiforms, scandentians, dermopterans, adapiforms, and extant strepsirrhines. Scale bars = 2 mm.

nonhomologous, are consequently transformed into geometrically homologous landmarks and can be used to compare shapes (Gunz and Mitteroecker, 2013). Specimens from the left foot were mirrored before placing the landmarks. Anatomical landmarks and sliding semilandmarks of curves were placed manually on each 3D surface using the software Landmark v. 3.0.0.6 (Wiley, 2006), while the remaining analyses were performed in R v. 4.3.0 (R Core Team, 2023). To carry out the sliding-semilandmark procedure, the R package morpho v.2.11 (Schlager, 2017) was used. To do so, it is first required to create a template for each bone, following the pipeline presented in Cornette et al. (2013), with 25 anatomical landmarks, 195 sliding semilandmarks on curves, and 130 sliding semilandmarks on surfaces for the astragalus and 20 anatomical landmarks, 100 sliding semilandmarks on curves, and 49 sliding semilandmarks on surfaces for the calcaneus. All the sliding semilandmarks of each template,

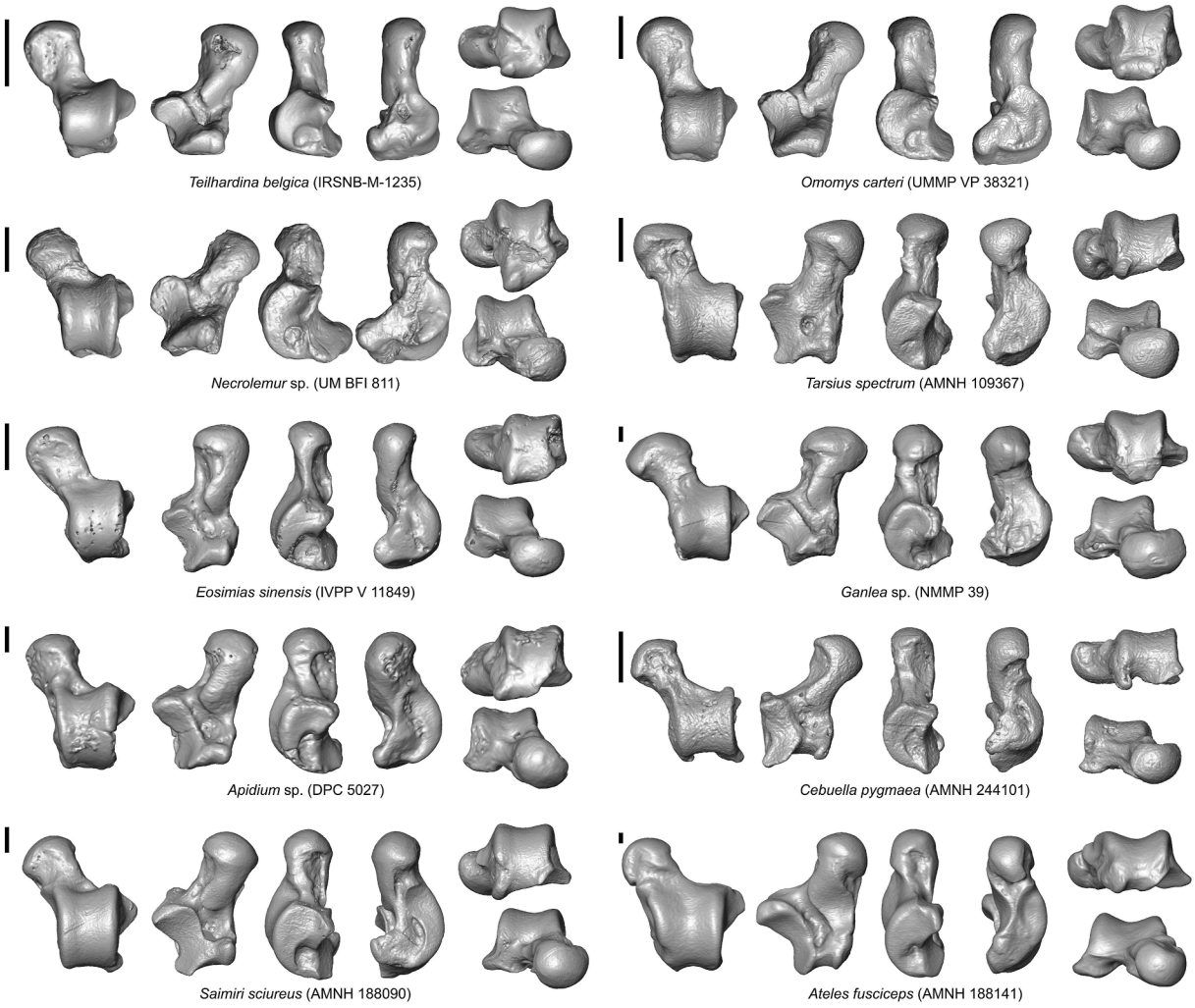


Figure 2. Selected sample of astragali belonging to extant and extinct haplorhines. Scale bars = 2 mm.

based on the homology between the anatomical landmarks and the curves, are projected onto the specimens using a thin-plate spline deformation (Gunz and Mitteroecker, 2013) using the function 'placePatch' of the package morpho. Before this step, all specimens were decimated to a maximum of 50,000 faces using the software Avizo v. 8.1.1 (Visualization Sciences Group, Merignac) to facilitate the projection and sliding procedures, as well as their visualization in the subsequent analyses. After projecting the sliding semilandmarks on surfaces, four thin-plate spline relaxation procedures were performed using the function 'slider3d' of the package morpho. The first relaxation was performed against the template, whereas the other three were performed against the Procrustes consensus obtained from the previous iteration. After the relaxation procedure, a generalized Procrustes superimposition (Rohlf and Slice, 1990) was performed using the function 'gpagen' of the package geomorph v. 4.0.6 (Adams and Otarola and Castillo, 2013).

Astragalar/calcaneal shape variation To assess astragalar and calcaneal shape variation across the sample, a principal component analysis (PCA) was performed on the species-mean Procrustes shape coordinates using the 'gm.prcomp' function of the package 'geomorph'. To decide how many principal components (PCs) should be considered as relevant for the analysis, a barplot depicting the variance explained by each PC was built following Hammer and Harper (2024). Phylogenetic signal was calculated employing two different methods, Blomberg's K (Blomberg et al., 2003) and Pagel's lambda (Pagel, 1999), using the 'phylosig' function of the package 'phytools' v. 2.1–1 (Revell, 2012). Additionally, a phylogenetic PCA (Revell, 2009; Polly et al., 2013) was also performed on the species-mean Procrustes shape coordinates using the 'gm.prcomp' function of the package 'geomorph'. Compared to a standard PCA, a phylogenetic PCA allows us to calculate PCs that are oriented by the nonphylogenetic component of variation, allowing us to take into account the phylogenetic nonindependence among species. Therefore, differences between PCA and phylogenetic PCA scatterplots might indicate that factors other than the phylogenetic structure of the sample account for phenotypic variation. Principal components obtained from the phylogenetic PCA will be used as shape data to calculate branch-specific evolutionary rates to address the evolution of astragalar and calcaneal morphology across the primate phylogenetic tree (see subsection 2.5).

Influence of size and foot type on astragalar/calcaneal shape The correlation between tarsal size, defined as the natural log-transformed (ln) centroid size (CS), and ln body mass (BM) was first examined to identify the presence of allometric effects

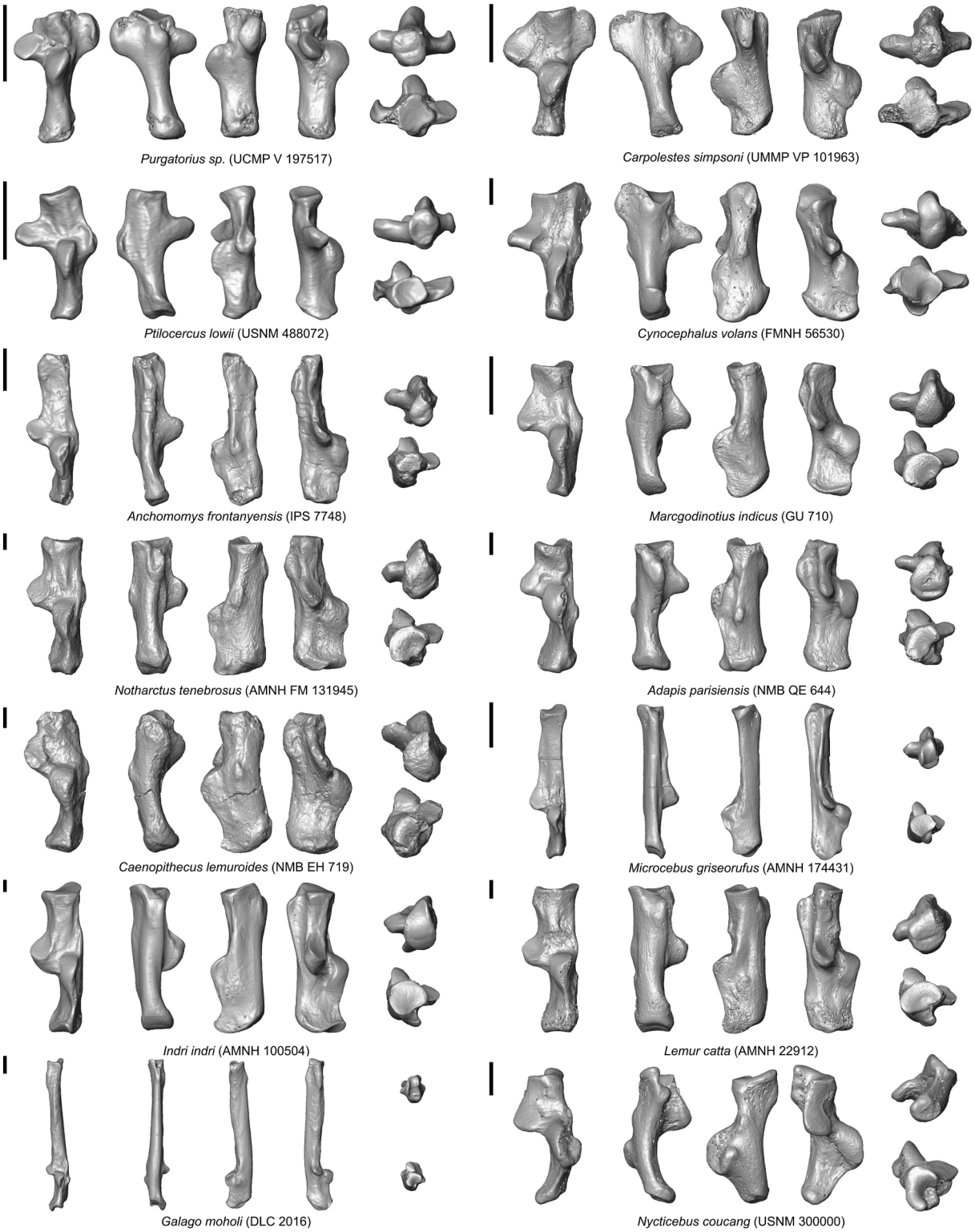


Figure 3. Selected sample of different calcanei belonging to plesiadapiforms, scandentians, dermopterans, adapiforms, and extant strepsirrhines. Scale bars = 3 mm.

between these two variables (see SOM Table S3 for details on the BM). For the calcaneus, this analysis was repeated without galagids and tarsiers as they are clear outliers in the linear regression. After that, a series of allometric regressions of the resulting PCs vs. ln CS or ln BM were calculated using a phylogenetic generalized least squares analysis with the 'pgls' function in the package 'caper' v. 1.0.3 (Orme et al., 2023). Shape differences based on the PCs between tarsi-fulcrumators and metatarsi-fulcrumators and the interaction term between size and foot type variables were also examined.

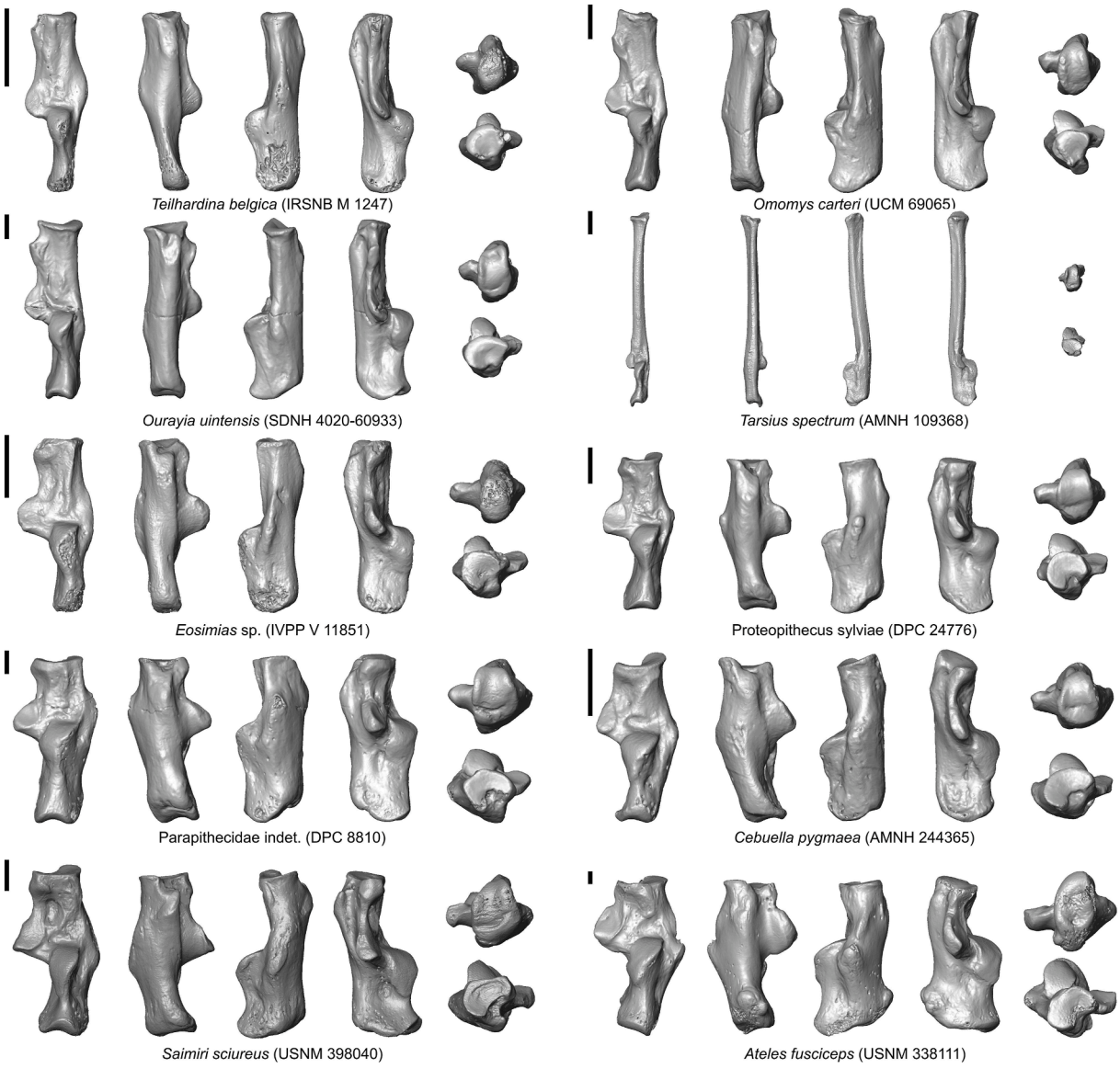


Figure 4. Selected sample of different calcanei belonging to extant and extinct haplorhines. Scale bars = 3 mm.

2.3. Covariation between astragalar/calcaneal shape and locomotor behavior in extant euprimates

To study the covariance between astragalar/calcaneal shape and locomotor behavior, a two-block partial least squares (PLS) analysis (Rohlf and Corti, 2000) was implemented using the functions 'two.b.pls' of the package geomorph and 'pls2b' of the package morpho. This type of analysis uses 3D landmark data and performs a singular value decomposition, which decomposes the covariance matrix of the two blocks of variables into two matrices of eigenvectors (one for each block of data) and a matrix of eigenvalues (the square roots of eigenvectors; Rohlf and Corti, 2000; Bookstein et al., 2003). The two blocks of data consisted of (1) the astragalar/calcaneal shape (Procrustes shape coordinates) averaged by species and (2) locomotor percentages for the 78 species included in the extant comparative sample. The significance of each linear combination is assessed by comparing the singular value to those obtained after resampling. If the PLS covariation coefficient is higher than the ones obtained from permutated blocks, its associated p value is significant. (The α level of significance was set at <0.05).

2.4. Reconstruction of extinct primate locomotor behavior

Prediction of locomotor percentages Although the standard version of two-block PLS is conceptualized as a symmetric analysis that does not allow for predictive outcomes (Zelditch et al., 2012), there is another version of this analysis more comparable to a regression, known as PLS regression, which allows the generation of predictive models (Wold et al., 2001). Similar approaches have already been applied in archaeology and paleoanthropology (e.g., Archer et al., 2018; Bastir et al., 2019; Torres-Tamayo et al., 2020) and in the reconstruction of extinct primate locomotion, using the navicular bone (Monclús-Gonzalo et al., 2023), the astragalus (Monclús-Gonzalo et al., 2025), or the ulna (Raventós-Izard et al., 2025) as a predictor. Therefore, a PLS regression approach was applied to estimate the locomotor behavior of the 37 Paleogene taxa based on their astragalar/calcaneal shape. To do so, the two

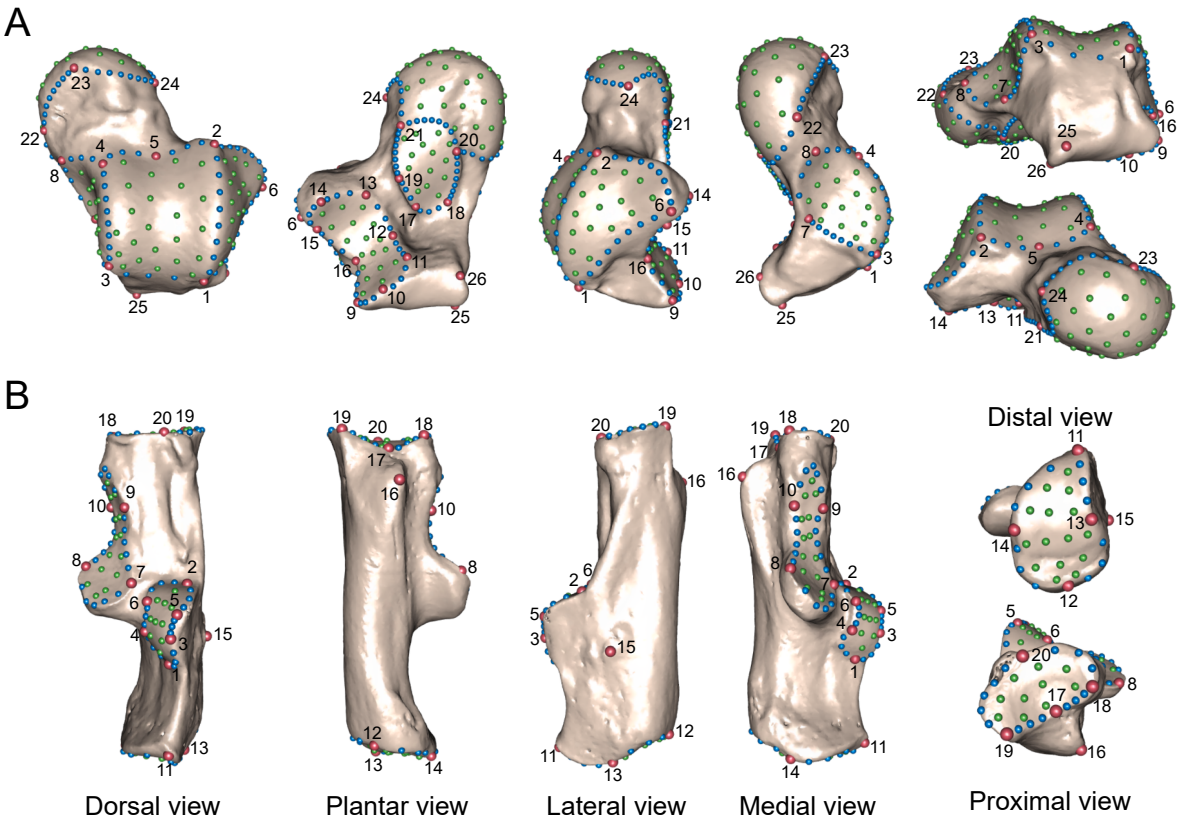


Figure 5. Landmark configuration of the astragalus (A) and the calcaneus (B). Red points represent anatomical landmarks (see Tables 2 and 3), blue points represent curve semilandmarks, and light green points represent surface semilandmarks. Views for both bones are indicated in the calcaneus. The two specimens used as a reference are right-sided and belong to the species *Lemur catta*: DLC 6848 (A) and AMNH 170739 (B). (For interpretation of the references to color in this figure legend, the reader is referred to the web version of this article.)

Table 2
Definition of the 26 anatomical landmarks (LMs) used for the astragalus.

LM	Definition
1	Proximalmost point of the lateral trochlear rim
2	Distalmost point of the lateral trochlear rim
3	Proximalmost point of the medial trochlear rim
4	Distalmost point of the medial trochlear rim
5	Point of maximum concavity on the lateral side of the junction between the astragalar body and the astragalar neck
6	Tip of the lateral astragalar process
7	Point of maximum concavity between LM3 and LM8
8	Distalmost point of the plantar aspect of the medial tibial facet
9	Proximalmost point of the ectal facet
10	Point of maximum curvature between LM9 and LM11
11	Proximomedialmost point of the ectal facet
12	Point of maximum curvature between LM11 and LM13
13	Distalmost point of the ectal facet
14	Point of maximum curvature between LM13 and LM15
15	Proximolateralmost point of the ectal facet
16	Point of maximum curvature between LM15 and LM9
17	Proximalmost point of the sustentacular facet
18	Proximomedialmost point of the sustentacular facet
19	Proximolateralmost point of the sustentacular facet
20	Medialmost joint of the sustentacular and the navicular facets
21	Lateralmost joint of the sustentacular and navicular facets
22	Proximalmost point of the navicular facet on the medial side of the astragalar neck
23	Proximodorsalmost point of the navicular facet
24	Proximalmost point of the navicular facet on the lateral side of the astragalar neck
25	Point of maximum curvature on the proximalmost point of the medial side of the astragalus
26	Plantarmost point of the m. Flexor Hallucis Longus groove on the medial side of the astragalus, below LM25

To visualize placement of the LMs on the bone, see Figure 5.

Table 3
Definition of the 20 anatomical landmarks (LMs) used for the calcaneus.

LM	Definition
1	Proximalmost point of the ectal facet
2	Distalmost point of the ectal facet
3	Proximolateralmost point of the ectal facet
4	Proximomedialmost point of the ectal facet
5	Dorsalmost point of the ectal facet
6	Medialmost point of the ectal facet
7	Proximolateralmost point of the sustentacular facet
8	Proximomedialmost point of the sustentacular facet
9	Distolateralmost point of the sustentacular facet
10	Distomedialmost point of the sustentacular facet
11	Dorsalmost point of the proximal facet
12	Plantarmost point of the proximal facet
13	Lateralmost point of the proximal facet
14	Medialmost point of the proximal facet
15	Lateralmost point of the peroneal tubercle
16	Plantarmost point of the calcaneal tubercle
17	Most concave point of the cuboid facet
18	Dorsomedialmost point of the cuboid facet
19	Plantolateralmost point of the cuboid facet
20	Dorsalmost point of the cuboid facet

To visualize placement of the LMs on the bone, see Figure 5. Landmarks includsed in the restricted configuration (see Material and Methods section) are denoted with an asterisk.

sets of eigenvectors generated by the singular warp analysis performed on each covariance analysis were used. The species-mean Procrustes shape coordinates of every extinct taxon are projected onto the latent space generated after the singular warp analysis. After that, the coefficients obtained from the linear regression of the original latent variables can be used to estimate the variables corresponding to the second block of data. The resulting new latent variables can be projected back to obtain the scores of each behavioral category. To calculate the locomotor percentages, the arcsin square root transformation must be reverted and the resulting values normalized to ensure that their total sum is equal to 100. To check the accuracy of this method, a leave-one-out cross-validation approach was applied on the extant species set. The leave-one-out subsampling approach removes each extant individual one by one from the original sample and performs the analysis again with the remaining extant species to compare the original behavioral data compiled from the literature with the predictions and assess the error generated during the estimation procedure (Kuhn and Johnson, 2013). Based on the cross-validated results, the mean absolute error (i.e., the arithmetic average of the absolute errors) was computed to assess our prediction results using the extant sample (Willmott and Matsuura, 2005).

Ancestral reconstruction Ancestral states of the locomotor repertoire for each node of the phylogenetic tree were estimated with the function 'mvgls' and 'estim' of the package 'mvMORPH' v. 1.1.6 (Clavel et al., 2015). Four evolutionary models (Brownian motion, Ornstein-Uhlenbeck, Early Burst, and Pagel's lambda transformation) were computed and compared using the Generalized Information Criterion with the function 'GIC' of the package 'mvMORPH,' selecting the evolutionary model with the lowest GIC to calculate the ancestral locomotor reconstruction (Konishi and Kitagawa, 1996).

2.5. Rates of morphological evolution

To investigate the morphological evolution of the astragalus and the calcaneus, branch-specific evolutionary rates were estimated using the variable rates model in BayesTraits v3 (http://www.evolution.rdg.ac.uk/). The first 36 PCs from the phylogenetic PCA of species-mean Procrustes shape coordinates for the astragalus and the first 25 PCs for the calcaneus were used as input. These PCs accounted for >95% of the total variation in astragalar/calcaneal shape. Five independent chains for 200 million interactions were ran, sampling every 10,000 iterations and discarding the first 25 million iterations as burn-in. Trace plots were examined to ensure stationarity and retain only chains that stabilized after burn-in. Effective sample sizes of the posterior distributions (effective sample size < 100) and chain convergence were assessed using Gelman and Rubin's diagnostic, using the functions 'effectiveSize' and 'Gelman.diag' in the package 'coda' v0.19-41 (Plummer et al., 2005). The verification of chain convergence is crucial to detect large deviations and ensuring similar between-chain variances (Gelman and Rubin, 1992). Results were visualized on the phylogeny using the 'mytreebybranch' function (https://github.com/anjgoswami/salamanders/blob/master/mytreerateplotter.R). Branch-specific average rates were obtained using the 'rjpp' function in the package 'btrtools' v0.0.0.9000 (https://github.com/hferg/btrtools/tree/master/R).

2.6. Shape visualization

To visualize the shape differences in astragalar and calcaneal shape between the extremes of the PC and PLS axes, a thin-plate spline deformation of the 3D models of an astragalus and a calcaneus was carried out using the functions 'shape.predictor' and 'plotRefToTarget' of the package geomorph and 'shade3d' of the package rgl 1.1.3 (Adler and Murdoch, 2020). Displacement heatmaps were calculated to illustrate mesh distances between extreme landmark configurations using the function 'mehsdist' of the package morpho. This function first calculates the distances between the vertices of the reference mesh and that of the target mesh. Then, distances are given a negative value if inside the reference mesh or a positive value if outside (Bærentzen and Aanæs, 2002). The functions 'mshape' and 'findMeanSpec' of the package geomorph were used to find the most suitable astragalar and calcaneal specimens to use as reference. The specimens selected were an astragalus of *Plecturocebus moloch* (AMNH 244363) and a calcaneus of *Eulemur albifrons* (AMNH 170717).

3. Results

3.1. Astragalar shape variation

The first four PCs of the standard PCA performed on the species-mean Procrustes shape coordinates of the astragalus were chosen as the most meaningful and accounted for up to 59% of the total variance (SOM Fig. S2), differentiating species by phylogenetic group, locomotor behavior, and foot type.

The PC1 (accounting for 18% of the total variance, Fig. 6A) indicates differences in astragalar body shape (mediolaterally broader and dorsoplantarly lower toward negative scores and narrower and higher toward positive scores), trochlear wedging (broader distally than proximally in negative scores and more parallel rims in positive scores), development of a posterior trochlear shelf (PTS; more developed in positive than in negative scores), fibular facet shape (steeper in negative scores and more sloping in positive ones), relative size of the medial tibial facet (smaller and without reaching the plantar edge toward negative scores and larger and reaching the plantar edge in positive scores), proximodistal elongation of the neck (more elongated in positive scores than in negative scores), and head shape (smaller and more spherical in negative scores and larger and mediolaterally extended toward positive scores; Fig. 7). This axis separates extant haplorhines (negative scores) from extant strepsirrhines, scandentians, and dermopterans (intermediate to positive scores). As expected by the clear phylogenetic structure of PC1, a strong

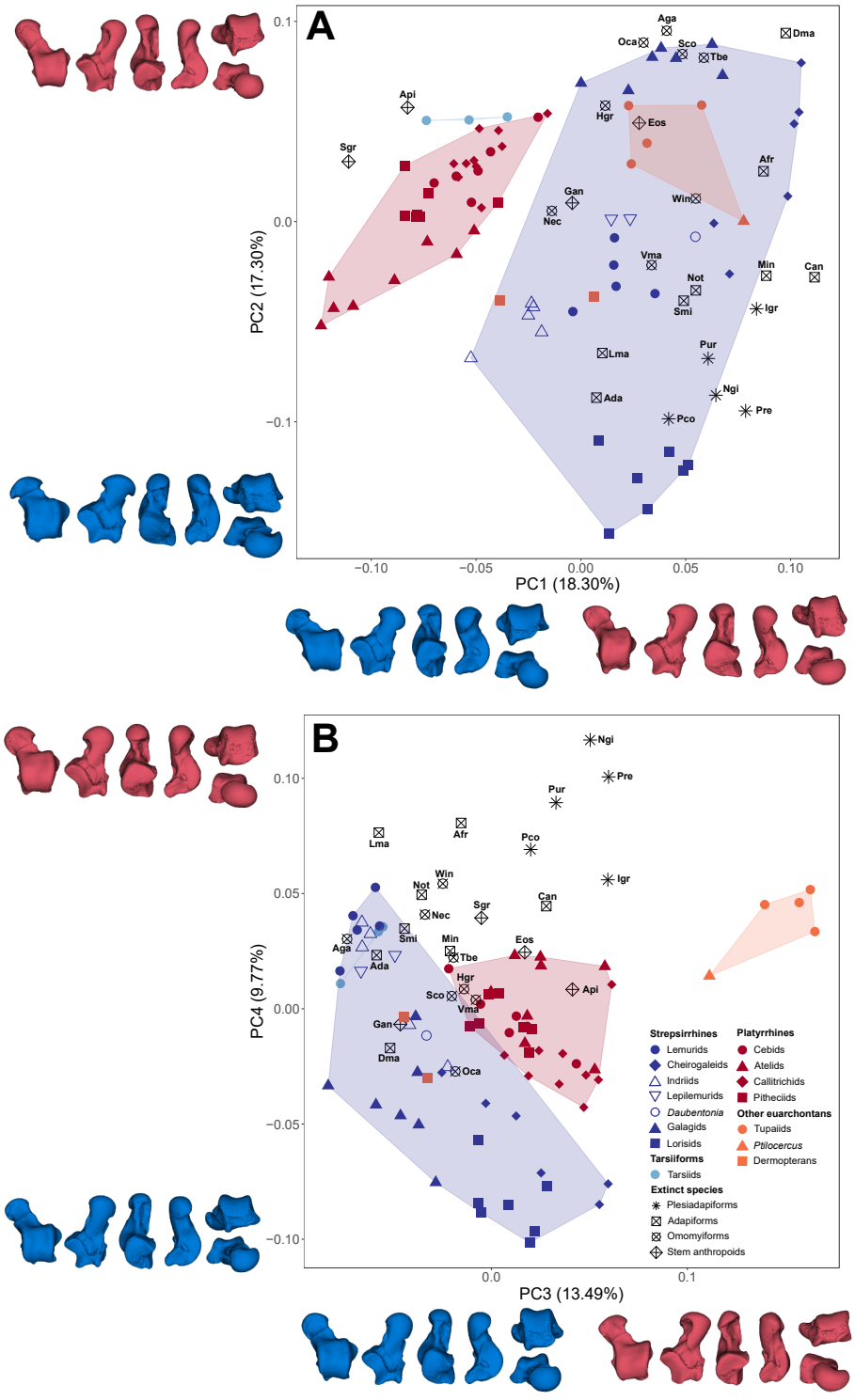


Figure 6. Results of the principal component analysis (PCA) performed on the species-mean Procrustes shape coordinates of the astragalus as depicted by bivariate plots of PC2 vs. PC1 (A) and PC4 vs. PC3 (B). Taxonomic groups are coded by color and symbol, as indicated in the legend. The percentage of variance explained by each PC is reported within parentheses. Astragalar shapes associated with minimum (blue) and maximum (red) values of each PC axis are plotted below each scatterplot (dorsal, plantar, lateral, medial, proximal, and distal views are shown, from left to right). Thin-plate splines correspond to an astragalus of *Plecturocebus moloch* (AMNH 244363). Abbreviations: Api = *Apidium*; Sgr = *Simonsius grangeri*; Gan = *Ganlea*; Eos = *Eosimias*; Nec = *Necrolemur*; Hgr = *Hemiacodon gracilis*; Sco = *Shoshonius cooperi*; Win = *Washakius insignis*; Oca = *Omomys carteri*; Aga = *Arapahovius gazini*; Vma = *Vastanomys major*; Tbe = *Teilhardina belgica*; Dma = *Djebelemur martinezi*; Afr = *Anchomomys frontanyensis*; Ada = *Adapis* group; Lma = *Leptadapis magnus*; Smi = *Smilodectes*; Not = *Notharctus*; Can = *Cantius*; Min = *Marcgodinotius indicus*; Ngi = *Nanodectes gidleyi*; Pre = *Plesiadapis rex*; Pco = *Plesiadapis cookei*; Igr = *Ignacius graybullianus*; Pur = *Purgatorius*; PC = principal component. (For interpretation of the references to color in this figure legend, the reader is referred to the web version of this article.)

phylogenetic signal is found for this axis (Table 4). Along PC1, most fossil species are projected onto slight to moderate negative scores and overlap with extant strepsirrhines, scandentians, and dermopterans, with only the Afro-Arabian anthropoids (*Apidium* and *Simonsius grangeri*) overlapping with extant haplorhines. Compared to the standard PC1, the phylogenetic PC1 (accounting for 18% of the total variance; SOM Fig. S3A) emphasizes changes in the trochlear and neck shape (a larger and broader trochlea relative to the neck toward negative scores and a smaller and more square-shaped trochlea relative to the neck in positive scores) and does not discriminate haplorhines from the other groups. Astragalar size and BM are significantly correlated ($r^2 = 0.909$; $p < 0.001$; SOM Fig. S4), although they exhibit a slight positive allometric slope. A significant allometric relationship is found between PC1 and either ln CS or ln BM, indicating a moderate negative correlation that accounts for 17–19% of the total variance (Table 5, SOM Figs. S5A–6A). Neither significant differences in PC1 were found between tarsi-fulcrumators and metatarsi-fulcrumators nor a significant interaction was found between either size variable and foot type.

The PC2 (accounting for 17% of the total variance, Fig. 6A) reflects differences in trochlear shape (more proximodistally elongated and less grooved toward negative scores and shorter and more grooved toward positive scores), fibular facet shape (more sloping in negative scores and steeper in positive scores), ectal facet shape (less concave in negative scores than in positive scores), neck shape (proximodistally abbreviated and mediolaterally broader in negative scores and more elongated and narrower in positive scores), and head shape (larger and mediolaterally broader toward negative scores and smaller and more spherical toward positive scores; Fig. 7). Within each group—nonprimates, strepsirrhines, and haplorhines—PC2 differentiates those species with better climbing and/or suspensory abilities (lorisids, dermopterans, and atelids) from those that engage in more quadrupedal or leaping behaviors. Therefore, a lower (albeit still significant) phylogenetic signal is found for this axis (Table 4). Plesiadapiforms and adapines are projected onto negative scores, between lorisids and the other extant groups. Notharctines, *Marcgodinotius indicus* and *Vastanomys major* are located in intermediate scores, overlapping with atelids, most extant strepsirrhines (excluding galagids and some cheirogaleids), and dermopterans. Conversely, fossil anthropoids, the remaining omomyiforms, *Anchomomys frontanyensis* and *D. martinezi* are projected onto positive scores. Given the lower phylogenetic component of the standard PC2, the phylogenetic PC2 (accounting for 11% of the total variation; SOM Fig. S3A) similarly discriminates more climbing and/or suspensory species (positive scores) from leapers and quadrupeds (negative scores). The PC2 is significantly correlated with both ln CS and ln BM (Table 5; SOM Figs. S5B–6B), suggesting a slight negative allometric correlation explaining up to 8–9% of the total variation. Significant differences in PC2 are found between tarsi-fulcrumators and metatarsi-fulcrumators, but the interaction between either size variable and foot type remains nonsignificant.

Table 4
Phylogenetic signal computed for the most explanatory principal components (PCs) derived from the species-mean Procrustes shape coordinates of each bone.

PC	Statistic	Astragalus	*p*	Calcaneus	*p*
		Phylogenetic signal		Phylogenetic signal	
1	K	1.854	**<0.001**	2.891	**<0.001**
	λ	0.975	**<0.001**	1.000	**<0.001**
2	K	1.035	**<0.001**	1.211	**<0.001**
	λ	0.993	**<0.001**	0.948	**<0.001**
3	K	0.867	**<0.001**	–	–
	λ	0.939	**<0.001**	–	–
4	K	1.369	**<0.001**	–	–
	λ	0.963	**<0.001**	–	–

Abbreviations: K = Blomberg's K; λ = Pagel's lambda.
Significant results (p <0.05) are indicated in bold.

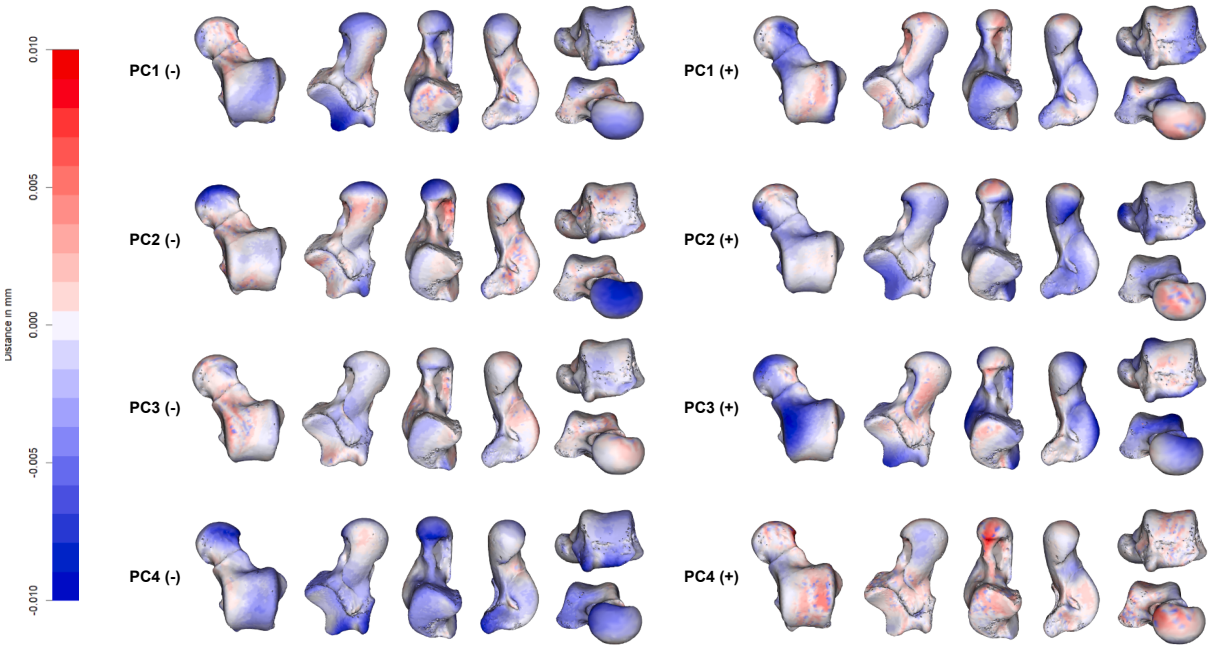


Figure 7. Displacement heatmaps illustrating mesh distances between the mean astragalar shape of each PC axis depicted in Figure 6 against the shapes associated with the minimum (−) and maximum (+) values. Blue and red indicate regions of contraction and expansion, respectively, based on the position of the extreme astragalar shapes (minimum or maximum values) relative to the mean shape along each PC axis. Abbreviation: PC = principal component. (For interpretation of the references to color in this figure legend, the reader is referred to the web version of this article.)

Table 5
Results of the phylogenetic generalized least squares (PGLS) analyses between astragalar/calcaneal shape and natural log-transformed (ln) centroid size (CS) or body mass (BM).

PC	Model	Astragalus		F	*p*	Calcaneus		F	*p*
		R^2	Df			R^2	Df		
1	ln CS	0.174	97	21.640	**<0.001**	−0.010	96	0.004	0.608
	ln BM	0.186	97	23.320	**<0.001**	0.082	96	9.694	**0.002**
	Foot type	−0.006	97	0.461	0.499	0.099	96	11.670	**0.001**
	ln CS × foot type	0.166	95	7.503	0.992	0.084	94	3.955	0.924
	ln BM × foot type	0.183	95	8.331	0.366	0.269	94	12.900	**0.006**
2	ln CS	0.088	97	10.480	**0.002**	0.107	96	12.630	**0.001**
	ln BM	0.084	97	9.980	**0.002**	0.005	96	1.451	0.231
	Foot type	0.049	97	6.037	**0.016**	−0.009	96	0.110	0.741
	ln CS × foot type	0.158	95	7.140	0.166	0.111	94	5.031	0.370
	ln BM × foot type	0.144	95	6.509	0.333	−0.004	94	0.870	0.303
3	ln CS	0.019	97	2.921	0.091	–		–	–
	ln BM	0.039	97	5.021	**0.027**	–		–	–
	Foot type	0.104	97	12.420	**0.001**	–		–	–
	ln CS × foot type	0.134	95	6.037	0.242	–		–	–
	ln BM × foot type	0.155	95	6.987	0.247	–		–	–
4	ln CS	−0.009	97	0.129	0.720	–		–	–
	ln BM	−0.006	97	0.402	0.528	–		–	–
	Foot type	0.036	97	4.662	**0.033**	–		–	–
	ln CS × foot type	0.063	95	3.187	**0.037**	–		–	–
	ln BM × foot type	0.050	95	2.719	0.094	–		–	–

Abbreviations: F = Fischer's F; Df = degrees of freedom; R^2 = adjusted coefficient of determination.
Astragalar and calcaneal shape are represented by the principal components (PCs) derived from the species-mean Procrustes shape coordinates of each bone. Additionally, the interaction between ln CS or ln BM and foot type was assessed too.[a]
[a] Significant results ($p < 0.05$) are indicated in bold.

The PC3 (accounting for 13% of the total variance, Fig. 6B) separates scandentians (very positive scores) from the other extant groups (slightly positive to negative scores). Shape differences associated with this axis are related to astragalar body shape (proximodistally shorter and lower medial side in positive scores than in negative scores), development of the trochlear rims (less developed in positive scores than in negative ones), and head shape (more dorsoplantarly compressed and laterally extended in positive scores than in negative scores; Fig. 7). A moderate phylogenetic signal, similar to that of PC2, is found for PC3 (Table 4). Fossil species are located in negative to slightly positive scores, thus overlapping with extant euprimates and dermopterans. Among fossil species, plesiadapiforms are the ones projected onto more positive scores, closer to scandentians. Unlike standard PC3, phylogenetic PC3 (accounting for 8% of the total variation; SOM Fig. S3B) discriminates plesiadapiforms (except for *Plesiadapis cookei*) from the other extant and extinct groups, resembling standard PC4. Only significant allometric relationship is found between PC3 and ln BM (Table 5; SOM Figs. S5C–S6C), although it is likely an artifact derived from the markedly different scores of scandentians. Conversely, strong significant differences in PC3 are found between tarsi-fulcrumators and metatarsi-fulcrumators, although the interaction between either size variable and foot type is nonsignificant.

The PC4 (accounting for 10% of the total variance, Fig. 6B) indicates differences between astragalar body (lower toward negative scores and higher toward positive ones), trochlear shape (more grooved and distally abbreviated in positive scores and shallower and more distally elongated in negative scores), fibular facet shape (more sloping in negative scores and steeper in positive ones), neck (narrower and more elongated in negative scores than in positive ones), and head shape (smaller relative to neck in negative scores than in positive ones; Fig. 7). The PC4 separates plesiadapiformes (very positive scores) from the extant groups (negative to slightly positive scores), with most adapiforms, omomyiforms, and early anthropoids being also projected onto slightly to moderately positive scores. A strong phylogenetic signal is found for this axis, indicating that phylogeny highly influences the distribution of species along PC4 (Table 4). Phylogenetic PC4 (accounting for 6% of the total variation; SOM Fig. S3B) resembles standard PC4, but it places greater emphasis on distal trochlear elongation, a feature that distinguishes notharctids (positive scores) due to their extreme development of the PTS. No significant correlation between PC4 and either ln CS or ln BM is found (Table 5; SOM Figs. S5D–S6D). Conversely, significant differences in PC4 are found between tarsi-fulcrumators and metatarsi-fulcrumators, as well as the interaction between ln CS and foot type, although this result is likely an artifact derived from the moderately positive scores of scandentians.

3.2. Calcaneal shape variation

The first two PCs of the standard PCA performed on the species-mean Procrustes shape coordinates of the calcaneus were chosen as the most meaningful and account for up to 82% of the total variance (SOM Fig. S7), differentiating species by phylogenetic group, locomotor behavior, and foot type.

The PC1 (accounting for 76% of the total variance; Fig. 8) is mostly associated with distal calcaneal elongation (abbreviated distal calcaneus toward negative scores and very elongated distal calcaneus toward positive scores; Fig. 9). This axis separates extant species depending on their degree of calcaneal elongation: scandentians, dermopterans, platyrrhines, lorisids, indriids, and *Daubentonia madagascariensis* are all projected in negative scores; lemurids, cheirogaleids, and lepilemurids are located along intermediate to slightly positive scores; and galagids and tarsiids are in the most positive scores of the axis. A strong phylogenetic signal is found for this axis, as evinced by the clear phylogenetic distribution of species along PC1 (Table 4). Plesiadapiforms (except for *C. simpsoni*) and adapines are projected onto very negative scores, outside the distribution of extant groups. Most adapiforms (except for *An. frontanyensis*), the Afro-Arabian anthropoids, and *C. simpsoni* are in slightly negative scores, overlapping with lorisids, indriids, *Da. madagascariensis*, platyrrhines, and nonprimate euarchontans. Omomyiforms, *Eosimias* and *An. frontanyensis* are projected onto slightly

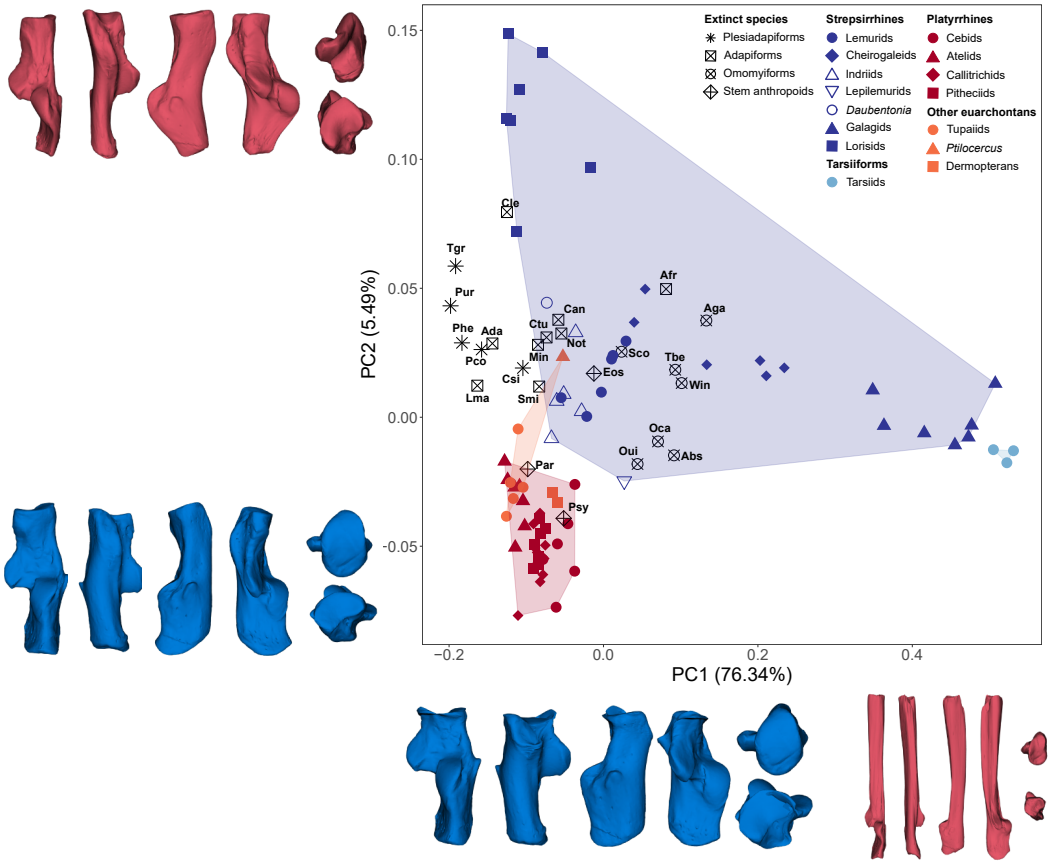


Figure 8. Results of the principal component analysis (PCA) performed on the species-mean Procrustes shape coordinates of the calcaneus as depicted by bivariate plots of PC2 vs. PC1. Taxonomic groups are coded by color and symbol, as indicated in the legend. The percentage of variance explained by each PC is reported within parentheses. Calcaneal shapes associated with minimum (blue) and maximum (red) values of each PC axis are plotted below each scatterplot (dorsal, plantar, lateral, medial, proximal, and distal views are shown, from left to right). Thin-plate splines correspond to a calcaneus of *Eulemur albifrons* (AMNH 170717). Abbreviations: Par = Parapithecidae indet; Psy = *Proteopithecus sylviae*; Eos = *Eosimias*; Oui = *Ouraya uintensis*; Sco = *Shoshonius cooperi*; Win = *Washakius insignis*; Oca = *Omomys carteri*; Abs = *Absarokius*; Aga = *Arapahovius gazini*; Tbe = *Teilhardina belgica*; Afr = *Anchomomys frontanyensis*; Ada = *Adapis* group; Lma = *Leptadapis magnus*; Cle = *Caenopithecus lemuroides*; Ctu = *Copelemur tutus*; Smi = *Smilodectes*; Not = *Notharctus*; Can = *Cantius*; Min = *Marcgodinotius indicus*; Csi = *Carpolestes simpsoni*; Pco = *Plesiadapis cookei*; Phe = *Phenacolemur*; Tgr = *Tinimomys graybulliensis*; Pur = *Purgatorius*; PC = principal component. (For interpretation of the references to color in this figure legend, the reader is referred to the web version of this article.)

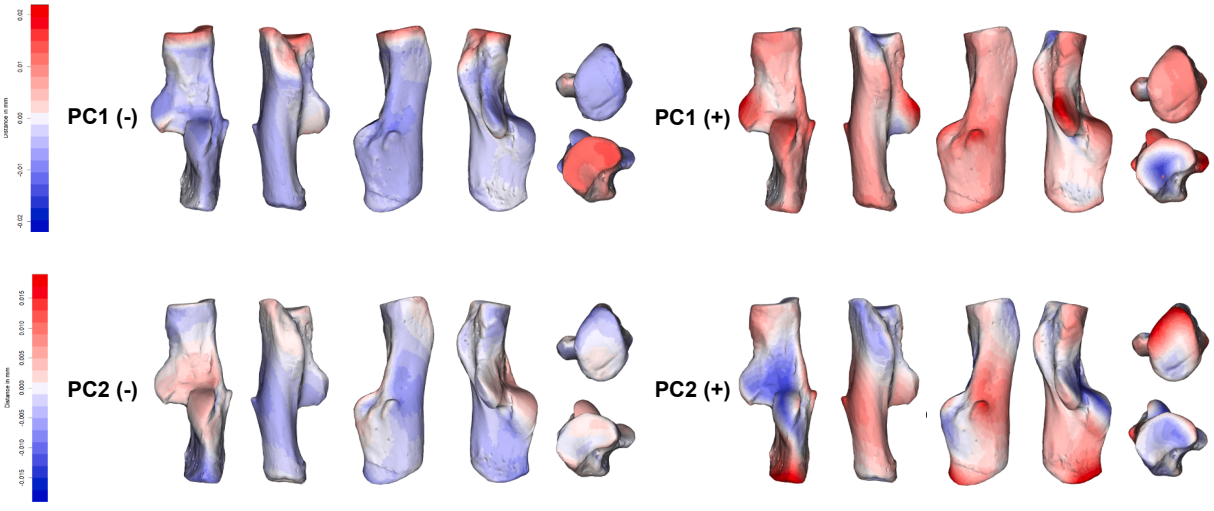


Figure 9. Displacement heatmaps illustrating mesh distances between the mean calcaneal shape of each PC axis depicted in Figure 8 against the shapes associated with the minimum (−) and maximum (+) values. Blue and red indicate regions of contraction and expansion, respectively, based on the position of the extreme calcaneal shapes (minimum or maximum values) relative to the mean shape along each PC axis. Abbreviation: PC = principal component. (For interpretation of the references to color in this figure legend, the reader is referred to the web version of this article.)

positive scores, overlying with lemurids and cheirogaleids. Despite the strong phylogenetic signal found for the standard PC1, the phylogenetic PC1 (accounting for 41% of the total variation; SOM Fig. S8) reflects the same distribution as proximodistal elongation is still the main source of variation for this bone even when the phylogenetic structure of the sample is considered. Nevertheless, it is remarkable that the amount of variance explained by this axis is only slightly more than half (41%) than that in the standard PCA (76%), suggesting that considering phylogenetic nonindependence among species improves the resolution for assessing aspects of calcaneal shape variation beyond distal elongation. Calcaneal size and BM are significantly correlated ($r^2 = 0.667$; $p < 0.001$; SOM Fig. S9). However, it is evident from the visualization of the scatterplot that galagids and tarsiers, which engage in a specialized locomotor behavior called vertical clinging and leaping (VCL), are outliers from the common trend exhibited by the rest of the sample. If galagids and tarsiers are removed from the analysis, the determination coefficient improves substantially ($r^2 = 0.919$; $p < 0.001$; SOM Fig. S10). A significant allometric relationship is found between PC1 and ln BM, but not with ln CS as the size variable (Table 5; SOM Fig. S11A, B). Significant differences are also found in PC1 between tarsi-fulcrumators and metatarsi-fulcrumators, and the interaction between ln BM and foot type is significant as well, explaining up to 27% of the total variance.

The PC2 (accounting for 5% of the total variance; Fig. 8) reflects changes in the shape and orientation of the ectal facet (more saddle shaped toward negative scores and more rounded and oblique toward positive scores), shape and orientation of the sustentacular facet (narrower and more dorsally oriented in negative scores and mediolaterally broader and medially oriented toward positive scores), position of the peroneal tubercle (more distally in negative scores than in positive ones), shape and orientation of the tuber calcanei (straighter, mediolaterally broader, and dorsoplantarly higher in negative scores and medially oriented and dorsoplantarly lower in positive scores), shape of the cuboid facet (flatter in negative scores and more concave in positive scores), and plantar edge shape (straighter in negative scores and more concave toward positive scores; Fig. 9). The PC2 separates lorisids (very positive scores) from extant anthropoids, tarsiids, and nonprimate euarchontans (negative scores). The remaining extant strepsirrhines are located between these groups in slightly positive scores. Most fossil species are projected onto slightly positive scores as well, largely overlapping with extant lemuroids and galagids. *Caenopithecus lemuroides* overlies with lorisids in more positive scores than any other fossil species, and the Afro-Arabian anthropoids fall within platyrrhine variation in negative scores. Compared to PC1, this axis has a weaker (albeit significant) phylogenetic signal (Table 4). As expected from the only moderately strong phylogenetic signal, the phylogenetic PC1 (accounting for 10% of the total variation; SOM Fig. S8) depicts a similar distribution of the species, separating the most climbing and/or suspensory species of each group—lorisids, atelids, and *Ptilocercus lowii*—from the most quadrupedal ones. Remarkably, the phylogenetic PC2 differs from the standard PC2 by associating distal calcaneal elongation with positive scores too. This association may explain the greater amount of variance explained by this axis than the standard PC2. Unlike PC1, the only significant allometric relationship is found between PC2 and ln CS (Table 5; SOM Figs. S11C, D), explaining up to 11% of the total variance. Neither significant differences in PC2 were found between tarsi-fulcrumators and metatarsi-fulcrumators nor a significant interaction was found between either size variable and foot type.

3.3. Astragalar shape as a predictor for locomotion

The covariation between astragalar shape and locomotor behavior is significant and explains up to 92% of covariance in the first two PLS axes (Table 6). Mean absolute error resulting from the cross-validated results performed on the extant species set reveals that the analysis accurately predicted all five locomotor variables (Table 7; SOM Fig. S12; SOM Table S4).

The first axis (PLS1; Fig. 10A) resembles PC2 (Fig. 6A) and discriminates between the more suspensory lorisids, atelids, dermopterans, and *Da. madagascariensis*, with more positive scores of the shape axis, and specialized VCL species (i.e., tarsiers, galagids, lepilemurids, and indriids). The group of more suspensory primates is characterized by a dorsoplantarly low astragalar body, a proximodistally elongated and slightly grooved trochlea, a laterally sloping fibular facet, a flat and slightly laterally oriented ectal facet, a proximodistally short and mediolaterally broad neck, and a relatively large and mediolaterally expanded head (Fig. 11). Conversely, the specialized leaping species possess a dorsoplantarly high astragalar body, a proximodistally abbreviated trochlea, a relatively deep trochlear groove, a comparatively steep fibular facet, a concave and plantarly oriented ectal facet, a proximodistally elongated and mediolaterally narrow astragalar neck, and a spherical astragalar head (Fig. 11). Plesiadapiforms display positive scores, suggesting that suspensory behaviors were an important component of their locomotor repertoire. Among fossil euprimates, the *Adapis* group exhibits the most positive scores, followed by *V. major* and *M. indicus*, indicating that suspension was also an important component of their locomotor repertoires. Notharctines, *L. magnus* and *Ganlea* are projected onto slightly positive scores, overlapping with more generalized species. The remaining species (*Eosimias*, the parapithecids, *An. frontanyensis*, *D. martinezi*, and most omomyiforms in exclusion of *V. major*) are plotted toward more negative values of the shape axis, indicating higher percentages of leaping behavior.

The second axis (PLS2; Fig. 10B) exhibits a clear phylogenetic pattern that nevertheless is also correlated with different

Table 6
Results of the two-block partial least squares (2B-PLS) between species-mean Procrustes shape coordinates of astragalar and calcaneal shape and quantified locomotor data.[a]

Bone	Latent variables	Singular value	% covariation	r-PLS	*p*
Astragalus	PLS1*	0.017	63.298	0.790	**<0.001**
	PLS2*	0.011	28.410	0.731	**<0.001**
	PLS3	0.006	7.371	0.666	**<0.001**
	PLS4	0.002	0.696	0.489	0.164
	PLS5	0.001	0.224	0.497	**0.026**
Calcaneus	PLS1*	0.039	88.463	0.565	**<0.001**
	PLS2*	0.012	8.964	0.753	**<0.001**
	PLS3	0.006	2.397	0.713	**<0.001**
	PLS4	0.001	0.125	0.413	0.177
	PLS5	0.001	0.051	0.467	0.015

Abbreviations: r-PLS = correlation coefficient between PLS scores.
[a] Significant results ($p < 0.05$) are indicated in bold, while the most explanatory PLS axes are denoted with asterisks.

Table 7
Mean absolute error (MAE)[a] calculated for the entire comparative sample after comparing the original locomotor values compiled for each extant species with the predicted ones using a leave-one-out cross-validation approach.

	Astragalus	Calcaneus
Q	0.172	0.184
C	0.101	0.095
L	0.174	0.162
S	0.138	0.134
CC	0.136	0.122

Abbreviations: Q = quadrupedalism; C = climbing; L = leaping; S = suspension; CC = clawed clinging/climbing.
[a] MAE is defined as the arithmetic average of the absolute errors.

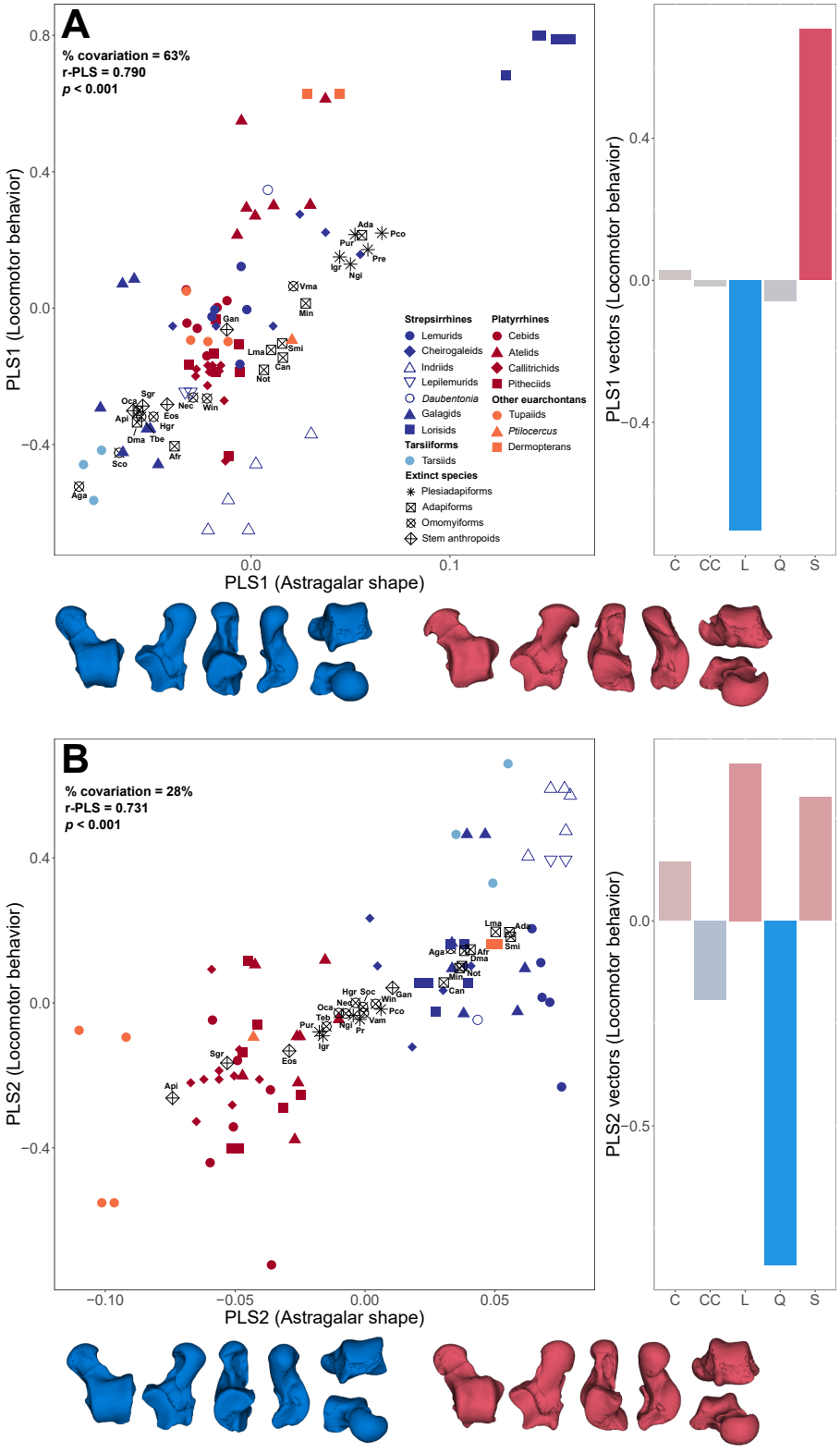


Figure 10. Results of the partial least squares regression (PLSR) for the first (PLS1; A) and second (PLS2; B) sets of linear combinations between the species-mean Procrustes shape coordinates (astragalar shape) and quantified locomotor data. The vectors of the first (A) or second (B) PLS axis of the locomotor variables are plotted to the right of each scatterplot. Taxonomic groups are coded by color and symbol, as indicated in the legend. Astragalar shapes associated with minimum (blue) and maximum (red) values of covariation are plotted below each scatterplot (dorsal, plantar, lateral, medial, proximal, and distal views are shown, from left to right). Thin-plate splines correspond to an astragalus of *Plecturocebus moloch* (AMNH 244363). Abbreviations: Q = quadrupedalism; C = climbing; L = leaping; S = suspension; CC = clawed clinging/climbing; Api = *Apidium*; Sgr = *Simonsius grangeri*; Gan = *Ganlea*; Eos = *Eosimias*; Nec = *Necrolemur*; Hgr = *Hemiacodon_gracilis*; Sco = *Shoshonius cooperi*; Win = *Washakius insignis*; Oca = *Omomys carteri*; Aga = *Arapahovius gazini*; Vma = *Vastanomys major*; Tbe = *Teilhardina belgica*; Dma = *Djebelemur martinezi*; Afr = *Anchomomys frontanyensis*; Ada = *Adapis* group; Lma = *Leptadapis magnus*; Smi = *Smilodectes*; Not = *Notharctus*; Can = *Cantius*; Min = *Marcgodinotius indicus*; Ngi = *Nanodectes gidleyi*; Pre = *Plesiadapis rex*; Pco = *Plesiadapis cookei*; Igr = *Ignacius graybullianus*; Pur = *Purgatorius*; PLS = partial least squares; r-PLS = correlation coefficient between PLS scores. (For interpretation of the references to color in this figure legend, the reader is referred to the web version of this article.)

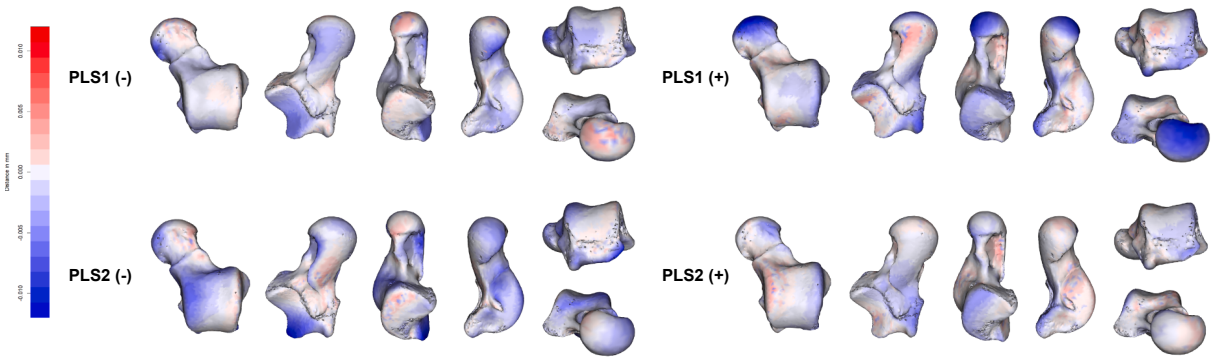


Figure 11. Displacement heatmaps illustrating mesh distances between the mean astragalar shape of each PLS shape axis depicted in Figure 10 against the shapes associated with the minimum (−) and maximum (+) values. Blue and red indicate regions of contraction and expansion, respectively, based on the position of the extreme astragalar shapes (minimum or maximum values) relative to the mean shape along each PLS shape axis. PLS = partial least squares. (For interpretation of the references to color in this figure legend, the reader is referred to the web version of this article.)

locomotor behaviors, resembling PC3 (Fig. 6B). Species with higher percentages of quadrupedalism, such as tree shrews and most platyrrhines, exhibit the most negative values along the shape axis, associated with a dorsoplantarly low astragalar body, a flat and slightly wedged trochlea (wider distally than proximally) with an elevated lateral rim, a steep fibular facet, a restricted medial tibial facet, an only slightly concave ectal facet, and a laterally tilted head (Fig. 11). In contrast, those species (strepsirrhines, dermopterans, and tarsiids) with a higher proportion of suspensory behaviors, leaping, and climbing, which can be interpreted as an emphasis in a 'grasp-leaping' behavior in euprimates, display the most positive scores and exhibit a dorsoplantarly high astragalar body, a moderately grooved trochlea with equally high parallel rims, a sloping fibular facet, a broad and dorsoplantarly extended medial tibial facet, a moderately concave ectal facet, and a head comparably oriented in the horizontal plane (Fig. 11). Plesiadapiforms, *Ganlea*, and most omomyiforms are projected onto intermediate scores between the two clusters formed by platyrrhines (negative scores) and strepsirrhines and tarsiers (positive scores). This indicates no predominance in their locomotor behavior of neither quadrupedalism nor a combination of suspensory and climbing and/or leaping behaviors typical of most extant prosimians. Conversely, *Eosimias* and the parapithecids are projected onto negative scores, overlapping with platyrrhines and suggesting an important quadrupedal component in their locomotor repertoire, whereas adapiforms and *Arapahovius gazini* fall with the extant strepsirrhine/tarsier cluster, indicating greater frequencies of suspensory, leaping, and climbing behaviors.

3.4. Calcaneal shape as a predictor for locomotion

There is significant covariation between calcaneal shape and locomotor behavior and explains 97% of the total covariance in the first two PLS axes (Fig. 12; Table 6). Mean absolute error resulting from the cross-validated results performed on the extant species set reveals that the analysis accurately predicted all five locomotor variables (Table 7; SOM Fig. S13; SOM Table S5).

The first axis (PLS1; Fig. 12A) is primarily related to distal calcaneal elongation, resembling PC1 (Fig. 8A). Species associated with high percentages of either quadrupedalism or suspension, in positive scores, are characterized by a proximodistally short distal calcaneus with mediolaterally wide ectal and sustentacular facets and a dorsoplantarly high and concave cuboid facet with a comparatively deep cuboid pit (Fig. 13). Conversely, leaping behaviors, exhibited by galagids and tarsiers (small VCL species), in negative scores, are associated with an extreme proximodistal elongation of the distal part of the calcaneus and mediolaterally narrow and restricted ectal and sustentacular facets (Fig. 13). Larger-bodied specialized VCL species, namely indriids and *Lepilemur*, are clear outliers of the trend observed in the scatterplot, displaying relatively positive scores in the shape axis and negative scores in the locomotor axis. Neither indriids nor lepilemurids exhibit extreme proximodistal elongation of the distal calcaneus. Plesiadapiforms display very positive scores, indicating that quadrupedalism and suspension were frequent behaviors in their locomotor repertoire. Omomyiforms and the small-sized adapiform *An. frontanyensis* overlap between cheirogaleids and non-indriid lemuroids, suggesting moderate use of climbing and leaping behaviors, without reaching the extremes exhibited by galagids and tarsiers. In contrast, the remaining adapiforms fall among anthropoids, indicating a higher frequency of quadrupedalism in their locomotion. *Caenopithecus lemuroides* is located very close to lorisids, denoting a similar type of locomotion. Early anthropoids are projected closer to adapiforms, except for *Eosimias*, which overlaps with omomyiforms.

The second axis (PLS2; Fig. 12B) resembles PC2 (Fig. 8) and phylogenetic PC2 (SOM Fig. S8), separating the most suspensory species (lorisids, atelids, and dermopterans) from the most quadrupeds (tupaiids, pitheciids, and cebids), as well as clawed clingers (callitrichids). Suspensory species, in most positive scores, are associated with a rounded and oblique ectal facet, mediolaterally broad and medially oriented sustentacular facet, a very proximally located peroneal tubercle, a medially oriented and dorsoplantarly low tuber calcanei, a very concave cuboid facet, and a concave plantar edge (Fig. 13). Conversely, quadrupedal species, in negative scores, exhibit a saddle-shaped ectal facet, a narrow and dorsally oriented sustentacular facet, a distally positioned peroneal tubercle, a straight, stout, and mediolaterally broad tuber calcanei, a flat cuboid facet, and a straight plantar edge (Fig. 13). Plesiadapiforms are distributed along the shape axis in a gradient, ranging from *Purgatorius* (negative scores) to *C. simpsoni* (positive scores), indicating distinct proportions of quadrupedal and suspensory behaviors within their locomotor repertoire depending on the species. Most adapiforms and omomyiforms are projected onto slightly negative to slightly positive scores, indicating a predominance of quadrupedalism over suspension, albeit some species like *Ca. lemuroides*, *M. indicus*, *Ar. gazini*, and *An. frontanyensis* are in more positive scores, suggesting a greater reliance in suspensory locomotion. Within anthropoids, the Afro-Arabian anthropoids are distinguished by their very negative scores, whereas *Eosimias* overlaps with adapiforms and omomyiforms in slightly positive scores. This result suggests that while the former probably

engaged in mostly quadrupedal locomotion with little to no suspension, *Eosimias* exhibited a more versatile locomotor behavior that included some degree of suspensory locomotion.

3.5. Variation in the locomotor behavior of Paleogene primates

Variation in the predicted percentages of locomotion in Paleogene primates not only supports the existence of a diverse array of locomotor behaviors among the various primate groups represented in this study but, in some cases, also denotes different estimates for some locomotor categories depending on the bone used as a predictor (Figs. 14–16; Tables 8 and 9).

When astragalar shape is used as a predictor, all plesiadapiform species are reconstructed displaying a very similar locomotor repertoire, with an important quadrupedal component (42–47%), and moderate amounts of climbing (14–22%), leaping (15–24%), and suspension (15–20%). No clawed clinging/climbing behavior is inferred for plesiadapiforms when astragalar shape is utilized as a predictor. This locomotor profile approaches the condition exhibited by *Cheirogaleus*, as well as that of the most arboreal tree shrews (*P. lowii* and *Tupaia minor*). Contrarily, when calcaneal shape is used as a predictor, plesiadapiforms reveal a different picture: on the one hand, *Purgatorius*, *Tinimomys graybulliensis*, and *Phenacolemur* (i.e., nonplesiadapoid plesiadapiforms) are characterized by relatively high amounts of quadrupedalism (60–67%) followed by small amounts of the other behaviors (>15%), except for clawed clinging/climbing. The only exception to this is *T. graybulliensis*, which is inferred to suspend more than the other two (19%). On the other hand, the locomotor repertoire of *Pl. cookei* and *C. simpsoni* (i.e., plesiadapoids) is dominated by quadrupedalism (42–49%) and suspension (26–32%), with only moderate amounts of climbing (15%) and traces of leaping (2–4%). Contrasting with nonplesiadapoid species, both *Pl. cookei* and *C. simpsoni* are inferred to participate in some degree of scansorial behavior as well (6–9%). The former nonplesiadapoid species mostly resembles extant tupaiids in their inferred locomotor repertoire. In contrast, plesiadapoids (particularly *C. simpsoni*) approach the locomotor profile of lorisids and other suspensory species (e.g., dermopterans and *Da. madagascariensis*).

Among early euprimates, adapiforms are the group exhibiting the most diverse locomotor behavior. Overall, three different main locomotor repertoires can be inferred from their estimated locomotion. The first one, exhibited by most species, is that of an arboreal quadruped and leaper, characterized by higher percentages (mostly above 30%) for both locomotor behaviors. When astragalar shape is used as a predictor, most notharctines, *M. indicus, L. magnus,* as well as *An. frontanyensis* and *D. martinezi* for both bones, concur with this locomotor profile. Remarkably, when astragalar shape is used as the predictor, higher values for leaping behavior are recovered (40–58%), whereas when calcaneal shape is utilized, comparatively higher percentages for suspension (up to 16%) are obtained for these species. Compared to extant species, they are better analogized to lemurids (in the case of notharctines and *L. magnus*) and to *Mirza* and *Microcebus* (*M. indicus*, *An. frontanyensis*, and *D. martinezi*). The second locomotor profile, characterized by a high quadrupedal component (49–55%), is represented by the *Adapis* group, *L. magnus*, and *Copelemur tutus* when calcaneal shape is used as the predictor. In this case, they are better analogized to small quadrupedal anthropoids (e.g., *Saimiri*, *Cebus*, and *Callicebus*), which participate in different arboreal behaviors (climbing, leaping, and suspension) but mainly move quadrupedally above relatively large supports. Lastly, the third locomotor profile is characterized by a high proportion of suspension (28–30%) and relatively low values for the other behaviors, particularly leaping. *Marcgodinotius indicus* and *Ca. lemuroides* fit this locomotor profile when calcaneal shape is used as a predictor and the *Adapis* group, when astragalar shape is used as a predictor. They resemble extant lorisids, *Daubentonia*, and *Cheirogaleus* due to their inferred emphasis on suspension.

Omomyiforms consistently exhibit a very homogeneous locomotor repertoire when either astragalar or calcaneal shape is used as the predictor. All omomyiforms display high percentages of leaping behavior (39–64%), followed by moderate amounts of quadrupedalism (20–39%) and climbing (12–23%). Compared with extant species, omomyiforms most closely resemble *Microcebus* and the most generalized galagids (i.e., those that more rarely engage in VCL behaviors). The only exception is *V. major*, which is inferred to have relied more on quadrupedalism (41%) and to have been a less frequent leaper (27%). In addition, moderate amounts of climbing (20%) and suspension (12%) indicate a more generalized behavior for this species, approaching that of *Otolemur*.

Anthropoids are reconstructed as mostly relying on quadrupedalism (43–55%) and leaping (30–42%), with small amounts of climbing in their locomotor repertoire as well (12–15%). Remarkably, they are inferred not to participate in suspensory behaviors at all. This locomotor profile is exhibited by parapithecids, *Proteopithecus sylviae*, and *Eosimias* when astragalar shape is used as the predictor, resembling the locomotor repertoire exhibited by extant small platyrrhines (e.g., *Saimiri*, *Cebus*, and *Callicebus*). Contrarily, when calcaneal shape is used as the predictor, *Ganlea* and *Eosimias* display less emphasis on quadrupedalism (28–31%), higher amounts of leaping (36–39%), and moderate frequency of climbing (19–20%). In addition, they are inferred to have moved using suspension as well (6–13%). This results in *Eosimias* (as predicted from calcaneal shape) approaching the condition exhibited by extant cheirogaleids, whereas *Ganlea* is better analogized to extant lemurids and *Otolemur*.

3.6. The evolution of astragalar and calcaneal shape in relation to locomotor changes among early primates

Branch-specific rate reconstructions (Fig. 17A, B) indicate that the transition from plesiadapiforms to euprimates exhibits very high evolutionary rates, the highest across the entire tree in the case of the calcaneus. Plesiadapiform branches are also characterized by very high evolutionary rates, particularly plesiadapoids. Similarly, adapiforms and omomyiforms display high evolutionary rates. Among the former, *Ca. lemuroides* and adapines exhibit particularly high evolutionary rates for the calcaneus, while the other species do not show increased rates compared to the branch leading from the euprimate LCA, suggesting less morphological change. In contrast, evolutionary rates for the astragalus remain consistently high across all adapiform species. Omomyiforms display increased evolutionary rates for both bones, with further increases in the branch leading to crown tarsiiforms. Remarkably, evolutionary rates in the branch leading to anthropoids are consistently low, indicating little morphological change between the euprimate/haplorrhine and anthropoid LCAs. However, in both bones, the lineage leading to the clade comprised by crown anthropoids and Afro-Arabian parapithecids and proteopithecids—to the exclusion of *Eosimias* and *Ganlea*—is characterized by increased evolutionary rates, suggesting significant morphological changes were occurring along this branch. Additionally, extant groups that exhibit specialized locomotor behaviors—such as lorisids, galagids, atelids, and tarsiids—display higher evolutionary rates at the base of their clades than other groups. This pinpoints that evolutionary rates of astragalar and calcaneal morphology are informative about locomotor transitions.

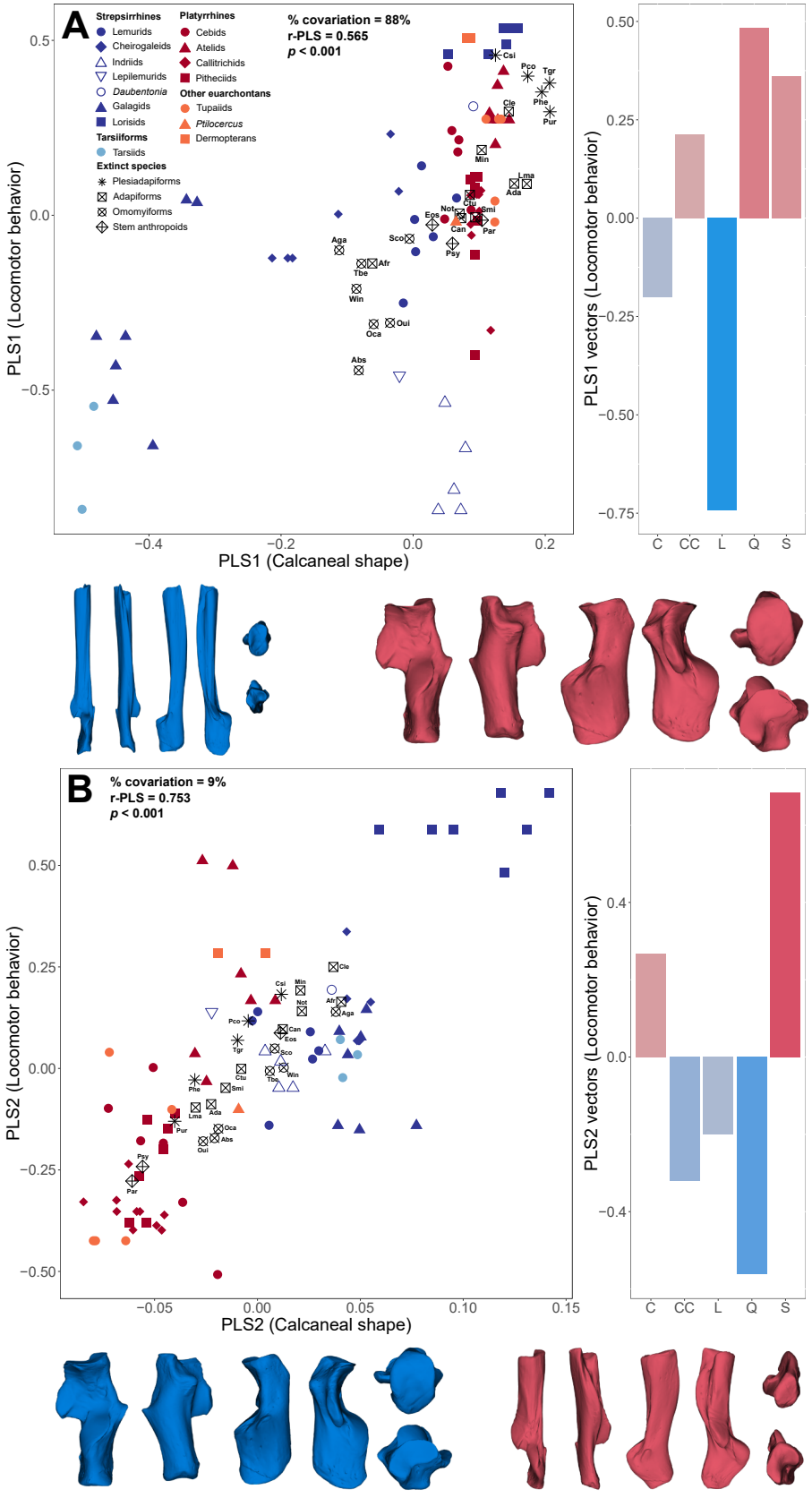


Figure 12. Results of the partial least squares regression (PLSR) for the first (PLS1; A) and second (PLS2; B) sets of linear combinations between the species-mean Procrustes shape coordinates (calcaneal shape) and quantified locomotor data. The vectors of the first (A) or second (B) PLS axis of the locomotor variables are plotted to the right of each scatterplot. Taxonomic groups are coded by color and symbol, as indicated in the legend. Calcaneal shapes associated with minimum (blue) and maximum (red) values of covariation are plotted below each scatterplot (dorsal, plantar, lateral, medial, and proximal views are shown, from left to right). *Eulemur albifrons* (AMNH 170717). Abbreviations: Q = quadrupedalism; C = climbing; L = leaping; S = suspension; CC = clawed clinging/climbing; Par = Parapithecidae indet; Psy = *Proteopithecus sylviae*; Eos = *Eosimias*;

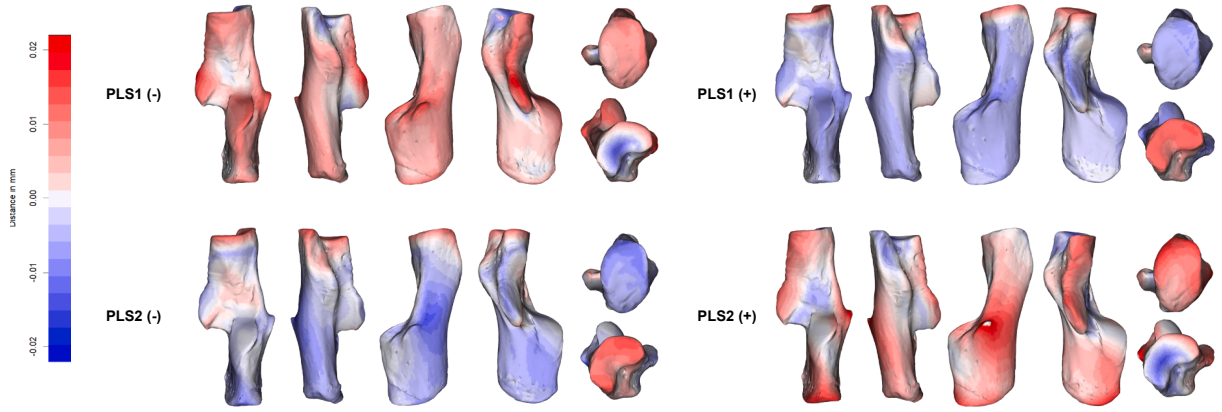


Figure 13. Displacement heatmaps illustrating mesh distances between the mean calcaneal shape of each PLS shape axis depicted in Figure 12 against the shapes associated with the minimum (−) and maximum (+) values. Blue and red indicate regions of contraction and expansion, respectively, based on the position of the extreme calcaneal shapes (minimum or maximum values) relative to the mean shape along each PLS shape axis. PLS = partial least squares. (For interpretation of the references to color in this figure legend, the reader is referred to the web version of this article.)

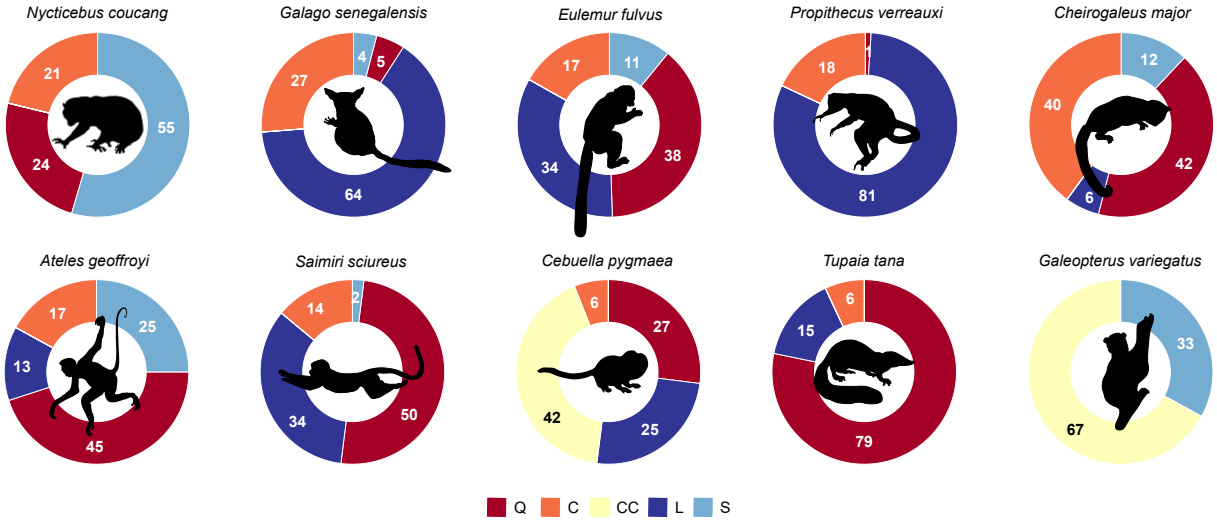


Figure 14. Donut charts summarizing the locomotor repertoire of a representative sample of the main primate groups (and close relatives) from the extant comparative sample. Abbreviations: Q = quadrupedalism; C = climbing; L = leaping; S = suspension; CC = clawed clinging/climbing. (For interpretation of the references to color in this figure, the reader is referred to the web version of this article.)

Increases in the rates of morphological evolution in both bones are reflected by the ancestral locomotor reconstructions (Fig. 17C, D; Table 10). The locomotor repertoires of the euarchont and primate LCAs are estimated to be very similar, dominated by quadrupedalism (39–49%) and lower amounts of the other locomotor variables (<26%). Conversely, the euprimate LCA shows an important increase in leaping behavior (22–32%). The strepsirrhine, tarsiiform, and anthropoid LCAs are reconstructed as more habitual leapers (24–43%) than the euprimate LCA, suggesting further increases in leaping behavior occurring in the different euprimate lineages. More specifically, the tarsiiform LCA shows the highest percentages of leaping behavior, whereas the anthropoid LCA exhibits comparatively higher percentages of quadrupedal locomotion (39–40%). Lastly, the strepsirrhine LCA is reconstructed as engaging in substantially higher suspension (12–17%) than either the tarsiiform or anthropoid LCAs.

4. Discussion

4.1. Functional morphology of the astragalocalcaneal complex

Comparative anatomy is a powerful tool to elucidate the relationship between the shape of a given structure (e.g., the hindfoot) and function (which might provide hints of the 'biological role', sensu Bock and von Wahlert, 1965). If this correlation is found to be strong, it allows us to provide reliable morphofunctional inferences—as it may be expected that similar selective pressures lead to similar anatomical adaptations (Lauder, 1986).

Oui = *Ourayia uintensis*; Sco = *Shoshonius cooperi*; Win = *Washakius insignis*; Oca = *Omomys carteri*; Abs = *Absarokius*; Aga = *Arapahovius gazini*; Tbe = *Teilhardina belgica*; Afr = *Anchomomys frontanyensis*; Ada = *Adapis* group; Lma = *Leptadapis magnus*; Cle = *Caenopithecus lemuroides*; Ctu = *Copelemur tutus*; Smi = *Smilodectes*; Not = *Notharctus*; Can = *Cantius*; Min = *Marcgodinotius indicus*; Csi = *Carpolestes simpsoni*; Pco = *Plesiadapis cookei*; Phe = *Phenacolemur*; Tgr = *Tinimomys graybulliensis*; Pur = *Purgatorius*; PLS = partial least squares; r-PLS = correlation coefficient between PLS scores. (For interpretation of the references to color in this figure legend, the reader is referred to the web version of this article.)

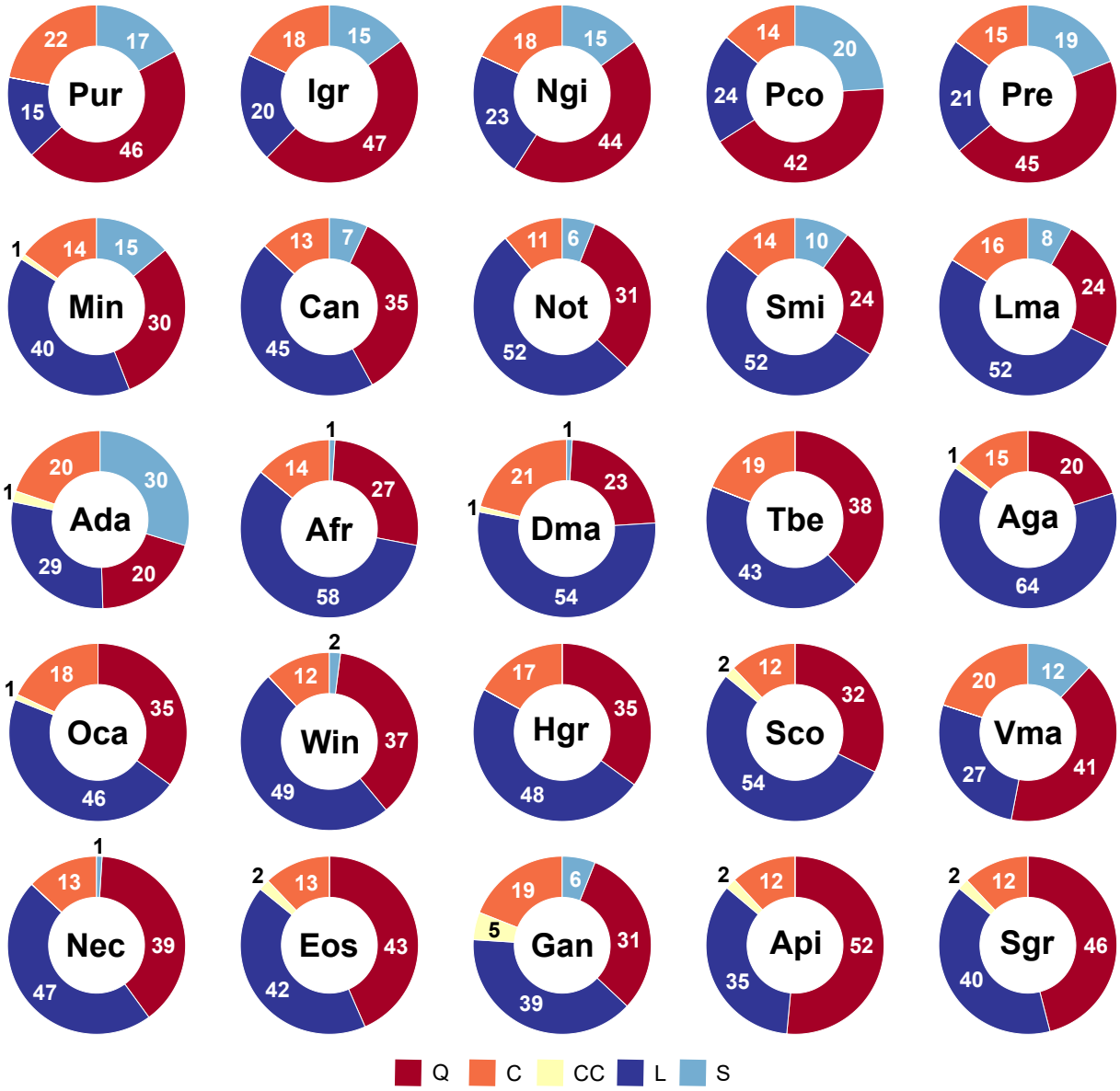


Figure 15. Donut charts summarizing the estimated locomotor repertoires of the extinct Paleogene taxa based on astragalar shape. Abbreviations: Q = quadrupedalism; C = climbing; L = leaping; S = suspension; CC = clawed clinging/climbing. Api = *Apidium*; Sgr = *Simonsius grangeri*; Gan = *Ganlea*; Eos = *Eosimias*; Nec = *Necrolemur*; Hgr = *Hemiacodon_gracilis*; Sco = *Shoshonius cooperi*; Win = *Washakius insignis*; Oca = *Omomys carteri*; Aga = *Arapahovius gazini*; Vma = *Vastanomys major*; Tbe = *Teilhardina belgica*; Dma = *Djebelemur martinezi*; Afr = *Anchomomys frontanyensis*; Ada = *Adapis* group; Lma = *Leptadapis magnus*; Smi = *Smilodectes*; Not = *Notharctus*; Can = *Cantius*; Min = *Marcgodinotius indicus*; Ngi = *Nanodectes gidleyi*; Pre = *Plesiadapis rex*; Pco = *Plesiadapis cookei*; Igr = *Ignacius graybullianus*; Pur = *Purgatorius*. (For interpretation of the references to color in this figure, the reader is referred to the web version of this article.)

Below, the main morphofunctional relationships between the hindfoot and locomotor behavior among primates (and their closest relatives) are discussed on the basis of both the correlations observed between tarsal shape and function and their relevance regarding plesiadapiform and early euprimate locomotor behavior.

In line with previous studies, our results indicate that the shape of the facets that conform the different joints constituting the ankle and tarsal elongation encompasses most functional information to reliably predict the locomotor behavior in extinct species (e.g., Szalay and Decker, 1974; Conroy and Rose, 1983; Moyà-Solà et al., 2012; Boyer and Seiffert, 2013; Boyer et al., 2013b, 2015; Parr et al., 2014; Yapuncich et al., 2017, 2019; Yapuncich and Granatosky, 2021). Our analyses show a strong correlation between astragalar/calcaneal shape and suspensory behaviors, such as a dorsoplantarly low astragalar body, a proximodistally elongated and slightly grooved trochlea, a laterally sloping fibular facet, a flat and slightly laterally oriented ectal facet, a proximodistally short and mediolaterally broad neck, a relatively large and mediolaterally expanded head (for the astragalus), a rounded an oblique ectal facet, mediolaterally broad and medially oriented sustentacular facet, a very proximally located peroneal tubercle, a medially oriented and dorsoplantarly low tuber calcanei, a very concave cuboid facet, and a concave plantar edge (for the calcaneus). Previous studies have shown that suspensory species (lorisids, atelids, dermopterans, *Daubentonia*, and *Cheirogaleus*) exhibit many to all of these features to some degree (Sarmiento, 1983; Gebo, 1989a; Boyer and Seiffert, 2013; Yapuncich and Granatosky, 2021), resulting in increased foot mobility that allows them to engage in different types of slow locomotion dominated by cautious climbing along with other types of progression, such as bridging movements to cross spatial gaps in

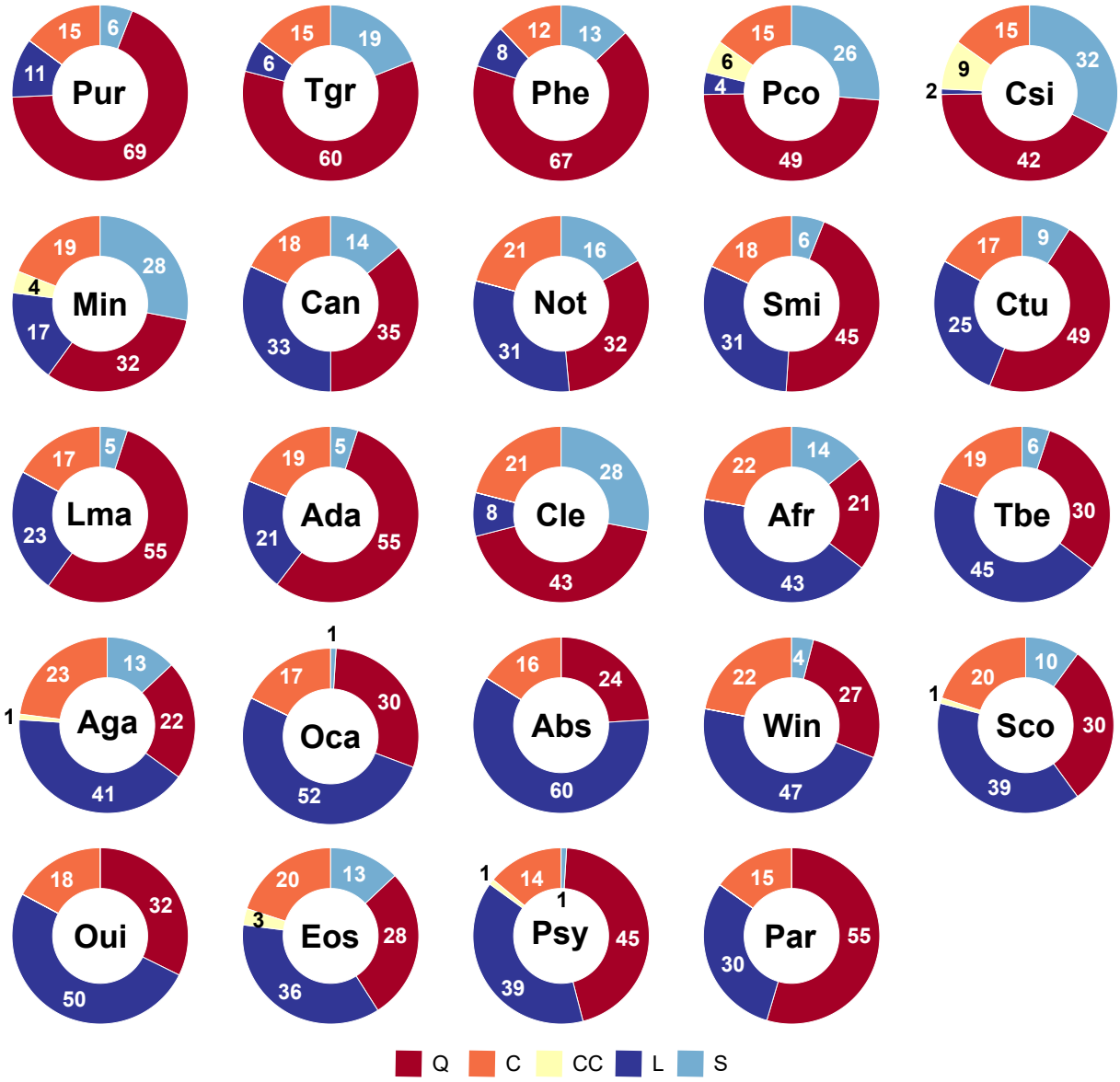


Figure 16. Donut charts summarizing the estimated locomotor repertoires of the extinct Paleogene taxa based on calcaneal shape. Abbreviations: Q = quadrupedalism; C = climbing; L = leaping; S = suspension; CC = clawed clinging/climbing. Par = Parapithecidae indet; Psy = *Proteopithecus sylviae*; Eos = *Eosimias*; Oui = *Ourayia uintensis*; Sco = *Shoshonius cooperi*; Win = *Washakius insignis*; Oca = *Omomys carteri*; Abs = *Absarokius*; Aga = *Arapahovius gazini*; Tbe = *Teilhardina belgica*; Afr = *Anchomomys frontanyensis*; Ada = *Adapis* group; Lma = *Leptadapis magnus*; Cle = *Caenopithecus lemuroides*; Ctu = *Copelemur tutus*; Smi = *Smilodectes*; Not = *Notharctus*; Can = *Cantius*; Min = *Marcgodinotius indicus*; Csi = *Carpolestes simpsoni*; Pco = *Plesiadapis cookei*; Phe = *Phenacolemur*; Tgr = *Tinimomys graybulliensis*; Pur = *Purgatorius*. (For interpretation of the references to color in this figure, the reader is referred to the web version of this article.)

the canopy and below-branch suspension (Gebo, 1987a; Oxnard et al., 1990; Youlatos and Meldrum, 2011; Youlatos et al., 2018). Some of these features (such as the medial bending of the tuber calcanei or a mediolaterally broader trochlea and calcaneal ectal facets) are found in some extinct species, including, *M. indicus*, *Ca. lemuroides*, and the *Adapis* group (Godinot, 1991; Seiffert et al., 2015; Dunn et al., 2016; Llera Martín et al., 2022). Additionally, as indicated by the allometric regressions, body size appears to influence certain climbing-related features, particularly in the astragalus (e.g., lower astragalar body and relatively larger facet areas than in fast-leaping and quadrupedal species). This pattern may stem from the distinct biomechanical constraints faced by larger-bodied species (Demes and Günther, 1989; Preuschoft et al., 1996), as exemplified by atelids and indriids compared to smaller platyrrhines and strepsirrhines, respectively (Fleagle and Mittermeier, 1980; Gebo and Dagosto, 1988). Lorisids are outliers from this allometric regression, representing the most extreme morphology for these features irrespective of their body size (Gebo, 1989a).

Conversely, specialized leapers display the opposite condition, characterized by features functionally related to foot stability (Gebo, 1987b, 1988; Boyer et al., 2013b), such as a dorsoplantarly high astragalar body, a proximodistally abbreviated trochlea, a relatively deep trochlear groove, a comparatively steep fibular facet, a concave and plantarly oriented ectal facet, a proximodistally elongated and mediolaterally narrow astragalar neck, a spherical astragalar head (in the astragalus), mediolaterally narrow and restricted calcaneal ectal and sustentacular facets, and a straight calcaneal plantar edge (in the calcaneus). However, as climbing and clinging on vertical substrates is interwoven with leaping behavior in the case of VCL species (tarsiers, galagids, and

Table 8
Estimated locomotor percentages using species-mean Procrustes shape coordinates of astragalar shape as a predictor.

Family	Species	Q	C	L	S	CC
Plesiadapiformes:						
Purgatoriidae	*Purgatorius* sp.	46	22	15	17	0
Paromomyidae	*Ignacius graybullianus*	48	18	20	15	0
Plesiadapidae	*Nannodectes gidleyi*	44	18	23	15	0
Plesiadapidae	*Plesiadapis cookei*	42	14	20	24	0
Plesiadapidae	*Plesiadapis rex*	45	15	21	19	0
Omomyiformes:						
Incertae sedis	*Teilhardina belgica*	38	19	43	0	0
Incertae sedis	*Vastanomys major*	41	20	27	12	0
Omomyidae	*Arapahovius gazini*	20	14	64	0	1
Omomyidae	*Necrolemur* sp.	39	13	47	1	0
Omomyidae	*Hemiacodon gracilis*	35	17	48	0	0
Omomyidae	*Omomys carteri*	35	18	46	0	1
Omomyidae	*Shoshonius cooperi*	32	12	53	0	2
Omomyidae	*Washakius insignis*	37	12	49	2	0
Adapiformes:						
Notharctidae	*Marcgodinotius indicus*	30	15	40	14	1
Notharctidae	*Cantius* sp.	35	13	45	7	0
Notharctidae	*Notharctus* sp.	31	11	52	6	0
Notharctidae	*Smilodectes* sp.	24	14	52	10	0
Notharctidae	*Anchomomys frontanyensis*	27	14	58	1	0
Adapidae	*'Adapis* group'	20	20	29	30	2
Adapidae	*Leptadapis magnus*	24	16	51	8	0
Stem Lemuriformes:						
Djebelemuridae	*Djebelemur martinezi*	23	21	54	1	1
Anthropoidea:						
Eosimiidae	*Eosimias* sp.	43	12	42	0	2
Amphipithecidae	*Ganlea* sp.	31	19	39	6	5
Parapithecidae	*Apidium* sp.	52	12	35	0	2
Parapithecidae	*Simonsius grangeri*	46	12	40	0	2

Abbreviations: Q = quadrupedalism; C = climbing; L = leaping; S = suspension; CC = clawed clinging/climbing.

Table 9
Estimated locomotor percentages using species-mean Procrustes shape coordinates of calcaneal shape as a predictor.

Family	Species	Q	C	L	S	CC
Plesiadapiformes:						
Purgatoriidae	*Purgatorius* sp.	69	15	11	6	0
Micromomyidae	*Tinimomys graybulliensis*	60	15	6	19	0
Paromomyidae	*Phenacolemur* sp.	67	12	8	13	0
Plesiadapidae	*Plesiadapis cookei*	48	15	4	26	6
Carpolestidae	*Carpolestes simpsoni*	42	15	1	32	9
Omomyiformes:						
Incertae sedis	*Teilhardina belgica*	30	19	45	5	0
Omomyidae	*Absarokius* sp.	24	16	60	0	0
Omomyidae	*Arapahovius gazini*	22	23	41	13	1
Omomyidae	*Omomys carteri*	30	18	52	1	0
Omomyidae	*Ourayia uintensis*	32	17	50	0	0
Omomyidae	*Shoshonius cooperi*	30	20	39	10	1
Omomyidae	*Washakius insignis*	27	22	47	4	0
Adapiformes:						
Notharctidae	*Marcgodinotius indicus*	32	19	17	28	4
Notharctidae	*Cantius* sp.	35	18	33	14	0
Notharctidae	*Copelemur tutus*	47	17	27	9	0
Notharctidae	*Notharctus* sp.	32	21	31	17	0
Notharctidae	*Smilodectes* sp.	45	18	31	6	0
Notharctidae	*Anchomomys frontanyensis*	21	22	42	14	0
Adapidae	*'Adapis* group'	56	19	21	5	0
Adapidae	*Leptadapis magnus*	55	17	23	5	0
Adapidae	*Caenopithecus lemuroides*	43	21	8	28	0
Anthropoidea:						
Eosimiidae	*Eosimias* sp.	28	20	36	13	3
Parapithecidae	*Parapithecidae* indet.	54	15	30	0	0
Proteopithecidae	*Proteopithecus sylviae*	45	14	39	1	1

Abbreviations: Q = quadrupedalism; C = climbing; L = leaping; S = suspension; CC = clawed clinging/climbing.

indriids) and clawed clinging callitrichids (Gebo, 1987a; Oxnard et al., 1990; Youlatos, 1999), this results in an admixture of morphological features associated with leaping (functionally linked to increasing the lever arm or the stability of the tarsal joints) and climbing (increasing the mobility of the foot). More precisely, strepsirrhines that engage in specialized VCL behavior, such as galagids and indriids (excluding more 'occasional' leapers such as cheirogaleids and some lemurids), exhibit clear adaptations for climbing vertical substrates (e.g., a sloping fibular facet, contrasting with the steeper shape found in haplorhines), which paradoxically contribute to greater foot mobility (Beard et al., 1988; Gebo and Dagosto, 1988; Gebo, 2011).

Generalized arboreal quadrupeds (e.g., lemurids, cheirogaleids, and many nonatelid platyrrhines) lack the extreme morphological adaptations found in either slow climbing/suspensory or specialized VCL species (Gebo, 1988). Our analyses show that quadrupedal species exhibit a dorsoplantarly low astragalar body, a flat and slightly wedged trochlea (wider distally than proximally) with an elevated lateral rim, a steep fibular facet, a restricted medial tibial facet, an only slightly concave ectal facet, a laterally tilted head (in the astragalus), a saddle-shaped ectal facet, a narrow and dorsally oriented sustentacular facet, a distally positioned peroneal tubercle, a straight, stout, and mediolaterally broad tuber calcanei, a flat cuboid facet, and a straight plantar edge (in the calcaneus). This set of features provides stability at the ankle (less concomitant mediolateral movements during plantarflexion or dorsiflexion) and increases the power arm of the triceps surae (facilitating force transmission, which is greater in the context of quadrupedal locomotion on large substrates; Conroy and Rose, 1983; Gebo, 1986, 1989b; Strasser, 1988). Early anthropoids and some adapiforms exhibit many of these features, suggesting that above-branch quadrupedal running on large and horizontal substrates was an important component of their locomotor behavior (Fleagle, 1980; Conroy and Rose, 1983; Gebo and Simons, 1987; Gebo, 1989b; Godinot, 1991; Fleagle and Simons, 1995). In addition, scandentians, regardless of their locomotor repertoire, that grade from mainly arboreal to more terrestrial forms, exhibit much reduced foot mobility and grasping capabilities, resembling some of those found in small quadrupedal primates (Sargis, 2001, 2002a, 2002b; Youlatos et al., 2017; Granatosky et al., 2022). As already suggested, astragalar and calcaneal shape of the most primitive (nonplesiadapoid) plesiadapiforms match some of the features exhibited by scandentians, evincing the potential of tree shrews as extant analogues of the ancestral euarchontan positional behavior (Sargis, 2001; Gebo, 2004; Bloch et al., 2007; Godinot, 2007; Sargis et al., 2007).

As previously stated, an elongated calcaneus is associated to habitual leaping behavior (Hall-Craggs, 1965; Decker and Szalay, 1974; Gebo, 1988; Dagosto, 1988, 2007; Moyà-Solà et al., 2012; Boyer et al., 2013b; Marigó et al., 2016; Monclús-Gonzalo et al., 2023). Proximodistal elongation of the distal calcaneus results in an increase of the lever arm of the foot, which is required to generate enough force to leap efficiently (Morton, 1924; Gebo, 1988). However, because of the different biomechanical constraints associated with distinct BMs, different anatomical solutions are exhibited by taxa (Demes and Günther, 1989). Small-bodied leapers (considered 'foot-powered leapers') exhibit elongation of the distal segments of the hind limb (the tarsus), whereas larger-bodied leapers (regarded 'thigh-powered leapers') display a more elongated proximal hind limb segment and use the foot solely as a force transducer (Gebo and Dagosto, 1988; Demes and Günther, 1989; Demes et al., 1996). Additionally, the type of foot (in relation to the location of the fulcrum; Morton, 1924) also

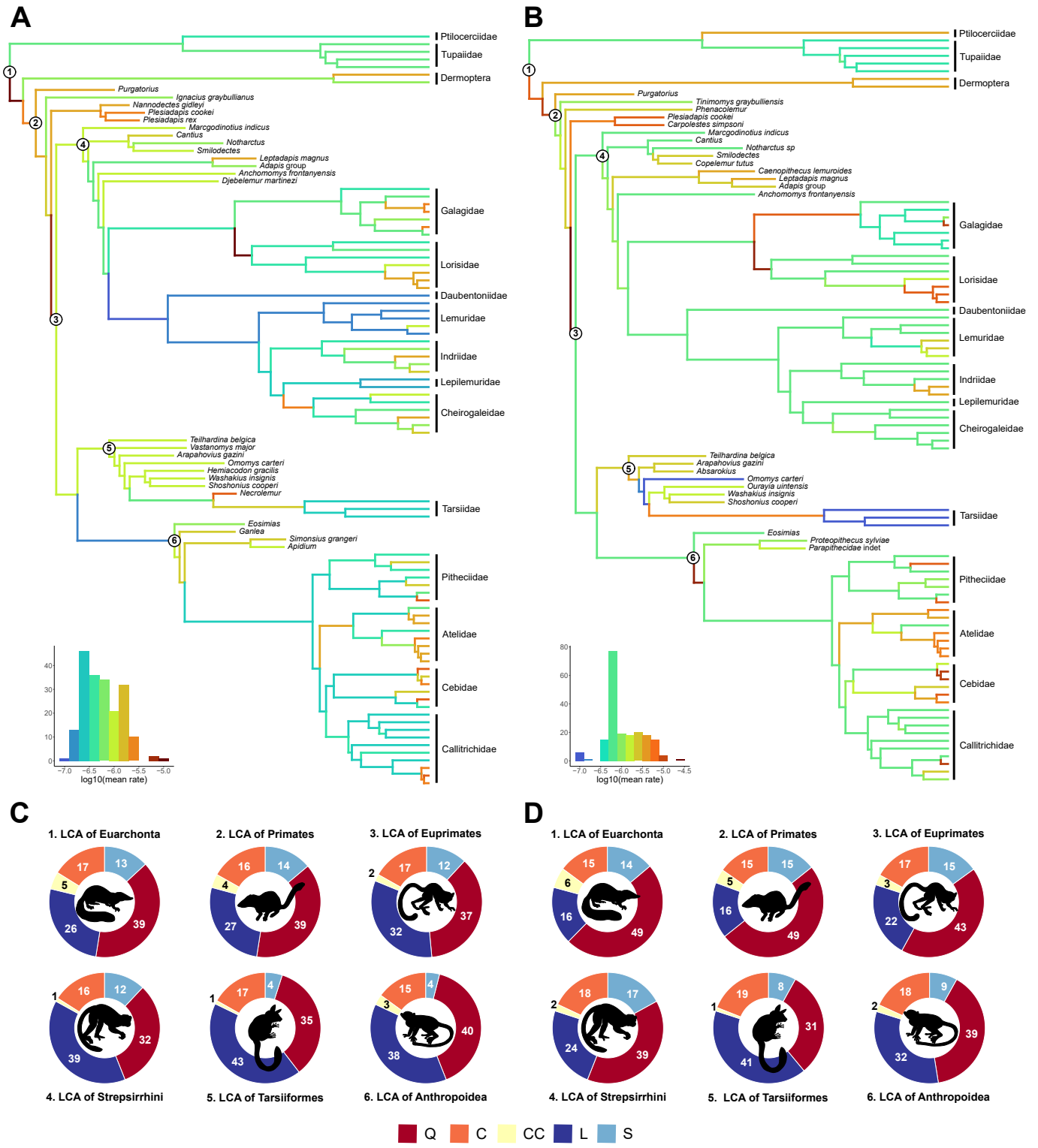


Figure 17. Branch-specific evolutionary rates for astragalar (A) and calcaneal (B) shape in extant and extinct primates. Branch rates are coded by color. (Warmer colors indicate faster evolutionary rates, while cooler colors represent slower evolutionary rates.) Below, each phylogenetic tree donut charts summarizes the estimated locomotor repertoires for each last common ancestor (LCA) based on astragalar (C) calcaneal (D) shape. Abbreviations: Q = quadrupedalism; C = climbing; L = leaping; S = suspension; CC = clawed clinging/climbing. (For interpretation of the references to color in this figure legend, the reader is referred to the web version of this article.)

influences the degree of proximodistal elongation of the tarsus (Moyà-Solà et al., 2012). Most nonprimate generalized mammals, including close relatives of primates such as scandentians and dermopterans, as well as anthropoids and likely plesiadapiforms, possess a metatarsi-fulcrumating foot. This group is characterized by a fulcrum placed distally in the foot, on the heads of metatarsals or even more distally up to the phalanges (Morton, 1924). Conversely, extant strepsirrhines and tarsiers, as well as early

Table 10
Estimated locomotor percentages of the internal nodes representing the last common ancestor (LCA) of euarchontans, primates, euprimates, strepsirrhines, tarsiiforms, and anthropoids.

LCA	Q	C	L	S	CC
Astragalus:					
Euarchonta	39	17	26	13	5
Primates	39	16	27	14	4
Euprimates	37	17	32	12	2
Strepsirrhini	32	16	39	12	1
Tarsiiformes	35	17	43	4	1
Anthropoidea	40	15	38	4	3
Calcaneus:					
Euarchonta	49	15	16	14	6
Primates	49	15	16	15	5
Euprimates	43	17	22	15	3
Strepsirrhini	39	18	24	17	2
Tarsiiformes	31	19	41	8	1
Anthropoidea	39	18	32	9	2

Abbreviations: Q = quadrupedalism; C = climbing; L = leaping; S = suspension; CC = clawed clinging/climbing.

euprimates (adapiforms and omomyiforms), exhibit a tarsi-fulcrumating foot, characterized by a much more proximally placed fulcrum (on the distal tarsal bones). The more proximal placement of the fulcrum provides improved grasping abilities at the cost of losing the part of the lever constituted by the metatarsus. Therefore, tarsi-fulcrumators require further elongation of the tarsal elements to compensate the loss of load arm, even if they are not specialized VCL species (Moyà-Solà et al., 2012). For this reason, small-bodied tarsi-fulcrumating primates are more prone to exhibit proximodistally elongated calcanei, even if they are not specialized leapers. In contrast, metatarsi-fulcrumating habitual leapers, as it is the case of many small platyrrhines and cercopithecoids, do not display a very elongated calcaneus. The results of our analyses concur with previous studies that extreme proximodistal elongation of the mid-tarsal region (including the distal calcaneus) in the case of small-bodied species with a tarsi-fulcrumating foot (e.g., tarsiers, galagids, and some cheirogaleids) is an adaptation for leaping behavior (Hall-Craggs, 1965; Dagosto, 1988; Gebo, 1988; Moyà-Solà et al., 2012; Boyer et al., 2013b; Monclús-Gonzalo et al., 2023) that can be found to different degrees among extinct tarsi-fulcrumating primates, indicating emphasis on leaping (Decker and Szalay, 1974; Dagosto, 1983; Covert, 1988; Gebo, 1988; Godinot, 1991; Gebo et al., 1991, 2001, 2012; Covert and Hamrick, 1993; Dagosto et al., 1999; Seiffert et al., 2015; Dunn et al., 2016; Marigó et al., 2016; Llera Martín et al., 2022). This is further supported by our allometric analyses that indicate significant differences in calcaneal shape (mainly driven by distal calcaneal elongation) between tarsi- and metatarsi-fulcrumating species in relation to body size (Moyà-Solà et al., 2012; Boyer et al., 2013b).

4.2. The locomotor behavior of Paleogene primates

Plesiadapiforms Our locomotor estimates for plesiadapiforms indicate a relatively generalized locomotor repertoire dominated by quadrupedalism, combined with lower percentages of climbing, leaping, and suspensory behaviors, concurring with a relatively mobile ankle, capable of extensive movements of inversion and eversion and adapted to the arboreal milieu (Szalay and Decker, 1974; Chester et al., 2015, 2017, 2019). Compared to most euprimates, plesiadapiforms are reconstructed as more suspensory and less prone to leap (Szalay and Dagosto, 1980; Dagosto, 1988, 2007). Nevertheless, the distinct relative amounts of quadrupedalism, leaping, and suspension predicted for each species, as well as the information provided by other skeletal elements of the postcranium, suggests that plesiadapiforms displayed considerable locomotor diversity (Bloch and Boyer, 2007; Bloch et al., 2007).

Purgatorius, the earliest known plesiadapiform (Van Valen and Sloan, 1965; Clemens, 1974; Wilson Mantilla et al., 2021), is reconstructed as having a locomotor repertoire largely analogous to that of extant arboreal tree shrews (Sargis, 2001, 2002a; Sargis et al., 2007; Chester et al., 2015). However, based on astragalar shape, it exhibits substantial amounts of suspensory behaviors (17%), suggesting a more deliberate type of locomotion for this species than for extant tree shrews. In contrast, calcaneal shape indicates that *Purgatorius* would have been the most quadrupedal plesiadapiform in our sample (69%)—which may be interpreted as a plesiomorphic condition of the ancestral euarchontan locomotor behavior. Extensive quadrupedalism in *Purgatorius* is supported by several calcaneal features, such as the relatively restricted ectal and sustentacular facets, and the dorsoplantarly lower and proximodistally elongated tuber calcanei, resembling those exhibited by tree shrews (Godinot, 2007).

Estimated locomotor percentages for *T. graybulliensis*, solely based on calcaneal shape, suggest a different locomotor behavior to that of *Purgatorius*, emphasizing more suspensory behaviors (19%). This concurs with the view, based on some features at the pelvis resembling those of taxa that frequently engage in suspensory behaviors (such as dermopterans and lorisids), that micromomyids might have been capable of some sort of below-branch suspensory behaviors (Bloch and Boyer, 2007).

We did not find evidence of a 'callitrichid-like' locomotor behavior in paromomyids, which has been inferred due to similarities in body size, exudativory diet, and locomotor repertoire (Garber, 1992; Vinyard et al., 2003; Youlatos and Meldrum, 2011). Our results, based on an astragalus of *Ignacius graybullianus* and a calcaneus of *Phenacolemur*, do not recover percentages of clawed clinging/climbing for these two species, as would be expected from the analysis of the rest of their postcranial skeleton (Bloch and Boyer, 2007; Bloch et al., 2007). In contrast, they are reconstructed as versatile quadrupeds, comparable to the other plesiadapiforms. Nevertheless, given that most features associated with vertical clinging/climbing are found in the trunk and forelimbs, our results do not unambiguously rule out this locomotor behavior and instead, given the less importance of suspensory locomotion (13–15%) inferred for this group, concur with the view that they were also adept pronograde bounders (Bloch and Boyer, 2007; Bloch et al., 2007).

Plesiadapids are consistently reconstructed as generalized arboreal quadrupeds capable of engaging in substantial amounts of suspensory behavior. The results based on the calcaneus of *Pl. cookei* suggest a more frequent use of suspension (26%) and claw clinging/climbing postures (6%), as indicated by the proximodistally long calcaneal ectal facet and dorsoplantarly high tuber calcanei. This result is consistent with its greater inferred BM (Boyer and Gingerich, 2019) as well as with the analysis of other regions of its postcranial skeleton, such as phalangeal proportions and humeral morphology, which resemble those of dermopterans and sloths (Hamrick, 2001; Boyer and Gingerich, 2019).

Calcaneal shape in *C. simpsoni* indicates a marked increase in the utilization of suspensory behaviors (32%) compared to the other plesiadapiforms, supporting the view that this animal had a more deliberate locomotion, which some have analogized to the extant didelphid *Caluromys* (Bloch and Boyer, 2002; Sargis et al., 2007). Similarities between the calcaneal shape of *Carpolestes* and extant suspensory species like dermopterans and lorisids, such as a rounded and oblique ectal facet, a mediolaterally broad and medially oriented sustentacular facet, a more proximally

(compared to other plesiadapiforms) peroneal tubercle, and a proportionally short and a dorsoplantarly high tuber calcanei, are indicative of a very mobile ankle better adapted to accommodate the foot into different postures on differently oriented supports and endure tensile forces during suspension rather than resist large loads derived from a more quadrupedal locomotion. This concurs with other features of the postcranial skeleton, such as the possession of long fingers and an opposable hallux with a nail instead of a claw—which have been related to the ability to grasp small branches and variously interpreted as either homologous or convergent with euprimates (Bloch and Boyer, 2002; Gebo, 2004; Sargis et al., 2007).

Adapiforms Adapiforms are predicted to have exhibited the most diverse locomotor behavior among early euprimates, with species characterized by substantial quadrupedalism accompanied by moderate amounts of leaping, climbing, and suspension; some species inferred to engage more in leaping behavior; and others exhibited a great suspensory component accompanied by climbing, quadrupedalism, and a little leaping behavior. These more extensive locomotor differences may be related with greater differences in body size as well as an occupation of different ecological niches (Godinot, 1998; Gunnell et al., 2008).

Asiadapines, represented by *M. indicus*, are reconstructed as arboreal quadrupeds with less leaping proclivity than in later and more derived adapiforms (Boyer et al., 2013b, 2015; Marigó et al., 2016; Ni et al., 2016). Its predicted low leaping component is explained by many astragalar features (e.g., a proximodistally long trochlea, the lack of a developed PTS, and a mediolaterally expanded and a dorsoplantarly low astragalar head) as well as by its relatively short distal calcaneal region, indicating an abbreviated tarsus, especially when compared with similarly sized adapiforms such as *An. frontanyensis* (Marigó et al., 2016, 2020). Furthermore, locomotor percentages based on calcaneal shape yield substantial suspensory behavior (28%), which is supported by several calcaneal traits resembling lorisids, including a large and more proximally located (compared to other adapiforms) peroneal tubercle, a medially oriented tuber calcanei, a slightly concave calcaneal plantar edge, a rounded ectal facet, and a broad and medially facing sustentacular facet (Gebo, 1988, 1989a). This result is consistent with previous studies that argue for a cautious locomotion with very little leaping behavior for this species (Boyer et al., 2013b), although other suggest a more generalized quadrupedal locomotion (Rose et al., 2009; Dunn et al., 2016; Llera Martín et al., 2022).

Our results do not support the view that notharctines were specialized in VCL like extant indriids and *Lepilemur* (Walker, 1974; Rose and Walker, 1985; Covert, 1995; Schmitt, 1996). This hypothesis has been already contested due to the lack of several key features of the distal tarsus and metatarsus associated with a derived adductor grasping mode (Gebo, 1985), which is at odds with an extensive use of vertical substrates (Gebo et al., 1991). In addition, the relatively long hind limbs, characteristic of notharctines, do not necessarily refer to adaptations for leaping behavior (Preuschoft et al., 1998). Conversely, the notharctines analyzed here (*Cantius*, *Notharctus*, *Smilodectes*, and *Co. tutus*) are reconstructed as above-branch quadrupeds resembling extant lemurids, with substantial amounts of quadrupedalism and leaping in their inferred locomotor repertoire, concurring with previous studies (Gregory, 1920; Decker and Szalay, 1974; Rose and Walker, 1985; Covert, 1988; Gebo, 1988; Gebo et al., 1991). Inferences based on astragalar shape yield higher percentages of leaping behavior (45–52%), whereas calcaneal shape distinguishes *Cantius* and *Notharctus*, characterized by higher suspensory behavior (14–16%), from *Smilodectes* and *Co. tutus*, which are reconstructed as more quadrupedal (45–49%).

Locomotor percentages based on astragalar shape discriminate *L. magnus* from the *Adapis* group because of the more lorisid-like features in the astragalus of the latter (Dagosto, 1983). These results suggest that *L. magnus* was likely an above-branch quadrupedal runner (24%) and leaper (52%), while specimens included in the *Adapis* group displayed more suspensory behaviors (30%), approaching those of extant lorisids (Dagosto, 1983; Gebo, 1988). Conversely, locomotor percentages based on calcaneal shape depict a more homogeneous locomotor behavior for adapines, vastly dominated by quadrupedalism (55%) and convergent to that displayed by anthropoids (Godinot, 1991). This result is explained by the presence of several features in the adapine calcaneus (such as a longer and stouter tuber calcanei, indicating strong plantarflexion) related to quadrupedal locomotion (Godinot, 1991). The overall picture of adapines indicates that these animals moved quadrupedally engaging in less leaping behavior than notharctines, with at least some of the specimens included in the *Adapis* group displaying adaptations for a cautious slow climbing locomotion (Dagosto, 1983; Bacon and Godinot, 1998; Boyer et al., 2013a; Marigó et al., 2019).

As previously suggested by Seiffert et al. (2015), our locomotor estimations based on its calcaneal shape indicate that *Ca. lemuroides* displayed a slow-climbing locomotor repertoire, characterized by considerable amounts of climbing (21%) and suspensory (28%) behaviors. This result is supported by the presence of several adaptations that facilitate rotational movements within the foot (required to habitually hold an inverted foot to navigate across complex arboreal settings), such as concave calcaneal plantar edge, a dorsoplantarly high cuboid facet with a deep cuboid pit, a dorsomedially inclined sustentacular facet, a rounded and oblique ectal facet, and a medially angled and plantarly projecting tuber calcanei. The latter feature is expected to allow for digital flexion because of increasing the mechanical advantage of the flexor digitorum brevis muscle (Sarmiento, 1983).

In agreement with previous studies, our results support marked leaping adaptations in the astragalus and calcaneus of *An. frontanyensis* and *D. martinezi* (43–58%; Marivaux et al., 2013; Marigó et al., 2016, 2020; Monclús-Gonzalo et al., 2023). Features in the astragalus (a dorsoplantarly tall astragalar body, a relatively narrow and proximodistally elongated astragalar neck, and a developed PTS) and the calcaneus (moderate proximodistal elongation of the distal portion, comparable to that of some contemporaneous omomyiforms) are associated with active arboreal locomotion (Gebo, 1988). Nevertheless, other calcaneal features of *An. frontanyensis* (such as a rounded and proximodistally elongated ectal facet, a relatively concave plantar calcaneal edge, and a medially bended tuber calcanei) are indicative of better climbing abilities (21%) and higher mobility of the foot (as suggested by its predicted suspensory locomotion, 14%) than in some omomyiform species with similar distal calcaneal elongation. This concurs with the view that sympatric omomyiforms and adapiforms with similar locomotor profiles may have nevertheless partitioned their niches by substrate preference (Marigó et al., 2020).

Omomyiforms The results for most omomyiforms analyzed here (*Teilhardina belgica*, *Ar. gazini*, *Hemiacodon gracilis*, *Omomys carteri*, *Ourayia uintensis*, *Shoshonius cooperi*, *Washakius insignis*, and *Absarokius*) support an active locomotor behavior dominated by leaping (39–64%) and quadrupedalism (20–39%), in agreement with previous studies (Szalay, 1976; Savage and Waters, 1978; Gebo, 1988; Covert and Hamrick, 1993; Dagosto and Schmid, 1996; Anemone and Covert, 2000; Dunn et al., 2006; Rose et al., 2011; Gebo et al., 2012, 2015). Together with several astragalar features (such as a dorsoplantarly high astragalar body and a narrow and elongated astragalar neck), the moderately elongated calcaneus of omomyiforms, falling within the cheirogaleid range, is the most

prominent feature related with increased leaping behavior. Nevertheless, omomyiforms do not exhibit the extreme elongation displayed by the specialized small VCL species (galagids and tarsiers), suggesting an overall active yet not specialized VCL locomotor behavior for these species (Dagosto, 1988; Gebo, 1988; Boyer et al., 2013b; Monclús-Gonzalo et al., 2023). Only a calcaneus specimen attributed to *Necrolemur*, which is broken distally and could not be included in this study, exhibits a proximodistal elongation comparable to that of galagids and tarsiers (Godinot and Dagosto, 1983).

An astragalus attributed to *V. major* (GU 800) departs from the overall omomyiform locomotor profile discussed earlier. Our locomotor estimates indicate a more generalized locomotor repertoire, dominated by quadrupedal locomotion (41%) and exhibiting less emphasis for leaping behavior (27%). This result concurs with recent studies carried out on the available material attributed to this species (Dunn et al., 2016; Llera Martín et al., 2022).

Early anthropoids Our locomotor estimates concur with previous studies that highlighted the morphological and behavioral shift toward a more quadrupedal locomotion in early anthropoids (Fleagle, 1980; Conroy and Rose, 1983; Gebo and Simons, 1987; Gebo, 1989b; Fleagle and Simons, 1995). However, the Asian taxa (*Eosimias* and *Ganlea*) still retain astragalar and calcaneal features that lack the derived anthropoid condition displayed by the Afro-Arabian taxa, resulting in locomotor repertoires that depart from the latter group and, instead, more closely resemble those of strepsirrhines and tarsiiforms (Gebo et al., 2000, 2001; Marivaux et al., 2003, 2010).

Eosmiids resemble omomyiforms in having a high astragalar body, a reduced PTS (absent from early anthropoids from Afro-Arabia), a shallow trochlea with parallel rims, a mediolaterally narrow astragalar neck, and a moderately long astragalar neck (Gebo et al., 2000, 2001; Gebo and Dagosto, 2004). Our locomotor estimates based on astragalar shape indicate considerable amounts of leaping (42%) and quadrupedalism (43%). Conversely, locomotor estimates based on calcaneal shape yield substantial suspensory (13%) and climbing (20%) components, resembling similar-sized adapiforms like *An. frontanyensis* and *M. indicus*. This is supported by several features (a rounded ectal facet, a moderately concave plantar edge, and a slightly medially bended tuber calcanei) that are associated with relatively mobile ankle (Gebo, 1988). Overall, our locomotor estimates concur with the view that eosimiids fill the morphological and behavioral gap between the earliest euprimates and more derived anthropoids from Afro-Arabia (Gebo, 1986; Dagosto, 1990; Gebo and Dagosto, 2004).

Ganlea is reconstructed as a generalized arboreal quadruped, with substantial amounts of leaping (39%) and quadrupedalism (31%), as well as non-negligible percentages of climbing (19%) and suspensory behaviors (6%). This result is consistent with the mosaic morphology exhibited by its astragalus, displaying features associated with leaping (e.g., a dorsoplantarly high astragalar body, parallel trochlear rims, and a straight and moderately elongated astragalar neck) and others more tightly related to increased mobility at the upper ankle joint (such as a relatively shallow trochlear groove; Marivaux et al., 2003, 2010). Given the purported more basal anthropoid position of eosmiids and amphipithecids in relation to Afro-Arabian parapithecids and proteopithecids (Beard et al., 2009; Coster et al., 2013; Jaeger et al., 2020; Chaimanee et al., 2024), this agrees with the view that a more generalized locomotor behavior with less emphasis on quadrupedalism might be plesiomorphic for anthropoids (Gebo et al., 2000, 2001; Gebo and Dagosto, 2004).

Locomotor estimations based on astragalar and calcaneal shape consistently reconstruct parapithecids and proteopithecids as above-branch arboreal quadrupeds and leapers similar to extant small platyrrhines such as *Cebus* or *Saimiri* (Fleagle, 1980; Gebo and Simons, 1987; Gebo, 1989b; Simons and Seiffert, 1999; Seiffert and Simons, 2001; Gladman et al., 2013). The reconstructed locomotor profile, vastly dominated by quadrupedalism (55–45%) and leaping (35–40%), reflects the presence of many astragalar (a broad trochlear surface with moderate wedging, a marked notch on the astragalar neck, a lack of PTS, and a medial tibial facet forming a small cup-like concavity) and calcaneal features (abbreviated distal calcaneal elongation, a lateral extension of the cuboid facet, and a stout and mediolaterally broad tuber calcanei), indicative of an ankle capable of high degrees of dorsiflexion but less prone to use inverted postures like strepsirrhines or tarsiers (Conroy and Rose, 1983). Compared with the contemporaneous and larger-sized parapithecids, *Pr. sylviae* is reconstructed as a more agile leaper, in agreement with its more proximodistally elongated calcaneal distal region and overall more gracile morphology (Seiffert and Simons, 2001; Gladman et al., 2013).

4.3. Origin and diversification of euprimates in the light of locomotor behavior

Fossil evidence suggests that the emergence of euprimates was marked by profound anatomical modifications, including the acquisition of a complete postorbital bar, convergent orbits, higher encephalization, relatively long digits, opposable hallux and pollex, nails instead of claws, and adaptations for leaping behavior (Cartmill, 1974, 1992; Szalay et al., 1987; Rose, 1994; Silcox et al., 2015). At the hindfoot, several adaptations for strong pedal grasping and leaping behavior (e.g., development of a PTS, a more sloping fibular facet, tarsal elongation) distinguish early euprimates from plesiadapiforms (Dagosto, 1988, 2007; Rose, 1994; Boyer and Seiffert, 2013; Boyer et al., 2013b; Yapuncich et al., 2017, 2019). Our results align with this, as evidenced by the increased evolutionary rates for both astragalar and calcaneal shape along the lineage leading to the first euprimates. However, the lack of any transitional species displaying a mixture of archaic (i.e., plesiadapiform-like) and derived (i.e., euprimate-like) traits hampers testing among competing hypotheses about the original selection pressures that drove the origin and early diversification of euprimates (Silcox et al., 2015). To date, only a single species, *C. simpsoni*, could fill in this 'transitional' gap (Bloch and Boyer, 2002). Based on the features displayed by this species, combining adaptations for strong pedal grasping (opposable hallux with a nail) with the lack of euprimate-like visual or leaping adaptations, Bloch and Boyer (2002) concluded that small-branch specialization would have preceded visual and leaping-related adaptations. Our results provide further support to this hypothesis as our locomotor estimates based on the calcaneus of *C. simpsoni* yielded the highest percentage of suspensory locomotion among plesiadapiforms, concurring with a mobile ankle adapted to a more deliberate type of locomotion, as would be required to engage in the fine branch milieu. Additionally, we also found particularly high evolutionary rates describing plesiadapoid evolution, pinpointing to the substantial morphological changes already occurring prior the emergence of euprimates (Sargis et al., 2007). Altogether, these results are consistent with the terminal branch feeding hypothesis (Rasmussen, 1990), suggesting that adaptation to the fine branch milieu was critical in the early stages of primate evolution.

Of the various locomotor categories investigated here, leaping behavior within the arboreal canopy is the one that most consistently discriminates between plesiadapiforms and euprimates—and, thus, the most relevant for characterizing the locomotor shift that occurred during the plesiadapiform-euprimate

transition. Albeit lacking in some extant euprimates (lorisids and hominids), leaping is widespread and most characteristic of this group (Dagosto, 1988, 2007). This is confirmed by our results as we only obtained substantial percentages of leaping for euprimate specimens. Habitual leaping may be thus considered synapomorphic for euprimates, even though this does not imply that the euprimate LCA was necessarily an adept leaper. These results, in line with previous studies, are consistent with the 'grasp-leaping' hypothesis (Szalay and Dagosto, 1980). The locomotor estimate for the euprimate LCA concurs with only moderate leaping capabilities (22–32%). Indeed, the percentages of leaping inferred for the most basal species in this study, such as *Te. belgica*, *V. major*, and *M. indicus* (Rose et al., 2009, 2011; Dunn et al., 2016; Llera Martín et al., 2022), are substantially lower than those of more derived species, thereby rejecting the existance of specialized leaping behavior during the emergence of euprimates. This view is further supported by a partial skeleton of the basal haplorrhine *Archicebus achilles* described by Ni et al. (2013), which has been reconstructed as a generalized arboreal quadruped instead of a committed leaper—but see Boyer et al.'s (2017a) interpretation of an astragalus of *Donrussellia provincialis* for an alternate view on the importance of leaping among the earliest euprimates. On the other hand, euprimates from various clades (e.g., most omomyiforms and later crown tarsiiforms, galagids, *D. martinezi*, and *An. frontanyensis*) exhibit substantially higher leaping percentages than other members of their respective clades, supporting the independent evolution of specialized leaping adaptations among various extant and extinct euprimate lineages (Boyer et al., 2013b). This is further exemplified by our locomotor estimates (strepsirrhine LCA = 24–39%; tarsiiform LCA = 41–43%; anthropoid LCA = 32–38%) and by the increased evolutionary rates in the branches leading to these groups, suggesting substantial morphological changes associated with the acquisition of more specialized leaping behavior, which probably was absent in the euprimate LCA. Conversely, the low evolutionary rates observed in the branch leading from the euprimate LCA to *Eosimias*, along with the similarity between its locomotor estimates and those of the euprimate LCA, suggest that this early anthropoid could be a reasonably good analogue of the euprimate LCA, even if it already exhibited some derived anthropoid adaptations (Gebo et al., 2000, 2001).

5. Summary and conclusions

We quantitatively analyzed the shape of the astragalus and calcaneus in a broad sample of extant and extinct primates (and close relatives) by means of a high-density sliding semilandmark 3D geometric morphometric approach for the first time. We also investigated the functional relationship between tarsal shape and locomotion using an extensive locomotor dataset of extant species compiled from the literature. Based on the covariation between tarsal shape and locomotion, we made locomotor inferences about early primates and, on this basis, critically evaluated their exhibited locomotor diversity and the potential locomotor changes that might have occurred during the origin and early diversification of euprimates. Concurring with previous studies, our results indicate that the shape of these bones is an excellent predictor of the locomotor repertoire of extant species. In particular, the shape of the facets involved in the mobility at the main joints of the proximal tarsus is indicative of adaptations for different locomotor behaviors. In turn, the elongation of the distal region of the calcaneus is correlated with agile grasp-leaping locomotion in many primates, although biomechanical factors such as BM and foot type may also influence calcaneal proportions.

Plesiadapiforms are reconstructed as generalized arboreal animals with substantial amounts of quadrupedalism and suspensory behaviors. Calcaneal shape further indicates an evolutionary trend toward decreased quadrupedalism and higher reliance on suspensory behaviors in plesiadapoids (*C. simpsoni* and *Pl. cookei*)—supporting the view that locomotor changes were already underway before the LCA of euprimates. Most early euprimates differ from plesiadapiforms in their higher emphasis on leaping. Adapiforms exhibit a diverse locomotor behavior, with some species estimated to have exhibited extensive suspensory behaviors (like extant lorisids, *Daubentonia*, and some cheirogaleids), some characterized as more quadrupedal and resembling anthropoids, and others displaying a more generalized locomotor pattern (similar to extant lemurids and cheirogaleids, depending on their body size). Omomyiforms display moderate percentages of leaping and extensive use of small substrates but lack extreme adaptations for VCL. They rather resemble the most leaping cheirogaleids except for the lack of frequent suspensory behaviors, thus being better envisioned as quadrupedal leapers with less ability to suspend or move deliberately than most strepsirrhines. Finally, early anthropoids are reconstructed as more quadrupedal than both adapiforms and omomyiforms. However, basalmost anthropoids (eosimiids) and *Ganlea* are intermediate in locomotion between omomyiforms and the late Eocene/early Oligocene Afro-Arabian anthropoids.

Overall, our results based on the astragalus and calcaneus indicate that early primates exhibited a very diverse array of locomotor repertoires. Moreover, the estimated locomotor percentages for euprimates differ significantly from those of plesiadapiforms, with the former showing a notably higher predicted leaping behavior. This provides further evidence of a major locomotor shift during the early evolution of euprimates, concurring with the 'grasp-leaping' hypothesis. While no plesiadapiform recovered so far exhibits adaptations for frequent leaping behavior, our results support that some plesiadapoid species displayed a more deliberate locomotion, particularly *C. simpsoni*. We therefore conclude that our results are consistent with the view that the adaptation to the fine branch milieu, as proposed by the terminal branch feeding hypothesis, preceded the leaping specializations exhibited by the earliest euprimates. As suggested by our locomotor estimations, several euprimate lineages further developed these leaping adaptations, some of them reaching very high levels of specialization, for example, extant VCL species. However, leaping behavior, even if not a specialized form, was already present during the origin of euprimates. Future research in other anatomical areas will be required to better determine the original selective pressures underpinning the profound locomotor shift that occurred during the origin and early diversification of euprimates.

Declaration of competing interest

The authors certify that they have no conflict of interest.

Acknowledgments

This article is part R + D + I projects PID2020-116908GB-I00 and PID2020-117289GB-I00 financed by the Agencia Estatal de Investigación (MCIN/AEI/10.13039/501100011033). It has also been supported by CERCA Programme/Generalitat de Catalunya, the Departament de Cultura of the Generalitat de Catalunya (CLT0009_22_000022), the Agència de Gestió d'Ajust Universitaris i de Recerca (AGAUR) of the Generalitat de Catalunya (consolidated research groups 2022 SGR 01188 and 2022 SGR 00620), a Ramón y Cajal grant (RYC2021-034366-I to J.M.) funded by the Agencia

Estatal de Investigación (MCIN/AEI/10.13039/501100011033) and the European Union NextGenerationEU/PRTR, and a Joan Oró FI AGAUR fellowship (2021 FI_B 00524, 2022 FI_B1 00131, and 2023 FI-3 00131 to O.M.G.) funded by the Secretaria d'Universitats i Recerca of the Generalitat de Catalunya and the European Social Fund. We thank the team of the online repository Morphosource, MorphoMuseuM and the following institutions for providing access to specimens: American Museum of Natural History (AMNH), Duke Lemur Center Division of Fossil Primates (DLC), National Museum of Natural History (NMNH), Institut des Sciences de l'Evolution de Montpellier (ISEM), Muséum National d'Histoire Naturelle (MNHN), University of California Museum of Paleontology (UCMP), University of Michigan Museum of Paleontology (MI), Hemvati Nandan Bahuguna Garhwal University (HNBGU), Institut Català de Paleontologia Miquel Crusafont (ICP), United States Geological Survey (USGS), Museum of the Office National des Mines (ONM), Royal Belgian Institute of Natural Sciences (IRSNB), Carnegie Museum of Natural History (CMNH), Museo Argentino de Ciencias Naturales (MACN), Institute of Vertebrate Paleontology and Paleoanthropology (IVPP), National Museum of Myanmar Primates (NMMP), Naturhistorisches Museum Basel (NGiB), University of Colorado (CU), University of Zurich (UZH), San Diego Natural History Museum (SDNH), Caribbean Primate Research Center (CPRC), Harvard Museum Comparative Zoology (MCZ), Field Museum of Natural History (FMNH), Yale Peabody Museum of Natural History (YPM), University of Nebraska State Museum (USNM), and Stony Brook University (SBU). We acknowledge the Magnetic Resonance Imaging (MRI) platform member of the national infrastructure France-BioImaging supported by the French National Research Agency (ANR-10-INBS-04, 'Investments for the future'), the labex Centre Méditerranéen de l'Environnement et de la Biodiversité (CEMEB) (ANR-10-LABX-0004) and Digital and hardware solutions for the environmental and life sciences (NUMEV) (ANR-10-LABX-0020). We also thank James Thostenson (American Museum of Natural History (AMNH)) and Brian Reuther for having scanned the two *Teilhardina belgica* specimens (IRSNB 1235 and IRSNB 26857-01). This article is part of the Ph.D. dissertation of O.M.G. within the Geology Ph.D. Program of the Universitat Autònoma de Barcelona.

Author contributions

Oriol Monclús-Gonzalo: Writing – review & editing, Writing – original draft, Methodology, Investigation, Funding acquisition, Formal analysis, Data curation, Conceptualization. **David M. Alba:** Writing – review & editing, Supervision, Funding acquisition. **Anne-Claire Fabre:** Writing – review & editing. **Judit Marigó:** Writing – review & editing, Supervision, Funding acquisition.

Supplementary online material

Supplementary Online Material related to this article can be found at https://doi.org/10.1016/j.jhevol.2025.103730.

References

Adams, D.C., Otárola-Castillo, E., 2013. Geomorph: An r package for the collection and analysis of geometric morphometric shape data. Methods Ecol. Evol. 4, 393–399.
Adler, D., Murdoch, D., 2020. Rgl: 3D visualization using openGL. https://github.com/dmurdoch/rgl. https://dmurdoch.github.io/rgl/.
Anemone, R.L., Covert, H.H., 2000. New skeletal remains of *Omomys* (Primates, Omomyidae): Functional morphology of the hindlimb and locomotor behavior of a Middle Eocene primate. J. Hum. Evol. 38, 607–633.
Archer, W., Pop, C.M., Rezek, Z., Schlager, S., Lin, S.C., Weiss, M., Dogandžić, T., Desta, D., McPherron, S.P., 2018. A geometric morphometric relationship predicts stone flake shape and size variability. Archaeol. Anthropol. Sci. 10, 1991–2003.
Arnold, C., Matthews, L.J., Nunn, C.L., 2010. The 10kTrees website: A new online resource for primate phylogeny. Evol. Anthropol. 19, 114–118.
Bacon, A.M., Godinot, M., 1998. Analyse morphofonctionnelle des fémurs et des tibias des «*Adapis*» du Quercy: Mise en évidence de cinq types morphologiques. Folia Primatol. 69, 1–21.
Bærentzen, J.A., Aanæs, H., 2002. Generating Signed Distance Fields From Triangle Meshes. Technical University of Denmark. http://www.imm.dtu.dk/pubdb/p.php?1833.
Bardua, C., Felice, R.N., Watanabe, A., Fabre, A.-C., Goswami, A., 2019. A practical guide to sliding and surface semilandmarks in morphometric analyses. Integr. Org. Biol. 1, obz016.
Bastir, M., Torres-Tamayo, N., Palancar, C.A., Lois-Zlolniski, S., García-Martínez, D., Riesco-López, A., Vidal, D., Blanco-Pérez, E., Barash, A., Nalla, S., Martelli, S., 2019. Geometric morphometric studies in the human spine. In: Been, E., Gómez-Olivencia, A., Ann Kramer, P. (Eds.), Spinal Evolution. Springer, Cham, pp. 361–386.
Beard, K.C., 1989. Postcranial anatomy locomotor adaptations and paleoecology of early Cenozoic Plesiadapidae, Paromomyidae and Micromomyidae (Eutheria, Dermoptera). Ph.D. Dissertation, Johns Hopkins University School of Medicine.
Beard, K.C., 2008. The oldest North American primate and mammalian biogeography during the Paleocene–Eocene thermal maximum. Proc. Natl. Acad. Sci. U.S.A. 105, 3815–3818.
Beard, K.C., Wang, J., 2004. The eosimiid primates (Anthropoidea) of the Heti Formation, Yuanqu Basin, Shanxi and Henan Provinces, People's Republic of China. J. Hum. Evol. 46, 401–432.
Beard, K.C., Dagosto, M., Gebo, D.L., Godinot, M., 1988. Interrelationships among primate higher taxa. Nature 331, 712–714.
Beard, K.C., Qi, T., Dawson, M.R., Wang, B., Li, C., 1994. A diverse new primate fauna from middle Eocene fissure-fillings in southeastern China. Nature 368, 604–609.
Beard, K.C., Tong, Y., Dawson, M.R., Wang, J., Huang, X., 1996. Earliest complete dentition of an anthropoid primate from the late middle Eocene of Shanxi Province, China. Science 272, 82–85.
Beard, K.C., Marivaux, L., Chaimanee, Y., Jaeger, J.J., Marandat, B., Tafforeau, P., Soe, A.N., Tun, S.T., Kyaw, A.A., 2009. A new primate from the Eocene Pondaung Formation of Myanmar and the monophyly of Burmese amphipithecids. Proc. R. Soc. B 276, 3285–3294.
Bloch, J.I., Boyer, D.M., 2002. Grasping primate origins. Science 298, 1606–1610.
Bloch, J.I., Boyer, D.M., 2007. New skeletons of Paleocene-Eocene Plesiadapiformes: A diversity of arboreal positional behaviors in early primates. In: Ravosa, M.J., Dagosto, M. (Eds.), Primate Origins: Adaptations and Evolution. Springer, New York, pp. 535–581.
Bloch, J.I., Silcox, M.T., Boyer, D.M., Sargis, E.J., 2007. New Paleocene skeletons and the relationship of plesiadapiforms to crown-clade primates. Proc. Natl. Acad. Sci. U.S.A. 104, 1159–1164.
Blomberg, S.P., Garland Jr, T., Ives, A.R., 2003. Testing for phylogenetic signal in comparative data: Behavioral traits are more labile. Evolution 57, 717–745.
Bock, W.J., Von Wahlert, G., 1965. Adaptation and the form-function complex. Evolution 19, 269–299.
Bookstein, F.L., 1997. Landmark methods for forms without landmarks: Morphometrics of group differences in outline shape. Med. Image Anal. 1, 225–243.
Bookstein, F.L., Gunz, P., Mitteræcker, P., Mitteroecker, P., Prossinger, H., Schaefer, K., Horst, S., 2003. Cranial integration in *Homo*: Singular warps analysis of the midsagittal plane in ontogeny and evolution. J. Hum. Evol. 44, 167–187.
Boyer, D.M., Seiffert, E.R., 2013. Patterns of astragalar fibular facet orientation in extant and fossil primates and their evolutionary implications. Am. J. Phys. Anthropol. 151, 420–447.
Boyer, D.M., Gingerich, P.D., 2019. Skeleton of late Paleocene *Plesiadapis cookei* (Mammalia, Euarchonta): Life history, locomotion, and phylogenetic relationships. Univ. Michigan Pap. Paleontol. 38, 1–269.
Boyer, D.M., Seiffert, E.R., Simons, E.L., 2010. Astragalar morphology of *Afradapis*, a large adapiform primate from the earliest late Eocene of Egypt. Am. J. Phys. Anthropol. 143, 383–402.
Boyer, D.M., Yapuncich, G.S., Chester, S.G., Bloch, J.I., Godinot, M., 2013a. Hands of early primates. Am. J. Phys. Anthropol. 152, 33–78.
Boyer, D.M., Seiffert, E.R., Gladman, J.T., Bloch, J.I., 2013b. Evolution and allometry of calcaneal elongation in living and extinct primates. PLoS One 8, e67792.
Boyer, D.M., Yapuncich, G.S., Butler, J.E., Dunn, R.H., Seiffert, E.R., 2015. Evolution of postural diversity in primates as reflected by the size and shape of the medial tibial facet of the talus. Am. J. Phys. Anthropol. 157, 134–177.
Boyer, D.M., Toussaint, S., Godinot, M., 2017a. Postcrania of the most primitive euprimate and implications for primate origins. J. Hum. Evol. 111, 202–211.
Boyer, D.M., Gunnell, G.F., Kaufman, S., McGeary, T.M., 2017b. Morphosource: Archiving and sharing 3-D digital specimen data. Paleontol. Soc. Pap. 22, 157–181.
Cartmill, M., 1974. Rethinking primate origins. Science 184, 436–443.
Cartmill, M., 1992. New views on primate origins. Evol. Anthropol. 1, 105–111.
Chaimanee, Y., Chavasseau, O., Beard, K.C., Kyaw, A.A., Soe, A.N., Sein, C., Lazzari, V., Marivaux, L., Marandat, B., Swe, M., Rugbumrung, M., 2012. Late Middle Eocene primate from Myanmar and the initial anthropoid colonization of Africa. Proc. Natl. Acad. Sci. U.S.A. 109, 10293–10297.
Chaimanee, Y., Chavasseau, O., Lazzari, V., Soe, A.N., Sein, C., Jaeger, J.-J., 2024. Early anthropoid primates: New data and new questions. Evol. Anthropol. 33, e22022.

Chester, S.G.B., Bloch, J.I., Boyer, D.M., Clemens, W.A., 2015. Oldest known euarchontan tarsals and affinities of Paleocene *Purgatorius* to primates. Proc. Natl. Acad. Sci. U.S.A. 112, 1487–1492.
Chester, S.G.B., Williamson, T.E., Bloch, J.I., Silcox, M.T., Sargis, E.J., 2017. Oldest skeleton of a plesiadapiform provides additional evidence for an exclusively arboreal radiation of stem primates in the Paleocene. R. Soc. Open Sci. 4, 170329.
Chester, S.G., Williamson, T.E., Silcox, M.T., Bloch, J.I., Sargis, E.J., 2019. Skeletal morphology of the early Paleocene plesiadapiform *Torrejonia wilsoni* (Euarchonta, Palaechthonidae). J. Hum. Evol. 128, 76–92.
Chester, S.G., Williamson, T.E., Crowell, J.W., Silcox, M.T., Bloch, J.I., Sargis, E.J., 2025. New remarkably complete skeleton of *Mixodectes* reveals arboreality in a large Paleocene primatomorphan mammal following the Cretaceous-Paleogene mass extinction. Sci. Rep. 15, 8041.
Clavel, J., Escarguel, G., Merceron, G., 2015. mvMORPH: an R package for fitting multivariate evolutionary models to morphometric data. Methods Ecol. Evol. 6, 1311–1319.
Clemens, W.A., 1974. *Purgatorius*, an early paromomyid primate (Mammalia). Science 184, 903–905.
Conroy, G.C., Rose, M.D., 1983. The evolution of the primate foot from the earliest primates to the Miocene hominoids. Foot Ankle 3, 342–364.
Cornette, R., Baylac, M., Souter, T., Herrel, A., 2013. Does shape co-variation between the skull and the mandible have functional consequences? A 3D approach for a 3D problem. J. Anat. 223, 329–336.
Coster, P., Beard, K.C., Soe, A.N., Sein, C., Chaimanee, Y., Lazzari, V., Valentin, X., Jaeger, J.J., 2013. Uniquely derived upper molar morphology of Eocene Amphipithecidae (Primates: Anthropoidea): Homology and phylogeny. J. Hum. Evol. 65, 143–155.
Covert, H.H., 1988. Ankle and foot morphology of *Cantius mckennai*: Adaptations and phylogenetic implications. J. Hum. Evol. 17, 57–70.
Covert, H.H., 1995. Locomotor adaptations of Eocene primates: Adaptive diversity among the earliest prosimians. In: Alterman, L., Doyle, G.A., Izard, M.K. (Eds.), Creatures of the Dark. Springer, Boston, pp. 495–509.
Covert, H.H., Hamrick, M.W., 1993. Description of new skeletal remains of the early Eocene anaptomorphine primate *Absarokius* (Omomyidae) and discussion about its adaptative profile. J. Hum. Evol. 25, 351–362.
Crowell, J.W., Wible, J.R., Chester, S.G., 2024. Basicranial evidence suggests picrodontid mammals are not stem primates. Biol. Lett. 20, 20230335.
Dagosto, M., 1983. Postcranium of *Adapis parisiensis* and *Leptadapis magnus* (Adapiformes, Primates). Adaptational and phylogenetic significance. Folia Primatol. 41, 49–101.
Dagosto, M., 1988. Implications of postcranial evidence for the origin of euprimates. J. Hum. Evol. 17, 35–56.
Dagosto, M., 1990. Models for the origin of the anthropoid postcranium. J. Hum. Evol. 19, 121–139.
Dagosto, M., 2007. The postcranial morphotype of primates. In: Ravosa, M.J., Dagosto, M. (Eds.), Primate Origins: Adaptations and Evolution. Springer, New York, pp. 489–534.
Dagosto, M., Schmid, P., 1996. Proximal femoral anatomy of omomyiform primates. J. Hum. Evol. 30, 29–56.
Dagosto, M., Gebo, D.L., Beard, K.C., 1999. Revision of the Wind River faunas, early Eocene of central Wyoming. Part 14. Postcranium of *Shoshonius cooperi* (Mammalia: Primates). Ann. Carnegie Mus. 68, 175–211.
Decker, R.L., Szalay, F.S., 1974. Origins and function of the pes in the Eocene Adapidae (Lemuriformes, Primates). In: Jenkins, F.A. (Ed.), Primate Locomotion. Academic Press, New York, pp. 261–291.
Demes, B., Günther, M.M., 1989. Biomechanics and allometric scaling in primate locomotion and morphology. Folia Primatol. 53, 125–141.
Demes, B., Jungers, W.L., Fleagle, J.G., Wunderlich, R.E., Richmond, B.G., Lemelin, P., 1996. Body size and leaping kinematics in Malagasy vertical clingers and leapers. J. Hum. Evol. 31, 367–388.
Dunn, R.H., Sybalsky, J.M., Conroy, G.C., Rasmussen, D.T., 2006. Hindlimb adaptations in *Ourayia* and *Chipetaia*, relatively large-bodied omomyine primates from the Middle Eocene of Utah. Am. J. Phys. Anthropol. 131, 303–310.
Dunn, R.H., Rose, K.D., Rana, R.S., Kumar, K., Sahni, A., Smith, T., 2016. New euprimate postcrania from the early Eocene of Gujarat, India, and the strepsirrhine–haplorhine divergence. J. Hum. Evol. 99, 25–51.
Fleagle, J.G., 1980. Locomotor behavior of the earliest anthropoids: A review of the current evidence. Z. Morph. Anthrop. 71, 149–156.
Fleagle, J.G., Mittermeier, R.A., 1980. Locomotor behavior, body size, and comparative ecology of seven Surinam monkeys. Am. J. Phys. Anthropol. 52, 301–314.
Fleagle, J.G., Kay, R.F., 1988. The phyletic position of the Parapithecidae. J. Hum. Evol. 16, 483–532.
Fleagle, J.G., Simons, E.L., 1995. Limb skeleton and locomotor adaptations of *Apidium phiomense*, an Oligocene anthropoid from Egypt. Am. J. Phys. Anthropol. 97, 235–289.
Garber, P.A., 1992. Vertical clinging, small body size, and the evolution of feeding adaptations in the Callitrichinae. Am. J. Phys. Anthropol. 88, 469–482.
Gebo, D.L., 1985. The nature of the primate grasping foot. Am. J. Phys. Anthropol. 67, 269–277.
Gebo, D.L., 1986. Anthropoid origins—The foot evidence. J. Hum. Evol. 15, 421–430.
Gebo, D.L., 1987a. Locomotor diversity in prosimian primates. Am. J. Primatol. 13, 271–281.
Gebo, D.L., 1987b. Functional anatomy of the tarsier foot. Am. J. Phys. Anthropol. 73, 9–31.
Gebo, D.L., 1988. Foot morphology and locomotor adaptation in Eocene primates. Folia Primatol. 50, 3–41.
Gebo, D.L., 1989a. Postcranial adaptation and evolution in Lorisidae. Primates 30, 347–367.
Gebo, D.L., 1989b. Locomotor and phylogenetic considerations in anthropoid evolution. J. Hum. Evol. 18, 201–233.
Gebo, D.L., 2004. A shrew-sized origin for primates. Am. J. Phys. Anthropol. 125, 40–62.
Gebo, D.L., 2011. Vertical clinging and leaping revisited: Vertical support use as the ancestral condition of strepsirrhine primates. Am. J. Phys. Anthropol. 146, 323–335.
Gebo, D.L., Simons, E.L., 1987. Morphology and locomotor adaptations of the foot in early Oligocene anthropoids. Am. J. Phys. Anthropol. 74, 83–101.
Gebo, D.L., Dagosto, M., 1988. Foot anatomy, climbing, and the origin of the Indriidae. J. Hum. Evol. 17, 135–154.
Gebo, D.L., Dagosto, M., 2004. Anthropoid origins: Postcranial evidence from the Eocene of Asia. In: Ross, C.F., Kay, R.F. (Eds.), Anthropoid Origins: New Visions. Kluwer Academic, New York, pp. 369–380.
Gebo, D.L., Dagosto, M., Rose, K.D., 1991. Foot morphology and evolution in early Eocene *Cantius*. Am. J. Phys. Anthropol. 86, 51–73.
Gebo, D.L., Dagosto, M., Beard, K.C., Qi, T., Wang, J., 2000. The oldest known anthropoid postcranial fossils and the early evolution of higher primates. Nature 404, 276–278.
Gebo, D.L., Dagosto, M., Beard, K.C., Qi, T., 2001. Middle Eocene primate tarsals from China: Implications for haplorhine evolution. Am. J. Phys. Anthropol. 116, 83–107.
Gebo, D.L., Smith, T., Dagosto, M., 2012. New postcranial elements for the earliest Eocene fossil primate *Teilhardina belgica*. J. Hum. Evol. 63, 205–218.
Gebo, D.L., Smith, R., Dagosto, M., Smith, T., 2015. Additional postcranial elements of *Teilhardina belgica*: The oldest European primate. Am. J. Phys. Anthropol. 156, 388–406.
Gelman, A., Rubin, D.B., 1992. Inference from iterative simulation using multiple sequences. Stat. Sci. 7, 457–511.
Gladman, J.T., Boyer, D.M., Simons, E.L., Seiffert, E.R., 2013. A calcaneus attributable to the primitive late Eocene anthropoid *Proteopithecus sylviae*: Phenetic affinities and phylogenetic implications. Am. J. Phys. Anthropol. 151, 372–397.
Godinot, M., 1991. Toward the locomotion of two contemporaneous *Adapis* species. Z. Morphol. Anthropol. 78, 387–405.
Godinot, M., 1998. A summary of adapiform systematics and phylogeny. Folia Primatol. 69, 218–249.
Godinot, M., 2007. Primate origins: A reappraisal of historical data favoring tupaiid affinities. In: Ravosa, M.J., Dagosto, M. (Eds.), Primate Origins: Adaptations and Evolution. Springer, New York, pp. 83–142.
Godinot, M., Dagosto, M., 1983. The astragalus of *Necrolemur* (Primates, Microchoerinae). J. Paleontol. 57, 1321–1324.
Godinot, M., Beard, K.C., 1991. Fossil primate hands: A review and an evolutionary inquiry emphasizing early forms. Hum. Evol. 6, 307–354.
Granatosky, M.C., Toussaint, S.L.D., Young, M.W., Panyutina, A., Youlatos, D., 2022. The northern treeshrew (Scandentia: Tupaiidae: *Tupaia belangeri*) in the context of primate locomotor evolution: A comprehensive analysis of gait, positional, and grasping behavior. J. Exp. Zool. A. 337, 645–665.
Gregory, W.K., 1920. On the structure and relations of *Notharctus*, an American Eocene primate. Mem. Am. Mus. Nat. Hist. 3, 49–243.
Gunnell, G.F., Miller, E.R., 2001. Origin of Anthropoidea: Dental evidence and recognition of early anthropoids in the fossil record, with comments on the Asian anthropoid radiation. Am. J. Phys. Anthropol. 114, 177–191.
Gunnell, G.F., Ciochcon, R.L., 2008. Revisiting primate postcrania from the Pondaung Formation of Myanmar: The purported anthropoid astragalus. In: Fleagle, J.G., Gilbert, C.C. (Eds.), Elwyn Simons: A Search for Origins. Springer, New York, pp. 211–228.
Gunnell, G.F., Rose, K.D., Rasmussen, D.T., 2008. Euprimates. In: Janis, C.M., Gunnell, G.F., Uhen, M.D. (Eds.), Evolution of Tertiary Mammals of North America, vol. 2. Cambridge University Press, Cambridge, pp. 239–261.
Gunz, P., Mitteroecker, P., 2013. Semilandmarks: A method for quantifying curves and surfaces. Hystrix 24, 103–109.
Gunz, P., Mitteroecker, P., Bookstein, F.L., 2005. Semilandmarks in three dimensions. In: Slice, E.D. (Ed.), Modern Morphometrics in Physical Anthropology. Kluwer Academic/Plenum Publishers, New York, pp. 73–98.
Hall-Craggs, E.C.B., 1965. An osteometric study of the hind limb of the Galagidae. J. Anat. Lond. 99, 119–126.
Hammer, Ø., Harper, D.A., 2024. Paleontological Data Analysis. John Wiley & Sons, Chichester.
Hamrick, M.W., 2001. Primate origins: Evolutionary change in digital ray patterning and segmentation. J. Hum. Evol. 40, 339–351.
Hoffstetter, R., 1977. Phylogénie des Primates. Confrontation des résultats obtenus par les diverses voies d'approche du problème. Bull. Mem. Soc. Anthropol. Paris 13, 327–346.
Hunt, K.D., Cant, J.H.C., Gebo, D.L., Rose, M.D., Walker, S.E., Youlatos, D., 1996. Standardized descriptions of primate locomotor and postural modes. Primates 37, 363–387.
Jaeger, J.J., Sein, C., Gebo, D.L., Chaimanee, Y., Nyein, M.T., Oo, T.Z., Aung, M.M., Suraprasit, K., Rugbumrung, M., Lazzari, V., Soe, A.N., 2020. Amphipithecine primates are stem anthropoids: Cranial and postcranial evidence. Proc. R. Soc. B 287, 20202129.

Kay, R.F., Ross, C., Williams, B.A., 1997. Anthropoid origins. Science 275, 797–804.
Kay, R.F., Schmitt, D., Vinyard, C.J., Perry, J.M., Shigehara, N., Takai, M., Egi, N., 2004. The paleobiology of Amphipithecidae, south Asian late Eocene primates. J. Hum. Evol. 46, 3–25.
Kemp, A.D., 2024a. Effects of binocular cue availability on leaping performance in *Cheirogaleus medius*: Implications for primate origins. J. Exp. Biol. 227, jeb245434.
Kemp, A.D., 2024b. Effect of binocular visual cue availability on fruit and insect grasping performance in two cheirogaleids: Implications for primate origins hypotheses. J. Hum. Evol. 188, 103456.
Kirk, E.C., Lemelin, P., Hamrick, M.W., Boyer, D.M., Bloch, J.I., 2008. Intrinsic hand proportions of euarchontans and other mammals: Implications for the locomotor behavior of plesiadapiforms. J. Hum. Evol. 55, 278–299.
Konishi, S., Kitagawa, G., 1996. Generalised information criteria in model selection. Biometrika 83, 875–890.
Kuhn, M., Johnson, K., 2013. Over-fitting and model tuning. In: Kuhn, M., Johnson, K. (Eds.), Applied Predictive Modeling. Springer, New York, pp. 61–92.
Lauder, G.V., 1986. Homology, analogy, and the evolution of behavior. In: Nitecki, M., Kitchell, J. (Eds.), The Evolution of Behavior. Oxford University Press, Oxford, pp. 9–40.
Lebrun, R., Orliac, M.J., 2016. MorphoMuseuM: An online platform for publication and storage of virtual specimens. Paleontol. Soc. Pap. 22, 183–195.
Llera Martín, C.J., Rose, K.D., Sylvester, A.D., 2022. A morphometric analysis of early Eocene Euprimate tarsals from Gujarat, India. J. Hum. Evol. 164, 103141.
López-Torres, S., Selig, K.R., Prufrock, K.A., Lin, D., Silcox, M.T., 2017. Dental topographic analysis of paromomyid (Plesiadapiformes, Primates) cheek teeth: More than 15 million years of changing surfaces and shifting ecologies. Hist. Biol. 30, 76–88.
Marigó, J., Roig, I., Seiffert, E.R., Moyà-Solà, S., Boyer, D.M., 2016. Astragalar and calcaneal morphology of the middle Eocene primate *Anchomomys frontanyensis* (Anchomomyini): Implications for early primate evolution. J. Hum. Evol. 91, 122–143.
Marigó, J., Verrière, N., Godinot, M., 2019. Systematic and locomotor diversification of the *Adapis* group (Primates, Adapiformes) in the late Eocene of the Quercy (Southwest France), revealed by humeral remains. J. Hum. Evol. 126, 71–90.
Marigó, J., Minwer-Barakat, R., Moyà-Solà, S., Boyer, D.M., 2020. First navicular remains of a European adapiform (*Anchomomys frontanyensis*) from the Middle Eocene of the Eastern Pyrenees (Catalonia, Spain): Implications for early primate locomotor behavior and navicular evolution. J. Hum. Evol. 139, 102708.
Marivaux, L., Chaimanee, Y., Ducrocq, S., Marandat, B., Sudre, J., Soe, A.N., Tun, S.T., Htoon, W., Jaeger, J.J., 2003. The anthropoid status of a primate from the late middle Eocene Pondaung Formation (Central Myanmar): Tarsal evidence. Proc. Natl. Acad. Sci. U.S.A. 100, 13173–13178.
Marivaux, L., Beard, K.C., Chaimanee, Y., Dagosto, M., Gebo, D.L., Guy, F., Marandat, B., Khaing, K., Kyaw, A.A., Oo, M., Sein, C., Soe, A.N., Swe, M., Jaeger, J.-J., 2010. Talar morphology, phylogenetic affinities, and locomotor adaptation of a large-bodied amphipithecid primate from the late middle Eocene of Myanmar. Am. J. Phys. Anthropol. 143, 208–222.
Marivaux, L., Tabuce, R., Lebrun, R., Ravel, A., Adaci, M., Mahboubi, M., Bensalah, M., 2011. Talar morphology of azibiids, strepsirhine-related primates from the Eocene of Algeria: Phylogenetic affinities and locomotor adaptation. J. Hum. Evol. 61, 447–457.
Marivaux, L., Ramdarshan, A., Essid, E.M., Marzougui, W., Ammar, H.K., Lebrun, R., Marandat, B., Merzeraud, G., Tabuce, R., Vianey-Liaud, M., 2013. *Djebelemur*, a tiny pre-tooth-combed primate from the Eocene of Tunisia: A glimpse into the origin of crown strepsirhines. PLoS One 8, e80778.
Marivaux, L., Lebrun, R., Tabuce, R., 2018. 3D models related to the publication: *Djebelemur*, a tiny pre-tooth-combed primate from the Eocene of Tunisia: A glimpse into the origin of crown strepsirhines. MorphoMuseum 4, e77.
Miller, E.R., Gunnell, G.F., Martin, R.D., 2005. Deep time and the search for anthropoid origins. Am. J. Phys. Anthropol. 128, 60–95.
Monclús-Gonzalo, O., Alba, D.M., Duhamel, A., Fabre, A.-C., Marigó, J., 2023. Early euprimates already had a diverse locomotor repertoire: Evidence from ankle bone morphology. J. Hum. Evol. 181, 103395.
Monclús-Gonzalo, O., Pal, S., Püschel, T.A., Urciuoli, A., Vinuesa, V., Robles, J.M., Almécija, S., Alba, D.M., 2025. A dryopithecine talus from the Late Miocene of the Vallès-Penedès Basin (NE Iberian Peninsula): Morphometric affinities and evolutionary implications for hominoid locomotion. Am. J. Phys. Anthropol. 186, e70043.
Morse, P.E., Chester, S.G., Boyer, D.M., Smith, T., Smith, R., Gigase, P., Bloch, J.I., 2019. New fossils, systematics, and biogeography of the oldest known crown primate *Teilhardina* from the earliest Eocene of Asia, Europe, and North America. J. Hum. Evol. 128, 103–131.
Morton, D.J., 1924. Evolution of the human foot II. Am. J. Phys. Anthropol. 7, 1–52.
Moyà-Solà, S., Köhler, M., Alba, D.M., Roig, I., 2012. Calcaneal proportions in primates and locomotor inferences in *Anchomomys* and other Palaeogene Euprimates. Swiss J. Palaeontol. 131, 147–159.
Ni, X., Gebo, D.L., Dagosto, M., Meng, J., Tafforeau, P., Flynn, J.J., Beard, K.C., 2013. The oldest known primate skeleton and early haplorhine evolution. Nature 498, 60–64.
Ni, X., Li, Q., Li, L., Beard, K.C., 2016. Oligocene primates from China reveal divergence between African and Asian primate evolution. Science 352, 673–677.
Orme, D., Freckleton, R., Thomas, G., Petzoldt, T., Fritz, S., Isaac, N., Pearse, W., 2023. caper: Comparative Analyses of Phylogenetics and Evolution in R. R package version 1.0.3. https://CRAN.R-project.org/package=caper.
Oxnard, C.E., Crompton, R.H., Lieberman, S.S., 1990. Animal Lifestyles and Anatomies. University of Washington Press, Seattle.
Pagel, M., 1999. Inferring the historical patterns of biological evolution. Nature 401, 877–884.
Parr, W.C.H., Soligo, C., Smaers, J., Chatterjee, H.J., Ruto, A., Cornish, L., Wroe, S., 2014. Three-dimensional shape variation of talar surface morphology in hominoid primates. J. Anat. 225, 42–59.
Pina, M., Salesa, M.J., Antón, M., 2011. Functional anatomy of the calcaneum and talus in Cercopithecinae (Mammalia, Primates, Cercopithecidae). Estud. Geol. 67, 385–394.
Plummer, M., Best, N., Cowles, K., Vines, K., 2005. CODA: Convergence diagnosis and output analysis for MCMC. R News 6, 7–11.
Polly, P.D., Lawing, A.M., Fabre, A.C., Goswami, A., 2013. Phylogenetic principal components analysis and geometric morphometrics. Hystrix 24, 33–41.
Preuschoft, H., Witte, H., Christian, A., Fischer, M., 1996. Size influences on primate locomotion and body shape, with special emphasis on the locomotion of 'small mammals'. Folia Primatol. 66, 93–112.
Preuschoft, H., Günther, M.M., Christian, A., 1998. Size dependence in prosimian locomotion and its implications for the distribution of body mass. Folia Primatol. 69, 60–81.
Prufrock, K.A., López-Torres, S., Silcox, M.T., Boyer, D.M., 2016. Surfaces and spaces: Troubleshooting the study of dietary niche space overlap between North American stem primates and rodents. Surf. Topogr. 4, 024005.
Püschel, T.A., Gladman, J.T., Bobe, R., Sellers, W.I., 2017. The evolution of the platyrrhine talus: A comparative analysis of the phenetic affinities of the Miocene platyrrhines with their modern relatives. J. Hum. Evol. 111, 179–201.
Püschel, T.A., Marcé-Nogué, J., Gladman, J.T., Bobe, R., Sellers, W.I., 2018. Inferring locomotor behaviours in Miocene New World monkeys using finite element analysis, geometric morphometrics and machine-learning classification techniques applied to talar morphology. J. R. Soc. Interface 15, 20180520.
Püschel, T.A., Marcé-Nogué, J., Gladman, J., Patel, B.A., Almécija, S., Sellers, W.I., 2020. Getting its feet on the ground: Elucidating *Paralouatta*'s semi-terrestriality using the virtual morpho-functional toolbox. Front. Earth Sci. 8, 79.
R Core Team, 2023. R: A language and environment for statistical computing. R Foundation for Statistical Computing, Vienna.
Rasmussen, D.T., 1990. Primate origins: Lessons from a neotropical marsupial. Am. J. Primatol. 22, 263–277.
Raventós-Izard, G., Monclús-Gonzalo, O., Moyà-Solà, S., Alba, D.M., Arias-Martorell, J., 2025. Ulnar morphology of *Pliobates cataloniae* (Pliopithecoidea: Crouzeliidae): Insights into catarrhine locomotor diversity and forelimb evolution. J. Hum. Evol. 202, 103663.
Revell, L.J., 2009. Size-correction and principal components for interspecific comparative studies. Evolution 63, 3258–3268.
Revell, L.J., 2012. phytools: An R package for phylogenetic comparative biology (and other things). Methods Ecol. Evol. 3, 217–223.
Rohlf, F.J., Slice, D., 1990. Extensions of the Procrustes method for the optimal superimposition of landmarks. Syst. Zool. 39, 40–59.
Rohlf, F.J., Corti, M., 2000. Use of two-block partial least-squares to study covariation in shape. Syst. Biol. 49, 740–753.
Rose, K.D., 1994. The earliest primates. Evol. Anthropol. 3, 159–173.
Rose, K.D., Walker, A., 1985. The skeleton of early Eocene *Cantius*, oldest lemuriform primate. Am. J. Phys. Anthropol. 66, 73–89.
Rose, K.D., Rana, R.S., Sahni, A., Kumar, K., Missiaen, P., Singh, L., Smith, T., 2009. Early Eocene primates from Gujarat, India. J. Hum. Evol. 56, 366–404.
Rose, K.D., Chester, S.G., Dunn, R.H., Boyer, D.M., Bloch, J.I., 2011. New fossils of the oldest North American euprimate *Teilhardina brandti* (Omomyidae) from the Paleocene–Eocene thermal maximum. Am. J. Phys. Anthropol. 146, 281–305.
Rosenberger, A.L., Preuschoft, H., 2012. Evolutionary morphology, cranial biomechanics and the origins of tarsiers and anthropoids. Paleobiodivers. Paleoenviron. 92, 507–525.
Sargis, E.J., 2001. The grasping behaviour, locomotion and substrate use of the tree shrews *Tupaia minor* and *T. tana* (Mammalia, Scandentia). J. Zool. Lond. 253, 485–490.
Sargis, E.J., 2002a. Functional morphology of the hindlimb of tupaiids (Mammalia, Scandentia) and its phylogenetic implications. J. Morphol. 254, 149–185.
Sargis, E.J., 2002b. The postcranial morphology of *Ptilocercus lowii* (Scandentia, Tupaiidae): An analysis of primatomorphan and volitantian characters. J. Mammal. Evol. 9, 137–160.
Sargis, E.J., Boyer, D.M., Bloch, J.I., Silcox, M.T., 2007. Evolution of pedal grasping in Primates. J. Hum. Evol. 53, 103–107.
Sarmiento, E.E., 1983. The significance of the heel process in anthropoids. Int. J. Primatol. 4, 127–152.
Savage, D.E., Waters, B.T., 1978. A new omomyid primate from the Wasatch Formation of southern Wyoming. Folia Primatol. 30, 1–29.
Schlager, S., 2017. Morpho and Rvcg-shape analysis in R. In: Zheng, G., Li, S., Szekely, G. (Eds.), Statistical Shape and Deformation Analysis: Methods, Implementation and Applications. Academic Press, London, pp. 217–256.
Schmitt, D., 1996. Humeral head shape as an indicator of locomotor behavior in extant strepsirhines and Eocene adapids. Folia Primatol. 67, 137–151.
Seiffert, E.R., Simons, E.L., 2001. Astragalar morphology of late Eocene anthropoids from the Fayum Depression (Egypt) and the origin of catarrhine primates. J. Hum. Evol. 41, 577–606.
Seiffert, E.R., Simons, E.L., Fleagle, J.G., 2000. Anthropoid humeri from the late Eocene of Egypt. Proc. Natl. Acad. Sci. U.S.A. 97, 10062–10067.

Seiffert, E.R., Simons, E.L., Simons, C.V., 2004. Phylogenetic, biogeographic, and adaptive implications of new fossil evidence bearing on crown anthropoid origins and early stem catarrhine evolution. In: Ross, C.F., Kay, R.F. (Eds.), Anthropoid Origins: New visions. Kluwer Academic, New York, pp. 157–181.
Seiffert, E.R., Simons, E.L., Clyde, W.C., Rossie, J.B., Attia, Y., Bown, T.M., Chatrath, P., Mathison, M.E., 2005. Basal anthropoids from Egypt and the antiquity of Africa's higher primate radiation. Science 310, 300–304.
Seiffert, E.R., Costeur, L., Boyer, D.M., 2015. Primate tarsal bones from Egerkingen, Switzerland, attributable to the middle Eocene adapiform *Caenopithecus lemuroides*. PeerJ 3, e1036.
Sigé, B., Jaeger, J.-J., Sudre, J., Vianey-Liaud, M., 1990. *Altiatlasius koulchii* n. gen. et sp., primate Omomyidé du Paléocène supérieur du Maroc, et les origines des euprimates. Palaeontographica A 214, 31–56.
Silcox, M.T., López-Torres, S., 2017. Major questions in the study of primate origins. Annu. Rev. Earth Planet Sci. 45, 113–137.
Silcox, M.T., Boyer, D.M., Bloch, J.I., Sargis, E.J., 2007. Revisiting the adaptive origins of primates (again). J. Hum. Evol. 53, 321–324.
Silcox, M.T., Sargis, E.J., Bloch, J.I., Boyer, D.M., 2015. Primate origins and supraordinal relationships: Morphological evidence. In: Henke, W., Tatterstall, I. (Eds.), Handbook of Paleoanthropology, 2nd ed. Springer, Heidelberg, pp. 1053–1081.
Silcox, M.T., Bloch, J.I., Boyer, D.M., Chester, S.G.B., López-Torres, S., 2017. The evolutionary radiation of plesiadapiforms. Evol. Anthropol. 26, 74–94.
Simons, E.L., Seiffert, E.R., 1999. A partial skeleton of *Proteopithecus sylviae* (Primates, Anthropoidea): First associated dental and postcranial remains of an Eocene anthropoidean. C. R. Acad. Sci. Paris 329, 921–927.
Smith, T., Rose, K.D., Gingerich, P.D., 2006. Rapid Asia–Europe–North America geographic dispersal of earliest Eocene primate *Teilhardina* during the Paleocene–Eocene thermal maximum. Proc. Natl. Acad. Sci. U.S.A. 103, 11223–11227.
Sokal, R., Rohlf, F., 1995. Biometry: The Principles and Practice of Statistics in Biological Research, 3rd ed. Freeman, New York.
Strasser, E., 1988. Pedal evidence for the origin and diversification of cercopithecid clades. J. Hum. Evol. 17, 225–245.
Su, A., Zeiniger, A., 2022. The primate ankle and hindfoot. In: Zeiniger, A., Hatala, K. G., Wunderlich, R.E., Schmitt, D. (Eds.), The Evolution of the Primate Foot. Anatomy, Function, and Palaeontological Evidence. Springer, Cham, pp. 21–45.
Sussman, R.W., 1991. Primate origins and the evolution of angiosperms. Am. J. Primatol. 23, 209–223.
Sussman, R.W., Raven, P.H., 1978. Pollination by lemurs and marsupials: An archaic coevolutionary system. Science 200, 731–736.
Sussman, R.W., Rasmussen, D.T., Raven, P.H., 2012. Rethinking primate origins again. Am. J. Primatol. 75, 95–106.
Szalay, F.S., 1976. Systematics of the Omomyidae (Tarsiiformes, Primates): Taxonomy, phylogeny, and adaptations. Bull. Am. Mus. Nat. Hist. 156, 157–450.
Szalay, F.S., Decker, R.L., 1974. Origins, evolution, and function of the tarsus in late Cretaceous Eutheria and Paleocene primates. In: Jenkins, F.A. (Ed.), Primate Locomotion. Academic Press, New York, pp. 223–259.
Szalay, F.S., Delson, E., 1979. Evolutionary History of the Primates. Academic Press, New York.
Szalay, F.S., Dagosto, F.S., 1980. Locomotor adaptations as reflected on the humerus of Paleogene primates. Folia Primatol. 34, 1–45.
Szalay, F.S., Drawhorn, G., 1980. Evolution and diversification of the Archonta in an arboreal milieu. In: Luckett, W.P. (Ed.), Comparative Biology and Evolutionary Relationships of Tree Shrews. Plenum Press, New York, pp. 133–169.
Szalay, F.S., Rosenberger, A.L., Dagosto, M., 1987. Diagnosis and differentiation of the Order Primates. Yearb. Phys. Anthropol. 30, 75–105.
Torres-Tamayo, N., Schlager, S., García-Martínez, D., Sanchis-Gimeno, J.A., Nalla, S., Ogihara, N., Oishi, M., Martelli, S., Bastir, M., 2020. Three-dimensional geometric morphometrics of thorax-pelvis covariation and its potential for predicting the thorax morphology: A case study on Kebara 2 Neandertal. J. Hum. Evol. 147, 102854.
Van Valen, L., Sloan, R.E., 1965. The earliest primates. Science 150, 743–745.
Vinyard, C.J., Wall, C.E., Williams, S.H., Hylander, W.L., 2003. Comparative functional analysis of skull morphology of tree-gouging primates. Am. J. Phys. Anthropol. 120, 153–170.
Walker, A., 1974. Locomotor adaptations in past and present prosimian primates. In: Jenkins, F.A. (Ed.), Primate Locomotion. Academic Press, New York, pp. 349–381.
Wiley, D., 2006. Landmark Editor 3.0. Institute for Data Analysis and Visualization. University of California, Davis.
Willmott, C.J., Matsuura, K., 2005. Advantages of the mean absolute error (MAE) over the root mean square error (RMSE) in assessing average model performance. Clim. Res. 30, 79–82.
Wilson Mantilla, G.P., Chester, S.G., Clemens, W.A., Moore, J.R., Sprain, C.J., Hovatter, B.T., Mitchell, W.S., Mans, W.W., Mundil, R., Renne, P.R., 2021. Earliest Palaeocene purgatoriids and the initial radiation of stem primates. R. Soc. Open Sci. 8, 210050.
Wold, S., Sjöström, M., Eriksson, L., 2001. PLS-regression: A basic tool of chemometrics. Chemometr. Intell. Lab. Syst. 58, 109–130.
Yapuncich, G.S., Granatosky, M.C., 2021. Footloose: Articular surface morphology and joint movement potential in the ankles of lorisids and cheirogaleids. Am. J. Phys. Anthropol. 175, 876–894.
Yapuncich, G.S., Seiffert, E.R., Boyer, D.M., 2017. Quantification of the position and depth of the flexor hallucis longus groove in euarchontans, with implications for the evolution of primate positional behavior. Am. J. Phys. Anthropol. 163, 367–406.
Yapuncich, G.S., Feng, H.F., Dunn, R.H., Seiffert, E.R., Boyer, D.M., 2019. Vertical support use and primate origins. Sci. Rep. 9, 12341.
Yapuncich, G.S., Chester, S.G.B., Bloch, J.I., Boyer, D.M., 2022. The feet of Paleogene primates. In: Zeiniger, A., Hatala, K.G., Wunderlich, R.E., Schmitt, D. (Eds.), The Evolution of the Primate Foot. Anatomy, Function, and Palaeontological Evidence. Springer, Cham, pp. 277–319.
Youlatos, D., 1999. Comparative locomotion of six sympatric primates in Ecuador. Ann. Sci. Nat. 20, 161–168.
Youlatos, D., Meldrum, J., 2011. Locomotor diversification in New World monkeys: Running, climbing, or clawing along evolutionary branches. Anat. Rec. 294, 1991–2012.
Youlatos, D., Karantanis, N.E., Panyutina, A., 2017. Pedal grasping in the northern smooth-tailed treeshrew *Dendrogale murina* (Tupaiidae, Scandentia): Insights for euarchontan pedal evolution. Mammalia 81, 61–70.
Youlatos, D., Widayati, K.A., Tsuji, Y., 2018. Foot postures and grasping of free-ranging Sunda colugos (*Galeopterus variegatus*) in West Java, Indonesia. Mamm. Biol. 95, 164–172.
Zelditch, M.L., Swiderski, D.L., Sheets, H.D., 2012. Geometric Morphometrics for Biologists. A Primer, 2nd ed. Academic Press, Amsterdam.

Supplementary Online Material (SOM):

Reconstruction of the locomotor repertoire of early primates in the light of astragalar and calcaneal shape

Oriol Monclús-Gonzalo[a,*], David M. Alba[a], Anne-Claire Fabre[b,c,d], Judit Marigó[e,a,*]

[a] *Institut Català de Paleontologia Miquel Crusafont (ICP-CERCA), Universitat Autònoma de Barcelona, Edifici ICTA-ICP, c/ Columnes s/n, 08193 Cerdanyola del Vallès, Barcelona, Spain*

[b] *Naturhistorisches Museum Bern, 3005 Bern, Switzerland*

[c] *Institute of Ecology and Evolution, University of Bern, 3012 Bern, Switzerland*

[d] *Life Sciences Department, Vertebrates Division, Natural History Museum, London SW7 5BD, UK*

[e]*Universitat Autònoma de Barcelona, Departament de Geologia, 08193 Cerdanyola del Vallès, Barcelona, Spain*

[*] Corresponding authors.

Email address: oriol.monclus@icp.cat (O. Monclús-Gonzalo) and judit.marigo@uab.cat (J. Marigó)

Author contributions

Oriol Monclús-Gonzalo: Writing – review & editing, Writing – original draft, Methodology, Investigation, Funding acquisition, Formal analysis, Data curation, Conceptualization. David M. Alba: Writing – review & editing, Supervision, Funding acquisition. Anne-Claire Fabre: Writing – review & editing. Judit Marigó: Writing – review & editing, Supervision, Funding acquisition.

SOM S1

Supplementary methods

Phylogenetic tree

A phylogenetic tree including all extant primates was downloaded from 10kTrees Project v.3 (Arnold et al., 2010). The different fossil species included in our study were added to the tree using the function 'bind.tip' of the package phytools v. 0.7-20 (Revell, 2012). The chronostratigraphic range reported in The Paleobiology Database (https://paleobiodb.org/) was used to estimate the branch lengths of extinct species. Extinct branches were grafted onto the base tree by sampling randomly within the length of the sister branch.

The inclusion of plesiadapiforms within Primates, as well as their actual relationship with euprimates, is still a matter of debate. However, here we follow the most recent and accepted hypothesis, which considers pleasiadapiforms as a paraphyletic assemblage of stem primates, more closely related to euprimates than to other euarchontans (Bloch et al., 2007; Silcox et al., 2007). Thus, we conferred *Purgatorius* the most basal position, followed by *Tinimomys graybulliensis* (Micromomyidae), *Ignacius graybullianus* and *Phenacolemur* (Paromomyidae), and considered plesiadapoids (plesiadapids and *Carpolestes simpsoni*) as the sister taxon of euprimates.

Despite some studies suggesting that adapiforms are ancestral or closely related to anthropoids (Franzen et al., 2009; Gingerich et al., 2010), most specialists consider them stem strepsirrhines (Beard et al., 1988; Seiffert et al., 2009; Williams et al., 2010), and we follow the latter view. Asiadapines, represented here by *Marcgodinotius indicus*, appear to be among the most primitive known adapiforms, and in most phylogenetic studies are placed between *Donrussellia* and other adapiform groups (Rose et al., 2009; Ni et al., 2016; Boyer et al., 2017). Notharctines (*Cantius*, *Copelemur tutus*, *Smilodectes* and *Notharctus*) form an independent clade of North American adapiforms. Only *Cantius* is also recorded from Europe, but the two species included in our study (*Cantius abditus* and *C. trigonodus*) are exclusive form North America (Rose and Walker, 1985; Rose et al., 1999). Within notharctines, phylogenetic analyses support a clade consisting of *Copelemur* and *Smilodectes*, with *Notharctus* often viewed as having evolved from *Cantius*

(Gunnnell, 2002). European adapids in our study include *Caenopithecus lemuroides*, *Leptadapis magnus*, and *Adapis parisiensis*. The latter has often been considered a basket case, as many remains attributed to this species probably belong to several taxa (e.g., see Godinot, 1991; Marigó et al., 2019). Most phylogenetic studies usually place adapids closer to extant strepsirrhines than North American notharctines, forming an independent European clade (Marigó et al., 2016; Seiffert et al., 2018), although sometimes they are viewed as sister clades (Ni et al., 2016). There are two main hypotheses regarding the placement of *Anchomomys frontanyensis* within adapiforms. The first one links this species with asiadapines and other European cercamoniines (Marigó et al., 2011). The second suggests that *A. frontanyensis* is more related to African taxa (aziibids, djebelemurids) than to other adapiforms (Marigó et al., 2016). In this study, we follow the latter hypothesis. Lastly, *Djebelemur martinezi* is regarded as a stem lemuriform closely related to extant strepsirrhines (Marivaux et al., 2013).

Omomyiforms are regarded as stem haplorrhines whose exact relationship with extant tarsiers and anthropoids is still a matter of debate, although most studies consider them tarsiiforms (Rosenberger and Preuschof, 2012; Ni et al., 2013; 2016). *Teilhardina belgica* is the most basal omomyiform in our study, followed by *Vastanomys major*, which is postcranially primitive but more derived than other omomyiforms dentally (Rose et al., 2009). Anaptomorphines (*Arapahovius gazini* and *Absarokius*) and omomyines (*Omomys carteri*, *Washakius insignis*, *Shoshonius cooperi*, *Hemiacodon gracilis* and *Ourayia uintensis*) are placed as two independent clades (Tornow, 2008; Ni et al., 2016). *Necrolemur* is placed as the sister taxon of extant tarsiers, as microchoerines exhibit some adaptations in their postcranial skeleton that resemble extant tarsiers (Rosenberger, 1985, 2011; Rosenberger and Preuschoft, 2012; Ni et al., 2016), although some consider that these are parallelisms (Dagosto and Gebo, 1994; Anemone and Covert, 2000).

Eosimiids are placed as the most basal anthropoids, in agreement with previous studies (Gebo et al., 2000, 2001; Gebo and Dagosto, 2004). Amphipithecids, an Asian radiation of early anthropoids, are usually regarded as stem anthropoids by most (Beard et al., 2009; Chaimanee, 2012, 2024) despite some studies rejecting their anthropoid status (Ciochcon and Gunnell, 2002; Gunnell and Ciochcon, 2008). In this study, we follow the former hypothesis and consider *Ganlea*

a stem anthropoid, more derived than eosimiids but less than the Afro-Arabian anthropoids (proteopithecids and parapithecids; Fleagle and Meldrum, 1988; Ford, 1990; Kay et al., 2008).

Locomotor categories

Eleven locomotor variables were compiled based on the minimum possible number of authors to maximize data standardization. However, as a result of the wide range of locomotor behaviors exhibited by primates and their close relatives, the field studies consulted sometimes used different locomotor categories (to emphasize those behaviors of greatest interest in a given taxon). We encountered two main problems: (1) different names for the same behavior; and (2) subcategorizations of specific locomotor categories. Below, we describe in detail the eleven categories used and justify those problems that we encountered while preparing the dataset. Locomotor categories (quadrupedalism, climbing, leaping, suspension, and clawed clinging) are defined following qualitative descriptions in Hunt et al. (1996).

Quadrupedalism is the most widespread locomotor behavior among primates and close relatives. It is performed on horizontal or oblique substrates (<45°). Most quadrupedal activities require a relatively large substrate diameter and pronograde postures with the torso parallel to the substrate. Most authors divide quadrupedalism in different subcategories, which we considered together: quadrupedal walking, trotting, running, bounding, and galloping (e.g., Gebo, 1987; Dagosto and Yamashita, 1998; Youlatos, 1999).

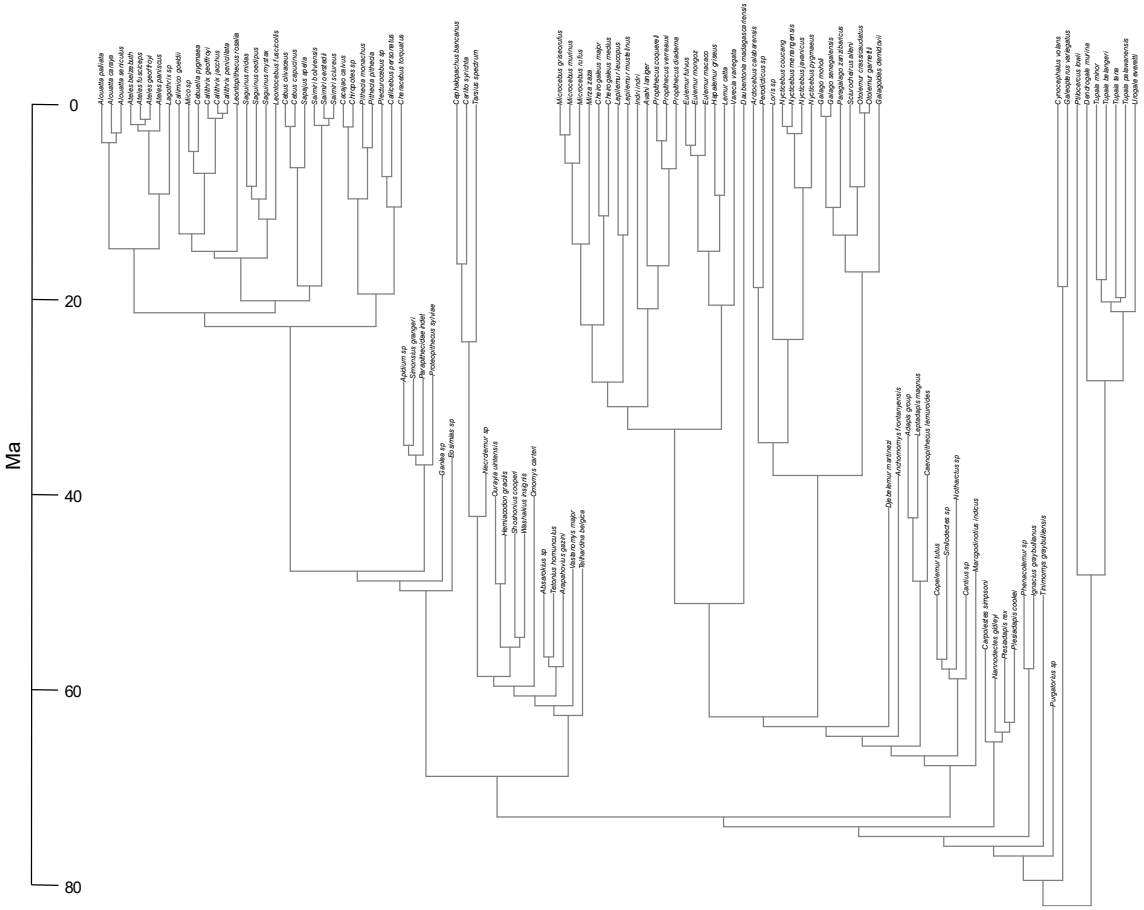
Climbing, in a strict sense, generally requires the ascension or descension of angled substrates (>45°). We do not include within this category those behaviors that require the use of claws (see clawed clinging below). In contrast, following Gebo and Chapman (1995), we also include clambering and scrambling within this category. Under this more general definition, our climbing category could be defined as a movement up or down a vertical or steeply inclined substrate or through irregular and intertwined small supports (= clambering sensu Cant, 1987). Other works (Walker, 2005; Youlatos et al., 2019) also distinguished clambering and scrambling from climbing. Crompton and Andau (1986) distinguished four different subcategories within

climbing: 1) quadrumanous climbing; 2) bipedal climbing; 3) quadrumanous descent; and 4) sliding down, and Youlatos (1999) separated oblique from vertical ascents/descents.

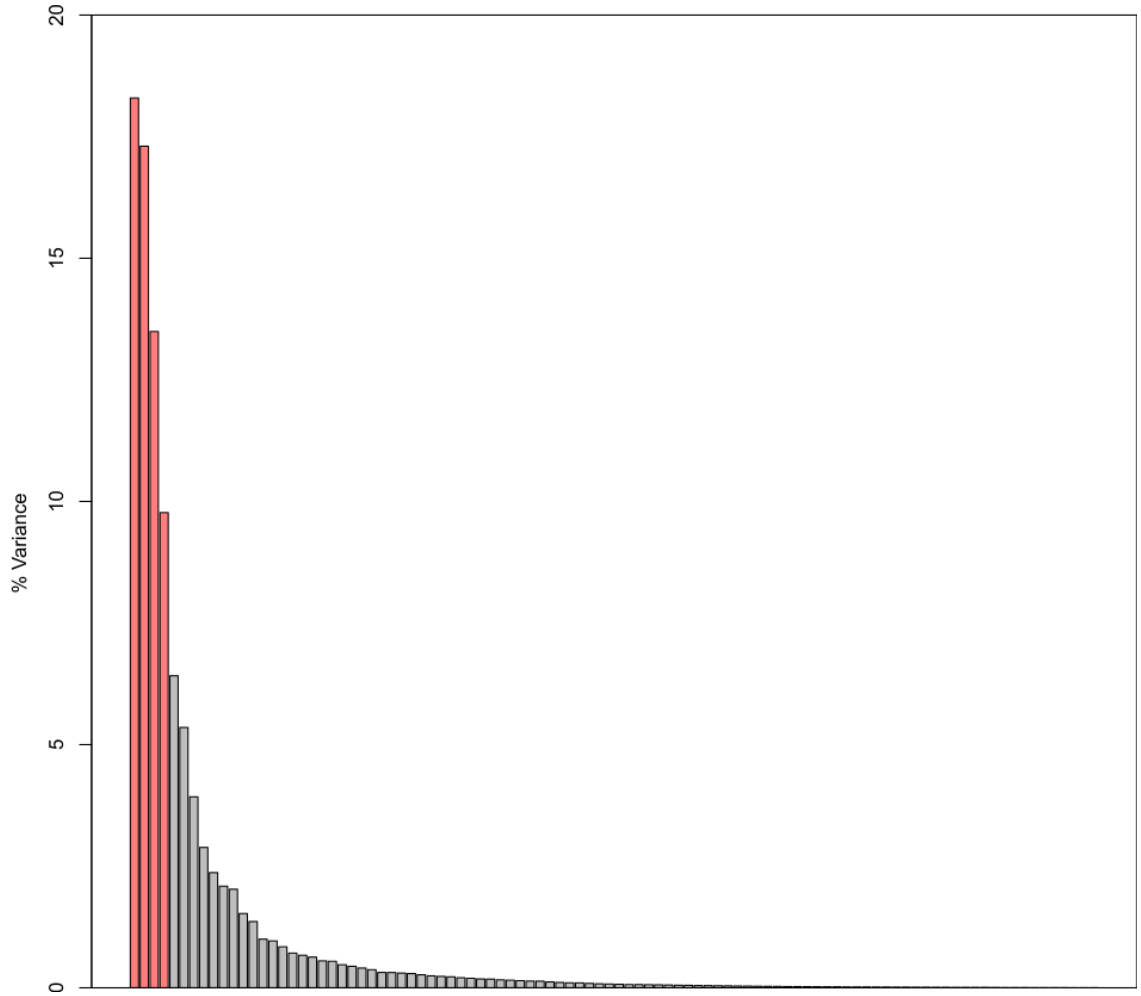
Leaping is characterized by an initial propulsive phase (in which the hindlimbs are required to be flexed back; in some variations of this type of behavior forelimbs are also involved), an airborne phase in which the body is held horizontally or inclined, and a relatively precise landing on a second support. The initial and final supports can either be arboreal or terrestrial substrates, and the initial position of the body can also vary from pronograde to orthograde. Several authors (Crompton and Andau, 1986; Walker, 2005) distinguished hopping (which is often subdivided into 'frog-hopping' and 'kangaroo-hopping', depending on the involvement of the forelimbs) from leaping. Youlatos (1999) and Lawler (2006) used a special category for those leaps performed on a vertical direction (i.e., 'vertical leap'). Within our leaping category we also included continuous leap and dropping, distinguished in Walker (2005), although in the case of the latter, the hindlimbs are barely used for propulsion and there is little horizontal movement, as it involves primarily vertical displacements.

Suspension includes all locomotor activities in which all or part of the animal's body mass is primarily held by at least one of the limbs in tension. It is important to emphasize that very different behaviors can be encompassed within this general locomotor category, and not all of them might have the same impact on the shape of the hindfoot. For example, those which are forelimb-dominated are less likely to condition astragalar or calcaneal shape (although we still might be able to assess the effects of this particular behavior, for example in the form of joints less committed to bear large loads). Several authors (Gebo, 1987; Youlatos, 1999) included bridging in their locomotor categories, either as a subcategory of climbing or scrambling/clambering activities, suspensory behaviors, or as a separate category. Cantilevering, which is defined as a specific subtype of suspensory behavior in which the grasping feet are holding on a substrate and the body is leaning across a gap to grasp another support, is presented in several studies as an independent category (Crompton and Andau, 1986; Gebo, 1987; Warren and Crompton, 1997). Gebo (1987) also distinguishes bimanualism as a subcategory of forelimb-dominated suspension.

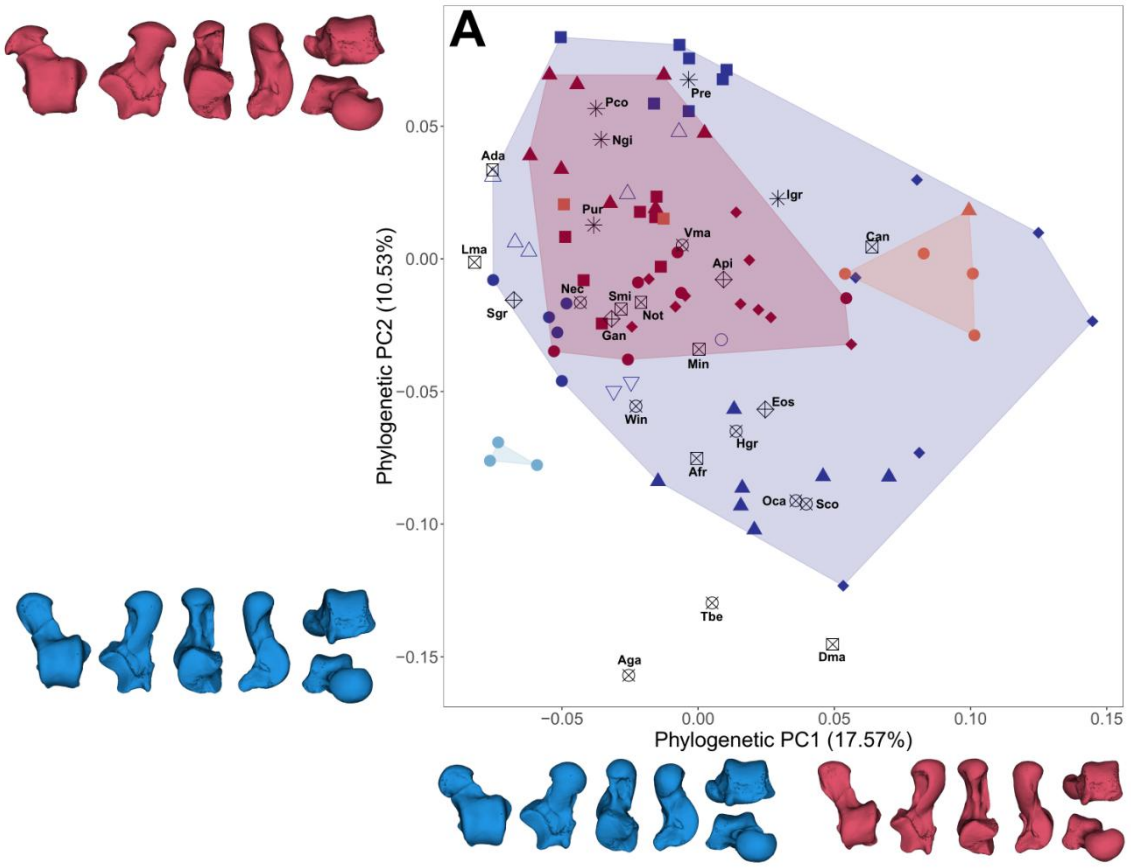
Clawed clinging and clawed climbing includes all locomotor activities involving the use of claws to cling, climb, and bound along mainly vertical trunks. Youlatos (1999) referred to it as scansorial behavior, whereas Youlatos and Meldrum (2011) used the term clawed locomotion. Moreover, Youlatos et al. (2019) subdivided clawed clinging in three different subcategories: bound claw climbing, claw climbing, and claw clinging.

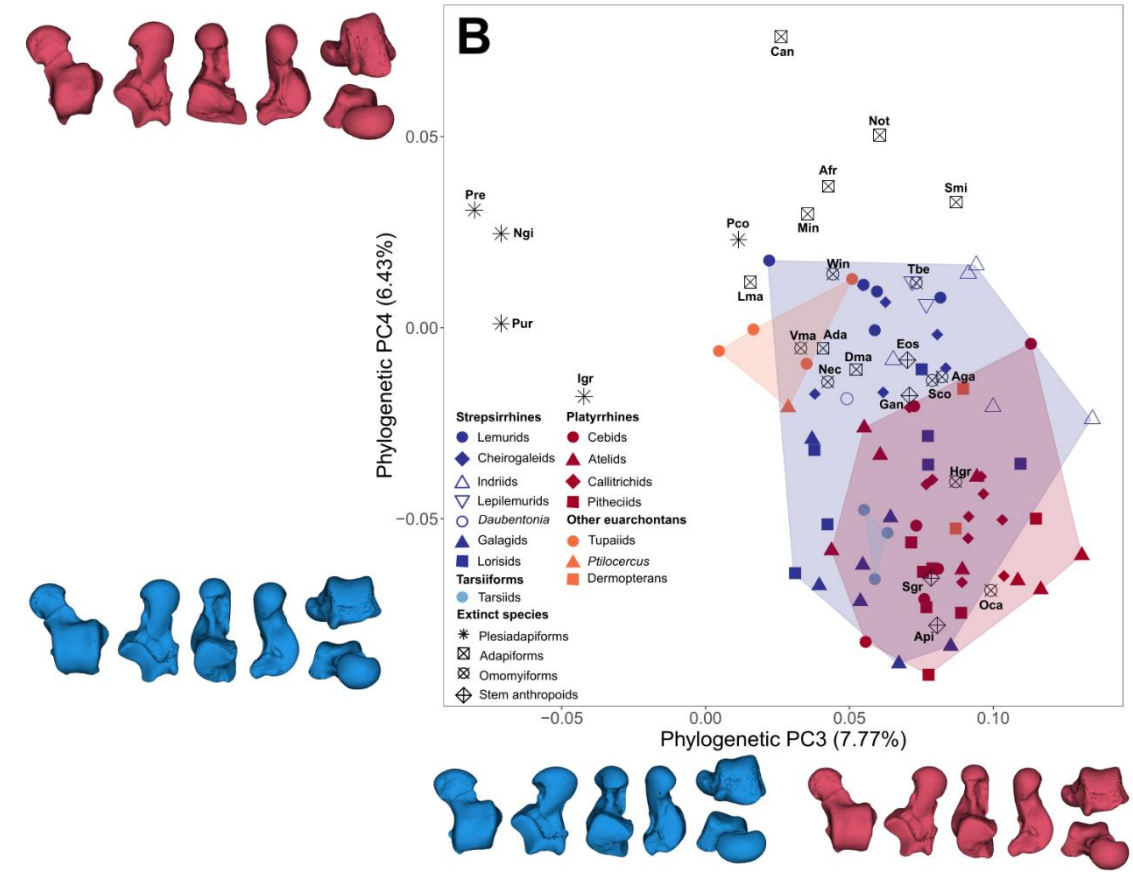


SOM Figure S1. Phylogenetic tree of the extant and extinct species included in the analyses. The phylogenetic tree was downloaded from 10kTrees Project v. 3 (Arnold et al., 2010). The fossil taxa were added manually to the tree by sampling randomly within the length of the sister branch and following the chronostratigraphic range provided in The Paleobiology Database (https://paleobiodb.org/).

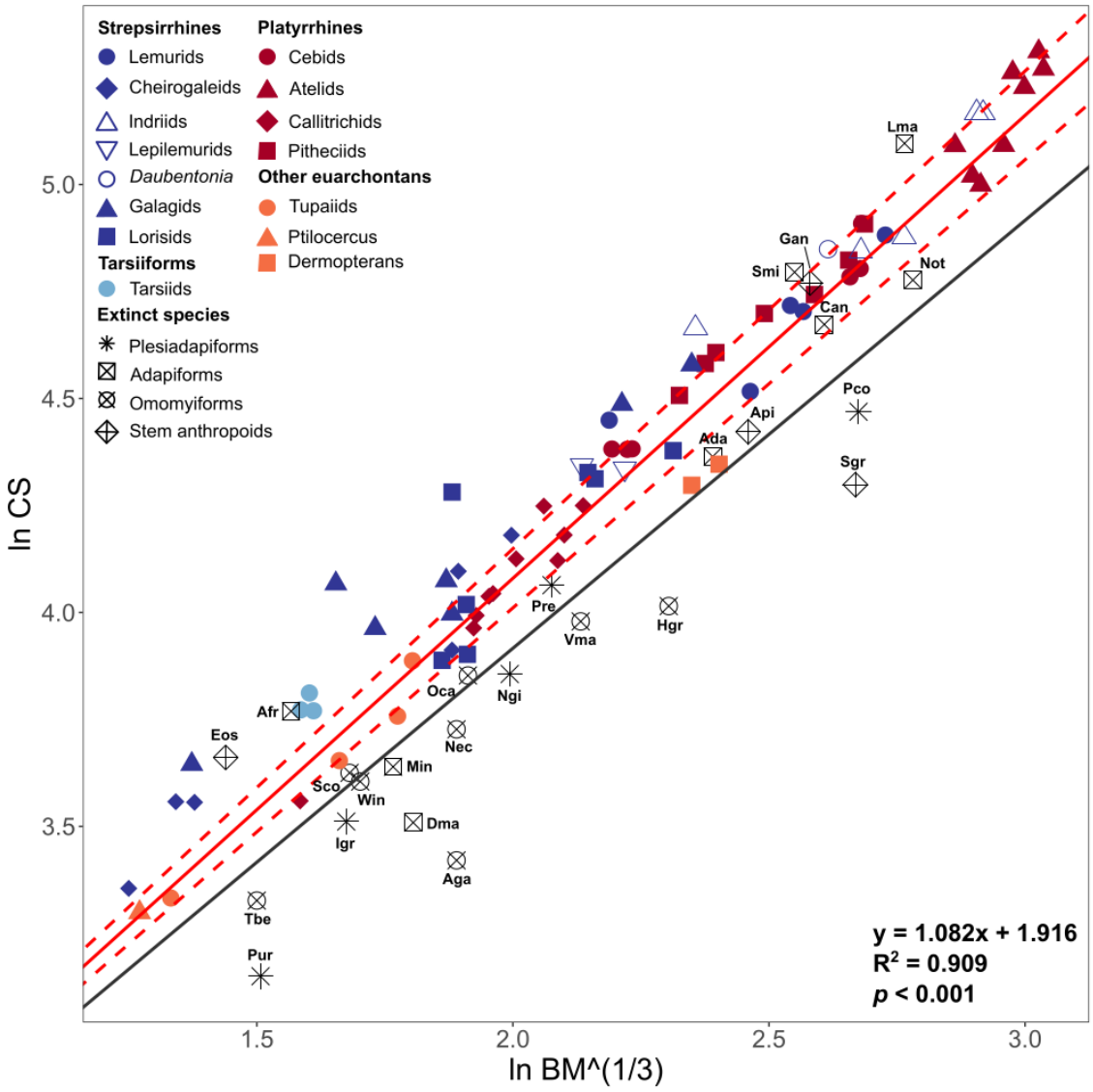


SOM Figure S2. Barplot depicting the decreasing amount of variance explained by each axis of the principal component analysis performed on the species-mean Procrustes shape coordinates of the astragalus. The first four components (in red) were used in subsequent analyses on astragalar shape.


A
Phylogenetic PC2 (10.53%)
Phylogenetic PC1 (17.57%)
0.05
0.00
−0.05
−0.10
−0.15
−0.05
0.00
0.05
0.10
0.15
Pco
Pre
Ngi
Ada
Igr
Pur
Vma
Can
Lma
Api
Nec
Smi
Not
Sgr
Gan
Min
Eos
Win
Hgr
Afr
Oca
Sco
Tbe
Aga
Dma

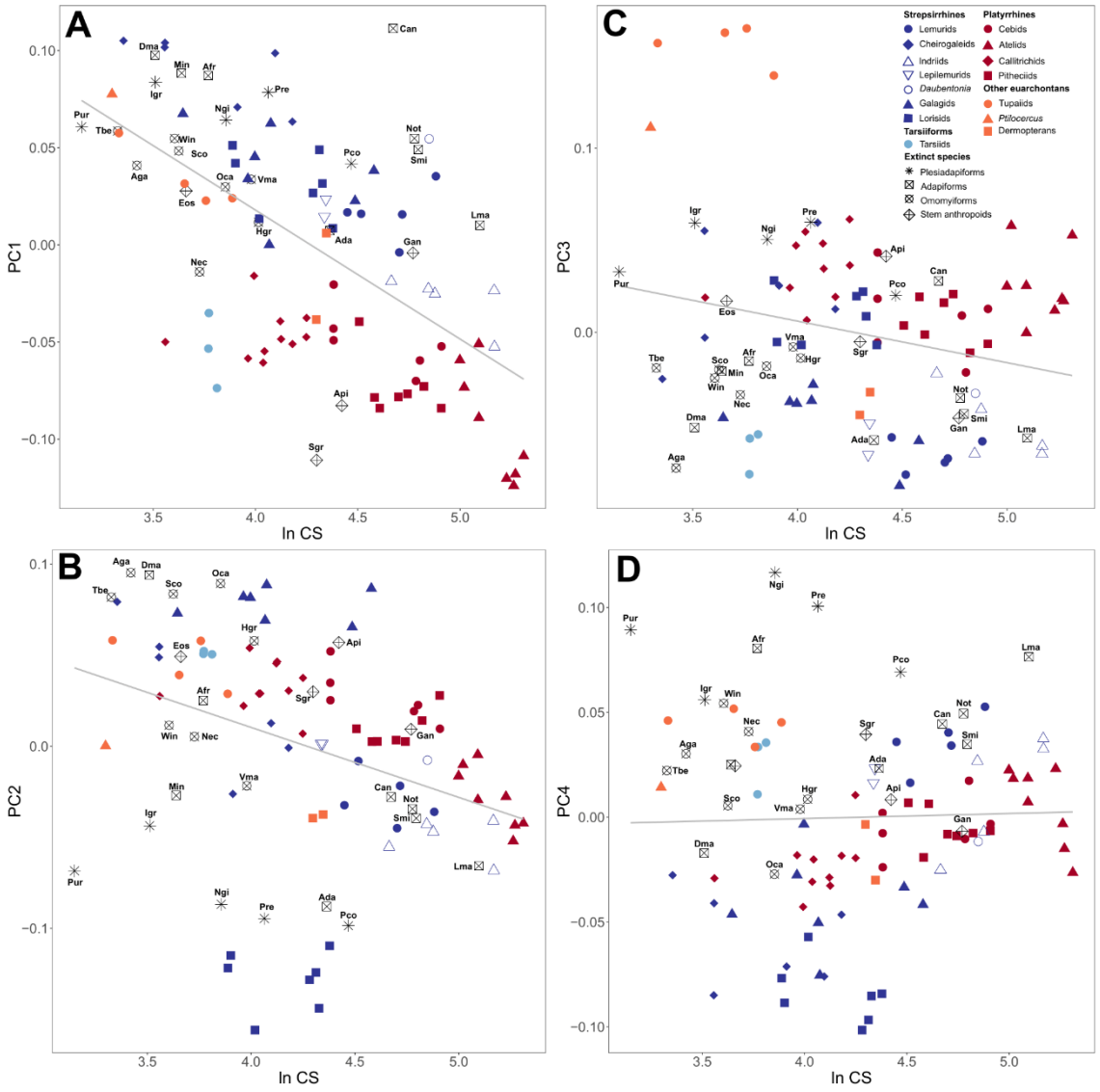

B
Phylogenetic PC4 (6.43%)
Phylogenetic PC3 (7.77%)
0.05
0.00
−0.05
−0.05
0.00
0.05
0.10
Can
Not
Afr
Smi
Pre
Min
Ngi
Pco
Win
Tbe
Lma
Pur
Vma
Ada
Eos
Dma
Nec
Aga
Igr
Sco
Gan
Hgr
Sgr
Oca
Api
Strepsirrhines
Lemurids
Cheirogaleids
Indriids
Lepilemurids
Daubentonia
Galagids
Lorisids
Tarsiiforms
Tarsiids
Extinct species
Plesiadapiforms
Adapiforms
Omomyiforms
Stem anthropoids
Platyrrhines
Cebids
Atelids
Callitrichids
Pitheciids
Other euarchontans
Tupaiids
Ptilocercus
Dermopterans

SOM Figure S3. Results of the phylogenetic principal component analysis (PCA) performed on the species-mean Procrustes shape coordinates of the astragalus as depicted by bivariate plots of PC2 vs. PC1 (A) and PC4 vs. PC3 (B). Taxonomic groups are color and symbol-coded, as indicated in the legend. The percentage of variance explained by each PC is reported within parentheses. Astragalar shapes associated with minimum (blue) and maximum (red) values of each PC axis are plotted below each scatterplot (dorsal, plantar, lateral, medial, proximal, and distal views are shown, from left to right). Thin plate splines correspond to an astragalus of *Plecturocebus moloch* (AMNH 244363). Abbreviations: Api= *Apidium*; Sgr = *Simonsius grangeri*; Gan = *Ganlea*; Eos = *Eosimias*; Nec = *Necrolemur*; Hgr = *Hemiacodon_gracilis*; Sco = *Shoshonius cooperi*; Win = *Washakius insignis*; Oca = *Omomys carteri*; Aga = *Arapahovius gazini*; Vma = *Vastanomys major*; Tbe = *Teilhardina belgica*; Dma = *Djebelemur martinezi*; Afr = *Anchomomys frontanyensis*; Ada = *Adapis* group; Lma = *Leptadapis magnus*; Smi = *Smilodectes*; Not = *Notharctus*; Can = *Cantius*; Min= *Marcgodinotius indicus*; Ngi = *Nanodectes gidleyi*; Pre = *Plesiadapis rex*; Pco = *Plesiadapis cookei*; Igr = *Ignacius graybullianus*; Pur = *Purgatorius*.



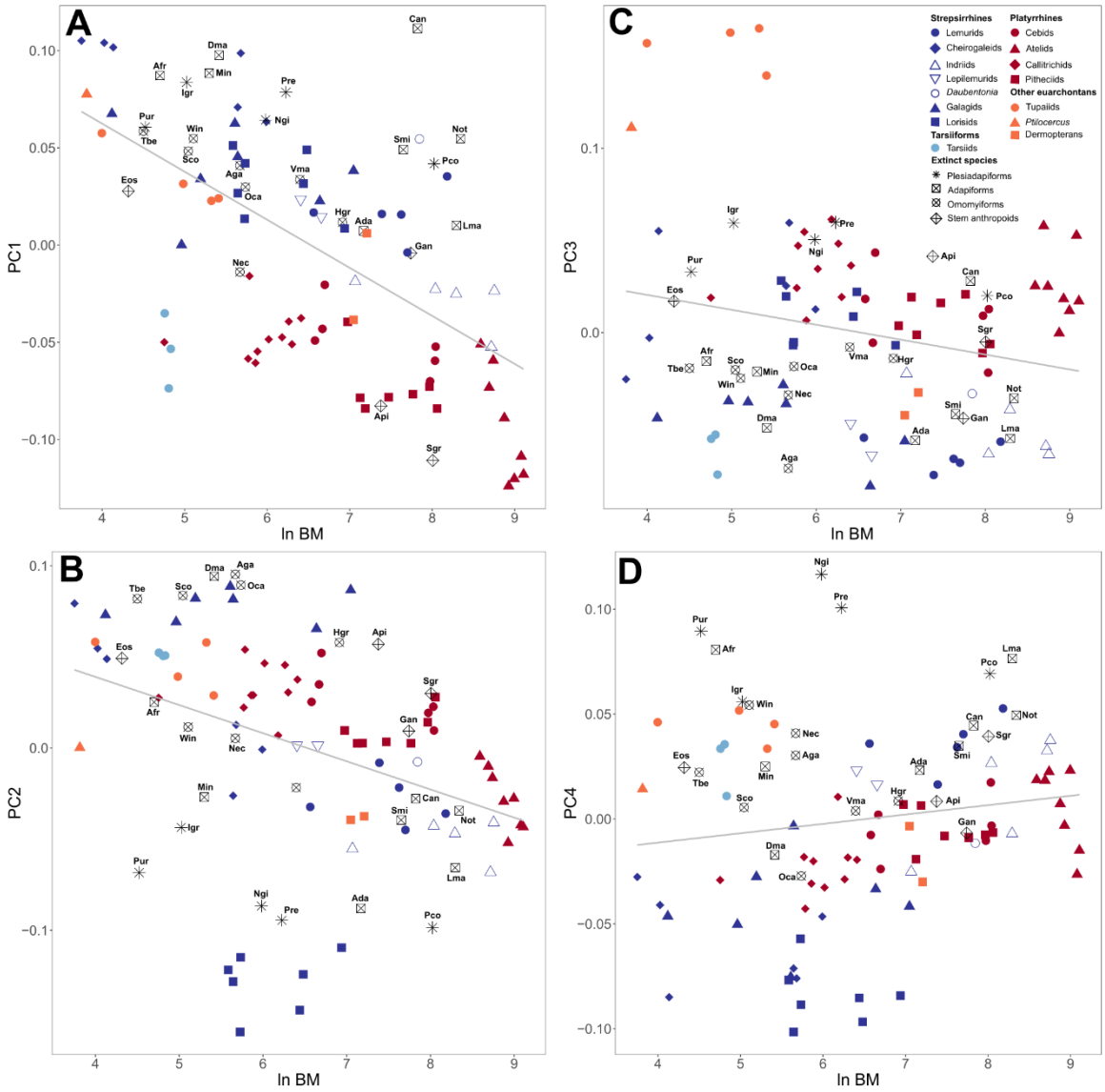
SOM Figure S4. Bivariate regression between log-transformed centroid size (ln CS) of the astragalus and log-transformed cube root of the body mass (ln $BM^{1/3}$). Taxonomic groups are color and symbol-coded, as indicated in the legend. The intercept and the slope, as well as the r^2 and the p-value are indicated in the scatterplot. The black line indicates the regression line of the data. The red line indicates the expected regression line (slope = 1) under an isometric relationship between ln CS and ln $BM^{1/3}$ and the dashed red lines indicate the upper and lower 95% confidence intervals. Abbreviations: Api= *Apidium*; Sgr = *Simonsius grangeri*; Gan = *Ganlea*; Eos = *Eosimias*; Nec = *Necrolemur*; Hgr = *Hemiacodon_gracilis*; Sco = *Shoshonius cooperi*; Win = *Washakius insignis*; Oca = *Omomys carteri*; Aga = *Arapahovius gazini*; Vma = *Vastanomys major*; Tbe = *Teilhardina belgica*; Dma = *Djebelemur martinezi*; Afr = *Anchomomys*

frontanyensis; Ada = *Adapis* group; Lma = *Leptadapis magnus*; Smi = *Smilodectes*; Not = *Notharctus*; Can = *Cantius*; Min= *Marcgodinotius indicus*; Ngi = *Nanodectes gidleyi*; Pre = *Plesiadapis rex*; Pco = *Plesiadapis cookei*; Igr = *Ignacius graybullianus*; Pur = *Purgatorius*.



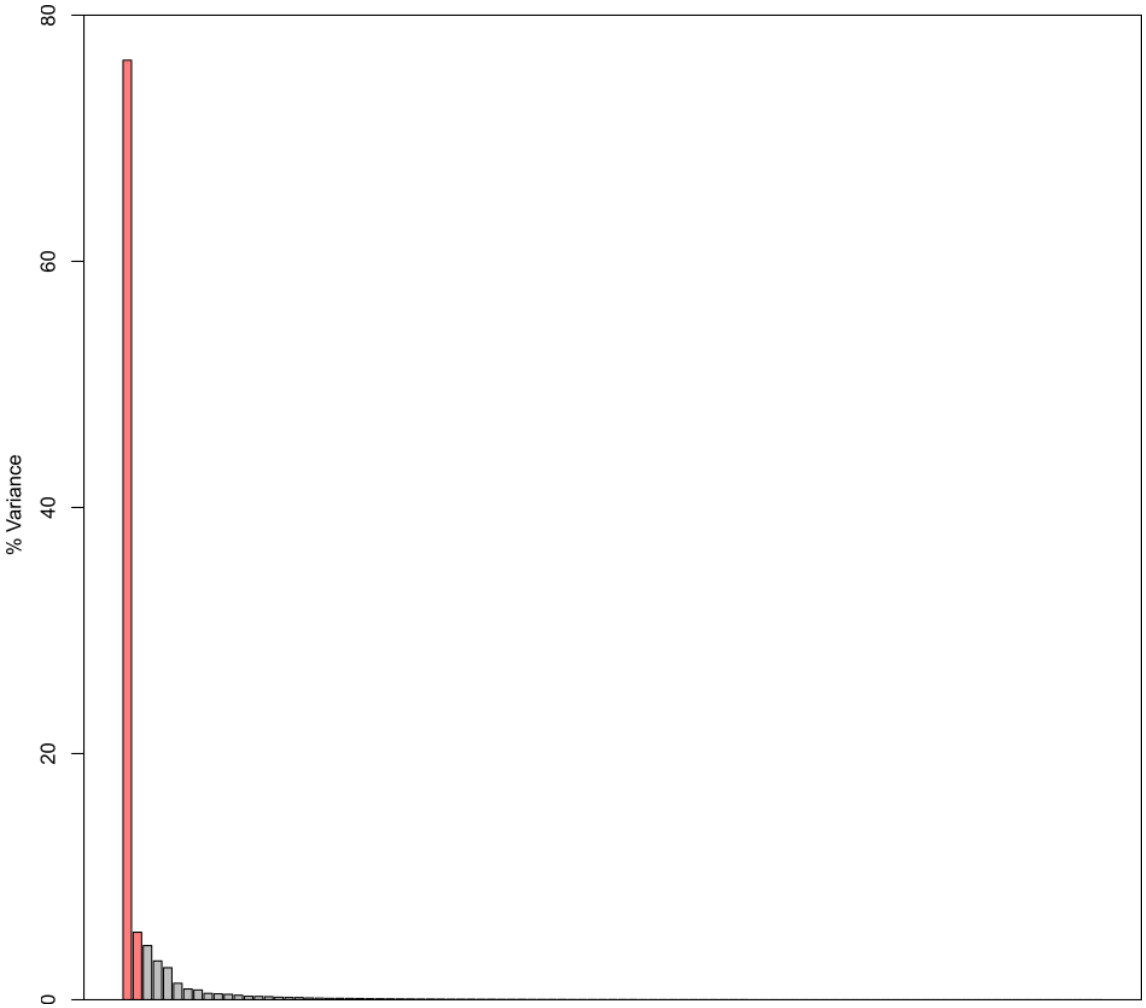
SOM Figure S5. Bivariate plots between the first four principal components (PCs; A–D, respectively) of the principal component analysis performed on the species-mean Procrustes shape coordinates of the astragalus and log-transformed centroid size (ln CS). Taxonomic groups are color and symbol-coded, as indicated in the legend. The grey line indicates the regression line of the data. Abbreviations: Api= *Apidium*; Sgr = *Simonsius grangeri*; Gan = *Ganlea*; Eos = *Eosimias*; Nec = *Necrolemur*; Hgr = *Hemiacodon_gracilis*; Sco = *Shoshonius cooperi*; Win = *Washakius insignis*; Oca = *Omomys carteri*; Aga = *Arapahovius gazini*; Vma = *Vastanomys major*; Tbe = *Teilhardina belgica*; Dma = *Djebelemur martinezi*; Afr = *Anchomomys frontanyensis*; Ada = *Adapis* group; Lma = *Leptadapis magnus*; Smi = *Smilodectes*; Not =

Notharctus; Can = *Cantius*; Min= *Marcgodinotius indicus*; Ngi = *Nanodectes gidleyi*; Pre = *Plesiadapis rex*; Pco = *Plesiadapis cookei*; Igr = *Ignacius graybullianus*; Pur = *Purgatorius*.

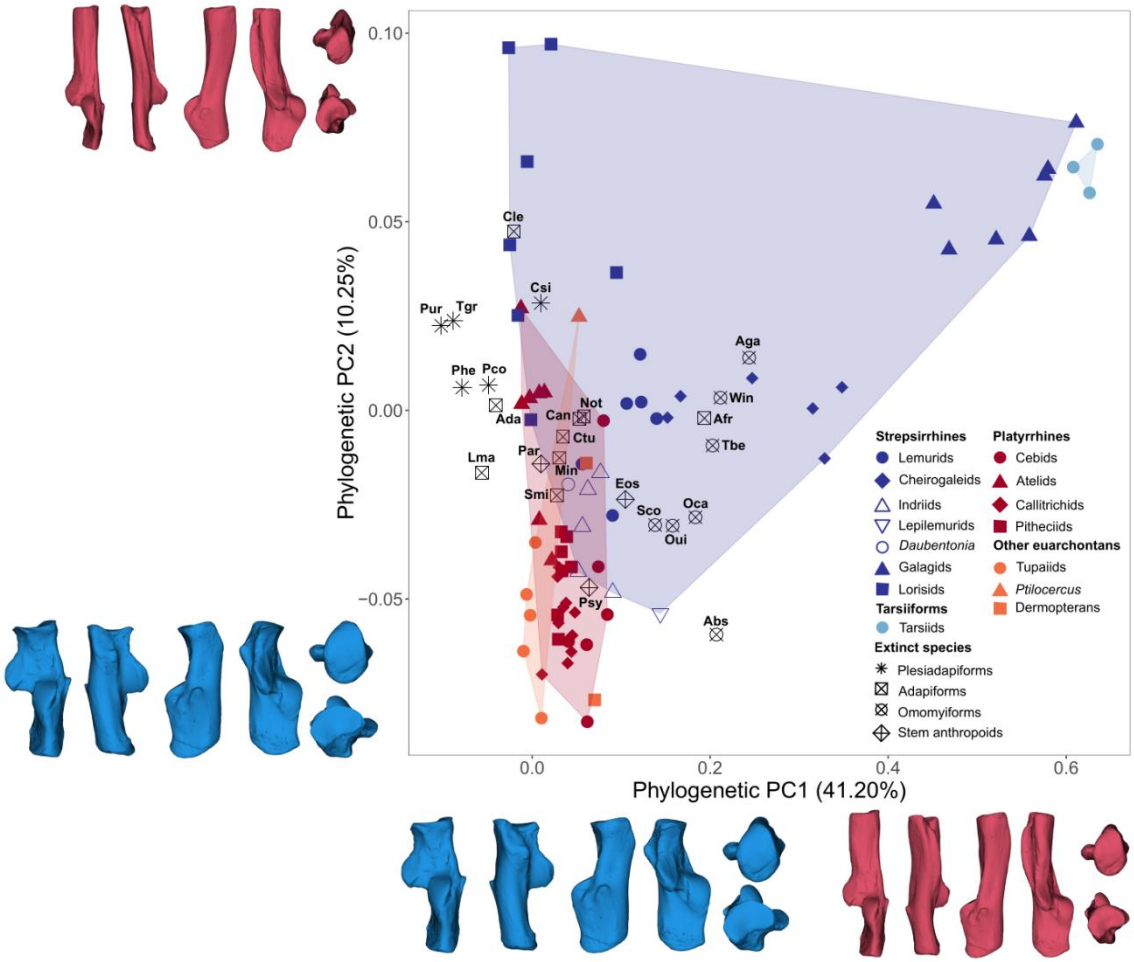


SOM Figure S6. Bivariate plots between the first four principal components (PCs; A–D, respectively) of the principal component analysis performed on the species-mean Procrustes shape coordinates of the astragalus and log-transformed body mass (ln BM). Taxonomic groups are color and symbol-coded, as indicated in the legend. The grey line indicates the regression line of the data. Abbreviations: Api= *Apidium*; Sgr = *Simonsius grangeri*; Gan = *Ganlea*; Eos = *Eosimias*; Nec = *Necrolemur*; Hgr = *Hemiacodon_gracilis*; Sco = *Shoshonius cooperi*; Win = *Washakius insignis*; Oca = *Omomys carteri*; Aga = *Arapahovius gazini*; Vma = *Vastanomys major*; Tbe = *Teilhardina belgica*; Dma = *Djebelemur martinezi*; Afr = *Anchomomys frontanyensis*; Ada = *Adapis* group; Lma = *Leptadapis magnus*; Smi = *Smilodectes*; Not =

Notharctus; Can = *Cantius*; Min= *Marcgodinotius indicus*; Ngi = *Nanodectes gidleyi*; Pre = *Plesiadapis rex*; Pco = *Plesiadapis cookei*; Igr = *Ignacius graybullianus*; Pur = *Purgatorius*.

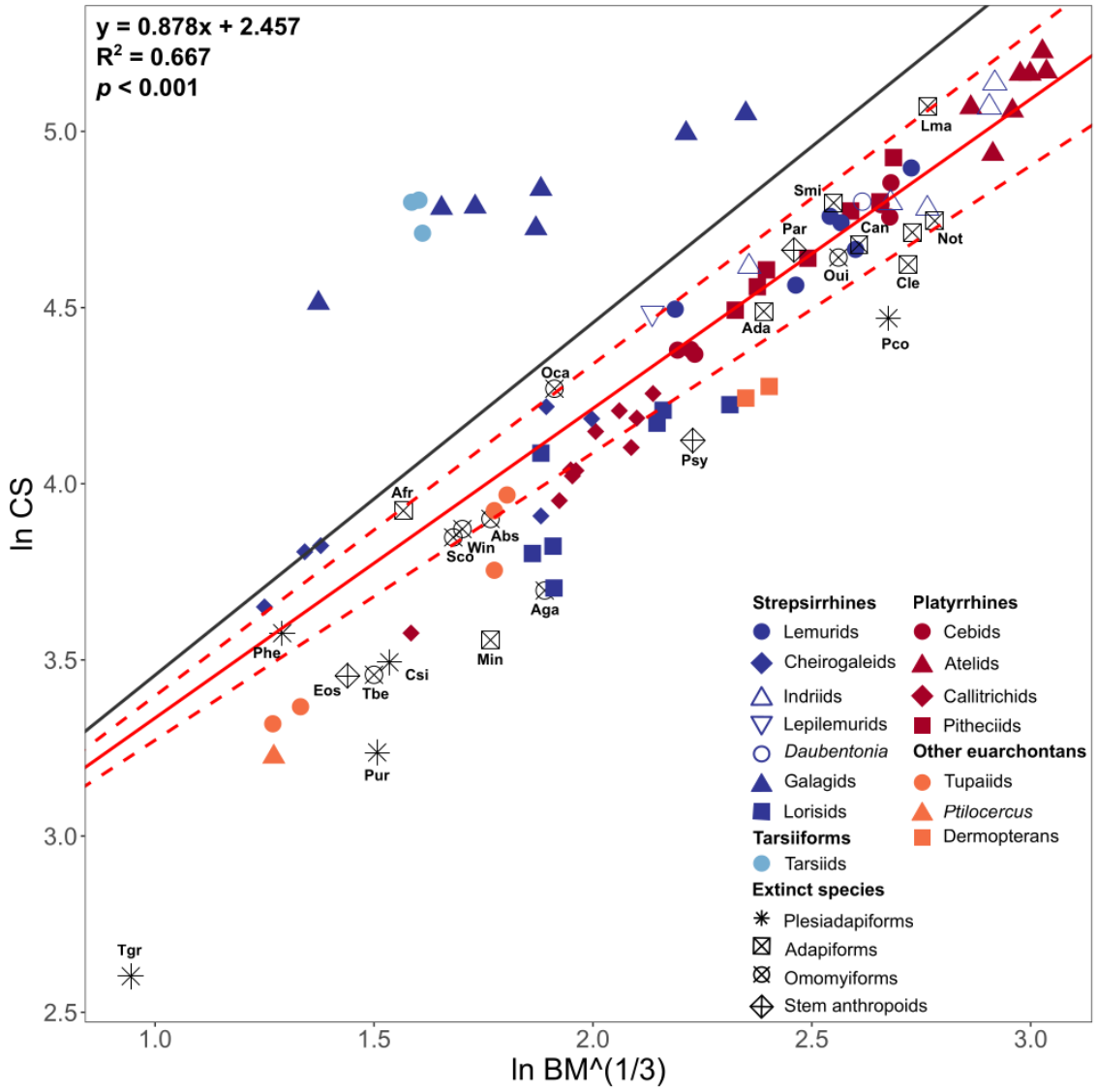


SOM Figure S7. Barplot depicting the decreasing amount of variance explained by each axis of the principal component analysis performed on the species-mean Procrustes shape coordinates of the calcaneus. The first two components (in red) were used in subsequent analyses on calcaneal shape.



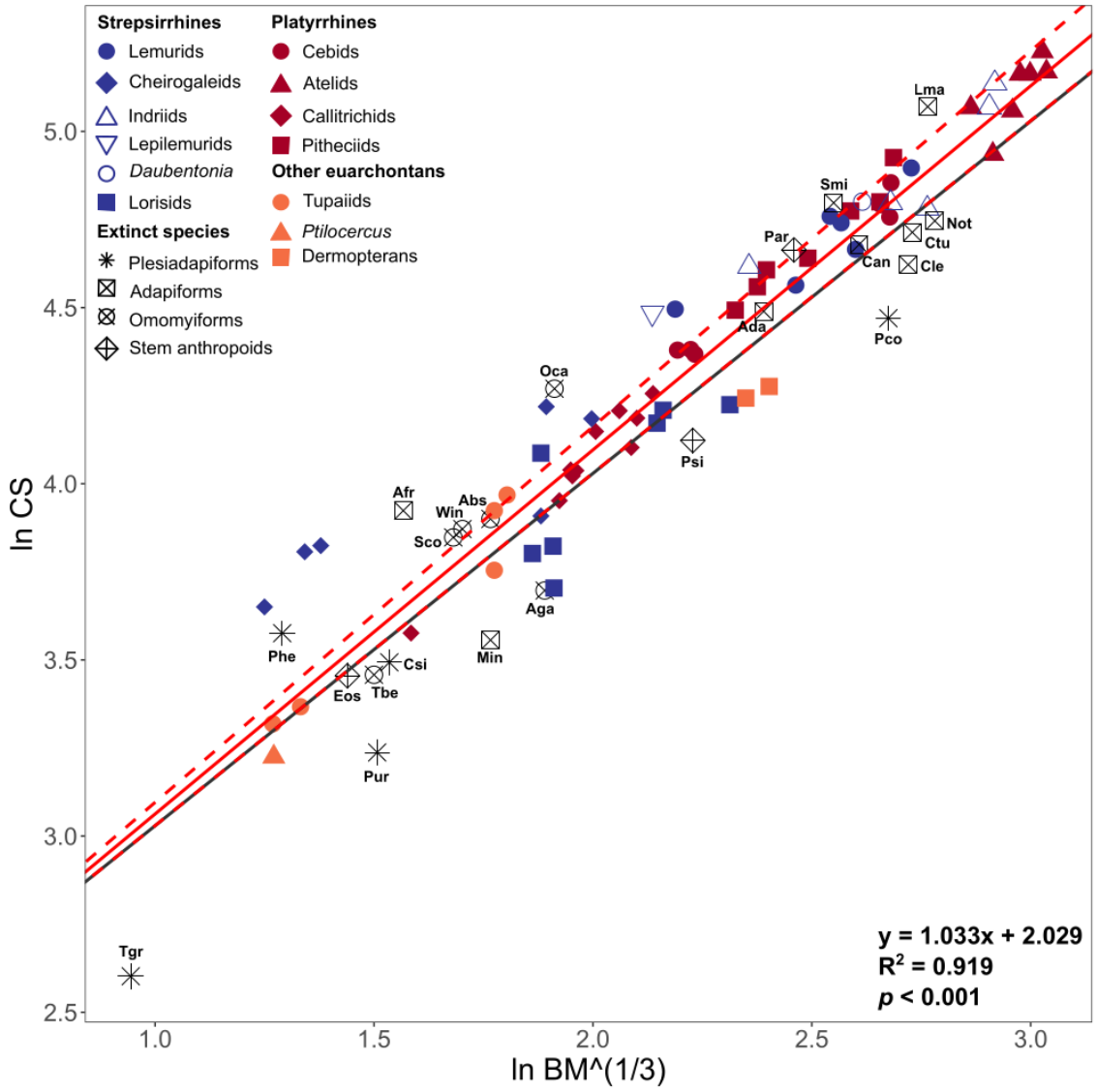
SOM Figure S8. Results of the phylogenetic principal component analysis (PCA) performed on the species-mean Procrustes shape coordinates of the calcaneus as depicted by bivariate plots of PC2 vs. PC1. Taxonomic groups are color and symbol-coded, as indicated in the legend. The percentage of variance explained by each PC is reported within parentheses. Calcaneal shapes associated with minimum (blue) and maximum (red) values of each PC axis are plotted below each scatterplot (dorsal, plantar, lateral, medial, proximal, and distal views are shown, from left to right). Thin plate splines correspond to a calcaneus of *Eulemur albifrons* (AMNH 170717). Abbreviations: Par = Parapithecidae indet; Psy = *Proteopithecus sylviae*; Eos = *Eosimias*; Oui = *Ourayia uintensis*; Sco = *Shoshonius cooperi*; Win = *Washakius insignis*; Oca = *Omomys carteri*; Abs = *Absarokius*; Aga = *Arapahovius gazini*; Tbe = *Teilhardina belgica*; Afr = *Anchomomys frontanyensis*; Ada = *Adapis* group; Lma = *Leptadapis magnus*; Cle = *Caenopithecus lemuroides*; Ctu = *Copelemur tutus*; Smi = *Smilodectes*; Not = *Notharctus*; Can = *Cantius*; Min =

Marcgodinotius indicus; Csi = *Carpolestes simpsoni*; Pco = *Plesiadapis cookei*; Phe = *Phenacolemur*; Tgr = *Tinimomys graybulliensis*; Pur = *Purgatorius*.



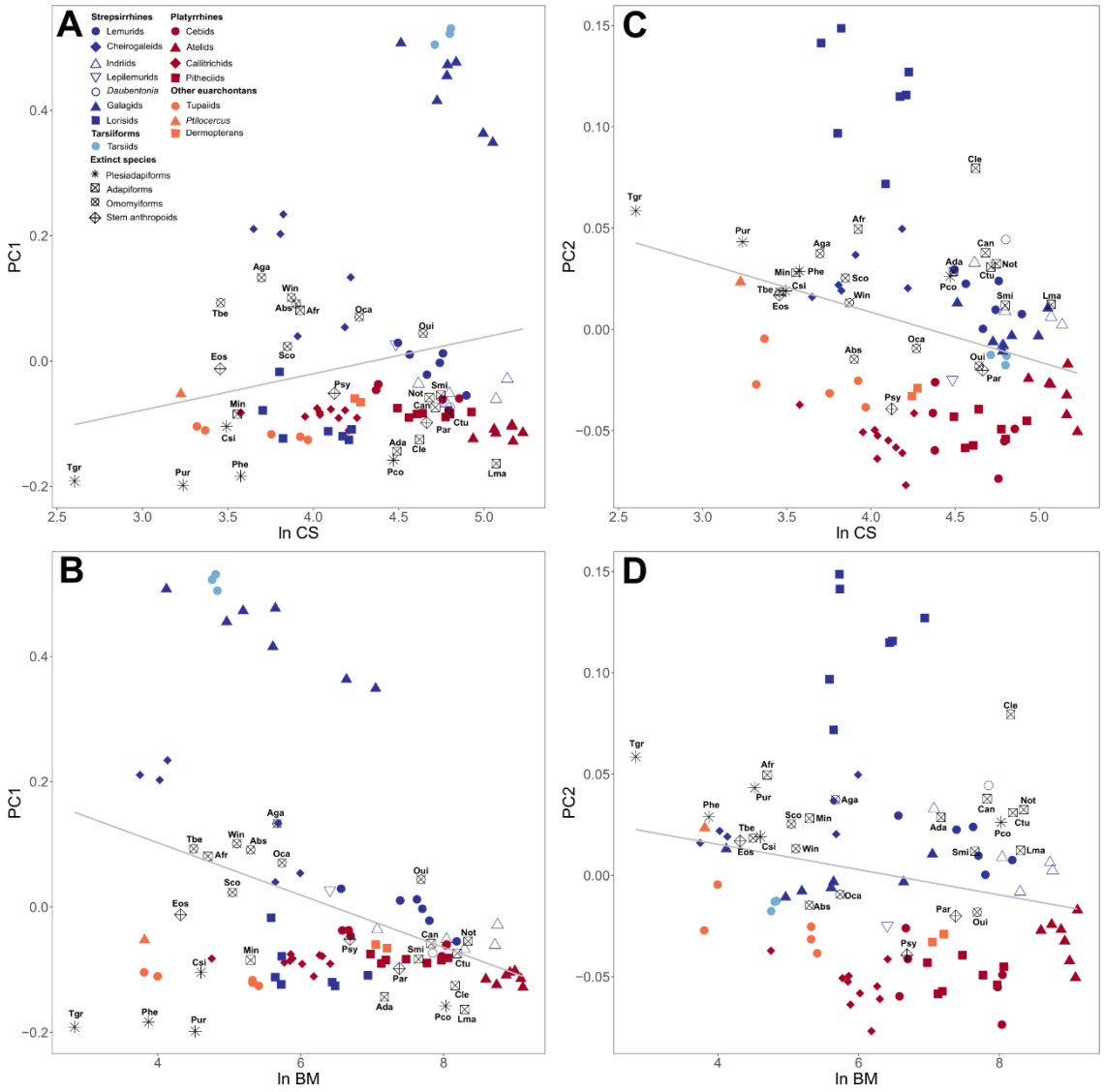
SOM Figure S9. Bivariate regression between log-transformed centroid size (ln CS) of the calcaneus and log-transformed cube root of the body mass (ln $BM^{1/3}$). Taxonomic groups are color and symbol-coded, as indicated in the legend. The intercept and the slope, as well as the r^2 and the p-value are indicated in the scatterplot. The black line indicates the regression line of the data. The red line indicates the expected regression line (slope = 1) under an isometric relationship between ln CS and ln $BM^{1/3}$ and the dashed red lines indicate the upper and lower 95% confidence intervals. Note that the small vertical clinger and leapers (galagids and tarsiids) clearly depart from the best-fit line displayed by other species. Abbreviations: Par = Parapithecidae indet; Psy = *Proteopithecus sylviae*; Eos = *Eosimias*; Oui = *Ourayia uintensis*; Sco = *Shoshonius cooperi*; Win = *Washakius insignis*; Oca = *Omomys carteri*; Abs = *Absarokius*; Aga = *Arapahovius gazini*;

Tbe = *Teilhardina belgica*; Afr = *Anchomomys frontanyensis*; Ada = *Adapis* group; Lma = *Leptadapis magnus*; Cle = *Caenopithecus lemuroides*; Ctu = *Copelemur tutus*; Smi = *Smilodectes*; Not = *Notharctus*; Can = *Cantius*; Min = *Marcgodinotius indicus*; Csi = *Carpolestes simpsoni*; Pco = *Plesiadapis cookei*; Phe = *Phenacolemur*; Tgr = *Tinimomys graybulliensis*; Pur = *Purgatorius*.



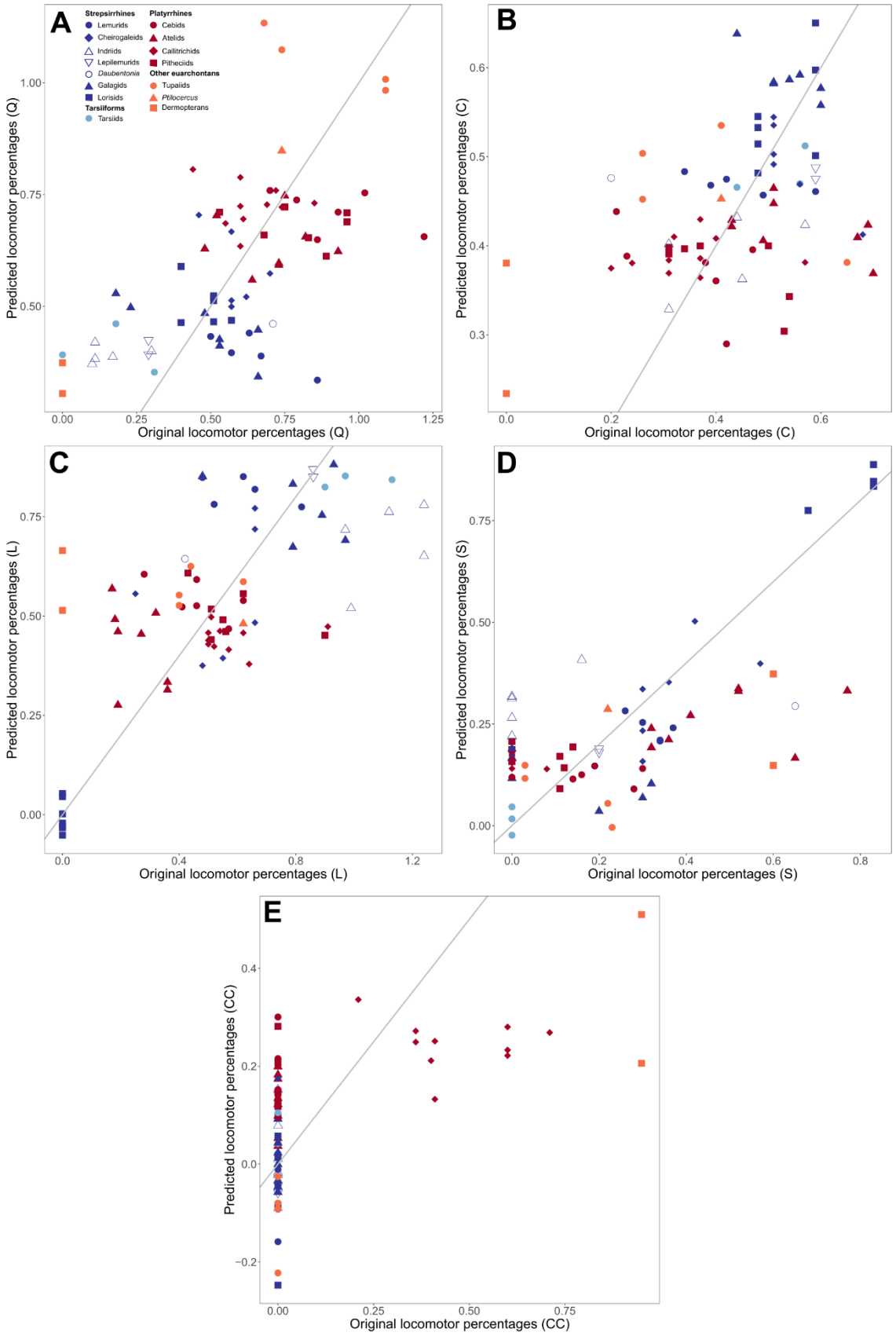
SOM Figure S10. Bivariate regression between log-transformed centroid size (ln CS) of the calcaneus and log-transformed cube root of the body mass (ln $BM^{1/3}$) after removing small VCL (galagids and tarsiids). Taxonomic groups are color and symbol-coded, as indicated in the legend. The intercept and the slope, as well as the r^2 and the *p*-value are indicated in the scatterplot. The black line indicates the regression line of the data. The red line indicates the expected regression line (slope = 1) under an isometric relationship between ln CS and ln $BM^{1/3}$ and the dashed red lines indicate the upper and lower 95% confidence intervals. Abbreviations: Par = Parapithecidae indet; Psy = *Proteopithecus sylviae*; Eos = *Eosimias*; Oui = *Ourayia uintensis*; Sco = *Shoshonius cooperi*; Win = *Washakius insignis*; Oca = *Omomys carteri*; Abs = *Absarokius*; Aga = *Arapahovius gazini*; Tbe = *Teilhardina belgica*; Afr = *Anchomomys frontanyensis*; Ada = *Adapis*

group; Lma = *Leptadapis magnus*; Cle = *Caenopithecus lemuroides*; Ctu = *Copelemur tutus*; Smi = *Smilodectes*; Not = *Notharctus*; Can = *Cantius*; Min = *Marcgodinotius indicus*; Csi = *Carpolestes simpsoni*; Pco = *Plesiadapis cookei*; Phe = *Phenacolemur*; Tgr = *Tinimomys graybulliensis*; Pur = *Purgatorius*.



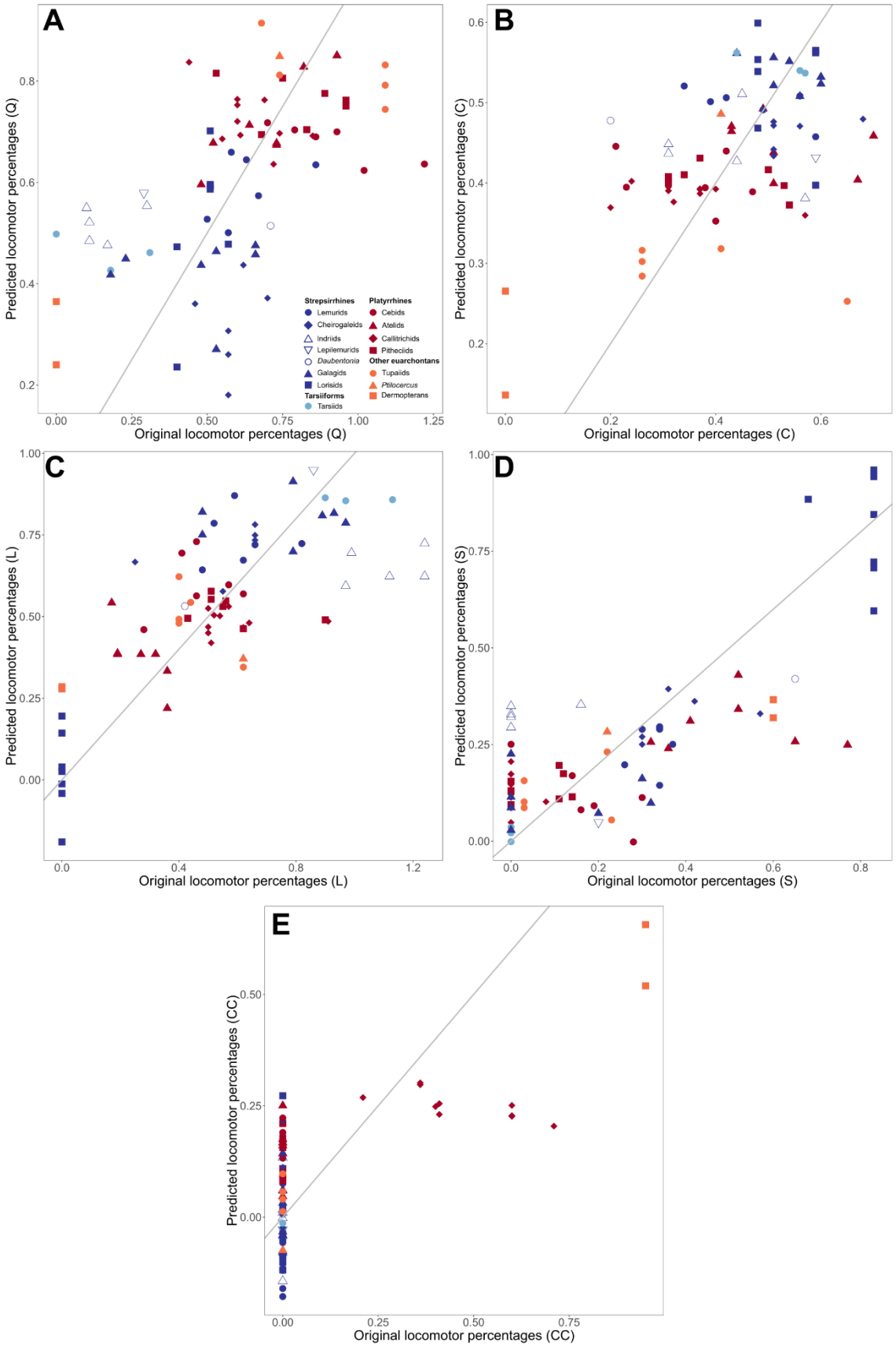
SOM Figure S11. Bivariate plots between the first two principal components (PCs; A and B, and C and D, respectively) of the principal component analysis performed on the species-mean Procrustes shape coordinates of the astragalus and log-transformed centroid size (ln CS; A and C) or log-transformed body mass (ln BM; B and D). Taxonomic groups are color and symbol-coded, as indicated in the legend. The grey line indicates the regression line of the data. Abbreviations: Par = Parapithecidae indet; Psy = *Proteopithecus sylviae*; Eos = *Eosimias*; Oui = *Ourayia uintensis*; Sco = *Shoshonius cooperi*; Win = *Washakius insignis*; Oca = *Omomys carteri*; Abs = *Absarokius*; Aga = *Arapahovius gazini*; Tbe = *Teilhardina belgica*; Afr = *Anchomomys frontanyensis*; Ada = *Adapis* group; Lma = *Leptadapis magnus*; Cle = *Caenopithecus lemuroides*; Ctu = *Copelemur tutus*; Smi = *Smilodectes*; Not = *Notharctus*; Can = *Cantius*; Min =

Marcgodinotius indicus; Csi = *Carpolestes simpsoni*; Pco = *Plesiadapis cookei*; Phe = *Phenacolemur*; Tgr = *Tinimomys graybulliensis*; Pur = *Purgatorius*.



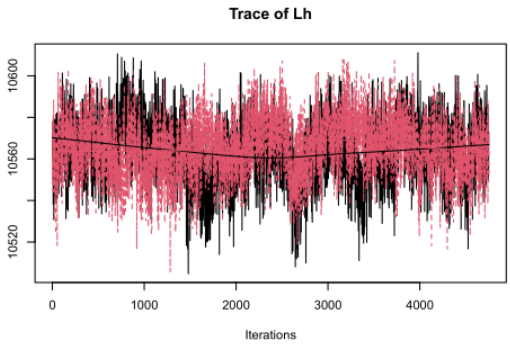
SOM Figure S12. Bivariate plots between the original locomotor percentages and the predicted ones using astragalar shape as a predictor after 'leave-one-out cross-validation' was performed

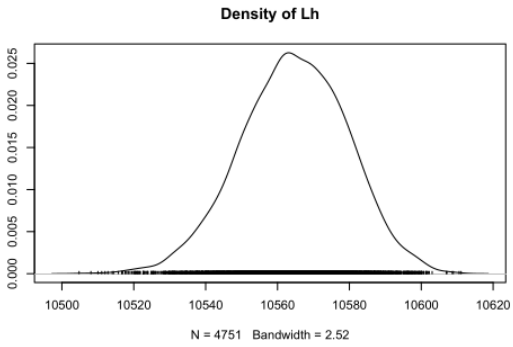
on the extant comparative sample for each locomotor variable: A) quadrupedalism (Q); B) climbing (C); C) leaping (L); D) suspension (S); E) clawed clinging/cimbing (CC).

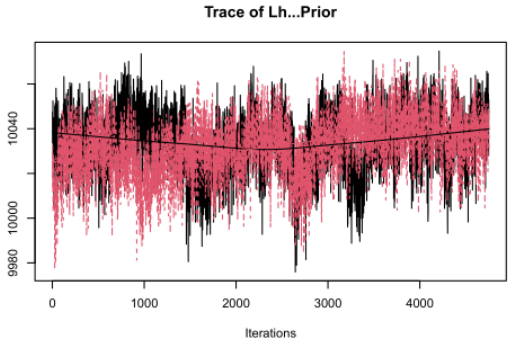


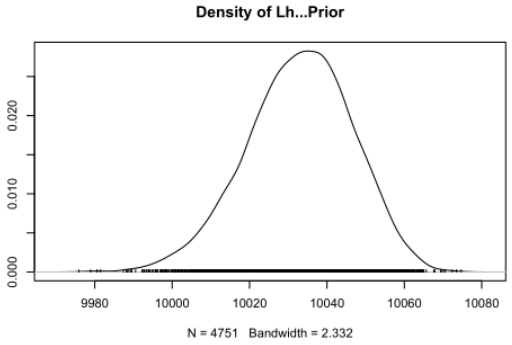
SOM Figure S13. Bivariate plots between the original locomotor percentages and the predicted ones using calcaneal shape as a predictor after 'leave-one-out cross-validation' was performed on

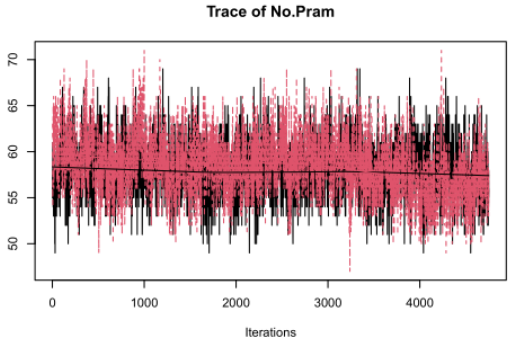
the extant comparative sample for each locomotor variable: A) quadrupedalism (Q); B) climbing (C); C) leaping (L); D) suspension (S); E) clawed clinging/cimbing (CC).

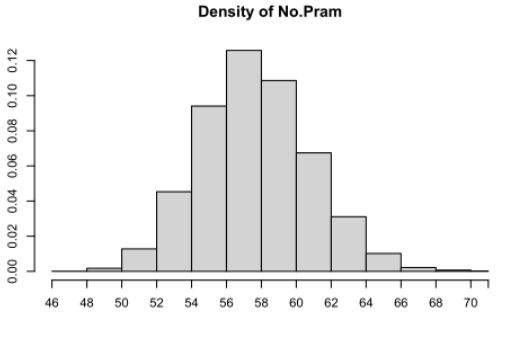

Trace of Lh
10600
10560
10520
0
1000
2000
3000
4000
Iterations

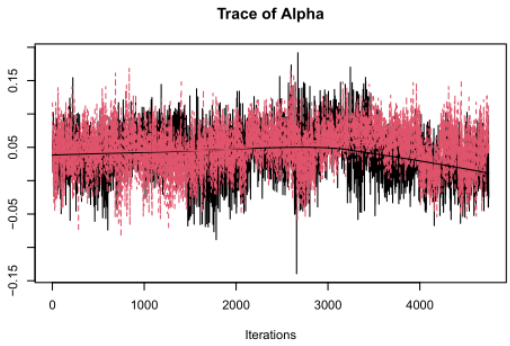

Density of Lh
0.025
0.020
0.015
0.010
0.005
0.000
10500
10520
10540
10560
10580
10600
10620
N = 4751 Bandwidth = 2.52

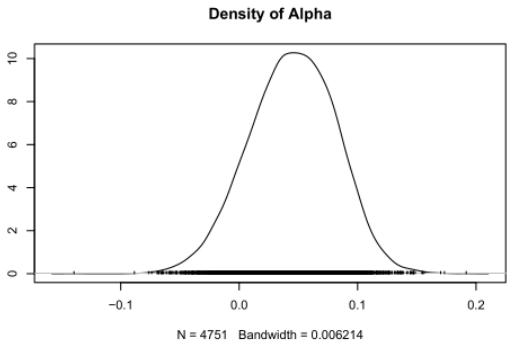

Trace of Lh...Prior
10040
10000
9980
0
1000
2000
3000
4000
Iterations

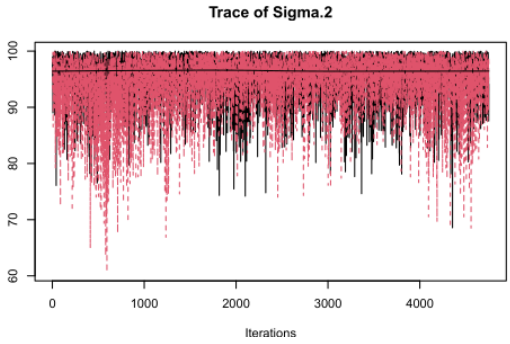

Density of Lh...Prior
0.020
0.010
0.000
9980
10000
10020
10040
10060
10080
N = 4751 Bandwidth = 2.332

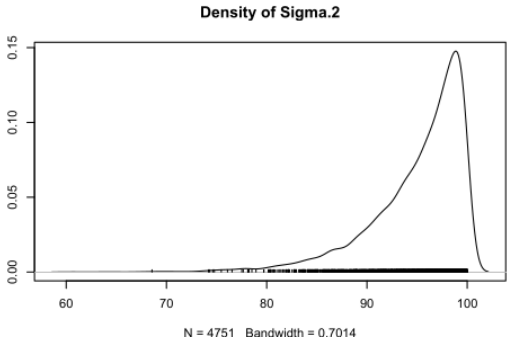

Trace of No.Pram
70
65
60
55
50
0
1000
2000
3000
4000
Iterations


Density of No.Pram
0.12
0.10
0.08
0.06
0.04
0.02
0.00
46
48
50
52
54
56
58
60
62
64
66
68
70

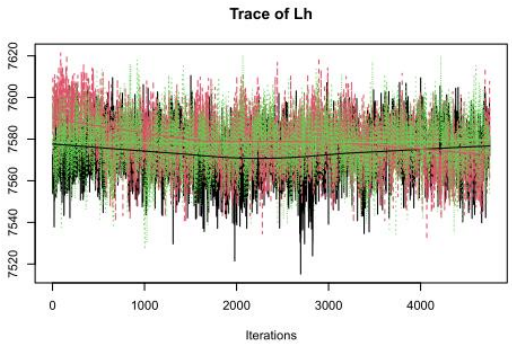

Trace of Alpha
0.15
0.05
−0.05
−0.15
0
1000
2000
3000
4000
Iterations

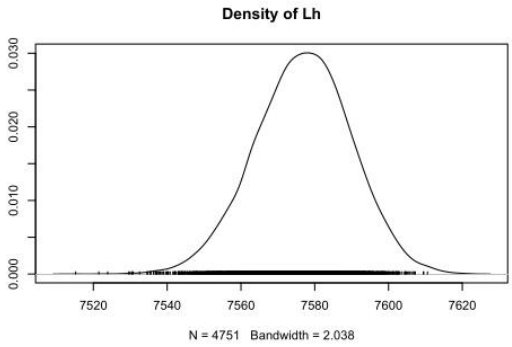

Density of Alpha
10
8
6
4
2
0
−0.1
0.0
0.1
0.2
N = 4751 Bandwidth = 0.006214

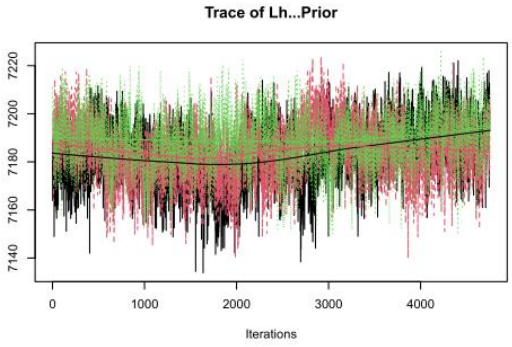

Trace of Sigma.2
100
90
80
70
60
0
1000
2000
3000
4000
Iterations

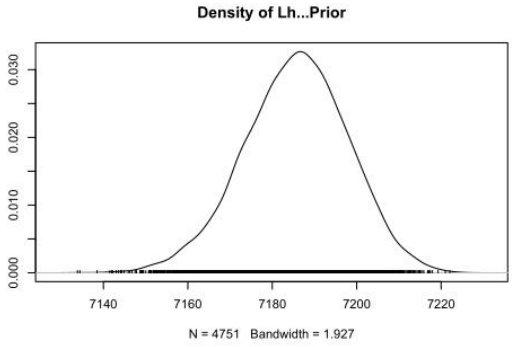

Density of Sigma.2
0.15
0.10
0.05
0.00
60
70
80
90
100
N = 4751 Bandwidth = 0.7014

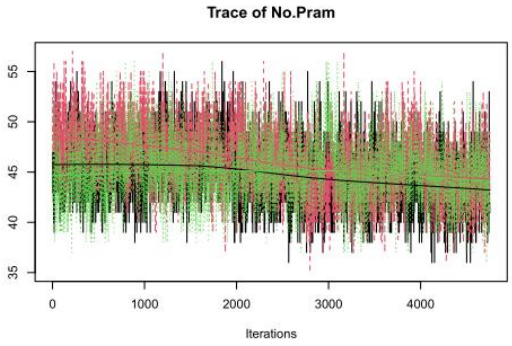
SOM Figure S14. Trace plots and comparison of several independent runs for the entire astragalus data set. See SOM Tables S6-7 for effective sample size for each run and Gelman and Rubin's convergence diagnostic.

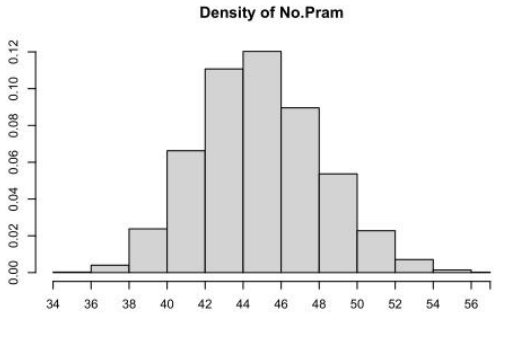

Trace of Lh
Iterations

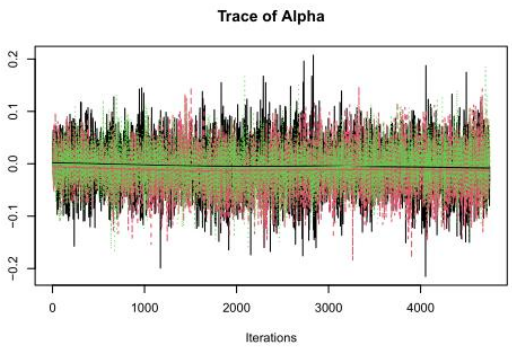

Density of Lh
N = 4751 Bandwidth = 2.038

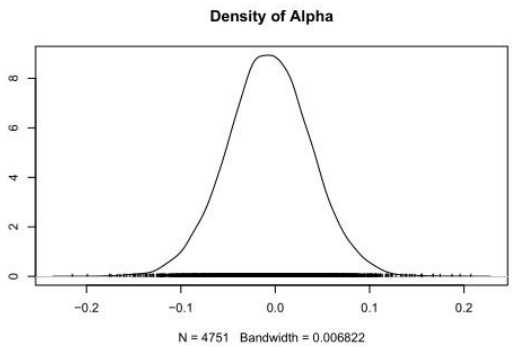

Trace of Lh...Prior
Iterations

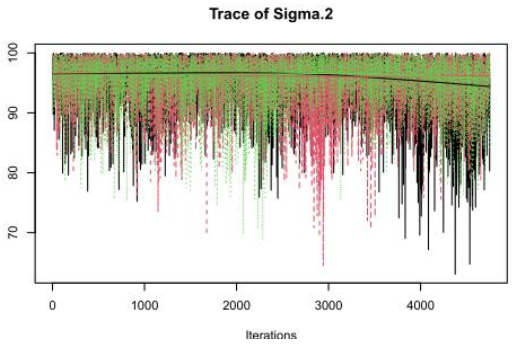

Density of Lh...Prior
N = 4751 Bandwidth = 1.927

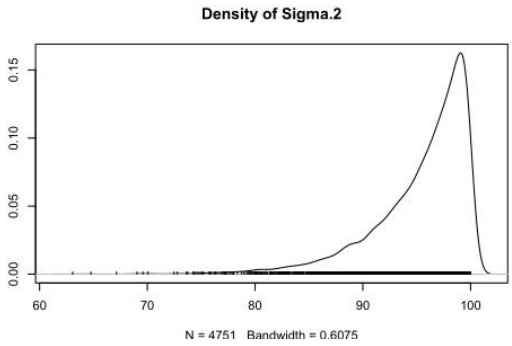

Trace of No.Pram
Iterations


Density of No.Pram


Trace of Alpha
Iterations


Density of Alpha
N = 4751 Bandwidth = 0.006822


Trace of Sigma.2
Iterations


Density of Sigma.2
N = 4751 Bandwidth = 0.6075

SOM Figure S15. Trace plots and comparison of several independent runs for the entire calcaneus data set. See SOM Tables S8-9 for effective sample size for each run and Gelman and Rubin's convergence diagnostic.

SOM Table S1

Complete list of all the specimens comprising the studied sample, including taxonomic identification, institutions where they are housed, and archival resource keys (ARKs) and digital object identifiers (DOIs) when available. (Provided separately as an Excel file.)

SOM Table S2

Extant comparative sample and their quantified locomotor behavior.

Group	Family	Species	Astragali	Calcanei	Q	C	L	S	CC	Source for locomotor behavior
Scandentia	Ptilocerciidae	*Ptilocercus lowii*	3	4	46	16	34	5	0	Based on *Tupaia minor*
Scandentia	Tupaiidae	*Dendrogale murina*	0	1	78	7	15	0	0	Based on *Tupaia tana*
Scandentia	Tupaiidae	*Tupaia belangeri*	2	6	40	37	18	5	0	Granatosky et al. (2022)
Scandentia	Tupaiidae	*Tupaia minor*	1	1	46	16	34	5	0	Sargis (2001)
Scandentia	Tupaiidae	*Tupaia palawanensis*	1	0	78	7	15	0	0	Based on *Tupaia tana*
Scandentia	Tupaiidae	*Tupaia tana*	0	1	78	7	15	0	0	Sargis (2001)
Scandentia	Tupaiidae	*Urogale everetti*	2	1	78	7	15	0	0	Based on *Tupaia tana*
Dermoptera	Cynocephalidae	*Cynocephalus volans*	5	2	0	0	0	33	67	Based on *Galeopterus variegatus*
Dermoptera	Cynocephalidae	*Galeopterus variegatus*	1	1	0	0	0	33	67	Youlatos et al. (2019)
Lemuriformes	Cheirogaleidae	*Cheirogaleus major*	3	4	42	40	6	12	0	Gebo (1987)
Lemuriformes	Cheirogaleidae	*Cheirogaleus medius*	2	7	34	28	21	17	0	Gebo (1987)
Lemuriformes	Cheirogaleidae	*Microcebus griseorufus*	12	0	29	24	38	9	0	Based on *Microcebus murinus*
Lemuriformes	Cheirogaleidae	*Microcebus murinus*	4	10	29	24	38	9	0	Gebo (1987)
Lemuriformes	Cheirogaleidae	*Microcebus rufus*	3	10	29	24	38	9	0	Based on *Microcebus murinus*
Lemuriformes	Cheirogaleidae	*Mirza zaza*	3	12	20	24	27	29	0	Gebo (1987). Based on *Mirza coquereli*
Lemuriformes	Daubentoniidae	*Daubentonia madagascariensis*	6	7	43	4	17	37	0	Curtis and Feistner (1994)

Lemuriformes	Galagidae	*Galago moholi*	12	9	21	18	60	0	0	Crompton (1983)
Lemuriformes	Galagidae	*Galago senegalensis*	8	7	5	26	64	4	0	Gebo (1987)
Lemuriformes	Galagidae	*Galagoides demidovii*	5	3	26	24	51	0	0	Gebo (1987)
Lemuriformes	Galagidae	*Otolemur crassicaudatus*	11	4	38	32	21	9	0	Crompton (1983)
Lemuriformes	Galagidae	*Otolemur garnettii*	3	4	38	32	21	9	0	Based on *Otolemur crassicaudatus*
Lemuriformes	Galagidae	*Paragalago zanzibaricus*	2	2	26	24	51	0	0	Based on *Galagoides demidovii*
Lemuriformes	Galagidae	*Sciurocheirus alleni*	1	2	3	28	68	0	0	Based on *Cephalopachus bancanus*
Lemuriformes	Indriidae	*Avahi laniger*	6	6	9	19	70	3	0	Warren and Crompton (1997). Based on *Avahi occidentalis*
Lemuriformes	Indriidae	*Indri indri*	3	2	1	9	89	0	0	Based on *Propithecus diadema*
Lemuriformes	Indriidae	*Propithecus coquereli*	2	2	3	29	68	0	0	Williams (2007)
Lemuriformes	Indriidae	*Propithecus diadema*	2	2	1	18	81	0	0	Dagosto and Yamashita (1998)
Lemuriformes	Indriidae	*Propithecus verreauxi*	6	3	1	18	81	0	0	Lawler (2006)
Lemuriformes	Lemuridae	*Eulemur fulvus*	22	20	39	17	34	11	0	Gebo (1987)
Lemuriformes	Lemuridae	*Eulemur macaco*	0	2	30	28	31	11	0	Gebo (1987)
Lemuriformes	Lemuridae	*Eulemur mongoz*	5	6	29	22	38	11	0	Gebo (1987)
Lemuriformes	Lemuridae	*Hapalemur griseus*	19	21	23	15	54	9	0	Gebo (1987)
Lemuriformes	Lemuridae	*Lemur catta*	8	7	58	11	25	7	0	Gebo (1987)
Lemuriformes	Lemuridae	*Varecia variegata*	3	4	35	31	21	13	0	Gebo (1987)
Lemuriformes	Lepilemuridae	*Lepilemur leucopus*	3	5	8	31	57	4	0	Warren and Crompton (1997). Based on *Lepilemur edwardsi*

Lemuriformes	Lepilemuridae	*Lepilemur mustelinus*	5	0	8	31	57	4	0	Warren and Crompton (1997). Based on *Lepilemur edwardsi*
Lemuriformes	Lorisidae	*Arctocebus calabarensis*	4	2	15	31	0	54	0	Based on *Loris* sp.
Lemuriformes	Lorisidae	*Loris* sp.	7	8	15	31	0	54	0	Gebo (1987)
Lemuriformes	Lorisidae	*Nycticebus coucang*	7	7	24	21	0	55	0	Gebo (1987)
Lemuriformes	Lorisidae	*Nycticebus javanicus*	1	1	24	21	0	55	0	Based on *Nycticebus coucang*
Lemuriformes	Lorisidae	*Nycticebus menangensis*	2	4	24	21	0	55	0	Based on *Nycticebus coucang*
Lemuriformes	Lorisidae	*Nycticebus pygmaeus*	4	5	24	21	0	55	0	Based on *Nycticebus coucang*
Lemuriformes	Lorisidae	*Perodicticus sp.*	16	10	29	31	0	40	0	Gebo (1987)
Tarsiiformes	Tarsiidae	*Carlito syrichta*	4	2	9	29	61	0	0	Dagosto et al. (2001)
Tarsiiformes	Tarsiidae	*Cephalopachus bancanus*	2	2	3	28	68	0	0	Crompton and Andau (1986)
Tarsiiformes	Tarsiidae	*Tarsius spectrum*	3	4	0	18	82	0	0	Mackninnon and Mackinnon (1980)
Platyrrhini	Atelidae	*Alouatta caraya*	7	2	54	24	10	12	0	Youlatos and Meldrum (2011)
Platyrrhini	Atelidae	*Alouatta palliata*	9	8	64	22	4	10	0	Youlatos and Meldrum (2011)
Platyrrhini	Atelidae	*Alouatta seniculus*	5	0	46	40	3	10	0	Youlatos and Meldrum (2011)
Platyrrhini	Atelidae	*Ateles belzebuth*	5	4	21	39	3	37	0	Youlatos and Meldrum (2011)
Platyrrhini	Atelidae	*Ateles fusciceps*	15	12	45	18	13	25	0	Based on *Ateles geoffroyi*
Platyrrhini	Atelidae	*Ateles geoffroyi*	7	10	45	18	13	25	0	Youlatos and Meldrum (2011)
Platyrrhini	Atelidae	*Ateles paniscus*	3	4	25	24	4	48	0	Youlatos and Meldrum (2011)
Platyrrhini	Atelidae	*Lagothrix* sp.	15	14	36	41	7	16	0	Youlatos and Meldrum (2011)

Platyrrhini	Callitrichidae	*Callimico goeldii*	12	11	18	4	62	0	16	Youlatos and Meldrum (2011)
Platyrrhini	Callitrichidae	*Callithrix geoffroyi*	2	2	32	13	23	0	32	Based on *Callithrix jacchus*
Platyrrhini	Callitrichidae	*Callithrix jacchus*	7	7	32	13	23	0	32	Youlatos and Meldrum (2011)
Platyrrhini	Callitrichidae	*Callithrix penicillata*	2	0	32	13	23	0	32	Based on *Callithrix jacchus*
Platyrrhini	Callitrichidae	*Cebuella pygmaea*	9	10	27	6	25	0	42	Youlatos and Meldrum (2011)
Platyrrhini	Callitrichidae	*Leontocebus fuscicollis*	10	10	43	9	35	0	12	Youlatos and Meldrum (2011)
Platyrrhini	Callitrichidae	*Leontopithecus rosalia*	9	9	46	15	24	0	15	Youlatos and Meldrum (2011)
Platyrrhini	Callitrichidae	*Mico* sp.	4	4	32	13	23	0	32	Based on *Callithrix jacchus*
Platyrrhini	Callitrichidae	*Saguinus midas*	7	4	33	29	26	0	12	Youlatos and Meldrum (2011)
Platyrrhini	Callitrichidae	*Saguinus mystax*	3	3	57	9	29	0	4	Youlatos and Meldrum (2011)
Platyrrhini	Callitrichidae	*Saguinus oedipus*	10	9	40	10	34	1	16	Youlatos (1999). Based on *Saguinus tripartitus*.
Platyrrhini	Cebidae	*Cebus capucinus*	2	2	64	17	16	4	0	Youlatos and Meldrum (2011)
Platyrrhini	Cebidae	*Cebus olivaceus*	3	2	42	21	29	9	0	Youlatos and Meldrum (2011)
Platyrrhini	Cebidae	*Saimiri boliviensis*	3	3	73	5	20	2	0	Youlatos and Meldrum (2011)
Platyrrhini	Cebidae	*Saimiri oerstedii*	2	2	88	4	8	0	0	Youlatos and Meldrum (2011)
Platyrrhini	Cebidae	*Saimiri sciureus*	7	6	50	14	34	3	0	Youlatos and Meldrum (2011)
Platyrrhini	Cebidae	*Sapajus apella*	6	3	57	15	20	8	0	Youlatos and Meldrum (2011)
Platyrrhini	Pitheciidae	*Cacajao calvus*	12	10	40	26	34	1	0	Youlatos and Meldrum (2011)

Platyrrhini	Pitheciidae	*Callicebus personatus*	1	2	67	9	24	0	0	Based on *Cheracebus torquatus*
Platyrrhini	Pitheciidae	*Cheracebus torquatus*	2	2	67	9	24	0	0	Youlatos and Meldrum (2011)
Platyrrhini	Pitheciidae	*Chiropotes* sp.	10	9	60	11	27	1	0	Walker (2005)
Platyrrhini	Pitheciidae	*Pithecia monachus*	2	5	47	23	28	2	0	Youlatos and Meldrum (2011)
Platyrrhini	Pitheciidae	*Pithecia pithecia*	8	7	26	13	61	0	0	Youlatos and Meldrum (2011)
Platyrrhini	Pitheciidae	*Plecturocebus* sp.	17	13	55	27	17	1	0	Youlatos and Meldrum (2011)
		Total	440	412						

Abbreviations: Q = quadrupedalism; C = climbing; L = leaping; S = suspension; CC = clawed clinging/climbing.

SOM Table S3

Body mass compiled for the extant and fossil sample.

Family	Species	BM[a]	Source for BM
Ptilocerciidae	*Ptilocercus lowii*	45.3	Sargis (2002)
Tupaiidae	*Dendrogale murina*	45	Sargis (2002)
Tupaiidae	*Tupaia belangeri*	205.3	Based on *Tupaia tana*
Tupaiidae	*Tupaia minor*	54.4	Sargis (2002)
Tupaiidae	*Tupaia palawanensis*	146	Based on one specimen from the Smithsonian National Museum of Natural History (USNM 477786)
Tupaiidae	*Tupaia tana*	205.3	Sargis (2002)
Tupaiidae	*Urogale everetti*	224	Sargis (2002)
Cynocephalidae	*Cynocephalus volans*	1350	Shepherd and Shepherd (2012)
Cynocephalidae	*Galeopterus variegatus*	1150	Shepherd and Shepherd (2012)
Cheirogaleidae	*Cheirogaleus major*	400	Fleagle (2013)
Cheirogaleidae	*Cheirogaleus medius*	282.5	Fleagle (2013)
Cheirogaleidae	*Microcebus griseorufus*	62.5	Fleagle (2013)
Cheirogaleidae	*Microcebus murinus*	56	Fleagle (2013)
Cheirogaleidae	*Microcebus rufus*	42.5	Fleagle (2013)
Cheirogaleidae	*Mirza zaza*	293	Fleagle (2013)
Daubentoniidae	*Daubentonia madagascariensis*	2555	Fleagle (2013)
Galagidae	*Galago moholi*	180	Fleagle (2013)
Galagidae	*Galago senegalensis*	282.5	Fleagle (2013)
Galagidae	*Galagoides demidovii*	61.5	Fleagle (2013)
Galagidae	*Otolemur crassicaudatus*	1150	Fleagle (2013)
Galagidae	*Otolemur garnettii*	764	Fleagle (2013)
Galagidae	*Paragalago zanzibaricus*	143	Fleagle (2013)
Galagidae	*Sciurocheirus alleni*	273	Fleagle (2013)
Indriidae	*Avahi laniger*	1175	Fleagle (2013)
Indriidae	*Indri indri*	6335	Fleagle (2013)
Indriidae	*Propithecus coquereli*	3990	Fleagle (2013)
Indriidae	*Propithecus diadema*	6100	Fleagle (2013)
Indriidae	*Propithecus verreauxi*	3100	Fleagle (2013)

Lemuridae	*Eulemur fulvus*	2050	Fleagle (2013)
Lemuridae	*Eulemur macaco*	2440	Fleagle (2013)
Lemuridae	*Eulemur mongoz*	1620	Fleagle (2013)
Lemuridae	*Hapalemur griseus*	709	Fleagle (2013)
Lemuridae	*Lemur catta*	2210	Fleagle (2013)
Lemuridae	*Varecia variegata*	3575	Fleagle (2013)
Lepilemuridae	*Lepilemur leucopus*	605.5	Fleagle (2013)
Lepilemuridae	*Lepilemur mustelinus*	777	Fleagle (2013)
Lorisidae	*Arctocebus calabarensis*	309	Fleagle (2013)
Lorisidae	*Loris* sp.	266.5	Fleagle (2013). Based on *Loris lydekkerianus*
Lorisidae	*Nycticebus coucang*	652.5	Fleagle (2013)
Lorisidae	*Nycticebus javanicus*	626	Nekaris (2008)
Lorisidae	*Nycticebus menangensis*	282.5	Fleagle (2013)
Lorisidae	*Nycticebus pygmaeus*	307	Fleagle (2013)
Lorisidae	*Perodicticus sp.*	1031.5	Fleagle (2013); average between *Perodicticus potto* and *Perodicticus edwardsi*
Tarsiidae	*Carlito syrichta*	125.5	Fleagle (2013)
Tarsiidae	*Cephalopachus bancanus*	122.5	Fleagle (2013)
Tarsiidae	*Tarsius spectrum*	116.5	Fleagle (2013)
Atelidae	*Alouatta caraya*	5375	Fleagle (2013)
Atelidae	*Alouatta palliata*	6250	Fleagle (2013)
Atelidae	*Alouatta seniculus*	5950	Fleagle (2013)
Atelidae	*Ateles belzebuth*	8070	Fleagle (2013)
Atelidae	*Ateles fusciceps*	9025	Fleagle (2013)
Atelidae	*Ateles geoffroyi*	7535	Fleagle (2013)
Atelidae	*Ateles paniscus*	8775	Fleagle (2013)
Atelidae	*Lagothrix* sp.	7150	Fleagle (2013)
Callitrichidae	*Callimico goeldii*	483.5	Fleagle (2013)
Callitrichidae	*Callithrix geoffroyi*	359	Fleagle (2013)
Callitrichidae	*Callithrix jacchus*	320.5	Fleagle (2013)
Callitrichidae	*Callithrix penicillata*	325.5	Fleagle (2013)
Callitrichidae	*Cebuella pygmaea*	116	Fleagle (2013)
Callitrichidae	*Leontocebus fuscicollis*	350.5	Fleagle (2013)

Callitrichidae	*Leontopithecus rosalia*	609	Fleagle (2013)
Callitrichidae	*Mico* sp.	346.5	Fleagle (2013)
Callitrichidae	*Saguinus midas*	545	Fleagle (2013)
Callitrichidae	*Saguinus mystax*	524.5	Fleagle (2013)
Callitrichidae	*Saguinus oedipus*	411	Fleagle (2013)
Cebidae	*Cebus capucinus*	3110	Fleagle (2013)
Cebidae	*Cebus olivaceus*	2905	Fleagle (2013)
Cebidae	*Saimiri boliviensis*	811	Fleagle (2013)
Cebidae	*Saimiri oerstedii*	788.5	Fleagle (2013)
Cebidae	*Saimiri sciureus*	720.5	Fleagle (2013)
Cebidae	*Sapajus apella*	3085	Fleagle (2013)
Pitheciidae	*Cacajao calvus*	3165	Fleagle (2013)
Pitheciidae	*Callicebus personatus*	1325	Fleagle (2013)
Pitheciidae	*Cheracebus torquatus*	1245	Fleagle (2013)
Pitheciidae	*Chiropotes* sp.	2885	Fleagle (2013)
Pitheciidae	*Pithecia monachus*	2360	Fleagle (2013)
Pitheciidae	*Pithecia pithecia*	1760	Fleagle (2013)
Pitheciidae	*Plecturocebus* sp.	1070	Fleagle (2013); based on *Plecturocebus moloch*
Purgatoriidae	*Purgatorius* sp.	92	Fleagle (2013)
Micromomyidae	*Tinimomys graybulliensis*	17	Fleagle (2013)
Paromomyidae	*Ignacius graybullianus*	152	Fleagle (2013)
Paromomyidae	*Phenacolemur* sp.	48	Fleagle (2013)
Plesiadapidae	*Nannodectes gidleyi*	396	Fleagle (2013)
Plesiadapidae	*Plesiadapis cookei*	3055	Fleagle (2013)
Plesiadapidae	*Plesiadapis rex*	506	Fleagle (2013)
Carpolestidae	*Carpolestes simpsoni*	100	Bloch and Gingerich (1998)
Incertae sedis	*Teilhardina belgica*	90	Fleagle (2013)
Incertae sedis	*Vastanomys major*	600	Fleagle (2013); based on *Asiadapis* (similarly sized according to Rose et al., 2009)
Omomyidae	*Absarokius* sp.	200	Fleagle (2013)
Omomyidae	*Arapahovius gazini*	290	Fleagle (2013)
Omomyidae	*Necrolemur* sp.	290	Fleagle (2013); based on *Necrolemur antiquus*
Omomyidae	*Hemiacodon gracilis*	1005	Fleagle (2013)

Omomyidae	*Omomys carteri*	310	Fleagle (2013)
Omomyidae	*Ourayia uintensis*	2170	Fleagle (2013)
Omomyidae	*Shoshonius cooperi*	155	Fleagle (2013)
Omomyidae	*Washakius insignis*	165	Fleagle (2013)
Notharctidae	*Marcgodinotius indicus*	200	Fleagle (2013)
Notharctidae	*Cantius* sp.	2500	Fleagle (2013); average between *Cantius abditus* and *Cantius frugivorous*
Notharctidae	*Copelemur tutus*	3600	Fleagle (2013)
Notharctidae	*Notharctus* sp.	4200	Fleagle (2013); based on *Notharctus tenebrosus*
Notharctidae	*Smilodectes* sp.	2100	Fleagle (2013); based on *Smilodectes gracilis*
Notharctidae	*Anchomomys frontanyensis*	110	Fleagle (2013)
Adapidae	*'Adapis* group*'*	1300	Fleagle (2013)
Adapidae	*Leptadapis magnus*	4000	Fleagle (2013)
Adapidae	*Caenopithecus lemuroides*	3500	Fleagle (2013)
Djebelemuridae	*Djebelemur martinezi*	225	Fleagle (2013)
Eosimiidae	*Eosimias* sp.	75	Fleagle (2013)
Amphipitheciidae	*Ganlea* sp.	2300	Fleagle (2013)
Parapithecidae	*Apidium* sp.	1600	Fleagle (2013)
Parapithecidae	*Simonsius grangeri*	3000	Fleagle (2013)
Parapithecidae	*Parapithecidae* indet.	1600	Based on *Apidium*
Proteopithecidae	*Proteopithecus sylviae*	800	Fleagle (2013)

SOM Table S4

Mean absolute error calculated for each extant species to assess the error generated during the estimation procedure in the covariation analysis between species-mean Procrustes shape coordinates of astragalar shape and quantified locomotor data.

	Q	C	L	S	CC
Alouatta caraya	0.165	0.063	0.188	0.148	0.098
Alouatta palliata	0.308	0.084	0.271	0.081	0.174
Alouatta seniculus	0.003	0.267	0.312	0.128	0.053
Arctocebus calabarensis	0.063	0.007	0.002	0.006	0.043
Ateles belzebuth	0.148	0.261	0.399	0.484	0.037
Ateles fusciceps	0.138	0.008	0.046	0.183	0.183
Ateles geoffroyi	0.134	0.001	0.026	0.190	0.135
Ateles paniscus	0.183	0.045	0.086	0.438	0.122
Avahi laniger	0.100	0.087	0.471	0.248	0.152
Cacajao calvus	0.021	0.226	0.064	0.019	0.281
Callicebus personatus	0.251	0.081	0.008	0.158	0.118
Callimico goeldii	0.366	0.175	0.437	0.160	0.277
Callithrix geoffroyi	0.034	0.006	0.042	0.171	0.320
Callithrix jacchus	0.124	0.016	0.071	0.180	0.367
Callithrix penicillata	0.188	0.060	0.061	0.175	0.378
Carlito syrichta	0.042	0.058	0.075	0.046	0.042
Cebuella pygmaea	0.135	0.141	0.097	0.185	0.441
Cebus capucinus	0.219	0.130	0.113	0.043	0.300
Cebus olivaceus	0.059	0.074	0.102	0.159	0.152
Cephalopachus bancanus	0.281	0.090	0.117	0.023	0.017
Cheirogaleus major	0.127	0.267	0.306	0.007	0.119
Cheirogaleus medius	0.099	0.091	0.105	0.083	0.148

Cheracebus torquatus	0.271	0.088	0.069	0.207	0.148
Chiropotes sp.	0.278	0.057	0.059	0.061	0.208
Cynocephalus volans	0.374	0.381	0.514	0.227	0.744
Daubentonia madagascariensis	0.249	0.276	0.224	0.356	0.021
Eulemur fulvus	0.281	0.055	0.231	0.132	0.092
Eulemur mongoz	0.174	0.033	0.159	0.130	0.011
Galago moholi	0.004	0.198	0.136	0.116	0.033
Galago senegalensis	0.267	0.047	0.049	0.164	0.057
Galagoides demidovii	0.119	0.072	0.042	0.166	0.046
Galeopterus variegatus	0.305	0.234	0.665	0.452	0.440
Hapalemur griseus	0.068	0.078	0.045	0.046	0.086
Indri indri	0.272	0.019	0.460	0.220	0.078
Lagothrix sp.	0.081	0.331	0.185	0.139	0.199
Lemur catta	0.525	0.143	0.261	0.022	0.088
Leontocebus fuscicollis	0.039	0.074	0.261	0.183	0.088
Leontopithecus rosalia	0.018	0.008	0.013	0.140	0.189
Lepilemur leucopus	0.134	0.102	0.009	0.010	0.058
Lepilemur mustelinus	0.102	0.115	0.010	0.020	0.043
Loris sp.	0.189	0.060	0.053	0.004	0.247
Microcebus griseorufus	0.097	0.019	0.177	0.036	0.175
Microcebus murinus	0.057	0.007	0.059	0.066	0.096
Microcebus rufus	0.071	0.025	0.111	0.142	0.103
Mirza zaza	0.244	0.034	0.156	0.172	0.055
Nycticebus coucang	0.010	0.034	0.033	0.015	0.057
Nycticebus javanicus	0.045	0.053	0.031	0.058	0.014
Nycticebus menangensis	0.003	0.002	0.052	0.005	0.123
Nycticebus pygmaeus	0.013	0.065	0.021	0.017	0.083

Otolemur crassicaudatus	0.213	0.023	0.372	0.231	0.001
Otolemur garnettii	0.318	0.042	0.371	0.217	0.043
Paragalago zanzibaricus	0.104	0.074	0.116	0.167	0.092
Perodicticus sp.	0.102	0.089	0.045	0.095	0.096
Pithecia monachus	0.028	0.100	0.099	0.053	0.119
Pithecia pithecia	0.180	0.030	0.448	0.187	0.148
Plecturocebus sp.	0.177	0.197	0.178	0.022	0.128
Propithecus coquereli	0.217	0.147	0.253	0.318	0.017
Propithecus diadema	0.309	0.092	0.588	0.313	0.011
Propithecus verreauxi	0.271	0.008	0.358	0.266	0.022
Ptilocercus lowii	0.108	0.043	0.139	0.067	0.090
Saguinus midas	0.085	0.189	0.078	0.163	0.111
Saguinus mystax	0.119	0.059	0.155	0.155	0.126
Saguinus oedipus	0.037	0.090	0.163	0.059	0.159
Saimiri boliviensis	0.266	0.158	0.066	0.025	0.216
Saimiri oerstedii	0.564	0.228	0.325	0.119	0.096
Saimiri sciureus	0.052	0.001	0.081	0.035	0.141
Sapajus apella	0.211	0.039	0.132	0.190	0.202
Sciurocheirus alleni	0.349	0.032	0.279	0.189	0.023
Tarsius spectrum	0.391	0.026	0.287	0.017	0.105
Tupaia belangeri	0.454	0.269	0.185	0.234	0.080
Tupaia minor	0.334	0.125	0.034	0.165	0.222
Tupaia palawanensis	0.082	0.244	0.153	0.086	0.091
Urogale everetti	0.107	0.192	0.127	0.118	0.026
Varecia variegata	0.190	0.129	0.369	0.129	0.159

Abbreviations: Q = quadrupedalism; C = climbing; L = leaping; S = suspension; CC = clawed clinging/climbing.

SOM Table S5

Mean absolute error calculated for each extant species to assess the error generated during the estimation procedure in the covariation analysis between species-mean Procrustes shape coordinates of calcaneal shape and quantified locomotor data.

	Q	C	L	S	CC
Alouatta caraya	0.008	0.072	0.065	0.120	0.061
Alouatta palliata	0.080	0.002	0.195	0.064	0.047
Arctocebus calabarensis	0.073	0.028	0.042	0.113	0.086
Ateles belzebuth	0.116	0.266	0.372	0.392	0.161
Ateles fusciceps	0.053	0.034	0.141	0.090	0.167
Ateles geoffroyi	0.056	0.040	0.027	0.178	0.175
Ateles paniscus	0.158	0.111	0.198	0.521	0.250
Avahi laniger	0.254	0.061	0.295	0.193	0.143
Cacajao calvus	0.014	0.133	0.157	0.086	0.210
Callicebus personatus	0.198	0.098	0.043	0.130	0.109
Callimico goeldii	0.397	0.169	0.425	0.048	0.179
Callithrix geoffroyi	0.164	0.023	0.025	0.086	0.374
Callithrix jacchus	0.153	0.017	0.050	0.147	0.372
Carlito syrichta	0.151	0.033	0.036	0.021	0.026
Cebuella pygmaea	0.136	0.162	0.016	0.174	0.506
Cebus capucinus	0.230	0.020	0.284	0.098	0.089
Cebus olivaceus	0.018	0.081	0.027	0.187	0.133
Cephalopachus bancanus	0.247	0.020	0.115	0.036	0.006
Cheirogaleus major	0.328	0.200	0.417	0.034	0.006
Cheirogaleus medius	0.183	0.089	0.163	0.058	0.023
Cheracebus torquatus	0.209	0.090	0.067	0.094	0.165
Chiropotes sp.	0.114	0.070	0.019	0.001	0.156

Cynocephalus volans	0.365	0.265	0.279	0.234	0.431
Daubentonia madagascariensis	0.196	0.278	0.112	0.230	0.048
Dendrogale murina	0.346	0.024	0.222	0.057	0.027
Eulemur fulvus	0.096	0.086	0.053	0.044	0.115
Eulemur macaco	0.080	0.052	0.280	0.196	0.178
Eulemur mongoz	0.069	0.001	0.060	0.050	0.053
Galago moholi	0.043	0.121	0.081	0.087	0.033
Galago senegalensis	0.219	0.011	0.113	0.128	0.042
Galagoides demidovii	0.259	0.011	0.091	0.226	0.059
Galeopterus variegatus	0.240	0.136	0.285	0.281	0.294
Hapalemur griseus	0.027	0.111	0.096	0.011	0.119
Indri indri	0.375	0.127	0.516	0.294	0.017
Lagothrix sp.	0.073	0.241	0.115	0.099	0.143
Lemur catta	0.225	0.181	0.266	0.062	0.160
Leontocebus fuscicollis	0.084	0.080	0.159	0.173	0.059
Leontopithecus rosalia	0.043	0.008	0.091	0.206	0.152
Lepilemur leucopus	0.289	0.158	0.089	0.152	0.027
Loris sp.	0.164	0.193	0.012	0.015	0.272
Mico sp.	0.120	0.022	0.032	0.151	0.349
Microcebus griseorufus	0.310	0.034	0.122	0.050	0.112
Microcebus murinus	0.263	0.038	0.089	0.030	0.073
Microcebus rufus	0.390	0.076	0.074	0.011	0.216
Mirza zaza	0.100	0.068	0.027	0.240	0.143
Nycticebus coucang	0.192	0.074	0.039	0.123	0.101
Nycticebus javanicus	0.086	0.059	0.143	0.108	0.119
Nycticebus menangensis	0.077	0.012	0.195	0.234	0.023
Nycticebus pygmaeus	0.083	0.119	0.190	0.130	0.085

Otolemur crassicaudatus	0.184	0.068	0.270	0.138	0.077
Otolemur garnettii	0.202	0.077	0.340	0.221	0.040
Paragalago zanzibaricus	0.066	0.046	0.124	0.029	0.080
Perodicticus sp.	0.092	0.025	0.026	0.204	0.039
Pithecia monachus	0.056	0.083	0.012	0.025	0.092
Pithecia pithecia	0.286	0.061	0.410	0.155	0.081
Plecturocebus sp.	0.126	0.168	0.065	0.055	0.168
Propithecus coquereli	0.306	0.189	0.376	0.328	0.134
Propithecus diadema	0.411	0.138	0.616	0.349	0.010
Propithecus verreauxi	0.450	0.013	0.497	0.321	0.003
Ptilocercus lowii	0.109	0.076	0.249	0.063	0.074
Saguinus midas	0.083	0.210	0.038	0.121	0.063
Saguinus mystax	0.158	0.085	0.039	0.113	0.058
Saguinus oedipus	0.073	0.056	0.153	0.022	0.155
Saimiri boliviensis	0.396	0.165	0.103	0.029	0.190
Saimiri oerstedii	0.584	0.236	0.180	0.251	0.181
Saimiri sciureus	0.086	0.014	0.051	0.079	0.222
Sapajus apella	0.170	0.047	0.269	0.282	0.175
Sciurocheirus alleni	0.238	0.052	0.183	0.114	0.032
Tarsius spectrum	0.498	0.122	0.272	0.001	0.013
Tupaia belangeri	0.234	0.397	0.103	0.175	0.013
Tupaia minor	0.072	0.092	0.275	0.011	0.057
Tupaia tana	0.298	0.056	0.092	0.126	0.040
Urogale everetti	0.258	0.042	0.080	0.072	0.097
Varecia variegata	0.015	0.132	0.163	0.120	0.057

Abbreviations: Q = quadrupedalism; C = climbing; L = leaping; S = suspension; CC = clawed clinging/climbing.

SOM Table S6

Effective sample size (EES) for the two independent chains ran for the Bayesian analysis performed to account for astragalar shape evolution.

	Likelihood	Likelihood + prior	Number of parameters	Alpha	Sigma2
Run 1	93.886	67.708	839.036	82.895	1628.822
Run 2	173.593	86.457	199.753	101.313	401.165

SOM Table S7

Gelman and Rubin's convergence diagnostic test on two independent chains ran for the Bayesian analysis performed to account for astragalar shape evolution. The multivariate potential scale reduction factor is equal to 1.23.

	Point estimations	Upper confidence limits
Likelihood	1.03	1.15
Likelihood + Prior	1.01	1.05
Number of parameters	1	1
Alpha	1.06	1.26
Sigma2	1.02	1.07

SOM Table S8

Effective sample size (EES) for three independent chains ran for the Bayesian analysis performed to account for astragalar shape evolution.

	Likelihood	Likelihood + prior	Number of parameters	Alpha	Sigma2
Run 1	152.2227	76.6688	210.418	4459.34	332.4371
Run 2	132.5841	77.58816	122.02439	2539.044	485.316
Run 3	665.213	274.0262	322.7462	2945.205	646.3398

SOM Table S9

Gelman and Rubin's convergence diagnostic test on three independent chains ran for the Bayesian analysis performed to account for calcaneal shape evolution. The multivariate potential scale reduction factor is equal to 1.05.

	Point estimations	Upper confidence limits
Likelihood	1.03	1.09
Likelihood + Prior	1.01	1.04
Number of Parameters	1.02	1.08
Alpha	1.01	1.02
Sigma2	1.02	1.04

SOM References

Anemone, R.L., Covert, H.H., 2000. New skeletal remains of *Omomys* (Primates, Omomyidae): functional morphology of the hindlimb and locomotor behavior of a Middle Eocene primate. J. Hum. Evol. 38, 607–633.

Arnold, C., Matthews, L.J., Nunn, C.L., 2010. The 10kTrees website: A new online resource for primate phylogeny. Evol. Anthropol. 19, 114–118.

Beard, K.C., Dagosto, M., Gebo, D.L., Godinot, M., 1988. Interrelationships among primate higher taxa. Nature 331, 712–714.

Beard, K.C., Marivaux, L., Chaimanee, Y., Jaeger, J.J., Marandat, B., Tafforeau, P., Soe, A.N., Tun, S.T., Kyaw, A.A., 2009. A new primate from the Eocene Pondaung Formation of Myanmar and the monophyly of Burmese amphipithecids. Proc. R. Soc. B 276, 3285–3294.

Bloch, J.I., Gingerich, P.D., 1998. *Carpolestes simpsoni*, new species (Mammalia, Proprimates) from the late Paleocene of the Clark's Fork Basin, Wyoming. Contrib. Mus. Paleontol. Univ. Mich 30, 131–162.

Bloch, J.I., Silcox, M.T., Boyer, D.M, Sargis, E.J., 2007. New Paleocene skeletons and the relationship of plesiadapiforms to crown-clade primates. Proc. Natl. Acad. Sci. USA 104, 1159–1164.

Boyer, D.M., Toussaint, S., Godinot, M., 2017. Postcrania of the most primitive euprimate and implications for primate origins. J. Hum. Evol. 111, 202–211.

Cant, J.G., 1987. Positional behavior of female Bornean orangutans (*Pongo pygmaeus*). Am. J. Primatol. 12, 71–90.

Chaimanee, Y., Chavasseau, O., Beard, K.C., Kyaw, A.A., Soe, A.N., Sein, C., Lazzari, V., Marivaux, L., Marandat, B., Swe, M. and Rugbumrung, M., 2012. Late Middle Eocene primate from Myanmar and the initial anthropoid colonization of Africa. Proc. Natl. Acad. Sci. USA 109, 10293–10297.

Chaimanee, Y., Chavasseau, O., Lazzari, V., Soe, A.N., Sein, C., Jaeger, J.-J., 2024. Early anthropoid primates: New data and new questions. Evol. Anthropol. 33, e22022.

Ciochcon, R.L., Gunnell, G.F., 2002. Eocene primates from Myanmar: Historical perspectives on the origin of Anthropoidea. Evol. Anthropol. 11, 156–168.

Crompton, R.H., 1983. Age differences in locomotion of two subtropical Galaginae. Primates 24, 241–259.

Crompton, R.H., Andau, P.M., 1986. Locomotion and habitat utilization in free-ranging *Tarsius bancanus*: a preliminary report. Primates 27, 337–355.

Curtis, D.J., Feistner, A.T., 1994. Positional behaviour in captive aye-ayes (*Daubentonia madagascariensis*). Folia Primatol. 62, 155–159.

Dagosto, M., Gebo, D.L., 1994. Postcranial anatomy and the origin of the Anthropoidea. In: Fleagle, J.G., Kay, R.F. (Eds.), Anthropoid Origins. Plenum Press, New York, pp. 567–593.

Dagosto, M., Yamashita, N., 1998. Effect of habitat structure on positional behavior and support use in three species of lemur. Primates 39, 459–472.

Dagosto, M., Gebo, D.L., Dolino, C., 2001. Positional behavior and social organization of the Philippine tarsier (*Tarsius syrichta*). Primates 42, 233–243.

Doran, D.M., Itani, J., Foundation, W.-G., 1996. Comparative positional behavior of the African apes. In: McGrew, W.C., Marchant, L.F., Nishida, T., (Eds.), Great Ape Societies. Cambridge University Press, Cambridge, pp. 213–224.

Dunham, N.T., 2015. Ontogeny of positional behavior and support use among *Colobus angolensis palliatus* of the Diani Forest, Kenya. Primates 56, 183–192.

Fleagle, J.G., Meldrum, D.J., 1988. Locomotor behavior and skeletal morphology of two sympatric pitheciine monkeys, *Pithecia pithecia* and *Chiropotes satanas*. Am. J. Primatol. 16, 227–249.

Ford, S.M., 1990. Locomotor adaptations of fossil platyrrhines. J. Hum. Evol. 19, 141–173.

Franzen, J.L., Gingerich, P.D., Habersetzer, J., Hurum, J.H., Von Koenigswald, W., Smith, B.H., 2009. Complete primate skeleton from the middle Eocene of Messel in Germany: morphology and paleobiology. PLoS One 4, e5723.

Gebo, D.L., 1987. Locomotor diversity in prosimian primates. Am. J. Primatol. 13, 271–281.

Gebo, D.L., Dagosto, M., 2004. Anthropoid origins: Postcranial evidence from the Eocene of Asia. In: Ross, C.F., Kay, R.F. (Eds.), Anthropoid Origins: New visions. Kluwer Academic, New York, pp. 369–380.

Gebo, D.L., Dagosto, M., Beard, K.C., Qi, T., Wang, J., 2000. The oldest known anthropoid postcranial fossils and the early evolution of higher primates. Nature 404, 276–278.

Gebo, D.L., Dagosto, M., Beard, K.C., Qi, T., 2001. Middle Eocene primate tarsals from China: Implications for haplorhine evolution. Am. J. Phys. Anthropol. 116, 83–107.

Gingerich, P.D., Franzen, J.L., Habersetzer, J., Hurum, J.H. and Smith, B.H., 2010. *Darwinius masillae* is a haplorhine — Reply to Williams et al. (2010). J. Hum. Evol. 59, 574–579.

Godinot, M., 1991. Toward the locomotion of two contemporaneous *Adapis* species. Z. Morphol. Anthropol. 78, 387–405

Granatosky, M.C., Toussaint, S.L., Young, M.W., Panyutina, A., Youlatos, D., 2022. The northern treeshrew (Scandentia: Tupaiidae: *Tupaia belangeri*) in the context of primate locomotor evolution: A comprehensive analysis of gait, positional, and grasping behavior. J. Exp. Zool. 337, 645–665.

Gunnell, G.F., 2002. Notharctine primates (Adapiformes) from the early to middle Eocene (Wasatchian–Bridgerian) of Wyoming: Transitional species and the origins of *Notharctus* and *Smilodectes*. J. Hum. Evol. 43, 353–380.

Gunnell, G.F., Ciochcon, R.L., 2008. Revisiting primate postcrania from the Pondaung Formation of Myanmar: The purported anthropoid astragalus. In: Gleagle, J.G., Gilbert, C.C. (Eds.), Elwyn Simons: A Search for Origins. Springer, New York, pp. 211–228.

Hunt, K.D., Cant, J.G., Gebo, D.L., Rose, M.D., Walker, S.E., Youlatos, D., 1996. Standardized descriptions of primate locomotor and postural modes. Primates 37, 363–387.

Kay, R.F., Fleagle, J.G., Mitchell, T.R.T., Colbert, M., Bown, T., Powers, D.W., 2008. The anatomy of *Dolichocebus gaimanensis*, a stem platyrrhine monkey from Argentina. J. Hum. Evol. 54, 323–382.

Lawler, R.R., 2006. Sifaka positional behavior: ontogenetic and quantitative genetic approaches. Am. J. Phys. Anthropol. 131, 261–271.

MacKinnon, J., MacKinnon, K., 1980. The behavior of wild spectral tarsiers. Int. J. Primatol. 1, 361–379.

Marigó, J., Minwer-Barakat, R., Moyà-Solà, S., 2011. New *Anchomomys* (Adapoidea, Primates) from the Robiacian (Middle Eocene) of northeastern Spain. Taxonomic and evolutionary implications. J. Hum. Evol. 60, 665–672.

Marigó, J., Roig, I., Seiffert, E.R., Moyà-Solà, S., Boyer, D.M., 2016. Astragalar and calcaneal morphology of the middle Eocene primate *Anchomomys frontanyensis* (Anchomomyini): Implications for early primate evolution. J. Hum. Evol. 91, 122–143.

Marigó, J., Verrière, N., Godinot, M., 2019. Systematic and locomotor diversification of the *Adapis* group (Primates, Adapiformes) in the late Eocene of the Quercy (Southwest France), revealed by humeral remains. J. Hum. Evol. 126, 71–90.

Marivaux, L., Ramdarshan, A., Essid, E.M., Marzougui, W., Ammar, H.K., Lebrun, R., Marandat, B., Merzeraud, G., Tabuce, R., Vianey-Liaud, M., 2013. *Djebelemur*, a tiny pre-tooth-combed primate from the Eocene of Tunisia: A glimpse into the origin of crown strepsirhines. PLoS One 8, e80778.

Ni, X., Gebo, D.L., Dagosto, M., Meng, J., Tafforeau, P., Flynn, J.J., Beard, K.C., 2013. The oldest known primate skeleton and early haplorhine evolution. Nature 498, 60–64.

Ni, X., Li, Q., Li, L., Beard, K.C., 2016. Oligocene primates from China reveal divergence between African and Asian primate evolution. Science 352, 673–677.

Off, E.C., Gebo, D.L., 2005. *Galago* locomotion in Kibale National Park, Uganda. Am. J. Primatol. 66, 189–195.

Rawson, B.M., 2009. The socio-ecology of the black-shanked douc (*Pygathrix nigripes*) in Mondulkiri Province, Cambodia. Ph.D. Dissertation, The Australian National University.

Revell, L.J., 2012. phytools: an R package for phylogenetic comparative biology (and other things). Methods Ecol. Evol. 3, 217–223.

Rogers, L.D., Nekaris, K.A.I., 2011. Behaviour and habitat use of the Bengal slow loris *Nycticebus bengalensis* in the dry dipterocarp forests of Phnom Samkos Wildlife Sanctuary, Cambodia. Cambodian J. Nat. Hist. 2011, 104–133.

Rose, K.D., Walker, A., 1985. The skeleton of early Eocene *Cantius*, oldest lemuriform primate. Am. J. Phys. Anthropol. 66, 73–89.

Rose, K.D., MacPhee, R.D., Alexander, J.P., 1999. Skull of early Eocene *Cantius abditus* (Primates: Adapiformes) and its phylogenetic implications, with a reevaluation of "*Hesperolemur*" *actius*. Am. J. Phys. Antropol. 109, 523–539.

Rose, K.D., Rana, R.S., Sahni, A., Kumar, K., Missiaen, P., Singh, L., Smith, T., 2009. Early Eocene primates from Gujarat, India. J. Hum. Evol. 56, 366–404.

Rosenberger, A.L., 1985. In favor of the *Necrolemur*-tarsier hypothesis. Folia Primatol. 45, 179–194.

Rosenberger, A.L., 2011. The face of *Strigorhysis*: implications of another tarsier-like, large-eyed Eocene North American tarsiiform primate. Anat. Rec. 294, 797-812.

Rosenberger, A.L., Preuschoft, H., 2012. Evolutionary morphology, cranial biomechanics and the origins of tarsiers and anthropoids. Palaeobio. Palaeoenv. 92, 507–525.

Sargis, E.J., 2001. The grasping behaviour, locomotion and substrate use of the tree shrews *Tupaia minor* and *T. tana* (Mammalia, Scandentia). J. Zool. 253, 485–490.

Seiffert, E.R., Perry, J.M., Simons, E.L., Boyer, D.M., 2009. Convergent evolution of anthropoid-like adaptations in Eocene adapiform primates. Nature 461, 1118–1121.

Seiffert, E.R., Boyer, D.M., Fleagle, J.G., Gunnell, G.F., Heesy, C.P., Perry, J.M., Sallam, H.M., 2018. New adapiform primate fossils from the late Eocene of Egypt. Hist. Biol. 30, 204–226.

Silcox, M.T., Boyer, D.M., Bloch, J.I., Sargis, E.J., 2007. Revisiting the adaptive origins of primates (again). J. Hum. Evol. 53, 321–324.

Tornow, M.A., 2008. Systematic analysis of the Eocene primate family Omomyidae using gnathic and postcranial data. Bull. Peabody Mus. Nat. Hist. 49, 43–129.

Walker, S.E., 2005. Leaping behavior of *Pithecia pithecia* and *Chiropotes satanas* in eastern Venezuela. Am. J. Primatol. 66, 369–387.

Williams, A.E., 2007. Ontogeny of locomotion in *Propithecus verreauxi*. Honors thesis, James Madison University.

Williams, B.A., Kay, R.F., Kirk, E.C., Ross, C.F., 2010. *Darwinius masillae* is a strepsirrhine—a reply to Franzen et al.(2009). J. Hum. Evol. 59, 567–573.

Youlatos, D., 1999. Positional behavior of *Cebuella pygmaea* in Yasuni National Park, Ecuador. Primates 40, 543–550.

Youlatos, D., Meldrum, J., 2011. Locomotor diversification in New World monkeys: Running, climbing, or clawing along evolutionary branches. Anat Rec. 294, 1991–2012.

Youlatos, D., Widayati, K.A., Tsuji, Y., 2019. Foot postures and grasping of free-ranging Sunda colugos (*Galeopterus variegatus*) in West Java, Indonesia. Mamm. Biol. 95, 164–172.

Chapter 5:

A dryopithecine talus from Abocador de Can Mata (Vallès-Penedès Basin, NE Iberian Peninsula): Morphometric affinities and evolutionary implications for hominoid locomotion.

Reproduced from:

Monclús-Gonzalo, O., Pal, S., Püschel, T.A., Urciuoli, A., Vinuesa, V., Robles, J.M., Almécija, S., Alba, D.M., 2025. A dryopithecine talus from Abocador de Can Mata (Vallès-Penedès Basin, NE Iberian Peninsula): Morphometric affinities and evolutionary implications for hominoid locomotion. Am. J. Biol. Anthropol. 186, e70043. https://doi.org/10.1002/ajpa.70043

Check for updates

American Journal of Biological Anthropology

WILEY

AMERICAN JOURNAL OF BIOLOGICAL ANTHROPOLOGY

RESEARCH ARTICLE OPEN ACCESS

A Dryopithecine Talus From Abocador de Can Mata (Vallès-Penedès Basin, NE Iberian Peninsula): Morphometric Affinities and Evolutionary Implications for Hominoid Locomotion

Oriol Monclús-Gonzalo[1] | Shubham Pal[1] | Thomas A. Püschel[2] | Alessandro Urciuoli[1,3,4] | Víctor Vinuesa[1] | Josep M. Robles[1] | Sergio Almécija[1,5,6] | David M. Alba[1]

[1]Institut Català de Paleontologia Miquel Crusafont (ICP-CERCA), Universitat Autònoma de Barcelona, Barcelona, Spain | [2]Institute of Human Sciences, School of Anthropology, University of Oxford, Oxford, UK | [3]Department of Paleontology, University of Zurich, Zurich, Switzerland | [4]Departamento de Ciencias de la Vida, Universidad de Alcalá, Cátedra de Otoacústica Evolutiva y Paleoantropología (HM Hospitales-UAH), Madrid, Spain | [5]Division of Anthropology, American Museum of Natural History, New York, New York, USA | [6]New York Consortium in Evolutionary Primatology, New York, New York, USA

Correspondence: Oriol Monclús-Gonzalo (oriol.monclus@icp.cat) | David M. Alba (david.alba@icp.cat)

Received: 11 December 2024 | **Revised:** 3 March 2025 | **Accepted:** 24 March 2025

Funding: This paper is part of R+D+I projects PID2020-116908GBI00 and PID2020-117289GBI00, funded by the Agencia Estatal de Investigación of the Spanish Ministerio de Ciencia e Innovación (MCIN/AEI/10.13039/501100011033/). Our research has also been supported by the CERCA Programme/Generalitat de Catalunya, the Agència de Gestió d'Ajuts Universitaris i de Recerca of the Generalitat de Catalunya (research groups 2021 SGR 00620 to D.M.A. and J.M.R., 2021 SGR 01188 to O.M.G., and 2022 SGR 01184 to V.V.), the Departament de Cultura of the Generalitat de Catalunya (CLT0009_22_000018), the Leverhulme Trust Early Career Fellowship (ECF-2018-264) to T.A.P., a Margarita Salas postdoctoral fellowship funded by the European Union-NextGenerationEU to A.U., and a Joan Oró FI AGAUR fellowship (2021 FI_B 00524, 2022 FI_B1 00131, and 2023 FI-3 00131 to O.M.G.) funded by the Secretaria d'Universitats i Recerca of the Generalitat de Catalunya and the European Social Fund.

Keywords: functional morphology | geometric morphometrics | locomotion | Miocene apes | talus

ABSTRACT

Objectives: The functional interpretation of postcranial remains of Middle Miocene great apes from Europe (dryopithecines) suggests a combination of quadrupedalism and orthograde behaviors without modern analogs. We provide further insights based on an isolated dryopithecine talus (IPS85037) from the Middle Miocene (11.7 Ma) Abocador de Can Mata locality ACM/C8-B* (Vallès-Penedès Basin, NE Iberian Peninsula), which represents the most complete one known to date.

Material and Methods: We compare the specimen with an extant anthropoid sample ($n = 68$) and the stem hominoid *Ekembo heseloni* (KMN RU 2036, ~18 Ma, Kenya) using 3D geometric morphometrics. For the two fossil tali, we assess their phenetic affinities using a between-group principal components analysis (bgPCA), estimate body mass based on centroid size, and make locomotor inferences using a partial least-squares regression (PLSR) between talar shape and locomotor repertoire.

Results: Its large inferred body mass (~38 kg) and the possession of several modern hominoid-like features (albeit combined with more plesiomorphic traits) support the attribution of IPS85037 to a male dryopithecine. The bgPCA indicates that IPS85037 falls close to the extant hominoid variation and is less cercopithecoid-like than that of *Ekembo*, whose inferred locomotor repertoire is vastly dominated by quadrupedalism (81%). In contrast, the locomotor repertoire inferred from IPS85037 combines important quadrupedal (32%) and vertical climbing/clambering (50%) components with only moderate suspension (10%).

This is an open access article under the terms of the Creative Commons Attribution-NonCommercial-NoDerivs License, which permits use and distribution in any medium, provided the original work is properly cited, the use is non-commercial and no modifications or adaptations are made.

© 2025 The Author(s). *American Journal of Biological Anthropology* published by Wiley Periodicals LLC.

Discussion: Our results align with previous inferences derived from other postcranial elements of Middle Miocene dryopithecines and, given their classification as crown hominoids, support the hypothesis that certain suspensory adaptations shared by extant hylobatids and hominids likely evolved independently.

1 | Introduction

1.1 | The Talus of Miocene Apes

The talus plays an important role in primate posture and locomotion, being involved in body weight transmission and stability/mobility at the ankle joint—including foot flexion-extension and abduction-adduction at the talocrural joint, pronation-supination at the subtalar joint, and flexion-extension at the midtarsal joint (Lewis 1980a, 1980b). Accordingly, talar morphology is tightly linked to foot function and substrate preference (Turley and Frost 2013; Parr et al. 2014), and these differences can even be characterized among closely related taxa (Dunn et al. 2014; Knigge et al. 2015; Friesen et al. 2024). Hence, the talus is of great value for making locomotor inferences in extinct primates (e.g., Day and Wood 1968, 1969; Lisowski et al. 1974, 1976; Alba et al. 2014; Marigó et al. 2016; Püschel et al. 2017; Püschel et al. 2018; Püschel et al. 2020).

Among hominoids (the ape and human clade), much emphasis has been devoted to the interpretation of talar morphology in fossil hominins in relation to bipedal adaptations (e.g., Day and Wood 1968; Latimer et al. 1987; Parr et al. 2014; Sorrentino et al. 2020). For Miocene apes, talar morphology has been mostly related to different types of arboreal behaviors, including the distinction between plesiomorphic (i.e., "monkey-like") quadrupedalism and more apomorphic (i.e., modern "ape-like") behaviors such as vertical climbing, suspension, and knuckle-walking (Day and Wood 1969; Lisowski et al. 1974, 1976; Langdon 1986). However, further insight into the evolution of talar morphology in extant hominoid lineages is hampered by the scarcity of fossil tali attributable to crown members of this group. On the other hand, there is a relatively good record of fossil tali of both putative stem catarrhines (Le Gros Clark and Thomas 1951; Harrison 1982; Morbeck 1983; Begun 1987; Leakey and Leakey 1987; Rose et al. 1992; Kordos and Begun 2001) and hominoids (Le Gros Clark and Leakey 1951; Le Gros Clark 1952; Harrison 1982; Walker and Pickford 1983; Hill and Ward 1988; Leakey et al. 1988; Ward et al. 1993; McCrossin 1994; Rose et al. 1996; Ward 1998; Ishida et al. 2004; Dunsworth 2006; Nakatsukasa et al. 2012; Russo et al. 2024) from the Early to Middle Miocene of Africa. In the Miocene of Eurasia, ape tali are more scarce, being restricted to the great apes (hominids) from the Late Miocene—one talus attributed to *Sivapithecus* (Pilbeam et al. 1977; Pilbeam et al. 1980; Morbeck 1983; Madar 1996) and an undescribed talus attributed to *Rudapithecus* (Kordos and Begun 2001; Begun 2002, 2009)—as well as *Oreopithecus* (Straus 1963; Szalay and Langdon 1986)—of controversial systematic affinities but currently interpreted as a likely stem hominoid (Pugh 2022; Urciuoli and Alba 2023; Alba, Urciuoli, et al. 2024).

To inform the evolution of ape locomotion, here we describe an unpublished talus (IPS85037) from the latest Middle Miocene of Abocador de Can Mata local stratigraphic sequence, previously attributed (without being described or figured) by Alba et al. (2017: table 2; 2022: SOM Table S6) to Dryopithecinae indet. The subfamily Dryopithecinae sensu Alba (2012) is an extinct group of Middle to Late Miocene great apes from Europe that is sometimes distinguished at the tribe rank (i.e., Dryopithecini) by some other authors (e.g., Begun 2009). Although they are generally considered extinct great apes (i.e., Hominidae; Alba 2012; Begun 2015; Urciuoli et al. 2021; Urciuoli and Alba 2023), as supported by cladistic analyses (Alba et al. 2015; Pugh 2022), it is still uncertain whether they constitute a clade or a paraphyletic assemblage (Alba 2012; Almécija et al. 2021). A consensus has yet to be reached as to whether dryopithecines are stem hominids (Andrews 1992; Casanovas-Vilar et al. 2011; Alba 2012; Alba et al. 2015) or crown hominids more closely related to either pongines (Moyà-Solà and Köhler 1993, 1995, 1996; Agustí et al. 1996) or hominines (Begun 2002, 2009, 2015, 2018; Begun et al. 2012). However, most recent cladistic analyses support the view that dryopithecines are stem hominids, with Late Miocene hispanopithecins (*Hispanopithecus* and *Rudapithecus*) occupying a more derived position toward crown hominids than the Middle Miocene dryopithecines (Pugh 2022). The dryopithecine talus described here was found isolated in a locality that has yielded no further primate remains (Alba et al. 2017). The size of the specimen discounts an attribution to the small-bodied catarrhines that have been recovered from ACM (Alba, Moyà-Solà, et al. 2010; Alba et al. 2015; Alba, Moyà-Solà, et al. 2012; Bouchet et al. 2024), but does not enable a conclusive assignment to any of the large-bodied dryopithecines recorded from slightly older sediments from the ACM sequence (Moyà-Solà et al. 2004; Moyà-Solà, Köhler, et al. 2009; Moyà-Solà, Alba, et al. 2009; Alba 2012; Alba and Moyà-Solà 2012; Alba et al. 2013, 2020; Alba, Bouchet, et al. 2024), namely *Pierolapithecus catalaunicus*, *Anoiapithecus brevirostris*, or *Dryopithecus fontani*.

Based on comparisons with extant anthropoid primates by means of three-dimensional geometric morphometric (3DGM) techniques, we evaluate the closest morphological affinities of the ACM dryopithecine talus and make locomotor inferences based on the covariation between talar shape and locomotor behavior, as well as additional morphofunctional considerations. During the last decade, 3DGM has been increasingly applied to the study of catarrhine talar morphology (Turley and Frost 2013), with emphasis on extant hominoids (Parr et al. 2011; Parr et al. 2014; Knigge et al. 2015; Friesen et al. 2024) and extinct hominins (Rosas et al. 2017; Sorrentino et al. 2020). However, to our knowledge, this is the first study where a Miocene ape talus is analyzed by means of 3DGM. All dryopithecines for which postcranial elements are available show a mosaic of plesiomorphic and apomorphic features that do not match the body plan found in any living ape—reflecting combinations of positional behaviors that have no modern analog (e.g., Alba 2012; Ward 2015; Almécija et al. 2021). Consequently, we predict that IPS85037 will not closely resemble the talar morphology of

any extant ape lineage. Instead, we expect that it will exhibit a mosaic morphology combining plesiomorphic ("monkey-like") and apomorphic (modern "hominoid-like") features. In addition, Middle Miocene dryopithecins are considered to be postcranially less derived than Late Miocene hispanopithecins, including *Danuvius* (Alba 2012; Almécija et al. 2021; Urciuoli and Alba 2023)—presumably lacking the suspensory specializations of the latter (Moyà-Solà et al. 2004; Moyà-Solà et al. 2005; Almécija et al. 2007; Almécija et al. 2009; Alba, Almécija, et al. 2010; Böhme et al. 2019; Pina et al. 2019; but see Begun and Ward 2005; Deane and Begun 2008, 2010). Thus, we also predict that IPS85037 will lack adaptations for suspensory locomotion, contrary to later hispanopithecins. Therefore, despite not being attributable to genus rank, the ACM dryopithecine talus not only provides new insight into the locomotor adaptations of dryopithecines but also contributes to a better understanding of talar morphology evolution and its locomotor implications in crown hominoids.

1.2 | Age and Geological Background

The ACM local stratigraphic sequence is located at els Hostalets de Pierola (Catalonia, Spain), in the Penedès sector of the Vallès-Penedès Basin (NE Iberian Peninsula). This basin is a Neogene half-graben limited by the Pre-Littoral and Littoral Catalan Coastal Ranges, close to Barcelona, that has yielded a rich fossil vertebrate record from the Early to the Late Miocene (Casanovas-Vilar, Madern, et al. 2016). The sedimentary deposits of the basin are broadly structured in two complexes of continental units, with intercalated marine and transitional units (Casanovas-Vilar, Madern, et al. 2016). The ACM stratigraphic sequence belongs to the upper continental complexes, which are Middle to Late Miocene in age (Alba et al. 2006, 2017; Moyà-Solà, Alba, et al. 2009; Casanovas-Vilar, Garcés, et al. 2016; Casanovas-Vilar, Madern, et al. 2016; Casanovas-Vilar et al. 2022). The sediments from ACM predominantly consist of mudstones, which were deposited in the distal-to-marginal, inter-fan zones of the coalescing alluvial fan systems of Olesa and els Hostalets de Pierola (Moyà-Solà, Köhler, et al. 2009; Casanovas-Vilar, Garcés, et al. 2016; Alba et al. 2017).

Based on litho-, bio-, and magnetostratigraphic correlation, the ACM sequence spans from 12.6 to 11.1 Ma (Middle to Late Miocene) and covers the Mammal Neogene (MN) zones MN6 (late portion), MN7+8, and MN9 (earliest portion), being correlated to the late Aragonian and earliest Vallesian (Casanovas-Vilar, Garcés, et al. 2016; Alba et al. 2017, 2022). The primate fossil talus described here was found isolated in the framework of paleontological surveillance performed during the construction of Sector B of Cell 8 of the Can Mata landfill in 2014. Its exact stratigraphic position (locality ACM/C8-B*) relative to the ACM composite sequence (Alba et al. 2017, 2022) was recorded, enabling a correlation with the base of normal polarity subchron C5r.2n, with an interpolated age of 11.65 Ma (Alba et al. 2022) that coincides with the Middle/Late Miocene (Serravallian/Tortonian) boundary (Raffi et al. 2020). Isotopic and mesowear data from the ACM fauna suggest that the time span comprised between 11.7 and 11.6 Ma at ACM was characterized by greater habitat heterogeneity than previous periods (DeMiguel et al. 2021), which might explain the coexistence between large-bodied dryopithecines and the small-bodied crouzeliid *Pliobates* around this time (Alba et al. 2017; DeMiguel et al. 2021).

2 | Materials and Methods

2.1 | Studied Material and Comparative Sample

IPS85037 (Figure 1A–E) is housed at the Institut Català de Paleontologia Miquel Crusafont (ICP) in Sabadell, Spain. The fossil was compared with a broad sample of extant anthropoids using 3DGM techniques. The extant comparative sample comprises 68 tali from 22 primate species across 14 genera, providing good phylogenetic coverage (Table 1; see Figure 2 for a representation of the main groups and Table S1 for further details). A talus of the Early Miocene hominoid *Ekembo heseloni* (KMN-RU 2036) was also included in the comparative sample (Walker and Pickford 1983) to gain insight into the stem hominoid condition. Additionally, the morphological affinities between IPS85037 and other relevant tali from Miocene apes and extinct catarrhines are assessed to understand better the evolution of hominoid talar morphology and its locomotor implications.

2.2 | Surface Scanning

3D virtual models of the specimens from the comparative sample were derived from surface scans obtained using a Geomagic Capture scanner (3D Systems, Rock Hill, USA) and subsequently cleaned using Geomagic Wrap 2019 (3D Systems, Rock Hill, USA). In turn, IPS85037 was scanned using a NextEngineTM 3D scanner HD (NextEngine Inc., Santa Monica, USA) using high definition (HD) settings following the protocol detailed by Hammond et al. (2016). The scanner's range was adjusted to Macro settings and the highest possible resolution (160 points per square inch). The three final scans obtained—one 360° scan and two bracket scans (top and bottom)—were fused in Scan Studio PRO v. 1.7.3 (NextEngine Inc., Santa Monica, USA) to obtain the final surface mesh, which underwent postprocessing following standard protocols (Tocheri et al. 2011; Hammond et al. 2016) using Geomagic Studio 12 (3D Systems, Rock Hill, USA). Since the talus virtual models included in the comparative sample were from the left side (or had been mirrored to appear as such), the 3D model of IPS85037 was mirrored to perform the analyses. The virtual model from the described specimen is available from MorphoSource (File S1). Similarly, the talus belonging to *E. heseloni* (KMN RU 2036) was scanned from the original specimen using the same procedure as for IPS85037.

2.3 | Geometric Morphometrics

Landmark protocol To perform the 3DGM analyses, 36 landmarks were placed following a protocol devised to capture the overall talar shape (Figure 3; Table 2). All landmarks are type II/III except for landmark 32 (type I). The 3D models were landmarked using Landmark Editor v. 3.0.0.6 (Wiley et al. 2005). All analyses were performed in the statistical software R v. 4.4.0 (R Core Team 2024), using the visual interface RStudio desktop v. 2023.3.0.386 (RStudio Inc., Boston, USA). In addition,

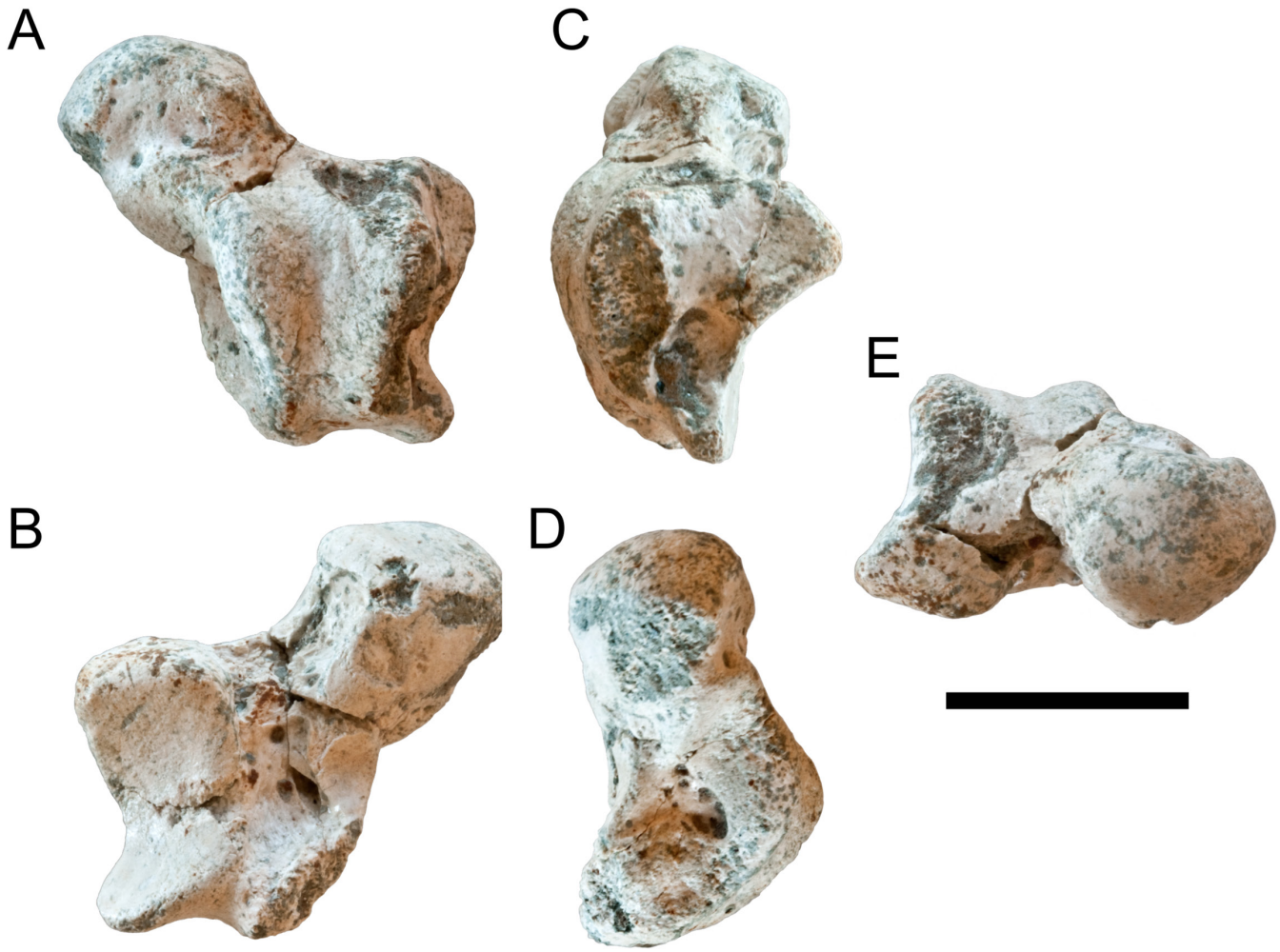


FIGURE 1 | IPS85037, right talus of Dryopithecini indet. from ACM/C8-B*, in dorsal (A), plantar (B), lateral (C), medial (D), and distal (E) views. Scale bar equals 2 cm.

a table with a list of 11 talar measurements using linear metrics (following Youlatos 1999) is provided for comparative purposes (Table 3). A generalized Procrustes analysis (GPA) was performed to obtain the Procrustes-aligned coordinates using "gpagen" function of "geomorph" package v. 4.0.7 (Adams and Otárola-Castillo 2013).

To confirm the repeatability of the landmark coordinate digitization used for geometric morphometric analyses (Shearer et al. 2017), intra- and inter-observer repeatability tests were performed by placing the same landmarks by four different researchers (Figure S1A) and four times by the same researcher (Figure S1B), respectively. Procrustes distances (Tables S2 and S3) and per-landmark variance (Figure S2; Table S4) were calculated. No significant differences were found between the intra- and inter-observer conditions ($t = 1.4035$, $p = 0.1651$), indicating that the landmark configuration is repeatable by different researchers.

Principal components analysis A between-group principal components analysis (bgPCA; Culhane et al. 2002) was performed on the Procustes-aligned coordinates using the "groupPCA" function of "Morpho" package v. 2.12 (Schlager 2017). Four groups were defined a priori: platyrrhines, cercopithecoids, hylobatids, and hominids. Unlike a standard PCA, a bgPCA maximizes variance along the axes based on the centroids (averages) of the groups defined a priori, with the scores of individual specimens being subsequently plotted post hoc onto the morphospace, thereby enhancing group distinction. The data from the fossil 3D models (IPS85037 and KMN-RU 2036) were projected a posteriori on each analysis. Bivariate plots among between-group principal components (bgPCs) were plotted using the "ggplot2" package v. 3.5.1 (Wickham 2016). For visualization purposes, a thin-plate spline deformation of the 3D model of a reference talus was carried out using the functions "shape.predictor" and "tps3d" of the "geomorph" and "Morpho" packages, respectively, and "shade3d" of the "rgl" package1.1.3 (Adler and Murdoch 2020). The "mshape" and "findMeanSpec" functions of the package "geomorph" were used to find the closest specimen to the sample mean to use as the reference. The specimen selected was a talus of *Pan paniscus* (RMCA 27698).

To assess the presence of allometric effects, the three resulting bgPCs were regressed using the ordinary least-squares method (OLS) against natural log-transformed (ln) centroid size of the talus for each specimen using the "procD.lm" function in "geomorph" and plotted using the package "ggplot2." To address the concerns about potentially spurious grouping

TABLE 1 | Summary of the comparative sample of extant anthropoid tali used in this study.

Main group	Species	Males	Females	Total
Platyrrhini	*Alouatta palliata*	1	1	2
Platyrrhini	*Alouatta seniculus*	1	1	2
Platyrrhini	*Ateles fusciceps*	2	2	4
Platyrrhini	*Cebus apella*	3	1	4
Cercopithecidae	*Colobus guereza*	2	2	4
Cercopithecidae	*Macaca artoides*	0	1	1
Cercopithecidae	*Macaca fascicularis*	1	0	1
Cercopithecidae	*Macaca mulatta*	1	1	2
Cercopithecidae	*Nasalis larvatus*	1	1	2
Cercopithecidae	*Papio anubis*	1	1	2
Cercopithecidae	*Papio hamadryas*	0	1	1
Hylobatidae	*Hylobates agilis*	0	1	1
Hylobatidae	*Hylobates klossii*	1	0	1
Hylobatidae	*Nomascus concolor*	1	0	1
Hylobatidae	*Symphalangus syndactylus*	1	2	3
Hominidae	*Gorilla beringei*	5	2	7
Hominidae	*Gorilla gorilla*	3	3	6
Hominidae	*Homo sapiens*	2	2	4
Hominidae	*Pan paniscus*	2	2	4
Hominidae	*Pan troglodytes*	5	3	8
Hominidae	*Pongo abelii*	1	1	2
Hominidae	*Pongo pygmaeus*	3	3	6
Total		37	31	68

when bgPCA is applied to highly multidimensional datasets (Bookstein 2019; Cardini et al. 2019)—such as those coming from 3DGM analyses—we designed the sample to include groups with a large number of individuals (Rohlf 2021). We also followed Cardini and Polly's (2020) recommendation to perform a cross-validated bgPCA on the raw data using the "groupPCA" function of the package "Morpho." With the same aim in mind, we also computed group mean differences for the raw shape data, regular bgPCA scores, and cross-validated bgPCA scores using the "lm.rrpp" function of the R package "RRPP" v. 2.0.0 (Collyer and Adams 2018). In addition, a standard PCA was performed to evaluate the differences between the bgPCA and a standard PCA using "prcompfast" function of "Morpho." In this second case, 3D data of IPS85037 and KMN-RU 2036 were projected a posteriori onto the morphospace defined by extant taxa.

Finally, we computed the typicality probabilities of group membership for the fossil specimens using the "typprobClass" function of the "Morpho" package. Unlike posterior probabilities, which are customarily calculated in discriminant analyses and assume that classified individuals belong to one of the a priori defined groups, typicality probabilities evaluate the similarity of a specimen to each group separately. Although the classification of each specimen is similarly based on the highest probability, the typicality probabilities also represent the p value to test the null hypothesis of group membership (separately for each group). Thus, even if the highest typicality probability denotes the highest morphometric affinities, it might still indicate that the specimen does not fit within the variation of the group if $p < 0.05$.

2.4 | Body Mass Estimation

Talus size, as captured using either linear measurements (e.g., Tsubamoto et al. 2016), articular areas (e.g., Yapuncich et al. 2015), or centroid size in 3DGM analyses (e.g., Parr et al. 2014), has been established as a suitable proxy of body mass (BM). We followed the latter approach to estimate BM for the described dryopithecine talus. As the comparative sample does not include individuals of known BM, mean data (Table S5) for both males and females of each species were taken from the literature (Smith and Jungers 1997). In the

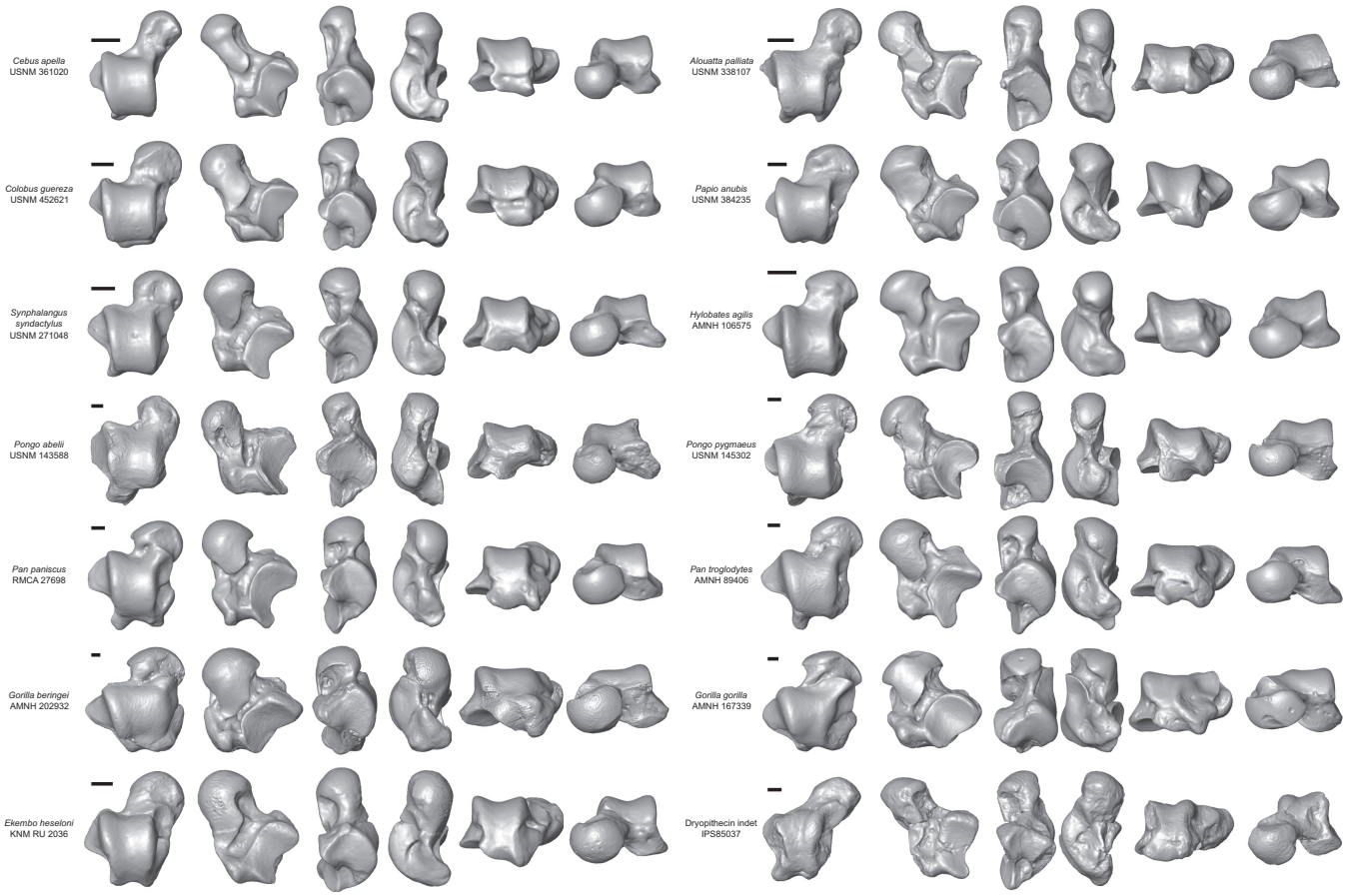


FIGURE 2 | Render images of the talus of Dryopithecini indet. from ACM/C8-B* (IPS85037) as compared to that of *Ekembo heseloni* (KMN RU 2036) and a selected sample of tali from extant anthropoids included in the comparative sample; from left to right, in dorsal, plantar, lateral, medial, and distal views. Scale bars equal 5 mm.

case of polytypic species, the average of subspecies BM means was computed for each sex. To estimate BM, allometric regressions of ln BM vs. ln centroid size were performed using an OLS regression with the "lm" function of the "stats" package. Body mass estimates for IPS85037 and KMN-RU 2036 were derived from the best-fit regression line by further applying the quasi-maximum likelihood estimator (QMLE) to account for the logarithmic transformation bias (Smith 1993). The latter was computed as $QMLE = \exp(SEE^2/2)$, where SEE is the standard error of estimate of the regression. 50% and 95% confidence intervals (CIs) were computed for each BM estimate of the fossil specimen.

2.5 | Partial Least-Squares Regression

Previous studies (e.g., Püschel et al. 2018, 2020; Llera Martín et al. 2022) have shown that it is possible to distinguish between main locomotor modes and substrate preferences using tarsal shape, as well as to infer the locomotor behavior of fossil primates on its basis. These studies discretized locomotor categories or substrate preferences into a limited number of categories to enable the application of different classification algorithms. Although certainly valuable, these approaches have limitations that arise from the fact that any classification scheme is a simplification of the actual locomotor repertoire displayed by any primate species, which includes a variety of locomotor behaviors. Other studies have overcome such limitations using two-block partial least-squares analysis (2B-PLS; Rohlf and Corti 2000), which enables the assessment of major patterns of covariation between a shape data matrix (e.g., talar shape) and a locomotor behavior data matrix (e.g., Almécija et al. 2015; Fabre et al. 2017; Fabre et al. 2018; Fabre et al. 2019; Püschel et al. 2017). These studies have shown that it is possible to find strong covariation patterns between behavioral data (e.g., locomotion) and the shape of certain skeletal elements, which may be used to make paleobiological inferences. However, the aforementioned works only focused on extant species and did not try to infer the locomotor behavior of extinct taxa. In addition, the standard version of 2B-PLS in the morphometric literature is a symmetric analysis that, in its classic formulation, does not allow predictions (Zelditch et al. 2012). However, there is a type of partial least-squares analysis more comparable to regression, known as partial least-squares regression (PLSR), that allows the generation of predictive models (Wold et al. 2001). This method has been previously applied in geometric morphometrics to predict one block of shape variables from another one (e.g., Schlager 2013; Archer et al. 2018; Bastir et al. 2019; Torres-Tamayo et al. 2020), and recently has been used to estimate the locomotor behavior of early primate species, yielding a good predictive performance (Monclús-Gonzalo et al. 2023). Therefore, we applied a PLSR approach to infer the locomotor behavior of the two Miocene apes included in the studied and comparative samples based on their talar shape.

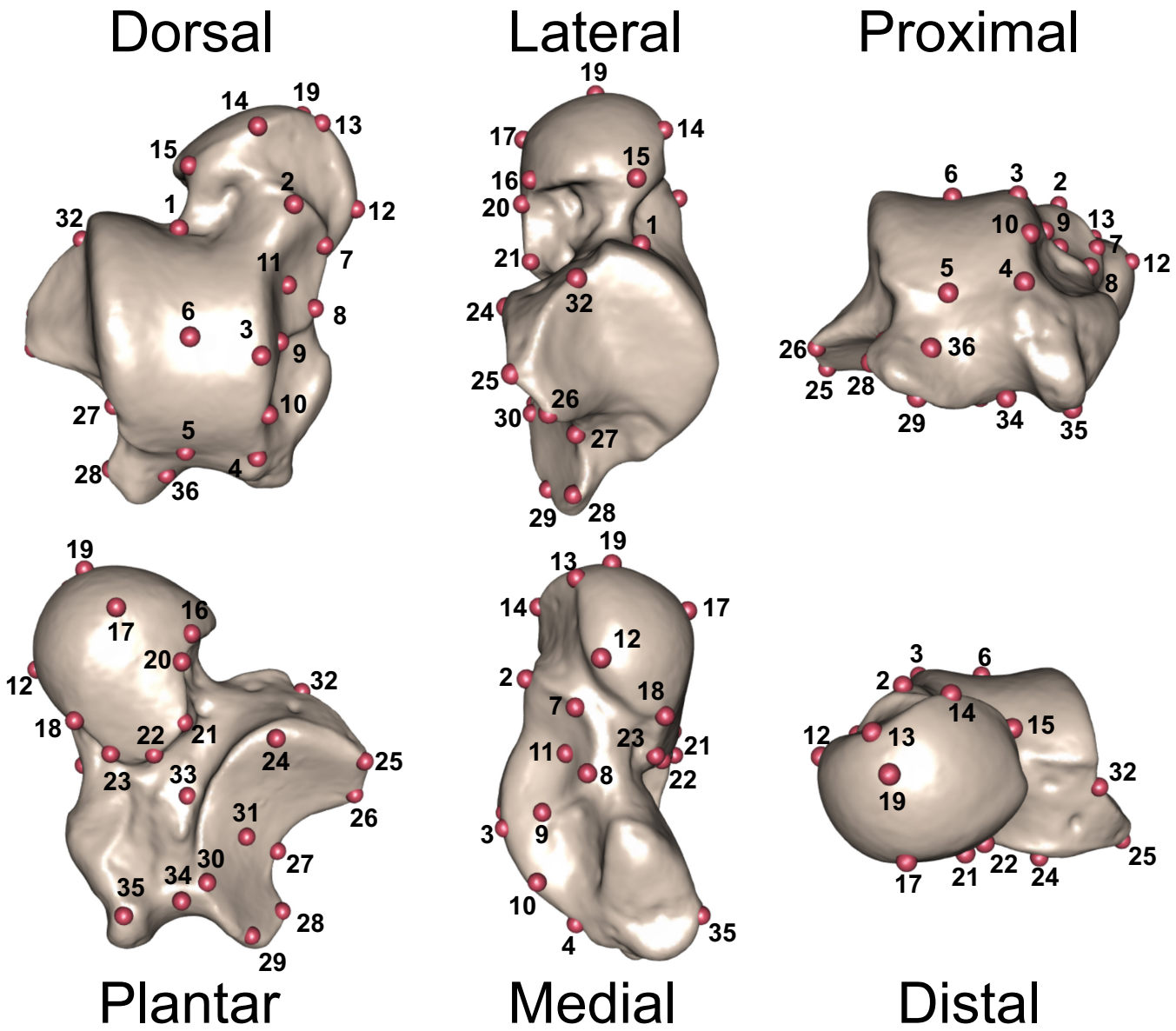


FIGURE 3 | Landmark configuration utilized in this study (see Table 2 for landmark definitions). The specimen used as reference corresponds to the talus of *Pan paniscus* (RMCA 27698).

The two blocks of data consisted of (1) talar shape (Procrustes-aligned coordinates) averaged by species and (2) locomotor mode percentages (LMPs)—that is, the percentage time a species spends performing a certain locomotor behavior—for the 21 extant species included in the extant comparative sample. Locomotor data were taken from the literature (see references in Table S6). Five locomotor modes were distinguished: (1) quadrupedal walking, bounding, and running; (2) clambering and vertical climbing; (3) leaping, dropping, and hopping; (4) bridging, brachiation, and suspensory locomotion; and (5) bipedal walking. Because the locomotor data came from different sources, and not all behaviors reported in the original studies were considered, we rounded the LMPs to percentages for those species that included small amounts of locomotor modes not considered in this study, ensuring that they add up to 100%. In addition, to ensure that our locomotor predictions were between 0% and 100%, we first converted the percentages to proportions by dividing them by 100 and then we applied a logit transformation, which can be defined as ln $[P/(1–P)]$, where P is a proportion (Cramer 2003). This transformation was done prior to carrying out the PLSR to avoid nonsensical results (e.g., LMPs higher than 100% or lower than 0%). Given that ln (0) is undefined, we added 1% to any LMP equal to 0 and then we rounded up the LMPs again to ensure that they added up to 100% before carrying out the logit transformation.

The PLSR is based on the same basic machinery as the standard 2B-PLS, which means that it finds the principal components of covariation between the blocks of variables by means of decomposing the covariance matrix of the two blocks into two sets of eigenvectors (one for each set of variables) and eigenvalues, using a singular value decomposition to generate a matrix of singular values (the square roots of the eigenvalues), a matrix of eigenvectors for the first set of variables and the transpose of the matrix of eigenvectors for the second set of variables (Rohlf and Corti 2000). We carried out this step by using the "two.b.pls" function of the "geomorph" package, and we ran 9999 iterations for significance testing. The PLSR

TABLE 2 | Definition of the 36 landmarks used in this study.

Landmark	Name/Structure	Description
1	Trochlear surface	Point of maximum concavity on distal margin
2		Most disto-tibial point
3		Most dorsally convex point along tibial border
4		Most proximo-tibial point
5		Point of most inflection along the proximal margin
6		Most proximal point along the trochlear groove between 1 and 5
7	Tibial malleolar surface	Most disto-tibal point
8		Most proximo-plantar point
9		Point of most inflection along margin between 8 & 10
10		Most proximal point
11		Most concave point on distal portion of surface
12	Talar head	Most dorso-tibial point
13		Most distal point along dorsal margin
14		Most dorsally convex point along margin between 13 and 15
15		Most fibular point
16		Point of most distal inflection along ridge between 15 and 20
17		Most distal point along margin with anterior subtalar facet
18		Most planto-tibial point
19		Most distally extending point on surface
20	Anterior subtalar surface	Point of most inflection on disto-fibular margin
21		Most fibularly extending point
22		Most convex point along margin between 21 and 23
23		Most proximo-tibial point
24	Posterior subtalar surface	Most disto-tibial point
25		Most disto-fibular point
26		Most convex point along margin between 25 and 27
27		Point of most inflection on proximo-fibular margin
28		Point of greatest convexity along margin between 27 and 29
29		Most proximo-fibular point
30		Most proximo-tibial point
31		Most plantarly concave point around center of surface
32	Fibular malleolar surface	Distal junction of the lateral trochlear rim and the fibular malleolar surface
33	Sulcus tali	Deepest point at the level of maximum tibial concavity
34		Deepest point around tibio-fibular axis
35		Tip of tibial margin
36	Posterior process	Midpoint root on proximo-dorsal side

works by regressing the first block of variables on the vector obtained from the scores for the second block of variables (i.e., the LMPs were regressed on the talar shape values that were projected onto the obtained singular vectors). This step was done using the "procD.lm" function of the same package (9999 iterations were used). To obtain LMP predictions, the talar

TABLE 3 | Talar linear measurements for IPS85037 (following Youlatos 1999).

	AS1	AS2	AS3	AS4	AS5	AS6	AS7	AS8	AS9	AS10	AS11
IPS85037	8.7	8.6	14.5	36.5	4.8	20.7	15.5	17.1	14.3	(17.8)	(13.2)

Abbreviations: AS1 = length of tibial malleolar surface on the dorsomedial plane; AS2 = length of the neck on the dorsolateral plane; AS3 = maximum length of the neck and head; AS4 = maximum length of the talus; AS5 = height of the posterior subtalar facet; AS6 = length of the posterior subtalar facet; AS7 = length of the head; AS8 = height of the head, perpendicular to the former measurement; AS9 = maximum length of the neck on the dorsal plane; AS10 = distal length of the trochlea; AS11 = proximal length of the trochlea.

shape values were projected onto the obtained singular vectors and then multiplied by a matrix consisting of the linear model coefficients. This process was done with the talar shape (Procrustes-aligned coordinates) averaged for extinct species to derive locomotor inferences (i.e., estimated percentages for the various locomotor modes). Given that, prior to the PLSR, the LMPs were subjected to a logit transformation, the obtained predictions were transformed back into percentages by applying an inverse logit transformation, defined as exp(X)/[1 + exp(X)], where X corresponds to a logit transformed value. The obtained predictions were then rounded up again to ensure that they added to 100%. To assess the PLSR predictive performance, we performed a "leave-one-out cross-validation" (LOOCV), which means that separate analyses were carried out for each one of the predictions, excluding the particular individual for which the prediction was being calculated (Kuhn and Johnson 2013). Using these cross-validated results, we computed the mean absolute error (MAE; i.e., the arithmetic average of the absolute errors) to assess our prediction results using the extant sample (Willmott and Matsuura 2005).

Additionally, the talus specimen closest to the multivariate mean of the talar shape dataset (*Pan paniscus*, RMCA 27698) was warped to represent the covariation between shape and LMPs along the first singular vectors (following the same procedure as that explained above to visualize the shapes associated to the negative and positive extremes of each axis of the bgPCA). A principal component analysis (PCA) was carried out with the LMPs using the "prcomp" function of the R package "stats." The PCA scores and the loadings of each locomotor variable were assembled in the same scatterplot (as a biplot). The estimated locomotor repertoires of IPS85037 and KMN RU 2036 were projected onto the PCA to visualize their placement within the "ecospace" defined by extant species' locomotor behavior. The direction and length of each vector indicate the region of the scatterplot in which the locomotor variable is more represented. As a result, those specimens projected the furthest in the direction of a given vector are those whose locomotor repertoire possesses the highest percentage in the direction of the corresponding locomotor variable.

3 | Results

3.1 | Description

The right talus IPS85037 (Figure 1A–E) is well preserved except for minor damage on the lateral edge of the trochlea, the medial tubercle, the posterior calcaneal facet, and the medial edge of the talar head, as well as a crack at the level of the neck. The talar body is dorsoplantarly taller than mediolaterally wide. The trochlea is wedge-shaped (broader anteriorly than posteriorly), displays a moderately deep central groove, and has a slightly dorsoplantarly higher lateral trochlear rim compared to the medial one. The groove for the flexor hallucis longus tendon is placed in a mid-trochlear position, flanked by a well-developed posterior lateral tubercle and a similarly developed (but somewhat damaged) posterior medial tubercle. The articular facet with the fibula is relatively dorsoplantarly tall and moderately expanded laterally. The medial tibial facet is moderately steep and does not reach the plantar side of the bone. The neck is relatively long and slender, medially angled, has a subsquare cross-section almost as wide as high, and displays a strong medial orientation. The posterior calcaneal facet is relatively shallow, subsquare (except for its proximal edge, which tapers toward the medial tubercle), slightly concave, and obliquely oriented. The sulcus tali is relatively broad and shallow. The anterior calcaneal facet is continuous and mediolaterally narrow, extending up to the anterior end of the sulcus tali. The talar head, relatively small and ovoid, bears a markedly convex articular surface that extends more laterally than medially and shows a slight medial torsion.

3.2 | Comparison With Stem Catarrhine and Other Miocene Ape Tali

The trochlear morphology of IPS85037, like that of stem catarrhines and other Miocene apes, exhibits an anteriorly broad articular facet and a relatively deep trochlear depth comparable to the dendropithecid *Simiolus enjiessi* (Leakey and Leakey 1987; Rose et al. 1992), the pliopithecoid *Pliopithecus antiquus* (see Senut 2012), and most Miocene hominoids (*E. heseloni*, *Ekembo nyanzae*, *Equatorius africanus*, *Nacholapithecus kerioi*, and *Sivapithecus sivalensis*; MacInnes 1943; Le Gros Clark and Leakey 1951; Pilbeam et al. 1980; Harrison 1982; Walker and Pickford 1983; Leakey and Leakey 1987; Rose et al. 1992, 1996; McCrossin 1994; Madar 1996; Ishida et al. 2004; Nakatsukasa et al. 2012). It differs from the dendropithecid *Dendropithecus maccinesi* (Le Gros Clark and Thomas 1951) and the nyanzapithecid *Rangwapithecus gordoni* (DeSilva 2008) in displaying a deeper trochlear groove. The lateral trochlear rim of IPS85037 is only slightly higher than the medial rim, as in extant hominoids (particularly orangutans and hylobatids; Turley and Frost 2013), dendropithecids (*D. maccinesi* and *S. enjiessi*; Le Gros Clark and Thomas 1951; Leakey and Leakey 1987; Rose et al. 1992), *Oreopithecus* (Szalay and Langdon 1986), and the stem pongine *Si. sivalensis* (Pilbeam et al. 1980; Madar 1996). Conversely, the lateral trochlear rim of IPS85037 is less prominent than that of extant cercopithecoids (Strasser 1988), pliopithecoids (*P. antiquus* and *Anapithecus hernyaki*; Begun 1987; Senut 2012), and several stem hominoids (*Turkanapithecus kalakolensis*, *E. heseloni*, *E. nyanzae*, *Eq. africanus*, and *N. kerioi*; Harrison 1982; Walker and Pickford 1983; Leakey and Leakey 1987; Ward

et al. 1993; McCrossin 1994; Ishida et al. 2004; Nakatsukasa et al. 2012).

Posteriorly, IPS85037 displays a deep and well-defined groove for the tendon of the m. flexor hallucis longus, and a rather well-developed posterior lateral tubercle. This condition is also met by the stem hominoid *Proconsul major* and *Orepithecus* (Harrison 1982; Szalay and Langdon 1986; DeSilva 2008). IPS85037 further resembles the afropithecid *N. kerioi* in the well-developed lateral posterior tubercle (Ishida et al. 2004; Nakatsukasa et al. 2012). Conversely, the condition of IPS85037 is markedly distinct from the shallow groove displayed by pliopithecoids (Begun 1987; Senut 2012) and the afropithecid *Eq. africanus* (McCrossin 1994). Moreover, IPS85037 resembles extant hominoids in the less concave facet for the medial tibial malleolus and the lack of a dorsal ridge on the talar neck (Conroy and Rose 1983). In the latter feature, IPS85037 is similar to *R. gordoni*, *Pr. major*, and *O. bambolii* (Harrison 1982; Szalay and Langdon 1986; DeSilva 2008) but different from the deeply cupped facet and the pronounced dorsal ridge exhibited by pliopithecoids (*P. antiquus* and *Epipliopithecus vindobonensis*; Zapfe 1958; Senut 2012), dendropithecids (*Micropithecus songhorensis* and *S. enjiessi*; Le Gros Clark and Thomas 1951; Leakey and Leakey 1987; Rose et al. 1992) and several stem hominoids (*E. heseloni*, *E. nyanzae*, *Eq. africanus*, and *N kerioi*; MacInnes 1943; Le Gros Clark and Leakey 1951; Harrison 1982; Walker and Pickford 1983; Leakey and Leakey 1987; Rose et al. 1992, 1996; McCrossin 1994; Ishida et al. 2004; Nakatsukasa et al. 2012), which resemble instead the extant cercopithecoids (Le Gros Clark and Leakey 1951; Harrison 1982).

IPS85037 resembles most stem catarrhines and Miocene apes in the gracile and moderately elongate neck (Harrison 1982), with the exception of *O. bambolii*, which resembles extant hominoids (excluding orangutans) in the extremely abbreviated neck (Szalay and Langdon 1986). In contrast, IPS85037 resembles *O. bambolii* and differs from other Miocene apes and stem catarrhines in the medially angled neck, albeit less markedly so than in *O. bambolii* (Szalay and Langdon 1986). IPS85037 resembles the pliopithecoid *P. antiquus* (Senut 2012), as well as the stem hominoids *T. kalakolensis* (Leakey and Leakey 1987) and *Pr. major* (Harrison 1982; DeSilva 2008) in the small and spherical head. In contrast, IPS85037 differs in this regard from dendropithecids (*D. maccinesi* and *S. enjiessi*; Le Gros Clark and Thomas 1951; Leakey and Leakey 1987; Rose et al. 1992) and several Miocene apes (*E. heseloni*, *E. nyanzae*, *Eq. africanus*, *N. kerioi*, and *O. bambolii*; MacInnes 1943; Le Gros Clark and Leakey 1951; Harrison 1982; Walker and Pickford 1983; Szalay and Langdon 1986; Rose et al. 1996; Ward et al. 1993; McCrossin 1994; Ishida et al. 2004; Nakatsukasa et al. 2012), which exhibit mediolaterally broad and large heads like those of extant cercopithecoids and African apes.

IPS85037 has a relatively flat and proximodistally elongated posterior calcaneal facet, comparable to that of orangutans (Langdon 1986). In this regard, IPS85037 differs from stem catarrhines and Miocene apes except for *O. bambolii* (Harrison 1982; Conroy and Rose 1983; Langdon 1986), which, like IPS85037, possesses a shallow and elongated facet (Szalay and Langdon 1986). Moreover, IPS85037 displays a small divergence between the posterior calcaneal facet and the long axis of the trochlea, matching extant hominoids, the pliopithecoid *An. hernyaki* (Begun 1987), *N. kerioi* (Ishida et al. 2004; Nakatsukasa et al. 2012), and *Si. sivalensis* (Pilbeam et al. 1980; Madar 1996). The sulcus tali of IPS85037, separating the anterior calcaneal facet from the posterior, is intermediate between the condition of extant great apes (deep and narrow) and gibbons and non-hominoid anthropoids (shallow and broad; Harrison 1982). Finally, IPS85037 resembles stem catarrhines and most other Miocene apes in the anteromedially L-shaped anterior calcaneal facet (Harrison 1982), except for *O. bambolii*, which differs from IPS85037 and resembles extant hominoids in possessing a crescent-shaped facet (Szalay and Langdon 1986).

3.3 | Morphometric Comparisons

The bgPCA (Figure 4) correctly classifies 100% of cases in the four extant groups defined a priori (platyrrhines, cercopithecoids, hylobatids, and hominids), whereas the bgPCA with cross-validation (Figure S3A,B) correctly classifies 94% of cases (Tables S7 and S8). The similarities between standard PC scores (Figure S4A,B) and standard and cross-validated bgPC scores suggest that discrimination is not spurious. In addition, significant group differences in the raw shape data indicate the presence of group structure in our sample ($R^2 = 0.23$, $p < 0.001$). Even if the amount of variance increases considerably when group differences are computed for bgPC ($R^2 = 0.77$, $p < 0.001$) and cross-validated bgPC scores ($R^2 = 0.71$, $p < 0.001$), the overall similarities between the Z-scores computed for the raw data ($Z = 6.49$), bgPC scores ($Z = 13.79$), and cross-validated bgPC scores ($Z = 12.01$) allow us to reject the presence of spurious grouping in the analysis.

The bgPC1 (62% of total variance; Figure 4A,B) reflects differences in talar body shape (broader and stouter toward positive scores vs. slenderer toward negative scores), wedging of the trochlea (broader anteriorly than posteriorly toward positive scores vs. subparallel rims toward negative scores), the shape of the posterior calcaneal facet (slenderer and medially tapered toward negative scores and broader and more squared toward positive scores), the anterior calcaneal facet (proximodistally longer and mediolaterally narrow toward positive scores and broader and more proximodistally restricted toward negative scores), proximodistal elongation and robusticity of the talar neck (shorter and more robust toward positive scores and proximodistally longer and slenderer toward negative scores), and the relative size of the talar head (smaller and more spherical toward negative scores). This axis separates platyrrhines (negative end of the axis) from cercopithecoids (moderately negative scores) as well as hylobatids (moderately negative or positive scores) and hominids (mostly positive scores), with hylobatids partly overlapping with both cercopithecoids and hominids. A significant allometric relationship is found between bgPC1 and talus size, indicating a strong positive correlation that accounts for 78% of the variance (Figure S5A, Table 4). This result parallels the rough gradient of decreasing body size observed along bgPC1, although hylobatids exhibit comparably more positive scores (overlapping with the lower end of great apes) than expected given their body size, while monkeys (especially platyrrhines), in contrast, display lower bgPC1 values than that expected on this basis.

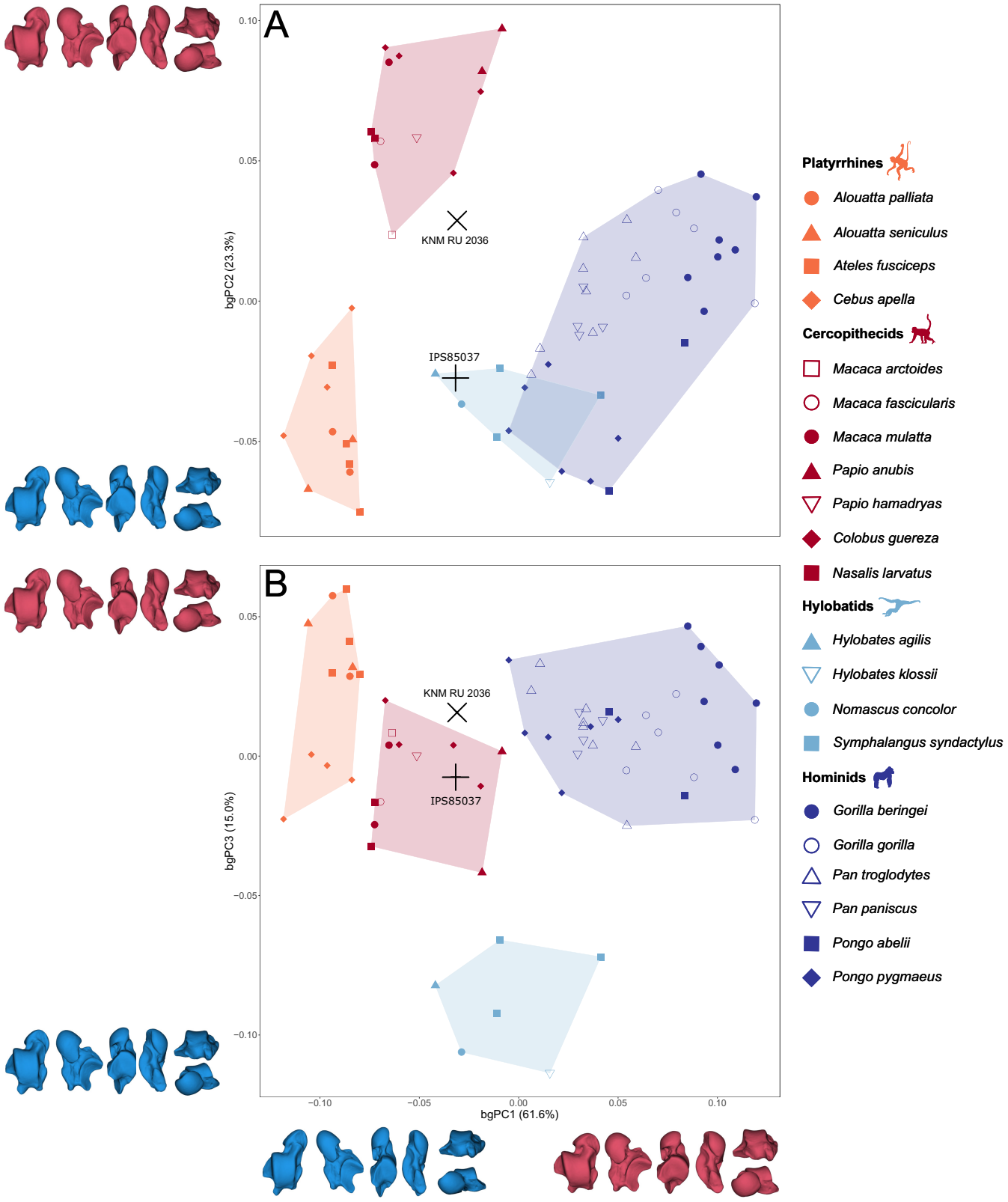


FIGURE 4 | Results of the between-group principal components analysis (bgPCA) as depicted by a bivariate plot of bgPC2 vs. bgPC1 (A) and bgPC3 vs. bgPC1 (B). The groups distinguished a priori are indicated by color-coded convex hulls, and each species is denoted by different symbols, as indicated in the legend. Fossil specimens (whose scores are projected a posteriori) are indicated by a cross (×) sign (KMN RU 2036) and a plus (+) sign (IPS85037). The percentage of variance explained by each bgPC is reported within parentheses. Talar shapes associated with minimum (blue) and maximum (red) values of each bgPC axis are plotted below each scatterplot (dorsal, plantar, lateral, medial, proximal, and distal views are shown from left to right). Thin plate spline warps are based on a talus of *Pan paniscus* (RMCA 27698).

TABLE 4 | Ordinary least-squares regressions of between-group principal components (bgPCs) vs. log-transformed centroid size (ln CS).[a]

bgPC	Slope	Intercept	r^2	Z	p
bgPC1	0.141	−0.611	0.758	6.777	**< 0.001**
bgPC2	0.011	−0.046	0.010	0.195	0.439
bgPC3	0.026	−0.113	0.093	2.008	**0.016**

Note: Z = effect sizes (computed as standard deviates of Fischer's F).
[a]Significant results ($p < 0.05$) are indicated in bold.

The bgPC2 (23% of the variance; Figure 4A) is driven by the shape of the talar body (negative scores are associated with a shallower and more dorsoplantarly compressed trochlea and positive scores with a deeper and dorsoplantarly higher trochlea), the relative height of the lateral rim (more symmetrical rims toward negative scores and distinctly dorsoplantarly higher lateral rim, compared to the medial rim, associated with positive scores), the size of the posterior lateral tubercle and the development of the groove for the flexor hallucis longus tendon (smaller tubercle and less well-developed groove toward positive scores), the shape of the posterior calcaneal facet (mediolaterally broader facet more extended medially than laterally toward positive scores), and the anterior calcaneal facet (more concave toward negative scores). This axis separates the more arboreal and/or suspensory species (platyrrhines, hylobatids, and orangutans), which display negative scores, from the more cursorial cercopithecoids (positive scores). African apes display intermediate scores and overlap slightly with cercopithecoids and only minimally (especially in the case of chimpanzees) with other platyrrhines, hylobatids, and orangutans. Unlike bgPC1, bgPC2 is not significantly correlated with talar centroid size (Figure S5B; Table 4), indicating that shape changes along this axis are not affected by size-scaling effects. The bgPC2 seemingly reflects differences in locomotor behavior, with the most arboreal and suspensory hominoids (hylobatids and orangutans) overlapping with the suspensory platyrrhines (*Ateles* and, to a lesser extent, *Alouatta*). Non-suspensory platyrrhines (*Cebus*) also overlap with hylobatids and orangutans, but remarkably exhibit less negative scores than either *Ateles* or *Alouatta*. The bgPC2 shows a locomotor gradient, with terrestrial and semiterrestrial species displaying more positive scores than arboreal ones—except for committed arboreal cercopithecoids such as *Colobus* or *Nasalis*, which cluster with (semi)terrestrial cercopithecoids instead of other arboreal species.

The bgPC3 (15% of total variance; Figure 4B) reflects differences in the shape of the trochlea (increased wedging toward positive scores), the size of the lateral posterior tubercle, and the depth of the groove for the flexor hallucis longus tendon (larger tubercle and deeper groove toward positive scores), and the shape of the anterior calcaneal facet (proximodistally more elongated toward positive values). This axis clearly discriminates hylobatids (very negative scores) from the rest of the comparative sample (which extensively overlaps from intermediate to moderately positive scores). The bgPC3 is significantly correlated with talus size (Figure S5C; Table 4). However, allometric effects can be excluded as the main driver of variation along this axis, as they only explain 8% of shape variance—as further illustrated by the overlap between great apes with the much smaller monkeys and the segregation of hylobatids from all monkeys irrespective of size.

Along bgPC1, both IPS85037 and KMN-RU 2036, characterized by a mediolaterally narrow and dorsoplantarly high astragalar body and a proximodistally elongated neck, overlap with hylobatids and cercopithecoids (Figure 4). Regarding bgPC2 (Figure 4A), IPS85037 closely approaches the variation of hylobatids and overlaps with that of the suspensory orangutans and atelids, as well as cebids. In contrast, KMN-RU 2036 displays a more positive score that approaches the cercopithecoid condition and overlaps with the knuckle-walking African apes. The different scores along bgPC2 can be explained by differences in talar shape between the two fossil specimens. IPS85037 shows some remarkable similarities with the tali of pongines and hylobatids, such as a slightly prominent lateral rim, a well-developed groove for the flexor hallucis longus tendon, and medial and lateral tubercles, a shallow and slightly angled (relative to the long axis of the bone) posterior calcaneal facet, a proximodistally elongated and medially angled neck, and a spherical and convex talar head. In contrast, KMN-RU 2036 more closely approaches the cercopithecoid condition in these regards. Finally, both IPS85037 and KMN-RU 2036 are distinguished from hylobatids along bgPC3 (Figure 4B), as both tali display a relatively wedged and dorsoplantarly deeper trochlea, as well as a more developed groove for the flexor hallucis longus tendon, similarly to the remaining taxa. The differences between the two fossil tali are further confirmed by the typicality probabilities (Table 5), with IPS85037 showing greatest affinities with platyrrhines but further matching the great ape variation, whereas KMN-RU 2036 is classified as a cercopithecoid despite not being incompatible either with the platyrrhine variation.

3.4 | Body Mass Estimation

The allometric equation derived to estimate body size is reported in Table 6. The BM estimate for IPS85037 is 38 kg (95%

TABLE 5 | Typicality probabilities[a] for individual fossil specimens based on a between-group principal component analysis on the Procrustes-aligned coordinates of each talar specimen carried out using four groups distinguished a priori among the extant comparative sample.

	Cercopithecidae	Hominidae	Hylobatidae	Platyrrhini
IPS85037	0.002	**0.041**	0.002	**0.104**
KNM RU 2036	**0.163**	0.004	< 0.001	**0.060**

[a]They indicate the probability of obtaining the score of each fossil specimen given membership in one of the a priori designed groups. Typicality probabilities above significance ($p \geq 0.05$) are bolded, while those below ($p < 0.05$) denote outliers to the distribution of each group.

TABLE 6 | Body mass (BM) estimates (in kg) based on centroid size (CS) using an ordinary least-squares allometric regression[a] of sex-species means (SOM Table S2).

	ln CS	BM estimate	CI (95%)	CI (50%)
IPS85037	4.476	38.008	34.695–41.637	36.863–39.189
KMN RU 2036	4.106	13.460	12.505–14.489	13.132–13.797

[a]ln BM = 2.808 × ln CS – 8.953 (r^2 = 0.963; p < 0.001; standard error of estimate = 0.213; quasi-maximum likelihood estimate = 1.023).

TABLE 7 | Results of the two-block partial least-squares (PLS) regression between talar shape and quantified locomotor data.[a]

Latent variable	Singular value	% covariance	r-PLS	*p*
PLS1	0.151	76.564	0.917	**< 0.001**
PLS2	0.067	15.066	0.868	**0.004**
PLS3	0.043	6.290	0.746	**0.008**
PLS4	0.022	1.577	0.749	0.206
PLS5	0.012	0.504	0.740	0.210

[a]Significant results (p < 0.05) are indicated in bold.

CI = 35–42 kg), thus being roughly the average size of a female orangutan (Smith and Jungers 1997). Conversely, the BM estimate for KMN RU 2036 is 13 kg (95% CI = 12–14 kg), comparable to male siamangs and slightly larger than most atelids, and similar to male macaques as well as female baboons (Smith and Jungers 1997).

3.5 | Partial Least-Squares Regression

The covariation between talar shape and locomotor behavior is significant and explains a considerable amount (92%) of covariance in the first two PLS axes (Table 7). The PLSR predictive performance is presented in Figure S6A–E and Tables S9 and S10.

The first axis (PLS1; Figure 5A; 77% of covariance) discriminates between most suspensory species (*Pongo*, hylobatids), in the most positive scores of the shape axis, and the most quadrupedal ones (African apes, cercopithecoids), located at the negative side of the axis. Platyrrhines, which engage in a more generalized locomotor behavior—including moderate amounts of arboreal quadrupedalism, climbing, and clambering, as well as some leaping (although some species, particularly atelids, also display tail-assisted suspensory behaviors)—are located in intermediate scores of the shape axis. Suspensory species are associated with a proximodistally longer trochlea, more symmetrical rims, a more laterally flaring fibular facet with a more gently inclined slope, a deeper groove for the flexor fibularis tendon and more developed posterior lateral tubercle, a shallower, narrower, and more elongated posterior calcaneal facet, a shallower sulcus talus, and a smaller and more spherical talar head. Conversely, most quadrupedal species exhibit a mediolaterally wider (and proximodistally shorter) trochlea, a higher lateral rim, a steeper fibular facet (in which only the base is laterally protruding), a shallower groove for the flexor fibularis and a less developed posterior lateral tubercle, a more concave and shorter posterior calcaneal facet, a deeper sulcus tali, and a larger talar head. IPS85037 is projected onto intermediate scores, overlapping with platyrrhines, which indicates that its locomotor behavior likely included moderate amounts of quadrupedalism and climbing/clambering, and only a moderate proportion of suspensory behaviors. In contrast, KMN-RU 2036 displays very negative scores, close to the negative end of the axis, suggesting that its locomotor repertoire was dominated by quadrupedalism.

The second axis (PLS2; Figure 5B) discriminates the larger-bodied great apes on positive scores, thus being associated with slower-paced locomotion involving climbing, clambering, and suspensory movements, but completely lacking leaping from the lightly built platyrrhines, cercopithecoids, and gibbons. These latter habitually engage in swifter movements—such as fast quadrupedal progressions, brachiation, and leaping. Siamangs, despite their relatively small body size—comparable to many male macaques, female baboons, and the larger platyrrhine species—exhibit more positive scores than other hylobatids, in agreement with their generally slower and less acrobatic locomotor behavior. Positive scores are associated with a stouter talar shape, a more marked wedging of the anterior part of the trochlea, a shorter (and semilunar-shaped) anterior calcaneal facet, and a shorter and more medially angled neck. Contrarily, negative scores are associated with a slenderer and more gracile talar shape, parallel trochlear rims, a proximodistally longer anterior calcaneal facet, and a longer and less medially angled neck. IPS85037 falls closer to siamangs and great apes, suggesting that it similarly engaged in slower and more cautious locomotion without leaping (not surprisingly, given its large BM) and with high amounts of climbing and clambering. In contrast, KMN-RU 2036 (in accordance with its smaller BM) is located in more negative scores, overlapping with some of the larger-sized platyrrhines and cercopithecoids, which suggests a more agile locomotion (compatible with some degree of leaping) with less climbing/clambering than IPS85037 as well as extant great apes and siamangs.

The estimated locomotor repertoire for the hominoid to which IPS85037 belonged (Figure 6 and Table 8) includes large percentages of vertical climbing/clambering (CL = 50%) and quadrupedalism (QWR = 32%), and a comparatively restricted suspensory component (S = 11%). This locomotor profile, characterized by higher amounts of vertical climbing/clambering and quadrupedalism but lacking substantial suspensory behaviors, approaches the condition of two extant species: *Alouatta seniculus* (QWR = 46%; CL = 41%; S = 10%) and *Pan paniscus* (QWR = 36%; CL = 51%; S = 9%). In contrast, KMN RU 2036 is reconstructed as possessing a remarkably different locomotor repertoire, dominated by quadrupedalism (QWR = 81%), and with much lower percentages of vertical climbing/clambering (CL = 9%) and suspension (S = 2%).

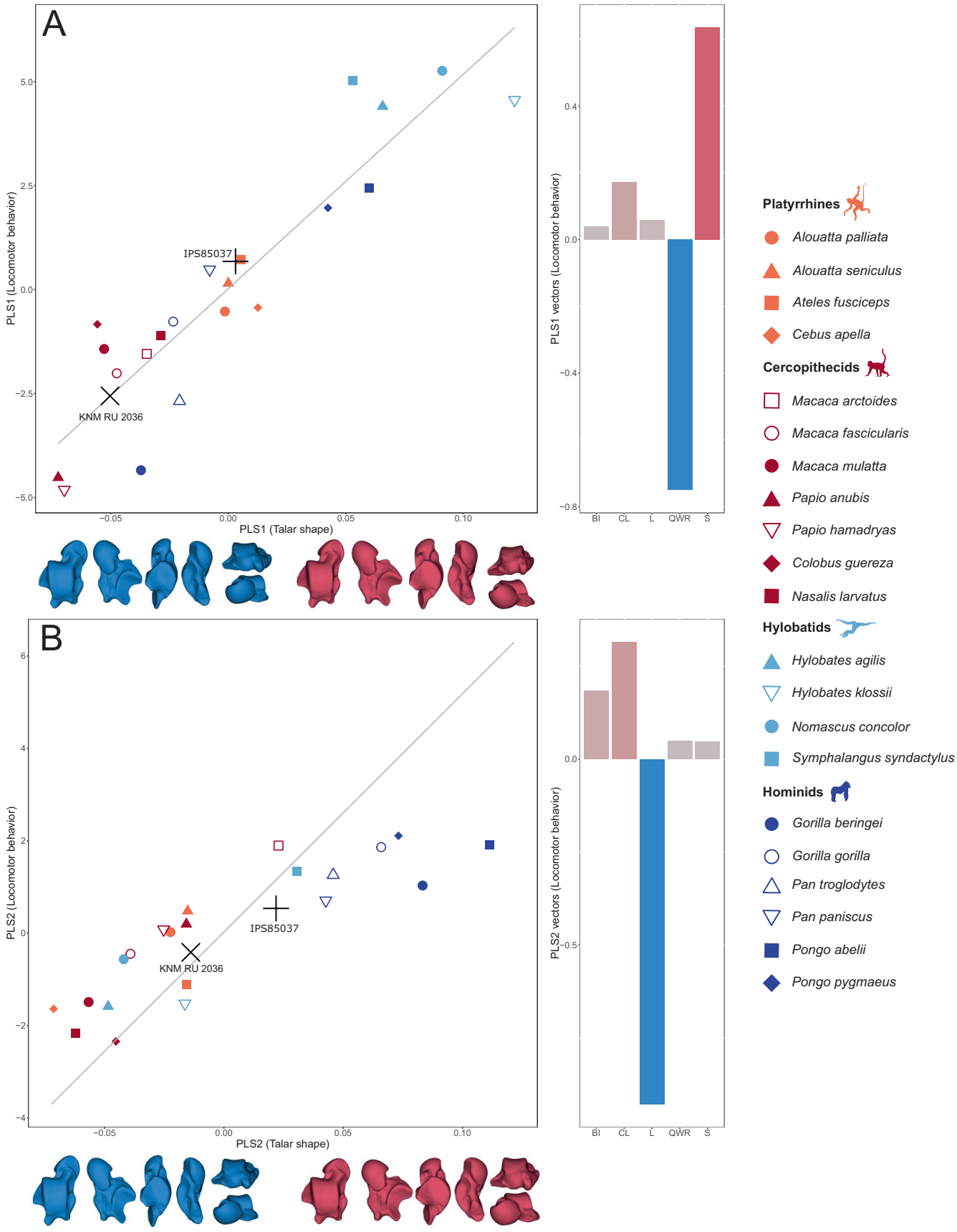


FIGURE 5 | Legend on next page.

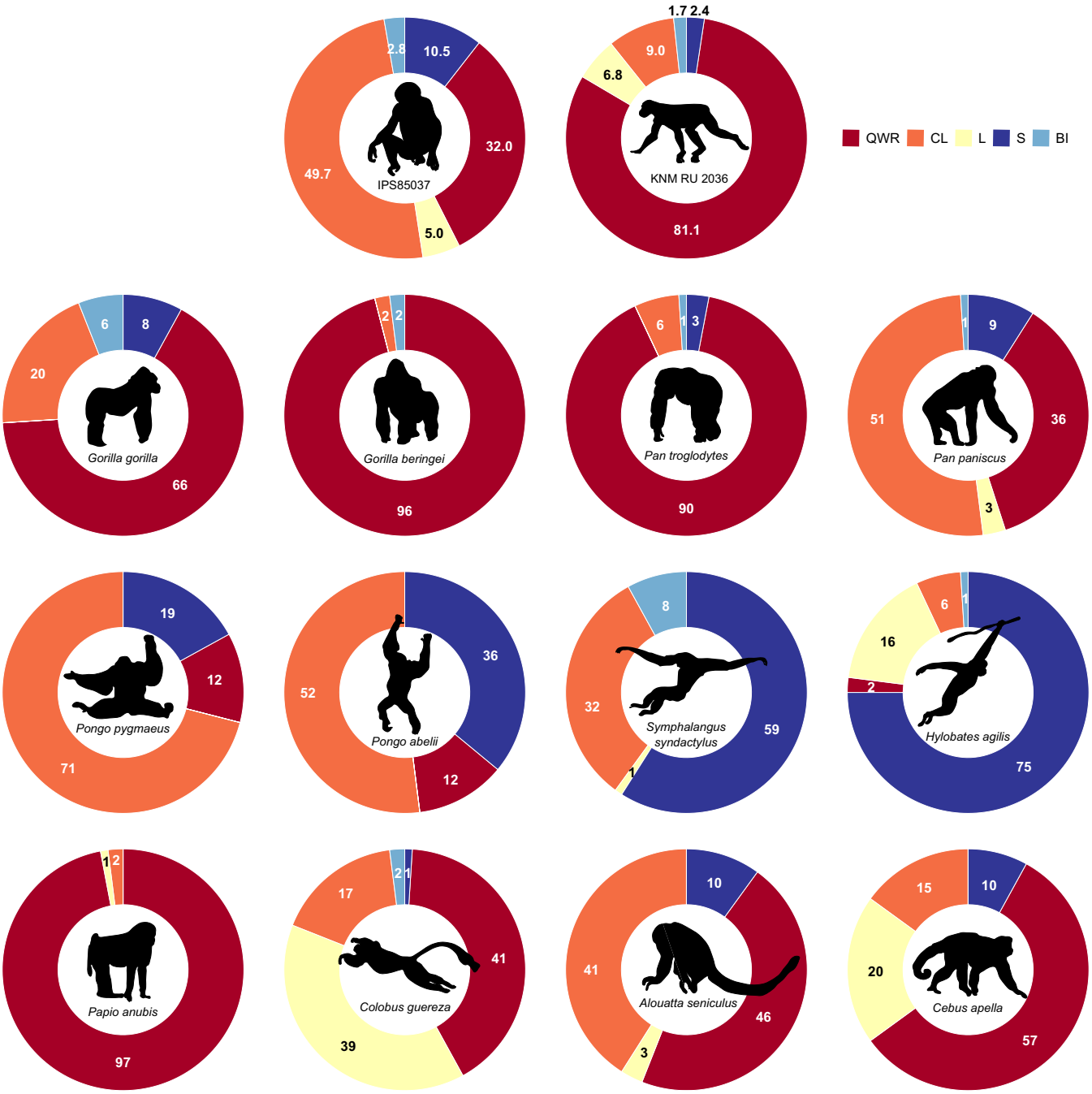


FIGURE 6 | Donut charts summarizing the estimated locomotor repertoires of the Dryopithecini indet (IPS85037) and *Ekembo heseloni* (KMN RU 2036), as well as representatives of the main anthropoid groups from the extant comparative sample (Table S6). BI = bipedal walking; CL = clambering, and vertical climbing; L = leaping, dropping, and hopping; QWR = quadrupedal walking, bounding, and running; S = bridging, brachiation, and suspensory locomotion.

FIGURE 5 | Results of the two-block partial least squares for the first (PLS1; A) and second (PLS2; B) set of linear combinations between the species-mean Procrustes-aligned coordinates quantified locomotor data. The vectors of the first (A) or second (B) PLS axis of the locomotor variables (LMPs) are plotted to the right of each scatterplot. The groups distinguished a priori are color-coded, and each species is denoted by different symbols, as indicated in the legend. Fossil specimens (whose scores are projected a posteriori) are indicated by a cross (×) sign (KMN RU 2036) and a plus (+) sign (IPS85037). Talar shape associated and magnified 3 times with minimum (blue) and maximum (red) values of covariation are plotted below each scatterplot (dorsal, plantar, lateral, medial, proximal, and distal views are shown, from left to right). Thin-plate spline warps are based on a talus of *Pan paniscus* (RMCA 27698). BI = bipedal walking; CL = clambering, and vertical climbing; L = leaping, dropping, and hopping; QWR = quadrupedal walking, bounding, and running; S = bridging, brachiation, and suspensory locomotion.

The PCA carried out on the locomotor percentages of the extant primate species distributes taxa according to their locomotor repertoire (Figure 7; Table S11). The first axis (PC1), which accounts for 41% of the total variance, discriminates quadrupedal species (platyrrhines, cercopithecoids, and African apes; most negative scores) from suspensory ones (orangutans and hylobatids; most positive scores). The second axis (PC2), which accounts for 26% of the total variance, separates those species with some leaping capabilities (including several platyrrhines, cercopithecoids and hylobatids, except for the larger-bodied siamangs; most positive scores) from those taxa with a more proclivity for climbing/clambering locomotion and lacking leaping behaviors (*Alouatta*, siamangs, and great apes; most negative scores). IPS85037 is projected closer to *Pan paniscus* and *Alouatta seniculus*, whereas the mainly quadrupedal locomotor repertoire estimated for KMN-RU 2036 overlaps with the more quadrupedal extant species.

TABLE 8 | Estimated locomotor percentages for IPS85037 and KMN RU 2036 using talar shape as a predictor.

	QWR	CL	L	S	BI
IPS85037	32.0	49.7	5.0	10.5	2.8
KNM RU 2036	81.1	9.0	6.8	2.4	1.7

Abbreviations: BI = bipedal walking; CL = clambering and vertical climbing; L = leaping, dropping, and hopping; QWR = quadrupedal walking, bounding, and running; S = bridging, brachiation, and suspensory locomotion.

4 | Discussion

4.1 | Body Size, Sex Assignment, and Taxonomic Attribution

The talus IPS85037 displays several modern hominoid-like features (such as a wedge-shaped trochlea, broader anteriorly than posteriorly, well-developed posterior tubercles, an only slightly concave depression for the medial malleolus, a relatively flat, elongate and obliquely oriented posterior calcaneal facet and a medially angled talar neck) despite an overall "monkey-like" appearance (Harrison 1982; Langdon 1986; Gebo 1989; Drapeau 2022). This fact, coupled with its large body size, supports its attribution to a dryopithecine instead of any of the small-bodied catarrhines (*Pliopithecus* and *Pliobates*) recorded at ACM (Alba, Moyà-Solà et al. 2010, 2012; Alba et al. 2015; Bouchet et al. 2024). The estimated BM IPS85037 (~38 kg) is close to the average BM of female orangutans (Smith and Jungers 1997) and only slightly lower than estimates previously derived for other Vallès-Penedès dryopithecines: ~43 kg for *P. catalaunicus* from ACM/BCV1 (~12.0 Ma; Alba et al. 2022), based on a lumbar vertebra of the male holotype individual (Susanna et al. 2014); ~44 kg for *D. fontani* from ACM/C3-Az (~11.9 Ma; Alba et al. 2022), based on an isolated femur (Moyà-Solà, Köhler, et al. 2009); and ~39–40 kg for the male skeleton of *Hispanopithecus laietanus* from Can Llobateres 2 (~9.6 Ma; Casanovas-Vilar, Garcés, et al. 2016), based on vertebral and femoral measurements (Moyà-Solà et al. 2004; Moyà-Solà,

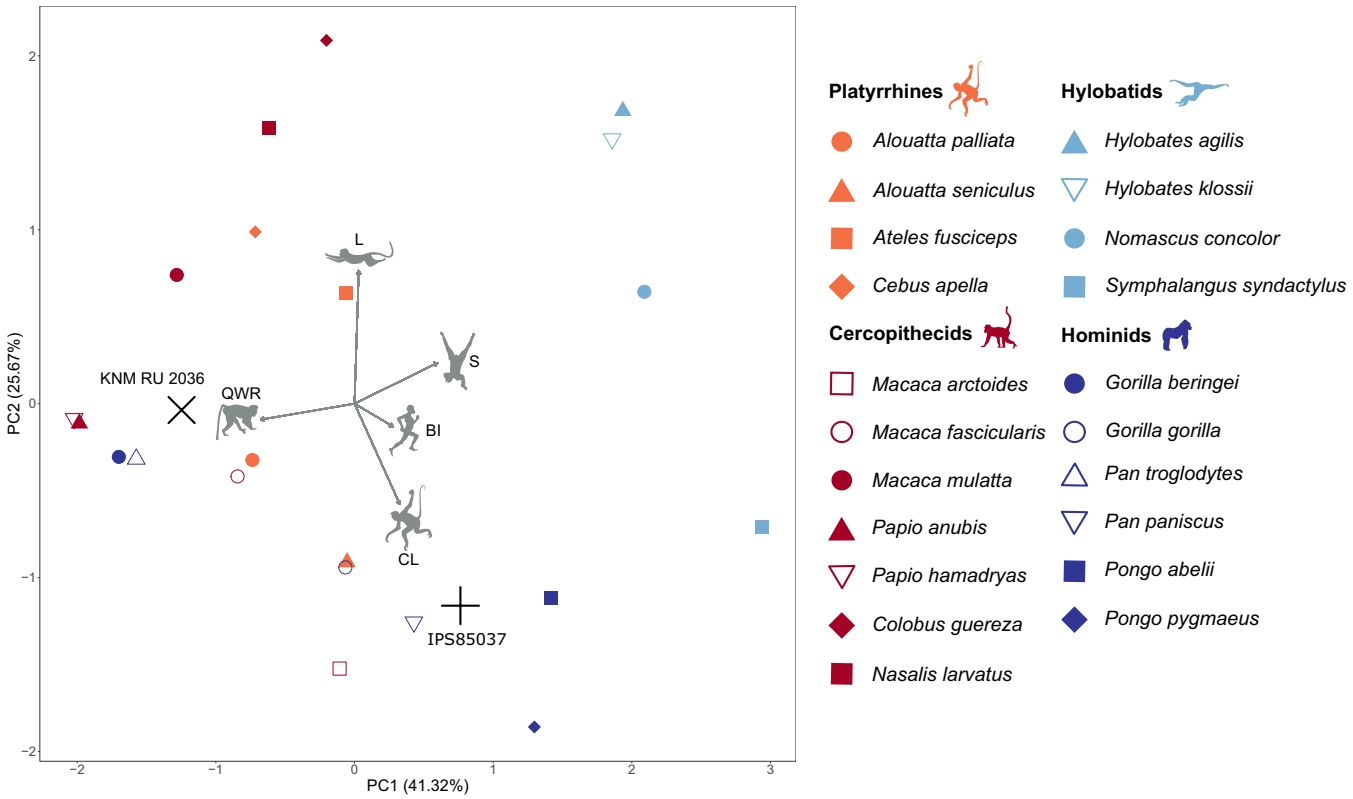


FIGURE 7 | Results of the principal components analysis (PCA) based on locomotor variables (LMPs) estimated for the fossil specimens as summarized by a bivariate plot of the first two PCs. The groups distinguished a priori are color-coded, and each species is denoted by different symbols, as indicated in the legend. Fossil specimens (whose scores are projected a posteriori) are indicated by a cross (×) sign (KMN RU 2036) and a plus (+) sign (IPS85037). The vectors of each locomotor variable are projected as gray arrows. BI = bipedal walking; CL = clambering and vertical climbing; L = leaping, droppping, and hopping; QWR = quadrupedal walking, bounding, and running; S = bridging, brachiation, and suspensory locomotion.

Köhler, et al. 2009; Susanna et al. 2014). These estimates indicate that Vallès-Penedès male dryopithecines were generally slightly smaller on average than extant male chimpanzees. Thus, although IPS85037 more closely resembles the average female body mass of orangutans, given the usually marked sexual size dimorphism of Miocene apes (Schrein 2006; Scott et al. 2009), roughly comparable to that of extant orangutans (with males about twice the size of females), attributing IPS85037 to a female individual would imply a BM of ~75 kg, much larger than previously recorded for any Vallès-Penedès hominoid. Therefore, based on the estimated BM, we conclude that IPS85037 most probably belonged to a male specimen.

With an estimated age of ~11.7 Ma, IPS85037 represents one of the two latest occurrences of dryopithecins at ACM, postdating the latest record of the small-bodied pliopithecid *Pliopithecus canmatensis*, and minimally predating that of the crouzeliid *Pliobates cataloniae* (Alba et al. 2017, 2022; DeMiguel et al. 2021). The lack of associated craniodental material, together with the fact that the talus is not recorded for any of the ACM dryopithecins, make it impossible to attempt a taxonomic assignment to genus rank. However, based on both body size (see above) and chronology, IPS85037 might belong to any of the dryopithecins recorded from slightly older deposits along the ACM stratigraphic sequence—*P. catalaunicus, A. brevirostris*, and *D. fontani* (Moyà-Solà et al. 2004; Moyà-Solà, Köhler, et al. 2009; Moyà-Solà, Alba, et al. 2009; Alba et al. 2013, 2020; Alba, Bouchet, et al. 2024)—which overall range from ~12.4 to 11.9 Ma (Alba et al. 2017, 2022). To our knowledge, IPS85037 is the first complete dryopithecine talus described in detail—the talus originally attributed to *Rudapithecus hungaricus* by Morbeck (1983) was subsequently reassigned to the pliopithecoid *Anapithecus* by Kordos and Begun (2001), while only an undescribed partial talus (RUD 135) is seemingly attributable to *R. hungaricus* (Begun 2002, 2009). For this reason, even if no genus attribution is warranted, the quantitative comparisons between IPS85037 and the tali of extant anthropoids and the stem hominoid *E. heseloni* (KMN-RU 2036), as well as the morphological comparisons with other recovered Miocene ape and stem catarrhine tali, provide invaluable insight into the locomotor repertoire of Miocene dryopithecines as well as for the evolution of crown-hominoid locomotion.

4.2 | Morphofunctional Inferences and Quantitative Comparisons With Extant Anthropoids

The morphology of IPS85037, as it is frequently the case of Miocene ape morphology (e.g., Moyà-Solà et al. 2004; Pugh et al. 2023), displays a mosaic of features that is unknown among extant anthropoids, combining an overall plesiomorphic appearance as compared with extant apes with some traits that more closely resemble the derived talar morphology of modern hominoids (Harrison 1982; Conroy and Rose 1983; Drapeau 2022). Among plesiomorphic traits, the possession of a dorsoplantarly high talar body along with a relatively deep trochlea suggests less conjunct rotation (adduction and abduction) at the talocrural joint during dorsi- and plantarflexion, indicating that the movement occurring at the upper ankle joint is mostly limited at the parasagittal plane (Langdon 1986; Ward 1998). Likewise, having an anteromedially L-shaped anterior calcaneal facet (resembling non-hominoid primates) has been associated with more limited inversion capabilities at the subtalar joint (Lewis 1980b)—contrasting with the crescent-shaped facet of extant hominoids, which has been related to increased inversion capabilities (Szalay and Langdon 1986).

Other features of IPS85037 that appear derived toward the crown hominoid condition are functionally related to high ranges of foot mobility and more powerful hallucal grasping (Langdon 1986; Drapeau 2022). For instance, IPS85037 resembles extant hominoids (particularly orangutans and hylobatids) in the possession of a more symmetrical trochlea, with a lateral rim that is only slightly dorsoplantarly higher than the medial one (Langdon 1986). The functional significance of this character is unclear, although it has been suggested that the presence of a prominent lateral rim might increase the amount of abduction accompanying the dorsiflexion of the foot (Strasser 1988). This, in turn, may be related to effective weight transfer during inversion and favor arboreal behavior, as concluded from studies performed in extant catarrhines (Turley and Frost 2013; Dunn et al. 2014; Knigge et al. 2015). However, it is noteworthy that this feature is more marked in terrestrial cercopithecines and African apes than in more arboreal cercopithecines, colobines, and Asian apes, suggesting a possible relationship with the use of terrestrial and/or larger horizontal substrates—as an adaptation for foot stabilization during walking and running, by limiting foot abduction and maintaining the foot in the parasagittal plane (Langdon 1986). The anterior widening of the trochlea in IPS85037 may be related to dorsiflexion during vertical climbing by facilitating the close packing of the talocrural joint as in extant great apes (Conroy and Rose 1983; Langdon 1986; DeSilva 2008, 2009). Posteriorly, the groove for the flexor hallucis longus tendon and the moderate development of the lateral (which serves as the attachment of the posterior talofibular ligament) and medial (which increases the load of the m. flexor hallucis longus) posterior tubercles are variably present among Miocene apes and stem catarrhine tali (Harrison 1982; Drapeau 2022). Judging by the depth of the groove and the moderate development of the lateral posterior tubercle, which acts as the insertion of the posterior talofibular ligament (an important ankle stabilizer during dorsiflexion; Leardini et al. 2000), IPS85037 is inferred to have possessed a powerful hallucal grasping, resembling extant African apes and suggesting frequent use of vertical climbing (DeSilva 2008). A strong hallucal grasp is inferred in other Miocene apes as well (Harrison 1982; Langdon 1986; Ward et al. 1993; Dunsworth 2006). On the medial side, IPS85037 displays only a slightly concave facet for articulation with the medial malleolus of the tibia that does not project medially, contrary to the close-packed configuration during dorsiflexion found in cercopithecoids (Le Gros Clark and Leakey 1951; Conroy and Rose 1983; Harrison 1986). This suggests an ankle adapted for withstanding large loadings during extreme dorsiflexion (DeSilva 2008). Similarly, the lack of a dorsal ridge on the talar neck, which is inferred to act as a locking mechanism for stopping the tibia during dorsiflexion, further indicates an ankle with a mobile talocrural joint (Le Gros Clark and Leakey 1951; Harrison 1982).

The possession of an elongated talar neck, normally considered the plesiomorphic condition for anthropoids, has been

hypothesized to be driven by allometric effects (Harrison 1982). However, this explanation does not apply to IPS85037, given its great ape-like BM. Orangutans also display a considerably elongated talar neck so that the talar head is projected further than the calcaneus, increasing the supination capability at the midtarsal joint during arboreal locomotion (Harrison 1982; Gebo 1989). The relatively deep groove for the flexor hallucis longus tendon in IPS85037 suggests that the calcaneus of the same individual, as in orangutans, was not distally elongated, implying a similarly high degree of midtarsal supination. In addition, the talar neck of IPS85037 also exhibits a very marked medial angulation, which is functionally related to the transmission of the compressive forces toward the medial side of the foot, occurring in arboreal animals with strong hallucal grasping (Barnett 1955; Harrison 1982). The spherical shape of the talar head in IPS85037 (similar to that of orangutans in size but somewhat smaller than that of cercopithecoids and African apes) and the great extent of the lateral side of the head (associated with better eversion capabilities of the forefoot) indicate that IPS85037 lacks the typical dorsal translation of the navicular observed in extant apes and would have been less capable of coping with large compressive forces than extant hominoids (Szalay and Langdon 1986; Meldrum and Wunderlich 1998). In turn, the posterior calcaneal facet, which is shallow and gently curved (resembling that of orangutans), indicates greater laxity and mobility at this joint, associated with better inversion capabilities at the subtalar joint (Gomberg 1981; Langdon 1986; Yapuncich and Granatosky 2021). Finally, IPS85037 exhibits a small divergence between the posterior calcaneal facet and the long axis of the trochlea, facilitating the screw motion of the talus at the level of the subtalar joint and enhancing the inversion of the foot (Conroy and Rose 1983).

The predicted LMPs for IPS85037 using the 2B-PLS regression models indicate a locomotor repertoire dominated by vertical climbing/clambering and quadrupedalism, with some degree of suspension. In contrast, the LMPs predicted for KMN RU 2036 indicate a very different locomotor repertoire, vastly dominated by quadrupedalism and with only small amounts of vertical climbing/clambering. These estimated percentages cannot be taken at face value because they are based on a single bone, although the errors computed for the extant species are not particularly large, indicating that the talus is a reliable predictor for locomotor behavior. Furthermore, the results for KMN RU 2036—which match the locomotor profile of some colobine monkeys and non-atelid platyrrhines (Youlatos and Meldrum 2011; Hunt 2016)—are consistent with previous locomotor inferences for *Ekembo* based on its postcranial morphology (Le Gros Clark 1952; Conroy and Rose 1983; Rose 1983, 1988; Gebo et al. 1988, 2009; Ward 1993, 1997; Ward et al. 1995; Walker 1997; Dunsworth 2006; DeSilva 2008). The combination of locomotor modes estimated for IPS85037 approaches that of two extant species: *Alouatta seniculus* and *Pan paniscus*. The former seems to be the species that exhibits the highest percentages of clambering/climbing among atelids (and platyrrhines in general; Youlatos and Meldrum 2011), which has been related to the diversity of habitats exploited by this species (including gallery forests and different types of shrub woodlands; Schön Ybarra and Schön 1987). In turn, bonobos are the most generalized great apes in terms of locomotion (Doran 1993; Isler 2002; Ramos 2014). This is reflected by their pedal anatomy, which combines features related to high foot mobility (e.g., comparatively subequal lateral and medial talar rims, slightly concave posterior calcaneal facet, mediolaterally broad anterior calcaneal facet) and propulsion (such as relatively large heel to provide lever arm; Vereecke et al. 2005; Friesen et al. 2024). Compared to orangutans, which exhibit a slow and cautious locomotion dominated by orthograde clambering and forelimb-dominated suspension (Cant 1987; Manduell et al. 2011), bonobos engage much less frequently in suspensory behaviors and equally divide their time between the forest floor and the arboreal canopy (Ramos 2014). Similarly, to chimpanzees and gorillas, bonobos spend a great amount of their time on the ground, habitually moving quadrupedally using knuckle-walking, which is an unlikely behavior for IPS85037 based on the hand morphology of dryopithecines (Almécija et al. 2009; Alba, Almécija, et al. 2010). However, bonobos also engage in more arboreal quadrupedalism than chimpanzees, being primarily palmigrade (Doran 1993), a type of locomotor mode that was likely used by most Miocene apes to varying degrees (Rose 1994; Almécija et al. 2007, 2021, 2009; Alba, Almécija, et al. 2010, 2012; Alba 2012; Ward 2015). Moreover, the morphology of several pedal elements of bonobos (including the talus and the medial cuneiform) suggests that they possess a greater range of hallucal abduction compared to other African apes, offering an advantage for maintaining strong pedal grips while climbing more varied and smaller arboreal substrates (Friesen et al. 2024). Remarkably, some talar features of bonobos, providing them with greater versatility at the ankle and subtalar joints (such as the even lateral and medial trochlear rims and the slightly concave posterior calcaneal facet), are also present in IPS85037.

4.3 | Implications for the Evolution of Crown Hominoid Positional Behaviors

The feet of extant apes display increased mobility and prehensility as compared with those of other living anthropoids, in agreement with the more varied and non-stereotypical locomotor behaviors of the former, which may be interpreted as an adaptation for navigating across precarious and unpredictably oriented arboreal substrates (Conroy and Rose 1983; Hunt 1991, 2016; DeSilva 2008; Drapeau 2022). In accordance with this, extant ape tali are distinguished by numerous adaptations related to enhanced stability during inversion and dorsiflexion, accommodating the foot into different positions and providing strong anchorage to the substrate (Conroy and Rose 1983; Langdon 1986; Strasser 1988; Gebo 1989; Parr et al. 2014; Drapeau 2022). However, almost all recovered tali of different groups of Miocene apes and stem catarrhines (pliopithecoids and dendropithecids) lack evidence of a specialized modern hominoid-like derived morphology and, in most cases, exhibit remarkable morphological uniformity (Harrison 1982; Conroy and Rose 1983; Rose 1994; Drapeau 2022).

Talar morphology of stem catarrhines (e.g., pliopithecoids and dendropithecids) evinces a foot more adapted to stable dorsiflexion and inversion than earlier stem anthropoids (such as parapithecoids, oligopithecids, and propliopithecoids; Fleagle 1980; Fleagle and Simons 1983, 1995; Gebo and Simons 1987; Seiffert and Simons 2001) and extant cercopithecoids and non-suspensory platyrrhines, as indicated by the possession of a mediolaterally

broad talar head, although they still retain an overall plesiomorphic appearance, exemplified by their trochlear proportions, lack of lateral flaring of the fibular facet, and proximodistally elongated talar neck (Le Gros Clark and Thomas 1951; Harrison 1982; Rose et al. 1992). Consequently, they are reconstructed as arboreal quadrupeds with, in some cases, moderate climbing and suspensory capabilities, resembling extant atelids in some respects (Harrison 1982; Sarmiento 1983; Rose 1988, 1994; Rose et al. 1992; Alba et al. 2015; Arias-Martorell et al. 2015; Arias-Martorell et al. 2021). Stem hominoids overall still display a very plesiomorphic talar morphology, although they already exhibit some other derived hominoid-like features (e.g., a fibular facet that flares more laterally), indicating a foot better adapted for grasping supports in a greater variety of positions than earlier stem catarrhines (Conroy and Rose 1983; Walker 1997; Dunsworth 2006). For instance, proconsulids (*Proconsul* and *Ekembo*), despite their vastly disparate range of BM (from *Pr. africanus* and *E. heseloni*, estimated between 9 and 15 kg, to *Pr. major*, with a body mass around 60–90 kg, comparable to a female *Gorilla*; Harrison 1982; Rafferty et al. 1995), are reconstructed as primarily arboreal quadrupeds that engaged in some climbing and pronograde clambering, assisted by a strong hallux adapted to powerful grasping (Walker 1997; Ward 2015). Our estimated locomotor percentages for KMN RU 2036 (*E. heseloni*) are consistent with this view, obtaining a locomotor repertoire with a large quadrupedal component, little (but not insignificant) climbing and clambering, and a lack of suspensory behaviors. Only the largest species, *Pr. major*, exhibits some talar features (e.g., deep groove for the flexor hallucis longus, developed lateral and medial posterior tubercles), as well as other postcranial adaptations, suggesting a higher proclivity for vertical climbing and other antipronograde behaviors (DeSilva 2008). Other stem hominoids, such as the afropithecids *Eq. africanus* and *N. kerioi*, provide further evidence that a broad plesiomorphic appearance, except for some derived hominoid-like features (e.g., fibular facet that flares more laterally, mediolaterally expanded talar head), characterized ape talar morphology during the Early/Middle Miocene (McCrossin 1994; Rose et al. 1996; Ishida et al. 2004; Nakatsukasa et al. 2012).

Compared to earlier Miocene ape and stem catarrhine tali, IPS85037 appears to be more derived toward the extant hominoid condition in features associated with greater mobility at the talocrural joint (a relatively wedged trochlea, subequal talar rims, the lack of a dorsal tubercle on the neck, a less concave articular basin for the medial tibial malleolus), subtalar joint (a slightly angled, proximodistally elongated and shallow posterior calcaneal facet), and greater prehensility (a deep groove for the m. flexor hallucis longus tendon, a developed and prominent lateral posterior tubercle, and a medially angled talar neck). However, the overall gracile appearance of IPS85037, emphasized by the relatively elongated neck and the small head, as well as several plesiomorphic features (relatively deep trochlear groove, an L-shaped anteromedially located anterior calcaneal facet, a laterally extended articular facet for the navicular on the talar head) reveal that, independently of the acquisition of an orthograde body plan and a more forelimb-dominated locomotion, the structure of the foot remained relatively generalized during most of hominoid evolution, with only changes for increased mobility and stronger hallucal grasping but lacking clear-cut adaptations for suspensory behavior. A similar mosaic pattern is observed in the slightly younger stem pongine *Si. sivalensis*, revealing that the talocrural and subtalar joints had more limited inversion/eversion capabilities than in extant hominoids, but greater than in cercopithecoids (Pilbeam et al. 1980; Madar 1996). In contrast, the Late Miocene stem hominoid *O. bambolii* exhibits a uniquely derived hominoid-like talar morphology among Miocene apes (Szalay and Langdon 1986), which, together with other postcranial adaptations, has been associated with a wide array of antipronograde behaviors, including vertical climbing and suspension (Jungers 1987; Russo and Shapiro 2013; Hammond et al. 2020).

The mosaic morphology of IPS85037 concurs with the pattern combining plesiomorphic and crown hominoid-like derived traits exhibited by other anatomical regions attributed to the Vallès-Penedès dryopithecines, particularly *Pierolapithecus* (Moyà-Solà et al. 2004, 2005; Almécija et al. 2009; Alba, Almécija, et al. 2010; Hammond et al. 2013; Pina et al. 2014; Pina et al. 2020) and *Dryopithecus* (Moyà-Solà, Köhler, et al. 2009; Alba et al. 2011; Almécija et al. 2012; Pina et al. 2019), but also to a lesser extent *Hispanopithecus* (Moyà-Solà and Köhler 1996; Almécija et al. 2007; Alba, Almécija, et al. 2012; Tallman et al. 2013; Susanna et al. 2014). Regardless of the exact phylogenetic position of dryopithecines, either as stem hominids (Andrews 1992; Casanovas-Vilar et al. 2011; Alba 2012; Alba et al. 2015; Pugh 2022) or more closely related to pongines (Moyà-Solà and Köhler 1993, 1995, 1996; Agustí et al. 1996) or hominines (Begun 2002, 2009, 2015, 2018; Begun et al. 2012), the morphology and estimated locomotor repertoire of IPS85037 reinforce the numerous evidence (e.g., Tuttle 1975; Larson 1998; Alba 2012; Almécija et al. 2021) that adaptations for suspensory locomotion and an orthograde body plan did not evolve at the same time, but rather were acquired independently in different lineages during hominoid evolution.

5 | Conclusions

An isolated primate talus (IPS85037) from ACM dated to ~11.7 Ma (close to the Middle/Late Miocene boundary) is described and compared with a sample of extant anthropoids as well as the stem hominoid *E. heseloni* (KMN RU 2036). Body mass estimates based on talar size (close to a female orangutan) and the possession of some derived modern hominoid features suggest that the specimen belongs to a male dryopithecine, but an attribution to genus rank is precluded by the lack of comparative material. Talar shape, quantified by means of 3DGM, indicates that IPS85037 displays a mosaic of plesiomorphic and apomorphic features relative to crown hominoids, unknown among modern anthropoids but resembling other Miocene ape tali. Compared to KMN RU 2036, IPS85037 presents several characters associated with relatively more mobile talocrural and subtalar joints and evidence of strong hallucal grasping. This is confirmed by the locomotor repertoire inferred from the covariation between talar shape and locomotor percentages, which indicate important quadrupedal and clambering/climbing components but much more restricted suspensory behaviors. Within extant species, *Alouatta seniculus* and *Pan paniscus* concur the most with this locomotor repertoire. In contrast, locomotor estimations based on KMN RU 2036 shape indicate a locomotor repertoire vastly dominated by quadrupedalism, resembling extant

cercopithecoids. Both the morphology and locomotor repertoire inferred for IPS85037 are broadly consistent with previous inferences for the Middle Miocene dryopithecins *Pierolapithecus* and, to a lesser extent, *Dryopithecus* but differ from the greater emphasis on suspensory behaviors displayed by the younger hispanopithecins *Hispanopithecus*, *Danuvius*, and *Rudapithecus*.

Author Contributions

Oriol Monclús-Gonzalo: conceptualization (equal), formal analysis (lead), investigation (lead), methodology (supporting), writing – original draft (lead), writing – review and editing (supporting). **Shubham Pal:** formal analysis (supporting), investigation (supporting), writing – original draft (supporting). **Thomas A. Püschel:** methodology (lead), writing – review and editing (supporting). **Alessandro Urciuoli:** methodology (supporting), writing – review and editing (supporting). **Víctor Vinuesa:** data curation (supporting), methodology (supporting). **Josep M. Robles:** data curation (lead). **Sergio Almécija:** conceptualization (equal), data curation (equal), methodology (supporting), resources (lead), supervision (supporting), writing – review and editing (supporting). **David M. Alba:** conceptualization (equal), funding acquisition (lead), supervision (lead), writing – original draft (supporting), writing – review and editing (lead).

Acknowledgments

Fieldwork at ACM was defrayed by CESPA Gestión de Residuos, SAU. We thank Sergio Llácer (ICP) for assistance with 3D scanning of the described fossil specimen, Alejandro Serrano-Martínez for uploading the 3D models to MorphoSource, Júlia Arias-Martorell and Georgina Raventós-Izard for collaboration in the inter-observer repeatability test, and Eileen Westwig (AMNH) for access to extant comparative material. We further acknowledge the collaboration of the Centre de Restauració i Interpretació Paleontològica (Ajuntament dels Hostalets de Pierola) and the Servei d'Arqueologia i Paleontologia of the Generalitat de Catalunya. This article is part of the Ph.D. dissertation of O.M.G. within the Geology Ph.D. Program of the Universitat Autònoma de Barcelona.

Data Availability Statement

The described original fossil is available for study from the ICP, which is a registered museums recognized by the Generalitat de Catalunya, while its digital 3D model is available from MorphoSouce (https://doi.org/10.17602/M2/M713734). 3D landmark coordinates used in this study are openly available in figshare (https://figshare.com/s/fcc3e39fee03117ed06f).

References

Adams, D. C., and E. Otárola-Castillo. 2013. "Geomorph: An R Package for the Collection and Analysis of Geometric Morphometric Shape Data." *Methods in Ecology and Evolution* 4, no. 4: 393–399. https://doi.org/10.1111/2041-210X.12035.

Adler, D., and D. Murdoch. 2020. "Rgl: 3D Visualization Using openGL." https://github.com/dmurdoch/rgl. https://dmurdoch.github.io/rgl/.

Agustí, J., M. Köhler, S. Moyà-Solà, L. Cabrera, M. Garcés, and J. M. Parés. 1996. "Can Llobateres: The Pattern and Timing of the Vallesian Hominoid Radiation Reconsidered." *Journal of Human Evolution* 31, no. 2: 143–155. https://doi.org/10.1006/jhev.1996.0055.

Alba, D. M. 2012. "Fossil Apes From the Vallès-Penedès Basin." *Evolutionary Anthropology* 21: 254–269. https://doi.org/10.1002/evan.21312.

Alba, D. M., S. Almécija, I. Casanovas-Vilar, J. M. Méndez, and S. Moyà-Solà. 2012. "A Partial Skeleton of the Fossil Great Ape *Hispanopithecus laietanus* From Can Feu and the Mosaic Evolution of Crown-Hominoid Positional Behaviors." *PLoS One* 7: e39617. https://doi.org/10.1371/journal.pone.0039617.

Alba, D. M., S. Almécija, D. DeMiguel, et al. 2015. "Miocene Small-Bodied Ape From Eurasia Sheds Light on Hominoid Evolution." *Science* 350: aab2625. https://doi.org/10.1126/science.aab2625.

Alba, D. M., S. Almécija, and S. Moyà-Solà. 2010. "Locomotor Inferences in *Pierolapithecus* and *Hispanopithecus*: Reply to Deane and Begun (2008)." *Journal of Human Evolution* 59: 143–149. https://doi.org/10.1016/j.jhevol.2010.02.002.

Alba, D. M., F. Bouchet, J. Fortuny, et al. 2024. "New Remains of the Miocene Great Ape *Anoiapithecus brevirostris* From Abocador de Can Mata." *Journal of Human Evolution* 188: 103497. https://doi.org/10.1016/j.jhevol.2024.103497.

Alba, D. M., I. Casanovas-Vilar, M. Garcés, and J. M. Robles. 2017. "Ten Years in the Dump: An Updated Review of the Miocene Primate-Bearing Localities From Abocador de Can Mata (NE Iberian Peninsula)." *Journal of Human Evolution* 102: 12–20. https://doi.org/10.1016/j.jhevol.2016.09.012.

Alba, D. M., E. Delson, G. Carnevale, et al. 2014. "First Joint Record of *Mesopithecus* and cf. *Macaca* in the Miocene of Europe." *Journal of Human Evolution* 67: 1–18. https://doi.org/10.1016/j.jhevol.2013.11.001.

Alba, D. M., J. Fortuny, M. Pérez de los Ríos, et al. 2013. "New Dental Remains of *Anoiapithecus* and the First Appearance Datum of Hominoids in the Iberian Peninsula." *Journal of Human Evolution* 65: 573–584. https://doi.org/10.1016/j.jhevol.2013.07.003.

Alba, D. M., J. Fortuny, J. M. Robles, et al. 2020. "A New Dryopithecine Mandibular Fragment From the Middle Miocene of Abocador de Can Mata and the Taxonomic Status of '*Sivapithecus*' *occidentalis* From Can Vila (Vallès-Penedès Basin, NE Iberian Peninsula)." *Journal of Human Evolution* 145: 102790. https://doi.org/10.1016/j.jhevol.2020.102790.

Alba, D. M., and S. Moyà-Solà. 2012. "On the Identity of a Hominoid Male Upper Canine From the Vallès-Penedès Basin Figured by Pickford (2012)." *Estudios Geológicos* 68: 149–153. https://doi.org/10.3989/egeol.40900.180.

Alba, D. M., S. Moyà-Solà, and S. Almécija. 2011. "A Partial Hominoid Humerus From the Middle Miocene of Castell de Barberà (Vallès-Penedès Basin, Catalonia, Spain)." *American Journal of Physical Anthropology* 144: 365–381. https://doi.org/10.1002/ajpa.21417.

Alba, D. M., S. Moyà-Solà, I. Casanovas-Vilar, et al. 2006. "Los Vertebrados Fósiles del Abocador de Can Mata (els Hostalets de Pierola, l'Anoia, Cataluña), una Sucesión de Localidades del Aragoniense Superior (MN6 y MN7+8) de la Cuenca del Vallès-Penedès. Campañas 2002–2003, 2004 Y 2005." *Estudios Geológicos* 62, no. 1: 295–312. https://doi.org/10.3989/egeol.0662127.

Alba, D. M., S. Moyà-Solà, A. Malgosa, et al. 2010. "A New Species of *Pliopithecus* Gervais, 1849 (Primates: Pliopithecidae) From the Middle Miocene (MN8) of Abocador de Can Mata (Els Hostalets de Pierola, Catalonia, Spain)." *American Journal of Physical Anthropology* 141, no. 1: 52–75. https://doi.org/10.1002/ajpa.21114.

Alba, D. M., S. Moyà-Solà, J. M. Robles, and J. Galindo. 2012. "Brief Communication: The Oldest Pliopithecid Record in the Iberian Peninsula Based on New Material From the Vallès-Penedès Basin." *American Journal of Physical Anthropology* 147: 135–140. https://doi.org/10.1002/ajpa.21631.

Alba, D. M., J. M. Robles, I. Casanovas-Vilar, et al. 2022. "A Revised (Earliest Vallesian) age for the Hominoid-Bearing Locality of Can Mata 1 Based on New Magnetostratigraphic and Biostratigraphic Data From Abocador de Can Mata (Vallès-Penedès Basin, NE Iberian Peninsula)." *Journal of Human Evolution* 170: 103237. https://doi.org/10.1016/j.jhevol.2022.103237.

Alba, D. M., A. Urciuoli, A. S. Hammond, S. Almécija, L. Rook, and C. Zanolli. 2024. "Miocene Ape Evolution: Where Does *Oreopithecus* Fit

in?" *Bollettino della Societa Paleontologica Italiana* 63, no. 2: 153–182. https://doi.org/10.4435/BSPI.2024.01.

Almécija, S., D. M. Alba, and S. Moya-Sola. 2009. "*Pierolapithecus* and the Functional Morphology of Miocene Ape Hand Phalanges: Paleobiological and Evolutionary Implications." *Journal of Human Evolution* 57: 284–297. https://doi.org/10.1016/j.jhevol.2009.02.008.

Almécija, S., D. M. Alba, and S. Moyà-Solà. 2012. "The Thumb of Miocene Apes: New Insights From Castell de Barberà (Catalonia, Spain)." *American Journal of Physical Anthropology* 148: 436–450. https://doi.org/10.1002/ajpa.22071.

Almécija, S., D. M. Alba, S. Moyà-Solà, and M. Köhler. 2007. "Orang-Like Manual Adaptations in the Fossil Hominoid *Hispanopithecus laietanus*: First Steps Towards Great Ape Suspensory Behaviours." *Proceedings. Biological Sciences* 274, no. 1624: 2375–2384. https://doi.org/10.1098/rspb.2007.0750.

Almécija, S., A. S. Hammond, N. E. Thompson, K. D. Pugh, S. Moyà-Solà, and D. M. Alba. 2021. "Fossil Apes and Human Evolution." *Science* 372, no. 6542: eabb4363. https://doi.org/10.1126/science.abb4363.

Almécija, S., C. M. Orr, M. W. Tocheri, B. A. Patel, and W. L. Jungers. 2015. "Exploring Phylogenetic and Functional Signals in Complex Morphologies: The Hamate of Extant Anthropoids as a Test-Case Study." *Anatomical Record* 298: 212–229. https://doi.org/10.1002/ar.23079.

Andrews, P. 1992. "Evolution and Environment in the Hominoidea." *Nature* 360: 641–646. https://doi.org/10.1038/360641a0.

Archer, W., C. M. Pop, Z. Rezek, et al. 2018. "A Geometric Morphometric Relationship Predicts Stone Flake Shape and Size Variability." *Archaeological and Anthropological Sciences* 10: 1991–2003. https://doi.org/10.1007/s12520-017-0517-2.

Arias-Martorell, J., D. M. Alba, J. M. Potau, G. Bello-Hellegouarch, and A. Pérez-Pérez. 2015. "Morphological Affinities of the Proximal Humerus of *Epipliopithecus vindobonensis* and *Pliopithecus antiquus*: Suspensory Inferences Based on a 3D Geometric Morphometrics Approach." *Journal of Human Evolution* 80: 83–95. https://doi.org/10.1016/j.jhevol.2014.08.012.

Arias-Martorell, J., S. Almécija, A. Urciuoli, M. Nakatsukasa, S. Moyà-Solà, and D. M. Alba. 2021. "A Proximal Radius of *Barberapithecus huerzeleri* From Castell de Barberà: Implications for Locomotor Diversity Among Pliopithecoids." *Journal of Human Evolution* 157: 103032. https://doi.org/10.1016/j.jhevol.2021.103032.

Barnett, C. H. 1955. "Some Factors Influencing Angulation of the Neck of the Mammalian Talus." *Journal of Anatomy* 89: 225–230.

Bastir, M., N. Torres-Tamayo, C. A. Palancar, et al. 2019. "Geometric Morphometric Studies in the Human Spine." In *Spinal Evolution*, edited by E. Been, A. Gómez-Olivencia, and P. A. Kramer, 361–386. Springer. https://doi.org/10.1007/978-3-030-19349-2_16.

Begun, D. R. 1987. "A Review of the Genus *Dryopithecus*" (PhD diss., University of Pennsylvania).

Begun, D. R. 2002. "European Hominoids." In *The Primate Fossil Record*, edited by W. C. Hartwig, 339–368. Cambridge University Press.

Begun, D. R. 2009. "Dryopithecins, Darwin, de Bonis, and the European Origin of the African Apes and Human Clade." *Geodiversitas* 31: 789–816. https://doi.org/10.5252/g2009n4a789.

Begun, D. R. 2015. "Fossil Record of Miocene Hominoids." In *Handbook of Paleoanthropology*, edited by W. Henke and I. Tattersall, 1261–1332. Springer. https://doi.org/10.1007/978-3-642-39979-4_32.

Begun, D. R. 2018. "*Dryopithecus*." In *The International Encyclopedia of Biological Anthropology*, edited by W. Trevathan. John Wiley and Sons. https://doi.org/10.1002/9781118584538.ieba0143.

Begun, D. R., M. C. Nargolwalla, and L. Kordos. 2012. "European Miocene Hominids and the Origin of the African Ape and Human Clade." *Evolutionary Anthropology* 21: 10–23. https://doi.org/10.1002/evan.20329.

Begun, D. R., and C. V. Ward. 2005. "Comment on '*Pierolapithecus catalaunicus*, a New Middle Miocene Great Ape From Spain'." *Science* 208: 203c. https://doi.org/10.1126/science.1108139.

Böhme, M., N. Spassov, J. Fuss, et al. 2019. "A New Miocene Ape and Locomotion in the Ancestor of Great Apes and Humans." *Nature* 575: 489–493. https://doi.org/10.1038/s41586-019-1731-0.

Bookstein, F. L. 2019. "Pathologies of Between-Groups Principal Components Analysis in Geometric Morphometrics." *Evolutionary Biology* 46: 271–302. https://doi.org/10.1007/s11692-019-09484-8.

Bouchet, F., C. Zanolli, A. Urciuoli, et al. 2024. "The Miocene Primate *Pliobates* Is a Pliopithecoid." *Nature Communications* 15: 2822. https://doi.org/10.1038/s41467-024-47034-9.

Cant, J. G. 1987. "Positional Behavior of Female Bornean Orangutans (*Pongo pygmaeus*)." *American Journal of Primatology* 12: 71–90. https://doi.org/10.1002/ajp.1350120104.

Cardini, A., P. O'Higgins, and F. J. Rohlf. 2019. "Seeing Distinct Groups Where There Are None: Spurious Patterns From Between-Group PCA." *Evolutionary Biology* 46, no. 4: 303–316. https://doi.org/10.1007/s11692-019-09487-5.

Cardini, A., and P. D. Polly. 2020. "Cross-Validated Between Group PCA Scatterplots: A Solution to Spurious Group Separation?" *Evolutionary Biology* 47, no. 1: 85–95. https://doi.org/10.1007/s11692-020-09494-x.

Casanovas-Vilar, I., D. M. Alba, M. Garcés, J. M. Robles, and S. Moyà-Solà. 2011. "Updated Chronology for the Miocene Hominoid Radiation in Western Eurasia." *Proceedings of the National Academy of Sciences* 108: 5554–5559. https://doi.org/10.1073/pnas.1018562108.

Casanovas-Vilar, I., M. Garcés, J. A. van Dam, I. García Paredes, J. M. Robles, and D. M. Alba. 2016. "An Updated Biostratigraphy for the Late Aragonian and the Vallesian of the Vallès-Penedès Basin (Catalonia)." *Geologica Acta* 14: 195–217. https://doi.org/10.1344/GeologicaActa2016.14.3.1.

Casanovas-Vilar, I., S. Jovells-Vaqué, and D. M. Alba. 2022. "The Miocene High-Resolution Record of the Vallès-Penedès Basin (Catalonia)." In *NOW 25th Anniversary Meeting. Sabadell (Barcelona), 16–18 November 2022*, edited by I. Casanovas-Vilar and D. M. Alba, 79–122. Abstract Book & Fieldtrip Guide. Paleontol. Evol., Memòria Especial.

Casanovas-Vilar, I., A. Madern, D. M. Alba, et al. 2016. "The Miocene Mammal Record of the Vallès-Penedès Basin (Catalonia)." *Comptes Rendus Palevol* 15: 791–812. https://doi.org/10.1016/j.crpv.2015.07.004.

Collyer, M. L., and D. C. Adams. 2018. "RRPP: An R Package for Fitting Linear Models to High-Dimensional Data Using Residual Randomization." *Methods in Ecology and Evolution* 9, no. 7: 1772–1779. https://doi.org/10.1111/2041-210X.13029.

Conroy, G. C., and M. D. Rose. 1983. "The Evolution of the Primate Foot From the Earliest Primates to the Miocene Hominoids." *Foot & Ankle* 3: 342–364. https://doi.org/10.1177/107110078300300604.

Cramer, J. S. 2003. "The Origins and Developments of the Logit Model." In *Logit Models From Economics and Other Fields*, edited by J. S. Cramer, 149–158. Cambridge University Press. https://doi.org/10.1017/CBO9780511615412.010.

Culhane, A. C., G. Perriere, E. C. Considine, T. G. Cotter, and D. G. Higgins. 2002. "Between-Group Analysis of Microarray Data." *Bioinformatics* 18: 1600–1608. https://doi.org/10.1093/bioinformatics/18.12.1600.

Day, M. H., and B. A. Wood. 1968. "Functional Affinities of the Olduvai Hominid 8 Talus." *Man* 3, no. 3: 440–455. https://doi.org/10.2307/2798879.

Day, M. H., and B. A. Wood. 1969. "Hominoid Tali From East Africa." *Nature* 222: 591–592. https://doi.org/10.1038/222591a0.

Deane, A. S., and D. R. Begun. 2008. "Broken Fingers: Retesting Locomotor Hypotheses for Fossil Hominoids Using Fragmentary Proximal Phalanges and High-Resolution Polynomial Curve Fitting (HR-PCF)." *Journal of Human Evolution* 55: 691–701. https://doi.org/10.1016/j.jhevol.2008.05.005.

Deane, A. S., and D. R. Begun. 2010. "*Pierolapithecus* Locomotor Adaptations: A Reply to Alba et al.'s Comment on Deane and Begun (2008)." *Journal of Human Evolution* 59: 150–154. https://doi.org/10.1016/j.jhevol.2010.04.003.

DeMiguel, D., L. Domingo, I. M. Sánchez, I. Casanovas-Vilar, J. M. Robles, and D. M. Alba. 2021. "Palaeoecological Differences Underlie Rare Co-Occurrence of Miocene European Primates." *BMC Biology* 19: 6. https://doi.org/10.1186/s12915-020-00939-5.

DeSilva, J. M. 2008. "Vertical Climbing Adaptations in the Anthropoid Ankle and Midfoot: Implications for Locomotion in Miocene Catarrhines and Plio-Pleistocene Hominins" (PhD diss., University of Michigan).

DeSilva, J. M. 2009. "Functional Morphology of the Ankle and the Likelihood of Climbing in Early Hominins." *Proceedings of the National Academy of Sciences* 106: 6567–6572. https://doi.org/10.1073/pnas.0900270106.

Doran, D. M. 1993. "Comparative Locomotor Behavior of Chimpanzees and Bonobos: The Influence of Morphology on Locomotion." *American Journal of Physical Anthropology* 91: 83–98. https://doi.org/10.1002/ajpa.1330910106.

Drapeau, M. 2022. "Miocene Ape Feet." In *The Evolution of the Primate Foot*, edited by A. Zeininger, K. G. Hatala, R. E. Wunderlich, and D. Schmitt, 321–359. Springer. https://doi.org/10.1007/978-3-031-06436-4_13.

Dunn, R. H., M. W. Tocheri, C. M. Orr, and W. L. Jungers. 2014. "Ecological Divergence and Talar Morphology in Gorillas." *American Journal of Physical Anthropology* 153: 526–541. https://doi.org/10.1002/ajpa.22451.

Dunsworth, H. M. 2006. "*Proconsul heseloni* Feet From Rusinga Island, Kenya" (PhD diss., Pennsylvania State University).

Fabre, A. C., M. C. Granatosky, J. B. Hanna, and D. Schmitt. 2018. "Do Forelimb Shape and Peak Forces Co-Vary in Strepsirrhines?" *American Journal of Physical Anthropology* 167: 602–614. https://doi.org/10.1002/ajpa.23688.

Fabre, A. C., J. Marigó, M. C. Granatosky, and D. Schmitt. 2017. "Functional Associations Between Support Use and Forelimb Shape in Strepsirrhines and Their Relevance to Inferring Locomotor Behavior in Early Primates." *Journal of Human Evolution* 108: 11–30. https://doi.org/10.1016/j.jhevol.2017.03.012.

Fabre, A. C., L. Peckre, E. Pouydebat, and C. E. Wall. 2019. "Does the Shape of Forelimb Long Bones Co-Vary With Grasping Behaviour in Strepsirrhine Primates?" *Biological Journal of the Linnean Society* 127: 649–660. https://doi.org/10.1093/biolinnean/bly188.

Fleagle, J. G. 1980. "Locomotor Behavior of the Earliest Anthropoids: A Review of the Current Evidence." *Zeitschrift für Morphologie und Anthropologie* 71: 149–156.

Fleagle, J. G., and E. L. Simons. 1983. "The Tibio-Fibular Articulation in *Apidium phiomense*, an Oligocene Anthropoid." *Nature* 301: 238–239. https://doi.org/10.1038/301238a0.

Fleagle, J. G., and E. L. Simons. 1995. "Limb Skeleton and Locomotor Adaptations of *Apidium phiomense*, an Oligocene Anthropoid From Egypt." *American Journal of Physical Anthropology* 97: 235–289. https://doi.org/10.1002/ajpa.1330970303.

Friesen, S. E., R. P. Knigge, T. Jashashvili, W. E. Harcourt-Smith, M. J. Schoeninger, and M. W. Tocheri. 2024. "Shape Variation in the Talus and Medial Cuneiform of Chimpanzees and Bonobos." *American Journal of Biological Anthropology* 183, no. 3: e24571. https://doi.org/10.1002/ajpa.24571.

Gebo, D. L. 1989. "Locomotor and Phylogenetic Considerations in Anthropoid Evolution." *Journal of Human Evolution* 18: 201–233. https://doi.org/10.1016/0047-2484(89)90050-X.

Gebo, D. L., K. C. Beard, M. F. Teaford, et al. 1988. "A Hominoid Proximal Humerus From the Early Miocene of Rusinga Island, Kenya." *Journal of Human Evolution* 17: 393–401. https://doi.org/10.1016/0047-2484(88)90028-0.

Gebo, D. L., N. R. Malit, and I. O. Nengo. 2009. "New Proconsuloid Postcranials From the Early Miocene of Kenya." *Primates* 50: 311–319. https://doi.org/10.1007/s10329-009-0151-4.

Gebo, D. L., and E. L. Simons. 1987. "Morphology and Locomotor Adaptations of the Foot in Early Oligocene Anthropoids." *American Journal of Physical Anthropology* 74: 83–101. https://doi.org/10.1002/ajpa.1330740108.

Gomberg, D. N. 1981. "Form and Function of the Hominoid Foot" (PhD diss., University of Massachusetts).

Hammond, A. S., D. M. Alba, S. Almécija, and S. Moyà-Solà. 2013. "Middle Miocene *Pierolapithecus* Provides a First Glimpse Into Early Hominid Pelvic Morphology." *Journal of Human Evolution* 64: 658–666. https://doi.org/10.1016/j.jhevol.2013.03.002.

Hammond, A. S., J. M. Plavcan, and C. V. Ward. 2016. "A Validated Method for Modeling Anthropoid Hip Abduction In Silico." *American Journal of Physical Anthropology* 160: 529–548. https://doi.org/10.1002/ajpa.22990.

Hammond, A. S., L. Rook, A. D. Anaya, et al. 2020. "Insights Into the Lower Torso in Late Miocene Hominoid *Oreopithecus bambolii*." *Proceedings of the National Academy of Sciences* 117: 278–284. https://doi.org/10.1073/pnas.1911896116.

Harrison, T. 1982. "Small-Bodied Apes From the Miocene of East Africa" (PhD diss., University College London).

Harrison, T. 1986. "A Reassessment of the Phylogenetic Relationships of *Oreopithecus bambolii* Gervais." *Journal of Human Evolution* 15: 541–583. https://doi.org/10.1016/S0047-2484(86)80073-2.

Hill, A., and S. Ward. 1988. "Origin of the Hominidae: The Record of African Large Hominoid Evolution Between 14 My and 4 My." *Yearbook of Physical Anthropology* 31: 49–83. https://doi.org/10.1002/ajpa.1330310505.

Hunt, K. D. 1991. "Positional Behavior in the Hominoidea." *International Journal of Primatology* 12: 95–118. https://doi.org/10.1007/BF02547576.

Hunt, K. D. 2016. "Why Are There Apes? Evidence for the Co-Evolution of Ape and Monkey Ecomorphology." *Journal of Anatomy* 228: 630–685. https://doi.org/10.1111/joa.12454.

Ishida, H., Y. Kunimatsu, T. Takano, Y. Nakano, and M. Nakatsukasa. 2004. "*Nacholapithecus* Skeleton From the Middle Miocene of Kenya." *Journal of Human Evolution* 46: 69–103. https://doi.org/10.1016/j.jhevol.2003.10.001.

Isler, K. 2002. "Characteristics of Vertical Climbing in African Apes." *Senckenbergiana Lethaea* 82: 115–124. https://doi.org/10.1007/BF03043777.

Jungers, W. L. 1987. "Body Size and Morphometric Affinities of the Appendicular Skeleton in *Oreopithecus bambolii* (IGF 11778)." *Journal of Human Evolution* 16: 445–456. https://doi.org/10.1016/0047-2484(87)90072-8.

Knigge, R. P., M. W. Tocheri, C. M. Orr, and K. P. Mcnulty. 2015. "Three-Dimensional Geometric Morphometric Analysis of Talar Morphology in Extant Gorilla Taxa From Highland and Lowland Habitats." *Anatomical Record* 298: 277–290. https://doi.org/10.1002/ar.23069.

Kordos, L., and D. R. Begun. 2001. "Primates From Rudabánya: Allocation of Specimens to Individuals, Sex and Age Categories." *Journal of Human Evolution* 40: 17–39. https://doi.org/10.1006/jhev.2000.0437.

Kuhn, M., and K. Johnson. 2013. *Applied Predictive Modeling*. Springer. https://doi.org/10.1007/978-1-4614-6849-3.

Langdon, J. H. 1986. *Functional Morphology of the Miocene Hominoid Foot*. Karger.

Larson, S. G. 1998. "Parallel Evolution in the Hominoid Trunk and Forelimb." *Evolutionary Anthropology* 6: 87–99. https://doi.org/10.1002/(SICI)1520-6505(1998)6:3%3C87::AID-EVAN3%3E3.0.CO;2-T.

Latimer, B., J. C. Ohman, and C. O. Lovejoy. 1987. "Talocrural Joint in African Hominoids: Implications for *Australopithecus afarensis*." *American Journal of Physical Anthropology* 74: 155–175. https://doi.org/10.1002/ajpa.1330740204.

Le Gros Clark, W. E. 1952. "Report on Fossil Hominoid Material Collected by the British-Kenya Miocene Expedition, 1949-1951." *Proceedings of the Zoological Society of London* 122: 273–286. https://doi.org/10.1111/j.1096-3642.1952.tb00314.x.

Le Gros Clark, W. E., and L. S. B. Leakey. 1951. "The Miocene Hominoidea of East Africa." *Fossil Mammals of Africa* 1: 1–117.

Le Gros Clark, W. E., and D. P. Thomas. 1951. "Associated Jaws and Limb Bones of *Limnopithecus macinnesi*." *Fossil Mammals of Africa* 3: 1–27.

Leakey, R. E. F., and M. G. Leakey. 1987. "A New Miocene Small-Bodied Ape From Kenya." *Journal of Human Evolution* 16, no. 4: 369–387. https://doi.org/10.1016/0047-2484(87)90067-4.

Leakey, R. E. F., M. G. Leakey, and A. C. Walker. 1988. "Morphology of *Afropithecus turkanensis* From Kenya." *American Journal of Physical Anthropology* 76, no. 3: 289–307. https://doi.org/10.1002/ajpa.1330760303.

Leardini, A., J. J. O'Connor, F. Catani, and S. Giannini. 2000. "The Role of the Passive Structures in the Mobility and Stability of the Human Ankle Joint: A Literature Review." *Foot & Ankle* 21: 602–615. https://doi.org/10.1177/107110070002100715.

Lewis, O. J. 1980a. "The Joints of the Evolving Foot. Part I. The Ankle Joint." *Journal of Anatomy* 130: 527–543.

Lewis, O. J. 1980b. "The Joints of the Evolving Foot. Part II. The Intrinsic Joints." *Journal of Anatomy* 130: 833–857.

Lisowski, F. P., G. H. Albrecht, and C. E. Oxnard. 1974. "The Form of the Talus in Some Higher Primates: A Multivariate Study." *American Journal of Physical Anthropology* 41: 191–215. https://doi.org/10.1002/ajpa.1330410203.

Lisowski, F. P., G. H. Albrecht, and C. E. Oxnard. 1976. "African Fossil Tali: Further Multivariate Morphometric Studies." *American Journal of Physical Anthropology* 45: 5–18. https://doi.org/10.1002/ajpa.1330450103.

Llera Martín, C. J., K. D. Rose, and A. D. Sylvester. 2022. "A Morphometric Analysis of Early Eocene Euprimate Tarsals From Gujarat, India." *Journal of Human Evolution* 164: 103141. https://doi.org/10.1016/j.jhevol.2022.103141.

MacInnes, C. 1943. "Notes on the East African Miocene Primates." *Journal of the East African Uganda Natural History Society* 17: 141–181.

Madar, S. I. 1996. "The Postcranial Morphology of *Sivapithecus*, an Asian Large-Bodied Miocene Hominoid" (PhD diss., Kent State University).

Manduell, K. L., H. C. Morrogh-Bernard, and S. K. Thorpe. 2011. "Locomotor Behavior of Wild Orangutans (*Pongo pygmaeus wurmbii*) in Disturbed Peat Swamp Forest, Sabangau, Central Kalimantan, Indonesia." *American Journal of Physical Anthropology* 145: 348–359. https://doi.org/10.1002/ajpa.21495.

Marigó, J., I. Roig, E. R. Seiffert, S. Moyà-Solà, and D. M. Boyer. 2016. "Astragalar and Calcaneal Morphology of the Middle Eocene Primate *Anchomomys frontanyensis* (Anchomomyini): Implications for Early Primate Evolution." *Journal of Human Evolution* 91: 122–143. https://doi.org/10.1016/j.jhevol.2015.08.011.

McCrossin, M. 1994. "The Phylogenetic Relationships, Adaptations, and Ecology of *Kenyapithecus*" (PhD diss., University of California Berkeley).

Meldrum, D. J., and R. E. Wunderlich. 1998. "Midfoot Flexibility in Ape Foot Dynamics, Early Hominid Footprints, and Bipedalism." *American Journal of Physical Anthropology* 105, no. S26: 161. https://doi.org/10.1002/(SICI)1096-8644(1998)26+%3C100::AID-AJPA8%3E3.0.CO;2-7.

Monclús-Gonzalo, O., D. M. Alba, A. Duhamel, A. C. Fabre, and J. Marigó. 2023. "Early Euprimates Already Had a Diverse Locomotor Repertoire: Evidence From Ankle Bone Morphology." *Journal of Human Evolution* 181: 103395. https://doi.org/10.1016/j.jhevol.2023.103395.

Morbeck, M. E. 1983. "Miocene Hominoid Discoveries From Rudabánya: Implications From the Postcranial Skeleton." In *New Interpretations of Ape and Human Ancestry*, edited by R. L. Ciochon and R. S. Corruccini, 369–404. Plenum Press. https://doi.org/10.1007/978-1-4684-8854-8_14.

Moyà-Solà, S., D. M. Alba, S. Almécija, et al. 2009. "A Unique Middle Miocene European Hominoid and the Origins of the Great Ape and Human Clade." *Proceedings of the National Academy of Sciences* 106: 9601–9606. https://doi.org/10.1073/pnas.0811730106.

Moyà-Solà, S., and M. Köhler. 1993. "Recent Discoveries of *Dryopithecus* Shed New Light on Evolution of Great Apes." *Nature* 365, no. 6446: 543–545. https://doi.org/10.1038/365543a0.

Moyà-Solà, S., and M. Köhler. 1995. "New Partial Cranium of *Dryopithecus* Lartet, 1863 (Hominoidea, Primates) From the Upper Miocene of Can Llobateres, Barcelona, Spain." *Journal of Human Evolution* 29, no. 2: 101–139. https://doi.org/10.1006/jhev.1995.1049.

Moyà-Solà, S., and M. Köhler. 1996. "A *Dryopithecus* Skeleton and the Origins of Great-Ape Locomotion." *Nature* 379: 156–159. https://doi.org/10.1038/379156a0.

Moyà-Solà, S., M. Köhler, D. M. Alba, I. Casanovas-Vilar, and J. Galindo. 2004. "*Pierolapithecus catalaunicus*, a New Middle Miocene Great Ape From Spain." *Science* 306: 1339–1344. https://doi.org/10.1126/science.1103094.

Moyà-Solà, S., M. Köhler, D. M. Alba, I. Casanovas-Vilar, and J. Galindo. 2005. "Response to Comment on '*Pierolapithecus catalaunicus*, a New Middle Miocene Great Ape From Spain'." *Science* 308: 203d. https://doi.org/10.1126/science.1108433.

Moyà-Solà, S., M. Köhler, D. M. Alba, et al. 2009. "First Partial Face and Upper Dentition of the Middle Miocene Hominoid *Dryopithecus Fontani* From Abocador de Can Mata (Vallès-Penedès Basin, Catalonia, NE Spain): Taxonomic and Phylogenetic Implications." *American Journal of Physical Anthropology* 139: 126–145. https://doi.org/10.1002/ajpa.20891.

Nakatsukasa, M., Y. Kunimatsu, D. Shimizu, Y. Nakano, Y. Kikuchi, and H. Ishida. 2012. "Hind Limb of the *Nacholapithecus kerioi* Holotype and Implications for Its Positional Behavior." *Anthropological Science* 120, no. 3: 235–250. https://doi.org/10.1537/ase.120731.

Parr, W. C. H., H. J. Chatterjee, and C. Soligo. 2011. "Inter- and Intra-Specific Scaling of Articular Surface Areas in the Hominoid Talus." *Journal of Anatomy* 218: 386–401. https://doi.org/10.1111/j.1469-7580.2011.01347.x.

Parr, W. C. H., C. Soligo, J. Smaers, et al. 2014. "Three-Dimensional Shape Variation of Talar Surface Morphology in Hominoid Primates." *Journal of Anatomy* 225: 42–59. https://doi.org/10.1111/joa.12195.

Pilbeam, D. R., G. E. Meyer, C. Badgley, et al. 1977. "New Hominoid Primates From the Siwaliks of Pakistan and Their Bearing on Hominoid Evolution." *Nature* 270, no. 5639: 689–695. https://doi.org/10.1038/270689a0.

Pilbeam, D. R., M. D. Rose, C. Badgley, and B. Lipschutz. 1980. "Miocene Hominoids From Pakistan." *Postilla* 181: 1–94.

Pina, M., D. M. Alba, S. Moyà-Solà, and S. Almécija. 2019. "Femoral Neck Cortical Bone Distribution of Dryopithecin Apes and the Evolution of Hominid Locomotion." *Journal of Human Evolution* 136: 102651. https://doi.org/10.1016/j.jhevol.2019.102651.

Pina, M., S. Almécija, D. M. Alba, M. C. O'Neil, and S. Moyà-Solà. 2014. "The Middle Miocene Ape *Pierolapithecus catalaunicus* Exhibits Extant Great Ape-Like Morphometric Affinities on Its Patella: Inferences on Knee Function and Evolution." *PLoS One* 9: e91944. https://doi.org/10.1371/journal.pone.0091944.

Pina, M., D. DeMiguel, F. Puigvert, J. Marcé-Nogué, and S. Moyà-Solà. 2020. "Knee Function Through Finite Element Analysis and the Role of Miocene Hominoids in Our Understanding of the Origin of Antipronograde Behaviours: The *Pierolapithecus catalaunicus* Patella as a Case Study." *Palaeontology* 63, no. 3: 459–475. https://doi.org/10.1111/pala.12466.

Pugh, K. D. 2022. "Phylogenetic Analysis of Middle-Late Miocene Apes." *Journal of Human Evolution* 165: 103140. https://doi.org/10.1016/j.jhevol.2021.103140.

Pugh, K. D., S. A. Catalano, M. Pérez de los Ríos, et al. 2023. "The Reconstructed Cranium of *Pierolapithecus* and the Evolution of the Great Ape Face." *Proceedings of the National Academy of Sciences* 120: e2218778120. https://doi.org/10.1073/pnas.2218778120.

Püschel, T. A., J. T. Gladman, R. Bobe, and W. I. Sellers. 2017. "The Evolution of the Platyrrhine Talus: A Comparative Analysis of the Phenetic Affinities of the Miocene Platyrrhines With Their Modern Relatives." *Journal of Human Evolution* 111: 179–201. https://doi.org/10.1016/j.jhevol.2017.07.015.

Püschel, T. A., J. Marcé-Nogué, J. Gladman, B. A. Patel, S. Almécija, and W. I. Sellers. 2020. "Getting Its Feet on the Ground: Elucidating *Paralouatta*'s Semi-Terrestriality Using the Virtual Morpho-Functional Toolbox." *Frontiers in Earth Science* 8: 79. https://doi.org/10.3389/feart.2020.00079.

Püschel, T. A., J. Marcé-Nogué, J. T. Gladman, R. Bobe, and W. I. Sellers. 2018. "Inferring Locomotor Behaviours in Miocene New World Monkeys Using Finite Element Analysis, Geometric Morphometrics, and Machine-Learning Classification Techniques Applied to Talar Morphology." *Journal of the Royal Society Interface* 15, no. 146: 20180520. https://doi.org/10.1098/rsif.2018.0520.

R Core Team. 2024. *R: A Language and Environment for Statistical Computing*. R Foundation for Statistical Computing.

Rafferty, K. L., A. Walker, C. B. Ruff, M. D. Rose, and P. J. Andrews. 1995. "Postcranial Estimates of Body Weight in Proconsul, With a Note on a Distal Tibia of *P. major* From Napak, Uganda." *American Journal of Physical Anthropology* 97: 391–402. https://doi.org/10.1002/ajpa.1330970406.

Raffi, I., B. S. Wade, H. Pälike, et al. 2020. "The Neogene Period." In *Geologic Time Scale 2020*, edited by F. M. Gradstein, J. G. Ogg, M. D. Schmitz, and G. M. Ogg, 1141–1215. Elsevier. https://doi.org/10.1016/B978-0-12-824360-2.00029-2.

Ramos, G. L., III. 2014. "Positional Behavior of *Pan paniscus* at Lui Kotale, Democratic Republic of Congo" (PhD diss., Indiana University).

Rohlf, F. J. 2021. "Why Clusters and Other Patterns Can Seem to Be Found in Analyses of High-Dimensional Data." *Evolutionary Biology* 48: 1–16. https://doi.org/10.1007/s11692-020-09518-6.

Rohlf, F. J., and M. Corti. 2000. "Use of Two-Block Partial Least-Squares to Study Covariation in Shape." *Systematic Biology* 49: 740–753. https://doi.org/10.1080/106351500750049806.

Rosas, A., A. Ferrando, M. Bastir, et al. 2017. "Neandertal Talus Bones From El Sidrón Site (Asturias, Spain): A 3D Geometric Morphometrics Analysis." *American Journal of Physical Anthropology* 164: 394–415. https://doi.org/10.1002/ajpa.23280.

Rose, M. D. 1983. "Miocene Hominoid Postcranial Morphology. Monkey-Like, Ape-Like, Neither, or Both?" In *New Interpretations of Ape and Human Ancestry*, edited by R. L. Ciochon and R. S. Corruccini, 503–516. Plenum Press. https://doi.org/10.1007/978-1-4684-8854-8_15.

Rose, M. D. 1988. "Another Look at the Anthropoid Elbow." *Journal of Human Evolution* 17: 193–224. https://doi.org/10.1016/0047-2484(88)90054-1.

Rose, M. D. 1994. "Quadrupedalism in Some Miocene Catarrhines." *Journal of Human Evolution* 26: 387–411. https://doi.org/10.1006/jhev.1994.1025.

Rose, M. D., M. G. Leakey, R. E. F. Leakey, and A. C. Walker. 1992. "Postcranial Specimens of *Simiolus enjiessi* and Other Primitive Catarrhines From the Early Miocene of Lake Turkana, Kenya." *Journal of Human Evolution* 22, no. 3: 171–237. https://doi.org/10.1016/S0047-2484(05)80006-5.

Rose, M. D., Y. Nakano, and H. Ishida. 1996. "*Kenyapithecus* Postcranial Specimens From Nachola, Kenya." *African Studies Monographs Supplement* 24: 3–56. https://doi.org/10.14989/68384.

Russo, G. A., T. C. Prang, F. R. McGechie, et al. 2024. "An Ape Partial Postcranial Skeleton (KNM-NP 64631) From the Middle Miocene of Napudet, Northern Kenya." *Journal of Human Evolution* 192: 103519. https://doi.org/10.1016/j.jhevol.2024.103519.

Russo, G. A., and L. J. Shapiro. 2013. "Reevaluation of the Lumbosacral Region of *Oreopithecus bambolii*." *Journal of Human Evolution* 65: 253–265. https://doi.org/10.1016/j.jhevol.2013.05.004.

Sarmiento, E. E. 1983. "The Significance of the Heel Process in Anthropoids." *International Journal of Primatology* 4: 127–152. https://doi.org/10.1007/BF02743754.

Schlager, S. 2013. "Soft-Tissue Reconstruction of the Human Nose: Population Differences and Sexual Dimorphism" (PhD diss., Albert-Ludwigs-Universität Freiburg).

Schlager, S. 2017. "Morpho and Rvcg–Shape Analysis in R: R-Packages for Geometric Morphometrics, Shape Analysis and Surface Manipulations." In *Statistical Shape and Deformation Analysis: Methods, Implementation and Applications*, edited by G. Zheng, S. Li, and G. Székely, 217–256. Academic Press. https://doi.org/10.1016/B978-0-12-810493-4.00011-0.

Schön Ybarra, M. A., and M. A. Schön III. 1987. "Positional Behavior and Limb Bone Adaptations in Red Howling Monkeys (*Alouatta seniculus*)." *Folia Primatologica* 49: 70–89. https://doi.org/10.1159/000156310.

Schrein, C. M. 2006. "Metric Variation and Sexual Dimorphism in the Dentition of *Ouranopithecus macedoniensis*." *Journal of Human Evolution* 50: 460–468. https://doi.org/10.1016/j.jhevol.2005.11.007.

Scott, J. E., C. M. Schrein, and J. Kelley. 2009. "Beyond *Gorilla* and *Pongo*: Alternative Models for Evaluating Variation and Sexual Dimorphism in Fossil Hominoid Samples." *American Journal of Physical Anthropology* 140: 253–264. https://doi.org/10.1002/ajpa.21059.

Seiffert, E. R., and E. L. Simons. 2001. "Astragalar Morphology of Late Eocene Anthropoids From the Fayum Depression (Egypt) and the Origin of Catarrhine Primates." *Journal of Human Evolution* 41: 577–606. https://doi.org/10.1006/jhev.2001.0508.

Senut, B. 2012. "Les Restes Post-Crâniens des Pliopithecidae (Primates) de Sansan." *Mémoires du Muséum National D'histoire Naturelle* 203: 535–558.

Shearer, B. M., S. B. Cooke, L. B. Halenar, et al. 2017. "Evaluating Causes of Error in Landmark-Based Data Collection Using Scanners." *PLoS One* 12: e0187452.

Smith, R. J. 1993. "Bias in Equations Used to Estimate Fossil Primate Body Mass." *Journal of Human Evolution* 25: 31–41. https://doi.org/10.1006/jhev.1993.1036.

Smith, R. J., and W. L. Jungers. 1997. "Body Mass in Comparative Primatology." *Journal of Human Evolution* 32: 523–559. https://doi.org/10.1006/jhev.1996.0122.

Sorrentino, R., K. J. Carlson, E. Bortolini, et al. 2020. "Morphometric Analysis of the Hominin Talus: Evolutionary and Functional Implications." *Journal of Human Evolution* 142: 102747. https://doi.org/10.1016/j.jhevol.2020.102747.

Strasser, E. 1988. "Pedal Evidence for the Origin and Diversification of Cercopithecid Clades." *Journal of Human Evolution* 17: 225–245. https://doi.org/10.1016/0047-2484(88)90055-3.

Straus, W. L. 1963. "The Classification of *Oreopithecus*." In *Classification and Human Evolution*, edited by S. L. Washburn, 146–177. Routledge.

Susanna, I., D. M. Alba, S. Almécija, and S. Moyà-Solà. 2014. "The Vertebral Remains of the Late Miocene Great Ape *Hispanopithecus laietanus* From Can Llobateres 2 (Vallès-Penedès Basin, NE Iberian Peninsula)." *Journal of Human Evolution* 73: 15–34. https://doi.org/10.1016/j.jhevol.2014.05.009.

Szalay, F. S., and J. H. Langdon. 1986. "The Foot of *Oreopithecus*: An Evolutionary Assessment." *Journal of Human Evolution* 15: 585–621. https://doi.org/10.1016/S0047-2484(86)80074-4.

Tallman, M., S. Almécija, S. L. Reber, D. M. Alba, and S. Moyà-Solà. 2013. "The Distal Tibia of *Hispanopithecus laietanus*: More Evidence for Mosaic Evolution in Miocene Apes." *Journal of Human Evolution* 64: 319–327. https://doi.org/10.1016/j.jhevol.2012.07.009.

Tocheri, M. W., C. R. Solhan, C. M. Orr, et al. 2011. "Ecological Divergence and Medial Cuneiform Morphology in Gorillas." *Journal of Human Evolution* 60: 171–184. https://doi.org/10.1016/j.jhevol.2010.09.002.

Torres-Tamayo, N., S. Schlager, D. García-Martínez, et al. 2020. "Three-Dimensional Geometric Morphometrics of Thorax-Pelvis Covariation and Its Potential for Predicting the Thorax Morphology: A Case Study on Kebara 2 Neandertal." *Journal of Human Evolution* 147: 102854. https://doi.org/10.1016/j.jhevol.2020.102854.

Tsubamoto, T., N. Egi, M. Takai, Thaung-Htike, and Zin-Maung-Maung-Thein. 2016. "Body Mass Estimation From the Talus in Primates and Its Application to the Pondaung Fossil Amphipithecid Primates." *Historical Biology* 28: 27–34. https://doi.org/10.1080/08912963.2014.971783.

Turley, K., and S. R. Frost. 2013. "The Shape and Presentation of the Catarrhine Talus: A Geometric Morphometric Analysis." *Anatomical Record* 296: 877–890. https://doi.org/10.1002/ar.22696.

Tuttle, R. 1975. "Parallelism, Brachiation, and Hominoid Phylogeny." In *Phylogeny of the Primates*, edited by W. P. Luckett and F. S. Szalay, 447–480. Plenum Press. https://doi.org/10.1007/978-1-4684-2166-8_17.

Urciuoli, A., and D. M. Alba. 2023. "Systematics of Miocene Apes: State of the Art of a Neverending Controversy." *Journal of Human Evolution* 175: 103309. https://doi.org/10.1016/j.jhevol.2022.103309.

Urciuoli, A., C. Zanolli, S. Almécija, et al. 2021. "Reassessment of the Phylogenetic Relationships of the Late Miocene Apes *Hispanopithecus* and *Rudapithecus* Based on Vestibular Morphology." *Proceedings of the National Academy of Sciences of the United States of America* 118, no. 5: e2015215118. https://doi.org/10.1073/pnas.2015215118.

Vereecke, E. E., K. D'Août, R. Payne, and P. Aerts. 2005. "Functional Analysis of the Foot and Ankle Myology of Gibbons and Bonobos." *Journal of Anatomy* 206: 453–476. https://doi.org/10.1111/j.1469-7580.2005.00412.x.

Walker, A. 1997. "Proconsul. Function and Phylogeny." In *Function, Phylogeny and Fossils: Miocene Hominoid Evolution and Adaptation*, edited by D. R. Begun, C. V. Ward, and M. D. Rose, 209–224. Plenum Press. https://doi.org/10.1007/978-1-4899-0075-3_10.

Walker, A., and M. Pickford. 1983. "New Postcranial Fossils of *Proconsul africanus* and *Proconsul nyanzae*." In *New Interpretations of Ape and Human Ancestry*, edited by R. L. Ciochon and R. S. Corruccini, 325–351. Plenum Press. https://doi.org/10.1007/978-1-4684-8854-8_12.

Ward, C. V. 1993. "Torso Morphology and Locomotion in *Proconsul nyanzae*." *American Journal of Physical Anthropology* 92: 291–328. https://doi.org/10.1002/ajpa.1330920306.

Ward, C. V. 1997. "Functional Anatomy and Phyletic Implications of the Hominoid Trunk and Hindlimb." In *Function, Phylogeny and Fossils: Miocene Hominoid Evolution and Adaptation*, edited by D. R. Begun, C. V. Ward, and M. D. Rose, 101–130. Plenum Press. https://doi.org/10.1007/978-1-4899-0075-3_6.

Ward, C. V. 1998. "*Afropithecus*, *Proconsul*, and the Primitive Hominoid Skeleton." In *Primate Locomotion*, edited by E. Strasser, J. G. Fleagle, A. L. Rosenberger, and H. M. McHenry, 337–352. Plenum Press. https://doi.org/10.1007/978-1-4899-0092-0_18.

Ward, C. V. 2015. "Postcranial and Locomotor Adaptations of Hominoids." In *Handbook of Paleoanthropology*, edited by W. Henke and I. Tattersall, 2nd ed., 1363–1386. Springer Berlin Heidelberg. https://doi.org/10.1007/978-3-642-39979-4_34.

Ward, C. V., C. B. Ruff, A. Walker, M. F. Teaford, M. D. Rose, and I. O. Nengo. 1995. "Functional Morphology of *Proconsul* Patellas From Rusinga Island, Kenya, With Implications for Other Miocene-Pliocene Catarrhines." *Journal of Human Evolution* 29: 1–19. https://doi.org/10.1006/jhev.1995.1045.

Ward, C. V., A. Walker, M. F. Teaford, and I. Odhiambo. 1993. "Partial Skeleton of *Proconsul nyanzae* From Mfangano Island, Kenya." *American Journal of Physical Anthropology* 90: 77–111. https://doi.org/10.1002/ajpa.1330900106.

Wickham, H. 2016. *ggplot2: Elegant Graphics for Data Analysis*. Springer.

Wiley, D. F., N. Amenta, D. A. Alcantara, et al. 2005. "Evolutionary Morphing." In *VIS 05: IEEE Visualization 2005*, edited by C. T. Silva, E. Gröller, and H. E. Rushmeier, 431–438. Institute of Electrical and Electronics Engineers. https://doi.org/10.1109/VISUAL.2005.1532826.

Willmott, C. J., and K. Matsuura. 2005. "Advantages of the Mean Absolute Error (MAE) Over the Root Mean Square Error (RMSE) in Assessing Average Model Performance." *Climate Research* 30: 79–82. https://doi.org/10.3354/cr030079.

Wold, S., M. Sjöström, and L. Eriksson. 2001. "PLS-Regression: A Basic Tool of Chemometrics." *Chemometrics and Intelligent Laboratory Systems* 58, no. 2: 109–130. https://doi.org/10.1016/S0169-7439(01)00155-1.

Yapuncich, G. S., J. T. Gladman, and D. M. Boyer. 2015. "Predicting Euarchontan Body Mass: A Comparison of Tarsal and Dental Variables." *American Journal of Physical Anthropology* 157: 472–506. https://doi.org/10.1002/ajpa.22735.

Yapuncich, G. S., and M. C. Granatosky. 2021. "Footloose: Articular Surface Morphology and Joint Movement Potential in the Ankles of Lorisids and Cheirogaleids." *American Journal of Physical Anthropology* 175: 876–894. https://doi.org/10.1002/ajpa.24298.

Youlatos, D. 1999. "Étude Fonctionnelle Multivariée de l'Astragale et du Calcanéum de *Mesopithecus pentelici*, Wagner, 1839 (Cercopithecoidea, Primates)." *Primatologie* 2: 407–420.

Youlatos, D., and J. Meldrum. 2011. "Locomotor Diversification in New World Monkeys: Running, Climbing, or Clawing Along Evolutionary

Branches." *Anatomical Record* 294: 1991–2012. https://doi.org/10.1002/ar.21508.

Zapfe, H. 1958. "The Skeleton of *Pliopithecus* (*Epipliopithecus*) *vindobonensis* Zapfe and Hürzeler." *American Journal of Physical Anthropology* 16: 441–457. https://doi.org/10.1002/ajpa.1330160405.

Zelditch, M. L., D. L. Swiderski, and H. D. Sheets. 2012. *Geometric Morphometrics for Biologists. A Primer.* 2nd ed. Academic Press.

Supporting Information

Additional supporting information can be found online in the Supporting Information section.

Supplementary Information (SI):

A dryopithecine talus from Abocador de Can Mata (Vallès-Penedès Basin, NE Iberian Peninsula): Morphometric affinities and evolutionary implications for hominoid locomotion

Oriol Monclús-Gonzalo[1,*], Shubham Pal[1], Thomas A. Püschel[2], Alessandro Urciuoli[3,4,1], Víctor Vinuesa[1], Josep M. Robles[1], Sergio Almécija[5,6,1], David M. Alba[1,*]

[1] *Institut Català de Paleontologia Miquel Crusafont, Universitat Autònoma de Barcelona, Edifici ICTA-ICP, c/ Columnes s/n, Campus de la UAB, 08193 Cerdanyola del Vallès, Barcelona, Spain*

[2] *Institute of Human Sciences, School of Anthropology, University of Oxford, Oxford, OX2 6PE, UK*

[3] *Department of Paleontology, University of Zurich, Karl-Schmid-Strasse 4, 8006, Zurich, Switzerland*

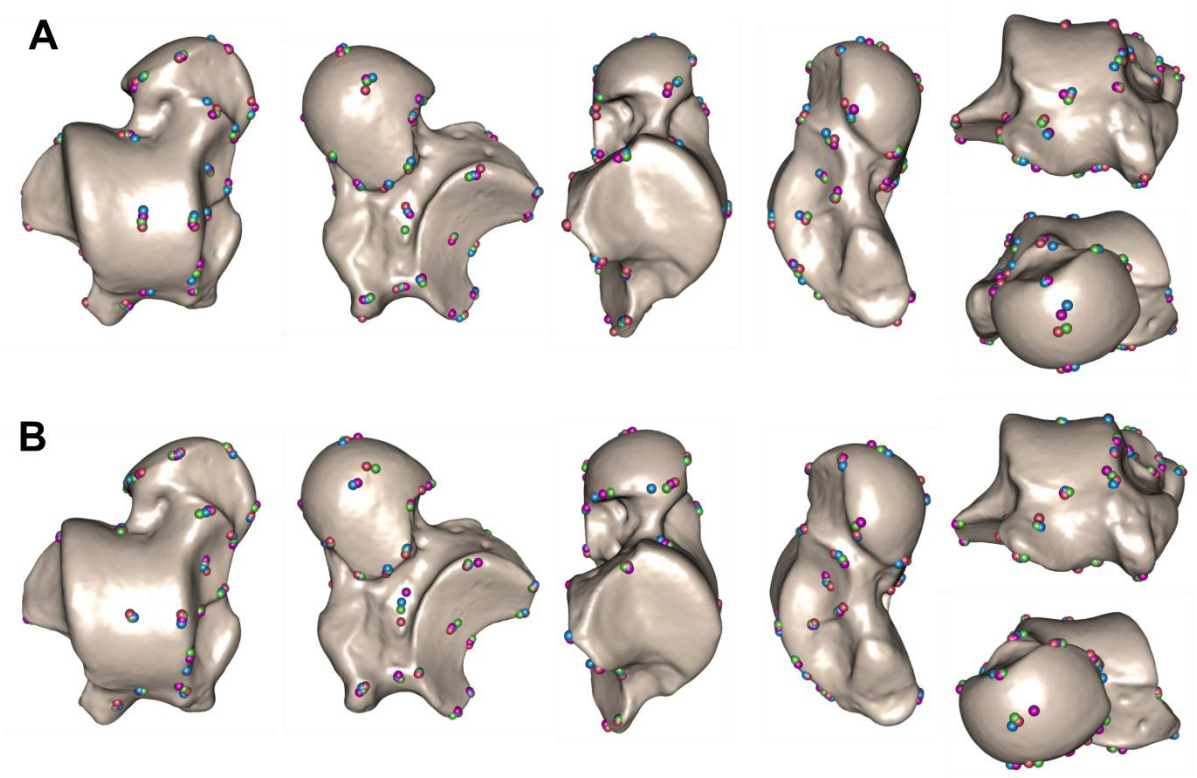
[4] *Universidad de Alcalá, Cátedra de Otoacústica Evolutiva y Paleoantropología (HM Hospitales-UAH), Departamento de Ciencias de la Vida, 28871 Alcalá de Henares, Madrid, Spain*

[5] *Division of Anthropology, American Museum of Natural History, New York, NY 10024, USA*

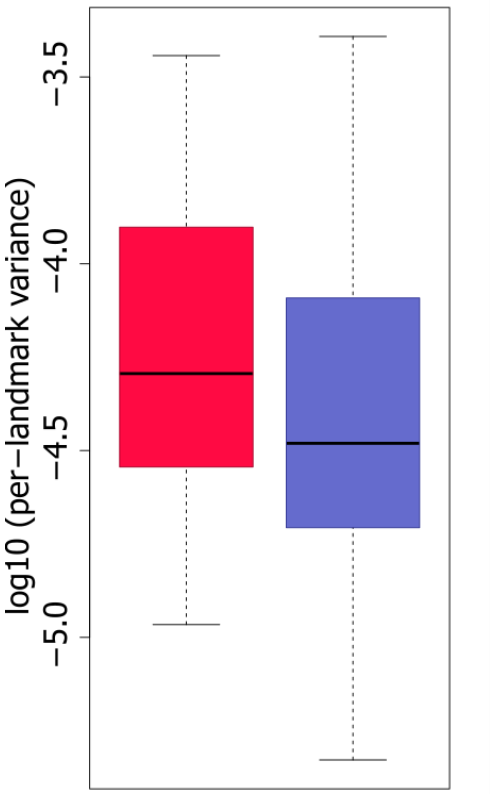
[6] *New York Consortium in Evolutionary Primatology, New York, USA*

*Corresponding authors.

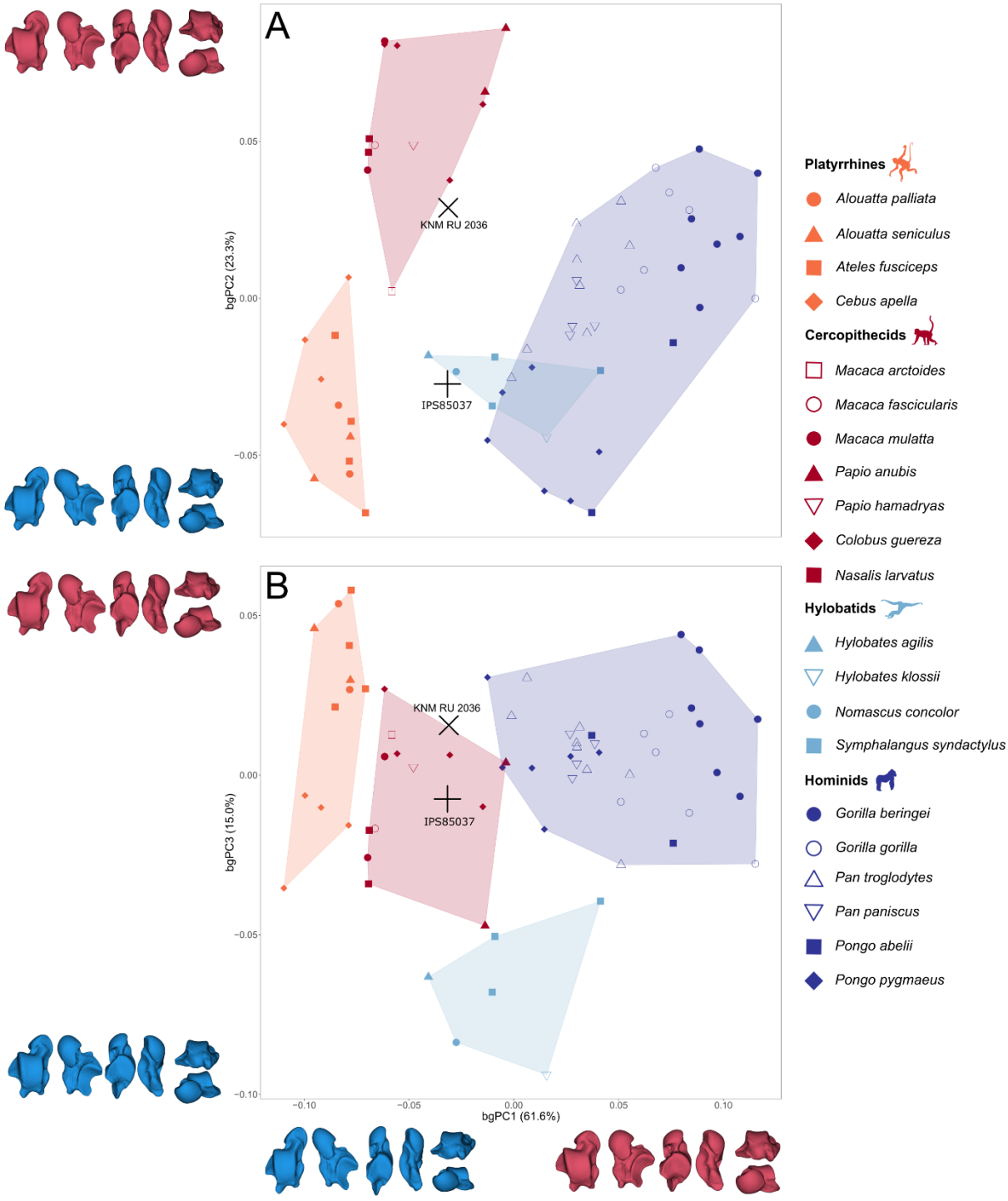
E-mail addresses: david.alba@icp.cat (D.M. Alba) and oriol.monclus@icp.cat (O. Monclús-Gonzalo).



SI FIGURE S1 Landmark coordinates placed onto RMCA 27698 by four different researchers (A) and by the same researcher four different times (B).

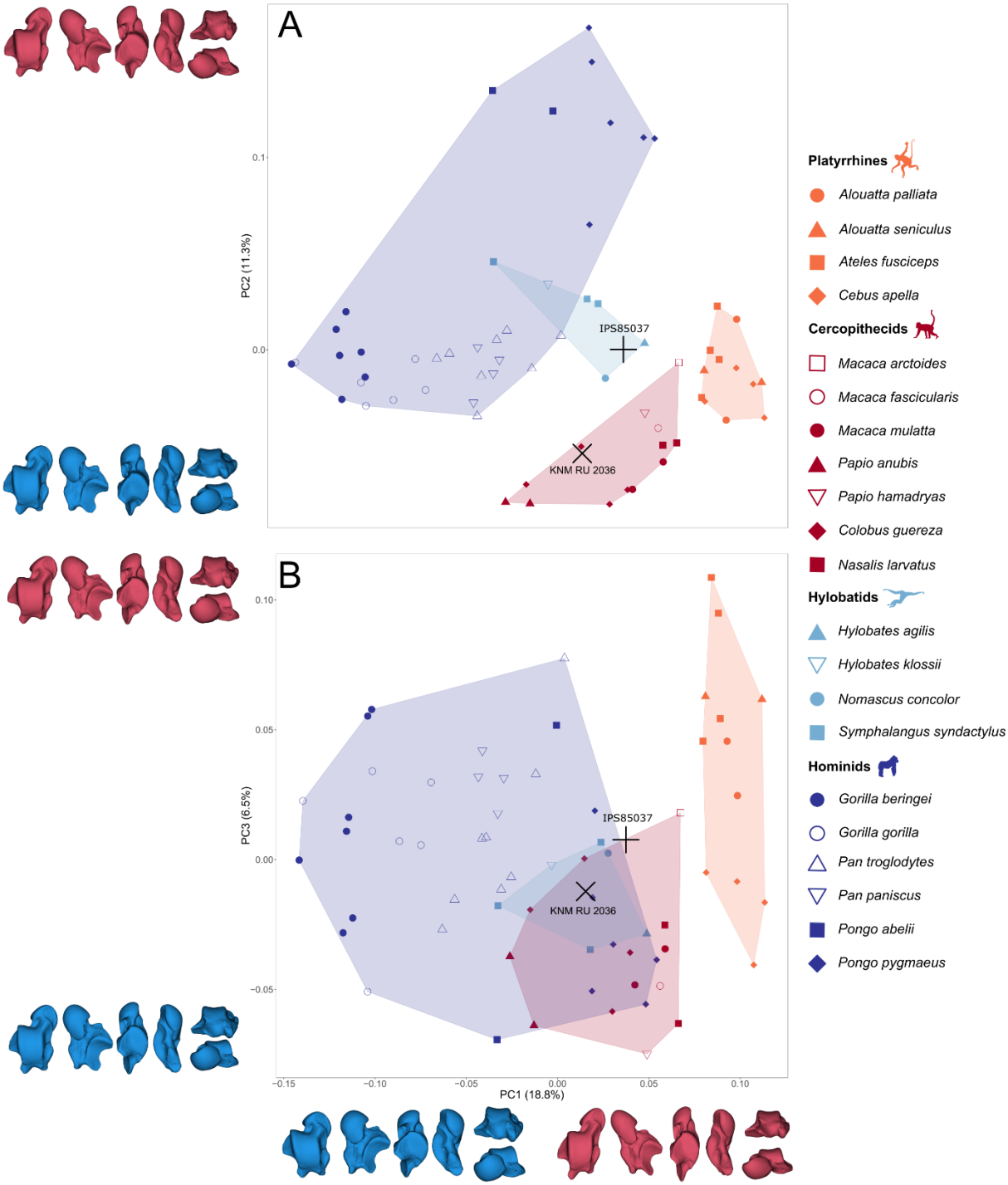


SI FIGURE S2 Boxplots displaying the amount of log10 per-landmark variance in each condition (red = inter-observer; blue = intra-observer).



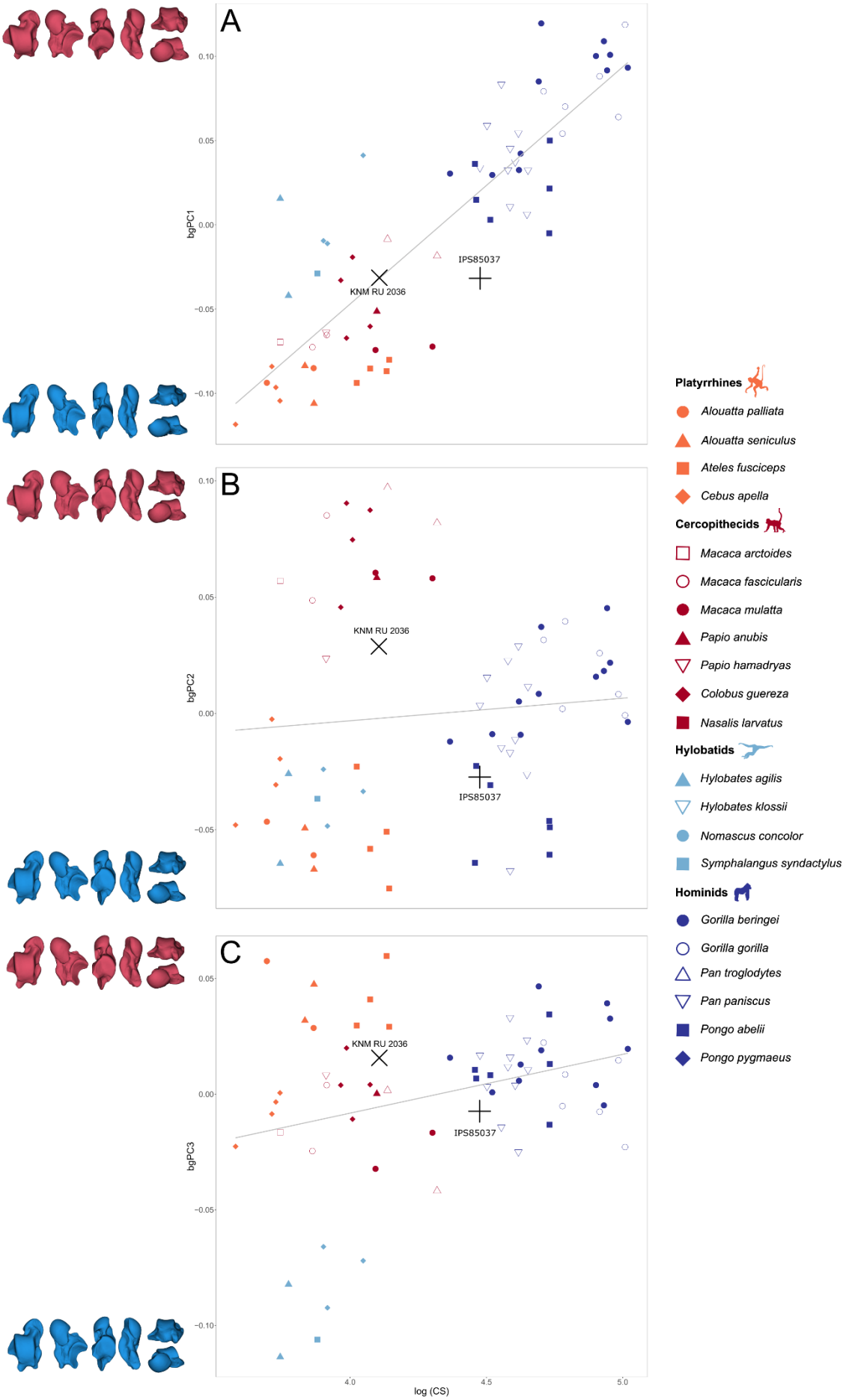
SI FIGURE S3 Results of the cross-validated between-group principal component analysis (bgPCA) as depicted by bivariate plots of bgPC2 vs. bgPC1 (A) and bgPC3 vs. bgPC1 (B). The groups distinguished a priori are indicated by color-coded convex hulls, and each species is denoted by different symbols, as indicated in the legend. Fossil specimens (whose scores are projected a posteriori) are indicated by a cross (╳) sign (KMN RU 2036) and a plus (+) sign

(IPS85037). The percentage of variance explained by each bgPC is reported within parentheses. Talar shapes associated with minimum (blue) and maximum (red) values of each bgPC axis are plotted below each scatterplot (dorsal, plantar, lateral, medial, proximal, and distal views are shown, from left to right). Thin plate splines are based on a talus of *Pan paniscus* (RMCA 27698).

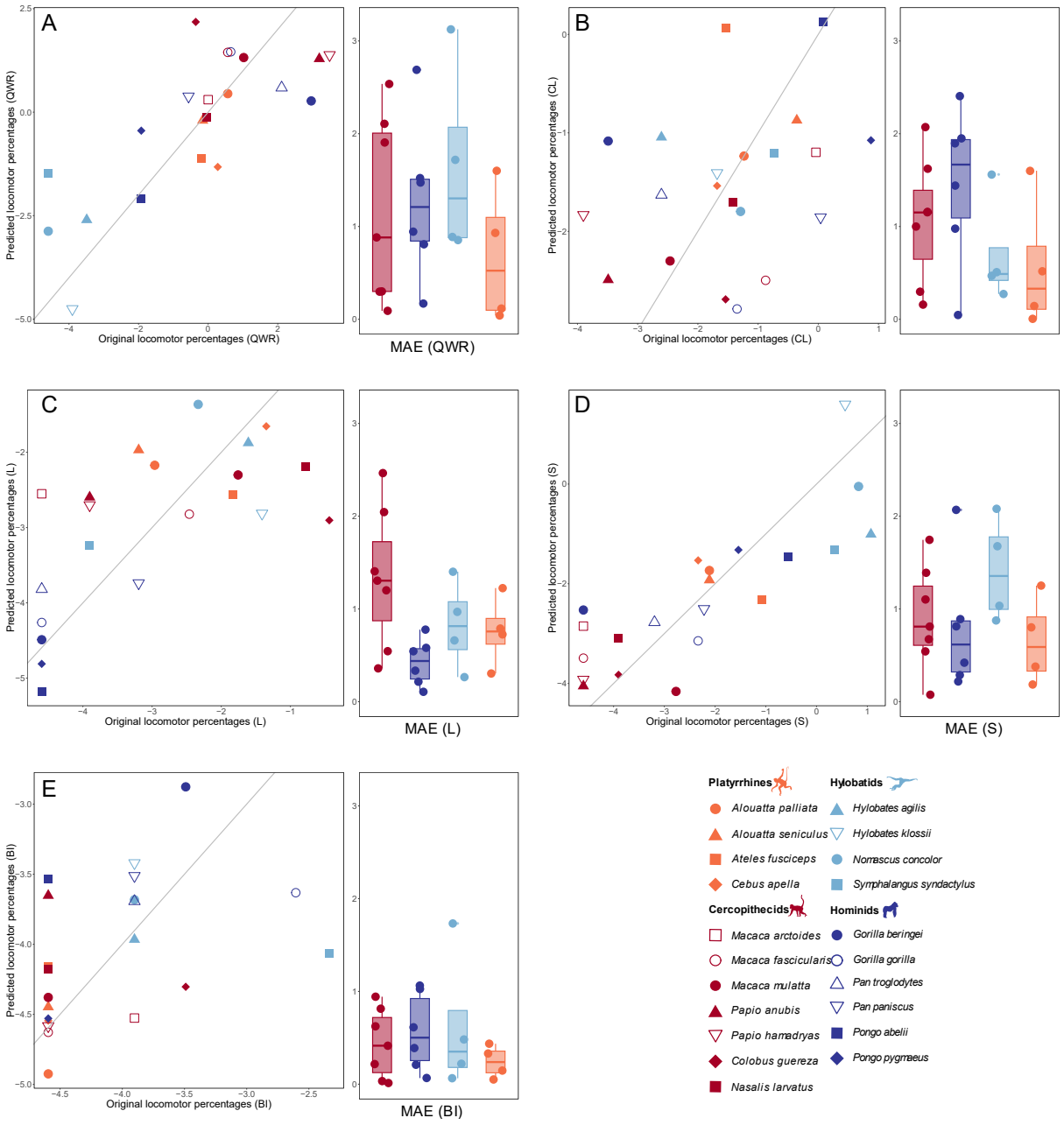


SI FIGURE S4 Results of the standard principal component analysis (PCA) as depicted by bivariate plots of PC2 vs. PC1 (A) and PC3 vs. PC1 (B). Taxonomic groups are indicated by color-coded convex hulls, and each species is denoted by different symbols, as indicated in the legend. Fossil specimens (whose scores are projected a posteriori) are indicated by a cross (╳) sign (KMN RU 2036) and a plus (+) sign (IPS85037). The percentage of variance explained by

each PC is reported within parentheses. Talar shapes associated with minimum (blue) and maximum (red) values of each PC axis are plotted below each scatterplot (dorsal, plantar, lateral, medial, proximal, and distal views are shown, from left to right). Thin plate splines are based on a talus of *Pan paniscus* (RMCA 27698).


A
B
C
bgPC1
bgPC2
bgPC3
log (CS)
KNM RU 2036
IPS85037
Platyrrhines
Alouatta palliata
Alouatta seniculus
Ateles fusciceps
Cebus apella
Cercopithecids
Macaca arctoides
Macaca fascicularis
Macaca mulatta
Papio anubis
Papio hamadryas
Colobus guereza
Nasalis larvatus
Hylobatids
Hylobates agilis
Hylobates klossii
Nomascus concolor
Symphalangus syndactylus
Hominids
Gorilla beringei
Gorilla gorilla
Pan troglodytes
Pan paniscus
Pongo abelii
Pongo pygmaeus

SI FIGURE S5 Bivariate plots between each between-group principal component (bgPC) and log-transformed centroid size (ln CS). The groups distinguished a priori are color-coded, and each species is denoted by different symbols, as indicated in the legend. Fossil specimens (whose scores are projected a posteriori) are indicated by a cross (╳) sign (KMN RU 2036) and a plus (+) sign (IPS85037). Talar shapes associated with minimum (blue) and maximum (red) values of each bgPC axis are plotted below each scatterplot (dorsal, plantar, lateral, medial, proximal, and distal views are shown, from left to right). Thin plate splines are based on a talus of *Pan paniscus* (RMCA 27698).



SI FIGURE S6 Bivariate plots between the original locomotor percentages and the predicted ones after 'leave-one-out cross-validation' was performed on the extant comparative sample for each locomotor variable: A) quadrupedal walking, bounding, and running (QWR); B) clambering and vertical climbing (CL); C) leaping, dropping, and hopping (L); D) bridging, brachiation, and suspensory locomotion (S); E) bipedal walking (BI) Boxplots displaying the mean absolute error (MAE) of each extant group are depicted next to each bivariate plot. The groups distinguished a priori are color-coded, and in the bivariate plots, each species is denoted by different symbols, as indicated in the legend.

SI TABLE S1 Details of the comparative sample of extant anthropoid tali used in this study.

Species	Sex	Catalog No.
Alouatta palliata	F	USNM 282798
Alouatta palliata	M	USNM 338107
Alouatta seniculus	F	AMNH 42316
Alouatta seniculus	M	AMNH 23333
Ateles fusciceps	F	USNM 338111
Ateles fusciceps	M	USNM 338112
Ateles fusciceps	F	AMNH 188135
Ateles fusciceps	M	AMNH 188140
Cebus apella	F	USNM 397940
Cebus apella	M	USNM 361020
Cebus apella	M	AMNH 188038
Cebus apella	M	AMNH 133606
Colobus guereza	M	USNM 452621
Colobus guereza	F	AMNH 52223
Colobus guereza	F	AMNH 52241
Colobus guereza	M	AMNH 52248
Gorilla beringei	F	RMCA 2263
Gorilla beringei	F	AMNH 54091
Gorilla beringei	M	USNM 239883
Gorilla beringei	M	USNM 395636
Gorilla beringei	M	AMNH 202932
Gorilla beringei	M	RMCA 8187
Gorilla beringei	M	USNM 397351

Gorilla gorilla	F	USNM 586541
Gorilla gorilla	F	AMNH 167339
Gorilla gorilla	F	AMNH 167340
Gorilla gorilla	M	CMNH 2767
Gorilla gorilla	M	USNM 176225
Gorilla gorilla	M	USNM 174722
Hylobates agilis	F	AMNH 106575
Hylobates klossii	M	AMNH 103344
Macaca arctoides	F	AMNH 112727
Macaca fascicularis	M	USNM 271168
Macaca mulatta	F	USNM 537241
Macaca mulatta	M	USNM 537253
Nasalis larvatus	F	USNM 536050
Nasalis larvatus	M	USNM 198276
Nomascus concolor	M	USNM 542282
Pan paniscus	F	AMNH 86857
Pan paniscus	M	SBU 87-1
Pan paniscus	F	RMCA 27698
Pan paniscus	M	RMCA 27696
Pan troglodytes	M	AMNH 89406
Pan troglodytes	F	USNM 176226
Pan troglodytes	F	USNM 176229
Pan troglodytes	M	USNM 395820
Pan troglodytes	M	USNM 176227
Pan troglodytes	M	USNM 220327

Pan troglodytes	M	USNM 481804
Pan troglodytes	F	USNM 220064
Papio anubis	F	USNM 384235
Papio anubis	M	USNM 384229
Papio hamadryas	F	RMCA A3-40-M-14
Pongo abelii	F	USNM 588109
Pongo abelii	M	USNM 143588
Pongo pygmaeus	F	USNM 145302
Pongo pygmaeus	F	USNM 153805
Pongo pygmaeus	M	USNM 145301
Pongo pygmaeus	M	USNM 153823
Pongo pygmaeus	F	USNM 142169
Pongo pygmaeus	M	USNM 145305
Symphalangus syndactylus	F	AMNH 106583
Symphalangus syndactylus	F	USNM 271048
Symphalangus syndactylus	M	AMNH 106581

Abbreviations: F = female; M = male; AMNH = American Museum of Natural History, New York, USA; CMNH = Cleveland Museum of Natural History, Cleveland, USA; RMCA = Royal Museum for Central Africa, Tervuren, Belgium; SBU = Stony Brook University, Stony Brook, USA; USNM = National Museum of Natural History (Smithsonian Institution), Washington D.C., USA.

SI TABLE S2 Procrustes distances between the consensus and the landmark configuration placed by four different researchers (inter-observer variability).

	R1	**R2**	**R3**	**R4**
Procrustes distance	0.059	0.050	0.043	0.041

SI TABLE S3 Procrustes distances between the consensus and the landmark configuration placed four times by the same researcher (intra-observer variability)

	1	**2**	**3**	**4**
Procrustes distance	0.050	0.044	0.045	0.048

SI TABLE S4 Log10 per-landmark variance in the inter-observer and intra-observer conditions.

Landmark	Log10 (per-landmark variance)	
	Inter-observer variability	Intra-observer variability
1	-3.89309	-4.563579
2	-3.99059	-4.224608
3	-4.30113	-4.377508
4	-3.59856	-4.006248
5	-4.28827	-4.845555
6	-4.01121	-4.629343
7	-4.17758	-3.862501
8	-4.46043	-4.405254
9	-4.53878	-4.981696
10	-4.05988	-3.605961
11	-4.96586	-4.32365
12	-3.69543	-3.981428
13	-4.66354	-4.830732
14	-4.53281	-4.633202
15	-3.8306	-3.592556
16	-3.99022	-3.560547
17	-4.34532	-3.414448
18	-4.29947	-4.453716
19	-3.64066	-3.698721
20	-4.78478	-4.785383
21	-4.31312	-4.560503

22	-4.40796	-4.542847
23	-4.72612	-4.944457
24	-3.90994	-4.176777
25	-4.80604	-4.737062
26	-4.57203	-4.675814
27	-4.1923	-4.507272
28	-4.82159	-5.322418
29	-3.82865	-4.627122
30	-4.5452	-5.3281
31	-4.60922	-4.283517
32	-4.54265	-4.624084
33	-3.53144	-3.391498
34	-4.22865	-4.786086
35	-3.44268	-4.27734
36	-3.89426	-4.286064

SI TABLE S5 Sex-species mean body mass (BM, in kg) and mean centroid size (CS) for the species included in the comparative sample. †

Species (sex)	BM	CS
Alouatta palliata (F)	5.32	40.22
Alouatta palliata (M)	7.16	47.75
Alouatta seniculus (F)	5.3	46.25
Alouatta seniculus (M)	6.87	47.81
Ateles fusciceps (F)	9.16	57.34
Ateles fusciceps (M)	8.89	62.70
Cebus apella (F)	2.52	35.86
Cebus apella (M)	3.65	41.58
Colobus guereza (F)	8.55	56.91
Colobus guereza (M)	11.7	53.31
Gorilla beringei (F)	97.5	109.57
Gorilla beringei (M)	162.5	141.23
Gorilla gorilla (F)	71.5	116.72
Gorilla gorilla (M)	170.4	144.05
Hylobates agilis (F)	5.82	43.55
Hylobates klossii (M)	5.67	42.24
Macaca arctoides (F)	8.4	49.97
Macaca fascicularis (M)	5.36	42.25
Macaca mulatta (F)	7.08	47.54
Macaca mulatta (M)	9.36	50.10
Nasalis larvatus (F)	9.82	59.92
Nasalis larvatus (M)	20.4	73.85

Nomascus concolor (M)	7.79	48.41
Pan paniscus (F)	33.2	85.36
Pan paniscus (M)	39.1	101.74
Pan troglodytes (F)	45.8	97.98
Pan troglodytes (M)	59.7	98.05
Papio anubis (F)	12.5	62.63
Papio anubis (M)	23.15	75.09
Papio hamadryas (F)	10.65	60.22
Pongo abelii (F)	35.6	95.07
Pongo abelii (M)	77.9	98.19
Pongo pygmaeus (F)	35.8	88.09
Pongo pygmaeus M	78.5	113.46
Symphalangus syndactylus F	10.7	49.87
Symphalangus syndactylus M	11.9	57.27

† BM data taken from Smith & Jungers (1997), whereas CS was computed from the specimens included in the comparative sample.

Abbreviations: F = female; M = male.

SI TABLE S6 Extant comparative sample and main references for their quantified locomotor behavior.

Species	QWR	CL	L	S	BI	References
Alouatta palliata	64	22	4	10	0	Youlatos & Meldrum (2011)
Alouatta seniculus	46	41	3	10	0	Youlatos & Meldrum (2011)
Ateles fusciceps	45	17	13	25	0	Youlatos & Meldrum (2011)
Cebus apella	57	15	20	8	0	Youlatos & Meldrum (2011)
Colobus guereza	41	17	39	1	2	Hunt (2016)
Gorilla beringei	96	2	0	0	2	Hunt (2004)
Gorilla gorilla	66	20	0	8	6	Doran (1996)
Hylobates agilis	2	6	16	75	1	Hunt (2016)
Hylobates klossii	1	15	19	64	1	Hunt (2016)
Macaca arctoides	50	49	0	0	1	Fooden (1990)
Macaca fascicularis	64	29	7	0	0	Cannon & Leighton (1994)
Macaca mulatta	74	7	14	5	0	Huang et al. (2015)
Nasalis larvatus	49	19	31	1	0	Hunt (2016)
Nomascus concolor	0	21	8	70	1	Fan, Scott, Fei, & Ma (2013)
Pan paniscus	36	51	3	9	1	Hunt (2004)
Pan troglodytes	90	6	0	3	1	Hunt (2016)
Papio anubis	97	2	1	0	0	Hunt (1992)
Papio hamadryas	98	1	1	0	0	Hunt (2016)
Pongo abelii	12	52	0	36	0	Sugardjito (1982)
Pongo pygmaeus	12	71	0	17	0	Cant (1987)
Symphalangus syndactylus	0	32	1	59	8	Hunt (2016)

Abbreviations: QWR = quadrupedal walking, bounding, and running; CL = clambering and vertical climbing; L = leaping, dropping, and hopping; S = bridging, brachiation, and suspensory locomotion; BI = bipedal walking.

SI TABLE S7 Number of correctly classified specimens (and percentages within parentheses) by the between-group principal component analysis for extant taxa.

	Cercopithecidae	**Hominidae**	**Hylobatidae**	**Platyrrhini**
Cercopithecidae	13 (100%)	0	0	0
Hominidae	0	33 (100%)	0	0
Hylobatidae	0	0	6 (100%)	0
Platyrrhini	0	0	0	12 (100%)

SI Table S8 Number of correctly classified specimens (and percentages within parentheses) by the between-group principal component analysis for extant taxa with cross-validation.

	Cercopithecidae	**Hominidae**	**Hylobatidae**	**Platyrrhini**
Cercopithecidae	12 (92.3%)	0	0	1 (7.7%)
Hominidae	0	32 (97.0%)		1 (3.0%)
Hylobatidae	0	1 (16.7%)	5 (83.3%)	0
Platyrrhini	0	0	0	12 (100%)

SI TABLE S9 Mean absolute error (MAE) calculated for the entire comparative sample after comparing the original locomotor values compiled for each extant species with the predicted ones using a leave-one-out cross-validation approach.

	MAE
QWR	1.191
CL	1.012
L	0.868
S	0.920
BI	0.471

Abbreviations: QWR = quadrupedal walking, bounding, and running; CL = clambering and vertical climbing; L = leaping, dropping, and hopping; S = bridging, brachiation, and suspensory locomotion; BI = bipedal walking.

SI TABLE S10 Mean absolute error calculated for each extant species.

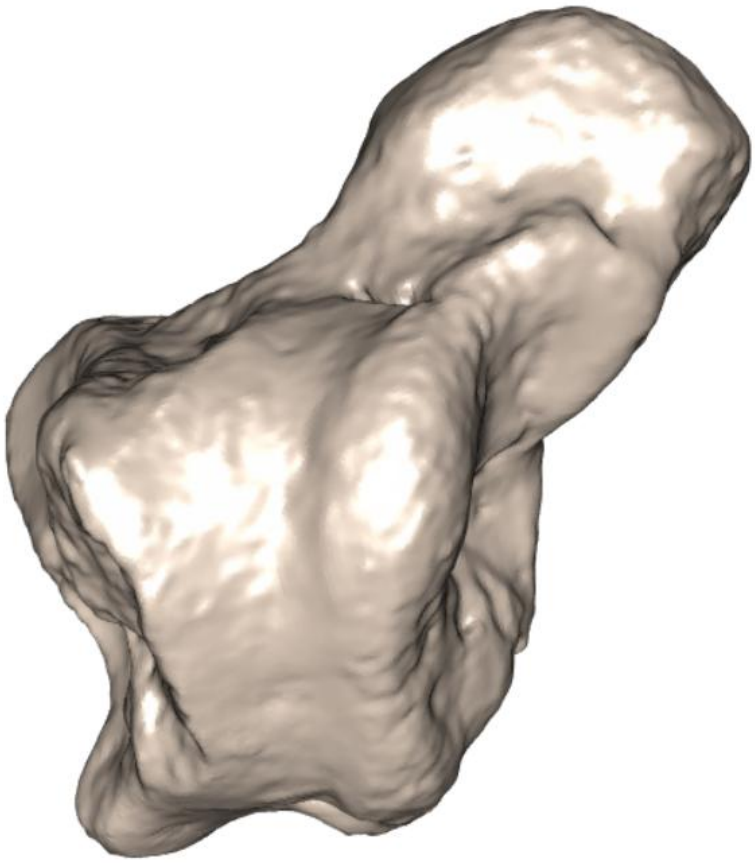
	QWR	CL	L	S	BI
Alouatta palliata	0.116	0.002	0.789	0.378	0.330
Alouatta seniculus	0.041	0.516	1.225	0.186	0.147
Ateles fusciceps	0.931	1.601	0.726	1.251	0.436
Cebus apella	1.600	0.143	0.305	0.802	0.050
Colobus guereza	2.537	1.151	2.465	0.075	0.814
Gorilla beringei	2.690	2.407	0.106	2.068	0.613
Gorilla gorilla	0.809	1.438	0.334	0.812	1.027
Hylobates agilis	0.888	1.561	0.266	2.080	0.064
Hylobates klossii	0.853	0.273	1.402	1.035	0.482
Macaca artoides	0.301	1.159	2.044	1.745	0.624
Macaca fascicularis	0.882	1.622	0.360	1.103	0.033
Macaca mulatta	0.298	0.161	0.544	1.390	0.216
Nasalis larvatus	0.091	0.296	1.405	0.810	0.415
Nomascus concolor	1.718	0.508	0.970	0.876	0.220
Pan paniscus	0.945	1.896	0.544	0.287	0.390
Pan troglodytes	1.521	0.976	0.777	0.421	0.209
Papio anubis	1.905	0.998	1.305	0.543	0.943
Papio hamadryas	2.108	2.069	1.201	0.673	0.012
Pongo abelii	0.169	0.048	0.581	0.891	1.063
Pongo pygmaeus	1.475	1.950	0.215	0.219	0.066
Symphalangus syndactylus	3.126	0.468	0.660	1.676	1.733

Abbreviations: QWR = quadrupedal walking, bounding, and running; CL = clambering and, vertical climbing; L = leaping, dropping, and hopping; S = bridging, brachiation, and suspensory locomotion; BI = bipedal walking.

SI TABLE S11 Locomotor variable loadings for the first two principal components (PCs) of the principal component analysis depicted in Figure 7.

	PC1	PC2
QWR	-0.676	-0.091
CL	0.327	-0.578
L	0.031	0.765
S	0.599	0.234
BI	0.278	-0.131

Abbreviations: QWR = quadrupedal walking, bounding, and running; CL = clambering and vertical climbing; L = leaping, dropping, and hopping; S = bridging, brachiation, and suspensory locomotion; BI = bipedal walking.



SI FILE S1 Rendering (in dorsal view) of the 3D virtual model of the right talus of Dryopithecini indet. from ACM/C8-B* (IPS85037), which is available from MorphoSource (https://doi.org/10.17602/M2/M713734).

SI References

Cannon, C.H., & Leighton, M. (1994). Comparative locomotor ecology of gibbons and macaques: Selection of canopy elements for crossing gaps. *American Journal of Physical Anthropology, 93*, 505–524. https://doi.org/10.1002/ajpa.1330930409

Cant, J.G. (1987). Positional behavior of female Bornean orangutans (*Pongo pygmaeus*). *American Journal of Primatology, 12*, 71–90. https://doi.org/10.1002/ajp.1350120104

Doran, D.M. (1996). Comparative positional behavior of the African apes. In W.C. McGrew, L.F. Marchant, & T. Nishida (Eds.), *Great ape societies* (pp. 213–224). Cambridge, Cambridge University Press.

Fan, P., Scott, M.B., Fei, H., & Ma, C. (2013). Locomotion behavior of Cao Vit gibbon (*Nomascus nasutus*) living in karst forest in Bangliang Nature Reserve, Guangxi, China. *Integrative Zoology, 8*, 356–364. https://doi.org/10.1111/j.1749-4877.2012.00300.x

Fooden, J. (1990). The bear macaque, *Macaca arctoides*: A systematic review. *Journal of Human Evolution, 19*, 607–686. https://doi.org/10.1016/0047-2484(90)90002-S

Huang, Z., Huang, C., Wei, H., Tang, H., Krzton, A., Ma, G., & Zhou, Q. (2015). Factors influencing positional behavior and habitat use of sympatric macaques in the limestone habitat of Nonggang, China. *International Journal of Primatology, 36*, 95–112. https://doi.org/10.1007/s10764-015-9813-9

Hunt, K.D. (1992). Positional behavior of *Pan troglodytes* in the Mahale Mountains and Gombe Stream National Parks, Tanzania. *American Journal of Physical Anthropology, 87*, 83–105. https://doi.org/10.1002/ajpa.1330870108

Hunt, K.D. (2004). The special demands of great ape locomotion and posture. In A.E. Russon & D.R. Begun (Eds.), *The evolution of thought: Evolutionary origins of great ape intelligence* (pp. 172–189). Cambridge, Cambridge University Press. https://doi.org/10.1017/CBO9780511542299.013

Hunt, K.D. (2016). Why are there apes? Evidence for the co-evolution of ape and monkey ecomorphology. *Journal of Anatomy, 228*, 630–685. https://doi.org/10.1111/joa.12454

Smith, R.J., & Jungers, W.L. (1997). Body mass in comparative primatology. *Journal of Human Evolution, 32*, 523–559. https://doi.org/10.1006/jhev.1996.0122

Sugardjito, J. (1982). Locomotor behavior of the Sumatran orangutan *Pongo pygmaeus abelii* at Ketambe, Gunung Leuser National Park. *Malaysian Naturalist Journal, 35*, 57–64.

Youlatos, D., & Meldrum, J. (2011). Locomotor diversification in New World monkeys: Running, climbing, or clawing along evolutionary branches. *Anatomical Record, 294*, 1991–2012. https://doi.org/10.1002/ar.21508

Chapter 6:

Discussion

Chapter 6. Discussion

6.1. Functional morphology of the hindfoot and the navicular bone

Foot morphology is expected to reflect the distinct functional demands required for the locomotor behaviors (e.g., quadrupedalism, leaping, climbing, suspension) that characterize the diverse locomotor repertoires of primates (e.g., Lewis, 1980a ,b; Conroy and Rose, 1983; Gebo, 1988, 1993b; DeSilva et al., 2019). Given that the function of morphological traits in fossil organisms cannot be directly assessed, comparative methods are required to provide a functional explanation of their significance (Bock, 1977). If a strong correlation is found between a morphological feature and a particular function, these methods allow to propose morphofunctional hypotheses that serve to make functional inferences for extinct species. Such inferences are strengthened by the expectation that similar selective pressures yield similar anatomical solutions (Lauder, 1986). Nevertheless, morphofunctional hypotheses based on form-function correlations among extant species must ideally be tested by means of other methods (such as biomechanics; Dunn, 2018).

In this section, the morphofunctional relationships between the hindfoot/ navicular bone and locomotor behavior in primates are examined. The results of the present dissertation demonstrate that there is significant covariation between tarsal shape, quantified using 3DGM, and locomotor behavior. These findings indicate that these bones can be employed to make inferences on the locomotor repertoire of fossil primates, underscoring the importance of applying the comparative method in 3DGM analyses to examine morphofunctional relationships in a quantified manner. Future studies should aim at incorporating additional sources of morphological data, including internal bone microstructure (Kivell, 2016), which largely reflects the ecophenotypic plasticity of the bone and, thus, might potentially reveal further insight into locomotion of extinct species. This is particularly interesting to compare the potential niche (as defined by adaptations based on heritable features, which reflect what an animal can do) and the realized niche (as defined by environmentally-driven features, which indicate that an animal actually did). Moreover, biomechanical studies should be conducted to test the morphofunctional hypotheses derived from the observed correlations between form and function in multivariate analyses. Such holistic approach offers the prospect to reliable test hypotheses of locomotor adaptation based on foot morphology in extinct primates.

6.1.1. The astragalus

The results presented in Chapter 4 and Chapter 5 support that the astragalus has a strong functional signal as a result of its key location between the leg and the rest of the foot, being involved in the three main tarsal joints (see Table 6.1. for a summary of the main morphofunctional relationships between astragalar shape and locomotor behavior discussed in this subsection). As shown in Chapter 4, astragalar shape is most dissimilar between specialized leaping and suspensory species. By contrast, species with more generalized locomotor repertoires exhibit intermediate morphologies between the other two. In Chapter 5, given the different training sample used (including only anthropoid species), the most divergent astragalar shapes discriminate suspensory taxa from (semi)terrestrial quadrupeds.

As expected, in both Chapters 4 and 5 suspensory behaviors are consistently associated with astragalar features that either increase the mobility at the main joints of this bone or enhance the efficiency of muscular stabilization during rotational movements and pedal grasping (e.g., Conroy and Rose, 1983; Gebo, 1988, 1989a,1993b; Meldrum, 1990; Youlatos and Meldrum, 2011; Püschel et al., 2017; Llera Martin et al., 2022). Among other features, slow climbing/suspensory species such as lorisids, atelids, hylobatids or orangutans exhibit a proximodistally elongated and slightly grooved trochlea, which facilitates dorsiflexion and plantarflexion at the UAJ. This is achieved because elongation of the articular facet extends the distance over which the tibia can translate over the astragalus, thereby increasing joint mobility (Hamrick, 1996; Yapuncich and Granatosky, 2021). All strepsirrhines (particularly those species with higher amounts of climbing and suspensory locomotion in their locomotor repertoire, such as lorisids), as well as atelids and hominoids to varying extents, show an angled, sloping fibular facet (Beard, 1988; Dagosto, 1988; Gebo, 1988; Turley and Frost, 2013; Knigge et al., 2015). This morphology increases the range of motion at the UAJ by allowing greater mobility of both the astragalus and the fibula, thereby reducing the rigidity of the mortise-and-tenon structure constituted by the astragalus, tibia and fibula (Lewis, 1980a; Gebo, 1993; Boyer and Seiffert, 2013). As a result, the UAJ can accommodate other movements besides dorsiflexion and plantarflexion, like inversion and eversion, to adopt a wider variety of foot postures (Dagosto, 1988, 2007; Gebo, 1988). The morphology of the medial tibial facet also reflects a less constrained UAJ in suspensory and slow climbing species, being shallow and comparatively large relative to astragalar size. As with the angled, sloping fibular facet, this morphology allows subtle rotational adjustments of the astragalus within the ankle mortise, an advantageous feature when the foot must accommodate to variable, oblique, and compliant supports (Dagosto, 1985; Gebo, 1993b; Boyer et al., 2015). A relatively wide and deep

groove for the FHL tendon, in addition to a well-developed lateral tubercle, is also found to be correlated with suspensory behaviors in Chapters 4 and 5. This result is consistent with previous evidence showing that species engaging in frequent hindlimb suspension and climbing behaviors (e.g., lorisids, atelids, hominoids) tend to exhibit deeper grooves and more prominent tubercles than either specialized leapers or more generalized pronograde quadrupeds (Harrison, 1982; Leardini et al., 2000; Seiffert et al., 2015). Suspensory locomotion is also correlated with a long and shallow ectal facet on the astragalus. As with the trochlea, elongation of the ectal facet expands the articular surface available for astragalocalcaneal motion, thereby enhancing inversion and eversion movements at the LAJ (Hamrick, 1996). This morphology has been documented in taxa that habitually engage in suspensory locomotion, climbing or bridging in relatively small and angled or vertical substrates, requiring joint mobility at the LAJ (e.g., Turley and Frost, 2013; Knigge et al., 2015; Püschel et al., 2017; Yapuncich and Granatosky, 2021; Friesen et al., 2024). The degree of concavity of the ectal facet on the astragalus has also been linked to locomotor behavior, although its functional significance remains debated. Some studies argue that a relatively shallow curvature of the facet is associated with terrestrial locomotion in catarrhines (Turley and Frost, 2013), consistent with loads perpendicular to the center of the joint (Hamrick, 1996). However, other studies (including this dissertation) report the opposite pattern, with shallower facets occurring in more suspensory taxa (e.g., Langdon, 1986; Meldrum, 1990; Knigge et al., 2015; Püschel et al., 2017; Friesen et al., 2024)—albeit, in arboreal species overall, those that engage in habitual leaping behavior exhibit a comparatively more concave ectal facet than those that do not (Turley and Frost, 2013). In addition to its length and curvature, the orientation of the ectal facet is also an important factor that determines the degree of screw motion that can be accomplished by the astragalus at the LAJ (Conroy and Rose 1983). In this regard, suspensory and cautious climbing species display a more obliquely oriented ectal facet on the astragalus relative to the long axis of the bone compared to other primates. This configuration facilitates mediolateral translation of the astragalus on the calcaneus during inversion–eversion, resulting in a subtalar axis angled relative to the long axis of the foot. Consequently, the sole can rotate inward during inversion and outward during eversion, increasing the flexibility of foot placement on variable supports (Lewis, 1980b; Gebo, 1993b). At the level of the astragalar neck, suspensory locomotion is associated with a pronounced medial angulation, in contrast to the condition observed in leaping or quadrupedal species. Marked medial angulation of the astragalar neck facilitates the transfer and absorption of compressive forces toward the medial side of the foot, which is consistent with enhanced pedal grasping in these species (Barnett, 1955; Harrison, 1982; Szalay and Langdon, 1986). In agreement with previous studies, the results in Chapters 4 and 5 indicate that a large and broad, mediolaterally expanded astragalar head characterizes several

suspensory and slow climbing species, such as lorisids and atelids (Gebo, 1988; Meldrum, 1990; Püschel et al., 2017). A relatively large astragalar head is also an important distinguishing feature in vertical climbers such as hylobatids and African apes, favoring mediolateral (as opposed to dorsoplantar) movements at the astragalonavicular joint in the TTJ (Szalay and Langdon, 1986).

In contrast, as shown in Chapter 4, specialized leaping species display astragalar features associated with enhanced foot stability (e.g., Gebo, 1987b, 1988, 1993b; Dagosto, 1988, 2007). For example, small-bodied VCL species like tarsiers and galagids exhibit a proximodistally abbreviated and moderately grooved trochlea, stabilizing the articulation between the tibia and the astragalus, and rendering the UAJ to functionally become hinge-like (Lewis, 1980a; Gebo, 1993b). Moreover, species that engage in substantial leaping behavior in general are characterized by the possession of a dorsoplantarly high astragalar body. This morphology reduces conjunct rotation at the UAJ during dorsi- and plantarflexion, thereby limiting the movement at this joint to the parasagittal plane—contrary to the condition observed in suspensory and cautious climbing species, which tend to have a comparatively dorsoplantarly lower astragalar body (Dagosto, 1985, 1988; Gebo, 1988). Additional trochlear features, including symmetrical rims and a relatively deep trochlear groove, are consistent in further reinforcing the stability at the UAJ by minimizing concomitant mediolateral movements during dorsi- and plantarflexion. Such constraints facilitate rapid parasagittal movements during take-off (Dagosto, 1988, 2007; Gebo, 1988). Furthermore, small-bodied specialized leapers among strepsirrhines stabilize the UAJ by possessing a comparatively steeper fibular facet, in contrast to less leaping-prone strepsirrhines that display a more angled, sloping facet. A comparatively steep facet allows the fibula to constitute a more upright lateral wall for the mortise formed by the astragalus, tibia and fibula, reinforcing the hinge-like configuration of the UAJ (Lewis, 1980a; Dagosto, 1985; Gebo, 1993; Boyer and Seiffert, 2013; Turley and Frost, 2013). As in the trochlea, the ectal facet is found to be similarly shortened, more concave and more plantarly oriented than in suspensory and cautious climbing species, facilitating a more stable axis of rotation and restricting the movement at the LAJ, resulting in a more efficient function of the joint in the parasagittal plane to enhance propulsion (Gebo, 1988; Yapuncich and Granatosky, 2021). In addition, specialized leapers display a proximodistally elongated astragalar neck, which, together with the elongation of other tarsal elements (see below for a more extended discussion in relation with the influence of foot type and the effect of body size), contribute to increase the effective length of hindlimb (Dagosto, 1988, 2007; Gebo, 1988). Lastly, the astragalar head tends to be smaller and more spherical in habitual leapers than in more suspensory or climbing species, a morphology that stiffens the astragalonavicular joint and increases midfoot rigidity, enhancing efficient force transference during rapid propulsion

(Gebo, 1988). A major challenge in functionally evaluating astragalar features associated with leaping behavior is that this locomotor mode is deeply intertwined with other behaviors requiring markedly different adaptations, most notably vertical clinging and climbing in vertical supports (e.g., tarsiers, galagids, indriids, sportive lemurs; e.g., Gebo, 1987a; 1988; Oxnard et al., 1990). As a result, astragalar shape exhibits an admixture of morphological features associated with leaping (linked to the stabilization of the ankle) and climbing (enhancing the rotation of the LAJ and TTJ in some species). This mosaic pattern is particularly evident in indriids, whose relatively large body size imposes additional biomechanical constraints (Demes and Gunther, 1989, Demes et al., 1996). Thus, their astragalar morphology reflects climbing adaptations to a greater degree than leaping, making them outliers in the analyses presented in Chapter 4 (similar deviations were observed for the calcaneus and navicular, see below), leading to an underestimation of the frequency of leaping in their locomotor repertoire during the LOOCV performed to assess the performance of the PLSR analysis. Consequently, this reveals a methodological limitation in the results of this dissertation, as distinguishing large-bodied VCL species from other large-bodied strepsirrhines with more generalized locomotor repertoires (e.g., lemurids) becomes problematic. This limitation is especially relevant when evaluating locomotor predictions for extinct primates that have been historically analogized to large-bodied VCL taxa, such as notharctines (Walker, 1974; Rose and Walker, 1985; Covert, 1995; Schmitt, 1996).

Generalized arboreal quadrupeds—including most lemurids, cheirogaleids, non-atelid platyrrhines and some cercopithecoids—lack the extreme morphological adaptations found in specialized leaping or suspensory species (Gebo, 1988). In contrast, as shown in Chapter 5, (semi)terrestrial quadrupeds—including several cercopithecoids and, to a lesser extent, African apes (which still require some midfoot mobility for habitual climbing and clambering)—display a markedly divergent astragalar morphology. Astragalar shape in these species reflects a combination of adaptations for foot stability (similarly to those of specialized leapers) and adaptations resisting the high loads of terrestrial cursorial locomotion (Strasser, 1988; Gebo, 1989b; Drapeau, 2022). In (semi)terrestrial cercopithecoids particularly, the astragalus is characterized by a relatively abbreviated trochlea. As in specialized leapers, this morphology restricts the proximodistal translation of the tibia over the calcaneus, enhancing stability at the UAJ (Lewis, 1980a; Gebo, 1993). Compared to the more symmetrical rims of more suspensory species, (semi)terrestrial quadrupeds possess a higher lateral rim than the medial rim. Some researchers have argued that this morphology may be related to an inverted grasping posture, as a prominent lateral rim could facilitate some abduction at the ankle accompanying dorsiflexion of the foot—which, in turn, could be related to effective weight transfer during inversion (Turley

and Frost, 2013; Dunn et al., 2014; Knigge et al., 2015). Nevertheless, the functional significance of this feature remains unclear, as others argue that it could be an adaptation for foot stabilization during quadrupedal locomotion in horizontal substrates, by limiting foot abduction and maintaining the foot on the parasagittal plane (Langdon, 1986; Strasser, 1988). As in specialized leapers, the UAJ is further stabilized by the possession of a steep fibular facet, which restricts fibular displacement and thus limits mediolateral ankle mobility (Lewis, 1980a; Gebo, 1993; Turley and Frost, 2013; Knigge et al., 2015). In African apes, this facet not only remains relatively steep but also flares laterally in its lower portion, creating a surface that resists excessive mediolateral movements (Conroy and Rose, 1983; Gebo, 1992b; DeSilva, 2009). The morphology of the medial tibial facet also reflects a close-packed configuration of the ankle during dorsi- and plantarflexion, as evinced by its medial flaring and well-developed malleolar cup for articulating with the tibia, which further contributes to stabilize the UAJ and restrict its mobility on the parasagittal plane (Harrison, 1982, 1987; Strasser, 1988). Evidence of relatively weak pedal grasping capacity in (semi)terrestrial quadrupeds is given by the relatively weak development of the posterior lateral tubercle—attachment site of the posterior talofibular ligament, an important stabilizer during dorsiflexion—and from the shallow groove for the FHL tendon (Harrison, 1982; Leardini et al., 1999; Yapuncich et al., 2017). These features are more pronounced in cercopithecoids than in African apes (Strasser, 1988; De Silva, 2008). The ectal facet of the astragalus is typically short and strongly concave in cercopithecoids. This morphology increases stability between the astragalus and the calcaneus, restricting the movements of the LAJ at the parasagittal plane (Lewis, 1980b; Conroy and Rose, 1983; Strasser, 1988; Turley and Frost, 2013). African apes, particularly *Gorilla*, also exhibit a relatively short ectal facet, although it is shallower than in cercopithecoids, reflecting both differences in body size and greater mobility at the LAJ (Turley and Frost, 2013; Knigge et al., 2015). As seen with some suspensory and slow climbing species, another key feature is the degree of medial deviation of the astragalar neck. In (semi)terrestrial cercopithecoids, the neck is less medially deviated than in more arboreal primates, stressing the less emphasis of grasping function and climbing behavior in their locomotor behavior compared to the latter (Szalay and Langdon, 1986). Notably, orangutans also exhibit a long and slightly deviated astragalar neck, despite engaging in little quadrupedalism and cursorial activities in general (Cant, 1987, Hunt, 1991). This morphology may help them withstand the longitudinal tensile stresses of pedal suspensory behaviors, where load bearing is largely supported by soft tissue structures (Szalay and Langdon, 1986).

Body size exerts a major influence on climbing and suspensory-related features of the astragalus. As shown in Chapter 4, larger-bodied primates tend to exhibit a dorsoplantarly lower

astragalar body, proximodistally shorter astragalar neck and relatively larger articular facet surfaces compared to smaller-bodied primates. This pattern reflects the expectation that larger animals require broader articular surfaces to accommodate higher joint reaction forces during locomotion (Ruff and Runestad, 1992). Biomechanical constraints also increase with size, as larger primates experience greater loads yet possess proportionally less available muscle force than smaller species, leading to different anatomical solutions and differences in their locomotor behaviors, which emphasize climbing and/or suspensory locomotion at the expense of grasp-leaping or above-branch quadrupedalism (Gebo, 1987a; Demes and Günther, 1989; Preuschoft et al., 1996; Youlatos and Meldrum, 2011). This distinction is exemplified by atelids and indriids, whose astragalar morphology contrasts with that of smaller platyrrhines and strepsirrhines, respectively, even if the latter are also specialized leapers (Fleagle and Mittermeier, 1980; Gebo and Dagosto, 1988). Regardless of body size, lorisids exhibit the most specialized astragalar morphology for slow, cautious climbing and suspension, characterized by a dorsoplantarly low body, a proximodistally short neck, and a large, mediolaterally expanded head (Gebo, 1988, 1989a). Conversely, some features that are commonly associated with leaping behavior, such as a dorsoplantarly high astragalar body and a proximodistally elongated astragalar neck—which effectively contributes to tarsal elongation and thereby lengthens the lever arm of the foot—may also be partly influenced by allometry. Indeed, species with relatively low reliance on leaping, such as some cheirogaleids (e.g., *Cheirogaleus*), nonetheless exhibit these traits (Moyà-Solà et al., 2012; Boyer et al., 2013). A similar allometric signal is observed among anthropoids in Chapter 5. Larger-bodied species, including hominids and, to a lesser extent, siamangs and atelids, exhibit features such as a stout astragalar body shape, a wedged trochlea (wider distally than proximally), and a short neck. These features are associated with slower-paced locomotion involving climbing, clambering and slow below-branch suspension (Langdon, 1986; Gebo, 1989b; Gebo, 1993a). A wedged trochlea, in particular, has been argued to enhance stability at the UAJ during dorsiflexion while permitting greater abduction and adduction during plantarflexion (Rose, 1983; Langdon, 1986). In contrast, smaller-bodied anthropoids, including hylobatids (other than siamangs), cercopithecoids, and non-atelid platyrrhines, exhibit a comparatively gracile astragalar body, parallel trochlear rims, and a relatively elongated neck. These features are linked to more agile locomotor repertoires, including rapid quadrupedalism, ricochetal brachiation, and leaping (Harrison, 1982; Turley and Frost, 2013). Orangutans are a notable exception to this pattern, as they exhibit a very elongated astragalar neck, comparable to that of much smaller-sized anthropoid species. This morphology projects the astragalar head further than the calcaneus, thereby enhancing inversion capability at the TTJ during arboreal locomotion (Harrison 1982; Szalay and Langdon, 1986; Gebo, 1989b).

Morphological variation in the astragalus also reflects the phylogenetic history of different primate groups (e.g., Beard et al., 1988; Dagosto, 1988, 2007). Broadly, strepsirrhines and haplorrhines exhibit distinct astragalar morphologies that correlate with some general differences in their locomotor behavior, particularly in their different emphasis on the utilization of vertical substrates, joint mobility and pedal grasping (Gebo, 1986a, 1988, 2011; Dagosto, 1988, 2007). One of the most consistent differences between strepsirrhines and haplorhines concerns the orientation of the astragalar fibular facet. In strepsirrhines, this facet tends to be obliquely sloping, whereas in haplorrhines (as well as in other eutherians) it is steep (Beard et al., 1988; Dagosto, 1988, 2007; Boyer and Seiffert, 2013). An obliquely sloping fibular facet increases UAJ mobility by allowing greater concomitant movement between the astragalus and fibula, rather than restricting motion to dorsiflexion and plantarflexion alone (Lewis, 1980a; Gebo, 1993b). This configuration is especially useful when navigating complex arboreal substrates, such as vertical or oblique supports. By contrast, a steep, vertically oriented fibular facet on the astragalus restricts the UAJ to primarily dorsiflexion and plantarflexion, thereby reducing mediolateral motion (Boyer and Seiffert, 2013). Such morphology is advantageous for anthropoids to engage in above-branch quadrupedalism and horizontal leaping, which requires stability during rapid loading on predominantly horizontal supports but does not require to accommodate the foot in so many different positions (Gebo, 1986a,1989b, 1993a). In most eutherians, including anthropoids and plesiadapiforms, the medial tibial facet is relatively restricted (dorsoplantarly shallow) and does not reach the plantar edge of the talus. In strepsirrhines and tarsiers, however, the medial tibial facet is comparatively larger (Dagosto, 1988, 1990; Gebo, 1993). Differences in the dimensions of the medial tibial facet between anthropoids and strepsirrhines and tarsiers reflect greater use of inverted foot postures and grasp-leaping in the latter group. This is expected because pedal inversion, which is a more habitual posture in strepsirrhines and tarsiers, generates higher compressive forces along the medial margin of the astragalus, requiring a larger facet to mitigate the risks associated with increased loadings on the medial side of the astragalus (Boyer et al., 2015a). Another distinguishing feature involves the position of the groove for the tendon of the FHL. In strepsirrhines, the groove lies lateral to the proximal trochlea, whereas in haplorrhines it is positioned at the midline of the bone (Beard et al., 1988). A laterally placed groove for the FHL indicates an habitually inverted foot and greater reliance on vertical supports compared to a more mid-trochlear position, as the former morphology is more advantageous for maintaining a straight path for the FHL tendon when the foot is positioned inverted (Gebo, 1986a, 2011; Yapuncich et al., 2017).

Table 6.1. Summary of the main morphofunctional relationships between astragalar shape and locomotor behavior.

Morphological feature	Condition	Functional explanation
Astragalar body (height)	High (specialized leapers/smaller-bodied species)	Constrains UAJ to parasagittal motion by limiting concomitant mediolateral movements
	Low (suspensory and slow climbing/larger-bodied species)	Permits greater mobility and rotational freedom at the UAJ
Trochlear shape (length and groove)	Elongated and slightly grooved (suspensory and slow climbers)	Facilitates mobility at the UAJ by increasing the range for dorsi- and plantarflexion
	Abbreviated and moderately grooved (specialized leapers and [semi]terrestrial quadrupeds)	Stabilizes the articulation between the tibia and the astragalus, more hinge-like joint
Trochlear rims (height)	High and symmetrical (specialized leapers)	Facilitates rapid parasagittal movements during take-off by reducing concomitant mediolateral movements
	Higher lateral rim ([semi]terrestrial quadrupeds, particularly cercopithecoids)	Facilitate abduction at the ankle accompanying dorsiflexion or promote parasagittal stability
Degree of trochlear wedging	Wedged (larger-bodied/suspensory and climbing species)	Stabilizes UAJ in dorsiflexion and allows abduction and adduction in plantarflexion.
	Parallel rims (smaller-sized species/specialized leapers)	Facilitate rapid locomotion (e.g., leaping, above-branch quadrupedalism)
FHL groove (width and depth) and lateral tubercle	Wide, deep groove + large tubercle (suspensory/slow climbing species)	Indicative of strong pedal grasping
	Shallow groove + weak tubercle ([semi]terrestrial quadrupeds)	Weak pedal grasping.
Position of the FHL groove	Lateral (strepsirrhines)	Maintains a straight tendon path during inversion, advantageous for foot inversion in vertical supports
	Midline (haplorrhines)	Indicates less habitual inverted foot position; higher reliance on horizontal substrates

Fibular facet (angle)	Sloping (strepsirrhines/suspensory and slow climbing species)	Allows greater concomitant movements between the astragalus and fibula, increasing the mobility at the UAJ
	Steep (haplorrhines/specialized leapers/[semi]terrestrial quadrupeds)	Reinforce the hinge-like configuration of the UAJ, constraining the joint to parasagittal motion
Medial tibial facet (extension)	Restricted (anthropoids)	Lower loadings on the medial side of the astragalus resulting from less inversion of the foot
	Large (strepsirrhines and tarsiers)	Indicates greater use of inverted foot postures and grasp-leaping, as a large facet allows to mitigate the increased loadings on the medial side of the astragalus
Medial tibial facet (shape)	Shallow (suspensory and slow climbing species)	Allows subtle rotational adjustments of the astragalus within the ankle mortise
	Medially flaring with well-developed malleolar cup ([semi]terrestrial quadrupeds)	Facilitates a close-packed configuration of the ankle during dorsi- and plantarflexion
Ectal facet (length, concavity and orientation	Long, shallow and oblique in relation to the direction of the long axis of the bone (suspensory and slow climbing species)	Increases astragalocalcaneal motion and facilitates mediolateral translation of the astragalus on the calcaneus
	Short, concave, and oriented in the direction of the long axis of the bone (specialized leapers/[semi]terrestrial quadrupeds	Restricted astragalocalcaneal motion and more stable axis of rotation
Neck (length and tilt)	Short and medially tilted (larger-bodied/suspensory and slow climbing species)	Enhances pedal grasping by increasing the transference and absorption of compressive forces to the medial side of the foot
	Long and less medially tilted (smaller-bodied/specialized leapers/[semi]terrestrial quadrupeds, although length is more variable in the latter case)	Lengthens the lever arm of the foot and/or indicates less emphasis on pedal grasping
	Long and less medially tilted (orangutans)	Enhances inversion capability at the TTJ by projecting the

		astragalar head further than the calcaneus
Head (size, shape and tilt)	Large, mediolaterally expanded head (suspensory and slow climbing species)	Favor mediolateral movements at the astragalonavicular joint in the TTJ
	Small, spherical head (specialized leapers)	Increases midfoot rigidity by stiffening the astragalonavicular joint (while allowing some mobility at the TTJ)
	Small, spherical head (orangutans)	Loads during pedal suspension are resisted primarily by the soft tissues

6.1.2. The calcaneus

The calcaneus, or heel bone, is a key element of the hindfoot involved in supporting the compressive loads generated by body weight and in transmitting forces between the hindfoot and the midfoot. It also constitutes part of the LAJ (via the ectal and sustentacular facets) and the TTJ (via the cuboid facet; Su and Zeininger, 2022). Accordingly, it is not surprising that the results presented in Chapter 4 indicate a strong functional signal in calcaneal shape (see Table 6.2. for a summary of the main morphofunctional relationships between calcaneal shape and locomotor behavior discussed in this subsection). In Chapter 4, specialized leaping and suspensory species exhibit the most divergent calcaneal shapes. By contrast, species with more generalized (e.g., grasp-leaping) locomotor repertoires exhibit intermediate morphologies.

In agreement with previous studies, this dissertation also found that calcaneal elongation is the main source of calcaneal shape variation across primates (e.g., Hall-Craggs, 1965b; Decker and Szalay, 1974; Gebo, 1988; Dagosto, 1988, 2007). Historically, calcaneal elongation has been linked to habitual leaping behavior and employed as a proxy for inferring this behavior in fossil taxa (e.g., Napier and Walker, 1967; Walker, 1974; Gebo, 1988; Moyà-Solà et al., 2012; Boyer et al., 2013; Marigó et al., 2016; Llera Martin et al., 2022). This association stems from the observation that proximodistal elongation of the distal calcaneal region—along with that of other tarsal elements that constitute the midfoot, such as the already discussed astragalar neck, the navicular (see below), or the cuboid—enhances the effective lever arm of the foot, thereby facilitating the generation of sufficient propulsive force for leaping (Morton, 1924; Gebo, 1988). However, calcaneal proportions in primates are strongly influenced by allometry, since species with distinct

body sizes face different biomechanical constraints (Jungers, 1984; Demes and Günther, 1989; Demes et al., 1996). For instance, only small-bodied VCL species, such as tarsiers and galagids (and, to a lesser extent, some cheirogaleids like *Microcebus*), exhibit extreme proximodistal elongation of the distal calcaneus, deviating markedly from the common allometric trend (Hall-Craggs, 1965b; Gebo, 1987b, 1989a; Moyà-Solà et al., 2012; Boyer et al, 2013). In contrast, larger-bodied species, most notably large-bodied specialized VCL like indriids and *Lepilemur*, employ the foot solely as a force transducer, overlapping in calcaneal proportions with non-leaping species (Gebo and Dagosto, 1988). Consequently, these species rely instead in elongating the proximal segment of the hindlimb to increase the lever arm (Demes and Günther, 1989; Demes et al., 1996). In fact, these allometric effects are very significant and need to be considered when evaluating the locomotor reconstructions of some fossil species. As explained in the previous subsection, indriids (in particular) pose a problem: their tarsal morphology, including the calcaneus (which is comparatively shorter than that of any other specialized leaper), reflect climbing adaptations to a greater degree than leaping ones (Gebo and Dagosto, 1988). For example, indriids exhibit very abbreviated distal calcaneus. As a result, they are found to be outliers in the covariation analyses presented in Chapter 4 between calcaneal shape and locomotor behavior. In addition, leaping behavior is underestimated for these species during the LOOCV tests to assess the performance of the PLSR analysis, leading to two undesirable effects. First, they obscure the distinction between large-bodied VCL species from other large-bodied strepsirrhines with more generalized locomotor repertoires. Secondly, and as a consequence of the first point, they can potentially inflate the predicted leaping percentages of those extinct species that resemble them morphologically (as well as to other large-bodied strepsirrhines, like lemurids), based on morphological features (i.e., short calcaneal elongation) that are not in fact linked to leaping behavior. For these reasons, such limitations must be carefully considered when evaluating locomotor predictions for extinct primates, especially notharctines—as these have been often compared to extant indriids by some researchers (Walker, 1974; Rose and Walker, 1985; Covert, 1995; Schmitt, 1996).

Calcaneal elongation also reflects the evolutionary history of different primate groups, as evinced by the more accentuated elongation in strepsirrhines and tarsiers than in anthropoids (Boyer et al., 2013). This distinction is best understood in relation to the distinct foot postures exhibited by these groups. Tarsi-fulcrumating species, such as strepsirrhines and tarsiers, are characterized by enhanced grasping abilities, which require the fulcrum of the foot to be positioned in a relatively proximal location, on the distal tarsal bones. However, while this configuration facilitates grasping, it reduces the effective lever arm of the forefoot. Therefore,

tarsi-fulcrumators require further elongation of the tarsal elements, including the distal calcaneus, to compensate for the loss of load arm (Morton, 1924). In contrast, metatarsi-fulcrumating species, including anthropoids as well as most nonprimate generalized mammals, like close relatives of primates such as scandentians and dermopterans, place the fulcrum more distally, on the metatarsal heads or the phalanges. In this case, there is no reduction in the available load arm, and, therefore, no further elongation of the tarsus is required (Morton, 1924). Based on this distinction, some authors have argued that calcaneal elongation should not be interpreted primarily as an adaptation to leaping, but rather as a consequence of possessing a grasping, tarsi-fulcrumating foot (Moyà-Solà et al., 2012). The results presented in Chapter 4 underscore this interpretation. However, the allometric analyses indicate a significant interaction between body mass and foot type, consistent with Boyer et al. (2013) that deviations in calcaneal elongation correlate with leaping only among tarsi-fulcrumators, not among metatarsi-fulcrumators.

In addition to distal calcaneal elongation, several other features are found to be correlated with leaping behavior. These are the possession of mediolaterally narrow and restricted calcaneal ectal and sustentacular facets, a dorsoplantarly high proximal facet on the tuber calcanei, and a straight calcaneal plantar edge. A short and mediolaterally narrow ectal facet reduces the potential range of motion at the LAJ, restricting the amount of helical motion between the astragalus and the calcaneus (Gebo and Simons, 1987; Gebo, 1988; Yapuncich and Granatosky, 2021). Likewise, a mediolaterally narrow and dorsally oriented sustentacular facet further restrict the movement at the LAJ to the parasagittal plane by limiting the rotational displacement of the head and neck of the astragalus on the calcaneus (Gebo and Simons, 1987). A dorsoplantarly high proximal facet of the tuber calcanei has also been linked to leaping behavior. This configuration expands the attachment area of the Achilles tendon, thereby increasing its length, resulting in an enhancement of the energy storage of this tendon and thus facilitating fast parasagittal movements during take-off (Gebo, 1987b, 1993b). Similarly, a straight calcaneal plantar edge stabilizes rapid, parasagittal motions required for rapid leaping behavior, by narrowing the foot in a more proximodistal direction (Gebo, 1986b).

Suspensory and slow climbing behaviors are associated with calcaneal features that enhance pedal grasping and facilitate inversion-eversion at the LAJ and TTJ, as concluded in Chapter 4. As with the astragalus, body size strongly influences climbing and suspensory-related features. For instance, they tend to have a comparatively abbreviated distal calcaneus relative to specialized leapers (Moyà-Solà et al., 2012; Boyer et al., 2013). This pattern reflects the expectation that calcaneal elongation will correlate negatively with body mass, as seen in atelids and in larger-

bodied strepsirrhines (including indriids, which, as discussed above, retain a climbing-adapted foot despite their VCL behavior; Gebo and Dagosto, 1988). Lorisids are a notable exception because, although relatively small-bodied (from 200 to 1400 g; Fleagle et al., 2025), also display a very short distal calcaneus (Gebo, 1988, 1989a). A short distal calcaneus changes hindfoot proportions by shortening the propulsion lever and increasing relative midfoot length. This results in a reduction of the lever arm used for propulsion and facilitates midfoot mobility at the TTJ via a more serial tarsus. A serial tarsus increases the ability of the foot to rotate and adapt to variable supports. Suspensory and slow climbing species also have a long, convex ectal facet, which expands the articular surface available for astragalocalcaneal motion and thereby increases inversion–eversion at the LAJ (Gebo, 1988; Hamrick, 1996; Yapuncich and Granatosky, 2021). For instance, among strepsirrhines, lorisids are particularly notable for an elongated, convex ectal facet (Gebo, 1989a). In platyrrhines, a proximodistally extended ectal facet likewise associates with suspensory behavior, reflecting a more mobile LAJ (Püschel et al., 2017). In these species, the sustentacular facet is mediolaterally broader and more medially oriented than in specialized leapers or habitual quadrupeds, consistent again with increased rotation at the LAJ, in this case between the astragalar neck and head and the distal calcaneus (Lewis, 1980b). Another distinguishing feature is the relative development of the peroneal tubercle, which acts as a muscle pulley for the peroneus longus tendon (an important hallux adductor; Gebo, 1993b; Godfrey et al., 1997). In suspensory and slow climbing species, this tubercle is prominent and enlarged, suggesting powerful hallucal grasping (Stern and Susman, 1983). Lorisids exemplify this condition, exhibiting an enlarged lateral peroneal tubercle and corresponding peroneal musculature (Gebo, 1989a). At the level of the tuber calcanei, suspensory and slow climbing species are characterized by an enlarged plantar tubercle. This feature, which is present in atelids, lorisids, and apes, provides the origin of the superficial head of the flexor digitorum brevis muscle (Sarmiento, 1983). A large origin process allows toe flexion that is less dependent on foot orientation, facilitating more diverse postures during deliberate climbing and suspension than in those species that lack a plantar tubercle (Sarmiento, 1983). Additionally, in lorisids the tuber calcanei displays a markedly plantar and medial orientation, which is associated with increased mechanical advantage of the superficial head of the flexor digitorum brevis muscle (Gebo, 1986b; Sarmiento, 1983; Seiffert et al., 2015). Lastly, the cuboid facet in suspensory and slow climbing species tends to be dorsoplantarly tall and deep. This allows the calcaneocuboid joint to act more as a pivot, facilitating adjunct inversion and eversion at the TTJ—at the expense of a more mediolateral translation (Conroy and Rose, 1983; Jenkins and McClearn, 1984; Gebo, 1989a). Compared to the straight calcaneal plantar edge exhibited by specialized leapers, suspensory and

slow climbing species, particularly lorisids, possess a very concave plantar edge, providing a compliant surface for foot placement in more variable types of substrates (Gebo, 1989a).

As with the astragalus, most generalized quadrupeds—including lemurids, most cheirogaleids, and several non-atelid platyrrhines—exhibit moderate morphological adaptations in the calcaneus compared to both specialized leapers and suspensory and slow climbing species (Gebo, 1988). For instance, proximodistal elongation of the calcaneus is markedly less marked than in leapers, yet generalized quadrupeds retain a longer distal calcaneus than suspensory and slow climbers, once allometric effects are considered (Moyà-Solà et al., 2012; Boyer et al., 2013). At the LAJ, the range of mediolateral movements is more restricted compared to that of suspensory and slow climbing species. This is suggested by the short, convex calcaneal ectal facet, as well as by the mediolaterally narrow and dorsally oriented sustentacular facet (Strasser, 1988; Harrison,1989). A similar pattern occurs in nonprimate euarchontans: *Ptilocercus lowii*, the most arboreal scandentian, exhibits a comparatively longer and more helical calcaneal ectal facet compared to that of other more terrestrial tupaiids, which are characterized by a correspondingly restricted LAJ (Sargis, 2002). A key feature that distinguishes habitual quadrupeds from either specialized leapers or suspensory and slow climbing species is the shape of the tuber calcanei. In the former, the tuber is straight, stout, and mediolaterally broad, increasing the lever arm of the triceps surae and thereby facilitating powerful loading of the foot during dorsi- and plantarflexion (Conroy and Rose, 1983; Strasser, 1988; Youlatos, 2003). In addition, quadrupeds also tend to exhibit a flatter cuboid facet compared to that of suspensory and slow climbing species, resulting in a less pivot-like calcaneocuboid joint. This indicates less rotational movements at the TTJ—consistent with their faster, above-branch quadrupedal locomotion (Conroy and Rose, 1983).

Table 6.2. Summary of the main morphofunctional relationships between calcaneal shape and locomotor behavior.

Morphological feature	Condition	Functional explanation
Distal calcaneal elongation	Proximodistally elongated distal calcaneus (especially in small-bodied VCL species; smaller-bodied tarsi-fulcrumators)	Increases lever arm of the foot, enhancing propulsive force for leaping. In tarsi-fulcrumators, it compensates for the loss of load arm due to the proximal position of the fulcrum

	Proximodistally short distal calcaneus (especially in suspensory and slow climbing species; more moderate in quadrupeds; larger-bodied tarsi-fulrumators and metatarsi-fulcrumators)	In suspensory and slow climbing species increases midfoot relative length and results in a more serial tarsus
Ectal facet (length, shape)	Proximodistally short (specialized leapers and quadrupeds)	Restricts the amount of helical motion between the astragalus and the calcaneus, thereby limiting the LAJ to the parasagittal plane
	Proximodistally long and convex	Expands the articular surface available for astragalocalcaneal motion; increases mediolateral rotation at the LAJ
Sustentacular facet (length, shape)	Proximodistally short and dorsally oriented	Limits movement of the astragalar neck and head on the calcaneus; constrains LAJ to parasagittal plane
	Mediolaterally broad and medially oriented	Increases rotational movement of the astragalar neck and head on calcaneus; enhances mediolateral rotation at the LAJ
Tuber calcanei (length, shape of the proximal facet)	Plantarly and medially oriented (especially lorisids)	Increased leverage for the flexor digitorum brevis muscle
	Proximodistally long and broad (quadrupeds)	Increases the power arm of the triceps surae muscles
	Dorsoplantarly high (specialized leapers)	Larger attachment site for the achilles tendon; increases tendon length and energy storage, which results in fast parasagittal movements during take-off
Development of a plantar tubercle (tuber calcanei)	Prominent (suspensory and slow climbing species)	Larger origin for the flexor digitorum brevis; allows toe flexion

		independently of foot posture
Cuboid facet	Flat (quadrupeds)	Less pivot-like calcaneocuboid joint; restricted mediolateral mobility at the TTJ
	Dorsoplantarly high and concave, pivot-like (suspensory and slow climbing species)	Facilitates adjunct inversion and eversion at the TTJ
Calcaneal plantar edge	Straight (specialized leapers and quadrupeds)	Narrows the foot in a proximodistal direction, stabilizes fast dorsi- and plantarflexion
	Concave (suspensory and slow climbing species)	Provides a less rigid, more compliant surface to position the foot in different surfaces

6.1.3. The navicular

Although the navicular is an important component for midfoot mobility—providing a bridge between the hindfoot and the cuneiforms and metatarsals—it has received relatively little attention in most studies about the functional morphology of the primate foot. The results presented in Chapter 3 indicate that the navicular has a strong functional signal that may be useful for inferring the locomotor behavior of extinct primates (see Table 6.3. for a summary of the main morphofunctional relationships between navicular shape and locomotor behavior discussed in this subsection). As previously noted with the calcaneus, the navicular exhibits the greatest shape differences between small-bodied specialized leapers and suspensory and slow climbing species, with generalized arboreal quadrupeds being somewhat intermediate in navicular shape.

The main source of navicular shape variation, as in other midfoot elements (e.g., astragalar neck, distal calcaneus, cuboid), is proximodistal elongation (Decker and Szalay, 1974; Gebo, 1986b, 1988; Dagosto, 1988, 2007). As explained in the previous subsection, elongation of the midfoot elements enhances the effective lever arm of the foot—which, in turn, facilitates the generation of propulsive force for leaping (Morton, 1924; Gebo, 1988). Navicular elongation follows the same allometric pattern as calcaneal elongation: only small-bodied VCL species display extreme proximodistal elongation of the navicular, whereas larger-bodied species (e.g., indriids, *Lepilemur*) are characterized by a markedly abbreviated navicular due to biomechanical

constraints derived from increased body size (Gebo and Dagosto, 1988; Demes and Gunther, 1989; Demes et al., 1996). As seen with the calcaneus, this scaling effect hinders the distinction between large-bodied VCL species from other similar-bodied species with more generalized locomotor repertoires. In addition, it also complicates the locomotor reconstructions of extinct taxa—e.g., notharctines, which resemble indriids in navicular proportions and may yield artificially high predicted leaping percentages. Moreover, the type of foot posture further influences the degree of navicular elongation. Overall, tarsi-fulcrumating species exhibit a greater range of variation compared to metatarsi-fulcrumating ones (Morton, 1924; Moyà-Solà et al., 2012; Boyer et al., 2013). As with the calcaneus, the results presented in Chapter 3 indicate that navicular elongation correlate only with leaping among tarsi-fulcrumators, not in metatarsi-fulcrumators. Additional features that characterize navicular shape in leaping species include a concave astragalar facet with a proximally protruding medial wall (which likely restricts mediolateral translations at the astragalonavicular joint), a relatively narrow cuboid facet (though strepsirrhines overall show broader facets than haplorrhines), and curved, relatively small cuneiform facets. Galagids are particularly prominent in the latter features, as they are characterized by a highly restricted morphology of the cuneiform facets that maximizes dorsiflexion and plantarflexion at these joints, at the cost of limiting the rotational mobility—which is accomplished via the calcaneocuboid joint (Gebo, 1987b, 1989a).

In contrast, suspensory and slow climbing primates exhibit a proximodistally abbreviated navicular combined with features that increase mobility at the astragalonavicular joint and the distal tarsal articulations. For instance, the astragalar facet is mediolaterally broader and shallower in suspensory and slow climbing species compared to specialized leapers, enhancing rotational movements at this joint (Decker and Szalay, 1974; Dagosto, 1986, 1988). Likewise, the cuboid and cuneiform facets are comparatively broader than in specialized leapers, enhancing mobility at the distal tarsal joints. Notably, lorisids exhibit a markedly oblique orientation of the entocuneiform facet on the navicular relative to the first metatarsal, which facilitates the abduction of the hallux (Dagosto, 1986; Gebo, 1989a). Among haplorrhines, atelids seem to follow the same morphology.

As already mentioned, some morphological features of the navicular reflect the phylogenetic history of different primate groups, distinguishing strepsirrhines from haplorrhines (Beard et al., 1988; Dagosto, 1988, 2007). This is particularly evident in the morphology of the cuneiform facets, which are more widely spaced and curved in strepsirrhines compared to haplorrhines. Similarly, the cuboid is broader in strepsirrhines and contacts the mesocuneiform facet—which is considered to be a synapomorphy of the suborder Strepsirrhini (Beard, 1988). The functional

explanation of this latter feature remains debated, as it has been proposed to stem from the morphology of the mesocuneiform itself (Gregory, 1920); as a lateral buttress for pedal flexors during grasping (Decker and Szalay, 1974); or as a mechanism facilitating inversion at the distal tarsal joints (Dagosto, 1988).

Table 6.3. Summary of the main morphofunctional relationships between navicular shape and locomotor behavior.

Morphological feature	Condition	Functional explanation
Navicular elongation	Proximodistally elongated navicular (especially in small-bodied VCL species; smaller-bodied tarsi-fulcrumators)	Increases the lever arm of the foot, enhancing propulsive force for leaping. In tarsi-fulcrumators, it compensates for the loss of load arm due to the proximal position of the fulcrum
	Proximodistally short navicular (especially in suspensory and slow climbing species; more moderate in quadrupeds; larger-bodied tarsi-fulrumators and metatarsi-fulcrumators)	In suspensory and slow climbing species increases midfoot relative length and results in a more serial tarsus
Astragalar facet (shape)	Concave, with proximally protruding medial wall (specialized leapers)	Restricts mediolateral translations at the TTJ
	Shallow, mediolaterally broad (suspensory and slow climbing species)	Enhances mobility at the TTJ
Cuneiform facets (shape)	Curved, restricted facets (specialized leapers except for tarsiers)	Limit rotational mobility at the distal tarsal joints
	Broad, spaced facets (suspensory and slow climbing species)	Enhance rotational mobility at the distal tarsal joints. In lorisids, the oblique orientation of the entocuneiform facet is associated with higher degrees of adduction of the hallux
Cuboid facet (shape, contact with the mesocuneiform facet)	Broad, contact with the mesocuneiform facet (strepsirrhines in general, albeit specialized leapers	Enhance rotational mobility at the distal tarsal joints. Different functional explanations have been given for the contact between the

	tend to have a narrower cuboid facet in comparison with more suspensory/climbing species)	cuboid and mesocuneiform facets: (1) structural consequence of mesocuneiform shape, (2) lateral buttress for pedal flexors in grasping, (3) to facilitate inversion at distal tarsal joints
	Narrow, no contact with the mesocuneiform facet (haplorrhines)	Limited mobility at the distal tarsal joints

6.2. Reconstruction of the locomotor behavior of Paleogene primates

6.2.1. Plesiadapiforms

Irrespective of their systematic position within Euarchonta, plesiadapiforms provide valuable information to understand the locomotor adaptations that may have characterized the ancestors of euprimates (Szalay and Decker, 1974; Dagosto, 1988, 2007; Szalay, 2007). Overall, plesiadapiforms are reconstructed as more suspensory and less prone to leaping than most euprimates, although evidence from calcaneal shape indicates considerable locomotor diversity in the group (Chapter 4), consistent with other regions of the skeleton (e.g., Bloch and Boyer, 2002, 2007; Bloch et al., 2007; Chester et al., 2017, 2019, 2025; Boyer and Gingerich, 2019).

When astragalar shape is used as a predictor, plesiadapiforms exhibit broadly similar locomotor repertoires, characterized by high amounts of quadrupedalism (42-47%), with moderate percentages of climbing, leaping, and suspensory locomotion (14-24%). This locomotor repertoire resembles that of the least prone-to-leap cheirogaleid species (*Cheirogaleus*) and the most arboreal scandentians (*Ptilocercus lowii* and *Tupaia minor*). These results concur with the view that plesiadapiforms already exhibited a relatively mobile UAJ and LAJ, which facilitated arboreal locomotion when compared with contemporaneous mammals retaining the primitive eutherian condition (Szalay and Decker, 1974; Szalay and Drawhorn, 1980; Szalay, 2007). Moreover, their relatively high percentages of climbing and suspensory behaviors—even compared with some euprimates—could be indicative of a habitual use of antipronograde postures by plesiadapiforms (Yapuncich and Granatosky, 2021).

Calcaneal shape reveals a slightly different picture, distinguishing nonplesiadapoid taxa (*Purgatorius*, *Tinimomys* and *Phenacolemur*) from plesiadapoids (*Plesiadapis* and *Carpolestes*).

The former resemble the reconstructions made using astragalar shape as a predictor, dominated by quadrupedalism and displaying small amounts of other behaviors. Notably, *Purgatorius* is reconstructed exhibiting the highest percentages for quadrupedalism, which is consistent with calcaneal features such as a relatively restricted ectal and sustentacular facets and a proximodistally elongated tuber calcanei—closely resembling those exhibited by extant scandentians, particularly the most cursorial species (Godinot, 2007). In contrast, plesiadapoids display more suspensory locomotion than their nonplesiadapoid counterparts (26–32%), pinpointing to a locomotor shift in more derived plesiadapiforms (Bloch and Boyer, 2002; Gebo, 2004; Sargis et al., 2007). Among plesiadapoids, *Plesiadapis cookei* is reconstructed with 26% suspensory locomotion, consistent with its relatively large body mass (1.8–2.2 kg; Gingerich and Gunnell, 2005; Boyer and Gingerich, 2019) and postcranial morphology (e.g., phalangeal proportions, scapular, and humeral features) resembling dermopterans and sloths (Hamrick, 2001; Bloch and Boyer, 2007; Boyer and Bloch, 2008). Meanwhile, *Carpolestes simpsoni* exhibits the highest suspensory values among plesiadapiforms (32%), in agreement with the evidence derived from other postcranial traits, including a divergent hallux bearing a nail rather than a claw (Bloch and Boyer, 2002).

The distinct locomotor reconstructions obtained from the astragalus and the calcaneus may be reflective of different macroevolutionary processes occurring at these bones. The results of this dissertation are consistent with the view that the UAJ remained relatively constrained in plesiadapiforms (and later in euprimates as well), retaining primitive eutherian features that favored parasagittal motion and cursorial abilities, whereas the LAJ and TTJ underwent key morphological changes required to enhance inversion-eversion and adduction-abduction to facilitate arboreal locomotion in the fine-branch milieu (Szalay and Dekcer, 1974; Szalay and Drawhorn, 1980; Szalay, 2007). For instance, *Carpolestes* already exhibits some of these changes, such as a proximodistally elongated, rounded and oblique ectal facet, a mediolaterally broad and medially oriented sustentacular facet, a proximally positioned peroneal tubercle, and a short and a dorsoplantarly high tuber calcanei, increasing astragalocalcaneal translation and enhancing pedal flexion (Hamrick, 1996; Yapuncich and Granatosky, 2021). If the LAJ and TTJ indeed underwent greater morphological change during plesiadapiform evolution than the UAJ, this may explain why calcaneal shape yields more distinct locomotor reconstructions across plesiadapiform species.

Interestingly, no plesiadapiforms are reconstructed as habitually engaging in scansorial locomotion, which contradicts some previous assumptions made in previous works (Bloch et al., 2007; Boyer and Bloch, 2008). Several reasons can be adduced, incuding that astragalar and

calcaneal shape are not very informative of this particular type of behavior, compared for instance to other elements of the foot, like the phalanges (e.g., Maiolino et al., 2023). It may also stem from the limited representation of scansorial taxa (e.g., callitrichids, dermopterans) in the comparative dataset, which probably reduced the accuracy of the analysis regarding predictions of this specific behavior (see Chapter 4). As a result, the only two species (*Plesiadapis cookei* and *Carpolestes simpsoni*) that exhibit non-negligible percentages of scansorial locomotion in the reconstructions based on calcaneal shape, likely just reflect similarities to dermopterans—such as an elongated ectal facet and high proximal facet of the tuber calcanei, which are typically associated with suspensory adaptations (Szalay and Drawhorn, 1980; Youlatos et al., 2019).

6.2.2. Adapiforms

Among early euprimate groups, adapiforms are inferred to have displayed the most diverse locomotor repertoires (Chapters 3 and 4). Broadly, three locomotor profiles can be distinguished. Most species exhibited a combination of quadrupedal and leaping behaviors, with moderate percentages of climbing and suspension. A second group is characterized by a locomotor repertoire dominated by quadrupedalism, somewhat similar to that of several early anthropoid species, particularly parapithecoids (see below), suggesting habitual above-branch quadrupedal locomotion. A third group is distinguished by their emphasis on suspension, accompanied by moderate percentages of climbing and quadrupedalism, but with little leaping involved. Notably, all adapiforms are distinguished from omomyiforms and early anthropoids by their higher reliance on suspension, which likely reflects greater pedal mobility and an emphasis on inverted postures on vertical or oblique supports in the former (Dagosto, 1988, 2007; Gebo, 2011).

Notharctines are reconstructed as generalized arboreal quadrupeds and leapers, although showing some differences among the various genera (Gebo, 1988; Boyer et al., 2013). Locomotor inferences also vary depending on the bone employed to make the prediction: astragalar shape yields higher leaping percentages compared to the other two bones. This difference is likely a consequence of the importance that tarsal elongation has in the calcaneus and navicular (in which is the main source of variation) compared to the astragalus. Additionally, as explained in the previous section, the inclusion of large VCL species such as indriids in the comparative sample could potentially inflate the predicted leaping percentages in notharctines that resemble them in tarsal morphology. While the results of this dissertation cannot reject the hypothesis that notharctines were specialized VCL (Walker, 1974; Rose and Walker, 1985; Covert, 1995; Schmitt,

1996), broader postcranial evidence, including other features of pedal morphology (such as the lack of a powerful adductor grasp; Gebo, 1985), supports the view (favored here) that notharctines were generalized arboreal quadrupeds with some leaping abilities but lacking VCL specializations (Decker and Szalay, 1974; Gebo, 1988; Boyer et al., 2013).

Within the Adapinae, the *Adapis* group also exhibits contrasting locomotor predictions depending on which bone is used. Conversely, in *Leptadapis magnus* the inferred locomotor repertoires are more similar to one another, albeit astragalar shape yields higher leaping percentages than calcaneal shape, as in notharctines. Astragalar shape in the *Adapis* group is consistent with a locomotor repertoire defined by moderately high percentages of climbing and suspensory locomotion, including a low astragalar body, long trochlea, gently sloping fibular facet, and mediolaterally broad head (Dagosto, 1983; Gebo, 1988; Godinot, 1991). In contrast, calcaneal shape for both the *Adapis* group and *Leptadapis* yields the highest percentages of quadrupedal locomotion among all adapiforms. This result is congruous with calcaneal shape, particularly the long tuber calcanei (comparable to that of some anthropoid species), which is associated with an increase of the power arm of the triceps surae muscles, facilitating loading at a parasagittal plane (Strasser, 1988; Youlatos, 2003). This discrepancy between the distinct locomotor signals exhibited by the ankle bones might reflect some trade-off as a result of distinct selective pressures acting on each bone—with the astragalus being more adapted for slow climbing and suspensory behaviors and the calcaneus better suited for quadrupedal locomotion. Furthermore, this discrepancy between the two bones might also be related to taxonomic issues within *"Adapis parisiensis*" (the species to which all specimens included in the *Adapis* group were originally referred), as there is abundant morphological evidence that it comprises several morphotypes with distinct locomotor adaptations (Godinot, 1991, 1998; Bacon and Godinot, 1998; Marigó et al., 2019). Thus, the astragali and calcanei might belong to different species characterized by distinct locomotor repertoires.

Caenopithecus lemuroides is reconstructed, based on calcaneal shape, as a primarily slow climbing animal with a greater quadrupedal component than extant lorisids (Seiffert et al., 2015). This interpretation is supported by several calcaneal features associated with enhanced joint mobility, including a dorsomedially inclined sustentacular facet, a rounded oblique ectal facet, and a dorsoplantarly high cuboid facet with a deep pit (Gebo, 1988, 1989a; Hamrick, 1996; Yapuncich and Granatosky, 2021). Notably, it also exhibits a medially angled, plantarly projecting tuber calcanei, which is linked to increased mechanical advantage of the superficial head of the flexor digitorum brevis muscle (Gebo, 1986b; Sarmiento, 1983; Seiffert et al., 2015).

Both *Anchomomys frontanyensis* and *Djebelemur martinezi* are reconstructed as habitual leapers with moderate quadrupedalism and climbing percentatges in their locomotor repertoire, resembling cheirogaleids such as *Microcebus* and *Mirza* (Boyer et al., 2013; Marigó et al., 2016, 2020). *Anchomomys frontanyensis* is particularly notable among adapiforms for its moderately elongated calcaneus and navicular, overlapping with omomyiforms in this regard (Marigó et al., 2016, 2020). Thus, it is likely that *Anchomomys frontanyensis* exhibited a leaping proclivity comparable to some omomyiform species, even if it was not a specialized leaper, as it does not deviate from the general allometric trend observed in tarsi-fulcrumators (like specialized small-bodied VCL species; Moyà-Solà et al., 2012; Boyer et al., 2013). *Anchomomys frontanyensis* is also distinguished from omomyiforms by some tarsal features (e.g., a moderately long ectal facet on the calcaneus, a slightly medially angled, plantarly projecting tuber calcanei, contact between the cuboid and mesocuneiform facets) related to greater joint mobility, resulting in moderate percentages of suspensory and climbing behaviors when calcaneal and navicular shape are used as predictors. This could be related with enhanced inversion capabilities in the foot of *Anchomomys frontanyensis* compared to contemporaneous sympatric omomyiform species, resulting in niche partitioning between them (Marigó et al., 2020). Conversely, astragalar shape in both *Anchomomys frontanyensis* and *Djebelemur martinezi* resembles more that of specialized leapers (e.g., a high astragalar body, almost parallel trochlear rims, proximodistally elongated neck), resulting in a predicted locomotor repertoire with higher leaping percentages than those predicted from calcaneal or navicular shape.

The locomotor reconstructions of *Marcgodinotius indicus*, particularly those derived from the calcaneus, are consistent with earlier studies suggesting little leaping proclivity in this species (Rose et al., 2009; Boyer et al., 2013; Dunn et al., 2016; Llera Martin et al. 2022). This interpretation is supported by the relatively short distal calcaneal region, especially when compared with similarly sized adapiforms such as *Anchomomys frontanyensis* (Marigó et al., 2016, 2020). Other calcaneal features are also indicative of habitual climbing and suspensory locomotion, including a medially oriented tuber calcanei, a slightly concave plantar edge, a rounded ectal facet, and a broad, medially facing sustentacular facet (Gebo, 1988, 1989a; Boyer et al., 2013). In contrast, predictions based on astragalar shape yield a relatively more generalized locomotor repertoire, with moderate percentages for leaping and quadrupedalism, compared to those made with the calcaneus (Rose et al., 2009; Dunn et al., 2016; Llera Martin et al., 2022). This discrepancy may reflect a trade-off between the bones that constitute the ankle of *Marcgodinotius indicus*, with calcaneal shape more associated with slow climbing and suspensory behavior compared to astragalar shape. Moreover, as mentioned earlier, among all adapiforms (except for *Adapis*

group), astragalar shape tends to yield higher percentages for leaping behavior compared to calcaneal or navicular shape, which is likely an effect of tarsal elongation and the morphological similarities shared with large VCL, particularly indriids (Gebo and Dagosto, 1988).

6.2.3. Omomyiforms

Omomyiforms are consistently reconstructed as more proficient leapers than adapiforms (Chapter 3 and 4), in agreement with previous studies (Szalay, 1975; Savage and Waters, 1978; Gebo, 1988; Covert and Hamrick, 1993; Dagosto and Schmid, 1996; Anemone and Covert, 2000; Dunn et al., 2006; Rose et al., 2011; Gebo et al., 2012a, 2015a). Nevertheless, they lack the extreme tarsal elongation characteristic of specialized small VCL species such as galagids and tarsiers, indicating that omomyiforms engaged in active yet not highly specialized VCL (Dagosto, 1988; Gebo, 1988; Boyer et al., 2013). In addition, omomyiforms are characterized by their low or nearly negligible percentages of suspensory locomotion, being more comparable to some early anthropoid species in this regard. This is supported by the absence of several tarsal features, interpreted as strepsirrhine synapomophies, that relate to increased mobility at the ankle joints and preferred use of inverted postures in vertical and oblique substrates—including a laterally positioned groove for the FHL tendon, a gently sloping fibular facet, and the lack of contact between the mesocuneiform and cuboid facets in the navicular (Beard, 1988; Dagosto, 1988, 2007; Gebo, 2011). Consequently, despite habitual comparisons to galagids and some cheirogaleid species, the absence of the aforementioned strepsirrhine synapomorphies make omomyiforms somewhat less analogous to these extant species compared to adapiforms like *Anchomomys frontanyensis*, which combined strong leaping proclivities with greater climbing and suspensory adaptations (Marigó et al., 2016, 2020).

The overall similarity in the predicted locomotor repertoires across omomyiform species is likely related to their comparable body sizes, which in most cases fall below 200 g (Fleagle et al., 2025). Even in larger-bodied taxa such as *Ourayia* and *Chipetaia* (>500 g), reconstructions consistently indicate habitual leaping, concurring with earlier works (Dunn et al., 2006; Dunn, 2010). This indicates that leaping was a pervasive component of omomyiform locomotion. Nonetheless, by analogy with extant galagids, it is not unlikely that larger-bodied omomyiforms engaged in more quadrupedal locomotion and preferred more horizontal substrates compared to smaller-bodied ones (Gebo, 1987a; Oxnard et al., 1990). This is supported by the results of the LOOCV analyses, which indicate that quadrupedalism is underestimated and leaping

overestimated in the largest-bodied galagid (*Otolemur*). Thus, while the PLSR analysis does not reveal this trend, it may be plausible that *Ourayia* and *Chipetaia* were less habitual leapers than other, smaller-bodied omomyiform species.

Despite the homogeneous locomotor repertoire of omoyiforms, some species deviate from this pattern. For example, based on navicular shape, *Tetonius homunculus* exhibits the highest percentages of quadrupedal locomotion and is classified as an arboreal quadruped in the discriminant analysis. This is supported by earlier studies on the astragalus and calcaneus of this taxon (not included in this dissertation), which noted features associated with climbing and suspensory behaviors, such as a relatively shorter distal calcaneus than in other omomyiforms (Gebo, 1988). Another species that stands out is *Vastanomys major*. Locomotor estimates for this species indicate a more generalized locomotor repertoire than in other omomyiforms, dominated by quadrupedal locomotion, moderate leaping percentages and the highest percentages of suspensory locomotion. These results are consistent with the somewhat distinct astragalar shape of this taxon (e.g., less steep fibular facet angle, more medially angled astragalar neck) as well as with the morphology of other postcranial remains, as reported in previous studies (Dunn et al., 2016; Llera Martin et al., 2022).

6.2.4. Early anthropoids

Among early anthropoids, locomotor reconstructions distinguish between Asian taxa, represented in this dissertation by *Eosimias* and *Ganlea*, and Afro-Arabian species, represented by parapithecoids (Chapter 4). Asian taxa are reconstructed as generalized arboreal quadrupeds with moderate percentages of climbing and suspensory behaviors along with quadrupedalism and leaping, resembling strepsirrhines and omomyiforms in these regards. Conversely, parapithecoids are consistently reconstructed as above-branch arboreal quadrupeds and leapers, with very similar locomotor repertoires to those of small to medium-sized platyrrhines like *Saimiri* or *Cebus*. These differences likely reflect the retention in Asian taxa of astragalar and calcaneal features absent from the more derived Afro-Arabian species (Fleagle, 1980; Gebo and Simons, 1987; Fleagle and Simons, 1995; Gebo et al., 2000, 2001, 2012b; Marivaux et al., 2003, 2010). These results concur with the view that the parapithecoid locomotor pattern—dominated by quadrupedalism and horizontal leaping—was preceded by a more generalized repertoire with stronger climbing and suspensory components, intermediate between that of adapiforms and omomyiforms and that of later, more derived anthropoids (Gebo and Dagosto, 2004).

The hindfoot morphology of *Eosimias* is somewhat intermediate between that of omomyiforms and more derived anthropoids, albeit each bone yields a moderately distinct locomotor signal (Gebo et al., 2000, 2001, 2012b). When astragalar shape is considered, the predicted locomotor repertoire closely resembles that of omomyiforms, with similar percentages of both quadrupedalism and leaping and absence of suspensory behaviors. This result is consistent with the astragalar morphology of *Eosimias*, which retains several omomyiform-like features—which are interpreted as primitive for euprimates (Gebo, 1986a; Beard, 1988)—such as a high astragalar body, a proximodistally short trochlea, a vertical fibular facet, and a mediolaterally narrow and moderately long neck (Dagosto, 1988, 2007; Gebo, 1988). In contrast, calcaneal shape yields higher percentages of climbing and suspensory locomotion, which may be explained by the presence of a mixture of derived anthropoid features (such as a relatively short distal length and a broad sustentaculum) with other traits that are suggestive of enhanced mobility (including a rounded ectal facet, a moderately concave plantar edge, and a slightly medially bended tuber calcanei; Gebo, 1986b; Seiffert et al., 2015). The other Asian taxon, *Ganlea*, is reconstructed with a generalized repertoire dominated by quadrupedalism and leaping, but also moderate percentages of climbing and suspension. This interpretation aligns with astragalar morphology, which combines features related to increased proclivity for leaping (e.g., a dorsoplantarly high astragalar body, parallel trochlear rims, a moderately elongated neck) with other characteristics that are associated with increased joint mobility (such as a shallow trochlea; Marivaux et al., 2003, 2010). Notably, the large astragalar head of *Ganlea* supports this reconstruction, as it indicates that the astragalar neck was able of enduring and transmitting large loadings in the medial direction of the foot (Szalay and Langdon, 1986).

Parapithecoids are consistently reconstructed as above-branch arboreal quadrupeds, in agreement with previous locomotor inferences based on tarsal morphology (e.g., Fleagle, 1980; Gebo and Simons, 1987; Fleagle and Simons, 1995). Overall, the hindfoot morphology of these taxa is suggestive of enhanced parasagittal movements to facilitate habitual dorsi- and plantarflexion at the expense of less rotational freedom at the main tarsal joints. Among parapithecoids, the proteopithecid *Proteopithecus sylviae* is reconstructed as having slightly greater leaping abilities than parapithecids, in agreement with its relatively more proximodistally elongated distal calcaneus (Seiffert and Simons, 2001; Boyer et al., 2013; Gladman et al., 2013).

6.3. Insights into primate origins and early evolution from tarsal evidence

Euprimates are characterized by a suit of adaptations not found in any other mammalian group, including higher encephalization, convergent orbits, a complete postorbital bar or septum, opposable hallux and pollex, and nails—at least on the hallux—rather than claws. Most species also show anatomical modifications for some degree of leaping behavior (Cartmill, 1974, 1992; Szalay et al., 1987; Rose, 1994b; Silcox et al., 2015). In particular, the hindfoot and navicular bone of euprimates exhibit features associated with strong pedal grasping and leaping, highlighting their relevance in the major anatomical reorganization that accompanied the origins and early evolution of euprimates (Dagosto, 1988, 2007). To account for the emergence of these traits, several adaptive hypotheses have been proposed, such as the "grasp-leaping" (Szalay, 1968; Szalay and Dagosto, 1980), the "(nocturnal) visual predator" (Cartmill, 1972, 1974a, b, 1992, 2012) or the "angiosperm coevolution" hypotheses (Sussman, 1991; Sussman and Raven, 1978; Sussman et al., 2013). Although not mutually exclusive (see Rassmussen, 1990), each one of these hypotheses underscores distinct selective pressures as the most critical in shaping the evolution of key euprimate adaptative complexes. More recently, stepwise models for the independent evolution of primate adaptative complexes have been proposed to accommodate these different hypotheses—beginning with feeding on the terminal branches and subsequently incorporating additional adaptations such as those associated with leaping behavior (Gebo, 2004; Sargis et al., 2007).

Locomotor reconstructions in Chapter 4 indicate that plesiadapiforms were generalized arboreal quadrupeds capable of engaging, to some extent, in suspensory and climbing locomotion. This concurs with previous studies arguing that plesiadapiforms already exhibited a relatively derived ankle compared with the primitive eutherian condition, enabling effective arboreal locomotion (Szalay and Decker, 1974; Szalay and Drawhorn, 1980; Chester et al., 2015). Whereas astragalar shape broadly yields a similar locomotor signal for all the members of this group included in the comparative sample, calcaneal shape reveals greater locomotor diversity. In particular, Chapter 4 reveals that plesiadapoids exhibit higher percentages of suspensory locomotion, while non-plesiadapoids are reconstructed as more strictly quadrupedal. This pattern suggests a locomotor shift from primarily quadrupedal animals, probably resembling extant scandentians to some degree, towards more adept climbers with enhanced grasping abilities, approaching the condition displayed by some arboreal marsupials like *Caluromys* (Rasmussen, 1990; Gebo, 2004; Sargis et al., 2007). This result concurs with the postcranial anatomy of

Carpolestes simpsoni, which combines adaptations for strong pedal grasping, such as an opposable hallux with a nail, with the absence of euprimate-like visual or leaping specializations (Bloch and Boyer, 2002). In addition, high evolutionary rates were detected in all three tarsal bones in both Chapters 3 and 4, indicating that substantial morphological changes occurred during plesiadapiform evolution. Changes in the function of a trait, or the evolution of a new trait with a novel function, can be associated with shifts in the rates of morphological evolution, accumulating morphological change as lineages diversify to fill new niches (e.g., Collar et al., 2010; Mahler et al., 2010; Higham et al., 2015; Botton-Divet and Nyakatura, 2021). Accordingly, changes in the rates of morphological evolution for the astragalus, calcaneus and navicular are also expected in those clades and lineages that evolved specialized locomotor repertoires, including slow climbers (lorisids), suspensory species (atelids) and VCL (tarsiers and galagids; Wainwright, 2007). Specifically, the astragalus seems to have been comparatively more stable, whereas calcaneal and navicular shape show greater evolvability. This might indicate that functional changes occurred primarily at the level of the LAJ and TTJ instead of the UAJ, which remained more conservative in the eutherian condition (Szalay and Decker, 1974; Lewis, 1980a, b; Szalay and Drawhorn, 1980). Such a pattern aligns with the terminal branch feeding hypothesis, a composite hypothesis between the (nocturnal) visual predator and the angiosperm coevolution hypotheses (Rasmussen, 1990), suggesting that adaptation to the fine branch milieu was critical in early stages of primate evolution. Moreover, this result still holds relevant if plesiadapiforms are shown not to be ancestral or closely related to euprimates. Still, a better understanding of plesiadapiform locomotor diversity and evolution will provide a scenario of convergent evolution as to how the ankle might have evolved from the primitive eutherian condition to that of an arboreal mammal specialized for terminal-branch environment on the arboreal canopy (Silcox, 2015).

Compared with plesiadapiforms, all early euprimates are reconstructed in Chapters 3 and 4 as exhibiting at least some degree of leaping behavior. Habitual leaping may therefore be considered a synapomorphy of Euprimates (Dagosto, 1988, 2007), in agreement with the "grasp-leaping" hypothesis (Szalay and Dagosto, 1980). This does not imply, however, that the LCA of euprimates was a highly specialized leaper, as ancestral reconstructions for its locomotor repertoire only yielded moderate leaping percentages (22–32%). Moreover, no early euprimate group shows clear-cut evidence of extreme VCL specializations. Additionally, if Vastan primates (including *Marcgodinotius* and *Vastanomys*, analyzed in this dissertation) are interpreted as basal representatives of their respective groups, as some authors suggest (Rose et al., 2009), the very low leaping percentages inferred for these taxa, along with the absence of adaptations for leaping behavior in their ankle morphology, further imply more limited leaping capabilities in the LCA of

euprimates (Rose et al., 2009; Dunn et al., 2016; Llera Martin et al., 2022). Notably, the basal position of the Vastan primates also concurs with the most plausible plaeobiogeographic scenario for the origin of euprimates, suggesting that the clade arose in Asia (Smith et al., 2006; Beard, 2008; Silcox, 2008; Rose et al., 2011; Morse et al., 2019). The recent discovery of a partial skeleton belonging to the basal haplorrhine *Archicebus achilles*—whose tarsal bones were not analyzed in this dissertation—further supports this view, as it has been described as lacking the leaping adaptations exhibited by other early tarsiiforms (Ni et al., 2013). On the other hand, leaping adaptations appear to have evolved independently in several euprimate lineages, including most tarsiiforms, galagids, indriids, *Lepilemur*, and several adapiform lineages (e.g., *Anchomomys frontanyensis*, *Djebelemur martinezi*, notharctines). Ancestral reconstructions of the locomotor repertoires of the strepsirrhine, tarsiiform and anthropoid LCAs further underscore the apparent independent evolution of enhanced leaping adaptations across crown primates. In addition, as mentioned above increases in the rates of morphological evolution in all three bones are observed in those lineages experiencing increases in their leaping behavior, indicating substantial morphological changes at the ankle in those groups showing leaping adaptations (Wainwright, 2007). The branch leading to the LCA of euprimates shows a similar pattern, correlating the morphological changes occurred at the onset of euprimate evolution with an initial, moderate increase in leaping behavior (Dagosto, 198, 2007). Given the persistent uncertainty surrounding early euprimate phylogenetic relationships and the presence of moderately long ghost lineages (Silcox and López-Torres, 2017), future discoveries of more complete fossil of early euprimates would hopefully shed further light on the locomotor adaptations that characterized the LCA of euprimates.

6.4. The evolution of crown-hominoid positional behaviors in the light of a dryopithecine astragalus from Abocador de Can Mata

6.4.1. Morphometric affinities, locomotor reconstruction and taxonomic attribution

Like most other Miocene ape astragali, IPS85037 from ACM displays a mosaic of traits not seen in any living anthropoid, combining several derived (hominoid-like) characteristics with an otherwise plesiomorphic ('monkey-like') morphology (Harrison, 1982; Conroy and Rose, 1983; Langdon, 1986; Gebo, 1989b; Drapeau, 2022). In Chapter 5, the morphology of IPS85037 is

analyzed in detail and compared to that of extant anthropoids (with special emphasis on extant hominoids) as well as other Miocene apes and stem catarrhines. Additionally, locomotor predictions based on shape and body mass estimates are carried out to confirm its initial taxonomic attribution and evaluate its morphofunctional implications.

Like in stem catarrhines and most Miocene apes, the trochlear morphology of IPS85037 is distally broader than proximally (wedged trochlea) and has a relatively deep trochlear groove. This morphology closely resembles that of some stem catarrhines—such as the dendropithecid *Simiolus enjiessi* and the pliopithecoid *Pliopithecus antiquus* (Leakey and Leakey, 1987; Rose et al., 1992; Senut, 2012)—as well as most Miocene hominoids for which astragalar morphology is known, including *Ekembo heseloni*, *Ekembo nyanzae*, *Equatorius africanus*, *Nacholapithecus kerioi*, and *Sivapithecus sivalensis* (MacInnes, 1943; Le Gros Clark and Leakey, 1951; Pilbeam et al., 1980; Harrison, 1982; Walker and Pickford, 1983; Leakey and Leakey, 1987; Rose et al., 1992, 1996; McCrossin, 1994; Madar, 1996; Ishida et al., 2004; Nakatsukasa et al., 2012). A dorsoplantarly high astragalar body combined with a relatively deep trochlea is indicative of less conjunct rotation at the UAJ during dorsi- and plantarflexion, effectively constraining movement to a parasagittal plane (Langdon, 1986; Ward, 1998). By contrast, a relatively wedged trochlea, which appears to be widespread among extinct hominoids, has been proposed to enhance stability during dorsiflexion while permitting greater abduction and adduction during plantarflexion (Rose, 1983; Langdon, 1986). As in extant hominoids, IPS85037 has a moderately symmetrical trochlea, with the lateral rim only slightly taller than the medial rim (Turley and Frost, 2013). A similar morphology is found in dendropithecids and the Miocene apes *Oreopithecus bambolii* and *Sivapithecus sivalensis* (Le Gros Clark and Thomas, 1951; Pilbeam et al., 1980; Szalay and Langdon, 1986; Leakey and Leakey, 1987; Rose et al., 1992; Madar, 1996). In contrast, the lateral rim of IPS85037 is less prominent than in extant cercopithecoids, pliopithecoids, and several stem hominoids, including *Turkanapithecus kalakolensis*, *Ekembo heseloni*, *Ekembo nyanzae*, *Equatorius africanus* and *Nacholapithecus kerioi* (Harrison, 1982; Walker and Pickford, 1983; Begun, 1987; Leakey and Leakey, 1987; Strasser, 1988; Ward et al., 1993; McCrossin, 1994; Ishida et al., 2004; Nakatsukasa et al., 2012; Senut, 2012). As explained above, the functional significance of this trait is unclear. Some authors proposed that it may facilitate abduction at the UAJ during dorsiflexion—facilitating weight transfer when the foot is in an inverted posture (Turley and Frost, 2013; Dunn et al., 2014; Knigge et al., 2015). However, its prevalence among (semi)terrestrial species, particularly in cercopithecoids, may instead be suggestive of promoting foot stabilization during quadrupedal locomotion along horizontal substrates, limiting abduction instead of favoring it (Strasser, 1988).

IPS85037 exhibits a deep, well-defined groove for the FHL tendon, like that of extant hominoids and the Miocene apes *Proconsul major* and *Oreopithecus bambolii* (Harrison, 1982; Szalay and Langdon, 1986; DeSilva, 2008). In contrast, pliopithecoids and the afropithecid *Equatorius africanus* display a shallow FHL groove (Begun, 1987; McCrossin, 1994; Senut, 2012). As discussed earlier, a relatively deep groove for the FHL tendon is associated with frequent climbing and hindlimb suspension in several extant primate groups (Harrison, 1982; Seiffert et al., 2015). Moreover, IPS85037 also possesses a well-developed lateral tubercle, comparable to that of the afropithecid *Nacholapithecus kerioi* (Ishida et al., 2004; Nakatsukasa et al., 2012). An enlarged lateral tubercle, which serves as the insertion of the posterior talofibular ligament—a key stabilizer of the ankle during dorsiflexion—is also functionally correlated with enhanced hindlimb suspension and inverted foot postures (Leardini et al., 2000). As in extant hominoids, particularly Asian apes, IPS85037 also shows a shallow medial tibial facet and lacks a dorsal ridge on the astragalar neck (Conroy and Rose, 1983). This condition is likewise exhibited by other Miocene apes such as *Rangwapithecus gordoni*, *Proconsul major* and *Oreopithecus bambolii* (Harrison, 1982; Szalay and Langdon, 1986; DeSilva, 2008). Conversely, pliopithecoids, dendropithecids, and several stem hominoids—including *Ekembo heseloni*, *Ekembo nyanzae*, *Equatorius africanus*, and *Nacholapithecus kerioi*—exhibit a more concave medial tibial facet and a pronounced dorsal ridge on the astragalar neck (MacInnes, 1943; Le Gros Clark and Leakey, 1951; Le Gros Clark and Thomas, 1951; Zapfe, 1958; Harrison, 1982; Walker and Pickford, 1983; Leakey and Leakey, 1987; Rose et al., 1992, 1996; McCrossin, 1994; Ishida et al., 2004; Nakatsukasa et al., 2012; Senut, 2012). The combination of a shallow medial tibial facet and the absence of a dorsal ridge on the astragalar neck is indicative of an ankle that does not lock into a close-packed configuration during dorsi- and plantarflexion, thereby enabling substantial mobility at the level of the UAJ (Conroy and Rose, 1983; Harrison, 1987; DeSilva, 2008).

The elongate, shallow ectal facet of IPS85037 closely resembles that of orangutans and atelids (Langdon, 1986; Turley and Frost, 2013; Püschel et al., 2017). Among stem catarrhines and Miocene apes, only *Oreopithecus bambolii* exhibits a comparable shallow and elongated ectal facet (Szalay and Langdon, 1986). Such configuration is functionally associated with greater mobility at the LAJ, facilitating increased astragalocalcaneal motion along the calcaneus and, thereby, enhancing the inversion and eversion capabilities of the foot (Langdon, 1986; Hamrick, 1996; Yapuncich and Granatosky 2021). Conversely, the sustentacular facet morphology of IPS85037 resembles that of most stem catarrhines and Miocene apes, being distomedially L-shaped (Harrison, 1982). Only *Oreopithecus bambolii* differs in that regard, approaching the

extant hominoid condition with a crescent-shaped facet (Szalay and Langdon, 1986). An L-shaped sustentacular facet is functionally linked with limited rotational mobility at the LAJ (Lewis, 1980b).

Most stem catarrhines and Miocene apes, including IPS85037, possess a moderately elongated neck, with the exception of *Oreopithecus bambolii*, which exhibits a markedly abbreviated neck (Harrison, 1982; Szalay and Langdon, 1986). The elongation of the astragalar neck is suggested to be driven by allometric effects (Harrison, 1982), and is typically regarded as a plesiomorphic anthropoid trait, functionally linked to enhanced leaping and quadrupedal locomotion (Gebo, 1989b). Among extant hominoids, only orangutans display a relatively elongated neck, which serves to further project the head further than the calcaneus, enhancing midtarsal rotational capabilities (Harrison 1982; Szalay and Langdon, 1986; Gebo 1989b). In relation to neck angulation, however, IPS85037 resembles *Oreopithecus bambolii* and African apes in displaying a very pronounced medial angulation (Szalay and Langdon, 1986). Such medial deflection of the neck is associated with a better transference and absorption of compressive forces along the medial side of the foot (Barnett 1955; Harrison 1982; Szalay and Langdon, 1986). As in orangutans, IPS85037 also bears a small, spherical astragalar head, smaller than that of other extant hominoids (excluding orangutans) and cercopithecoids. It also resembles the pliopithecoid *Pliopithecus antiquus* and the stem hominoids *Turkanapithecus kalakolensis* and *Proconsul major* in this regard (Harrison, 1982; Leakey and Leakey, 1987; DeSilva, 2008; Senut, 2012). Conversely, dendropithecoids and most Miocene apes possess larger and mediolaterally broader heads (MacInnes, 1943; Le Gros Clark and Leakey, 1951; Le Gros Clark and Thomas, 1951; Harrison, 1982; Walker and Pickford, 1983; Szalay and Langdon, 1986; Leakey and Leakey, 1987; Rose et al., 1992, 1996; Ward et al., 1993; McCrossin, 1994; Ishida et al., 2004; Nakatsukasa et al., 2012). The possession of a smaller, more spherical head suggests that IPS85037—like orangutans—would have been less capable of accommodating large compressive forces at the astragalonavicular joint than other extant hominoids, in which a broader talar head facilitates mediolateral movements (Szalay and Langdon 1986).

In Chapter 5, the body mass of IPS85037 is calculated based on centroid size, yielding an estimate of ~38 kg, similar to that of female orangutans and male bonobos (Smith and Jungers, 1997). This value is slightly lower to previous estimates reported for other dryopithecines from the Vallès-Penedès Basin, including *Pierolapithecus catalaunicus* (Susanna et al. 2014), *Dryopithecus fontani* (Moyà-Solà et al., 2009a; Alba et al., 2011), and *Hispanopithecus laietanus* (Moyà-Solà and Köhler, 1996 Moyà-Solà et al. 2004; Alba et al., 2012a; Susanna et al. 2014). Collectively, these results indicate that dryopithecines exhibited a significant degree of body size dimorphism, as seen in other Miocene and extant great apes (Plavcan, 2001). Consequently,

IPS85037 most probably belonged to a male individual, since attributing it to a female individual would imply a male body mass much larger than any other dryopithecine recorded so far. Given this estimated BM, it is unlikely that neck elongation resulted by allometric scaling (Harrison, 1982). Instead, as in orangutans, it could serve as a way for enhancing midtarsal rotation at the TTJ (Harrison 1982; Szalay and Langdon, 1986; Gebo 1989b).

The combination of locomotor modes inferred for IPS85037 includes moderate percentages of climbing and clambering (50%) and quadrupedalism (32%), and more restricted percentages for suspensory behavior (11%). This locomotor repertoire resembles that of two extant species—*Alouatta seniculus* and *Pan paniscus*—both of which exhibit a comparatively more versatile and generalized locomotor repertoires compared with other atelids and hominids. For instance, *Alouatta seniculus*, like other species of this genus, engages in substantially less suspensory locomotion than other atelids and, instead, relies more extensively on quadrupedal and clambering locomotion (Fleagle and Mittermeier, 1980; Schön Ybarra and Schön, 1987; Gebo, 1992a; Youlatos and Meldrum, 2011). Similarly, bonobos are far less suspensory than Asian apes, like *Gorilla* and *Pan troglodytes*, but, compared to the latter, bonobos seem to engage in more arboreal quadrupedalism than chimpanzees and gorillas, being primarily palmigrade (Doran 1993)—a locomotor mode that was likely used by Miocene apes to varying degrees (e.g., Rose 1994a; Almécija et al. 2007, 2009; Alba, et al. 2010c, 2012a; Alba 2012; Ward 2015). Notably, several pedal elements of bonobos, including the astragalus and entocuneiform, are indicative of a greater range of hallucal abduction compared to other African apes, suggesting adaptation for climbing on smaller and more varied substrates (Friesen et al. 2024). However, it is necessary to remark that neither *Alouatta seniculus* nor *Pan paniscus* are perfect analogues of IPS85037. *Alouatta seniculus* has a prehensile tail that is used in tail-assisted suspension during feeding postures (e.g., Gebo, 1992a), whereas hominoids do lack an external tail (which is considered a synapomorphy of the group; Ward et al., 1991; Nakatsukasa et al., 2003, 2004). Moreover, the estimated body mass of IPS85037 (~38 kg) is roughly four times that of *Alouatta seniculus*, implying that it would have used different substrate types and sizes (Preuschoft, 2002). In the case of *Pan paniscus*, the most significant difference with IPS85037 is that the former spends around half of their traveling time on the ground, moving quadrupedally via knuckle-walking (Doran 1993). This is an unlikely behavior for dryopithecines, based on lack of terrestrial adaptations on their hand morphology (Almécija et al. 2009; Alba et al. 2010c).

Altogether, the locomotor predictions reported in Chapter 5 are consistent with the observed morphology of IPS85037, which combines features associated with relatively mobile main tarsal joints along with an overall plesiomorphic morphology, as seen in other Miocene apes (Harrison,

1982; Drapeau, 2022). Considering its morphology, body size and chronology (~11.7 Ma, representing one of the two latest dryopithecine occurrences at ACM; Alba et al. 2017, 2022), IPS85037 might belong to any of the three dryopithecin species recorded from slightly older deposits along the ACM stratigraphic sequence (*Pierolapithecus catalaunicu*s, *Anoiapithecus brevirostris*, and *Dryopithecus fontani*; Moyà-Solà et al., 2004; Moyà-Solà, et al., 2009a,b; Alba et al. 2013, 2020, 2024), differing from the younger hispanopithecins (*Hispanopithecus laietanus* and *Hispanopithecus crusafonti*) in their inferred greater emphasis on suspensory behaviors (Moyà-Solà and Köhler, 1996; Almécija et al., 2007; Alba et al., 2012a). The absence of associated craniodental material and the lack of a documented astragalus for any dryopithecin species precludes a taxonomic assignment to genus rank.

6.4.2. Evolutionary implications for hominoid locomotion

Stem hominoids from the Early to Middle Miocene of Africa—such as *Proconsul*, *Ekembo*, *Afropithecus*, *Equatorius* and *Nacholapithecus*—as well as other early catarrhines (pliopithecoids and dendropithecids), generally exhibit a pronograde body plan primarily associated with quadrupedal locomotion (e.g., Ward, 1993, 2015; Nakatsukasa, 2004; Nakatsukasa and Kunimatsu, 2009; Russo et al., 2024). Likewise, almost all recovered astragali from these taxa show no evidence of the specialized, modern hominoid-like morphology, and, instead, display striking morphological uniformity (e.g., Harrison, 1982; Walker, 1997; Nakatsukasa et al., 2012; Ward, 2015; Drapeau, 2022). This pattern contrasts sharply with the postcranial morphology of extant apes, which are characterized by a suite of adaptations for below-branch, forelimb-dominated locomotion, including high intermembral indices and orthograde body plans (Ward, 2015). At the astragalus, and despite some differences between the different genera, extant apes share numerous adaptations associated with enhanced mobility of the main joints, allowing the foot to adopt multiple positions to provide strong anchorage to the substrate (Drapeau, 2022). Albeit incipient, stem hominoids from Africa already show some 'ape-like' features in their postcranium, including the astragalus (e.g., a fibular facet that flares more laterally) and elsewhere in the foot (a moderately robust hallux), which is suggestive of some degree of forelimb-dominated locomotion and slightly higher reliance in antipronograde behaviors in these taxa compared to most other earlier stem catarrhines (Conroy and Rose 1983; Ward et al., 1993; Walker 1997; Ward, 2015). Locomotor estimates for KNM-RU 2036 (*Ekembo heseloni*), presented in Chapter 5, support

this view, yielding a locomotor repertoire dominated by quadrupedalism (81%), low percentages of climbing and clambering (9%), and an almost complete absence of suspensory behaviors (2%). Among stem hominoids, only *Morotopithecus bishopi* exhibits putative orthograde-related adaptations in its vertebral morphology (Gebo et al., 1997; MacLatchy et al., 2000; MacLatchy, 2004; Nakatsukasa, 2008), while the largest stem hominoid species recorded, *Proconsul major*, based on several distinctive ankle features (DeSilva, 2008), has been proposed to engage in greater amounts of vertical climbing and other antipronograde behaviors.

Relatively younger apes from the Middle to Late Miocene of Eurasia, including those from the Vallès-Penedès Basin, appear to resemble earlier African Miocene apes in retaining a substantial quadrupedal component in their locomotor repertoire (e.g., Alba, 2012). However, the first unambiguous evidence of an orthograde body plan (*Pierolapithecus catalaunicus*) and habitual below-branch suspensory locomotion (*Danuvius*, *Rudapithecus* and *Hispanopithecus* spp.) is found among these Middle to Late Miocene ape species, highlighting the mosaic nature of their postcranial morphology (Begun, 1992; Moyà-Solà and Köhler, 1996; Moyà-Solà et al., 2004; Almécija et al., 2007, 2009; Alba et al., 2010c, 2011, 2012a; Alba, 2012). Consistent with this pattern, the astragalar morphology of IPS85037 already exhibits several astragalar features associated with enhanced mobility and strong hallucal grasping, resembling extant apes. This is further confirmed by its inferred locomotor repertoire, reported in Chapter 5, which includes moderate proportions of climbing and clambering (50%) and quadrupedalism (32%), along with a smaller but non-negligible component of suspensory behaviors (11%). These results indicate a locomotor shift towards a more forelimb-dominated locomotion, with greater use of climbing and clambering locomotion, compared to earlier hominoids like *Ekembo heseloni*. Yet, IPS85037 also retains multiple plesiomorphic ('monkey-like') traits, such as a tall astragalar body and elongated neck—revealing that, independently of the acquisition of an orthograde body plan and the enhancement of forelimb dominated locomotion, foot morphology remained relatively generalized (compared to extant apes) during most of Miocene ape evolution (Harrison, 1982; Drapeau, 2022). The mosaic morphology of IPS85037, along with its inferred locomotor repertoire, aligns with previous interpretations for the Middle Miocene dryopithecins of the Vallès-Penedès Basin—*Pierolapithecus catalaunicus* and *Dryopithecus fontani*—but differs from the greater emphasis on suspensory behaviors inferred for the Late Miocene hispanopithecins (Moyà-Solà and Köhler, 1996; Moyà-Solà et al., 2004, 2009a; Almécija et al., 2007, 2009, 2012; Alba et al., 2010c, 2011, 2012a; Pina et al., 2012, 2019, 2020; Hammond et al., 2013; Tallman et al., 2013; Susanna et al., 2014). This concurs with the abundant evidence that adaptations for suspensory locomotion and orthograde body plan did not evolve together but rather were acquired in parallel

in different hominoid lineages (e.g., Tuttle 1975; Larson 1998b; Alba 2012; Almécija et al. 2021). A similar pattern is observed in the stem pongine *Sivapithecus sivalensis*, one of the few Middle to Late Miocene ape species for which the astragalus is recorded (Pilbeam et al., 1980). Like IPS85037, *Sivapithecus sivalensis* retains a mosaic astragalar morphology, and its ankle has been interpreted as less mobile than that of extant apes, but more mobile than in living cercopithecoids (Pilbeam et al., 1980; Madar, 1996). The only Miocene ape that exhibits an extant ape-like astragalar morphology is *Oreopithecus bambolii*, which exhibits a uniquely derived hominoid-like ankle, characterized by a highly mobile talocrural joint and a splayed forefoot (Szalay and Langdon 1986). These features are consistent with other adaptations in the postcranium that have led multiple researchers to propose different antipronograde behaviors for this species, including vertical climbing and suspension (Jungers, 1987; Russo and Shapiro, 2013; Hammond et al., 2020; see also Köhler and Moyà-Solà, 1997; Rook et al., 1999; for an alternative reconstruction of this species as a facultative biped). Nevertheless, the systematic status of *Oreopithecus bambolii* remains debated, with most authors considering that it is less closely related to extant great apes than dryopithecines are (e.g., Alba et al., 2024b). Given the scarcity of Late Miocene hominoid material, the discovery of new pedal elements attributable to Eurasian Middle to Late Miocene apes, such as dryopithecines, together with more thorough analyses of the available specimens, is of the utmost importance to better understand the locomotor repertoire of the last common ancestor of crown hominoids, as well as the subsequent evolution of diverging locomotor lineages along various lineages, including the emergence of habitual bipedalism in hominins (McNutt et al., 2018).

Chapter 7:

Conclusions

Chapter 7. Conclusions

1. The shape of the astragalus, calcaneus, and navicular is functionally related to locomotion among extant primates. Therefore, these bones can be used to make meaningful locomotor inferences for extinct primates. However, it is important to account for factors like phylogeny, body size, and foot type when investigating the relationship between tarsal shape and locomotor behavior.
2. Plesiadapiforms are reconstructed as predominantly quadrupedal with moderate percentages of climbing, leaping, and suspensory behaviors. However, the calcaneus reveals greater locomotor diversity, indicating that plesiadapiforms underwent a locomotor shift from primarily quadrupedal forms to more proficient climbers with enhanced grasping abilities.
3. Euprimates show moderate adaptations for leaping early on in their evolution, albeit specializations for enhanced leaping behavior arose convergently in different lineages. Specifically, adapiforms exhibit the most diverse locomotor repertoires among early euprimates, revealing greater pedal mobility and an emphasis on inverted postures compared to omomyiforms. The latter are reconstructed as proficient leapers, although less specialized than galagids and tarsiers.
4. Locomotor inferences highlight a clear contrast between Asian early anthropoids and Afro-Arabian parapithecoids. The former are interpreted as generalized arboreal quadrupeds, combining quadrupedalism and leaping with moderate climbing and suspension, whereas the latter exhibited a comparatively more derived anthropoid morphology associated with above-branch quadrupedalism and horizontal leaping.
5. The isolated astragalus of a Middle Miocene dryopithecin from ACM exhibits a mosaic morphology, combining derived (crown hominoid-like) features with plesiomorphic ('monkey-like') traits. Along with its inferred body mass, the inferred locomotor repertoire (dominated by vertical climbing, clambering and quadrupedalism) is consistent with previous inferences for dryopithecins based on other anatomical regions, reinforcing the view that suspensory adaptations evolved later than the orthograde body plan.

References

References

Abdi, H., 2010. Partial least squares regression and projection on latent structure regression (PLS Regression). Wiley Interdiscip. Rev. Comput. Stat. 2, 97–106.

Adams, D.C., 2014a. Quantifying and comparing phylogenetic evolutionary rates for shape and other high-dimensional phenotypic data. Syst. Biol. 63, 166–177.

Adams, D.C., 2014b. A method for assessing phylogenetic least squares models for shape and other high-dimensional multivariate data. Evolution 68, 2675–2688.

Adams, D.C., Collyer, M.L., 2015. Permutation tests for phylogenetic comparative analyses of high-dimensional shape data: what you shuffle matters. Evolution 69, 823–829.

Adams, D.C., Collyer, M.L., 2018. Multivariate phylogenetic comparative methods: evaluations, comparisons, and recommendations. Syst. Biol. 67, 14–31.

Adams, D.C., Collyer, M.L., 2019. Phylogenetic comparative methods and the evolution of multivariate phenotypes. Annu. Rev. Ecol. Evol. Syst. 50, 405–425.

Adams, D.C., Nistri, A., 2010. Ontogenetic convergence and evolution of foot morphology in European cave salamanders (Family: Plethodontidae). BMC Evol. Biol. 10, 216.

Adams, D.C., Rohlf, F.J., Slice, D.E., 2004. Geometric morphometrics: ten years of progress following the 'revolution'. Ital. J. Zool. 71, 5–16.

Adkins, R.M., Honeycutt, R.L., 1991. Molecular phylogeny of the superorder Archonta. Proc. Natl. Acad. Sci. USA 88, 10317–10321.

Agustí, J., Köhler, M., Moyà-Solà, S., Cabrera, L., Garcés, M., Parés, J.M., 1996. Can Llobateres: the pattern and timing of the Vallesian hominoid radiation reconsidered. J. Hum. Evol. 31, 143–155.

Agustí, J., Cabrera, L., Garces, M., Parés, J.M., 1997. The Vallesian mammal succession in the Vallès-Penedès basin (northeast Spain): Paleomagnetic calibration and correlation with global events. Palaeogeogr. Palaeoclimatol. Palaeoecol. 133, 149–180.

Aiello, L., Dean, C., 1990. An Introduction to Human Evolutionary Anatomy. Academic Press, San Diego.

Alba, D.M., 2012. Fossil apes from the Vallès-Penedès Basin. Evol. Anthropol. 21, 254–269.

Alba, D.M., Moyà-Solà, S., 2012. A new pliopithecid genus (Primates: Pliopithecoidea) from Castell de Barberà (Vallès-Penedès basin, Catalonia, Spain). Am. J. Phys. Anthropol. 147, 88–112.

Alba, D.M., Moyà-Solà, S., Malgosa, A., Casanovas-Vilar, I., Robles, J.M., Almécija, S., Galindo, J., Rotgers, C., Mengual, J.V.B., 2010a. A new species of *Pliopithecus* Gervais, 1849 (Primates:

Pliopithecidae) from the middle Miocene (mn8) of Abocador de Can Mata (els Hostalets de Pierola, Catalonia, Spain). Am. J. Phys. Anthropol. 141, 52–75.

Alba, D.M., Fortuny, J., Moyà-Solà, S., 2010b. Enamel thickness in the Middle Miocene great apes *Anoiapithecus*, *Pierolapithecus* and *Dryopithecus*. Proc. R. Soc. B 277, 2237–2245.

Alba, D.M., Almécija, S., Moyà-Solà, S., 2010c. Locomotor inferences in *Pierolapithecus* and *Hispanopithecus*: Reply to: Reply to Deane and Begun, 2008. J. Hum. Evol. 59, 143–149.

Alba, D.M., Moyà-Solà, S., Almécija, S., 2011. A partial hominoid humerus from the middle Miocene of Castell de Barberà (Vallès-Penedès Basin, Catalonia, Spain). Am. J. Phys. Anthropol. 144, 365–381.

Alba, D.M., Almécija, S., Casanovas-Vilar, I., Méndez, J.M., Moyà-Solà, S., 2012a. A partial skeleton of the fossil great ape *Hispanopithecus laietanus* from Can Feu and the mosaic evolution of crown-hominoid positional behaviors. PLoS One 7, e39617.

Alba, D.M., Casanovas-Vilar, I., Almécija, S., Robles, J.M., Arias-Martorell, J., Moyà-Solà, S., 2012b. New dental remains of *Hispanopithecus laietanus* (primates: Hominidae) from Can Llobateres 1 and the taxonomy of late Miocene hominoids from the Vallès-Penedès Basin (NE Iberian Peninsula). J. Hum. Evol. 63, 231–246.

Alba, D.M., Fortuny, J., de Los Rios, M.P., Zanolli, C., Almécija, S., Casanovas-Vilar, I., Robles, J.M., Moyà-Solà, S., 2013. New dental remains of *Anoiapithecus* and the first appearance datum of hominoids in the Iberian Peninsula. J. Hum. Evol. 65, 573–584.

Alba, D.M., Almécija, S., DeMiguel, D., Fortuny, J., de los Ríos, M.P., Pina, M., Robles, J.M., Moyà-Solà, S., 2015. Miocene small-bodied ape from Eurasia sheds light on hominoid evolution. Science 350, aab2625.

Alba, D.M., Casanovas-Vilar, I., Garcés, M., Robles, J.M., 2017. Ten years in the dump: An updated review of the Miocene primate-bearing localities from Abocador de Can Mata (NE Iberian Peninsula). J. Hum. Evol. 102, 12-20.

Alba, D.M., Casanovas-Vilar, I., Furió, M., García-Paredes, I., Angelone, C., Jovells-Vaqué, S., Luján, À.H., Almécija, S., Moyà-Solà, S., 2018. Can Pallars i Llobateres: A new hominoid-bearing locality from the late Miocene of the Vallès-Penedès Basin (NE Iberian Peninsula). J. Hum. Evol. 121, 193–203.

Alba, D.M., Fortuny, J., Robles, J.M., Bernardini, F., de Los Ríos, M.P., Tuniz, C., Moyà-Solà, S., Zanolli, C., 2020. A new dryopithecine mandibular fragment from the middle Miocene of Abocador de Can Mata and the taxonomic status of '*Sivapithecus*' *occidentalis* from Can Vila (Vallès-Penedès Basin, NE Iberian Peninsula). J. Hum. Evol. 145, 102790.

Alba, D.M., Robles, J.M., Casanovas-Vilar, I., Beamud, E., Bernor, R.L., Cirilli, O., DeMiguel, D., Galindo, J., Llopart, I., Pons-Monjo, G., Sánchez, I.M., 2022. A revised (earliest Vallesian) age for

the hominoid-bearing locality of Can Mata 1 based on new magnetostratigraphic and biostratigraphic data from Abocador de Can Mata (Vallès-Penedès Basin, NE Iberian Peninsula). J. Hum. Evol. 170, 103237.

Alba, D.M., Bouchet, F., Fortuny, J., Robles, J.M., Galindo, J., Luján, À.H., Moyà-Solà, S., Zanolli, C., 2024a. New remains of the Miocene great ape *Anoiapithecus brevirostris* from Abocador de Can Mata. J. Hum. Evol. 188, 103497.

Alba, D.M., Urciuoli, A., Hammond, A.S., Almécija, S., Rook, L., Zanolli, C., 2024b. Miocene ape evolution: Where does *Oreopithecus* fit in? Boll. Soc. Paleontol. Ital. 63, 153–182.

Alberch, P., Gould, S.J., Oster, G.F., Wake, D.B., 1979. Size and shape in ontogeny and phylogeny. Paleobiology 5, 296–317.

Albrecht, G.H., 1992. Assessing the affinities of fossils using canonical variates and generalized distances. Hum. Evol. 7, 49–69.

Albrecht, G.H., Gelvin, B.R., Hartman, S.E., 1993. Ratios as a size adjustment in morphometrics. Am. J. Phys. Anthropol. 91, 441–468.

Almécija, S., Alba, D.M., Moyà-Solà, S., Köhler, M., 2007. Orang-like manual adaptations in the fossil hominoid *Hispanopithecus laietanus*: first steps towards great ape suspensory behaviours. Proc. R. Soc. B 274, 2375–2384.

Almécija, S., Alba, D.M., Moyà-Solà, S., 2009. *Pierolapithecus* and the functional morphology of Miocene ape hand phalanges: paleobiological and evolutionary implications. J. Hum. Evol. 57, 284–297.

Almécija, S., Alba, D.M., Moyà-Solà, S., 2012. The thumb of Miocene apes: new insights from Castell de Barberà (Catalonia, Spain). Am. J. Phys. Anthropol. 148, 436–450.

Almécija, S., Orr, C.M., Tocheri, M.W., Patel, B.A., Jungers, W.L., 2015. Exploring phylogenetic and functional signals in complex morphologies: The hamate of extant anthropoids as a test-case study. Anat. Rec. 298, 212–229.

Almécija, S., Hammond, A.S., Thompson, N.E., Pugh, K.D., Moyà-Solà, S., Alba, D.M., 2021. Fossil apes and human evolution. Science 372, eabb4363.

Anapol, F., Turner, T.R., Mott, C.S., Jolly, C.J., 2005. Comparative postcranial body shape and locomotion in *Chlorocebus aethiops* and *Cercopithecus mitis*. Am. J. Phys. Anthropol. 127, 231–239.

Anderson, M.J., 2001. A new method for non-parametric multivariate analysis of variance. Austral Ecol. 26, 32–46.

Andrews, P., 1992. Evolution and environment in the Hominoidea. Nature 360, 641–646.

Andrews, P., Harrison, T., Martin, L., Delson, E., Bernor, R., 1996. Distribution and biochronology of European and southwest Asian Miocene catarrhines. In: R Bernor, R., Fahlbusch, V.,

Mittmann, H.W. (Eds.), The Evolution of Western Eurasian Neogene Mammal Faunas. Columbia University Press, New York, pp. 168–207.

Anemone, R.L., 1990. The VCL hypothesis revisited: patterns of femoral morphology among quadrupedal and saltatorial prosimian primates. Am. J. Phys. Anthropol. 83, 373–393.

Anemone, R.L., Covert, H.H., 2000. New skeletal remains of *Omomys* (Primates, Omomyidae): functional morphology of the hindlimb and locomotor behavior of a Middle Eocene primate. J. Hum. Evol. 38, 607–633.

Ankel-Simons, F., 2007. Primate Anatomy: An Introduction. Academic Press, New York.

Ankel-Simons, F., Fleagle, J.G., Chatrath, P.S., 1998. Femoral anatomy of *Aegyptopithecus zeuxis*, an early Oligocene anthropoid. Am. J. Phys. Anthropol. 106, 413–424.

Archer, W., Pop, C.M., Rezek, Z., Schlager, S., Lin, S.C., Weiss, M., Dogandžić, T., Desta, D., McPherron, S.P., 2018. A geometric morphometric relationship predicts stone flake shape and size variability. Archaeol. Anthropol. Sci. 10, 1991–2003.

Bachelier, L., 1900. Théorie de la spéculation. Ann. Sci. Éc. Norm. Supér. 3, 21–86.

Bacon, A.M., Godinot, M., 1998. Analyse morphofonctionnelle des fémurs et des tibias des «Adapis» du Quercy: mise en évidence de cinq types morphologiques. Folia Primatol. 69, 1–21.

Bajpai, S., Kay, R.F., Williams, B.A., Das, D.P., Kapur, V.V., Tiwari, B.N., 2008. The oldest Asian record of Anthropoidea. Proc. Natl. Acad. Sci. USA. 105, 11093–11098.

Bardua, C., Felice, R.N., Watanabe, A., Fabre, A.C., Goswami, A., 2019. A practical guide to sliding and surface semilandmarks in morphometric analyses. Integr. Org. Biol. 1, obz016.

Barnett, C.H., 1955. Some factors influencing angulation of the neck of the mammalian talus. J. Anat. 89, 225–230.

Barnett, C.H., Napier, J.R., 1952. The axis of rotation at the ankle joint in man. Its influence upon the form of the talus and the mobility of the fibula. J. Anat. 86, 1–9.

Bastir, M., Rosas, A., 2006. Correlated variation between the lateral basicranium and the face: a geometric morphometric study in different human groups. Arch. Oral Biol. 51, 814–824.

Bastir, M., Torres-Tamayo, N., Palancar, C.A., Lois-Zlolniski, S., García-Martínez, D., Riesco-López, A., Vidal, D., Blanco-Pérez, E., Barash, A., Nalla, S., Martelli, S., 2019. Geometric morphometric studies in the human spine. In: Been, E., Gómez-Olivencia, A., Ann Kramer, P. (Eds.), Spinal Evolution. Springer, Cham, pp. 361–386.

Beard, K.C., 1990. Gliding behaviour and palaeoecology of the alleged primate family Paromomyidae (Mammalia, Dermoptera). Nature 345, 340–341.

Beard, K.C., 1993a. Phylogenetic systematics of the Primatomorpha, with special reference to Dermoptera. In: Szalay, F.S., Novacaek, J., McKenna, M.C. (Eds.), Mammal Phylogeny: Placentals. Springer, New York, pp.129–150.

Beard, K.C., 1993b. Origin and evolution of gliding in early Cenozoic Dermoptera (Mammalia, Primatomorpha). In: MacPhee, R.D.E. (Ed.), Primates and their Relatives in Phylogenetic Perspective. Springer, New York, pp. 63–90.

Beard, K.C., 2008. The oldest North American primate and mammalian biogeography during the Paleocene–Eocene Thermal Maximum. Proc. Natl. Acad. Sci. USA 105, 3815–3818.

Beard, K.C., 2016. Out of Asia: anthropoid origins and the colonization of Africa. Annu. Rev. Anthropol. 45, 199–213.

Beard, K.C., Dagosto, M., Gebo, D.L., Godinot, M., 1988. Interrelationships among primate higher taxa. Nature 331, 712–714.

Beard, K.C., Tong, Y., Dawson, M.R., Wang, J., Huang, X., 1996. Earliest complete dentition of an anthropoid primate from the late middle Eocene of Shanxi Province, China. Science 272, 82–85.

Beard, K.C., Marivaux, L., Tun, S.T., Soe, A.N., Chaimanee, Y., Htoon, W., Marandat, B., Aung, H.H., Jaeger, J.J., 2007. New sivaladapid primates from the Eocene Pondaung Formation of Myanmar and the anthropoid status of Amphipithecidae. Bull. Carnegie Mus. Nat. Hist. 39, 67–76.

Beard, K.C., Marivaux, L., Chaimanee, Y., Jaeger, J.J., Marandat, B., Tafforeau, P., Soe, A.N., Tun, S.T., Kyaw, A.A., 2009. A new primate from the Eocene Pondaung Formation of Myanmar and the monophyly of Burmese amphipithecids. Proc. R. Soc. B 276, 3285–3294.

Beaudet, A., 2025. Investigating the primate fossil record using diffeomorphic deformation: what have we learnt? Bull. Mém. Soc. Anthropol. 37, 98–104.

Beaulieu, J.M., Jhwueng, D.C., Boettiger, C., O'Meara, B.C., 2012. Modeling stabilizing selection: expanding the Ornstein–Uhlenbeck model of adaptive evolution. Evolution 66, 2369–2383.

Begun, D.R., 1987. A review of the genus *Dryopithecus*. Ph.D. Dissertation, University of Pennsylvania.

Begun, D.R., 1992a. *Dryopithecus crusafonti* sp. nov., a new Miocene hominoid species from Can Ponsic (Northeastern Spain). Am. J. Phys. Anthropol. 87, 291–309.

Begun, D.R., 1992b. Miocene fossil hominids and the chimp-human clade. Science 257, 1929–1933.

Begun, D.R., 2002. European hominoids. In: Hartwig, W.C. (Ed.), The Primate Fossil Record. Cambridge University Press, Cambridge, pp. 339–368.

Begun, D.R., 2009. Dryopithecins, Darwin, de Bonis, and the European origin of the African apes and human clade. Geodiversitas 31, 789–816.

Begun, D.R., 2015. Fossil record of Miocene hominoids. In: Henke, W., Tattersall, I. (Ed.), Handbook of Paleoanthropology, 2nd ed. Springer, Heidelberg, pp. 1261–1332.

Begun, D.R, Ward, C.V., 2005. Comment on "*Pierolapithecus catalaunicus*, a new Middle Miocene great ape from Spain". Science 308, 203.

Begun, D.R., Moyà-Solà, S., Kohler, M., 1990. New Miocene hominoid specimens from Can Llobateres (Vallès Penedès, Spain) and their geological and paleoecological context. J. Hum. Evol. 19, 255–268.

Begun, D.R., Ward, C.V., Rose, M.D., 1997. Events in hominoid evolution. In: Begun, D.R., Ward, C.V., Rose, M.D. (Eds), Function, Phylogeny, and Fossils. Plenum Press, New York, pp. 389–415.

Begun, D.R., Nargolwalla, M.C., Kordos, L., 2012. European Miocene hominids and the origin of the African ape and human clade. Evol. Anthropol. 21, 10–23.

Benefit, B.R., 1999. *Victoriapithecus*: the key to Old World monkey and catarrhine origins. Evol. Anthropol. 7, 155–174.

Bertram, J.E., 2004. New perspectives on brachiation mechanics. Am. J. Phys. Anthropol. 125, 100–117.

Bezanson, M., 2009. Life history and locomotion in *Cebus capucinus* and *Alouatta palliata*. Am. J. Phys. Anthropol. 140, 508–517.

Bloch, J.I., Boyer, D.M., 2002. Grasping primate origins. Science 298, 1606–1610.

Bloch, J.I., Boyer, D.M., 2007. New skeletons of Paleocene-Eocene Plesiadapiformes: A diversity of arboreal positional behaviors in early primates. In: Ravosa, M.J., Dagosto, M. (Eds.), Primate Origins: Adaptations and Evolution. Springer, New York, pp. 535–581

Bloch, J.I., Silcox, M.T., Boyer, D.M, Sargis, E.J., 2007. New Paleocene skeletons and the relationship of plesiadapiforms to crown-clade primates. Proc. Natl. Acad. Sci. USA 104, 1159–1164.

Blomberg, S.P., Garland Jr, T., Ives, A.R., 2003. Testing for phylogenetic signal in comparative data: behavioral traits are more labile. Evolution 57, 717–745.

Blomberg, S.P., Rathnayake, S.I., Moreau, C.M., 2020. Beyond Brownian motion and the Ornstein-Uhlenbeck process: stochastic diffusion models for the evolution of quantitative characters. Am. Nat. 195, 145–165.

Bock, W.J., 1977. Adaptation and the comparative method. In: Hecht, M.K., Goody, P.C., Hecht, B.M. (Eds.), Major Patterns in Vertebrate Evolution. Plenum Press, New York, pp. 57–82.

Böhme, M., Spassov, N., Fuss, J., Tröscher, A., Deane, A.S., Prieto, J., Kirscher, U., Lechner, T., Begun, D.R., 2019. A new Miocene ape and locomotion in the ancestor of great apes and humans. Nature 575, 489–493.

Boinski, S., 1989. The positional behavior and substrate use of squirrel monkeys: ecological implications. J. Hum. Evol. 18, 659–677.

Bookstein, F.L., 1986. Size and shape spaces for landmark data in two dimensions. Stat. Sci. 1, 181–222.

Bookstein, F.L., 1989. " Size and shape": a comment on semantics. Syst. Zool. 38, 173–180.

Bookstein, F.L., 1991, Morphometric Tools for Landmark Data: Geometry and Biology. Cambridge University Press, Cambridge.

Bookstein, F.L., 1996. Biometrics, biomathematics and the morphometric synthesis. Bull. Math. Biol. 58, 313–365.

Bookstein, F.L., 1997. Landmark methods for forms without landmarks: morphometrics of group differences in outline shape. Med. Image Anal. 1, 225–243.

Bookstein, F.L., 2019. Pathologies of between-groups principal components analysis in geometric morphometrics. Evol. Biol. 46, 271–302.

Bookstein, F.L., Chernoff, B., Elder, R., Humphries, J., Smith, G., Strauss, R., 1985. Morphometrics in Evolutionary Biology. The Geometry of Size and Shape Change, with Examples from FishesThe Academy of Natural Sciences of Philadelphia, Philadelphia.

Bookstein, F.L., Gunz, P., Mitteroecker, P., Prossinger, H., Schaefer, K., Seidler, H., 2003. Cranial integration in *Homo*: Singular warps analysis of the midsagittal plane in ontogeny and evolution. J. Hum. Evol. 44, 167–187.

Botton-Divet, L., Nyakatura, J.A., 2021. Vertical clinging and leaping induced evolutionary rate shifts in postcranial evolution of tamarins and marmosets (Primates, Callitrichidae). BMC Ecol. Evol. 21, 132.

Botton-Divet, L., Houssaye, A., Herrel, A., Fabre, A.C., Cornette, R., 2015. Tools for quantitative form description; an evaluation of different software packages for semi-landmark analysis. PeerJ 3, e1417.

Bouchet, F., Zanolli, C., Urciuoli, A., Almécija, S., Fortuny, J., Robles, J.M., Beaudet, A., Moyà-Solà, S., Alba, D.M., 2024a. The Miocene primate *Pliobates* is a pliopithecoid. Nat. Commun. 15, 2822.

Bouchet, F., Zanolli, C., Skinner, M.M., Urciuoli, A., Fortuny, J., Almécija, S., Bernardini, F., Tuniz, C., Schillinger, B., Moyà-Solà, S., Alba, D.M., 2024b. Molar enamel–dentine junction shape of *Pliobates cataloniae* and other Iberian pliopithecoids. J. Hum. Evol. 195, 103581.

Boyer, D.M., Bloch, J.I., 2008. Evaluating the mitten-gliding hypothesis for Paromomyidae and Micromomyidae (Mammalia, “Plesiadapiformes”) using comparative functional morphology of new Paleogene skeletons. In: Sargis, E.J., Dagosto, M. (Eds.), Mammalian Evolutionary Morphology. Springer, Dordrecht, pp. 233–284.

Boyer, D.M., Gingerich, P.D., 2019. Skeleton of late Paleocene *Plesiadapis cookei* (Mammalia, Euarchonta): Life history, locomotion, and phylogenetic relationships. Univ. Mich. Pap. Paleontol. 38, 1–263.

Boyer, D.M., Seiffert, E.R., 2013. Patterns of astragalar fibular facet orientation in extant and fossil primates and their evolutionary implications. Am. J. Phys. Anthropol. 151, 420–447.

Boyer, D.M., Seiffert, E.R., Simons, E.L., 2010a. Astragalar morphology of *Afradapis*, a large adapiform primate from the earliest late Eocene of Egypt. Am. J. Phys. Anthropol. 143, 383–402.

Boyer, D.M., Evans, A.R., Jernvall, J., 2010b. Evidence of dietary differentiation among late Paleocene–early Eocene plesiadapids (Mammalia, Primates). Am. J. Phys. Anthropol. 142, 194–210.

Boyer, D.M., Seiffert, E.R., Gladman, J.T., Bloch, J.I., 2013. Evolution and allometry of calcaneal elongation in living and extinct primates. PLoS One 8, e67792.

Boyer, D.M., Yapuncich, G.S., Butler, J.E., Dunn, R.H., Seiffert, E.R., 2015a. Evolution of postural diversity in primates as reflected by the size and shape of the medial tibial facet of the talus. Am. J. Phys, Anthropol. 157, 134–177.

Boyer, D.M., Puente, J., Gladman, J.T., Glynn, C., Mukherjee, S., Yapuncich, G.S., Daubechies, I., 2015b. A new fully automated approach for aligning and comparing shapes. Anat. Rec. 298, 249–276.

Boyer, D.M., Toussaint, S., Godinot, M., 2017a. Postcrania of the most primitive euprimate and implications for primate origins. J. Hum. Evol. 111, 202–215.

Boyer, D.M., Gunnell, G.F., Kaufman, S., McGeary, T.M., 2017b. Morphosource: archiving and sharing 3-D digital specimen data. Paleontol. Soc. Pap. 22, 157–181.

Brown, R., 1828. A brief account of microscopical observations made in the months of June, July and August 1827, on the particles contained in the pollen of plants; and on the general existence of active molecules in organic and inorganic bodies. Phil. Mag. 4, 161-173.

Butler, M.A., King, A.A., 2004. Phylogenetic comparative analysis: a modeling approach for adaptive evolution. Am. Nat. 164, 683–695.

Byron, C.D., Covert, H.H., 2004. Unexpected locomotor behaviour: brachiation by an Old World monkey (*Pygathrix nemaeus*) from Vietnam. J. Zool. 263, 101–106.

Cabrera, L., Roca, E., Garcés, M., Porta, J. de, 2004. Estratigrafía y evolución tectonosedimentaria oligocena superior-neógena del sector central del margen catalán (Cadena Costero-Catalana). In: Vera, J.A. (Ed.), Geología de España. Sociedad Geológica de España / Instituto Geológico y Minero de España, Madrid, pp. 569–573.

Campbell, N.A., Atchley, W.R., 1981. The geometry of canonical variate analysis. Syst. Biol. 30, 268–280.

Campbell, C.J., Fuentes, A., MacKinnon, K.C., Bearder, S.K., Stumpf, R., 2010. Primates in Perspective. Oxford University Press, Oxford.

Cant, J.G.H., 1986. Locomotion and feeding postures of spider and howling monkeys: field study and evolutionary interpretation. Folia Primatol. 46, 1–14.

Cant, J.G., 1987. Positional behavior of female Bornean orangutans (*Pongo pygmaeus*). Am. J. Primatol. 12, 71–90.

Cant, J.G., 1988. Positional behavior of long-tailed macaques (*Macaca fascicularis*) in northern Sumatra. Am. J. Phys. Anthropol. 76, 29–37.

Cant, J.G., 1992. Positional behavior and body size of arboreal primates: a theoretical framework for field studies and an illustration of its application. Am. J. Phys. Anthropol. 88, 273–283.

Cant, J.G., Youlatos, D., Rose, M.D., 2001. Locomotor behavior of *Lagothrix lagothricha* and *Ateles belzebuth* in Yasunı National Park, Ecuador: general patterns and nonsuspensory modes. J. Hum. Evol. 41, 141–166.

Cardini, A., Polly, P.D., 2020. Cross-validated between group PCA scatterplots: A solution to spurious group separation? Evol. Biol. 47, 85–95.

Cardini, A., O'Higgins, P., Rohlf, F.J., 2019. Seeing distinct groups where there are none: spurious patterns from between-group PCA. Evol. Biol. 46, 303–316.

Cartmill, M., 1974a. Pads and claws in arboreal locomotion. In: Jenkins, F.A. (Ed.), Primate Locomotion. Academic Press, New York, pp. 45–83.

Cartmill, M., 1974b. Rethinking primate origins. Science 184, 436–443.

Cartmill, M., 1985. Climbing. In: Hilderbrand, M., Bramble, D.M., Liem, K.F., Wake, D.B. (Eds.), Functional Vertebrate Morphology. Harvard University Press, Cambridge, pp. 73–88.

Cartmill, M., 1992. New views on primate origins. Evol. Anthropol. 1, 105–111.

Cartmill, M., 2012. Primate origins, human origins, and the end of higher taxa. Evol. Anthropol. 21, 208–220.

Cartmill, M., 2018. A sort of revolution: Systematics and physical anthropology in the 20th century. Am. J. Phys. Anthropol. 165, 677–687.

Cartmill, M., Milton, K., 1977. The lorisiform wrist joint and the evolution of "brachiating" adaptations in the Hominoidea. Am. J. Phys. Anthropol. 47, 249–272.

Cartmill, M., Lemelin, P., Schmitt, D., 2002. Support polygons and symmetrical gaits in mammals. Zool. J. Linn. Soc. 136, 401–420.

Cartmill, M., Lemelin, P., Schmitt, D., 2007a. Understanding the adaptive value of diagonal-sequence gaits in primates: A comment on Shapiro and Raichlen, 2005. Am. J. Phys. Anthropol. 133, 822–825.

Cartmill, M., Lemelin, P., Schmitt, D., 2007b. Primate gaits and primate origins. In: Ravosa, M.J., Dagosto, M. (Eds.), Primate Origins: Adaptations and Evolution. Springer, New York, pp. 403–435.

Casanovas-Vilar, I., Alba, D.M., Garcés, M., Robles, J.M., Moyà-Solà, S., 2011. Updated chronology for the Miocene hominoid radiation in Western Eurasia. Proc. Natl. Acad. Sci. USA, 108, 5554–5559.

Casanovas-Vilar, I., Madern, A., Alba, D.M., Cabrera, L., García-Paredes, I., Van den Hoek Ostende, L.W., DeMiguel, D., Robles, J.M., Furió, M., van Dam, J., Garcés, M., 2016. The Miocene mammal record of the Vallès-Penedès basin (Catalonia). C. R. Palevol. 15, 791–812.

Casanovas-Vilar, I., Jovells-Vaqué, S., Alba, D.M., 2022. The Miocene high-resolution record of the Vallès-Penedès Basin (Catalonia). In: Casanovas-Vilar, I., Alba, D.M. (Eds.), NOW 25th Anniversary Meeting. Sabadell (Barcelona), 16–18 November 2022. Abstract Book & Fieldtrip Guide. Paleontol. Evol. mem. espec. 9, 79–122.

Cavalli-Sforza, L.L., Edwards, A.W., 1967. Phylogenetic analysis. Models and estimation procedures. Am. J. Hum. Genet. 19, 233–257.

Chaimanee, Y., Chavasseau, O., Beard, K.C., Kyaw, A.A., Soe, A.N., Sein, C., Lazzari, V., Marivaux, L., Marandat, B., Swe, M., Rugbumrung, M., 2012. Late Middle Eocene primate from Myanmar and the initial anthropoid colonization of Africa. Proc. Natl. Acad. Sci. USA. 109, 10293–10297.

Chaimanee, Y., Chavasseau, O., Lazzari, V., Soe, A.N., Sein, C., Jaeger, J.J., 2024. Early anthropoid primates: New data and new questions. Evol. Anthropol. 33, e22022.

Changizi, M.A., Shimojo, S., 2008. "X-ray vision" and the evolution of forward-facing eyes. J. Theor. Biol. 254, 756–767.

Charles-Dominique, P., Martin, R.D., 1970. Evolution of lemurs and lorises. Nature 227, 257–260.

Chatani, K., 2003. Positional behavior of free-ranging Japanese macaques (*Macaca fuscata*). Primates 44, 13–23.

Chatterjee, H.J., Ho, S.Y., Barnes, I., Groves, C., 2009. Estimating the phylogeny and divergence times of primates using a supermatrix approach. BMC Evol. Biol. 9, 1–19.

Chester, S.G., Bloch, J.I., Boyer, D.M., Clemens, W.A., 2015. Oldest known euarchontan tarsals and affinities of Paleocene *Purgatorius* to Primates. Proc. Natl. Acad. Sci. USA, 112, 1487–1492.

Chester, S.G., Williamson, T.E., Bloch, J.I., Silcox, M.T., Sargis, E.J., 2017. Oldest skeleton of a plesiadapiform provides additional evidence for an exclusively arboreal radiation of stem primates in the Palaeocene. R. Soc. Open Sci. 4, 170329.

Chester, S.G., Williamson, T.E., Silcox, M.T., Bloch, J.I., Sargis, E.J., 2019. Skeletal morphology of the early Paleocene plesiadapiform *Torrejonia wilsoni* (Euarchonta, Palaechthonidae). J. Hum. Evol. 128, 76–92.

Chester, S.G., Williamson, T.E., Crowell, J.W., Silcox, M.T., Bloch, J.I., Sargis, E.J., 2025. New remarkably complete skeleton of *Mixodectes* reveals arboreality in a large Paleocene primatomorphan mammal following the Cretaceous-Paleogene mass extinction. Sci. Rep. 15, 8041.

Ciochon, R.L., Gunnell, G.F., 2002. Eocene primates from Myanmar: historical perspectives on the origin of Anthropoidea. Evol. Anthropol. 11, 156–168.

Ciochon, R.L., Gunnell, G.F., 2004. Eocene large-bodied primates of Myanmar and Thailand: morphological considerations and phylogenetic affinities. In: Fleagle, J.G., Kay, R.F. (Eds.), Anthropoid Origins. Plenum Press, New York, pp. 249–282.

Clavel, J., Escarguel, G., Merceron, G., 2015. mvMORPH: an R package for fitting multivariate evolutionary models to morphometric data. Methods Ecol. Evol. 6, 1311–1319.

Clavel, J., Aristide, L., Morlon, H., 2019. A penalized likelihood framework for high-dimensional phylogenetic comparative methods and an application to new-world monkeys brain evolution. Syst. Biol. 68, 93–116.

Clavel, J., Morlon, H., 2020. Reliable phylogenetic regressions for multivariate comparative data: illustration with the MANOVA and application to the effect of diet on mandible morphology in phyllostomid bats. Syst. Biol. 69, 927–943.

Collar, D.C., Schulte, J.A., O'meara, B.C., Losos, J.B., 2010. Habitat use affects morphological diversification in dragon lizards. J. Evol. Biol. 23, 1033–1049.

Collyer, M.L., Adams, D.C., 2018. RRPP: An r package for fitting linear models to high-dimensional data using residual randomization. Methods. Ecol. Evol. 9, 1772–1779.

Collyer, M.L., Adams, D.C., 2021. Phylogenetically aligned component analysis. Methods Ecol. Evol. 12, 359–372.

Conroy, G.C., Rose, M.D., 1983. The evolution of the primate foot from the earliest primates to the Miocene hominoids. Foot Ankle 3, 342–364.

Cornwell, W., Nakagawa, S., 2017. Phylogenetic comparative methods. Curr. Biol. 27, R333–R336.

Courtenay, L.A., 2023. Can we restore balance to geometric morphometrics? A theoretical evaluation of how sample imbalance conditions ordination and classification. Evol. Biol. 50, 90–110.

Covert, H.H., 1988. Ankle and foot morphology of *Cantius mckennai*: Adaptations and phylogenetic implications. J. Hum. Evol. 17, 57–70.

Covert, H.H., 1995. Locomotor adaptations of Eocene primates: adaptive diversity among the earliest prosimians. In: Alterman, L., Doyle, G.A., Izard, M.K. (Eds.), Creatures of the Dark. Springer US, Boston, pp. 495-509.

Covert, H.H., Hamrick, M.W., 1993. Description of new skeletal remains of the early Eocene anaptomorphine primate *Absarokius* (Omomyidae) and discussion about its adaptative profile. J. Hum. Evol. 25, 351–362.

Cowles, M.K., Carlin, B.P., 1996. Markov chain Monte Carlo convergence diagnostics: a comparative review. J. Am. Stat. Assoc. 91, 883–904.

Crompton, R.H., 1983. Age differences in locomotion of two subtropical Galaginae. Primates 24, 241–259.

Crompton, R.H., 1995. "Visual predation," habitat structure, and the ancestral primate niche. In: Alterman, L., Doyle, G.A., Izard, M.K. (Eds.), Creatures of the Dark. Springer US, Boston, pp. 11–30.

Crompton, R.H., Andau, P.M., 1986. Locomotion and habitat utilization in free-ranging *Tarsius bancanus*: a preliminary report. Primates 27, 337–355.

Crompton, R.H., Sellers, W.I., 2007. A consideration of leaping locomotion as a means of predator avoidance in prosimian primates. In: Gursky, S.L., Nekaris, K.A.I. (Eds.), Primate Anti-Predator Strategies. Springer, Boston, pp. 127–145.

Crompton, R.H., Sellers, W.I., Günther, M.M., 1993. Energetic efficiency and ecology as selective factors in the saltatory adaptation of prosimian primates. Proc. R. Soc. B 254, 41–45.

Crompton, R.H., Blanchard, M.L., Coward, S., Alexander, R.M., Thorpe, S.K., 2010. Vertical clinging and leaping revisited: locomotion and habitat use in the western tarsier, *Tarsius bancanus* explored via loglinear modeling. Int. J. Primatol. 31, 958–979.

Crowell, J.W., Wible, J.R., Chester, S.G., 2024. Basicranial evidence suggests picrodontid mammals are not stem primates. Biol. Lett. 20, 20230335.

Curtis, D.J., Feistner, A.T., 1994. Positional behaviour in captive aye-ayes (*Daubentonia madagascariensis*). Folia Primatol. 62, 155–159.

Dagosto, M., 1983. Postcranium of *Adapis parisiensis* and *Leptadapis magnus* (Adapiformes, Primates). Adaptational and phylogenetic significance. Folia Primatol. 41, 49–101.

Dagosto, M., 1985. The distal tibia of primates with special reference to the Omomyidae. Int. J. Primatol. 6, 45–75.

Dagosto, M., 1986. The joints of the tarsus in the strepsirhine primates: functional, adaptive, and evolutionary implications. Ph.D. Dissertation, City University of New York.

Dagosto, M., 1988. Implications of postcranial evidence for the origin of euprimates. J. Hum. Evol. 17, 35–56.

Dagosto, M., 1993. Postcranial anatomy and locomotor behavior in Eocene primates. In: Gebo, D.L. (Ed.), Postcranial Adaptation in Nonhuman Primates. Northen Illinois University Press, DeKalb, pp. 199–219.

Dagosto, M., 2007. The postcranial morphotype of primates. In: Ravosa, M. J., Dagosto, M. (Eds.), Primate Origins: Adaptations and Evolution. Springer, New York, pp. 489–534.

Dagosto, M., Schmid, P., 1996. Proximal femoral anatomy of omomyiform primates. J. Hum. Evol. 30, 29–56.

Dagosto, M., Yamashita, N., 1998. Effect of habitat structure on positional behavior and support use in three species of lemur. Primates 39, 459–472.

Dagosto, M., Gebo, D.L., Beard, K.C., 1999. Revision of the Wind River faunas, early Eocene of central Wyoming. Part 14. Postcranium of *Shoshonius cooperi* (Mammalia: Primates). Ann. Carnegie Mus. 68, 175–211.

Dagosto, M., Gebo, D.L., Dolino, C., 2001. Positional behavior and social organization of the Philippine tarsier (*Tarsius syrichta*). Primates 42, 233–243.

Dagosto, M., Marivaux, L., Gebo, D.L., Beard, K.C., Chaimanee, Y., Jaeger, J.J., Marandat, B., Soe, A.N., Kyaw, A.A., 2010. The phylogenetic affinities of the Pondaung tali. Am. J. Phys. Anthropol. 143, 223–234.

Deane, A.S., Begun, D.R., 2008. Broken fingers: retesting locomotor hypotheses for fossil hominoids using fragmentary proximal phalanges and high-resolution polynomial curve fitting (HR-PCF). J. Hum. Evol. 55, 691–701.

Deane, A.S., Begun, D.R., 2010. *Pierolapithecus* locomotor adaptations: a reply to Alba et al.'s comment on Deane and Begun, 2008. J. Hum. Evol. 59, 150–154.

DeCasien, A.R., Williams, S.A., Higham, J.P., 2017. Primate brain size is predicted by diet but not sociality. Nat. Ecol. Evol. 1, 0112.

Decker, R.L., Szalay, F.S., 1974, Origins and function of the pes in the Eocene Adapidae (Lemuriformes, Primates). In: Jenkins, F.A. (Ed.), Primate Locomotion. Academic Press, New York, pp. 261–291.

Demes, B., Günther, M.M., 1989. Biomechanics and allometric scaling in primate locomotion and morphology. Folia Primatol. 53, 125–141.

Demes, B., Jungers, W.L., Selpien, K., 1991. Body size, locomotion, and long bone cross-sectional geometry in indriid primates. Am. J. Phys. Anthropol. 86, 537–547.

Demes, B., Larson, S.G., Stern Jr, J.T., Jungers, W.L., Biknevicius, A.R., Schmitt, D., 1994. The kinetics of primate quadrupedalism: "hindlimb drive" reconsidered. J. Hum. Evol. 26, 353–374.

Demes, B., Jungers, W.L., Fleagle, J.G., Wunderlich, R.E., Richmond, B.G., Lemelin, P., 1996. Body size and leaping kinematics in Malagasy vertical clingers and leapers. J. Hum. Evol. 31, 367–388.

DeSilva, J.M., 2008. Vertical climbing adaptations in the anthropoid ankle and midfoot: Implications for locomotion in Miocene catarrhines and Plio-Pleistocene hominins. Ph.D Dissertation, University of Michigan.

DeSilva, J.M., 2009. Functional morphology of the ankle and the likelihood of climbing in early hominins. Proc. Natl. Acad. Sci. USA. 106, 6567–6572.

DeSilva, J., McNutt, E., Benoit, J., Zipfel, B., 2019. One small step: A review of Plio-Pleistocene hominin foot evolution. Am. J. Phys. Anthropol. 168, 63–140.

Doran, D.M., 1993. Comparative locomotor behavior of chimpanzees and bonobos: the influence of morphology on locomotion. Am. J. Phys. Anthropol. 91, 83–98.

Drake, A.G., Klingenberg, C.P., 2008. The pace of morphological change: historical transformation of skull shape in St Bernard dogs. Proc. R. Soc. B 275, 71–76.

Drapeau, M., 2022. Miocene ape feet. In: Zeiniger, A., Hatala, K.G., Wunderlich, R.E., Schmitt, D. (Eds.), The Evolution of the Primate Foot. Springer, Cham, pp. 321–359.

Dryden, I.L, Mardia, K.V., 2016. Statistical Shape Analysis. John Wiley & Sons, New York.

Dunbar, R.I., 1998. The social brain hypothesis. Evol. Anthropol. 6, 178–190.

Dunbar, R.I., Shultz, S., 2007. Evolution in the social brain. Science 317, 1344–1347.

Dunn, R.H., 2010. Additional postcranial remains of omomyid primates from the Uinta Formation, Utah and implications for the locomotor behavior of large-bodied omomyids. J. Hum. Evol. 58, 406–417.

Dunn, R.H., 2018. Functional morphology of the postcranial skeleton. In: Croft, D., Su, D., Simpson, S. (Eds.), Methods in Paleoecology. Springer, Cham, pp. 23–36.

Dunn, R.H., Sybalsky, J.M., Conroy, G.C., Rasmussen, D.T., 2006. Hindlimb adaptations in *Ourayia* and *Chipetaia*, relatively large-bodied omomyine primates from the Middle Eocene of Utah. Am. J. Phys. Anthropol. 131, 303–310.

Dunn, R.H., Tocheri, M.W., Orr, C.M., Jungers, W.L., 2014. Ecological divergence and talar morphology in gorillas. Am. J. Phys. Anthropol. 153, 526–541.

Dunn, R.H., Rose, K.D., Rana, R.S., Kumar, K., Sahni, A., Smith, T., 2016. New euprimate postcrania from the early Eocene of Gujarat, India, and the strepsirrhine–haplorhine divergence. J. Hum. Evol. 99, 25–51.

Dunsworth, H.M., 2006. *Proconsul heseloni* feet from Rusinga Island. Ph.D Dissertation, The Pennsylvania State University.

Durrleman, S., Pennec, X., Trouvé, A., Ayache, N., Braga, J., 2012. Comparison of the endocranial ontogenies between chimpanzees and bonobos via temporal regression and spatiotemporal registration. J. Hum. Evol. 62, 74–88.

Dykyj, D., 1980. Locomotion of the slow loris in a designed substrate context. Am. J. Phys. Anthropol. 52, 577–586.

Eastman, J.M., Alfaro, M.E., Joyce, P., Hipp, A.L., Harmon, L.J., 2011. A novel comparative method for identifying shifts in the rate of character evolution on trees. Evolution 65, 3578–3589.

Egi, N., Takai, M., Shigehara, N., Tsubamoto, T., 2004. Body mass estimates for Eocene eosimiid and amphipithecid primates using prosimian and anthropoid scaling models. Int. J. Primatol. 25, 211–236.

Einstein, A., 1905. Über die von der molekularkinetischen Theorie der Wärme geforderte Bewegung von in ruhenden Flüssigkeiten suspendierten Teilchen. Ann. Phys. 17, 549–560.

Erikson GE. 1963. Brachiation in the New World monkeys and anthropoid apes. Symp. Zool. Soc. Lond. 10,135–164.

Erickson, C.J., 1991. Percussive foraging in the aye-aye, *Daubentonia madagascariensis*. Anim. Behav. 41, 793–801.

Evans, M.E., Smith, S.A., Flynn, R.S., Donoghue, M.J., 2009. Climate, niche evolution, and diversification of the "bird-cage" evening primroses (Oenothera, sections Anogra and Kleinia). Am. Nat. 173, 225-240.

Fabre, A.C., Marigó, J., Granatosky, M.C., Schmitt, D., 2017. Functional associations between support use and forelimb shape in strepsirrhines and their relevance to inferring locomotor behavior in early primates. J. Hum. Evol. 108, 11–30.

Fabre, A.C., Granatosky, M.C., Hanna, J.B., Schmitt, D., 2018. Do forelimb shape and peak forces co-vary in strepsirrhines? Am. J. Phys. Anthropol. 167, 602–614.

Fabre, A.C., Peckre, L., Pouydebat, E., Wall, C.E., 2019. Does the shape of forelimb long bones co-vary with grasping behaviour in strepsirrhine primates? Biol. J. Linn. Soc. 127, 649-–660.

Fabre, A.C., Bardua, C., Bon, M., Clavel, J., Felice, R.N., Streicher, J.W., Bonnel, J., Stanley, E.L., Blackburn, D.C., Goswami, A., 2020. Metamorphosis shapes cranial diversity and rate of evolution in salamanders. Nat. Ecol. Evol. 4, 1129–1140.

Fabre, A.C., Dowling, C., Portela Miguez, R., Fernandez, V., Noirault, E., Goswami, A., 2021. Functional constraints during development limit jaw shape evolution in marsupials. Proc. R. Soc. B 288, 20210319.

Falk, D., 2015. Evolution of the primate brain. In: Henke, W., Tattersall, I. (Eds.), Handbook of Paleoanthropology. Springer, Heidelberg, pp. 1495–1525.

Fan, P., Scott, M.B., Fei, H., Ma, C., 2013. Locomotion behavior of cao vit gibbon (*Nomascus nasutus*) living in karst forest in Bangliang Nature Reserve, Guangxi, China. Integr. Zool. 8, 356–364.

Felsenstein, J., 1973. Maximum-likelihood estimation of evolutionary trees from continuous characters. Am. J. Hum. Genet. 25, 471–492.

Felsenstein, J., 1985. Phylogenies and the comparative method. Am. Nat.125, 1–15.

Felsenstein, J., 1988. Phylogenies and quantitative characters. Annu. Rev. Ecol. Evol. Syst. 19, 445–471.

Fleagle, J.G., 1976. Locomotion and posture of the Malayan siamang and implications for hominoid evolution. Folia Primatol. 26, 245–269.

Fleagle, J.G., 1977. Locomotor behavior and muscular anatomy of sympatric Malaysian leaf-monkeys (*Presbytis obscura* and *Presbytis melalophos*). Am. J. Phys. Anthropol. 46, 297–307.

Fleagle, J.G., 1980. Locomotion and posture. In: Chivers, D.J. (Ed.) Malayan Forest Primates. Springer, Boston, pp. 191–208.

Fleagle, J.G., Kay, R.F., 1987. The phyletic position of the Parapithecidae. J. Hum. Evol. 16, 483–532.

Fleagle, J.G., Meldrum, D.J., 1988. Locomotor behavior and skeletal morphology of two sympatric pitheciine monkeys, *Pithecia pithecia* and *Chiropotes satanas*. Am. J. Primatol. 16, 227–249.

Fleagle, J.G., Mittermeier, R.A., 1980. Locomotor behavior, body size, and comparative ecology of seven Surinam monkeys. Am. J. Phys. Anthropol. 52, 301–314.

Fleagle, J.G., Seiffert, E.R., 2020. The phylogeny of primates. In: Kaas, J.H. (Ed.), Evolutionary Neuroscience. Academic Press, pp. 483–518.

Fleagle, J.G., Simons, E.L., 1995. Limb skeleton and locomotor adaptations of *Apidium phiomense*, an Oligocene anthropoid from Egypt. Am. J. Phys. Anthropol. 97, 235–289.

Fleagle, J.G., Baden, A.L., Gilbert, C.C., 2025. Primate Adaptation and Evolution 4th ed. Academic Press, San Diego.

Fontaine, R., 1990. Positional behavior in *Saimiri boliviensis* and *Ateles geoffroyi*. Am. J. Phys. Anthropol. 82, 485–508.

Foote, M., 1989. Perimeter-based Fourier analysis: a new morphometric method applied to the trilobite cranidium. J. Paleontol. 63, 880–885.

Foote, M., 1997. The evolution of morphological diversity. Annu. Rev. Ecol. Evol. Syst. 28, 129–152.

Forbanka, D.N., 2018. Microhabitat utilization by fork-marked dwarf lemurs (*Phaner* spp.) and needle-clawed galagos (*Euoticus* spp.) in primary and secondary forests. Am. J. Primatol. 80, e22864.

Ford, S.M., 1988. Postcranial adaptations of the earliest platyrrhine. J. Hum. Evol. 17, 155–192.

Fortuny, J., Zanolli, C., Bernardini, F., Tuniz, C., Alba, D.M., 2021. Dryopithecine palaeobiodiversity in the Iberian Miocene revisited on the basis of molar endostructural morphology. Palaeontology 64, 531–554.

Franzen, J.L., Gingerich, P.D., Habersetzer, J., Hurum, J.H., Von Koenigswald, W., Smith, B.H., 2009. Complete primate skeleton from the middle Eocene of Messel in Germany: morphology and paleobiology. PLoS One 4, e5723.

Freckleton, R.P., 2012. Fast likelihood calculations for comparative analyses. Methods Ecol. Evol. 3, 940–947.

Freckleton, R.P., Harvey, P.H., Pagel, M., 2002. Phylogenetic analysis and comparative data: a test and review of evidence. Am. Nat. 160, 712–726.

Friesen, S.E., Knigge, R.P., Jashashvili, T., Harcourt-Smith, W.E., Schoeninger, M.J., Tocheri, M.W., 2024. Shape variation in the talus and medial cuneiform of chimpanzees and bonobos. Am. J. Biol. Anthropol. 183, e24571.

Fruciano, C., 2016. Measurement error in geometric morphometrics. Dev. Genes. Evol., 226, 139–158.

Garber, P.A., 1980. Locomotor behavior and feeding ecology of the Panamanian tamarin (*Saguinus oedipus geoffroyi*, Callitrichidae, Primates). Int. J. Primatol. 1, 185–201.

Garber, P.A., 1987. Foraging strategies among living primates. Annu. Rev. Anthropol. 16, 339–364.

Garber, P.A., 1992. Vertical clinging, small body size, and the evolution of feeding adaptations in the Callitrichinae. Am. J. Phys. Anthropol. 88, 469–482.

Garber, P.A., Leigh, S.R., 2001. Patterns of positional behavior in mixed-species troops of *Callimico goeldii*, *Saguinus labiatus*, and *Saguinus fuscicollis* in northwestern Brazil. Am. J. Phys. Anthropol. 54, 17–31.

Gebo, D.L., 1985. The nature of the primate grasping foot. Am. Phys. Anthropol. 67, 269–277.

Gebo, D.L., 1986. Anthropoid origins—the foot evidence. J. Hum. Evol. 15, 421–430.

Gebo, D.L., 1987a. Locomotor diversity in prosimian primates. Am. J. Primatol. 13, 271–281.

Gebo, D.L., 1987b. Functional anatomy of the tarsier foot. Am. J. Phys. Anthropol. 73, 9–31.

Gebo, D.L., 1988. Foot morphology and locomotor adaptation in Eocene primates. Folia Primatol. 50, 3–41.

Gebo, D.L., 1989a. Postcranial adaptation and evolution in Lorisidae. Primates 30, 347–367.

Gebo, D.L., 1989b. Locomotor and phylogenetic considerations in anthropoid evolution. J. Hum. Evol. 18, 201–233.

Gebo, D.L., 1992a. Locomotor and postural behavior in *Alouatta palliata* and *Cebus capucinus*. Am. J. Primatol. 26, 277–290.

Gebo, D.L., 1992b. Plantigrady and foot adaptation in African apes: implications for hominid origins. Am. J. Phys. Anthropol. 89, 29–58.

Gebo, D.L., 1993a. Postcranial anatomy and locomotor adaptation in early African anthropoids. In: Gebo D.L. (Ed.), Postcranial Adaptation in Nonhuman Primates. Northern Illinois University Press, DeKalb, pp. 220–234.

Gebo, D.L., 1993b. Functional morphology of the foot in primates. In: Gebo D.L. (Ed.), Postcranial Adaptation in Nonhuman Primates. Northern Illinois University Press, DeKalb, pp.175–196.

Gebo, D.L., 1996. Climbing, brachiation, and terrestrial quadrupedalism: historical precursors of hominid bipedalism. Am. J. Phys. Anthropol. 101, 55–92.

Gebo, D.L., 2004. A shrew-sized origin for primates. Am. J. Phys. Anthropol. 125, 40–62.

Gebo, D.L., 2009. A response to Sargis et al. (2007). J. Hum. Evol. 57, 810–814.

Gebo, D.L., 2011. Vertical clinging and leaping revisited: vertical support use as the ancestral condition of strepsirrhine primates. Am. J. Phys. Anthropol. 146, 323–335.

Gebo, D.L., 2014. Primate Comparative Anatomy. Johns Hopkins University Press, Baltimore.

Gebo, D.L., Chapman, C.A., 1995. Positional behavior in five sympatric Old World monkeys. Am. J. Phys. Anthropol. 97, 49–76.

Gebo, D.L., Dagosto, M., 1988. Foot anatomy, climbing, and the origin of the Indriidae. J. Hum. Evol. 17, 135–154.

Gebo, D.L., Dagosto, M., 2004. Anthropoid origins: Postcranial evidence from the Eocene of Asia. In: Ross, C.F., Kay, R.F. (Eds.), Anthropoid Origins: New Visions. Kluwer Academic / Plenum Publishers, New York, pp. 369–380.

Gebo, D.L., Sargis, E.J., 1994. Terrestrial adaptations in the postcranial skeletons of guenons. Am. J. Phys. Anthropol. 93, 341–371.

Gebo, D.L., Simons, E.L., 1987. Morphology and locomotor adaptations of the foot in early Oligocene anthropoids. Am. J. Phys. Anthropol. 74, 83–101.

Gebo, D.L., Dagosto, M., Rose, K.D., 1991. Foot morphology and evolution in early Eocene *Cantius*. Am. J. Phys. Anthropol. 86, 51–73.

Gebo, D.L., MacLatchy, L., Kityo, R., Deino, A., Kingston, J., Pilbeam, D., 1997. A hominoid genus from the early Miocene of Uganda. Science 276, 401–404.

Gebo, D.L., Dagosto, M., Beard, K.C., Wang, J., 1999. A first metatarsal of *Hoanghonius stehlini* from the late middle Eocene of Shanxi Province, China. J. Hum. Evol. 37, 801–806.

Gebo, D.L., Dagosto, M., Beard, K.C., Qi, T., Wang, J., 2000. The oldest known anthropoid postcranial fossils and the early evolution of higher primates. Nature 404, 276–278.

Gebo, D.L., Dagosto, M., Beard, K.C., Qi, T., 2001. Middle Eocene primate tarsals from China: Implications for haplorhine evolution. Am. J. Phys. Anthropol. 116, 83–107.

Gebo, D.L., Gunnell, G.F., Ciochon, R.L., Takai, M., Egi, N., 2002. News and Views New eosimiid primate from Myanmar. J. Hum. Evol. 42, 549–553.

Gebo, D.L., Dagosto, M., Beard, K.C., Ni, X., 2008. New primate hind limb elements from the middle Eocene of China. J. Hum. Evol. 55, 999–1014.

Gebo, D.L., Smith, T., Dagosto, M., 2012a. New postcranial elements for the earliest Eocene fossil primate *Teilhardina belgica*. J. Hum. Evol. 63, 205–218.

Gebo, D.L., Dagosto, M., Ni, X., Beard, K.C., 2012b. Species diversity and postcranial anatomy of Eocene primates from Shanghuang, China. Evol. Anthropol. 21, 224–238.

Gebo, D.L., Smith, R., Dagosto, M., Smith, T., 2015a. Additional postcranial elements of *Teilhardina belgica*: The oldest European primate. Am. J. Phys. Anthropol. 156, 388–406.

Gebo, D.L., Beard, K.C., Ni, X., Dagosto, M., 2015b. Distal phalanges of *Eosimias* and *Hoanghonius*. J. Hum. Evol. 86, 92–98.

Gebo, D.L., Dagosto, M., Ni, X., Beard, K.C., 2017. Phalangeal morphology of Shanghuang fossil primates. J. Hum. Evol. 113, 38–82.

Gelman, A., Rubin, D.B., 1992. Inference from iterative simulation using multiple sequences. Stat. Sci. 7, 457–472.

Geyer, C.J., 2011. Introduction to Markov Chain Monte Carlo. In: Brooks, S., Gelman, A., Jones, G.L., Meng, X.-L., (Eds.), Handbook of Markov Chain Monte Carlo. Chapman & Hall/CRC, New York, pp., 3–48.

Gladman, J.T., Boyer, D.M., Simons, E.L., Seiffert, E.R., 2013. A calcaneus attributable to the primitive late Eocene anthropoid *Proteopithecus sylviae*: phenetic affinities and phylogenetic implications. Am. J. Phys. Anthropol. 151, 372–397.

Glassman, D.M., Wells, J.P., 1984. Positional and activity behavior in a captive slow loris: a quantitative assessment. Am. J. Primatol. 7, 121–132.

Gidley, J.W., 1923. Paleocene primates of the Fort Union, with discussion of relationships of Eocene primates. Proc. U. S. Natl. Mus. 63, 1–38.

Gilbert, C.C., Ortiz, A., Pugh, K.D., Campisano, C.J., Patel, B.A., Singh, N.P., Fleagle, J.G., Patnaik, R., 2020. New Middle Miocene ape (Primates: Hylobatidae) from Ramnagar, India fills major gaps in the hominoid fossil record. Proc. R. Soc. B 287, 20201655.

Gingerich, P.D., 1976. Cranial anatomy and evolution of early Tertiary Plesiadapidae (Mammalia, Primates). Univ. Mich. Pap. Paleontol. 15, 1–141.

Gingerich, P.D., 1981. Early Cenozoic Omomyidae and the evolutionary history of tarsiiform primates. J. Hum. Evol. 10, 345–374.

Gingerich, P.D., Gunnell, G.F., 2005. Brain of *Plesiadapis cookei* (Mammalia, Proprimates): surface morphology and encephalization compared to those of Primates and Dermoptera. Contrib. Mus. Paleontol. Univ. Mich. 31, 185–195.

Gittins, S.P., 1983. Use of the forest canopy by the agile gibbon. Folia Primatol. 40, 134–144.

Godfrey, L.R., Sutherland, M., Boy, D., Gomberg, N., 1991. Scaling of limb joint surface areas in anthropoid primates and other mammals. J. Zool. 223, 603–625.

Godfrey, L.R., Sutherland, M.R., Paine, R.R., Williams, F.L., Boy, D.S., Vuillaume-Randriamanantena, M., 1995. Limb joint surface areas and their ratios in Malagasy lemurs and other mammals. Am. J. Phys. Anthropol. 97, 11–36.

Godfrey, L.R., Jungers, W.L., Wunderlich, R.E., Richmond, B.G., 1997. Reappraisal of the postcranium of *Hadropithecus* (Primates, Indroidea). Am. J. Phys. Anthropol. 103, 529–556.

Godinot, M., 1991. Toward the locomotion of two contemporaneous *Adapis* species. Z. Morphol. Anthropol. 78, 387–405.

Godinot, M., 1994. Early North African primates and their significance for the origin of Simiiformes (=Anthropoidea). In: Fleagle, J.G., Kay, R.F. (Eds.), Anthropoid Origins. Plenum Press, New York, pp. 235–295.

Godinot, M., 1998. A summary of adapiform systematics and phylogeny. Folia Primatol. 69, 218–249.

Godinot, M., 2007. Primate origins: a reappraisal of historical data favoring tupaiid affinities. In: Ravosa, M.J., Dagosto, M. (Eds.), Primate Origins: Adaptations and Evolution. Springer, New York, pp. 83–142.

Godinot, M., Dagosto, M., 1983. The astragalus of *Necrolemur* (Primates, Microchoerinae). J. Paleontol. 57, 1321–1324.

Golpe Posse, J.M., 1993. Los Hispanopitecos (Primates, Pongidae) de los yacimientos del Vallès-Penedès (Cataluña, España). II: Descripción del material existente en el Instituto de Paleontología de Sabadell. Paleontol. Evol. 26–27, 151–224.

Goodall, C., 1991. Procrustes methods in the statistical analysis of shape. J. R. Stat. Soc. B. 53, 285–321.

Goswami, A., Clavel, J., 2025. Morphological evolution in a time of phenomics. Paleobiology 51, 195–213.

Gould, S.J., 1966. Allometry and size in ontogeny and phylogeny. Biol. Rev. 41, 587–638.

Gould, S.J., 1970. Evolutionary paleontology and the science of form. Earth-Sci. Rev. 6, 77–119.

Gower, J.C., 1975. Generalized procrustes analysis. Psychometrika 40, 33–51.

Grafen, A., 1989. The phylogenetic regression. Philos. Trans. R. Soc. B 326, 119–157.

Granatosky, M.C., 2018. A review of locomotor diversity in mammals with analyses exploring the influence of substrate use, body mass and intermembral index in primates. J. Zool. 306, 207–216.

Granatosky, M.C., Lemelin, P., Chester, S.G., Pampush, J.D., Schmitt, D., 2014. Functional and evolutionary aspects of axial stability in euarchontans and other mammals. J. Morphol. 275, 313–327.

Grand, T.I., 1967. The functional anatomy of the ankle and foot of the slow loris (*Nycticebus coucang*). Am. J. Phys. Anthropol. 26, 207–218.

Green, P.J., 1995. Reversible jump Markov chain Monte Carlo computation and Bayesian model determination. Biometrika 82, 711–732.

Gregory, W.K., 1920. On the structure and relations of *Notharctus*, an American Eocene primate. Mem. Am. Mus. Nat. Hist. 3, 49–243.

Groves, C.P., 2001. Primate Taxonomy. Smithsonian Institution Press, Washington DC.

Gunnell, G.F., Rose, K.D., 2002. Tarsiiformes: evolutionary history and adaptation. In: Hartwig, W.C. (Ed.), The Primate Fossil Record. Cambridge University Press, Cambridge, pp. 45–82.

Gunnell, G.F., Rose, K.D., Rasmussen, D.T., 2008. Euprimates. In: Janis, C.M., Gunnell, G.F., Uhen, M.D. (Eds.), Evolution of Tertiary Mammals of North America, Vol. 2. Cambridge University Press, Cambridge, pp. 239–261.

Gunz, P., Mitteroecker, P., 2013. Semilandmarks: a method for quantifying curves and surfaces. Hystrix 24, 103–109.

Gunz, P., Mitteroecker, P., Bookstein, F.L., 2005. Semilandmarks in three dimensions. In: Slice, D.E., (Ed.), Modern Morphometrics in Physical Anthropology. Kluwer Academic / Plenum Publishers, New York, pp.73–98.

Haines, A.J., Crampton, J.S., 2000. Improvements to the method of Fourier shape analysis as applied in morphometric studies. Palaeontology 43, 765–783.

Hall-Craggs, E.C.B., 1965a. An analysis of the jump of the Lesser Galago (*Galago senegalensis*). Proc. Zool. Soc. Lond. 147, 20–29.

Hall-Craggs, E.C.B., 1965b. An osteometric study of the hind limb of the Galagidae. J. Anat. 99, 119–126.

Hall-Craggs, E.C.B., 1966. Rotational movements in the foot of *Galago senegalensis*. Anat. Rec. 154, 287–293.

Hammond, A.S., Alba, D.M., Almécija, S., Moyà-Solà, S., 2013. Middle Miocene *Pierolapithecus* provides a first glimpse into early hominid pelvic morphology. J. Hum. Evol. 64, 658–666.

Hammond, A.S., Plavcan, J.M., Ward, C.V., 2016. A validated method for modeling anthropoid hip abduction *in silico*. Am. J. Phys. Anthropol. 160, 529–548.

Hammond, A.S., Rook, L., Anaya, A.D., Cioppi, E., Costeur, L., Moyà-Solà, S., Almécija, S., 2020. Insights into the lower torso in late Miocene hominoid *Oreopithecus bambolii*. Proc. Natl. Acad. Sci. USA 117, 278–284.

Hamrick, M.W., 1996. Articular size and curvature as determinants of carpal joint mobility and stability in strepsirhine primates. J. Morphol. 230, 113–127.

Hamrick, M.W., 2001. Primate origins: evolutionary change in digital ray patterning and segmentation. J. Hum. Evol. 40, 339–351.

Hansen, T.F., 1997. Stabilizing selection and the comparative analysis of adaptation. Evolution 51, 1341–1351.

Hansen, T.F., Martins, E.P., 1996. Translating between microevolutionary process and macroevolutionary patterns: the correlation structure of interspecific data. Evolution 50, 1404–1417.

Harcourt-Smith, W.E., Aiello, L.C., 2004. Fossils, feet and the evolution of human bipedal locomotion. J. Anat. 204, 403–416.

Harmon, L.J., Schulte, J.A., Larson, A., Losos, J.B., 2003. Tempo and mode of evolutionary radiation in iguanian lizards. Science 301, 961–964.

Harmon, L.J., Weir, J.T., Brock, C.D., Glor, R.E., Challenger, W., 2008. GEIGER: investigating evolutionary radiations. Bioinformatics 24, 129–131.

Harmon, L.J., Losos, J.B., Jonathan Davies, T., Gillespie, R.G., Gittleman, J.L., Bryan Jennings, W., Kozak, K.H., McPeek, M.A., Moreno-Roark, F., Near, T.J., Purvis, A., 2010. Early bursts of body size and shape evolution are rare in comparative data. Evolution 64, 2385–2396.

Harper, C.M., Ruff, C.B., Sylvester, A.D., 2022. Scaling and relative size of the human, nonhuman ape, and baboon calcaneus. Anat. Rec. 305, 100–122.

Harrison, T., 1982. Small-bodied apes from the Miocene of East Africa. Ph.D. Dissertation, University College London.

Harrison, T., 1987. A reassessment of the phylogenetic relationships of *Oreopithecus bambolii* Gervais. J. Hum. Evol. 15, 541–583.

Harrison, T., 1989. New postcranial remains of *Victoriapithecus* from the middle Miocene of Kenya. J. Hum. Evol. 18, 3–54.

Harrison, T., 1991. Some observations on the Miocene hominoids from Spain. J. Hum. Evol. 20, 515–520.

Harrison, T. 2010. Dendropithecoidea, Proconsuloidea, and Hominoidea (Catarrhini, Primates). In: Werderlin, L., Sanders, W.J. (Eds.), Cenozoic Mammals of Africa. University of California Press, Berkeley, pp. 429–469.

Harrison, T., Rook, L., 1997. Enigmatic anthropoid or misunderstood ape? The phylogenetic status of *Oreopithecus bambolii* reconsidered. In: Begun, D.R., Ward, C.V., Rose, M.D. (Eds.), Function, Phylogeny and Fossils: Miocene Hominoid Evolution and Adaptation. Plenum Press, New York, pp. 327–362.

Heard-Booth, A.N., Kuo, S., McNutt, E.J., DeSilva, J.M., 2022. The Primate Midfoot and Human Longitudinal Arch. In: Zeininger, A., Hatala, K.G., Wunderlich, R.E., Schmitt, D. (Eds.), The Evolution of the Primate Foot. Springer, Cham, pp. 47–72.

Hemingway, H.W., Burrows, A.M., Omstead, K.M., Zohdy, S., Pastor, J.F., Muchlinski, M.N., 2020. Vertical clinging and leaping ahead: how bamboo has shaped the anatomy and physiology of *Hapalemur*. Anat. Rec. 303, 295–307.

Higham, T.E., Birn-Jeffery, A.V., Collins, C.E., Hulsey, C.D., Russell, A.P., 2015. Adaptive simplification and the evolution of gecko locomotion: morphological and biomechanical consequences of losing adhesion. Proc. Natl. Acad. Sci. USA. 112, 809–814.

Hildebrand, M., 1967. Symmetrical gaits of primates. Am. J. Phys. Anthropol. 26, 119–130.

Hildebrand, M., 1985. Walking and running. In: Hildebrand, M., Bramble, D.M., Liem, K.F., Wake, D.B. (Eds.), Functional Vertebrate Morphology. Harvard University Press, Cambridge, pp. 38–57.

Ho, L.S.T., Ané, C., 2014. A linear-time algorithm for Gaussian and non-Gaussian trait evolution models. Syst. Biol. 63, 397–408.

Hoffstetter, R., 1977. Phylogénie des Primates. Confrontation des résultats obtenus par les diverses voies d'approche du problème. Bull. Mém. Soc. Anthropol. Paris 13, 327–346.

Hollihn, U., Jungers, W.L., 1984. Kinesiologische Untersuchungen zur Brachiation bei Weißhandgibbons (*Hylobates lar*). Z. Morph. Anthropol. 74, 275–293.

Hooker, J.J., 2001. Tarsals of the extinct insectivoran family Nyctitheriidae (Mammalia): evidence for archontan relationships. Zool. J. Linn. Soc. 132, 501–529.

Hooker, J.J., Russell, D.E., Phélizon, A., 1999. A new family of Plesiadapiformes (Mammalia) from the Old World lower Paleogene. Palaeontology 42, 377–407.

Hotelling, H., 1933. Analysis of a complex of statistical variables into principal components. J. Educ. Psychol. 24, 417–441.

Hunt, K.D., 1991. Positional behavior in the Hominoidea. Int. J. Primatol. 12, 95–118.

Hunt, K.D., 1992. Positional behavior of *Pan troglodytes* in the Mahale Mountains and Gombe Stream National Parks, Tanzania. Am. J. Phys. Anthropol. 87, 83–105.

Hunt, K.D., 2016. Why are there apes? Evidence for the co-evolution of ape and monkey ecomorphology. J. Anat. 228, 630–685.

Ishida, H., Kunimatsu, Y., Takano, T., Nakano, Y., Nakatsukasa, M., 2004. *Nacholapithecus* skeleton from the Middle Miocene of Kenya. J. Hum. Evol. 46, 69–103.

Jaeger, J.J., Thein, T., Benammi, M., Chaimanee, Y., Soe, A.N., Lwin, T., Tun, T., Wai, S., Ducrocq, S., 1999. A new primate from the middle Eocene of Myanmar and the Asian early origin of anthropoids. Science 286, 528–530.

Jaeger, J.J., Chavasseau, O., Lazzari, V., Naing Soe, A., Sein, C., Le Maître, A., Shwe, H., Chaimanee, Y., 2019. New Eocene primate from Myanmar shares dental characters with African Eocene crown anthropoids. Nat. Commun. 10, 3531.

Jaeger, J.J., Sein, C., Gebo, D.L., Chaimanee, Y., Nyein, M.T., Oo, T.Z., Aung, M.M., Suraprasit, K., Rugbumrung, M., Lazzari, V., Soe, A.N., 2020. Amphipithecine primates are stem anthropoids: cranial and postcranial evidence. Proc. R. Soc. B 287, 20202129.

Janecka, J.E., Miller, W., Pringle, T.H., Wiens, F., Zitzmann, A., Helgen, K.M., Springer, M.S., Murphy, W.J., 2007. Molecular and genomic data identify the closest living relative of primates. Science 318, 792–794.

Jastifer, J.R., Gustafson, P.A., 2014. The subtalar joint: biomechanics and functional representations in the literature. Foot 24, 203–209.

Jenkins, F.A., 1974. Tree shrew locomotion and the origins of primate arborealism. In: Jenkins, F.A. (Ed.), Primate Locomotion. Academic Press, New York, pp. 85–115.

Jenkins, F.A., McClearn, D., 1984. Mechanisms of hind foot reversal in climbing mammals. J. Morphol. 182, 197–219.

Jolliffe, I.T., 1982. A note on the use of principal components in regression. J. R. Stat. Soc. C 31, 300–303.

Jolliffe, I.T., 1986. Principal component analysis and factor analysis. In: Jolliffe, I.T. (Ed.), Principal Component Analysis. Springer, New York, pp. 115–128.

Jones, F.W., 1916. Arboreal man. E. Arnold, London.

Jungers, W.L., 1987. Body size and morphometric affinities of the appendicular skeleton in *Oreopithecus bambolii* (IGF 11778). J. Hum. Evol. 16, 445–456.

Jungers, W.L., Falsetti, A.B., Wall, C.E., 1995. Shape, relative size, and size-adjustments in morphometrics. Am. J. Phys. Anthropol. 38, 137–161.

Kamilar, J.M., Cooper, N., 2013. Phylogenetic signal in primate behaviour, ecology and life history. Philos. Trans. R. Soc. B 368, 20120341.

Kay, R.F., 1984. On the use of anatomical features to infer foraging behavior in extinct primates. In: Rodman, P.S., Cant, J.G.H. (Eds.), Adaptations for Foraging in Nonhuman Primates: Contributions to an Organismal Biology of Prosimians, Monkeys, and Apes. Columbia University Press, New York, pp. 21–53.

Kay, R.F., Cartmill, M., 1977. Cranial morphology and adaptations of *Palaechthon nacimienti* and other Paromomyidae (Plesiadapoidea,? Primates), with a description of a new genus and species. J. Hum. Evol. 6, 19–53.

Kay, R.F., Thorington Jr, R.W., Houde, P., 1990. Eocene plesiadapiform shows affinities with flying lemurs not primates. Nature 345, 342–344.

Kay, R.F., Thewissen, J.G.M., Yoder, A.D., 1992. Cranial anatomy of *Ignacius graybullianus* and the affinities of the Plesiadapiformes. Am. J. Phys. Anthropol. 89, 477–498.

Kemp, A.D., 2024. Effect of binocular visual cue availability on fruit and insect grasping performance in two cheirogaleids: Implications for primate origins hypotheses. J. Hum. Evol. 188, 103456.

Kendall, D.G., 1977. The diffusion of shape. Adv. Appl. Probab. 9, 428–430.

Kendall, D.G., 1984. Shape manifolds, procrustean metrics, and complex projective spaces. Bull. Lond. Math. Soc. 16, 81–121.

Klingenberg, C.P., 1998. Heterochrony and allometry: the analysis of evolutionary change in ontogeny. Biol. Rev. 73, 79–123.

Klingenberg, C.P., 2010. Evolution and development of shape: integrating quantitative approaches. Nat. Rev. Genet. 11, 623–635.

Klingenberg, C.P., 2016. Size, shape, and form: concepts of allometry in geometric morphometrics. Dev. Genes Evol. 226, 113–137.

Klingenberg, C.P., 2020. Walking on Kendall's shape space: understanding shape spaces and their coordinate systems. Evol. Biol. 47, 334–352.

Klingenberg, C.P., Ekau, W., 1996. A combined morphometric and phylogenetic analysis of an ecomorphological trend: pelagization in Antarctic fishes (Perciformes: Nototheniidae). Biol. J. Linn. Soc. 59, 143–177.

Klingenberg, C.P., Monteiro, L.R., 2005. Distances and directions in multidimensional shape spaces: implications for morphometric applications. Syst. Biol. 54, 678–688.

Kirk, E.C., 2006. Visual influences on primate encephalization. J. Hum. Evol. 5, 76–90.

Kirk, E.C., Cartmill, M., Kay, R.F., Lemelin, P., 2003. Comment on "Grasping primate origins". Science 300, 741.

Kivell, T.L., 2016. A review of trabecular bone functional adaptation: what have we learned from trabecular analyses in extant hominoids and what can we apply to fossils? J. Anat. 228, 569–594.

Kivell, T.L., Schmitt, D., 2009. Independent evolution of knuckle-walking in African apes shows that humans did not evolve from a knuckle-walking ancestor. Proc. Natl. Acad. Sci. USA. 106, 14241–14246.

Klenerman, L., Wood, B., 2006. The Human Foot. Springer, London.

Knigge, R.P., Tocheri, M.W., Orr, C.M., Mcnulty, K.P., 2015. Three-dimensional geometric morphometric analysis of talar morphology in extant gorilla taxa from highland and lowland habitats. Anat. Rec. 298, 277–290.

Köhler, M., Moyà-Solà, S., 1997. Ape-like or hominid-like? The positional behavior of *Oreopithecus bambolii* reconsidered. Proc. Natl. Acad. Sci. USA 94, 11747–11750.

Köhler, M., Moyà-Solà, S., Alba, D.M., 2001a. Brief communication: Cranial reconstruction of *Dryopithecus*. Am. J. Phys. Anthropol. 115, 284–288.

Köhler, M., Moyà-Solà, S., Alba, D.M., 2001b. Eurasian hominoid evolution in the light of recent *Dryopithecus* findings. In: de Bonis, L., Koufos, G.D., Andrews, P. (Eds.), Hominoid Evolution and Climatic Change in Europe, Vol. 2. Phylogeny of the Neogene Hominoid Primates of Eurasia. Cambridge University Press, Cambridge, pp. 192–212.

Köhler, M., Alba, D.M., Solà, S.M., MacLatchy, L., 2002. Taxonomic affinities of the Eppelsheim femur. Am. J. Phys. Anthropol. 119, 297–304.

Kuhner, M.K., 2009. Coalescent genealogy samplers: windows into population history. Trends Ecol. Evol. 24, 86–93.

Kuo, S., 2020. Foot and ankle functional morphology in anthropoid primates and Miocene hominoids. Ph.D. Dissertation, University of Missouri.

Lambert, J.E., 1998. Primate digestion: interactions among anatomy, physiology, and feeding ecology. Evol. Anthropol. 7, 8–20.

Langdon, J.H., 1986. Functional morphology of the Miocene hominoid foot. Contrib. Primatol. 22, 1–255.

Larney, E., Larson, S.G., 2004. Compliant walking in primates: elbow and knee yield in primates compared to other mammals. Am. J. Phys. Anthropol. 125, 42–50.

Larson, S.G., 1998a. Unique aspects of quadrupedal locomotion in nonhuman primates. In: Strasser, E., Fleagle, J.G., Rosenberger, A.L., McHenry, H.M. (Eds.), Primate Locomotion. Plenum Press, New York, pp. 157–173.

Larson, S.G., 1998b. Parallel evolution in the hominoid trunk and forelimb. Evol. Anthropol. 6, 87–99.

Larson, S.G., Schmitt, D., Lemelin, P., Hamrick, M., 2000. Uniqueness of primate forelimb posture during quadrupedal locomotion. Am. J. Phys. Anthropol. 112, 87–101.

Larson, S.G., Schmitt, D., Lemelin, P., Hamrick, M., 2001. Limb excursion during quadrupedal walking: how do primates compare to other mammals? J. Zool. 255, 353-365.

Lartet, E., 1856. Note sur un grand singe fossile qui se rattache au groupe des singes supérieurs. C. R. Acad. Sci. 43, 219–223.

Latimer, B., Ohman, J.C., Lovejoy, C.O., 1987. Talocrural joint in African hominoids: implications for *Australopithecus afarensis*. Am. J. Phys. Anthropol. 74, 155–175.

Lauder, G.V., 1986. Homology, analogy, and the evolution of behavior. In: Nitecki, M., Kitchell, J. (Eds.), The Evolution of Behavior. Oxford University Press, Oxford, pp. 9–40.

Lawler, R.R., 2006. Sifaka positional behavior: ontogenetic and quantitative genetic approaches. Am. J. Phys. Anthropol. 131, 261–271.

Le Gros Clark, W.E., 1934. Early Forerunners of Man. William Wood, Baltimore.

Le Gros Clark, W.E., 1959. The Antecedents of Man. Edinburgh University Press, Edinburgh.

Le Gros Clark, W.E., Leakey, L.S.B., 1951. The Miocene Hominoidea of East Africa. Foss. Mamm. Afr. 1, 1–117.

Le Gros Clark, W.E., Thomas, D., 1951. Associated jaws and limb bones of *Limnopithecus macinnesi*. Foss. Mamm. Afr. 3, 1–27.

Leakey, R.E., Leakey, M.G., 1987. A new Miocene small-bodied ape from Kenya. J. Hum. Evol. 16, 369–387.

Leardini, A., O'Connor, J.J., Catani, F., Giannini, S., 1999. A geometric model of the human ankle joint. J. Biomech. 32, 585–591.

Leardini, A., O'Connor, J.J., Catani, F., Giannini, S., 2000. The role of the passive structures in the mobility and stability of the human ankle joint: a literature review. Foot Ankle Int. 21, 602–615.

Lebrun, R., Orliac, M.J., 2016. MorphoMuseuM: An online platform for publication and storage of virtual specimens. Paleontol. Soc. Pap. 22, 183–195.

Lemelin, P., 1999. Morphological correlates of substrate use in didelphid marsupials: implications for primate origins. J. Zool. 247, 165–175.

Lemelin, P., Schmitt, D., 2007. Origins of grasping and locomotor adaptations in primates: Comparative and experimental approaches using an opossum model. In: Ravosa, M.J., Dagosto, M. (Eds.) Primate Origins: Adaptations and Evolution. Springer, New York, pp. 329–380.

Lemelin, P., Schmitt, D., Cartmill, M., 2003. Footfall patterns and interlimb co-ordination in opossums (Family Didelphidae): evidence for the evolution of diagonal-sequence walking gaits in primates. J. Zool. 260, 423–429.

Lessertisseur, J., Jouffroy, F.K., 1973. Tendances locomotrices des primates traduites par les proportions du pied. L'adaptation à la bipédie. Folia Primatol. 20, 125–160.

Lewis, O.J., 1964. The tibialis posterior tendon in the primate foot. J. Anat. 98, 209–218.

Lewis, O.J., 1980a. The joints of the evolving foot. Part I. The ankle joint. J. Anat. 130, 527–543.

Lewis, O.J., 1980b. The joints of the evolving foot. Part II. The intrinsic joints. J. Anat. 130, 833–857.

Lewton, K.L., Patel, B.A., 2020. Calcaneal elongation and bone strength in leaping galagids. Am. J. Phys. Anthropol. 171, 430-438.

Liu, F.G.R., Miyamoto, M.M., Freire, N.P., Ong, P.Q., Tennant, M.R., Young, T.S., Gugel, K.F., 2001. Molecular and morphological supertrees for eutherian (placental) mammals. Science 291, 1786–1789.

Llera Martín, C.J., Rose, K.D., Sylvester, A.D., 2022. A morphometric analysis of early Eocene Euprimate tarsals from Gujarat, India. J. Hum. Evol. 164, 103141.

Lockwood, C.A., 1999. Homoplasy and adaptation in the atelid postcranium. Am. J. Phys. Anthropol. 108, 459–482.

López-Torres, S., Selig, K.R., Prufrock, K.A., Lin, D., Silcox, M.T., 2018. Dental topographic analysis of paromomyid (Plesiadapiformes, Primates) cheek teeth: more than 15 million years of changing surfaces and shifting ecologies. Hist. Biol. 30, 76–88.

MacInnes, D.G., 1943. Notes on the east African Miocene primates. J. E. Afr. Uganda Nat. Hist. Soc. 17, 141–181.

MacConaill, M.A., 1953. The movements of bones and joints: 5. The significance of shape. J. Bone. Joint. Surg. Br. 35, 290–297.

MacConaill, M.A., 1973. A structuro-functional classification of synovial articular units. Ir. J. Med. Sci. 142, 19–26.

MacKinnon, J., MacKinnon, K., 1980. The behavior of wild spectral tarsiers. Int. J. Primatol. 1, 361–379.

MaClatchy, L., 2004. The oldest ape. Evol. Anthropol. 13, 90–103.

MaClatchy, L., Gebo, D., Kityo, R., Pilbeam, D., 2000. Postcranial functional morphology of *Morotopithecus bishopi*, with implications for the evolution of modern ape locomotion. J. Hum. Evol. 39, 159–183.

Madar, S. I. 1996. The postcranial morphology of *Sivapithecus*, an Asian large-bodied Miocene hominoid. Ph.D. Dissertation, Kent State University.

Madar, S.I., Rose, M.D., Kelley, J., MacLatchy, L., Pilbeam, D., 2002. New *Sivapithecus* postcranial specimens from the Siwaliks of Pakistan. J. Hum. Evol. 42, 705–752.

Maddison, W.P., 1991. Squared-change parsimony reconstructions of ancestral states for continuous-valued characters on a phylogenetic tree. Syst. Biol. 40, 304–314.

Mahler, D.L., Revell, L.J., Glor, R.E., Losos, J.B., 2010. Ecological opportunity and the rate of morphological evolution in the diversification of Greater Antillean anoles. Evolution 64, 2731–2745.

Maiolino, S.A., Chester, S.G., Boyer, D.M., Bloch, J.I., 2023. Functional morphology of plesiadapiform distal phalanges and implications for the evolution of arboreality in Paleogene euarchontans. J. Mamm. Evol. 30, 1107–1153.

Manter, J.T., 1941. Movements of the subtalar and transverse tarsal joints. Anat. Rec., 80, 397–410.

Marcus, L.F., 1990. Traditional morphometrics. In: Rohlf F.J., Bookstein F.L. (Eds.), Proceedings of the Michigan Morphometrics Workshop. The University of Michigan Museum of Zoology, Ann Arbor, pp. 77–122.

Marigó, J., Susanna, I., Minwer-Barakat, R., Madurell-Malapeira, J., Moyà-Solà, S., Casanovas-Vilar, I., Robles, J.M., Alba, D.M., 2014. The primate fossil record in the Iberian Peninsula. J. Iber. Geol. 40, 179–211.

Marigó, J., Roig, I., Seiffert, E.R., Moyà-Solà, S., Boyer, D.M., 2016. Astragalar and calcaneal morphology of the middle Eocene primate *Anchomomys frontanyensis* (Anchomomyini): Implications for early primate evolution. J. Hum. Evol. 91, 122–143.

Marigó, J., Verrière, N., Godinot, M., 2019. Systematic and locomotor diversification of the *Adapis* group (Primates, Adapiformes) in the late Eocene of the Quercy (Southwest France), revealed by humeral remains. J. Hum. Evol. 126, 71–90.

Marigó, J., Minwer-Barakat, R., Moyà-Solà, S., Boyer, D.M., 2020. First navicular remains of a European adapiform (*Anchomomys frontanyensis*) from the Middle Eocene of the Eastern Pyrenees (Catalonia, Spain): Implications for early primate locomotor behavior and navicular evolution. J. Hum. Evol. 139, 102708.

Marivaux, L., Chaimanee, Y., Ducrocq, S., Marandat, B., Sudre, J., Soe, A.N., Tun, S.T., Htoon, W., Jaeger, J.J., 2003. The anthropoid status of a primate from the late middle Eocene Pondaung Formation (Central Myanmar): tarsal evidence. Proc. Natl. Acad. Sci. USA 100, 13173–13178.

Marivaux, L., Beard, K.C., Chaimanee, Y., Dagosto, M., Gebo, D.L., Guy, F., Marandat, B., Khaing, K., Kyaw, A.A., Oo, M., Sein, C., 2010. Talar morphology, phylogenetic affinities, and locomotor adaptation of a large-bodied amphipithecid primate from the late middle Eocene of Myanmar. Am. J. Phys. Anthropol. 143, 208–222.

Marivaux, L., Tabuce, R., Lebrun, R., Ravel, A., Adaci, M., Mahboubi, M.H., Bensalah, M., 2011. Talar morphology of azibiids, strepsirhine-related primates from the Eocene of Algeria: Phylogenetic affinities and locomotor adaptation. J. Hum. Evol. 61, 447–457.

Marivaux, L., Ramdarshan, A., Essid, E.M., Marzougui, W., Ammar, H.K., Lebrun, R., Marandat, B., Merzeraud, G., Tabuce, R., Vianey-Liaud, M., 2013. *Djebelemur*, a tiny pre-tooth-combed primate from the Eocene of Tunisia: a glimpse into the origin of crown strepsirhines. PLoS One 8, e80778.

Marivaux, L., Lebrun, R., Tabuce, R., 2018. 3D models related to the publication: Djebelemur, a tiny pre-tooth-combed primate from the Eocene of Tunisia: A glimpse into the origin of crown strepsirhines. MorphMuseum 4, e77.

Marivaux, L., Negri, F.R., Antoine, P.O., Stutz, N.S., Condamine, F.L., Kerber, L., Pujos, F., Ventura Santos, R., Alvim, A.M., Hsiou, A.S., Bissaro Jr, M.C., 2023. An eosimiid primate of South Asian affinities in the Paleogene of Western Amazonia and the origin of New World monkeys. Proc. Natl. Acad. Sci. USA. 120, e2301338120.

Martin, R.D., 1968. Towards a new definition of primates. Man 3, 377–401.

Martin, R.D., 1986. Primates: a definition. In: Wood, B.A., Martin, L.B., Andrews, P. (Eds.), Major Topics in Primate and Human Evolution. Cambridge University Press, Cambridge, pp., 1–31.

Martin, R.D., 1990. Primate Origins and Evolution: A Phylogenetic Reconstruction. Princeton University Press, Princeton.

Martins, E.P., Hansen, T.F., 1997. Phylogenies and the comparative method: a general approach to incorporating phylogenetic information into the analysis of interspecific data. Am. Nat. 149, 646–667.

Martínez-Gómez, J., Song, M.J., Tribble, C.M., Kopperud, B.T., Freyman, W.A., Höhna, S., Specht, C.D., Rothfels, C.J., 2024. Commonly used Bayesian diversification methods lead to biologically meaningful differences in branch-specific rates on empirical phylogenies. Evol. Lett. 8, 189–199.

Mazel, F., Davies, T.J., Georges, D., Lavergne, S., Thuiller, W., Peres-Neto, P.R., 2016. Improving phylogenetic regression under complex evolutionary models. Ecology 97, 286–293.

McCrossin, M.L., 1994. The phylogenetic relationships, adaptations, and ecology of *Kenyapithecus*. Ph.D. Dissertation, University of California.

McCrossin, M.L., Benefit, B.R., 1997. On the relationships and adaptations of *Kenyapithecus*, a large-bodied hominoid from the Middle Miocene of Eastern Africa. In: Begun, D.R., Ward, C.V., Rose, M.D. (Eds.), Function, Phylogeny, and Fossils: Hominoid Evolution and Adaptation. Plenum Press, New York, pp. 241–267.

McCrossin, M.L., Benefit, B.R., Gitau, S.N., Palmer, A.K., Blue, K.T., 1998. Fossil evidence for the origins of terrestriality among Old World higher primates. In: Primate Locomotion. Plenum Press, New York, pp. 353–396.

McGhee, G.R. Jr., 2015. Limits in the evolution of biological form: a theoretical morphologic perspective. Interface Focus 5, 20150034.

McGraw, W.S., 1998. Comparative locomotion and habitat use of six monkeys in the Tai Forest, Ivory Coast. Am. J. Phys. Anthropol. 105, 493–510.

McNutt, E.J., Zipfel, B., DeSilva, J.M., 2018. The evolution of the human foot. Evol. Anthropol. 27, 197–217.

Meldrum, D.J., 1990. New fossil platyrrhine tali from the early Miocene of Argentina. Am. J. Phys. Anthropol. 83, 403–418.

Meldrum, D.J., Dagosto, M., White, J., 1997. Hindlimb suspension and hind foot reversal in *Varecia variegata* and other arboreal mammals. Am. J. Phys. Anthropol. 103, 85–102.

Michelson, J.D., Helgemo Jr, S.L., 1995. Kinematics of the axially loaded ankle. Foot Ankle Int. 16, 577–582.

Mittermeier, R.A., 1978. Locomotion and posture in *Ateles geoffroyi* and *Ateles paniscus*. Folia Primatol. 30, 161–193.

Mittermeier, R.A., Fleagle, J.G., 1976. The locomotor and postural repertoires of *Ateles geoffroyi* and *Colobus guereza*, and a reevaluation of the locomotor category semibrachiation. Am. J. Phys. Anthropol. 45, 235–255.

Mitteroecker, P., Bookstein, F., 2011. Linear discrimination, ordination, and the visualization of selection gradients in modern morphometrics. Evol. Biol. 38, 100–114.

Mitteroecker, P., Gunz, P., 2009. Advances in geometric morphometrics. Evol. Biol. 36, 235–247.

Mitteroecker, P., Schaefer, K., 2022. Thirty years of geometric morphometrics: Achievements, challenges, and the ongoing quest for biological meaningfulness. Am. J. Biol. Anthropol. 178, 181–210.

Mitteroecker, P., Gunz, P., Bernhard, M., Schaefer, K., Bookstein, F.L., 2004. Comparison of cranial ontogenetic trajectories among great apes and humans. J. Hum. Evol. 46, 679–698.

Mitteroecker, P., Gunz, P., Windhager, S., Schaefer, K., 2013. A brief review of shape, form, and allometry in geometric morphometrics, with applications to human facial morphology. Hystrix 24, 59-66.

Morse, P.E., Chester, S.G., Boyer, D.M., Smith, T., Smith, R., Gigase, P., Bloch, J.I., 2019. New fossils, systematics, and biogeography of the oldest known crown primate *Teilhardina* from the earliest Eocene of Asia, Europe, and North America. J. Hum. Evol. 128, 103–131.

Morton, D.J., 1924. Evolution of the human foot II. Am. J. Phys. Anthropol. 7, 1–52.

Mosimann, J.E., 1970. Size allometry: size and shape variables with characterizations of the lognormal and generalized gamma distributions. J. Am. Stat. Assoc. 65, 930–945.

Mosimann, J.E., 1975. Statistical problems of size and shape. I. Biological applications and basic theorems. In: Patil, G.P., Kotz, S., Ord, K. (Eds.), Statistical Distributions in Scientific Work 2. Springer, Dordrecht, pp. 187–217.

Moyà-Solà, S., Köhler, M., 1993. Recent discoveries of *Dryopithecus* shed new light on evolution of great apes. Nature 365, 543–545.

Moyà-Solà, S., Köhler, M., 1995. New partial cranium of *Dryopithecus* Lartet, 1863 (Hominoidea, Primates) from the upper Miocene of Can Llobateres, Barcelona, Spain. J. Hum. Evol. 29, 101–139.

Moyà-Solà, S., Köhler, M., 1996. A *Dryopithecus* skeleton and the origins of great-ape locomotion. Nature 379, 156–159.

Moyà-Solà, S., Pons Moyà, J., Köhler, M., 1990. Primates catarrinos (Mammalia) del Neogeno de la peninsula Ibérica. Paleont. i Evol. 23, 41–45.

Moyà-Solà, S., Köhler, M., Alba, D.M., 2001. *Egarapithecus narcisoi*, a new genus of Pliopithecidae (Primates, Catarrhini) from the Late Miocene of Spain. Am. J. Phys. Anthropol. 114, 312–324.

Moyà-Solà, S., Köhler, M., Alba, D.M., Casanovas-Vilar, I., Galindo, J., 2004. *Pierolapithecus catalaunicus*, a new Middle Miocene great ape from Spain. Science 306, 1339–1344.

Moyà-Solà, S., Kohler, M., Alba, D.M., Casanovas-Vilar, I., Galindo, J., 2005. Response to Comment on" *Pierolapithecus catalaunicus*, a new Middle Miocene great ape from Spain". Science 308, 203.

Moyà-Solà, S., Köhler, M., Alba, D.M., Casanovas-Vilar, I., Galindo, J., Robles, J.M., Cabrera, L., Garcés, M., Almécija, S., Beamud, E., 2009a. First partial face and upper dentition of the Middle Miocene hominoid *Dryopithecus fontani* from Abocador de Can Mata (Vallès-Penedès Basin, Catalonia, NE Spain): taxonomic and phylogenetic implications. Am. J. Phys. Anthropol. 139, 126–145.

Moyà-Solà, S., Alba, D.M., Almécija, S., Casanovas-Vilar, I., Köhler, M., De Esteban-Trivigno, S., Robles, J.M., Galindo, J., Fortuny, J., 2009b. A unique Middle Miocene European hominoid and the origins of the great ape and human clade. Proc. Natl. Acad. Sci. USA 106, 9601–9606.

Moyà-Solà, S., Köhler, M., Alba, D.M., Roig, I., 2012. Calcaneal proportions in primates and locomotor inferences in *Anchomomys* and other Palaeogene Euprimates. Swiss J. Palaeontol. 131, 147–159.

Murphy, W.J., Eizirik, E., Johnson, W.E., Zhang, Y.P., Ryder, O.A., O'Brien, S.J., 2001a. Molecular phylogenetics and the origins of placental mammals. Nature 409, 614–618.

Murphy, W.J., Eizirik, E., O'Brien, S.J., Madsen, O., Scally, M., Douady, C.J., Teeling, E., Ryder, O.A., Stanhope, M.J., de Jong, W.W., Springer, M.S., 2001b. Resolution of the early placental mammal radiation using Bayesian phylogenetics. Science 294, 2348–2351.

Nakatsukasa, M., 2004. Acquisition of bipedalism: the Miocene hominoid record and modern analogues for bipedal protohominids. J. Anat. 204, 385–402.

Nakatsukasa, M., 2008. Comparative study of Moroto vertebral specimens. J. Hum. Evol. 55, 581–588.

Nakatsukasa, M., Kunimatsu, Y., 2009. *Nacholapithecus* and its importance for understanding hominoid evolution. Evol. Anthropol. 18, 103–119.

Nakatsukasa, M., Tsujikawa, H., Shimizu, D., Takano, T., Kunimatsu, Y., Nakano, Y., Ishida, H., 2003. Definitive evidence for tail loss in *Nacholapithecus*, an East African Miocene hominoid. J. Hum. Evol. 45, 179–186.

Nakatsukasa, M., Ward, C.V., Walker, A., Teaford, M.F., Kunimatsu, Y., Ogihara, N., 2004. Tail loss in *Proconsul heseloni*. J. Hum. Evol. 46, 777–784.

Nakatsukasa, M., Kunimatsu, Y., Shimizu, D., Nakano, Y., Kikuchi, Y., Ishida, H., 2012. Hind limb of the *Nacholapithecus kerioi* holotype and implications for its positional behavior. Anthropol. Sci. 120, 235–250.

Napier, J.R., Napier, P.H., 1967. A Handbook of Living Primates. Academic Press, New York.

Napier, J.R., Walker, A.C., 1967. Vertical clinging and leaping-a newly recognized category of locomotor behaviour of primates. Folia Primatol. 6, 204–219.

Nekaris, K.A.I., Stevens, N.J., 2007. Not all lorises are slow: rapid arboreal locomotion in *Loris tardigradus* of southwestern Sri Lanka. Am. J. Primatol. 69, 113–121.

Nengo, I.O., Rae, T.C., 1992. New hominoid fossils from the early Miocene site of Songhor, Kenya. J. Hum. Evol. 23, 423–429.

Nengo, I., Tafforeau, P., Gilbert, C.C., Fleagle, J.G., Miller, E.R., Feibel, C., Fox, D.L., Feinberg, J., Pugh, K.D., Berruyer, C., Mana, S., 2017. New infant cranium from the African Miocene sheds light on ape evolution. Nature 548, 169–174.

Ni, X., Wang, Y., Hu, Y., Li, C., 2004. A euprimate skull from the early Eocene of China. Nature 427, 65–68.

Ni, X., Gebo, D.L., Dagosto, M., Meng, J., Tafforeau, P., Flynn, J.J., Beard, K.C., 2013. The oldest known primate skeleton and early haplorhine evolution. Nature 498, 60–64.

Ni, X., Li, Q., Li, L., Beard, K.C., 2016. Oligocene primates from China reveal divergence between African and Asian primate evolution. Science 352, 673–677.

Novacek, M.J., 1992. Fossils, topologies, missing data, and the higher level phylogeny of eutherian mammals. Syst. Biol. 41, 58–73.

Novacheck, T.F., 1998. The biomechanics of running. Gait. Post. 7, 77–95.

Nozaki, S., Amano, H., Oishi, M., Ogihara, N., 2021. Morphological differences in the calcaneus among extant great apes investigated by three-dimensional geometric morphometrics. Sci. Rep. 11, 20889.

Off, E.C., Gebo, D.L., 2005. *Galago* locomotion in Kibale National Park, Uganda. Am. J. Primatol. 66, 189–195.

O'Leary, M.A., Bloch, J.I., Flynn, J.J., Gaudin, T.J., Giallombardo, A., Giannini, N.P., Goldberg, S.L., Kraatz, B.P., Luo, Z.X., Meng, J., Ni, X., 2013. The placental mammal ancestor and the post–K-Pg radiation of placentals. Science 339, 662–667.

O'Meara, B.C., 2012. Evolutionary inferences from phylogenies: a review of methods. Annu. Rev. Ecol. Evol. Syst. 43, 267–285.

O'Meara, B.C., Ané, C., Sanderson, M.J., Wainwright, P.C., 2006. Testing for different rates of continuous trait evolution using likelihood. Evolution 60, 922–933.

Oxnard, C.E., 1978. One biologist's view of morphometrics. Annu. Rev. Ecol. Evol. Syst. 9, 219–241.

Oxnard, C.E., Crompton, R.H., Lieberman, S.S., 1990. Animal Lifestyles and Anatomies. University of Washington Press, Seattle.

Pagel, M., 1997. Inferring evolutionary processes from phylogenies. Zool. Scr. 26, 331–348.

Pagel, M., 1999. Inferring the historical patterns of biological evolution. Nature 401, 877–884.

Pagel, M.D., Harvey, P.H., 1988. Recent developments in the analysis of comparative data. Q. Rev. Biol. 63, 413–440.

Pagel, M., Meade, A., 2008. Modelling heterotachy in phylogenetic inference by reversible-jump Markov chain Monte Carlo. Philos. Trans. R. Soc. B 363, 3955–3964.

Paradis, E., 2014. An introduction to the phylogenetic comparative method. In: Garamszegi, L. (Ed.), Modern Phylogenetic Comparative Methods and Their Application in Evolutionary Biology. Springer, Berlin, pp. 3–18.

Parr, W.C.H., Soligo, C., Smaers, J., Chatterjee, H.J., Ruto, A., Cornish, L., Wroe, S., 2014. Three-dimensional shape variation of talar surface morphology in hominoid primates. J. Anat. 225, 42–59.

Patel, B.A., Seiffert, E.R., Boyer, D.M., Jacobs, R.L., St Clair, E.M., Simons, E.L., 2012. New primate first metatarsals from the Paleogene of Egypt and the origin of the anthropoid big toe. J. Hum. Evol. 63, 99–120.

Patel, B.A., Yapuncich, G.S., Tran, C., Nengo, I.O., 2017. Catarrhine hallucal metatarsals from the early Miocene site of Songhor, Kenya. J. Hum. Evol. 108, 176–198.

Pennell, M.W., Harmon, L.J., 2013. An integrative view of phylogenetic comparative methods: connections to population genetics, community ecology, and paleobiology. Ann. N. Y. Acad. Sci. 1289, 90–105.

Pereira, M.E., Seeligson, M.L., Macedonia, J.M., 1988. The behavioral repertoire of the black-and-white ruffed lemur, *Varecia variegata variegata* (Primates: Lemuridae). Folia Primatol. 51, 1–32.

Perez, S.I., Bernal, V., Gonzalez, P.N., 2006. Differences between sliding semi-landmark methods in geometric morphometrics, with an application to human craniofacial and dental variation. J. Anat. 208, 769–784.

Pérez de Los Ríos, M., Moyà-Solà, S., Alba, D.M., 2012. The nasal and paranasal architecture of the Middle Miocene ape *Pierolapithecus catalaunicus* (Primates: Hominidae): Phylogenetic implications. J. Hum. Evol. 63, 497–506.

Pilbeam, D. R., Rose, M. D., Badgley, C., Lipschutz, B., 1980. Miocene hominoids from Pakistan. Postilla 181, 1–94.

Pilbeam, D.R., Simons, E.L., 1971. Humerus of *Dryopithecus* from Saint Gaudens, France. Nature 229, 406–407.

Pina, M., Alba, D.M., Almécija, S., Fortuny, J., Moyà-Solà, S., 2012. Brief communication: Paleobiological inferences on the locomotor repertoire of extinct hominoids based on femoral neck cortical thickness: The fossil great ape *Hispanopithecus laietanus* as a test-case study. Am. J. Phys. Anthropol. 149, 142–148.

Pina, M., Almécija, S., Alba, D.M., O'Neill, M.C., Moyà-Solà, S., 2014. The Middle Miocene ape *Pierolapithecus catalaunicus* exhibits extant great ape-like morphometric affinities on its patella: Inferences on knee function and evolution. PLoS One 9, e91944.

Pina, M., 2016. Unravelling the positional behaviour of fossil hominoids: Morphofunctional and structural analysis of the primate hindlimb. Ph.D. Dissertation, Universitat Autònoma de Barcelona.

Pina, M., Alba, D.M., Moyà-Solà, S., Almécija, S., 2019. Femoral neck cortical bone distribution of dryopithecin apes and the evolution of hominid locomotion. J. Hum. Evol. 136, 102651.

Pina, M., DeMiguel, D., Puigvert, F., Marcé-Nogué, J., Moyà-Solà, S., 2020. Knee function through finite element analysis and the role of Miocene hominoids in our understanding of the origin of antipronograde behaviours: the *Pierolapithecus catalaunicus* patella as a case study. Palaeontology 63, 459–475.

Plavcan, J.M., 2001. Sexual dimorphism in primate evolution. Am. J. Phys. Anthropol. 116, 25–53.

Polk, J.D., 2002. Adaptive and phylogenetic influences on musculoskeletal design in cercopithecine primates. J. Exp. Biol. 205, 3399–3412.

Polly, P.D., Lawing, A.M., Fabre, A.C., Goswami, A., 2013. Phylogenetic principal components analysis and geometric morphometrics. Hystrix 24, 33–41.

Prang, T.C., 2016. Reevaluating the functional implications of *Australopithecus afarensis* navicular morphology. J. Hum. Evol. 97, 73–85.

Prang, T.C., 2024. The relative size of the calcaneal tuber reflects heel strike plantigrady in African apes and humans. Am. J. Bio. Anthropol. 183, e24865.

Preuschoft, H., 2002. What does "arboreal locomotion" mean exactly and what are the relationships between" climbing", environment and morphology? Z. Morphol. Anthropol. 83, 171–188.

Preuschoft, H., Witte, H., Christian, A., Fischer, M., 1996. Size influences on primate locomotion and body shape, with special emphasis on the locomotion of 'small mammals'. Folia Primatol. 66, 93–112.

Pugh, K.D., 2022. Phylogenetic analysis of Middle-Late Miocene apes. J. Hum. Evol. 165, 103140.

Pugh, K.D., Catalano, S.A., Pérez De Los Ríos, M., Fortuny, J., Shearer, B.M., Vecino Gazabón, A., Hammond, A.S., Moyà-Solà, S., Alba, D.M., Almécija, S., 2023. The reconstructed cranium of *Pierolapithecus* and the evolution of the great ape face. Proc. Natl. Acad. Sci. USA 120, e2218778120.

Püschel, T.A., Gladman, J.T., Bobe, R., Sellers, W.I., 2017. The evolution of the platyrrhine talus: A comparative analysis of the phenetic affinities of the Miocene platyrrhines with their modern relatives. J. Hum. Evol. 111, 179–201.

Püschel, T.A., Marcé-Nogué, J., Chamberlain, A.T., Yoxall, A., Sellers, W.I., 2020. The biomechanical importance of the scaphoid-centrale fusion during simulated knuckle-walking and its implications for human locomotor evolution. Sci. Rep. 10, 3526.

Qiao, Z., Zhou, L., Huang, J.Z., 2009. Sparse linear discriminant analysis with applications to high dimensional low sample size data. Int. J. Appl. Math. 39 48–60.

Raaum, R.L., 2015. Molecular evidence on primate origins and evolution. In: Henke, W., Tattersall, I. (Eds.), Handbook of Paleoanthropology. Springer, Heidelberg, pp. 1083–1135.

Rafferty, K.L., Ruff, C.B., 1994. Articular structure and function in *Hylobates*, *Colobus*, and *Papio*. Am. J. Phys. Anthropol. 94, 395–408.

Rasmussen, D.T., 1990. Primate origins: lessons from a neotropical marsupial. Am. J. Primatol. 22, 263–277.

Rasmussen, D.T., Sussman, R.W., 2007. Parallelisms among primates and possums. In: Ravosa, M.J., Dagosto, M. (Eds.), Primate Origins: Adaptations and Evolution. Springer, New York, pp. 775–803.

Raup, D.M., 1966. Geometric analysis of shell coiling: general problems. J. Paleontol. 40, 1178–1190.

Raventós-Izard, G., Monclús-Gonzalo, O., Moyà-Solà, S., Alba, D.M., Arias-Martorell, J., 2025. Ulnar morphology of *Pliobates cataloniae* (Pliopithecoidea: Crouzeliidae): Insights into catarrhine locomotor diversity and forelimb evolution. J. Hum. Evol. 202, 103663.

Remis, M., 1995. Effects of body size and social context on the arboreal activities of lowland gorillas in the Central African Republic. Am. J. Phys. Anthropol. 97, 413–433.

Revell, L.J., 2009. Size-correction and principal components for interspecific comparative studies. Evolution 63, 3258–3268.

Revell, L.J., 2012. phytools: an R package for phylogenetic comparative biology (and other things). Methods Ecol. Evol. 217–223.

Revell, L.J., 2014. Graphical methods for visualizing comparative data on phylogenies. In: Garamszegi, L. (Ed.), Modern Phylogenetic Comparative Methods and Their Application in Evolutionary Biology. Springer, Berlin, pp. 77–103).

Revell, L.J., Mahler, D.L., Peres-Neto, P.R., Redelings, B.D., 2012. A new phylogenetic method for identifying exceptional phenotypic diversification. Evolution 66, 135–146.

Reyment, R.A., 1985. Multivariate morphometrics and analysis of shape. J. Int. Assoc. Math. Geo. 17, 591–609.

Reynolds, T.R., 1985a. Mechanics of increased support of weight by the hindlimbs in primates. Am. J. Phys. Anthropol. 67, 335–349.

Reynolds, T.R., 1985b. Stresses on the limbs of quadrupedal primates. Am. J. Phys. Anthropol. 67, 351–362.

Ribot, F., Gibert, J., Harrison, T., 1996. A reinterpretation of the taxonomy of *Dryopithecus* from Vallès-Penedès, Catalonia (Spain). J. Hum. Evol. 31, 129–141.

Rohlf, F.J., 1967. Correlated characters in numerical taxonomy. Syst. Zool. 16, 109–126.

Rohlf, F. J., 1990. Morphometrics. Annu. Rev. Ecol. Syst. 21, 299–316.

Rohlf, F.J., 1993. Relative warp analysis and an example of its application to mosquito wings. In: Marcus, L.F., Bello, E., Garcia-Valdecasas, A. (Eds.), Contributions to morphometrics. Nabu Press, Charleston, pp. 131–159.

Rohlf, F.J., 1998. On applications of geometric morphometrics to studies of ontogeny and phylogeny. Syst. Biol. 47, 147–158.

Rohlf, F.J., 1999. Shape statistics: Procrustes superimpositions and tangent spaces. J. Classif. 16, 197–223.

Rohlf, F.J., 2001. Comparative methods for the analysis of continuous variables: geometric interpretations. Evolution 55, 2143–2160.

Rohlf F. J., 2002, Geometric morphometrics and phylogeny. In: MacLeod, N., Forey, P. L. (Eds.), Morphology, shape and phylogeny. Taylor and Francis, London, pp. 175–193.

Rohlf, F.J., 2021. Why clusters and other patterns can seem to be found in analyses of high-dimensional data. Evol. Biol. 48, 1–16.

Rohlf, F.J., Bookstein, F.L., 1987. A comment on shearing as a method for “size correction”. Syst. Zool. 36, 356–367.

Rohlf, F.J., Bookstein, F.L., 2003. Computing the uniform component of shape variation. Syst. Biol. 52, 66–69.

Rohlf, F.J., Corti, M., 2000. Use of two-block partial least-squares to study covariation in shape. Syst. Biol. 49, 740–753.

Rohlf, F.J., Marcus, L.F., 1993. A revolution in morphometrics. Trends Ecol. Evol. 8, 129–132.

Rohlf, F.J., Slice, D., 1990. Extensions of the Procrustes method for the optimal superimposition of landmarks. Syst. Zool. 39, 40–59.

Rolfe, S., Davis, C., Maga, A.M., 2021. Comparing semi-landmarking approaches for analyzing three-dimensional cranial morphology. Am. J. Phys. Anthropol. 175, 227–237.

Rook, L., Bondioli, L., Köhler, M., Moyà-Solà, S., Macchiarelli, R., 1999. *Oreopithecus* was a bipedal ape after all: evidence from the iliac cancellous architecture. Proc. Natl. Acad. Sci. USA 96, 8795–8799.

Rose, K.D., 1994a. The earliest primates. Evol. Anthropol. 3, 159–173.

Rose, K.D., Walker, A., 1985. The skeleton of early Eocene *Cantius*, oldest lemuriform primate. Am. J. Phys. Anthropol. 66, 73–89.

Rose, K.D., Bown, T.M., 1996. A new plesiadapiform (Mammalia: Plesiadapiformes) from the early Eocene of the Bighorn Basin, Wyoming. Ann. Carnegie Mus. 65, 305–319.

Rose, K.D., Rana, R.S., Sahni, A., Kumar, K., Missiaen, P., Singh, L., Smith, T., 2009. Early eocene primates from Gujarat, India. J. Hum. Evol. 56, 366–404.

Rose, K.D., Chester, S.G., Dunn, R.H., Boyer, D.M., Bloch, J.I., 2011. New fossils of the oldest North American euprimate *Teilhardina brandti* (Omomyidae) from the Paleocene–Eocene thermal maximum. Am. J. Phys. Anthropol. 146, 281–305.

Rose, M.D., 1973. Quadrupedalism in primates. Primates 14, 337–357.

Rose, M.D., 1977. Positional behaviour of olive baboons (*Papio anubis*) and its relationship to maintenance and social activities. Primates 18, 59–116.

Rose, M.D., 1983. Miocene hominoid postcranial morphology. In: Ciochon, R.L., Corruccini, R.S. (Eds.), New Interpretations of Ape and Human Ancestry. Plenum Press, New York, pp. 405–417.

Rose, M.D., 1993. Locomotor anatomy of Miocene Hominoids. In: Gebo, D.L. (Ed.), Postcranial adaptation in nonhuman primates. Northern Illinois University Press, DeKalb, pp. 252–272.

Rose, M.D., 1994b. Quadrupedalism in some Miocene catarrhines. J. Hum. Evol. 26, 387–411.

Rose, M.D., Leakey, M.G., Leakey, R.E.F., Walker, A.C., 1992. Postcranial specimens of *Simiolus enjiessi* and other primitive catarrhines from the early Miocene of Lake Turkana, Kenya. J. Hum. Evol. 22, 171–237.

Rose, M.D., Nakano, Y., Ishida, H., 1996. *Kenyapithecus* postcranial specimens from Nachola, Kenya. Afr. Study Monogr. 24, 3–56.

Rosenberger, A.L., 1983. Tale of tails: parallelism and prehensility. Am. J. Phys. Anthropol. 60, 103–107.

Rosenberger, A.L., Preuschoft, H., 2012. Evolutionary morphology, cranial biomechanics and the origins of tarsiers and anthropoids. Palaeobiodiv. Palaeoenviron. 92, 507–525.

Rosenberger, A.L., Stafford, B.J., 1994. Locomotion in captive *Leontopithecus* and *Callimico*: a multimedia study. Am. J. Phys. Anthropol. 94, 379–394.

Ross, C., 1996. Adaptive explanation for the origins of the Anthropoidea (Primates). Am. J. Primatol. 40, 205–230.

Rossie, J.B., Smith, T.D., Beard, K.C., Godinot, M., Rowe, T.B., 2018. Nasolacrimal anatomy and haplorhine origins. J. Hum. Evol. 114, 176–183.

Ruff, C.B., Runestad, J.A., 1992. Primate limb bone structural adaptations. Annu. Rev. Anthropol. 21, 407–433.

Runestad, J.A., 1997. Postcranial adaptations for climbing in Loridae (Primates). J. Zool. 242, 261–290.

Russo, G.A., Shapiro, L.J., 2013. Reevaluation of the lumbosacral region of *Oreopithecus bambolii*. J. Hum. Evol. 65, 253–265.

Russo, G.A., Prang, T.C., McGechie, F.R., Kuo, S., Ward, C.V., Feibel, C., Nengo, I.O., 2024. An ape partial postcranial skeleton (KNM-NP 64631) from the Middle Miocene of Napudet, northern Kenya. J. Hum. Evol. 192, 103519.

Sargis, E.J., 2002. Functional morphology of the hindlimb of tupaiids (Mammalia, Scandentia) and its phylogenetic implications. J. Morphol. 254, 149–185.

Sargis, E.J., Boyer, D.M., Bloch, J.I., Silcox, M.T., 2007. Evolution of pedal grasping in Primates. J. Hum. Evol. 53, 103–107.

Sarmiento, E.E., 1983. The significance of the heel process in anthropoids. Int. J. Primatol. 4, 127–152.

Sarmiento, E.E., 1988. Anatomy of the hominoid wrist joint: its evolutionary and functional implications. Int. J. Primatol. 9, 281–345.

Sarmiento, E.E., Marcus, L.F., 2000. The os navicular of humans, great apes, OH 8, Hadar, and *Oreopithecus*: Function, phylogeny, and multivariate analyses. Am. Mus. Novit. 3288, 1–38.

Savage, D.E., Waters, B.T., 1978. A new omomyid primate from the Wasatch Formation of southern Wyoming. Folia Primatol. 30, 1–29.

Schlager, S., 2017. Morpho and Rvcg-shape analysis in R. In: Zheng, G., Li, S., Szekely, G. (Eds.), Statistical Shape and Deformation Analysis: Methods, Implementation and Applications. Academic Press, London, pp. 217–256.

Schluter, D., Price, T., Mooers, A.Ø., Ludwig, D., 1997. Likelihood of ancestor states in adaptive radiation. Evolution 51, 1699–1711.

Schmidt, M., 2005. Hind limb proportions and kinematics: are small primates different from other small mammals? J. Exp. Biol. 208, 3367–3383.

Schmitt, D., 1996. Humeral head shape as an indicator of locomotor behavior in extant strepsirhines and Eocene adapids. Folia Primatol. 67, 137–151.

Schmitt, D., 1999. Compliant walking in primates. J. Zool. 248, 149–160.

Schmitt, D., 2003. Evolutionary implications of the unusual walking mechanics of the common marmoset (*C. jacchus*). Am. J. Phys. Anthropol. 122, 28–37.

Schmitt, D., Hanna, J.B., 2004. Substrate alters forelimb to hindlimb peak force ratios in primates. J. Hum. Evol. 46, 237–252.

Schmitt, D., Lemelin, P., 2002. Origins of primate locomotion: gait mechanics of the woolly opossum. Am. J. Phys. Anthropol. 118, 231–238.

Schmitt, D., Lemelin, P., 2004. Locomotor mechanics of the slender loris (*Loris tardigradus*). J. Hum. Evol. 47, 85–94.

Schmitt, D., Zeininger, A., Granatosky, M.C., 2016. Patterns, variability, and flexibility of hand posture during locomotion in primates. In: Kivell, T., Lemelin, P., Richmond, B., Schmitt, D. (Eds.), The Evolution of the Primate Hand. Springer, New York, pp. 345–369.

Schön Ybarra, M.A., Schön, III, M.A., 1987. Positional behavior and limb bone adaptations in red howling monkeys (*Alouatta seniculus*). Folia Primatol. 49, 70–89.

Scott, S.H., Winter, D.A., 1991. Talocrural and talocalcaneal joint kinematics and kinetics during the stance phase of walking. J. Biomech. 24, 743–752.

Shapiro, L.J., 2007. Morphological and functional differentiation in the lumbar spine of lorisids and galagids. Am. J. Primatol. 69, 86–102.

Seiffert, E.R., 2012. Early primate evolution in Afro-Arabia. Evol. Anthropol. 21, 239–253.

Seiffert, E.R., Simons, E.L., 2001. Astragalar morphology of late Eocene anthropoids from the Fayum Depression (Egypt) and the origin of catarrhine primates. J. Hum. Evol. 41, 577–606.

Seiffert, E.R., Simons, E.L., Fleagle, J.G., 2000. Anthropoid humeri from the late Eocene of Egypt. Proc. Natl. Acad. Sci. USA 97, 10062–10067.

Seiffert, E.R., Simons, E.L., Clyde, W.C., Rossie, J.B., Attia, Y., Bown, T.M., Chatrath, P., Mathison, M.E., 2005. Basal anthropoids from Egypt and the antiquity of Africa's higher primate radiation. Science 310, 300–304.

Seiffert, E.R., Perry, J.M., Simons, E.L., Boyer, D.M., 2009. Convergent evolution of anthropoid-like adaptations in Eocene adapiform primates. Nature 461, 1118–1121.

Seiffert, E.R., Simons, E.L., Boyer, D.M., Perry, J.M., Ryan, T.M., Sallam, H.M., 2010. A fossil primate of uncertain affinities from the earliest late Eocene of Egypt. Proc. Natl. Acad. Sci. USA. 107, 9712–9717.

Seiffert, E.R., Costeur, L., Boyer, D.M., 2015. Primate tarsal bones from Egerkingen, Switzerland, attributable to the middle Eocene adapiform *Caenopithecus lemuroides*. PeerJ 3, e1036.

Seiffert, E.R., Boyer, D.M., Fleagle, J.G., Gunnell, G.F., Heesy, C.P., Perry, J.M., Sallam, H.M., 2018. New adapiform primate fossils from the late Eocene of Egypt. Hist. Biol. 30, 204–226.

Seiffert, E.R., Tejedor, M.F., Fleagle, J.G., Novo, N.M., Cornejo, F.M., Bond, M., De Vries, D., Campbell Jr, K.E., 2020. A parapithecid stem anthropoid of African origin in the Paleogene of South America. Science 368, 194–197.

Senut, B., 2012. Les restes post-crâniens des Pliopithecidae (Primates) de Sansan. Mém. Mus. Hist. Nat. Paris. 203, 535–558.

Shen, L., Farid, H., McPeek, M.A., 2009. Modeling three-dimensional morphological structures using spherical harmonics. Evolution 63, 1003–1016.

Sidlauskas, B., 2008. Continuous and arrested morphological diversification in sister clades of characiform fishes: a phylomorphospace approach. Evolution 62, 3135–3156.

Sigé, B., Jaeger, J.-J., Sudre, J., Vianey-Liaud, M., 1990. *Altiatlasius koulchii* n. gen. et sp., primate Omomyidé du Paléocène supérieur du Maroc, et les origines des euprimates. Palaeontographica A 214, 31–56.

Silcox, M.T., 2001. A phylogenetic analysis of the Plesiadapiformes and their relationship to Euprimates and other archontans. Ph.D. Dissertation, The Johns Hopkins University.

Silcox, M.T., 2007. Primate taxonomy, plesiadapiforms, and approaches to primate origins. In: Ravosa, M.J., Dagosto, M. (Eds.), Primate Origins: Adaptations and Evolution. Springer, New York, pp. 143–178.

Silcox, M.T., 2008. The biogeographic origins of Primates and Euprimates: east, west, north, or south of Eden? In: Sargis, E.J., Dagosto, M. (Eds.), Mammalian Evolutionary Morphology: A Tribute to Frederick S. Szalay. Springer, Dordrecht, pp. 199–232.

Silcox, M.T., Gunnell, G.F., 2008. Plesiadapiformes. In: Janis, C. M. Gunnell, G. F., Uhen, M. D., (Eds.), Evolution of Tertiary Mammals of North America Vol. 2: Small Mammals, Xenarthrans, and Marine Mammals. Cambridge University Press, Cambridge, pp., 207–238.

Silcox, M.T., Rose, K.D., Walsh, S.L., 2002. New specimens of picromomyids (Plesiadapiformes, Primates) with description of a new species of *Alveojunctus*. Ann. Carnegie Mus. 71, 1–11.

Silcox, M.T., Dalmyn, C.K., Bloch, J.I., 2009. Virtual endocast of *Ignacius graybullianus* (Paromomyidae, Primates) and brain evolution in early primates. Proc. Natl. Acad. Sci. USA 106, 10987–10992.

Silcox, M.T., Benham, A.E., Bloch, J.I., 2010. Endocasts of *Microsyops* (Microsyopidae, Primates) and the evolution of the brain in primitive primates. J. Hum. Evol. 58, 505–521.

Silcox, M.T., Sargis, E.J., Bloch, J.I., Boyer, D.M., 2015. Primate origins and supraordinal relationships: Morphological evidence. In: Henke, W., Tatterstall, I. (Eds.), Handbook of Paleoanthropology. Springer, Heidelberg, pp. 1053–1081.

Silcox, M.T., Bloch, J.I., Boyer, D.M., Chester, S.G., López-Torres, S., 2017. The evolutionary radiation of plesiadapiforms. Evol. Anthropol. 26, 74–94.

Simons, E.L., 1962. Two new primate species from the African Oligocene. Postilla 64, 1–12.

Simons, E., 1995. Egyptian Oligocene primates: a review. Am. J. Phys. Anthropol. 38, 199–238.

Simons, E. L., Pilbeam, D. R., 1965. Preliminary revision of the Dryopithecinae (Pongidae, Anthropoidea). Folia Primatol. 3, 81–152.

Simons, E.L., Seiffert, E.R., 1999. A partial skeleton of *Proteopithecus sylviae* (Primates, Anthropoidea): first associated dental and postcranial remains of an Eocene anthropoidean. C. R. Acad. Sci. Paris 329, 921–927.

Simpson, G.G., 1945. The principles of classification and a classification of mammals. Bull. Am. Mus. Nat. Hist. 85, 1–350.

Slice, D.E., 2001. Landmark coordinates aligned by Procrustes analysis do not lie in Kendall's shape space. Syst. Biol. 50, 141–149.

Smaers, J.B., Mongle, C.S., Kandler, A., 2016. A multiple variance Brownian motion framework for estimating variable rates and inferring ancestral states. Biol. J. Linn. Soc. 118, 78–94.

Smith, G.E., 1924. The Evolution of Man. Oxford University Press, London.

Smith, R.J., 1993. Logarithmic transformation bias in allometry. Am. J. Phys. Anthropol. 90, 215–228.

Smith, R.J., Jungers, W.L., 1997. Body mass in comparative primatology. J. Hum. Evol. 32, 523–559.

Smith, T.D., Rose, K.D., Gingerich, P.D., 2006. Rapid Asia–Europe–North America geographic dispersal of earliest Eocene primate *Teilhardina* during the Paleocene–Eocene thermal maximum. Proc. Natl. Acad. Sci. USA 103, 11223–11227.

Smith, T.D., Rossie, J.B., Bhatnagar, K.P., 2007. Evolution of the nose and nasal skeleton in primates. Evol. Anthropol. 16, 132–146.

Sokal, R.R., Rohlf, F.J., 1995. Biometry. W.H. Freeman and Co., New York.

Song, S., Liu, L., Edwards, S.V., Wu, S., 2012. Resolving conflict in eutherian mammal phylogeny using phylogenomics and the multispecies coalescent model. Proc. Natl. Acad. Sci. USA 109, 14942–14947.

Springer, M.S., Murphy, W.J., Eizirik, E., O'Brien, S.J., 2003. Placental mammal diversification and the Cretaceous–Tertiary boundary. Proc. Natl. Acad. Sci. USA 100, 1056–1061.

Springer, M.S., Stanhope, M.J., Madsen, O., de Jong, W.W., 2004. Molecules consolidate the placental mammal tree. Trends Ecol. Evol. 19, 430–438.

Springer, M.S., Meredith, R.W., Gatesy, J., Emerling, C.A., Park, J., Rabosky, D.L., Stadler, T., Steiner, C., Ryder, O.A., Janečka, J.E., Fisher, C.A., 2012. Macroevolutionary dynamics and historical biogeography of primate diversification inferred from a species supermatrix. PLoS One 7, e49521.

Stayton, C.T., 2005. Morphological evolution of the lizard skull: a geometric morphometrics survey. J. Morphol. 263, 47–59.

Stern, J. T., 1976. Before bipedality. Yearb. Phys. Anthropol. 19, 59–68.

Stern J.T., Susman, R.L., 1983. The locomotor anatomy of *Australopithecus afarensis*. Am. J. Phys. Anthropol. 60, 279–317.

Stevens, J.L., Edgerton, V.R., Mitton, S., 1971. Gross anatomy of the hindlimb skeletal system of the *Galago senegalensis*. Primates 12, 313–321.

Strasser, E., 1988. Pedal evidence for the origin and diversification of cercopithecid clades. J. Hum. Evol. 17, 225–245.

Strauss, R.E., Bookstein, F.L., 1982. The truss: body form reconstructions in morphometrics. Syst. Biol, 31, 113–135.

Su, A., Zeininger, A., 2022. The primate ankle and hindfoot. In: Zeininger, A., Hatala, K.G., Wunderlich, R.E., Schmitt, D. (Eds.), The Evolution of the Primate Foot. Springer, Cham, pp. 21–45.

Sujardito, J., van Hoof, J., 1986. Age-sex class differences in the positional behavior of the Sumatran orangutan (*Pongo pygmaeus abelii*) in the Gunung Leuser National Park, Indonesia. Folia Primatol. 47, 14–25.

Susanna, I., Alba, D.M., Almécija, S., 2010. Las vertebras lumbares del gran simio anthropomorfo basal del Mioceno medio *Pierolapithecus catalaunicus* (Primates: Hominidae). Cidaris 30, 311–316.

Susanna, I., Alba, D.M., Almécija, S., Moyà-Solà, S., 2014. The vertebral remains of the late Miocene great ape *Hispanopithecus laietanus* from Can Llobateres 2 (Vallès-Penedès Basin, NE Iberian Peninsula). J. Hum. Evol. 73, 15–34.

Susman, R.L., 1974. Facultative terrestrial hand postures in an orangutan (*Pongo pygmaeus*) and pongid evolution. Am. J. Phys. Anthropol. 40, 27–37.

Sussman, R.W., 1991. Primate origins and the evolution of angiosperms. Am. J. Primatol. 23, 209–223.

Sussman, R.W., Raven, P.H., 1978. Pollination by lemurs and marsupials: an archaic coevolutionary system. Science 200, 731–736.

Sussman, R.W., Rasmussen, D.T., Raven, P.H., 2013. Rethinking primate origins again. Am. J. Primatol. 75, 95–106.

Swindler, D. R., 2002. Primate Dentition. An Introduction to the Teeth of Non-Human Primates. Cambridge University Press, Cambridge.

Symonds, M.R., Blomberg, S.P., 2014. A primer on phylogenetic generalised least squares. In: Garamszegi, L. (Ed.), Modern Phylogenetic Comparative Methods and Their Application in Evolutionary Biology. Springer, Berlin, pp. 105–130.

Szalay, F.S., 1968. The beginnings of primates. Evolution 22, 19–36.

Szalay, F.S., 1972. The paleobiology of the first primates. In: Tuttle, R. (Ed.), The Functional and Evolutionary Biology of Primates. Routledge, New York, pp. 3–35.

Szalay, F.S., 1975. Phylogeny, adaptations, and dispersal of the tarsiiform primates. In: Luckett, W.P., Szalay, F.S. (Eds.), Phylogeny of the Primates: A Multidisciplinary Approach. Plenum Press, New York, pp. 357–404.

Szalay, F.S., 2007. Ancestral locomotor modes, placental mammals, and the origin of Euprimates: Lessons from history. In: Ravosa, M. J., Dagosto, M. (Eds.), Primate Origins: Adaptations and Evolution. Springer, New York, pp. 457–487.

Szalay, F.S., Dagosto, M., 1980. Locomotor adaptations as reflected on the humerus of Paleogene primates. Folia Primatol. 34, 1–45.

Szalay, F.S., Dagosto, M., 1988. Evolution of hallucial grasping in the primates. J. Hum. Evol. 17, 1–33.

Szalay, F.S., Decker, L.D., 1974. Origins, evolution and function of the tarsus in Late Cretaceous Eutheria and Paleocene primates. In: Jenkins, F.A. (Ed.), Primate Locomotion. Academic Press, New York, pp. 223–259.

Szalay, F.S., Drawhorn, G., 1980. Evolution and diversification of the Archonta in an arboreal milieu. In: Luckett, W.P. (Ed.), Comparative Biology and Evolutionary Relationships of Tree Shrews. Springer, Boston, pp. 133–169.

Szalay, F.S., Langdon, J.H., 1986. The foot of *Oreopithecus*: an evolutionary assessment. J. Hum. Evol. 15, 585–621.

Szalay, F.S., Rosenberger, A.L., Dagosto, M., 1987. Diagnosis and differentiation of the order Primates. Yearb. Phys. Anthropol. 30, 75–105.

Tallman, M., Almécija, S., Reber, S.L., Alba, D.M., Moyà-Solà, S., 2013. The distal tibia of *Hispanopithecus laietanus*: More evidence for mosaic evolution in Miocene apes. J. Hum. Evol., 64, 319–327.

Terranova, C.J., 1996. Variation in the leaping of lemurs. Am. J. Primatol. 40, 145–165.

Thompson, D'A.W., 1915. Galileo and the principle of similitude. Nature 95, 426–427.

Thompson, D'A.W., 1917. On Growth and Form. Cambridge University Press, Cambridge.

Thorpe, S.K., Crompton, R.H., 2006. Orangutan positional behavior and the nature of arboreal locomotion in Hominoidea. Am. J. Phys. Anthropol. 131, 384–401.

Tocheri, M.W., Marzke, M.W., Liu, D., Bae, M., Jones, G.P., Williams, R.C., Razdan, A., 2003. Functional capabilities of modern and fossil hominid hands: Three-dimensional analysis of trapezia. Am. J. Phys. Anthropol. 122, 101–112.

Torres-Tamayo, N., Schlager, S., García-Martínez, D., Sanchis-Gimeno, J.A., Nalla, S., Ogihara, N., Oishi, M., Martelli, S., Bastir, M., 2020. Three-dimensional geometric morphometrics of thorax-pelvis covariation and its potential for predicting the thorax morphology: A case study on Kebara 2 Neandertal. J. Hum. Evol. 147, 102854.

Toussaint, S., Herrel, A., Ross, C.F., Aujard, F., Pouydebat, E., 2015. Substrate diameter and orientation in the context of food type in the gray mouse lemur, *Microcebus murinus*: implications for the origins of grasping in primates. Int. J. Primatol. 36, 583–604.

Turley, K., Frost, S.R., 2013. The shape and presentation of the catarrhine talus: a geometric morphometric analysis. Anat. Rec. 296, 877–890.

Tuttle, R.H., 1967. Knuckle-walking and the evolution of hominoid hands. Am. J. Phys. Anthropol. 26, 171–206.

Tuttle, R.H., 1969. Knuckle-walking and the problem of human origins: Studies on the hands of great apes and man lead to reevaluation of theories on hominoid evolution. Science 166, 953–961.

Tuttle, R.H., 1975. Parallelism, brachiation, and hominoid phylogeny. In: Luckett, W.P., Szalay, F.S. (Eds.), Phylogeny of the Primates. Plenum, New York, pp. 447–480.

Tuttle, R.H., 2014. Apes and Human Evolution. Harvard University Press, Cambridge.

Uhlenbeck, G.E., Ornstein, L.S., 1930. On the theory of the Brownian motion. Phys. Rev. 36, 823–841.

Urciuoli, A., Alba, D.M., 2023. Systematics of Miocene apes: State of the art of a neverending controversy. J. Hum. Evol. 175, 103309.

Usherwood, J.R., Bertram, J.E., 2003. Understanding brachiation: insight from a collisional perspective. J. Exp. Biol. 206, 1631–1642.

Venditti, C., Meade, A., Pagel, M., 2011. Multiple routes to mammalian diversity. Nature 479, 393–396.

Vereecke, E.E., D'Août, K., Aerts, P., 2006. Locomotor versatility in the white-handed gibbon (*Hylobates lar*): A spatiotemporal analysis of the bipedal, tripedal, and quadrupedal gaits. J. Hum. Evol. 50, 552–567.

Vidal, L.M., 1913. Sobre la presència del "*Dryopithecus*" en el Miocè superior del Pirineu català. Treb. Soc. Biol. 1, 247–256.

Vilensky, J.A., Larson, S.G., 1989. Primate locomotion: utilization and control of symmetrical gaits. Annu. Rev. Anthropol. 18, 17–35.

Villalta Comella, J.F. de, Crusafont Pairo, M., 1944. Dos nuevos antropomorfos del Mioceno español y su situación dentro de la moderna sistemática de los símidos. Not. Com. Inst. Geol. Min. Esp. 13, 1–51.

Waddell, P.J., Okada, N., Hasegawa, M., 1999. Towards resolving the interordinal relationships of placental mammals. Syst. Biol. 48, 1–5.

Wainwright, P.C., 2007. Functional versus morphological diversity in macroevolution. Annu. Rev. Ecol. Evol. Syst., 38, 381–401.

Walker, A., 1969. The locomotion of the lorises, with special reference to the potto. Afr. J. Ecol. 7, 1–5.

Walker, A., 1974. Locomotor adaptations in past and present prosimian primates. In: Jenkins, F.A. (Ed.), Primate Locomotion. Academic Press, New York, pp. 349–381.

Walker, A., 1997. *Proconsul*. In: Begun, D.R., Ward, C.V., Rose, M.D. (Eds.), Function, Phylogeny, and Fossils: Miocene Hominoid Evolution and Adaptation. Plenum Press, New York, pp. 209–224.

Walker, A., Pickford, M., 1983. New postcranial fossils of *Proconsul africanus* and *Proconsul nyanzae*. In: Ciochon, R.L., Corruccini, R.S. (Eds.), New Interpretations of Ape and Human Ancestry. Plenum Press, New York, pp. 325–351.

Walker, S.E., Ayres, J.M., 1996. Positional behavior of the white uakari (*Cacajao calvus calvus*). Am. J. Phys. Anthropol. 101, 161–172.

Ward, C.V., 1993. Torso morphology and locomotion in *Proconsul nyanzae*. Am. J. Phys. Anthropol. 92, 291–328.

Ward, C.V., 1998. *Afropithecus*, *Proconsul*, and the Primitive Hominoid Skeleton. In: Strasser, E., Fleagle, J.G., Rosenberger, A.L., McHenry, H.M. (Eds.), Primate Locomotion. Plenum Press, New York, pp. 337–352.

Ward, C.V., 2015. Postcranial and locomotor adaptations of hominoids. In: Henke, W., Tatterstall, I. (Eds.), Hanbook of Paleoanthropology, 2nd ed. Springer, Heidelberg, pp. 1363–1386.

Ward, C.V., Walker, A., Teaford, M.F., 1991. *Proconsul* did not have a tail. J. Hum. Evol. 21, 215–220.

Ward, C.V., Walker, A., Teaford, M.F., Odhiambo, I., 1993. Partial skeleton of *Proconsul nyanzae* from Mfangano island, Kenya. Am. J. Phys. Anthropol. 90, 77–111.

Ward, S.C., Sussman, R.W., 1979. Correlates between locomotor anatomy and behavior in two sympatric species of *Lemur*. Am. J. Phys. Anthropol. 50, 575–590.

Warren, R.D., Crompton, R.H., 1997. Locomotor ecology of *Lepilemur edwardsi* and *Avahi occidentalis*. Am. J. Phys. Anthropol. 104, 471–486.

Warton, D.I., Hui, F.K., 2011. The arcsine is asinine: the analysis of proportions in ecology. Ecology 92, 3–10.

Wells, J.P., Turnquist, J.E., 2001. Ontogeny of locomotion in rhesus macaques (*Macaca mulatta*): II. Postural and locomotor behavior and habitat use in a free-ranging colony. Am. J. Phys. Anthropol. 115, 80–94.

Wiener, N., 1923. Differential-space. J. Math. Phys. 2, 131–174.

Williams, B.A., Kay, R.F., Kirk, E.C., 2010. New perspectives on anthropoid origins. Proc. Natl. Acad. Sci. USA 107, 4797–4804.

Willmott, C.J., Matsuura, K., 2005. Advantages of the mean absolute error (MAE) over the root mean square error (RMSE) in assessing average model performance. Clim. Res. 30, 79–82.

Wilson Mantilla, G.P., Chester, S.G., Clemens, W.A., Moore, J.R., Sprain, C.J., Hovatter, B.T., Mitchell, W.S., Mans, W.W., Mundil, R., Renne, P.R., 2021. Earliest Palaeocene purgatoriids and the initial radiation of stem primates. R. Soc. Open Sci. 8, 210050.

Wold, H., 1966. Estimation of principal components and related models by iterative least squares. In: Krishnaiaah, P.R. (Ed.), Multivariate Analysis. Academic Press, New York, pp. 391–420.

Wold, S., Sjöström, M., Eriksson, L., 2001. PLS-regression: a basic tool of chemometrics. Chemom. Intell. Lab. Syst. 58, 109–130.

Woodward, A.S., 1914. On the lower jaw of an anthropoid ape (*Dryopithecus*) from the Upper Miocene of Lérida (Spain). Quart. J. Geol. Soc. 70, 316–320.

Wright, K.A., 2007. The relationship between locomotor behavior and limb morphology in brown (*Cebus apella*) and weeper (*Cebus olivaceus*) capuchins. Am. J. Phys. Anthropol. 69, 736–756.

Wright, K.A., Stevens, N.J., Covert, H.H., Nadler, T., 2008. Comparisons of suspensory behaviors among *Pygathrix cinerea*, *P. nemaeus*, and *Nomascus leucogenys* in Cuc Phuong National Park, Vietnam. Int. J. Primatol. 29, 1467–1480.

Yapuncich, G.S., Granatosky, M.C., 2021. Footloose: Articular surface morphology and joint movement potential in the ankles of lorisids and cheirogaleids. Am. J. Phys. Anthropol. 175, 876–894.

Yapuncich, G.S., Seiffert, E.R., Boyer, D.M., 2017. Quantification of the position and depth of the flexor hallucis longus groove in euarchontans, with implications for the evolution of primate positional behavior. Am. J. Phys. Anthropol. 163, 367–406.

Yapuncich, G.S., Feng, H.J., Dunn, R.H., Seiffert, E.R., Boyer, D.M., 2019. Vertical support use and primate origins. Sci. Rep. 9, 12341.

Yapuncich, G.S., Chester, S.G.B., Bloch, J.I., Boyer, D.M., 2022. The feet of Paleogene primates. In: Zeiniger, A., Hatala, K.G., Wunderlich, R.E., Schmitt, D. (Eds.), The Evolution of the Primate Foot. Anatomy, Function, and Palaeontological Evidence, 1st ed. Springer, Cham, pp. 277–319.

Youlatos, D., 1998. Positional behavior of two sympatric guianan capuchin monkeys, the brown capuchin (*Cebus apella*) and the wedge-capped capuchin (*Cebus olivaceus*). Mammalia 62, 351–366.

Youlatos, D., 1999. Comparative locomotion of six sympatric primates in Ecuador. Ann. Sci. Nat., B 20, 161–168.

Youlatos, D., 2003. Calcaneal features of the Greek Miocene primate *Mesopithecus pentelicus* (Cercopithecoidea: Colobinae). Geobios 36, 229–239.

Youlatos, D., 2008. Locomotion and positional behavior of spider monkeys. In: Campbell, C.J. (Ed.), Spider Monkeys. Behavior, Ecology and Evolution of the Genus *Ateles*. Cambridge University Press, Cambridge, pp. 185–219.

Youlatos, D., Meldrum, J., 2011. Locomotor diversification in New World monkeys: running, climbing, or clawing along evolutionary branches. Anat. Rec. 294, 1991–2012.

Youlatos, D., Widayati, K.A., Tsuji, Y., 2019. Foot postures and grasping of free-ranging Sunda colugos (*Galeopterus variegatus*) in West Java, Indonesia. Mamm. Biol. 95, 164–172.

Zanolli, C., Bouchet, F., Fortuny, J., Bernardini, F., Tuniz, C., Alba, D.M., 2023. A reassessment of the distinctiveness of dryopithecine genera from the Iberian Miocene based on enamel-dentine junction geometric morphometric analyses. J. Hum. Evol. 177, 103326.

Zapfe, H. 1958. The skeleton of *Pliopithecus* (*Epipliopithecus*) *vindobonensis* Zapfe and Hürzeler. Am. J. Phys. Anthropol. 16, 441–457.

Zelditch, M., Swiderski, D., Sheets, H.D., 2012. Geometric Morphometrics for Biologists: A Primer, 2nd. ed. Academic press, San Diego.

Zihlman, A.L., Underwood, C.E., 2013. Locomotor anatomy and behavior of patas monkeys (*Erythrocebus patas*) with comparison to vervet monkeys (*Cercopithecus aethiops*). Anat. Res. Int. 2013, 409534.

Zhu, W.W., Garber, P.A., Bezanson, M., Qi, X.G., Li, B.G., 2015. Age-and sex-based patterns of positional behavior and substrate utilization in the golden snub-nosed monkey (*Rhinopithecus roxellana*). Am. J. Primatol, 77, 98–108.



Life is short, and potential studies infinite.
We have a much better chance of accomplishing something significant
when we follow our passionate interests and work in areas
of deepest personal meaning.

Stephen Jay Gould (The Panda’s Thumb, 1980)